CHO cell engineering to develop new chassis for enhanced difficult to express recombinant protein production

2024

Phoebe Lee

A thesis submitted to the University of Kent for the degree of Doctor of Philosophy in Biochemistry

University of Kent

School of Biosciences

Declaration

No part of this thesis has been submitted in support of an application for any degree or other qualification of the University of Kent, or any other University or institution of learning.

Phoebe Lee **Date: 15/03/24**

Abstract

Recombinant biotherapeutic protein based therapies have been developed for the treatment of a range of diseases with several therapies successfully obtaining 'blockbuster' status of sales >US $1 Billion pa. Many of these molecules are IgG monoclonal antibodies (mAb) manufactured from *in vitro* cultured mammalian cell expression systems due to their ability to correctly synthesise, assemble, post-translationally modify and secrete the target molecule. Chinese hamster ovary (CHO) cells are the mammalian expression cell line of choice because of their ability to undertake 'human like' post-translation modifications, grow to high viable cell concentrations under fed-batch conditions with isolated cell lines able to produce high yields of target recombinant protein (up to 10 g/L). The CHO cell platform is mature for the production of well-expressed mAbs, but many mAbs and new format molecules such as fusion proteins and other designs remain difficult to express (DTE) in this, or any other host. This thesis describes approaches to engineer the CHO cell to manipulate glycolytic flux to enhance flux from pyruvate to acetyl-CoA, a metabolite that feeds the TCA cycle and fatty acid metabolism, both metabolic pathways known to impact CHO cell phenotype regarding growth and secretory recombinant protein productivity. The pyruvate dehydrogenase (PDH) complex, and pyruvate dehydrogenase kinases (PDKs) that regulate this, were targeted to investigate whether their manipulation impacted CHO cell growth and recombinant protein productivity using a model biotherapeutic DTE protein, Etanercept. The three PDH subunits, E1α, E1β and E2 were cloned, with and without N- and C-terminal tags and stably over-expressed in two host CHO cell lines, CHOS and CHOK1. Subunits were expressed individually and together. A triple mutant of the E1α subunit was generated where the three Ser residues phosphorylated by PDKs to regulate its activity were mutated to Ala residues. C-terminally tagged subunits were observed by western blot to be stably expressed better than N-terminally tagged. Immunoprecipitation experiments using the tag to determine if exogenous subunits were able to form complexes with other native subunits was inconclusive. Knockout (KO) of 3 of the PDKs that phosphorylate and inactivate the E1α subunit was undertaken using CRISPR/Cas9 paired gDNA gene editing approach. Guides that resulted in apparent KO were identified and then KO pools of the three individually targeted PDKs and a triple KO were generated. Multiple attempts to isolate single cell clones of KO cells did not recover and thus KO pools were generated. Reduction in gDNA and mRNA was observed in pools, particularly for PDK1 and PDK2, however complete KO in pools was not observed and no impact on PDK protein expression was apparent. Minipools that did not recover under these study conditions showed evidence of a greater target PDK KO. During batch culture and when transiently expressing Etanercept, the apparent gDNA amount of the PDK genes targeted for KO changed. This likely reflects the nature of the KO pools and that certain populations within the pool were preferentially advantaged under the culture and recombinant protein load allowing them to outgrow others. PDH over-expression resulted in cell pools achieving higher maximum viable cell concentrations and prolonged culture viability under batch culture conditions, but this did not lead to increased transient Etanercept production. Similarly, the PDK KO pools instead resulted in lower apparent cell specific Etanercept production. In both the PDH subunit and PDK KO pools there was evidence of changes in the glycolytic flux as determined by measuring extracellular glucose and lactate concentrations, but there was also cell and pool specific impacts. In conclusion, CHO cells can tolerate PDH subunit over-expression whilst, at least under the conditions investigated here, seem very susceptible to PDK KO. The evidence from this work suggests it is unlikely that manipulation of these components of energy metabolism using the approaches outlined in this thesis can deliver a new CHO chassis with a large enhancement in cell grow or DTE recombinant protein that cannot be achieved from the diversity that already exists within the CHO cell hosts, however alternative approaches may allow this to be achieved.

Acknowledgements

Better late than never!

Many people have helped me throughout my PhD, and I'd like to thank them for their guidance during these many years.

I would like to thank Professor Mark Smales for helping me throughout the process and for always providing support and feedback. The Smales lab have been a key part of my project and I value the time spent getting up to antics as well as the occasional bit of work.

Lab members past and present have made the PhD thoroughly enjoyable with a special thank you to Dr. James Bazeebo, Dr. Laura Dyball, Dr. Sarah Martin, Dr. Louis Darton, Kseniia Pidlisna and Jo Roobol. Your help and support have been essential, and I miss getting up to mischief with the gang. Thank you for your kindness and friendship throughout many ups and downs, it's safe to say a few tears have been shed.

Finally, I'd like to thank my family and friends for their continued support during this process. My mum (Maz) and dad (Baz), brother and Janet have supported me, especially financially, and patiently waited for me to finally finish being a student and get a proper job.

Dr. Ana Cooke, my work wife. Thank you for putting up with me, not only through lockdown but also general life. I miss our flat life and especially your baking.

Evie Haywood, you have supported me and always been there to cheer me up and listen to me rant. How I've not put you off your own PhD is beyond me. But we're quite the pair and can be best Dr gals together soon.

Jack, you have been incredible, your support and love has been amazing, and I am grateful for your kind words and patience, you're quite fab! I await my turn to return the favour.

This thesis has been quite a journey, and I can't say I'll miss it now it's finished!

Table of Contents

Declaration 2
Abstract 3
Acknowledgements 4
Table of Contents 5
List of Abbreviations 10
List of Figures 14
List of Tables 22
Chapter 1: Introduction 24
1.1 Recombinant proteins as therapeutics 24
1.2 Use of mammalian cell lines for the expression of recombinant proteins 28
1.3 CHO cell engineering to improve recombinant protein expression 37
1.4 Targets of CHO cell engineering to increase quality and quantity of biotherapeutic recombinant proteins produced from this expression system 43
1.5 Metabolic targets of CHO cell engineering to increase quality and quantity of recombinant proteins for biotherapeutics 47
1.6 The activity and structure of the pyruvate dehydrogenase complex 52
1.7 Aims of this study 57
Chapter 2: Materials and Methods 58
2.1 General Methods 58
2.2 Molecular Biology to generate gene constructs 58
2.2.1 Lysogeny Broth (LB media) 58
2.2.2 Super Optimal Broth (SOB media) 58
2.2.3 Super Optimal Broth with Catabolite Repression (SOC Media) 58
2.2.4 LB Agar plates 58
2.2.5 Generation of Calcium Competent DH5α cells 58
2.2.6 Transformation of DNA into Calcium Competent DH5α cells 58
2.2.7 Preparation of DNA 59
2.2.8 DNA Quantification 59
2.2.9 Polymerase Chain Reaction target amplification 59
2.2.10.1 Agarose Gel Electrophoresis 62
2.2.10.2 Purification of DNA from Agarose gel 62
2.2.11 Restriction digests 62
2.2.12 Dephosphorylation of a DNA backbone 62

2.2.13 DNA ligation 62
2.3 Mammalian Cell culture and sampling 62
2.3.1 Suspension Cell lines and maintenance 62
2.3.2 Cell sampling 63
2.3.3 Cryopreservation and revival of cells 63
2.3.4 Lipofectamine NovaCHOice® based Transfection of DNA in Mammalian Cells 63
2.3.5 Electroporation based Transfection of DNA in Mammalian Cells 64
2.3.6 Linearisation of DNA and DNA precipitation 64
2.3.7 Construction of Stable Cell Pools 64
2.3.8 Metabolite Analysis 64
2.3.9.1 RNA Extraction and cDNA generation 65
2.3.9.2 mRNA analysis using RTqPCR 65
2.3.10.1 gDNA extraction 68
2.3.10.2 gDNA analysis using qPCR 68
2.4 Protein analysis via SDS-PAGE and Western blotting 71
2.4.1 Cell lysis 71
2.4.2 Bradford Assay 71
2.4.3 Prepare samples for SDS-PAGE gel analysis 71
2.4.4 SDS-PAGE Gels 71
2.4.5 Western blots 72
2.4.6 Dot blots 74
2.4.7 Coomassie Staining 74
2.4.8 Western blot Densitometry analysis 74
2.4.9 Magnetic Immunoprecipitation using Invitrogen Dynabeads™ M-270 Epoxy 74
2.5 CRISPR/Cas9 Knock out of target genes 75
2.5.1 Annealing and phosphorylation of oligos for CRISPR/Cas9 gRNAs 75
2.5.2 Golden Gate Assembly cloning of CRISPR/Cas9 gRNAs into Cas9 vector 77
2.5.3 Single cell cloning by serial dilution 78
2.5.4 Fluorescence activated cell sorting 78
Chapter 3: Investigating the Overexpression of PDH Subunits and their Interactions with Endogenous Subunits 79
3.1 Introduction 79
3.2 Aims of this Chapter 81
3.3 Generation of a Hygromycin 3-Cassette Mammalian Expression Vector 82
3.4 Organisation of PDH Subunit Orientation and Order in the PEL1 Hygro 3 Cassette Vector 83
3.5 PCR Amplification of PDH Subunit Genes 84

3.6 Evaluation of Transient Protein Expression of PDH Subunits in CHOS Cells from PDH Generated Plasmid Constructs 88

3.7 Generation and Evaluation of CHOS and CHOK1 Cell Pools Stably Overexpressing the PDH Subunits 89

3.8 Assembly of the Hygromycin 3 Cassette Tag vector with Antigen Tags in Frame with Target Gene Open Reading Frames 93

3.9 Investigating Transient Expression of the PDH Subunits with N-Terminal Tags 94

3.10 Generation of Stably Expressing N- and C-Tagged PDH Subunit CHO Cell Pools 95

3.11 Evaluation of Recombinant Tagged PDH Subunit Expression in Stable CHO Cell Pools 96

3.12 Generation and Evaluation of CHOS and CHOK1 Cell Pools Stably Expressing an E1alpha PDH Subunit Serine Mutant 106

3.13 Creation and Evaluation of E1alpha Mutant Stably Expressing Cell Pools 108

3.14 Magnetic Bead Immunoprecipitation of the PDH Complex 113

3.15 Evaluation of PDH Subunit gDNA Expression in Stable CHO Cell Pools using qPCR 119

3.16 Discussion 125

Chapter 4: Investigating the Impact of CRISPR/Cas9 KO of PDKs 1-3 on CHO Cell Growth and PDH Expression 128

4.1 Introduction 128

4.2 Aims of this Chapter 129

4.3 Design of PDK1 and PDK2 gRNAs and assembly into the Cas9 plasmid backbone 130

4.4 Analysing Transient Transfection Efficiency of Cas9 Vectors into CHOK1 cells using Flow Cytometry 132

4.5 Evaluation of PDK gDNA in KO Cell Pools using qPCR 135

4.6 Evaluation of PDK mRNA Expression in KO Cell Pools using qRT-PCR 139

4.7 Repeat of the CRISPR/Cas9 Process in CHOS cells and with addition of PDK3 target gRNAs 143

4.8 Analysing Transient Transfection efficiency of Cas9 vectors into CHOS cells and comparison to CHOK1 cells using Flow Cytometry 143

4.9 Evaluation of PDK gDNA Amounts in KO Cell Pools using qPCR 146

4.10 Evaluation of PDK RNA Expression in KO Cell Pools using RTqPCR 150

4.11 Evaluation of PDK Protein Expression in KO Cell Pools 154

4.12 Evaluation of KO impact on PDH subunit gDNA Amounts in CHOS KO Cell Pools using qPCR 161

4.13 Single Cell Sorting for Selection of Monoclonal Cell Lines 168

4.14 FACS Sorting of Cell Pools 169

4.15 Evaluation of PDK Expression in KO Cell Pools with Differences in Recovery 177

4.16 Attempt Two at FACS Sorting of PDK KO Cell Pools 179

4.17 qPCR Screening of PDK gDNA Levels in Selected Cell Pools 184

4.18 General Discussion 186

Chapter 5: Investigating the Impact of PDH Cell Line Engineering on CHO Cell Phenotype and Difficult to Express (DTE) Protein Yields 189

5.1 Introduction 189

5.2 Aims of this Chapter 192

5.3 Analysis of cell growth during batch culture of CHO cell pools engineered to express tagged and untagged exogenous PDH subunits described in Chapter 3 192

5.4 Analysis of untagged and tagged PDH subunit overexpression cell pool IVC values across batch culture 200

5.5 Analysis of glucose concentrations in overexpression cell lines during batch culture 201

5.6 Analysis of lactate concentrations in PDH subunit overexpression cell pools during batch culture 204

5.7 Analysis of the yield of viable cells and lactate from glucose in PDH overexpression cell pools across batch culture 207

5.8 Analysis of ammonia concentrations in PDH subunit overexpression CHO cell pools during batch culture 209

5.9 Analysis of glutamine concentrations in PDH subunit overexpression CHO cell pools during batch culture 211

5.10 Analysis of glutamate concentrations in PDH subunit overexpression CHO cell pools during batch culture 213

5.11 Analysis of batch culture cell growth during transient Etanercept expression in the PDH subunit overexpression and PDK KO CHO cell pools 215

5.12 Investigating model DTE Etanercept expression from PDH subunit overexpression cell pools and PDK KO cell pools 223

5.13 Investigating transient cell specific model DTE Etanercept expression from tagged and untagged PDH subunit overexpression cell pools and PDK KO cell pools 225

5.14 Evaluation of PDH subunit gDNA in CHOS and CHOK1 control cell pools during the Etanercept production run using qPCR 227

5.15 Evaluation of impact of Etanercept production on PDH subunit gDNA amounts in CHOS PDK KO cell pools using qPCR 229

5.16 Evaluation of impact of Etanercept production on PDK gDNA amounts in CHOS PDK KO cell pools using qPCR 233

5.17 Evaluation of impact to expression of Lipid metabolism targets SCD1 and SREBF1 in PDH subunit overexpression cell pools and PDK KO cell pools 234

5.18 Discussion 237

Chapter 6: Overall Discussion 243

Bibliography 259

Appendix 275

Chapter 3 Appendices: 285

Chapter 4 Appendices:..293

List of Abbreviations

ACA	Anti Clumping Agent
ACC	Acetyl-CoA Carboxylase
ADC	Antibody Drug Conjugates
ADCC	Antibody-dependent Cell-mediated Cytotoxicity
AMD	Age-related Macular Degeneration
ANOVA	Analysis of Variance
ATP	Adenosine triphosphate
BAK	BCL-2 Homologous Antagonist Killer
BAX	BCL-2 Associated X Protein
BCL	B Cell Lymphoma Gene 2
BiTE	Bispecific T cell Engager
BLAST	Basic Local Alignment Search Tool
BP	Binding Protein
BSA	Bovine Serum Albumin
Cas	CRISPR Associated Protein
Caspases	Cysteine-dependent Aspartate Proteases
CDC	Complement-dependent Cytotoxicity
cDNA	Complementary DNA
CHO	Chinese Hamster Ovary
CMV	Cytomegalovirus
COVID	Corona Virus Disease
CRISPR	Clustered Regularly Interspaced Short Palindromic Repeats
DCA	Dichloroacetate
dCas9	Dead Cas9
DHFR	Dihydrofolate Reductase
DME	Diabetic Macular Edema
DMSO	Dimethylsulfoxide
DNA	Deoxyribonucleic Acid
DNAJC	DnaJ Homolog C
dNTP	Deoxyribonucleotide Triphosphate
DSB	Double Strand Break
DTE	Difficult to Express

E3bp	E3 Binding Protein
ECL	Enhanced Chemiluminescence
E. coli	*Escherichia coli*
EDTA	Ethylenediaminetetraacetic Acid
eGFP	Enhanced Green Fluorescent Protein
EMA	European Medicines Agency
EPSRC	Engineering and Physical Sciences Research Council
ER	Endoplasmic Reticulum
ERAD	ER Associated Degradation
FACS	Fluorescence-activated cell sorting
Fab	Fragment Antigen-binding
FAD	Flavin Adenine Dinucleotide
Fc	Fragment Crystallisable
FDA	US Food and Drug Administration
FUT 8	Fucosyltransferase 8
GAPDH	Glyceraldehyde-3-phosphate Dehydrogenase
gDNA	Genomic DNA
GFP	Green Fluorescent Protein
gRNA	Guide RNA
GS	Glutamine Synthetase
GSK	GlaxoSmithKline plc
HA	Human influenza hemagglutinin
HCl	Hydrogen Chloride
HDR	Homology Directed Repair
HEK	Human Embryonic Kidney
HSP	Heat Shock Protein
IDT	Integrated DNA Technologies
IMS	Industrial Methylated Spirit
IVC	Integral of Viable Cell Concentration
KO	Knock out
LB	Lysogeny Broth
LDH	Lactate Dehydrogenase
mAb	Monoclonal Antibody
MCS	Multiple Cloning Site

MPC	Mitochondrial Pyruvate Carrier
mRNA	Messenger RNA
MSX	Methionine Sulfoximine
MTX	Methotrexate
NAD	Nicotinamide Adenine Dinucleotide
NADH	Nicotinamide Adenine Dinucleotide + Hydrogen
NADPH	Nicotinamide Adenine Dinucleotide Phosphate
NCBI	National Center for Biotechnology Information
NEB	New England Biolabs
NHEJ	Non-homologous End Joining
NHS	National Health Service
NTC	No Template Control
OD	Optical Density
OPEN	Oligomerised Pool Engineering
PAM	Protospacer Adjacent Motif
PBS	Phosphate-buffered Saline
PC	Pyruvate Carboxylase
PCR	Polymerase Chain Reaction
PDH	Pyruvate Dehydrogenase
PDI	Protein Disulphide Isomerases
PDK	Pyruvate Dehydrogenase Kinase
PDP	Pyruvate Dehydrogenase Phosphatase
PEP	Phosphoenolpyruvate
PK	Pyruvate Kinase
PKM	Pyruvate Kinase Isozymes
PNK	Polynucleotide Kinase
PTM	Post-translational Modification
qPCR	Quantitative PCR
RNA	Ribonucleic Acid
RT	Reverse Transcriptase
RTC	Reverse Transcriptase Control
RTqPCR	Reverse Transcription Quantitative PCR
RVD	Repeat Variable Diresidues
SCD1	Stearoyl CoA Desaturase

scFvs	Single Chain Variable Fragments
SDS	Sodium Dodecyl sulfate
SDS PAGE	Sodium Dodecyl-sulfate Polyacrylamide Gel Electrophoresis
SOB	Super Optimal Broth
SOC	Super Optimal Broth with Catabolite Repression
SREBF1	Sterol Regulatory Element Binding Factor 1
TAE	Tris-acetate-EDTA
TALE	Transcription Activator like Effector
TALEN	Transcription Activator like Effector Nucleases
TBS	Tris-buffered Saline
TBST	Tris-buffered Saline with Tween
TCA	Tricarboxylic Acid Cycle
TEMED	Tetramethylethylenediamine
tPA	Tissue-type Plasminogen Activator
TPP	Thiamine Pyrophosphate
TSAP	Thermosensitive Alkaline Phosphatase
UPR	Unfolded Protein Response
XBP	X box Binding Protein
XIAP	X-Linked Inhibitory Apoptosis Protein
ZFN	Zinc Finger Nuclease

List of Figures

Figure 1.1 Cartoon of the classes of immunoglobulins and their structures alongside a typical monoclonal antibody labelled with its domains.

Figure 1.2 Cartoon structures of several antibody based biotherapeutic designs compared to a monoclonal antibody (mAb).

Figure 1.3.1 Cellular methods to repair a double stranded DNA break as a result of the activity of site-specific nucleases utilised in synthetic biology.

Figure 1.3.2 Activity of the CRISPR/Cas9 complex during a double strand break.

Figure 1.5.1 Overview of glycolysis.

Figure 1.5.2 Overview of pyruvate metabolism and connecting pathways.

Figure 1.6.1 Cartoon structure of the Pyruvate Dehydrogenase (PDH) complex assembly.

Figure 1.6.2 Reactions of the PDH complex converting pyruvate to acetyl-CoA and the switching from active (dephosphorylated) to inactive (phosphorylated) forms via the action of PDPs and PDKs respectively.

Figure 3.3.1 Schematic of the Hygro 3 Cassette plasmid PEL1 showing the unique enzymes used to clone genes into each of the separate cassettes 1, 2 and 3.

Figure 3.5.1 Restriction digest of PEL3 (E1α), Hygro 3 Cass backbone with the E1alpha subunit in cassette 1.

Figure 3.5.2 Restriction digest of PEL4 (E1β), Hygro 3 Cass backbone with the E1beta subunit in cassette 2.

Figure 3.5.3 Restriction digest of PEL5 (E2), Hygro 3 Cass backbone with the E2 subunit in cassette 3.

Figure 3.5.4 Restriction enzyme digest of all Hygro 3 Cass vectors with different combinations of PDH gene subunits in the three cassettes.

Figure 3.7.1 Overnight linearisation of plasmids using FspI enzyme in preparation for the generation of PDH subunit stably expressing CHOS and CHOK1 cell lines.

Figure 3.7.2 Western blot analysis of CHOS cells transfected with PDH subunit plasmids and subjected to hygromycin selection to isolate stably overexpressing PDH cell pools.

Figure 3.7.3 Western blot analysis of β-actin expression in CHOS PDH subunit engineered stable cell pools for expression of the PDH enzyme complex subunits.

Figure 3.7.4 Western blot analysis of CHOK1 cells engineered to stably overexpress PDH enzyme subunits.

Figure 3.8.1 Schematic of the Hygro 3 Cass Tag (PEL12) vector showing the unique enzymes enabling the N- or C-terminal tagging of the PDH enzyme complex genes of interest.

Figure 3.10.1 Agarose gel analysis after the linearisation of plasmid DNA after an overnight digest with FspI enzyme in preparation for the generation of stably expressing CHOS and CHOK1 cell pools expressing the different N- or C-terminally tagged PDH subunits.

Figure 3.11.1.1 Analysis of CHOS and CHOK1 cell pools engineered to stably express E1alpha N V5- (PEL13) and C- (PEL16) terminally tagged protein.

Figure 3.11.1.2 Densitometry of western blot signals showing the relative expression of E2, E3bp and E1alpha subunits in CHOS and CHOK1 cell pools engineered to stably express E1alpha N V5- (PEL13) and C- (PEL16) terminally tagged protein compared to control host cell lines and β-actin expression.

Figure 3.11.2.1 Analysis of CHOS and CHOK1 cell pools engineered to stably express E1beta N HA- (PEL14) and C- (PEL17) terminally tagged protein.

Figure 3.11.2.2 Densitometry of western blot signals showing the relative expression of E2, E3bp and E1alpha subunits in CHOS and CHOK1 cell pools engineered to stably express E1beta N HA- (PEL14) and C- (PEL17) terminally tagged protein compared to control host cell lines and β-actin expression.

Figure 3.11.3.1 Analysis of CHOS and CHOK1 cell pools engineered to stably express E2 N FLAG- (PEL15) and C- (PEL18) terminally tagged protein.

Figure 3.11.3.2 Densitometry of western blot signals showing the relative expression of E2, E3bp and E1alpha subunits in CHOS and CHOK1 cell pools engineered to stably express E2 N FLAG- (PEL15) and C- (PEL18) terminally tagged protein compared to control host cell lines and β-actin expression.

Figure 3.12.1 Restriction digests of PEL19 (E1αmutCV5), Hygro 3 Cass Tags backbone with the mutant E1alpha subunit in cassette 1 and linearisation using FspI in preparation for the generation of stably expressing CHOS and CHOK1 cell pools.

Figure 3.13.1 Evaluation of CHOS and CHOK1 cell pools engineered to stably express E1alpha N V5- and C-terminally tagged proteins (N-PEL13 and C-PEL16) alongside C-terminally V5 tagged E1alpha mutant (PEL19) stably expressing cells.

Figure 3.13.2 Densitometry of western blot signals showing the relative expression of E2, E3bp and E1alpha subunits in CHOS and CHOK1 cell lines engineered to stably express E1alpha N V5- (PEL13) and C- (PEL16) terminally tagged protein and C-terminally V5 tagged E1alpha mutant (PEL19) compared to control host cell lines and β-actin expression.

Figure 3.14.1 CHOS lysate samples from cell pools engineered to stably express E1beta N HA- (PEL14) and C- (PEL17) terminally tagged protein incubated with anti-HA antibody coupled Invitrogen Dynabeads™ M-270 Epoxy beads.

Figure 3.14.2 CHOS and CHOK1 lysate samples from cells engineered to express N- (PEL13) terminally and C- (PEL16) terminally tagged and C-terminally tagged mutant (PEL19) E1alpha PDH subunits incubated with anti-V5 antibody coupled Invitrogen Dynabeads™ M-270 Epoxy beads.

Figure 3.14.3 CHOS and CHOK1 lysate samples from cells engineered to express N- (PEL14) terminally and C- (PEL17) terminally tagged E1beta PDH subunits incubated with anti-HA antibody coupled Invitrogen Dynabeads™ M-270 Epoxy beads.

Figure 3.14.4 CHOS and CHOK1 lysate samples from cells engineered to express N- (PEL15) terminally and C- (PEL18) terminally tagged E2 PDH subunits incubated with anti-FLAG antibody coupled Invitrogen Dynabeads™ M-270 Epoxy beads.

Figure 3.15.1 Fold change in relative gDNA amount of the E1alpha PDH subunit in CHOS and CHOK1 cell pools engineered to stably express E1alpha (PEL3), E1alpha N V5- (PEL13) and C- (PEL16) terminally tagged proteins analysed via qPCR.

Figure 3.15.2 Fold change in relative amount of the E1beta PDH subunit in CHOS and CHOK1 cell pools engineered to stably express E1beta (PEL4), E1beta N HA- (PEL14) and C- (PEL17) terminally tagged proteins analysed via qPCR.

Figure 3.15.3 Fold change in relative amount of the E2 PDH subunit in CHOS and CHOK1 cell pools engineered to stably express E2 (PEL5), E2 N FLAG- (PEL15) and C- (PEL18) terminally tagged proteins analysed via qPCR.

Figure 4.3.1 gRNA positions for targeted CRISPR/Cas9 double strand breaks aiming to knockout target PDK genes of interest resulting in a reduction of expression and therefore activity.

Figure 4.4.1 Flow cytometry analysis of CHOK1 cells transfected with CRISPR/Cas9 plasmids containing the GFP gene and gRNAs targeting either Fut8 or PDK1 genes compared to CHOK1 host cells.

Figure 4.4.2 Flow cytometry analysis of CHOK1 cells transfected with CRISPR/Cas9 plasmids with gRNAs targeting either fut8 or PDK2 genes and with a GFP expression cassette compared to CHOK1 host cells.

Figure 4.5.1 qPCR products when testing primers for PDK genes with CHOS and CHOK1 gDNA.

Figure 4.5.2 Relative gDNA amount of PDK1 in CHOK1 cell pools expressing CRISPR/Cas9 KO plasmids with varied combinations of PDK1 targeting gRNAs analysed via qPCR.

Figure 4.5.3 Relative gDNA amount of PDK2 in CHOK1 cell pools expressing CRISPR/Cas9 KO plasmids with varied combinations of PDK2 targeting gRNAs analysed via qPCR.

Figure 4.5.4 Relative gDNA amount of fut8 in CHOK1 cell pools expressing CRISPR/Cas9 KO plasmids with fut8 targeting gRNAs analysed via qPCR.

Figure 4.6.1 qRT-PCR products when testing primers for PDK genes with CHOS and CHOK1 RNA.

Figure 4.6.2 Relative cDNA amount of PDK1 in CHOK1 cell pools expressing CRISPR/Cas9 KO plasmids with PDK1 targeting gRNAs analysed via qPCR from cDNA samples.

Figure 4.6.3 Relative cDNA amount of PDK2 in CHOK1 cell pools expressing CRISPR/Cas9 KO plasmids with PDK2 targeting gRNAs analysed via qPCR from cDNA samples.

Figure 4.8.1 Flow cytometry of GFP expression from CHOS cell pools transfected with CRISPR/Cas9 gRNAs targeting PDKs 1, 2, 3 and fut8 compared to the control CHOS host cell line.

Figure 4.8.2 Flow cytometry results from analysis of CHOK1 cell pools transfected with CRISPR/Cas9 gRNAs targeting PDKs 1, 2, 3 and fut8 compared to control cell lines.

Figure 4.9.1 Relative gDNA amount of PDK1 in CHOS and CHOkK1 cell pools transfected with CRISPR/Cas9 KO plasmids with PDK1 targeting gRNAs analysed via qPCR from gDNA samples.

Figure 4.9.2 Relative gDNA amount of PDK2 in CHOS and CHOK1 cell pools transfected with CRISPR/Cas9 KO plasmids with PDK2 targeting gRNAs analysed via qPCR from gDNA samples.

Figure 4.9.3 Relative gDNA amount of PDK3 in CHOS and CHOK1 cell pools transfected with CRISPR/Cas9 KO plasmids with PDK3 targeting gRNAs analysed via qPCR from gDNA samples.

Figure 4.9.4 Relative gDNA amount of fut8 in CHOS and CHOK1 cell pools transfected with CRISPR/Cas9 KO plasmids with fut8 targeting gRNAs analysed via qPCR from gDNA samples.

Figure 4.10.1 Relative amount of PDK1 mRNA in CHOS and CHOK1 cell pools transfected with CRISPR/Cas9 KO plasmids with PDK1 targeting gRNAs analysed via RTqPCR from RNA samples.

Figure 4.10.2 Relative amount of PDK2 mRNA in CHOS and CHOK1 cell pools transfected with CRISPR/Cas9 KO plasmids with PDK2 targeting gRNAs analysed via RTqPCR from RNA samples.

Figure 4.10.3 Relative amount of PDK3 mRNA in CHOS and CHOK1 cell pools transfected with CRISPR/Cas9 KO plasmids with PDK3 targeting gRNAs analysed via RTqPCR from RNA samples.

Figure 4.11.1 Western blot analysis of CHOS and CHOK1 cells transfected with CRISPR/Cas9 plasmids with gRNAs targeting PDKs 1, 2, 3 or all three (TRIPLE) when probed with an anti-PDK1 antibody.

Figure 4.11.2 Western blot protein analysis of CHOS and CHOK1 cells transfected with CRISPR/Cas9 plasmids with gRNAs targeting PDKs 1, 2, 3 or all three (TRIPLE) when probed with an anti-PDK2 antibody.

Figure 4.11.3 Western blot protein analysis of CHOS and CHOK1 cells transfected with CRISPR/Cas9 plasmids with gRNAs targeting PDKs 1, 2, 3 or all three (TRIPLE) when probed with an anti-PDK3 antibody.

Figure 4.11.4 Western blot protein analysis of CHOS and CHOK1 cells transfected with CRISPR/Cas9 plasmids with gRNAs targeting PDKs 1, 2, 3 or all three (TRIPLE) when probed with an anti-β-actin antibody.

Figure 4.11.5.1 Western blot protein analysis of CHOS and CHOK1 cells transfected with CRISPR/Cas9 plasmids with gRNAs targeting PDKs 1, 2, 3 or all three (TRIPLE) when probed with an anti-PDPc (D-11) antibody.

Figure 4.11.5.2 Densitometry of western blot signals showing the relative expression of PDP in CHOS and CHOK1 cell pools transfected with CRISPR/Cas9 plasmids with gRNAs targeting PDKs 1, 2, 3 or all three (TRIPLE) compared to control host cell lines and β-actin expression.

Figure 4.11.6.1 Western blot protein analysis of CHOS and CHOK1 cells transfected with CRISPR/Cas9 plasmids with gRNAs targeting PDKs 1, 2, 3 or all three (TRIPLE) when probed with an anti-PKLR antibody.

Figure 4.11.6.2 Densitometry of western blot signals showing the relative expression of PK in CHOS and CHOK1 cell pools transfected with CRISPR/Cas9 plasmids with gRNAs targeting PDKs 1, 2, 3 or all three (TRIPLE) compared to control host cell lines and β-actin expression.

Figure 4.12.1 Relative gDNA amount of PDH subunit E1alpha in CHOS cell pools transfected with CRISPR/Cas9 KO plasmids with PDK1, 2 and 3 targeting gRNAs analysed via qPCR from gDNA samples.

Figure 4.12.2 Relative gDNA amount of PDH subunit E1beta in CHOS cell pools transfected with CRISPR/Cas9 KO plasmids with PDK1, 2 and 3 targeting gRNAs analysed via qPCR from gDNA samples.

Figure 4.12.3 Relative gDNA amount of PDH subunit E2 in CHOS cell pools transfected with CRISPR/Cas9 KO plasmids with PDK1, 2 and 3 targeting gRNAs analysed via qPCR from gDNA samples.

Figure 4.12.4 Relative gDNA amount of PDH subunit E3bp in CHOS cell pools transfected with CRISPR/Cas9 KO plasmids with PDK1, 2 and 3 targeting gRNAs analysed via qPCR from gDNA samples.

Figure 4.12.5 Relative gDNA amount of PDP in CHOS cell pools transfected with CRISPR/Cas9 KO plasmids with PDK1, 2 and 3 targeting gRNAs analysed via qPCR from gDNA samples.

Figure 4.14.1 Dot blot analysis of CHOS and CHOK1 cells transfected with CRISPR/Cas9 plasmids with gRNAs targeting PDK1 or all three PDKs (TRIPLE) when probed with an anti-PDK1 antibody or anti-β-actin antibody.

Figure 4.14.2 Dot blot analysis of CHOS and CHOK1 cells transfected with CRISPR/Cas9 plasmids with gRNAs targeting PDK2 or all three PDKs (TRIPLE) when probed with an anti-PDK2 antibody or anti-β-actin antibody.

Figure 4.14.3 Dot blot analysis of CHOS and CHOK1 cell pools transfected with CRISPR/Cas9 plasmids with gRNAs targeting PDK3 or all three PDKs (TRIPLE) when probed with an anti-PDK3 antibody or anti-β-actin antibody.

Figure 4.14.4 The chosen CHOS and CHOK1 TRIPLE KO cell pools and the originating cell pool size.

Figure 4.14.5 Western blot protein analysis of CHOS and CHOK1 cells transfected with CRISPR/Cas9 plasmids with gRNAs targeting PDK 1 or all three PDKs (TRIPLE) when probed with an anti-PDK1 antibody and an anti-β-actin antibody.

Figure 4.14.6 Western blot protein analysis of CHOS cells transfected with CRISPR/Cas9 plasmids with gRNAs targeting all three PDKs (TRIPLE) when probed with an anti-PDK2 antibody and an anti-β-actin antibody.

Figure 4.14.7 Western blot protein analysis of CHOS and CHOK1 cells transfected with CRISPR/Cas9 plasmids with gRNAs targeting PDK 3 or all three PDKs (TRIPLE) when probed with an anti-PDK3 antibody and an anti-β-actin antibody.

Figure 4.15.1 Relative gDNA amount of PDK2 in selected CHOS and CHOK1 cell pools expressing CRISPR/Cas9 KO plasmids with PDK1 targeting gRNAs analysed via qPCR from gDNA samples.

Figure 4.16.1 Dot blot analysis of CHOS and CHOK1 cells transfected with CRISPR/Cas9 plasmids with gRNAs targeting PDK1 or all three PDKs (TRIPLE) when probed with an anti-PDK1 antibody or an anti-β-actin antibody.

Figure 4.16.2 Western blot analysis of CHOS and CHOK1 cells transfected with CRISPR/Cas9 plasmids with gRNAs targeting PDK2 when probed with an anti-PDK2 antibody or an anti-β-actin antibody.

Figure 4.16.3 Dot blot analysis of CHOS and CHOK1 cells transfected with CRISPR/Cas9 plasmids with gRNAs targeting PDK3 or all three PDKs (TRIPLE) when probed with an anti-PDK3 antibody or an anti-β-actin antibody.

Figure 4.16.4 Dot blot analysis of CHOS and CHOK1 cells transfected with CRISPR/Cas9 plasmids with gRNAs targeting all three PDKs (TRIPLE) when probed with an anti-PDK1 antibody and an anti-β-actin antibody or anti-PDK3 antibody and an anti-β-actin antibody.

Figure 4.17.1 Relative gDNA amount of PDK2 in selected CHOS and CHOK1 cell pools transfected with CRISPR/Cas9 KO plasmids with PDK1 targeting gRNAs analysed via qPCR from gDNA samples.

Figure 5.3.1 Viable cell number ($x10^6$) for CHOS cell pools stably expressing untagged and N- or C-terminally tagged PDH subunits E1alpha, E1beta or E2 generated in Chapter 3 over a 312 hour batch culture time course.

Figure 5.3.2 Average percentage culture viability for CHOS cell pools stably expressing untagged and N- or C-terminally tagged PDH subunits E1alpha, E1beta or E2 generated in Chapter 3 over a 312 hour batch culture time course together with the doubling time (Hours) over the first 96 hours of batch culture and peak cell density ($x10^6$).

Figure 5.3.3 Viable cell number ($x10^6$) for CHOK1 cell pools stably expressing untagged and N- or C-terminally tagged PDH subunits E1alpha, E1beta or E2 generated in Chapter 3 over a 312 hour batch culture time course.

Figure 5.3.4 Average Percentage Viability for CHOK1 cell lines stably expressing untagged and N- or C-terminally tagged PDH subunits E1alpha, E1beta or E2 generated in Chapter 3 over a 312 hour batch culture time course together with the doubling time (Hours) over the first 96 hours of batch culture and peak cell density ($x10^6$).

Figure 5.4.1 Integral of Viable Cell Concentration (IVC) of CHOS and CHOK1 cell pools over a 312 hour batch culture time course.

Figure 5.5.1 Glucose concentration (mmol) over culture time and cumulative glucose utilisation (QGlucose) over IVC for CHOS and CHOK1 overexpression cell pools generated in Chapter 3 over a 312 hour batch culture.

Figure 5.5.2 Specific utilisation of glucose for CHOS and CHOK1 PDH subunit overexpression cell pools.

Figure 5.6.1 Lactate concentration (mmol) over culture time and cumulative lactate production (QLactate) over IVC for CHOS and CHOK1 PDH subunit overexpression cell pools generated in Chapter 3 across a 312 hour batch culture.

Figure 5.6.2 Specific production of lactate for CHOS and CHOK1 PDH subunit overexpression cell pools.

Figure 5.7 Yield of viable cells per glucose (mmol) and yield of lactate (mmol) per glucose (mmol) over culture for CHOS and CHOK1 PDH subunit overexpression cell pools generated in Chapter 3 from a 312 hour batch culture.

Figure 5.8.1 Ammonia concentration (mmol) over culture time and cumulative ammonia production (QAmmonia) over IVC for CHOS and CHOK1 PDH subunit overexpression cell pools generated in Chapter 3 from a 312 hour batch culture.

Figure 5.8.2 Specific production of ammonia from CHOS and CHOK1 PDH subunit overexpression cell pools.

Figure 5.9.1 Glutamine concentration (mmol) over culture time and cumulative glutamine production (QGlutamine) over IVC for CHOS and CHOK1 PDH subunit overexpression cell pools generated in Chapter 3 from a 312 hour batch culture.

Figure 5.9.2 Specific utilisation of glutamine for CHOS and CHOK1 PDH subunit overexpression cell pools.

Figure 5.10.1 Glutamate concentration (mmol) over culture time and cumulative glutamate production (QGlutamate) over IVC for CHOS and CHOK1 PDH subunit overexpression cell pools generated in Chapter 3 from a 312 hour batch culture.

Figure 5.10.2 Specific production of glutamate for CHOS and CHOK1 PDH subunit overexpression cell pools.

Figure 5.11.1 Restriction test digest of Etanercept PEL11 plasmid using AvrII and BamHI fast digest enzymes.

Figure 5.11.2 Viable cell number ($x10^6$) for CHOS cell pools stably expressing C-terminally tagged PDH subunits E1beta (PEL17) or E2 (PEL18) and E1alpha mutant (PEL19) alongside CHOS PDK2 and PDK3 KO cell pools generated transiently expressing Etanercept over a 240 hour batch culture.

Figure 5.11.3 Average culture viability for CHOS cell pools stably expressing C-terminally tagged PDH subunits E1beta (PEL17) or E2 (PEL18) and E1alpha mutant (PEL19) alongside CHOS PDK2 and PDK3 KO cell pools transiently expressing Etanercept over a 240 hour batch culture.

Figure 5.11.4 Viable cell number ($x10^6$) for CHOK1 cell pools stably expressing N- or C-terminally tagged PDH subunits E1alpha (PEL13 & PEL16), E1beta (PEL14 & PEL17) or E2 (PEL15 & PEL18) and E1alpha Serine/Alanine mutant PEL19 transiently expressing Etanercept over a 240 hour batch culture.

Figure 5.11.5 Average culture viability for CHOK1 cell pools stably expressing N- or C-terminally tagged PDH subunits E1alpha (PEL13 & PEL16), E1beta (PEL14 & PEL17) or E2 (PEL15 & PEL18) and E1alpha Serine/Alanine mutant PEL19 transiently expressing Etanercept over a 240 hour batch culture.

Figure 5.12 Densitometry analysis from dot blot analysis of transient Etanercept production from edited CHOS and CHOK1 cells generated in Chapters 3 and 4 when probed with anti-γ chain antibody.

Figure 5.13.1 Integral of viable cell concentration (IVC) of CHOS and CHOK1 cells transiently producing Etanercept in a production run over a 240 hour batch culture time course.

Figure 5.13.2 Relative cell specific Etanercept production in CHOS and CHOK1 cell pools generated in Chapters 3 and 4.

Figure 5.14.1 Relative gDNA amount of PDH subunits E1alpha, E1beta, E2, E3BP and LDHa and PDP in CHOS and CHOK1 host control cell pools during batch culture compared to an Etanercept production run, analysed via qPCR from gDNA samples taken 144 hours into culture time.

Figure 5.15.1 Relative gDNA amount of PDH subunits E1alpha, E1beta, E2 and E3BP, LDHa and PDP in CHOS PDK KO cell lines during an Etanercept production run compared to CHOS host analysed via qPCR from gDNA samples taken 144 hours into culture time.

Figure 5.16.1 Relative gDNA amount of PDK1 and PDK2 in CHOS PDK KO cell pools during an Etanercept production run compared to CHOS host cells during an Etanercept production run analysed via qPCR from gDNA samples taken 144 hours into culture time.

Figure 5.17.1 Evaluation of SREBF1 and β-actin protein expression in CHOS and CHOK1 cell pools engineered to stably express E1alpha N V5- and C-terminally tagged and untagged proteins (N-PEL13, C-PEL16 and untagged PEL3) alongside the E1alpha serine/alanine mutant PEL19 cells.

Figure 5.17.2 Evaluation of SREBF1 and β-actin protein expression in CHOS and CHOK1 cell pools engineered to stably express E1beta N HA- and C-terminally tagged and untagged proteins (N-PEL14, C-PEL17 and untagged PEL4).

Appendix Figure 7.1.1 Western blot analysis of PDH subunit expression in CHOS cells harvested 72 hours after transfection with plasmids for the expression of PDH subunits via Merck NovaCHOice lipofectamine.

Appendix Figure 7.1.2 Western blot analysis of β-actin expression in CHOS cells harvested 72 hours after transfection with plasmids for the expression of PDH subunits via Merck NovaCHOice lipofectamine.

Appendix Figure 7.1.3 Western blot analysis of eGFP expression in CHOS cells harvested 72 hours after transfection with plasmids for the expression of PDH subunits via Merck NovaCHOice lipofectamine.

Appendix Figure 7.1.4 Percentage culture viability of CHOS cells transfected with different PDH constructs or a control 72 hours post-transfection.

Appendix Figure 7.1.5 Culture viability of CHOS and CHOK1 cells three days after transient transfection with the N-terminally tagged PDH subunit containing PEL13, 14 and 15.

Appendix Figure 7.1.6 Western blot protein analysis of CHOS and CHOK1 cells for transient expression of an N-terminally HA tagged E1beta subunit when probed with an anti-HA antibody.

Appendix Figure 7.1.7 Evaluation of CHOS and CHOK1 cell pools engineered to stably express E1alpha N V5- and C-terminally tagged proteins (N – PEL13, C - PEL16) respectively.

Appendix Figure 7.1.8 Evaluation of CHOS and CHOK1 cell pools engineered to stably express E1beta N HA- and C- terminally tagged proteins respectively (N- PEL14 and C- PEL17).

Appendix Figure 7.1.9 Evaluation of CHOS and CHOK1 cell pools engineered to stably express E2 N FLAG- and C -terminally tagged proteins (N-PEL15 and C-PEL18) respectively.

Appendix Figure 7.1.10 qPCR products when testing primers for PDH subunit genes with CHOS and CHOK1 gDNA.

Appendix Figure 7.1.11 qPCR products when testing primers for PDH subunit genes with CHOS gDNA.

List of Tables

Table 1.1 Advantages and disadvantages of cell based expression systems commonly used for the production of recombinant proteins and an example of their use in the biopharmaceutical industry.

Table 1.2 The top ten selling biopharmaceutical products of 2022 alongside the company that produced it, their sales in billions of US dollars and information about the molecule design, target and host cell production platform.

Table 1.3 Summary of key differences between double strand break synthetic biology based nucleases.

Table 1.4 Some of the cell engineering strategies and approaches investigated to improve recombinant protein production from CHO cells.

Table 1.6.1 Specificities of PDKs 1-4 when targeting PDH E1alpha subunit Serine residues 264, 271 and 203 for phosphorylation.

Table 2.2.1.1 Thermocycler Programme used for PCR with Phusion High Fidelity Polymerase.

Table 2.2.1.2 Thermocycler Programme used for PCR with Promega GoTaq® G2 Flexi DNA Polymerase.

Table 2.2.2 Primers used to amplify target genes including the addition of a tag when required.

Table 2.3.1 Thermocycler programme used to run all RTqPCR and qPCR plates.

Table 2.3.2 Primer sequences used for RTqPCR analysis.

Table 2.3.3 Primer sequences used for qPCR analysis.

Table 2.4.1 Details of Primary and Secondary Antibodies. Antibodies were diluted accordingly in 5% (w/v) BSA in TBST buffer.

Table 2.5.1.1 Thermocycler programme used for annealing and phosphorylation of oligos for CRISPR/Cas9 gRNAs.

Table 2.5.1.2 gRNAs sequences used for CRISPR/Cas9 targeting of specific genes of interest for KO.

Table 2.5.2 Thermocycler Programme used for Golden Gate assembly cloning of CRISPR/Cas9 gRNAs into the Cas9 vector.

Table 3.4.1 Restriction enzymes used for cloning of PDH subunits into different cassettes of the Hygro 3 Cass vector PEL1 and the insert size of each gene.

Table 3.4.2 The seven plasmids generated from PEL1 for overexpression of the different PDH subunits and combinations of these.

Table 3.8.1 Restriction enzymes used on the end of primers for PCR amplification, and subsequent digestion and ligation of PDH subunits into PEL2 in the specific cassette locations.

Table 3.11.1 Summary of the protein expression and resulting densitometry data of relative expression of PDH subunits presented in Figures 3.11.1.1 to 3.11.3.2.

Table 3.13.1 Summary of the protein expression and resulting densitometry data of relative expression of PDH subunits presented in Figures 3.13.1.1 and 3.13.1.2.

Table 3.12.1 Restriction enzymes used on the end of primers for PCR amplification, and subsequent digestion and ligation of the mutant E1alpha PDH subunit into PEL12 into cassette 1.

Table 4.10.1 The final gRNA pairs chosen for CRISPR/Cas9 targeted KO of PDKs 1, 2 and 3 in both CHOS and CHOK1 cell lines.

Table 5.1 CHOS and CHOK1 cell pools generated in Chapter 3 of this thesis and the gene engineered.

Appendix Table I Plasmids used throughout the cloning process to enable the expression of recombinant protein.

Chapter 1: Introduction

1.1 Recombinant proteins as therapeutics

The production of recombinant proteins is usually achieved by the introduction of recombinant DNA into a host cell, although other systems such as cell free systems can be used. The host cells gene expression machinery is then utilised to produce the protein of interest. Recombinant proteins produced in such a manner can be used for a wide range of applications including the assembly of enzymes for use in the food industry (Deckers et al., 2020) or as biocatalysts for applications in textiles (Jemli et al., 2016) and animal feed industries (Gifre et al., 2017). Alternatively, recombinant proteins can be manufactured industrially as biotherapeutics for use in the clinic as treatments for diseases such as cancer (Posner et al., 2019). When compared to traditional small molecule treatments, which are chemically synthesised drugs with a known molecular structure and show little batch to batch variation (Makurvet, 2021), clinically relevant biotherapeutic recombinant proteins are usually produced from a living biological organism (e.g. bacteria, fungi) or *in vitro* cultured cell expression system (e.g. mammalian cell, insect cells). Biotherapeutic recombinant proteins are highly specific in the role they clinically undertake meaning they are less likely to interfere with normal biological processes and have the potential for more complex activities compared to small molecules. In the case of replacement therapies, the molecule produced is as close to the 'human' protein as possible and in some cases identical (e.g. insulin). As these recombinant proteins are to be administered clinically into patients, their manufacture must be undertaken under much stricter and highly controlled conditions and processes compared to those destined for use as enzymes or in food products.

Recombinant protein based biotherapeutics can be categorised into multiple classes depending on their function and application (Leader et al., 2008). For example, these can be consider as belonging to 4 different groups. Group 1 are considered therapeutics with enzymatic or regulatory activity including those that replace deficient or abnormal protein, augment an existing pathway, or provide a novel function. Group 2 includes protein therapeutics with special targeting activity such as those that interfere with molecules or organisms or those that deliver other compounds or proteins to a specific site. Group 3 are protein vaccines that protect against foreign agents, treat autoimmune diseases and cancers. Group 4 includes proteins used for in vivo diagnostics to answer clinical questions. The activity of recombinant protein-based therapeutics can be used to assign them to one of two categories, agonists that act as replacement therapies and are required

at a low dosage or antagonists that act to block and prevent normal physiological function and are required at a higher dose (Rudge & Ladisch, 2020).

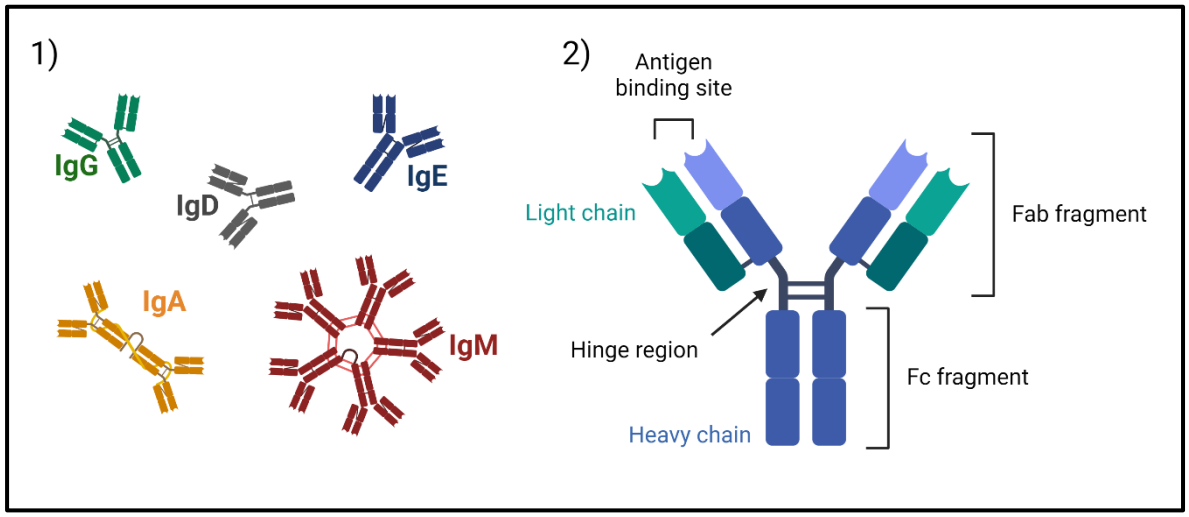

Figure 1.1 Cartoon representation of the classes of immunoglobulins and their structures (1) alongside a typical monoclonal antibody labelled with its domains (2). Created with BioRender.com.

Recombinant proteins also fall into classes based on format and structure. Antibodies or antibody-inspired designs bind to specific target molecules called antigens and act to inactivate pathogens or recognise non-self molecules and target these for destruction. Antibodies or immunoglobulins (Igs) are the result of an immune response and there are a number of different types or classes of Ig molecules; IgA, IgD, IgE, IgG, IgM. A typical monoclonal antibody (mAb) structure is made up of two antigen binding fragments (Fab) and a crystallisable fragment (Fc) that join together to form a Y shape. Figure 1.1 shows the classes of antibodies and the structure of the fragments as well as the light and heavy chains, antigen binding site and hinge region. The heavy and light chains are made up of constant and variable domains which allow target specificity. The majority of antibody therapies in the clinic or development are based on the IgG class of which there are 4 isotypes (IgG1-4) (Vidarsson et al., 2014). These IgGs can be manipulated or added to such as in the use of antibody drug conjugates (ADCs) (Sasso et al., 2023) which act to deliver a payload. Alternatively, the sections of the antibody structure can be used in antibody fragment based biotherapeutics such as fusion proteins or single chain variable fragments (Goulet & Atkins, 2020). Recombinant therapeutic proteins can also be enzymes that catalyse biochemical reactions in the body, coagulation factors involved in blood clotting, protein hormones such as insulin or cytokines such as interleukins or interferons that mediate cell to cell communication (Ebrahimi & Samanta, 2023).

The class, structure and action of a biotherapeutic must be considered when looking for industrially relevant candidates for the treatment of disease.

Biotherapeutic recombinant protein based treatments for use in the clinic are being used to treat an increasingly wide range of diseases and represent a large part of the multi-billion US dollar biotechnology industry. Production of these complex molecules usually relies on harnessing host cells as 'factories' for their expression. Prokaryotic cells such as *Escherichia coli* (*E. coli*) (Baeshen et al., 2015) or eukaryotic cells such as yeast (Gomes et al., 2018), animal (Zhu, 2011), insect (Mckenzie & Abbott, 2018) or plant (Karki et al., 2021) cells are amongst those used as host cell expression systems for the manufacture of biotherapeutic recombinant proteins. Each have their advantages and disadvantages for the production of recombinant proteins (Tripathi & Shrivastava, 2019), particularly at large and industrially relevant scales which are summarised in Table 1.1. Alternatively, research developments have been made for producing recombinant proteins using so called 'cell free systems' (K. H. Lee & Kim, 2018) with benefits including reduced cost, reliance on host cell growth and reduced potential for host intracellular functions to impact the protein product (Yue et al., 2023). However, currently this approach is not scalable to meet the large amounts of protein required for multiple treatments.

Table 1.1 Advantages and disadvantages of cell based expression systems commonly used for the production of recombinant proteins and an example of their use in the biopharmaceutical industry. Adapted from (Shanmugaraj et al., 2020).

Expression System	**Advantages**	**Disadvantages**	**Example use in Industry**
Bacteria (Prokaryotic)	High yield, scale up possible, large variety of genetic elements for plasmids	Limited post-translational modifications	Lucentis (Humanized IgG antibody Fragment to treat Neovascular (wet) age-related macular degeneration) Roche/Genentech, Novartis produced in *E. coli*
Yeast (Eukaryotic)	Rapid growth, simple and inexpensive media, post-translational modifications	Hyper glycosylation can occur, difficulties due to thick cell wall	Semglee (Insulin glargine yfgn to treat Diabetes mellitus) Biocon Biologics Inc. produced in *Pichia pastoris*
Mammalian (Eukaryotic)	Protein products secreted, post-translational modifications, suitable for complex molecules, existing regulatory approval	High cost of media and culture conditions, low to medium yield, additives required	Humira (Adalimumab to treat rheumatoid arthritis) AbbVie & Eisai, produced in Chinese hamster ovary cells
Insect (Eukaryotic)	High expression, folding and post-translational modifications	High cost, glycosylation profiles can be an issue	Supemtek (Quadrivalent influenza vaccine) Sanofi Pasteur produced in Sf9 insect cells
Plant (Eukaryotic)	High biomass accumulation, optimised growth conditions	Glycosylation profiles can be an issue, regulatory compliance issues	Covifenz (Corona virus-like particle vaccine) Medicago, GSK produced in *Nicotiana benthamiana*

The development of a new biotherapeutic protein, estimated to cost an average of $780 million over a 10-year development time (Farid et al., 2020), combines with the costs from industrial production challenges and specialist requirements to result in a large cost to the provider (e.g. NHS, insurance company, individual patient) which can limit the availability of specific treatment options. Rare and uncommon diseases that do not have a large enough treatable target market for industrial development can be left without treatment due to the lack of financial interest from biopharmaceutical companies as the large upfront costings will not be offset from treatment sales. For these reasons, alongside the wide variety of potential applications of biotherapeutic proteins, there is a drive to deliver new approaches that decrease the development time and production costs whilst increasing protein yields and treatment availability. These pressures were brought into further context by the COVID-19 global pandemic with a push to increase the availability and development speed of treatments and vaccines. The US Food and Drug Administration (FDA) and other regulatory bodies such as the European Medicines Agency (EMA) have worked to accelerate scientific advice, compliance checks and evaluation procedures (Walsh & Walsh, 2022) with the use of the accelerated approval pathways allowing early access to the market depending on reporting of study process and post approval studies (Hwang et al., 2022). These processes still have large upfront costs due to the production requirements and clinical studies required so can be considered risky due to the potential for removal of regulatory approval further down the clinical development pathway, however increased and more rapid patient treatment availability can result from these changes. Alongside changes to the regulatory framework, the development of enhanced manufacturing platforms for the recombinant biotherapeutics, particularly for those that are currently considered difficult to express (DTE), is required to meet the increasing demand for these medicines, lowering the development times and costs and increasing patient availability.

1.2 Use of mammalian cell lines for the expression of recombinant proteins

Cultured host cell expression systems have been used for the production of recombinant biotherapeutic proteins for many years. The first recombinant DNA product, Humulin® a recombinant form of human insulin, was approved by the FDA in 1982 and produced in prokaryotic *E. coli* cells (Kinch, 2015). The first FDA approved recombinant protein biotherapeutic produced in eukaryotic mammalian cells, Tissue Plasminogen Activator (tPA) used to treat acute ischemic stroke, was approved for market shortly after in 1986 and was produced in Chinese hamster ovary (CHO) cells (Williams et al., 1986). Eukaryotic, and in particular mammalian, cell lines offer multiple advantages when expressing recombinant DNA intended for production of complex biotherapeutics such as those with post-translational modifications that need to be

'human like' or that contain multiple chains with complex folding needs when compared to prokaryotic host cell systems. The ability to grow mammalian cells in suspension in large culture volumes in bioreactors (S. Xu et al., 2017) enables a scalable production process and the adaption of these cells to chemically defined, serum free media and reduces the potential for the presence of contaminants such as viruses in the final product (Marigliani et al., 2019). However, serum-free equivalent additives are often still required which can add to the production cost especially when compared to a bacterial system such as *E. coli* which can be cultured in considerably cheaper media and at similar large culture volumes.

Another advantage of mammalian cells is that they also secrete expressed recombinant protein out of the cell (Le et al., 2015) allowing product purification from the culture supernatant with product titres for a typical mAb design reaching up to 10 g/L in a fed batch process (Kunert & Reinhart, 2016). This contrasts to *E. coli* expression systems whereby the product needs to be recovered from inside the cell requiring extra downstream processing steps. Mammalian host cells also generate 'human protein-like' post-translational modifications (PTMs) (Zhu, 2011) such as phosphorylation, ubiquitination and of particular importance for many biotherapeutic proteins, glycosylation patterns (Bryan et al., 2021). Prokaryotic systems can often not produce patterns that are 'human protein-like' as they that lack the required enzymes and intracellular compartments to undertake such modifications (Ghaderi et al., 2012). Post-translational, co-translational and chemical modifications such as these are a key advantage of eukaryotic and mammalian cells over prokaryotic cell hosts when producing complex biotherapeutic protein designs that would otherwise require further processing steps after expression in prokaryotic hosts.

When considering glycosylation patterns, these can impact recombinant protein affinity, stability (Q. Zhou & Qiu, 2019) immunogenicity and the biologic activity and clearance rate of a biotherapeutic. Immunogenicity is an important consideration for recombinant proteins and their post-translation modifications. Proteins naturally have structurally heterogenous glycosylation patterns (Jefferis, 2016) which are often mirrored in recombinant proteins produced from a host cell system. As a result, maintaining glycosylation patterns between batches has been determined as a key critical quality attribute for industrial production. Optimisation of process strategies such as the feeding, culture duration, temperature, pH and dissolved oxygen are identified and maintained due to their potential to impact glycosylation (alongside other attributes such as titre, cell growth), and may have a larger impact on recombinant protein glycosylation than differences between cell clones (Hmiel et al., 2015). The glycans influence the half-lives of antibodies (and other proteins) and enhance their antibody-dependent cell-mediated cytotoxicity (ADCC) and

complement-dependent cytotoxicity (CDC) activity (Giddens et al., 2018). Glycoengineering strategies have been extensively explored in order to impact or tune the reproducibility of glycosylation and to impact recombinant protein activity. This approach is particularly relevant for non-mammalian and non-human cell lines that produce glycosylation patterns not expressed in humans which can lead to immune responses. For example, the presence of core fucose can impact recombinant protein ADCC by decreasing the affinity between the Fc region and receptor (Z. Wang et al., 2020). By combining cell engineering and glycoengineering, the Fut8 gene encoding α1,6-fucosyltransferase can be knocked out in CHO cells to create non-fucosylated proteins with enhanced ADCC activity (Yang et al., 2021). This issue can be removed by the use of human cell lines such as HeLa or human embryonic kidney 293 (HEK293) cells although the clinical use of these cell lines is not as extensive as other mammalian host cells such as CHO (Dumont et al., 2016).

It is important that the host cell system of choice matches the complexity of the biotherapeutic design so simpler, less intricate proteins may be successfully produced in a cheaper non-mammalian alternative. This thesis centres on the use of animal, and in particular mammalian cell lines, and their use for producing recombinant proteins for biotherapeutic applications notably those that are considered DTE.

Table 1.2 The top ten selling biopharmaceutical products of 2022 alongside the company that produced it, their sales in billions of US dollars and information about the molecule design, target and host cell production platform. Adapted from (Walsh & Walsh, 2022)**.**

Rank	Product	Company	Sales (Billions)	Molecule	Treatment Target	Production Platform
1	Comirnaty	Pfizer & BioNTech	36.8	COVID-19 Vaccine, mRNA	COVID-19 vaccine	Cell free, mRNA
2	Humira (adalimumab)	AbbVie & Eisai	21.2	mAb	Rheumatoid Arthritis	CHO
3	Spikevax (COVID-19 Vaccine, mRNA)	Moderna	17.7	COVID-19 Vaccine, mRNA	COVID-19 vaccine	Cell free, mRNA
4	Keytruda (pembrolizumab)	Merck	17.2	Humanised mAb	Head and neck squamous cell cancer	CHO
5	Stelara (ustekinumab)	Janssen (Johnson & Johnson)	9.5	mAb	Plaque psoriasis, psoriatic arthritis, Crohn's disease and ulcerative colitis	Murine
6	Eylea (aflibercept)	Regeneron, Bayer	9.4	Fusion protein	Neovascular (wet) age-related macular degeneration (AMD) and diabetic macular edema (DME)	CHO
7	Opdivo (nivolumab)	Bristol Myers Squibb, Ono	8.5	mAb	Melanoma and multiple other cancers	CHO
8	Ronapreve/Regen-Cov (casirivimab & imdevimab)	Roche, Regeneron	7.6	Mix of two Humanised mAbs	COVID-19	CHO
9	Trulicity (dulaglutide)	Eli Lilly	6.7	Fusion protein	Diabetes mellitus	CHO
10	Darzalex (daratumumab)	Janssen	6.0	Humanised mAb	Multiple myeloma and light chain amyloidosis	CHO

Mammalian cells were the most frequently used expression system for recombinant protein products from 2018-2022, with 67% of the approved biopharmaceuticals approved in the time period produced in mammalian cells and 89% of these were in CHO cells (Walsh & Walsh, 2022). Table 1.2 shows the 10 top selling biopharmaceutical products in 2022 where the presence of two COVID-19 mRNA based vaccines and a COVID-19 mAb based treatment highlight the impact the global pandemic had on the biopharmaceutical industry. CHO cells are shown to be the preferred host cell production system for many of these products which is likely due to the aforementioned benefits of the cells combined with the historical success of approvals from regulatory authorities of biotherapeutics produced in these hosts. However, as treatment aims are expanded for new diseases, innovative biotherapeutic designs are being created to meet the unique requirements for the generation of suitable treatments including identifying novel modes of action and the delivery of antibodies to difficult to reach sites of action (Carter & Lazar, 2017). These molecules can differ from the traditional mAb design and can often be considered DTE. The term DTE can be applied to many recombinant proteins including mAbs and membrane proteins with multiple factors influencing their expression. They are often characterised by low protein yields, low solubility and stability, misfolding and toxicity to the host cell system (Chen et al., 2023) as well as high levels of protein aggregation.

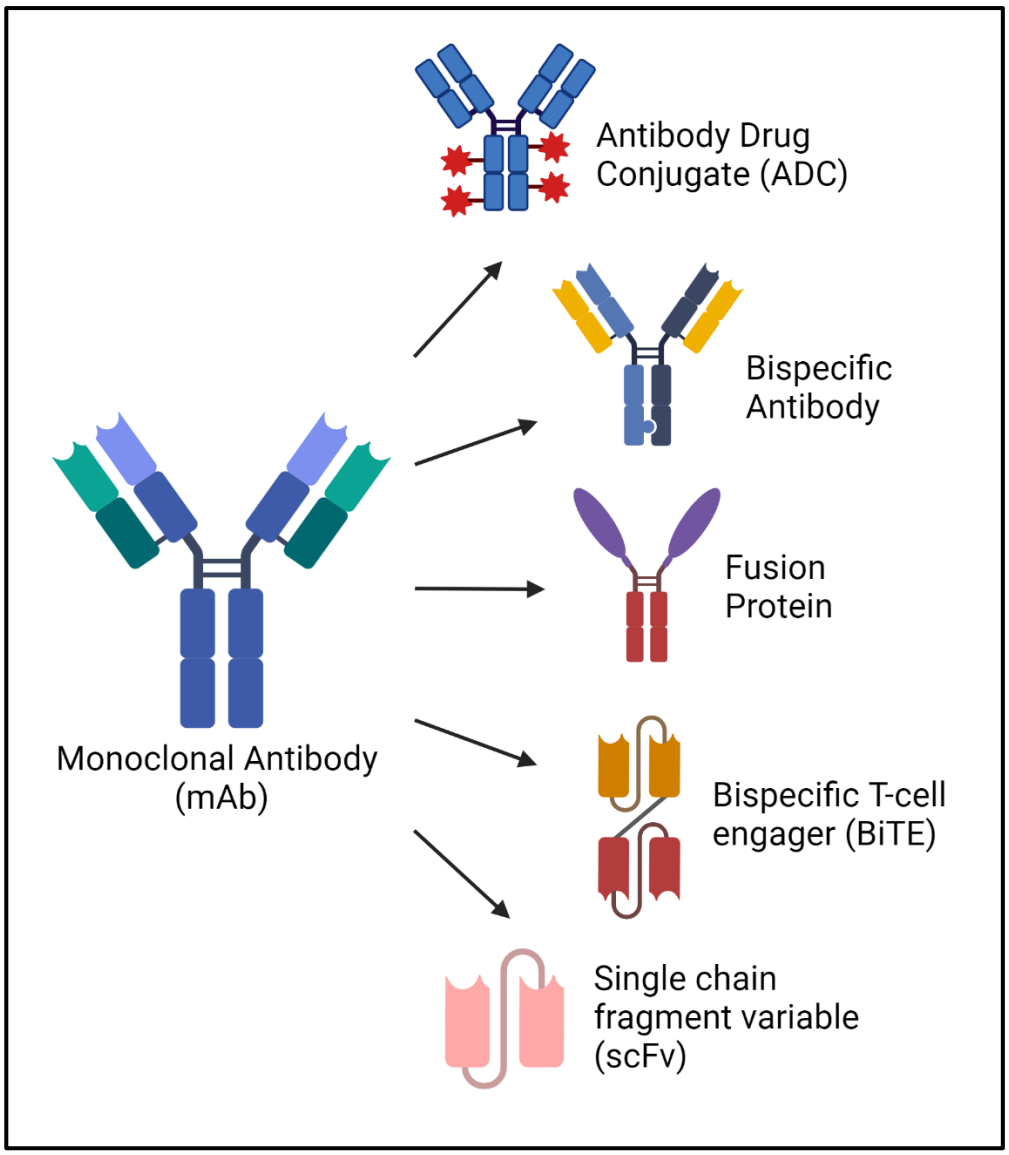

Figure 1.2 Cartoon structures of several antibody based biotherapeutic designs compared to a monoclonal antibody (mAb). Created with BioRender.com.

Figure 1.2 shows examples of different novel biotherapeutic designs based on the IgG format and their structure compared to the classic native mAb format. Antibody drug conjugates (ADCs) are a further variation on the classic mAb and act to deliver a cytotoxic chemical or warhead to the site of antibody binding, combining the potency of the chemical and the high selectivity and stability of mAbs (Beck et al., 2017). A variety of linkers can be used to attach a range of chemicals to the mAb. Different scaffolds are also being developed based upon multiple antigen binding sites such as bispecific antibodies capable of recognising two targets. ADCs offer the potential for a bystander effect killing neighbouring cells that may not be presenting disease relevant antigens but this alongside the chemical toxicity needs to be managed for specific target designs.

Bispecific and multispecific antibodies have the potential for binding two or more target recognition sites. There are two categories of multi specific molecules, non-obligate which bind two or more targets involved in a signalling pathway simultaneously such as a mix of antibodies or obligate that have multiple binding specificities included in a single molecule to achieve expected efficacies such as immune cell engagers or ADCs (Zhong et al., 2021). Multispecific antibodies can vary in structure and format depending on the structural building blocks chosen but increased design complexity can lead to challenges when expressing and correctly assembling the molecule design. However, this also allows the selection of specific advantageous structural components such as the Fc domain to increase the half-life of the molecule and influence other antibody effector functions associated with the Fc region such as antibody recycling, ADCC and CDC (Booth et al., 2018). This structural approach is seen in the design of fusion proteins where multiple ligands such as extracellular domains or receptors, peptides, cytokine traps or enzymes are attached to an Fc domain (Duivelshof et al., 2021). This attachment also allows the binding of the Fc domain to protein A or protein G which is advantageous for manufacturing steps such as purification (Rath et al., 2015).

A similar biotherapeutic design is the bispecific T cell engager (BiTE) which acts to bind both target antigens and T cells bringing them together to form an immune synapse inducing T cell mediated killing of target cells. BiTEs differ from bispecific antibodies in their format, consisting of two single chain variable fragments (scFvs) connected by small linker peptides (Goebeler & Bargou, 2020). Toxicities associated with BiTEs include the potential for cytokine release syndrome emphasising dosage as an important consideration for these treatments. Small chain variable fragments (scFvs) are an example of a protein scaffold that can be incorporated into BiTEs and other biotherapeutic protein products but can also be used as a standalone design. Co-expression of two scFvs can be used to form a bispecific fragment called a diabody with one-to-one antigen binding (Spiess et al., 2015). The format reduces molecular size enabling access to difficult to reach target sites although the lack of an Fc domain can lead to a short half life and therefore requires more frequent dosing.

Process development and optimisation of pharmacokinetics and safety also need to be considered with bispecific and multispecific antibody formats specifically when compared to a typical IgG mAb format. Requiring the correct assembly of multiple chains, bispecific and multispecific formats can lead to the formation of incorrect assemblies which can lead to protein aggregation resulting in cellular stress and enhanced immunogenicity for patients (W. Wang & Roberts, 2018). If the expressed heavy and light chains are of a similar size, the formation of homodimers can be an issue for protein purification methods. To encourage the heterodimerisation of bispecific antibody chains, methods to engineer the Fc region of the antibody such as the Knob in Hole mutations

have been used (H. Liu et al., 2017). This process forms mutations in one of the antibody heavy chain constant domains to reduce the formation of homodimers increasing yield of the correct heterodimer whilst reducing the purification steps and protein aggregate levels. Biosimilars are also emerging as key players in the biotherapeutic market. By taking advantage of the end of a particular products licensing and adapting the format or design, a biosimilar can act as an equivalent treatment creating competition within the industry, driving down prices and increasing treatment availability for patients (Azevedo et al., 2015).

The design and expression of novel biotherapeutic formats can vary depending on desired characteristics and pharmacokinetics as well as the host system used. Although they often show increasingly complex designs when compared to a mAb format, they are not necessarily immediately considered DTE and multiple biotherapeutics based on these structures have been industrially produced, approved for treatments and are available for patient treatments on the market. There is however a balance between the expression levels that make these treatments possible and the costings for their development. The identification of a DTE protein can result in the removal of the drug candidate or the cessation of product development for rare or uncommon diseases altogether. The expression of novel biotherapeutic designs is usually carried out in the same mammalian systems as those used for less complex designs that generate higher protein yields (Mathias et al., 2020). There is expectation that the platform processes developed for mAb expression translate for the expression of these non-native and DTE molecules, however this may not necessarily be the case. It is therefore important to identify characteristics of DTEs and develop approaches to improve protein expression in host cell systems to prevent the loss of drug candidates at the initial screening stages whilst aiming to reduce the costs and time associated with their development.

When aiming to increase the protein yield from a host cell system, multiple approaches have been taken outside the design of the biotherapeutic molecules themselves (Davy et al., 2017). Improvements to the DNA vector design can include codon optimisation of gene sequences to suit the relevant host cell expression system as well as the use of promoters and assembly of multiple expression cassettes to increase expression levels. This is particularly relevant with mAbs which require expression of both light and heavy chains for their assembly. Light chains are important in the folding and assembly of mAbs as excess heavy chains can become misfolded and form aggregates (Ho et al., 2015). It is therefore important to consider the ratios of the expression of these two components which becomes even more important when producing multispecific formats with multiple transgenes and their positions in the expression cassettes (Beal et al., 2023a).

One approach is to use inducible promoters that allows the culture to reach high viable cell numbers before 'switching on' expression of the target protein and can be of particular interest when the expression of the target is toxic to the cells (Kallunki et al., 2019). However, this approach is yet to be fully adopted when using mammalian expression systems due to the required use of inducible agents, for example the antibiotic tetracycline. The method of DNA delivery via transfection can also be varied using biological, chemical or physical processes, although electroporation is often the choice for industrial manufacture (M. M. Zhu et al., 2017). The site of DNA integration in stably expressing cell pools is also of interest when aiming to increase protein expression. Random integration creates highly heterogeneous expression in cell pools including those with very low or very high protein expression levels which require additional work to isolate high expressing clones (Hamaker & Lee, 2018). The use of site specific recombinases allows the creation of landing pads at sites with high expression levels where the same recombinases can be used to specifically insert target genes to that locus (Gaidukov et al., 2018) generating high producing cell lines. The use of chemically defined, serum free media for mammalian cell culture allows choice for individual cell lines with different medium designed for specific purposes such as high cell density growth, increased cell longevity or the enhancement of cell specific productivity (Pan et al., 2017). Media optimisation efforts aim to increase titre, maintain nutrient levels, optimise trace elements, salts and osmolarity whilst minimising accumulation of waste metabolites and avoiding cellular aggregation and clumping (Ritacco et al., 2018).

Small molecules can also be used as additives to improve process productivity and reduce production costs acting through multiple mechanisms such as impacting cell cycle and cellular redox regulation (Q. Zhang et al., 2023). These additives aim to keep a smaller number of high yielding cells at specific stages of the cell cycle to improve productivity, but their impact needs to be analysed fully before they are added to a production process. The use of on-line measurements during cell cultures for key factors such as pH, metabolite levels and dissolved oxygen also ensures that the cultures are constantly monitored during their growth with feedback loops ensuring negative impacts on the culture viabilities and cell numbers are avoided.

In a similar fashion the use of omics approaches such as metabolomics and proteomics ensures that samples taken throughout the culture course can be analysed for key quality attributes such as product quality and titre influencing future approaches to recombinant protein expression. Further development of bioreactors used for culturing mammalian cells whilst producing recombinant proteins has also led to improvements in production. By understanding how the cells interact with the macroenvironment inside the bioreactor and combining this with real time

process monitoring, the production culture can be adjusted throughout the process aiming to maintain high viabilities and cell numbers (Sharma et al., 2022). Novel bioreactor designs can combine with different culture styles such as perfusion culture for a continuous process with a constant flow in and out of the bioreactor (Bielser et al., 2018). These processes link to the downstream purification of recombinant proteins where improvements have been made to processes such as centrifugation and filtration methods allowing an improved purified protein yield from the same volume of cell culture.

Overall, these improvements to the different aspects of recombinant protein expression in mammalian cells have been driven by efforts to reduce production and development costs. Another alternative is to use engineering techniques to alter the host cells themselves. This thesis focuses on using synthetic biology based techniques to improve the expression of recombinant proteins such as those that are considered DTEs by altering the CHO cell host through multiple approaches including targeting its metabolism.

1.3 CHO cell engineering to improve recombinant protein expression

A benefit of using CHO cells as a mammalian host system for the expression of recombinant proteins is its malleable genome that allows for genetic manipulation and the use of cell engineering techniques with the aim of improving expression levels of recombinant proteins. CHO cells have high tolerance to genetic manipulations and adapt well to different manufacturing process scales (Dahodwala & Lee, 2019). A traditional approach of targeting one gene or protein for up or downregulation generates a specific response and can improve knowledge surrounding the role of that target of interest on the cell growth or protein production levels. However, a connected approach using a combination of synthetic biology and cell engineering enables the targeting of multiple genes in a target pathway to address protein complexes and their roles in recombinant protein expression.

The term synthetic biology is used to describe numerous approaches and biological techniques for the manipulation of genetic elements that control gene expression in cellular systems. By combining 'engineering principles with existing biotechnology techniques, such as DNA sequencing and genome editing, to modify organisms or create new ones' (Government Accountability Office US, 2023) synthetic biology can be used to alter an organism's genetic makeup to suit the individual system requirements such as those of large-scale industrial production of biotherapeutic proteins for the treatment of diseases such as cancer (Abil et al., 2015). As such, synthetic biology and cell engineering need not be restricted to living organisms

and can be applied to cells and cellular systems such as *in vitro* cultured mammalian cells used for the production of biotherapeutic proteins.

Synthetic biology techniques have been used to target many genes and pathways involved in controlling CHO cell growth, metabolism and recombinant protein expression with the aim of increasing expression of beneficial genes and/or reducing or knocking out expression of those that are disadvantageous in regards to these goals (Fischer et al., 2015). When aiming to overexpress a target gene of interest, its sequence is identified and codon optimised for the host cell system if the gene is not native. This is a key application of synthetic biology, with the introduction of non-native genes taken from other species which can be advantageous due to the host systems lack of regulatory elements to control the 'new' gene leading to high expression levels. However, high expression levels may be detrimental and therefore it is often necessary to 'tune' the level of expression to achieve the desired result (i.e. the highest expression, or constitutive expression may not always be the most appropriate). Once cloned into a mammalian expression vector, the plasmid DNA is delivered into the cells via transfection through a method such as lipid mediated or electroporation and appropriate expression levels driven by a promoter, often of viral origin. Expression can be transient for short term expression or stable, whereby the gene of interest is integrated into the host genome, for long term expression that is passed onto future cell generations.

If stably integrating DNA of interest into the host cell genome, a selection pressure is applied, such as the antibiotic hygromycin, so that only cells expressing the selection gene residing within the plasmid featuring a hygromycin resistance marker survive. To avoid the use of antibiotics in industrial processes, an alternative metabolic based selection marker is often used, for example the glutamine synthetase (GS) selection system. This process uses the activity of GS which catalyses the condensation of glutamate and ammonia to generate glutamine avoiding the accumulation of toxic waste product ammonia (Lin et al., 2019). This can then be used as a substrate for nucleotide synthesis, NADPH and other biosynthetic pathways involved in cellular integrity and function (Cruzat et al., 2018). CHO cells produce glutamine endogenously so a GS inhibitor methionine sulfoximine (MSX) is added to cultured cells to select those only expressing the target gene and the GS gene contained within it. Improvements to this selection process have led to the generation of GS knock out (KO) cell lines (Fan et al., 2012) that avoid any potential endogenous CHO cell GS gene expression and using weaker promoters designed to require a reduced concentration of MSX whilst still generating high producing cell lines (Fan et al., 2013).

These antibiotic or metabolic selection processes can lead to high levels of heterogeneity between cell pools so single cell cloning techniques are often used to select monoclonal cells expressing the target to a high level. However, care must be taken as high levels of expression of some gene targets may have a negative impact on factors such as cell growth and recombinant protein expression. This process can also be used to generate high producing cell lines expressing recombinant protein targets for use in large scale production processes and is often used in combination with targeted integration such as the use of the piggyBac transposase (Wei et al., 2022) so that the target gene or protein is inserted in an active transcription site resulting in high expression levels ultimately aiming to limit the clonal screening process required.

When aiming to knock the expression of a target gene down or out, synthetic biology techniques can also be used. These processes involve the use of site-specific targeted nucleases to cause double stranded DNA breaks and using the cellular repair methods of non-homologous end joining (NHEJ) or homology directed repair (HDR) to repair them, shown in Figure 1.3.1.

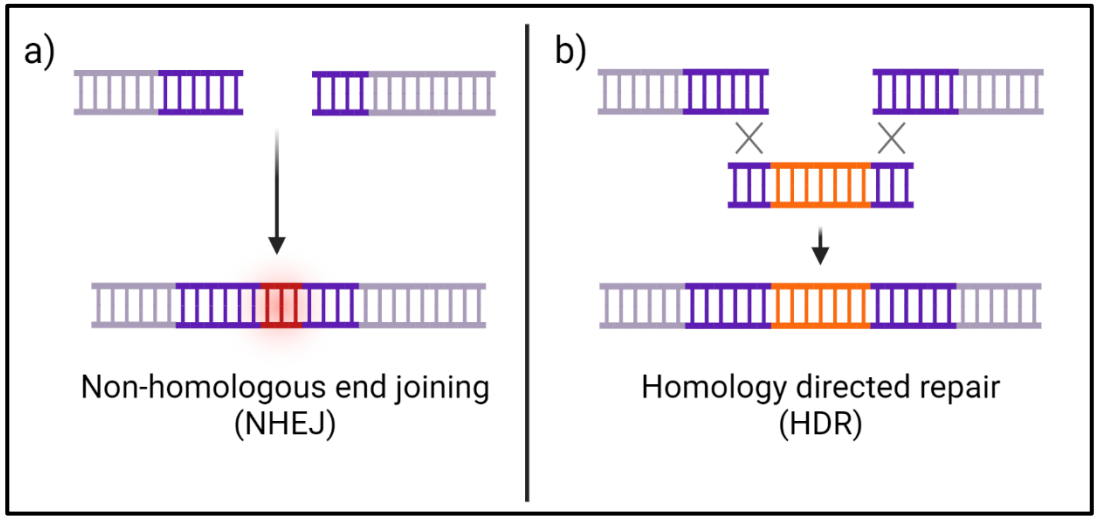

Figure 1.3.1 Cellular methods to repair a double stranded DNA break as a result of the activity of site-specific nucleases utilised in synthetic biology methods such as zinc finger nucleases (ZFNs), transcription activator like effector nucleases (TALENs) and clustered regularly interspaced short palindromic repeats (CRISPR)/Cas nucleases. a) Error prone non-homologous end joining (NHEJ) where no DNA template is given can result in gene mutations and disruption and b) homology directed repair (HDR) where a DNA template is provided to insert or impact the DNA sequence either to insert or replace a target gene. Created with BioRender.com.

Non-homologous end joining is an error prone mechanism that can be used to introduce small insertions or deletions at the target site disrupting the gene function via frame shift mutations. This approach can also lead to the deletion of large gene segments as well as inversions and

translocations which can also be achieved by the use of a pair of nucleases simultaneously cutting at either end of a gene (Schmieder et al., 2021). The unpredictability of results from using this process can be beneficial when studying the activity of a gene of interest but can cause issues such as the accumulation of aggregated protein due to the presence of a mutation causing target protein misfolding and the resulting imposed cellular stress. An alternative approach is the use of homology directed repair where a donor plasmid template is supplied with sequence homology to the target DNA to be inserted into a specific site. These templates can contain either transgenes or modified sequences such as additional gene copies or mutated protein sequences acting to replace target genes. This approach is of particular interest when looking to develop gene therapies where a patient's disease effected cells are targeted and faulty genes removed and/or replaced (J. Lee et al., 2020).

Table 1.3 Summary of key differences between synthetic biology based nucleases that result in double strand DNA breaks. Adapted from (H. X. Zhang et al., 2019).

	ZFNs	**TALENs**	**CRISPR/Cas9**
Target sequence (bp)	9-18	14-20	~23
Mechanism of target DNA recognition	DNA-protein interaction	DNA-protein interaction	DNA-RNA via Watson Crick base pairing
Enzyme engineering	Difficult. Libraries available but positional impact from neighbouring motifs	Simpler. TALE motif are well defined for different specificities	Simple. gRNA design based on target DNA complementarity
Size (kb)	~1	~3	~3.5-4.5

Zinc finger nucleases (ZFNs) are the result of the fusion of one of the most common classes of proteins in the human genome, zinc finger proteins, to the nonspecific DNA cleavage domain of the endonuclease FokI (Lanigan et al., 2020). The resulting zinc finger motifs have independent recognition sequences 3 nucleotides in length and can be used in tandem repeats joined by a linker to form a zinc finger protein. This recognises and cleaves target DNA sequences when a FokI dimer is formed on the opposite DNA strand, relying on NHEJ or HDR to repair the target sequence. Modular assembly is often used to assemble repeats although an oligomerised pool engineering (OPEN) strategy was developed with pre-selected pools to make custom array designs

simpler and take neighbouring motif interactions into account when thinking about target DNA specificity (Maeder et al., 2008). Zinc finger proteins can be combined with multiple domains to impact gene expression in a variety of ways with the use of DNA nucleases, activators, methylases or repressors. Another approach is the fusion with base editors such as cytidine deaminases to allow base editing (Fauser et al., 2024).

Although dimerisation of the FokI endonuclease is required for a DNA break to occur, off target effects can cause toxicity in cells due to the specificity of DNA binding and cleavage, the frequency and location of sites in the genome recognised by the ZFNs, as well as the alignment of neighbouring zinc finger motifs influencing others. Efforts to reduce the likelihood of off target effects have led to the design of charge based obligate heterodimer variants of the FokI nuclease (Doyon et al., 2010), the creation of zinc finger nickases (ZFNickases) that instead generate single strand breaks in DNA so only HDR can occur instead of the error prone NHEJ (E. Kim et al., 2010). Ultimately, the difficulty of constructing ZFNs arrays that can recognise all DNA triplet codes led to researchers looking to develop other more specific methods for generating DNA double strand breaks for the insertion or deletion of genes with fewer off target effects.

Transcription activator like effector nucleases (TALENs) are an alternate synthetic biology based approach for the genetic engineering of cellular DNA. Originating from a family of proteins produced by bacterial plant pathogens in the genus *Xanthomonas*, transcription activator like effector proteins, similarly to ZFNs, can be joined to a FokI endonuclease to result in double stranded DNA breaks which can be repaired using either NHEJ or HDR to introduce or impact gene sequences (Boti et al., 2023). TALENs are also modular with repeats around 34 bp long which act to contact and recognise amino acid residues at positions 12 and 13 known as the repeat variable diresidues (RVDs). Unlike ZFNs that recognise a DNA triplet, TALENs only recognise one bp with no overlap between motifs creating a substantially larger protein assembly compared to ZFNs with a highly repetitive structure also making their delivery into cells more difficult (Gaj et al., 2016). TALEN motifs can have different specificities which don't show impacts from the context of neighbours that are seen in ZFNs; they have also been shown to have improved specificity and reduced toxicity compared to ZFNs (Mussolino et al., 2014). However, the size and reduced options for delivery into cells (Holkers et al., 2013) has led to the use of methods other than TALENs for generating double stranded DNA breaks.

An alternate synthetic biology based approach to using modular protein assemblies to cause double stranded DNA breaks is the use of clustered regularly interspaced short palindromic repeats (CRISPR) with a CRISPR associated protein (Cas) nuclease. Derived from the bacterial

defensive immune system, the CRISPR system, unlike ZFNs and TALENs that use protein-DNA pairing, relies upon Watson-Crick base pairing of DNA and RNA sequences to cleave DNA via complementary RNA guides. CRISPR/Cas protein complexes come in two class types; Class I are multi protein effector complexes whilst Class II are single protein effectors. Class II are most commonly used in combination with a *Streptococcus pyogenes* Cas9 protein. The CRISPR/Cas9 system is made of two components, the Cas9 protein and a single guide RNA (gRNA) which must be immediately followed by a protospacer adjacent motif (PAM) site that is specific to, and essential for, compatibility with the Cas9 protein (H. Li et al., 2020) The PAM sequence is NGG in the case of the *Streptococcus pyogenes* Cas9 protein. These two components can be delivered to the cell in a variety of ways with the simplest being the encoding of both the Cas9 protein and gRNA in the same vector backbone avoiding multiple transfections and increasing stability (C. Liu et al., 2017). The sequence of the gRNA is changed to allow customisation of the cleavage site to suit the gene of interest enabling easy adaptation to different targets. This is a significant advantage of the CRISPR/Cas9 system over the modular designs of ZFNs and TALENs that require complete redesign for interactions and double strand breaks with different target genes whilst only the gRNA sequence needs to be changed for CRISPR/Cas9 targeting.

CRISPR/Cas also has the potential for multiplexing, where multiple sites are targeted via expression of numerous gRNAs and/or Cas nucleases for simultaneous editing, activation and inhibition of target genes in combination (Macarrón Palacios et al., 2024). Mutation in the Cas9 nuclease allows the creation of a Cas9 Nickase which cuts a single DNA strand instead of causing a double strand DNA break or the creation of a dead Cas9 (dCas9) that loses the catalytic function but still retains the ability to recognise target DNA sequences. These inactive dCas9 nucleases can be combined with transcription modifiers such as DNA methyltransferases to modulate transcription (Villiger et al., 2024a). Further research has led to the development of next generation Cas nucleases with increased specificity and activity aiming to reduce off target effects (Kovalev et al., 2024). Figure 1.3.2 depicts the CRISPR/Cas9 complex interacting with target DNA to cause a double strand DNA break.

Other variations of native Cas proteins can be used for different applications such as the use of the Cas13 which acts to target RNA for transcript regulation (Abudayyeh et al., 2017). Alternatively, the Cas7-11 protein is a designed fusion of a Cas11 domain with multiple Cas7 subunits which also acts to target RNA and has a reduced impact on resulting cell viability due to off target effects when compared to Cas13 (Özcan et al., 2021). The ease of design and adaptation for multiple targets has led to the extended use of the CRISPR/Cas system for genome editing compared to the use of ZFNs and TALENs . Nevertheless, for all three genome editing techniques off target effects

and specificity must be considered throughout these design and use of these systems, including when using CRISPR/Cas9 (Lopes & Prasad, 2023). The key differences between approaches are summarised in Table 1.3.

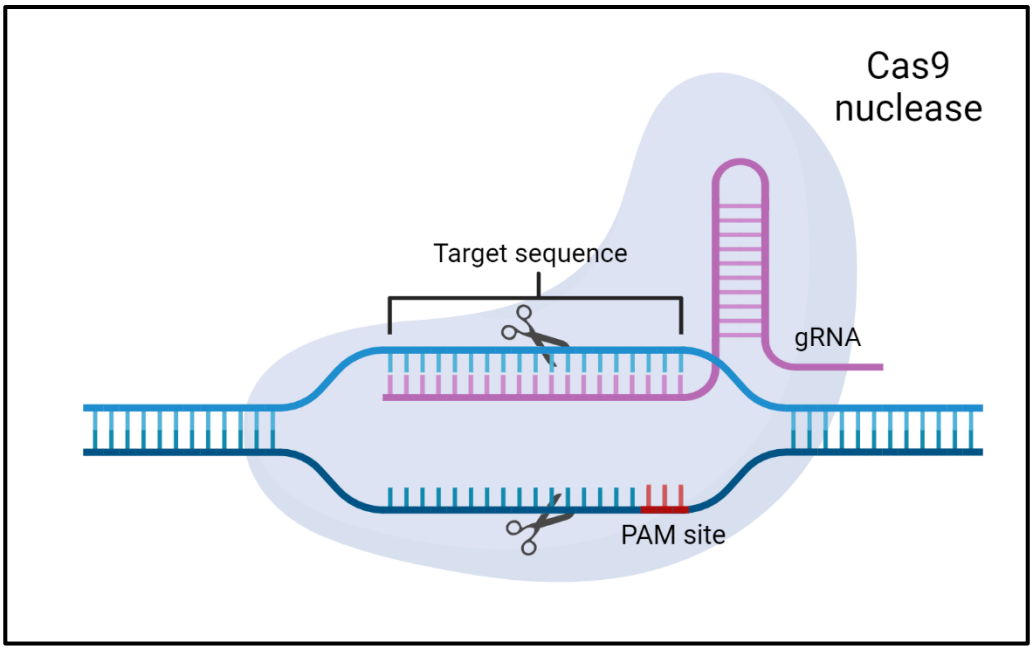

Figure 1.3.2 Activity and assembly of the CRISPR/Cas9 complex during a double strand break. The Cas protein binds to the specific gRNA via recognition of the PAM site to form a complex which shifts the Cas9 protein into an active conformation. The gRNA interacts with the target sequence via Watson-Crick RNA-DNA interactions that cause a second conformational change in the Cas9 protein to cleave the target DNA strands resulting in a double strand break ready for repair via NHEJ or HDR. Created with BioRender.com.

1.4 Targets of CHO cell engineering to increase quality and quantity of biotherapeutic recombinant proteins produced from this expression system

Many approaches have been taken to try and improve the production of recombinant proteins using CHO cells as the expression system of choice. Specifically with relation to genome engineering, the manipulation of the activity of various pathways that underpin secretory recombinant protein production has been explored including regulation of apoptosis, engineering of the Endoplasmic Reticulum (ER) and protein secretion, and the lipid composition of the cell. The majority of engineering approaches look to increase the maximum viable cell number that can be achieved, culture life span, cell specific productivity and ultimately increase recombinant protein yield and quality. Apoptosis in particular has been explored as cell death induced as a result of high stress conditions such as nutrient deficiency, temperature and osmolarity can be detrimental

to the production culture (Xiao et al., 2023) Apoptosis limits the viable cell numbers available to produce the target protein but also releases proteases, glycosylases and sialidases which can degrade the protein product as well as the accumulation of cell debris which can cause issues for downstream processing and purification. To avoid these issues, cultures are often harvested early resulting in a lower protein yield that involves fewer purification steps.

Improvements to cell culture media composition and feeding strategies as well as changes to bioreactor designs have improved viable cell concentrations and culture viabilities throughout the duration of culture. Specifically with regard to apoptosis, cell engineering has been utilised to impact gene expression of members of the B cell lymphoma gene 2 (BCL-2) protein family which act to inhibit the oligomerisation of BCL-2 homologous antagonist killer (BAK) and BCL-2 associated X protein (BAX) which go on to form pore structures in the Endoplasmic Reticulum (ER) or mitochondrial outer membrane leading to apoptosis and cell death. Approaches have been taken to either knock out the activity of BAK and BAX (Tang et al., 2022) or overexpress BCL-2 genes to block their activity (Gulce Iz et al., 2018). Results from these genome editing approaches show increased prolonged culture viability and, in some cases, enhanced protein yields (X. Zhang et al., 2018) suggesting a resistance to apoptosis allows the culture to maintain a higher culture viability over a longer period of time. A similar method involved cysteine-dependent aspartate proteases (Caspases) which have been targeted due to their role in apoptosis destroying structural proteins to promote dismantling of the cell (Zamaraev et al., 2017). Genetic engineering techniques have been applied in the form of CRISPR interference (CRISPRi) which was used to mediate gene expression of BAK, BAX and Casp3 resulting in CHO cells rescued from cell induced apoptosis (Xiong et al., 2019). Both approaches aim to delay cell death, extend cell culture span and therefore lead to an increase in production of recombinant proteins over the culture time.

Targeting the secretory pathway, and particularly the ER, is another approach often taken when using genome editing tools to increase recombinant protein expression. Protein secretion starts from the translocation of the polypeptide into the ER followed by protein folding and maturation in the ER lumen, trafficking to the Golgi for additional glycosylation processing and sorting before the protein is secreted (Y. Zhou et al., 2018). The core N-glycan structure is added onto Asn residues in a N-X-S/T motif (where N is asparagine, X is any amino acid except proline, S is serine, T is threonine) co-translationally. The ability to secrete recombinant proteins serves as a key advantage of the use of CHO cells for expression, however increasingly complex protein designs can lead to a more challenging expression process resulting in bottlenecks during this process such as the accumulation of misfolded proteins. ER associated degradation (ERAD) is a mechanism designed to remove unfolded proteins from the ER and degrade them, helping to prevent their

accumulation. This process is functionally linked to the unfolded protein response (UPR) and if the response is not sufficient to clear unfolded proteins, apoptosis will occur (Read & Schröder, 2021). Although cellular stress acts to influence apoptosis, a low level of stress can result in the induction of heat shock proteins (HSPs) as part of a cellular stress response. Chaperones such as HSPs act to stabilise folded proteins and help promote folding of unfolded or misfolded proteins. HSP27 plays a role in cytoskeleton stability, protein synthesis, redox potential and inhibiting apoptosis whilst HSP70 acts to inhibit mitochondria associated apoptosis (Henry et al., 2020). Increasing the expression of molecular chaperones such as HSPs aims to assist with protein folding, assembly, translocation and degradation under cellular stress whilst avoiding the aggregation of newly synthesised polypeptide chains into defective proteins (Z. M. Li et al., 2022). Aggregation is a key issue with biotherapeutic design with expression of some recombinant proteins producing up to 30-40% aggregates due to their sequence and structure (T. Xu et al., 2022).

Overexpression of HSPs, and in particular HSP27, in CHO cells has resulted in increased peak viable cell density and improved mAb production in fed batch cultures (Tan et al., 2015). Other molecular chaperones have been expressed in CHO such as protein disulphide isomerases (PDI) which act in the ER to catalyse the formation, cleavage and reformation of disulphide bonds which are essential during the production of recombinant proteins. However, overexpression of the PDIa4 protein showed no increase in antibody production suggesting a combination of multiple chaperones might be needed for an impact on antibody production levels (Komatsu et al., 2020). This approach was also investigated with the co-expression of multiple luminal chaperones; HSPA5, HSP90B1 and DNAJC3 that act to protect proteins from misfolding (Barzadd et al., 2022). HSP90B1 was co-expressed with other chaperones but showed no positive effect on secreted protein expression levels (Hansen et al., 2015), Similarly, overexpression of X box binding protein 1 (XBP1), a regulator of ER protein processing and the UPR, in CHO cells has shown mixed success at increasing secretory recombinant protein expression (Gutiérrez-González et al., 2019), however when expressed in combination with other transcription factors such as MYC, an increase to both viable cell density and recombinant protein production was reported (Latorre et al., 2023). It is of note that these approaches investigated different recombinant protein targets when determining the impact on expression levels which have different sequences, structures and therefore demands on the cell as a result of their expression.

Another approach utilising genetic engineering to improve recombinant protein expression in CHO cells involves targeting cellular lipids although this strategy has been less well studied. The ER is the main site for synthesis of sterols and phospholipids that constitute the bulk of lipid components of all biological membranes, with many enzymes and regulatory proteins involved in

lipid metabolism found in the ER (Han & Kaufman, 2016). Lipids play an important role in cellular growth as well as protein production and secretion. Their involvement in energy metabolism, vesicular transport, membrane structure, dynamics and signalling (Y. Zhang et al., 2017) makes the genes involved in their expression and regulation ideal targets for genetic engineering with the aim of increasing protein production. By overexpressing sterol regulatory element binding factor 1 (SREBF1) alongside stearoyl CoA desaturase (SCD1), which play a role in global transcriptional regulation of multiple genes involved in lipid metabolism and acts to modify cellular lipid content respectively, an increase in recombinant protein yields, increased cellular growth and culture longevity alongside an increased ER size was reported (Budge et al., 2020). These authors also showed that an overexpression of SREBF1 to high levels could be detrimental to the cell due to the high levels of lipid synthesis. Connecting the activity of the ER and the secretory pathway to lipid metabolism could therefore be a successful approach to increasing recombinant protein production.

Table 1.4 Some of the cell engineering strategies and approaches investigated to improve recombinant protein production from CHO cells. Adapted from (Lalonde & Durocher, 2017)**.**

Selection system	**Gene expression**	**Cell growth and proliferation**	**Protein folding and secretion**
GS/MSX	Site specific integration	Overexpression of anti-apoptosis genes BCL02, XIAP etc	UPR pathway
DHFR/ MTOPEN X	DSBs and repair via NHEJ or HDR via ZFNs/TALENs/CRISPR/Cas systems to introduce knock ins/outs	Down-regulation of apoptosis genes Caspases, BAK and BAX	Chaperones PDI, BiP, HSPs
Antibiotics e.g. Hygromycin/ puromycin	Codon optimisation		Lipid metabolism

1.5 Metabolic targets of CHO cell engineering to increase quality and quantity of recombinant proteins for biotherapeutics

Another target for genetic engineering, and the focus of this thesis, is cellular glucose metabolism and its role providing energy for cellular function and growth as well as recombinant protein production. Glucose usually acts as the main carbon source for i*n vitro* cultured cells and, along with its products, is used as the substrate for glycolysis subsequently providing intermediates into the tricarboxylic acid (TCA) or Kreb's cycle and finally oxidative phosphorylation, to generate Adenosine triphosphate (ATP) as well as precursors for amino acid and lipid biosynthesis. During glycolysis, a glucose molecule in the cell cytoplasm is converted into various intermediates via the action of multiple enzymes which conclude with the formation of two molecules of pyruvate from two molecules of phosphoenolpyruvate (PEP) via the activity of the pyruvate kinase (PK) enzyme, shown in Figure 1.5.1.

In aerobic glycolysis, the pyruvate molecules are then transported across the mitochondrial inner and outer membranes into the mitochondrial matrix via either the voltage dependent anion channel or porin and mitochondrial pyruvate carrier (MPC) respectively (McCommis & Finck, 2015). Here they are converted to acetyl-CoA molecules via the activity of the pyruvate dehydrogenase (PDH) enzyme complex. The acetyl-CoA molecules can be used to fuel multiple cellular activities including entering the TCA cycle or as fuel for amino acid biosynthesis and other pathways. It is because of this branch point between glycolysis and the TCA cycle, that pyruvate plays a key role in controlling glucose metabolism in the cell (Yiew & Finck, 2022). Alternatively, under anaerobic conditions the pyruvate molecules can be converted to lactate via the activity of lactate dehydrogenase (LDH). Although lactate is considered a waste product, this process regenerates NAD+ which is an important electron acceptor in pathways such as glycolysis. A further option is the conversion of pyruvate to oxaloacetate via the activity of pyruvate carboxylase through the process of anaplerosis which allows the replenishment of TCA cycle intermediates for processes such as gluconeogenesis, the urea cycle and lipid synthesis (Zangari et al., 2020). The potential outcomes after the production of pyruvate from glycolysis are shown in Figure 1.5.2.

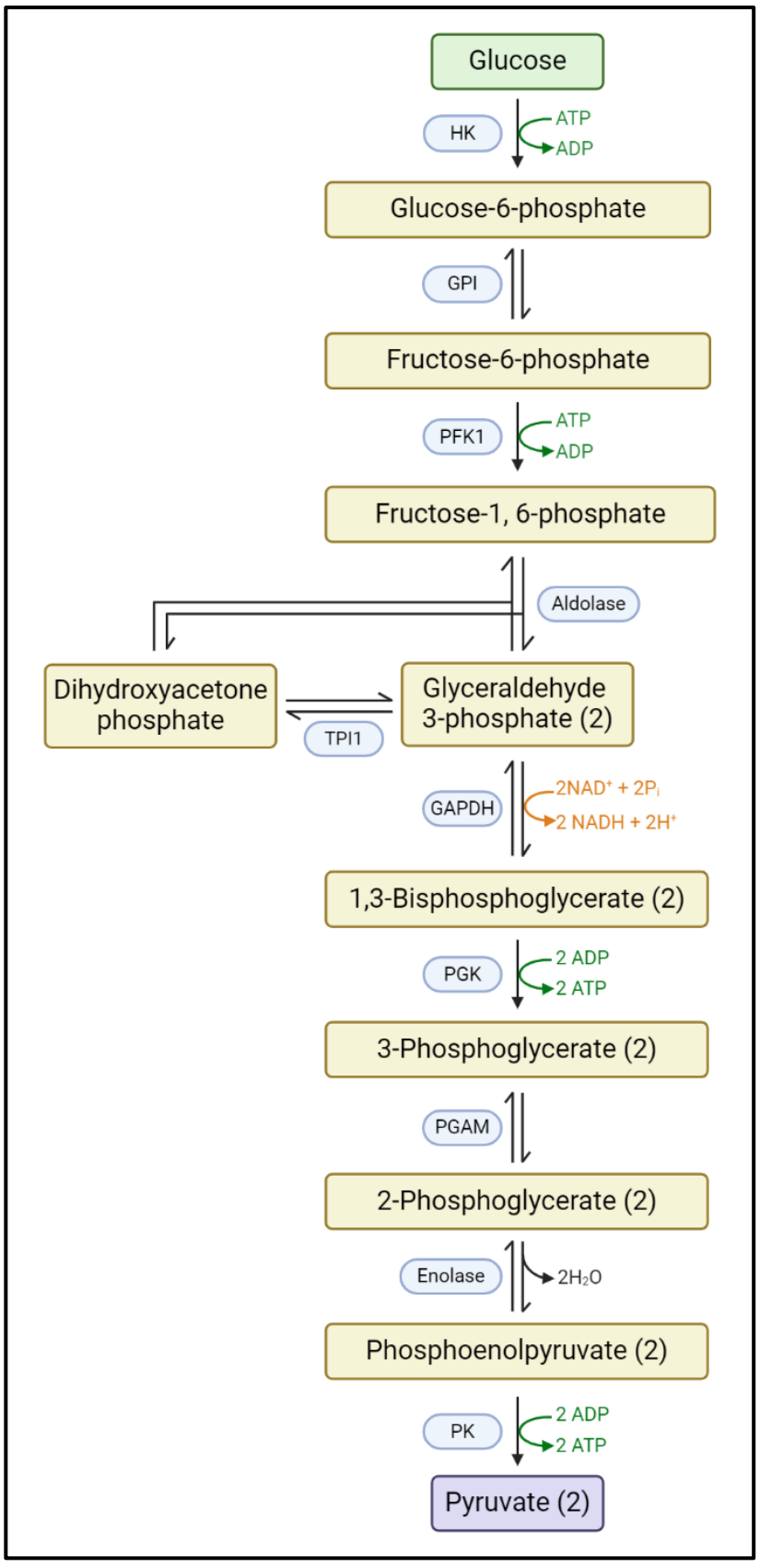

Figure 1.5.1 Overview of glycolysis which converts one molecule of glucose into two molecules of pyruvate whilst generating two molecules of ATP and two molecules of NADH. The glycolysis intermediates and enzyme abbreviations are shown. Created with BioRender.com.

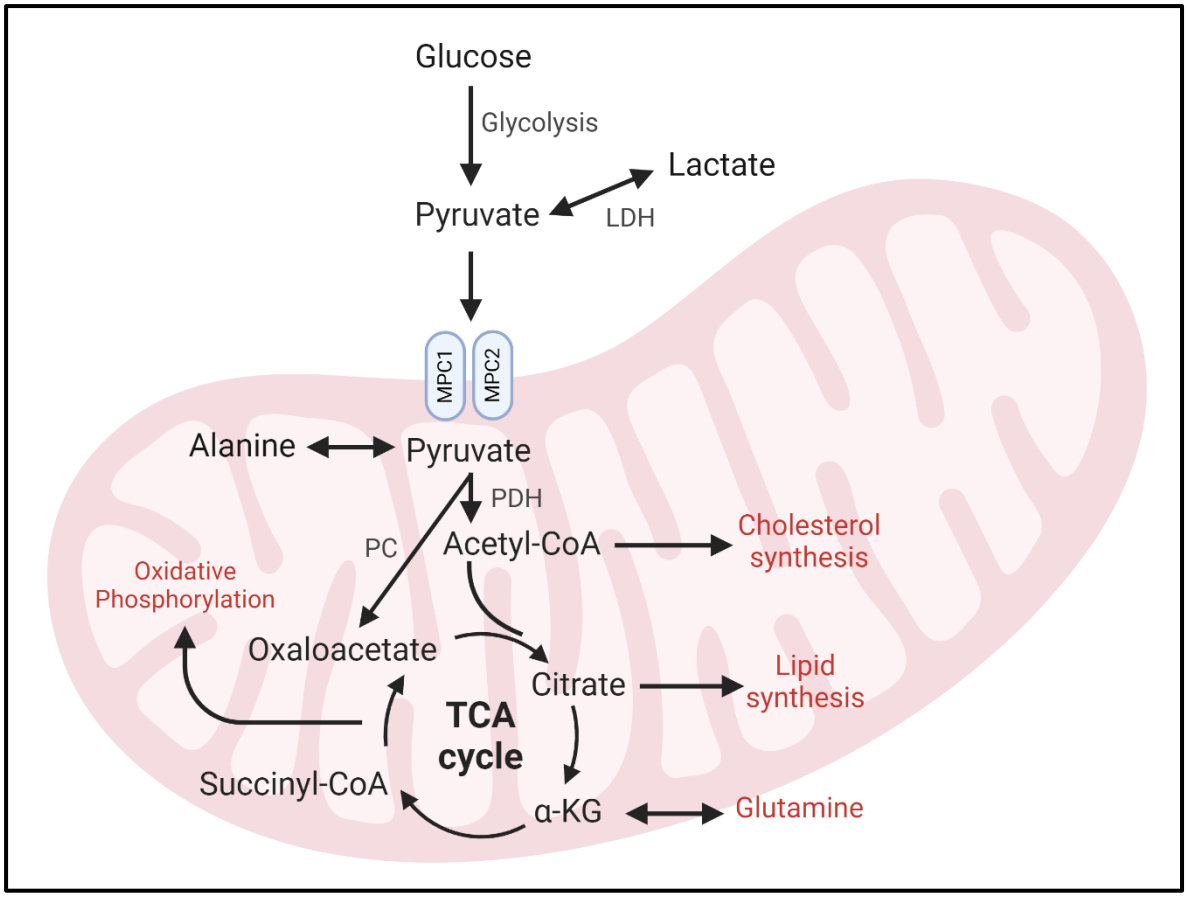

Figure 1.5.2 Overview of pyruvate metabolism and connecting pathways. In the cell cytoplasm, glucose is converted to pyruvate through multiple enzymatic steps during glycolysis, shown in Figure 1.5.1. Pyruvate is then transported into the mitochondrial matrix via the MPC where it can be converted into oxaloacetate for gluconeogenesis via the activity of PC or into acetyl-CoA via the activity of PDH for entry into the TCA cycle. Alternatively, pyruvate is transaminated to alanine via alanine transaminase. In the cytoplasm, LDH can also act to reduce pyruvate into lactate. Created with BioRender.com.

Glucose and pyruvate metabolism are of interest when culturing cells for recombinant protein production due to the fluctuations in glucose consumption and lactate production and ultimately consumption throughout a cell culture. A culture can be considered as consisting of three phases; exponential growth, stationary phase and decline, during which there is variation between consumption and production levels of both glucose and lactate as well as other key metabolites depending on factors such as the availability of nutrients due to media composition and clonal variation. The use of both targeted and untargeted metabolomics has enabled the tracking of metabolites throughout the CHO cell production (fed)batch culture linking their flux to mAb productivity (Alden et al., 2020). During exponential growth, cells show high consumption of glucose and glutamine resulting in high lactate production and biomass generation but lower

levels of mAb production (Coulet et al., 2022). During the stationary phase cells display lower glycolytic activity with an increased TCA flux whilst lactate is consumed and mAb production increases. Finally in the decline phase, metabolites become limiting due to their exhaustion and toxic products such as ammonia and lactate begin to accumulate negatively impacting cell number and culture viability as well as product quality. These distinct cell culture phases have led to the use of approaches to improve expression such as the use of inducible expression of recombinant proteins when the cultures are at high viability and cell number after the exponential growth phase (Sheikholeslami et al., 2014) and temperature shifts (e.g. from 37°C to 32°C) which act to limit cell growth after the exponential growth phase but keep the cells producing recombinant protein resulting in a longer culture span and increased protein yield (McHugh et al., 2020). .

An accumulation of lactate in the culture is toxic to cells and acts to increase the acidity of the media requiring the addition of base which in turn impacts the culture osmolarity, culture viability and product quality (Dean & Reddy, 2013). Rapidly growing cells demonstrate high glucose consumption and therefore need to regenerate both ATP and NAD+ to continue with glycolytic function resulting in the formation of lactate via the activity of LDH (Rogatzki et al., 2015). This process is known as the Warburg effect and is found in tumour cells actively increasing biomass where aerobic glycolysis results in the generation of lactate (Warburg et al., 1927). Further into a production culture, cells often signal a switch in metabolism from production to the consumption of lactate and have demonstrated the ability to co-metabolise both glucose and lactate (Liste-Calleja et al., 2015). The cause of this switch in lactate metabolism has been linked to multiple factors such as the depletion of glucose and/or glutamine, a pH or temperature shift, or coinciding with a change from exponential growth to the stationary culture phase (Hartley et al., 2018). This switch is suggested to be beneficial to recombinant protein production with cell cultures exhibiting a change to lactate consumption yielding higher protein titres compared to those that continued with high glucose consumption rates (Mulukutla et al., 2015).

To avoid the accumulation of lactate in the cell culture media and encourage the conversion of pyruvate to acetyl-CoA for entrance into the TCA cycle instead of to lactate, multiple approaches have been taken to control the activity of LDH. By focusing on the feeding regime during culture, clonal cell lines can be adapted to high lactate concentrations in the media or be supplemented with lactate during the culture leading to higher viable cell densities (Freund & Croughan, 2018). Changing the feed source from glucose to another sugar, as well as changing the make-up of media have been used to improve CHO cell culture in regard to lactate accumulation. Alternatively, supplementation of NAD+ with the aim of reducing the need for LDH based NAD+ regeneration reduced lactate yield and increased antibody titre (J. H. Lee et al., 2023).

Synthetic biology and cell engineering based approaches to reduce lactate accumulation have also been used to target and downregulate LDH expression (S. H. Kim & Lee, 2007) as well as increasing the expression of other proteins/enzymes that control glycolysis and adjoining metabolic pathways. The expression of a codon optimised pyruvate carboxylase from yeast resulted in a lower accumulation of lactate in batch culture whilst glucose consumption was maintained, suggesting an increase of pyruvate entry into the TCA cycle which also resulted in a higher mAb titre (Gupta et al., 2017). The expression of LDH-C, a subtype of LDH found in animal sperm which preferably converts lactate to pyruvate, was also expressed in CHO cells resulting in lower lactate production and alleviated apoptosis responses (Fu et al., 2016). Similarly, by targeting PK that acts in the final step of glycolysis to convert PEP to pyruvate, lactate accumulation can be reduced. Knocking out exon 9, involved in the alternative splicing required to form constantly active PKM1 instead of the regulated PKM2 isoform, resulted in a reduction of lactate accumulation in CHO cells (Tang et al., 2019).

Another waste product that accumulates over the culture period is ammonium which can impact culture viability and critical quality attributes such as glycosylation patterns (Savizi et al., 2021). Resulting from the metabolism of glutamine and other amino acids, efforts to reduce ammonium production from CHO cells, similarly to lactate, have often been approached through the control of amino acid components in cell media such as glutamine and glutamate, however this approach does not always lead to an increase in mAb titre (McAtee Pereira et al., 2018). Synthetic biology approaches have also been used to reduce ammonia build up through the generation of GS knockout (KO) cell lines. Although this KO process is primarily used as a metabolic selection for cell clones expressing the plasmid encoding the recombinant protein of interest, the resulting exogenous GS acts to catalyse the conversion of glutamate and ammonia to form glutamine providing energy for cells whilst reducing the ammonia levels in the culture and the potential for negative impacts on cell culture conditions due to its accumulation (Noh et al., 2017). Amino acid metabolism pathways are highly linked and intertwined. By approaching amino acid metabolism as a whole, the use of metabolomic methodologies has enabled the identification of gene candidates for disruption whilst maintaining a high viable cell concentration, growth and recombinant protein production, focusing on pathways extending from lactate and ammonia metabolism (Ley et al., 2019).

1.6 The activity and structure of the pyruvate dehydrogenase complex

Metabolic manipulation of cells often aims to drive activity away from glycolysis and lactate production and instead funnel intermediates through the TCA cycle and oxidative phosphorylation to generate ATP (Templeton et al., 2013). High glycolytic flux and lactate production during exponential growth where mAb production is limited and the switch to the consumption of lactate and high TCA cycling where mAb production is increased during stationary phase is a key target feature of strategies to increase recombinant protein production (Rish et al., 2022). Engineering to increase the activity of the TCA cycle and driving glucose metabolism away from lactate aims to provide precursors for biosynthesis and enhance the production of secretory recombinant protein yields. The production of acetyl-CoA from pyruvate via the activity of PDH is a key branch point between glycolysis and entry into the TCA cycle, avoiding the production of lactate and feeding substrates into various metabolic pathways such as the synthesis of fatty acids and amino acids (Ku et al., 2020). By increasing the activity of the PDH complex and therefore acetyl-CoA production, increased TCA cycle flux should occur limiting the need for glycolytic generation of ATP whilst avoiding lactate production, encouraging cell growth and recombinant protein production. An increase in cellular acetyl-CoA levels will also supply precursors for amino acid and lipid synthesis; lipid synthesis itself can support expansion of the ER and result in increased secretory recombinant protein production.

PDH is an enzyme complex made up of 3 core catalytic subunits; pyruvate dehydrogenase (E1) which in eukaryotes is heterotetrametric, made up of two protein subunits E1alpha and E1beta, dihydrolipoyl transacetylase (E2), and dihydrolipoyl dehydrogenase (E3) (Kozak et al., 2014). 60 copies of the E2 subunit form an icosahedral catalytic core of the complex with tandem repeat lipoyl domains followed by peripheral subunit binding domains that bind subunits E1 and E3 with the help of an additional E3 binding protein (E3bp) (Kumaran et al., 2013). Mammalian PDH complexes have two lipoyl per E2 subunit. Domains are separated via long flexible linker regions which create swinging arms that act to transfer catalytic intermediates between the active sites (Perham, 2000). Figure 1.6.1 depicts the structure of the PDH assembly.

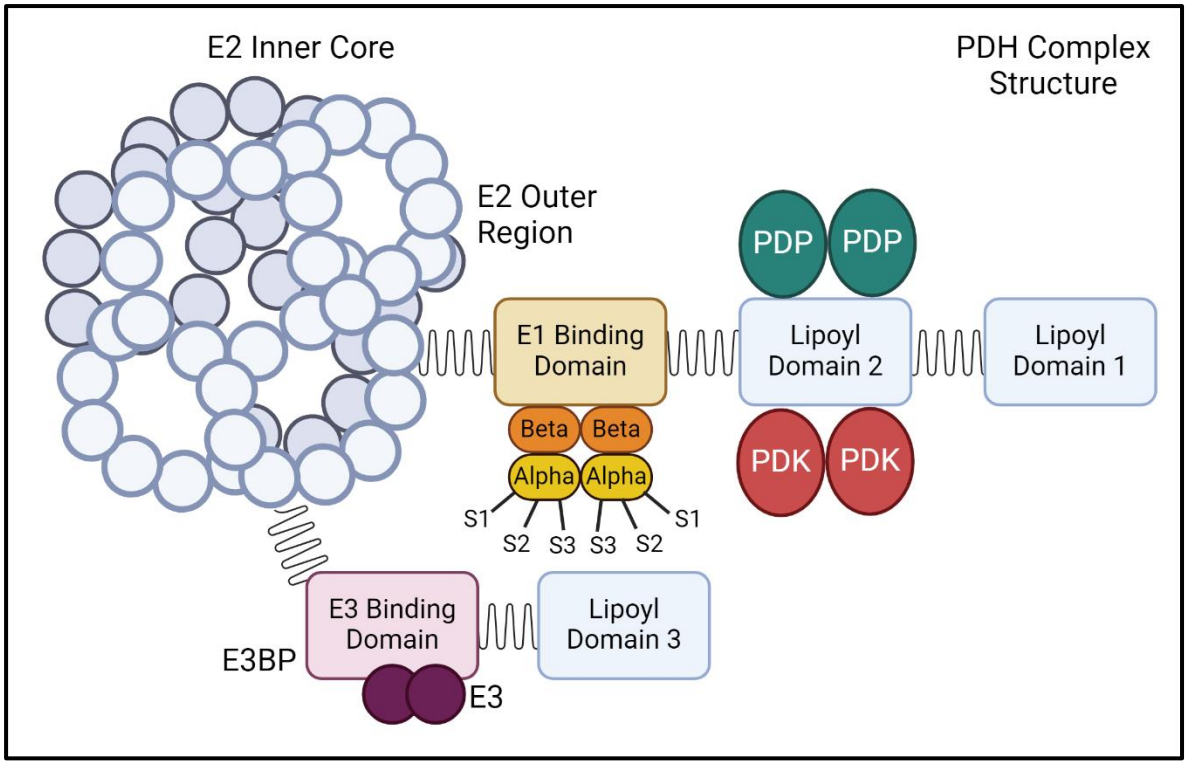

Figure 1.6.1 Cartoon structure of the Pyruvate Dehydrogenase (PDH) complex assembly. Serine residues, sites of regulation on E1alpha subunit: S1=264, S2=271, S3=203. E1 and E2 subunits targeted for overexpression in plasmids PEL3-9 and with either an N- or C-terminal tag in plasmids PEL13-18 in Chapter 3. E1alpha in cassette 1, E1beta in cassette 2 and E2 in cassette 3, full details in Tables 3.4.1 and 3.4.2. Adapted from (Harris et al., 2002). Created with BioRender.com.

PDH is a member of the keto acid dehydrogenase family and its activity requires multiple cofactors for its activity including Coenzyme A (CoA), NAD+, thiamine pyrophosphate (TPP, also referred to as thiamine diphosphate, ThDP) and lipoic acid (X. Liu et al., 2018). E1 catalyses the first and rate limiting step of PDH activity and is TPP dependent. The first step, the decarboxylation of pyruvate to carbon dioxide with the formation of a 2-alpha-hydroxyethylidene-TPP intermediate occurs with the reductive acetylation of the lipoyl groups covalently attached to the E2 subunit. The E2 subunit catalyses the transfer of an acetyl moiety to CoA forming acetyl-CoA. Finally, the E3 subunit transfers the electrons from the dihydrolipoyl moieties of E2 to FAD and then to NAD+ (Patel et al., 2014). The reactions of the PDH complex are shown in Figure 1.6.2. PDH is present in both the mitochondria and nucleus of the cell enabling its role in both acetyl-CoA generation and the generation of acetyl-CoA for histone acetylation to control gene expression (Sutendra et al., 2014).

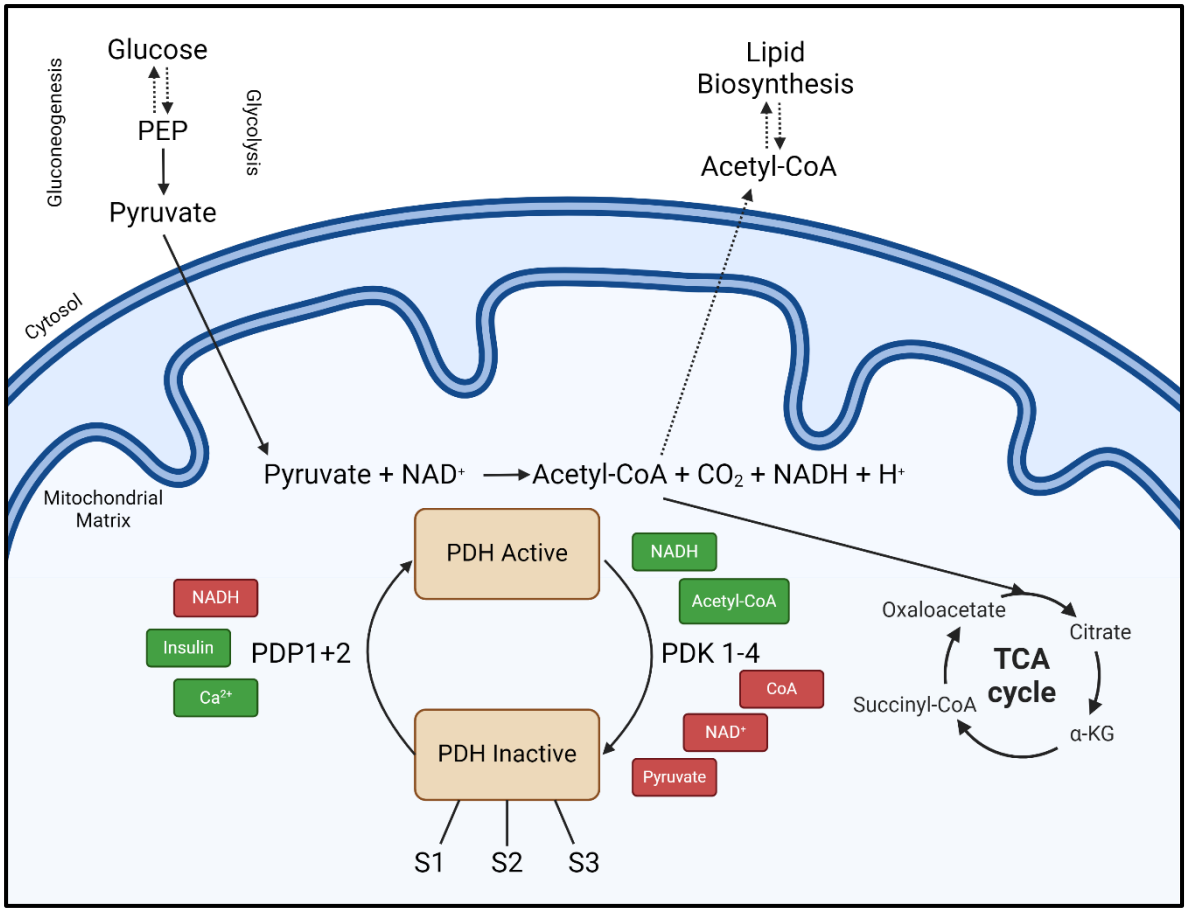

Figure 1.6.2 Reactions of the PDH complex converting pyruvate to acetyl-CoA and the switching from active (dephosphorylated) to inactive (phosphorylated) forms via the action of PDPs and PDKs respectively. Stimulants of PDH activity are shown in green with molecules that discourage PDH activity shown in red. Sites of regulation on E1alpha subunit: S1=264, S2=271, S3=203. Adapted from (Patel & Korotchkina, 2001). Created with BioRender.com.

Due to its pivotal role in the branching of substrates and intermediates through glycolysis and into the TCA cycle, the PDH complex is the subject of tight regulation via the phosphorylation activity of multiple kinases. Pyruvate dehydrogenase kinases (PDKs) 1-4 act to phosphorylate one of three serine residues on the E1alpha subunit Serine 264, 271 and 203 known as sites 1, 2 and 3 respectively. Sites 1 and 2 are located on a conserved phosphorylation loop A which forms a wall of the E1 active site and helps anchor TPP to the active site. Site 3 is located in a short loop segment known as phosphorylation loop B which provides coordination to an Mg^{2+} ion chelated by the diphosphate group of TPP (Kato et al., 2008). Upon TPP binding, the phosphorylation loops become ordered however phosphorylation via PDK activity maintains disorder even with TPP present preventing the recognition of substrates and enzymatic activity. Phosphorylation at one site alone is therefore enough to inactivate the whole complex (Holness & Sugden, 2003). PDKs

show limited tissue distribution with specific activity at each phosphorylation site which is summarised in Table 1.6. The PDKs bind to the lipoyl domains of E2 allowing them to phosphorylate the E1alpha Serine residues and regulate complex activity. Regulation of PDH activity via the activity of PDKs can be influenced by ratios of NADH to NAD+ and acetyl-CoA to CoA and the intracellular environment.

Table 1.6 Specificities of PDKs 1-4 when targeting PDH E1alpha subunit Serine residues 264, 271 and 203 for phosphorylation. Y shows phosphorylation activity at a specific residue whilst (*) shows highest specific activity for that Serine residue. Adapted from (Gray et al., 2014).

Site number (Serine residue)	PDK 1	PDK 2	PDK 3	PDK 4
1 (Ser264)	Y	Y *	Y	Y
2 (Ser271)	Y	Y	Y *	Y
3 (Ser203)	Y			

Dephosphorylation to reactivate the PDH complex occurs via the activity of pyruvate dehydrogenase phosphatases (PDPs), of which there are two isoforms, PDP1 and PDP2 (Roche & Hiromasa, 2007). Both isoforms require Mg^{2+} ions for their activity which reduce as mitochondrial ATP concentration decreases, suggesting a feedback loop to dephosphorylate and restart the PDH complex activity.

Feedback between PDH and the PDKs and PDPs that act to regulate its activity is key in cellular metabolism and allows flexibility when responding to varied nutrient conditions such as fasting or feeding (S. Zhang et al., 2014). It is because of this balance, and the key position of PDH linking glycolysis and the TCA cycle, that the complex has been a target of expression disruption aiming to increase pyruvate conversion to acetyl-CoA through PDH activity and away from lactate. Replacing glutamine in CHO cell media with pyruvate resulted in CHO cells with reduced glucose uptake and lactate production whilst maintaining cellular growth (Genzel et al., 2005). Similarly, supplying TCA cycle intermediates improved cellular metabolism. For example, alpha-ketoglutarate substitution for glutamine in the media resulted in a reduced ammonia accumulation and better sialylation of a fusion protein however gave lower cell growth but with enhanced recombinant protein yield (Ha

& Lee, 2014). Addition of alpha-ketoglutarate, malic acid or succinic acid had little effect when added to the basal media but additions during the stationary phase of growth improved lactate consumption, reduced ammonia accumulation and led to a higher cell specific productivity (X. Zhang et al., 2020). Addition of dichloroacetate (DCA) that acts to inhibit the activity of PDKs has also been used to increase the activity of PDH (Buchsteiner et al., 2018). Increasing PDH activity through reduced regulation resulted in increased peak viable cell densities, culture duration and final antibody titre with the addition of glucose extending culture time and doubling the recombinant protein yield. The improvements to cell growth and productivity from these media additives suggest an increase in TCA flux whilst limiting accumulation of lactate and ammonia is an appropriate approach when trying to engineer CHO cells.

Synthetic biology based approaches have also been used to impact PDH activity targeting the expression of functionally connected proteins as well as PDH itself. Targeting of MPCs that allow pyruvate entry into the mitochondria has been investigated to increase the movement of the PDH substrate leading to an increase in activity and flux into the TCA cycle away from lactate. Overexpression of the MPC1 and MPC2 subunits resulted in a reduction of overall lactate production and an increase in protein production (Bulté et al., 2020). Mutation of the PDH serine residues that are targeted for phosphorylation via PDKs allows the E1alpha subunit to remain active preventing PDK regulation. Changing the serine sites to alanine residues changes the polarity and hydrophobicity of the residues preventing their phosphorylation via PDKs and has been used to identify the specificities of PDKs for each of the serine residues (Kolobova et al., 2001a).

Alternatively, methods have been used to reduce or knock down expression of the PDKs. This has most frequently been completed alongside the knock down of LDH expression. Targeting both the PDKs and LDH aims to drive pyruvate metabolism through the TCA cycle by the reduction of entrance to other metabolic pathways. Small interfering RNAs (siRNAs) were used to target PDKs 1, 2 and 3 due to the low expression levels of PDK4 in CHO cells alongside LDHa (M. Zhou et al., 2011). This approach varied in knock down success with LDHa, PDK2 and 3 showing a stronger reduction in expression compared to PDK1. The use of a single siRNA vector to knock out the four targets resulted in lower lactate levels in cell culture and the maintenance of a more neutral pH. In a fed batch culture the knock down cells also showed a large increase in antibody production. A similar approach was taken using ZFNs targeting LDHa and PDKs 1, 2 and 3 (Yip et al., 2014). When targeting LDH alongside PDKs, no cell lines were generated with a complete knock out of expression suggesting the LDH activity regenerating NAD+ is essential for cellular growth and survival and that completely unregulated pyruvate metabolism is not sustainable. These

approaches substantiate the connections between glucose and pyruvate metabolism suggesting that manipulation of other pathways linked to PDH activity is possible but not to the extent of a complete knock out.

1.7 Aims of this study

Recombinant proteins for clinical use are most commonly produced in CHO cells as previously described (Shanmugaraj et al., 2020). An average yield for a mAb ranges from 1-10 g/L when grown in a batch culture resulting from process optimisation (Kunert & Reinhart, 2016). However, novel recombinant protein therapeutic designs can create challenges for their expression leading to these being difficult to express (DTE) (Saccardo et al., 2016). Using the same CHO cell host often results in a lower yield with high levels of aggregation for such DTE proteins, creating issues for cellular secretion and purification methods. This thesis set out to apply synthetic biology techniques to design new CHO cell host chassis' specifically to help produce such DTE recombinant proteins as well as improve expression yields of more traditional mAbs formats.

The PDH enzyme complex plays a key role in the branching of glycolysis and the TCA cycle as outlined above, converting pyruvate to acetyl-CoA which acts to provide precursors for multiple metabolic pathways including amino acid and lipid biosynthesis. These metabolic pathways have been linked to an increase in recombinant protein production (Budge et al., 2020). Here, the aiming was to increase the availability of cellular acetyl-CoA which may enhance lipid biosynthesis and thus improve secretory productivity of the cell, whilst driving pyruvate metabolism away from the waste product lactate. The activity of PDH and its regulation was targeted using traditional overexpression studies and CRISPR/Cas9 synthetic biology KO techniques. The impact of the genetic engineering was then analysed with cell pools transiently expressing a model DTE recombinant biotherapeutic protein Etanercept.

The work in this thesis therefore set out to engineer the CHO host cell. Specifically, the aims of the work were to:

1. Generate CHO cell lines stably overexpressing subunits of the PDH enzyme complex
2. Design gRNA pairs to target specific PDKs for knock out using CRISPR/Cas9
3. Transfect CHO cells with the relevant CRISPR/Cas9 gRNAs to generate knock out cell pools and lines
4. Analyse the impact on the expression of model DTE biotherapeutic protein, Etanercept, as a result of PDH targeted engineering as well as cellular metabolism and lipids

Chapter 2: Materials and Methods

2.1 General Methods

All materials used in this study were of analytical grade or higher unless otherwise stated.

2.2 Molecular Biology to generate gene constructs

For use in *E.coli* cell culture

2.2.1 Lysogeny Broth (LB media)

10g tryptone, 5g yeast, 10g sodium chloride was added to 1L of MilliQ water and autoclaved to sterilise.

2.2.2 Super Optimal Broth (SOB media)

20g tryptone, 5g yeast, 0.5g sodium chloride, 10 mL 0.25 M potassium chloride was added to 1L of MilliQ water, with 5 mL 2 M magnesium chloride added after sterilisation via autoclaving.

2.2.3 Super Optimal Broth with Catabolite Repression (SOC Media)

100µl 50% glucose was added per 10ml SOB media.

2.2.4 LB Agar plates

15g Agar was added to 1L LB media and autoclaved. After cooling the appropriate antibiotic was added. Ampicillin was added with a final concentration of 100µg/ml or Kanamycin was added with a final concentration of 50µg/ml. The medium was then poured to form plates.

2.2.5 Generation of Calcium Competent DH5α cells

DH5α cells were spread out onto an antibiotic free agar plate and left to grow overnight. One colony was picked and incubated overnight in 5ml LB media. 1ml of culture was added to two 500ml flasks containing 50ml SOB medium. These were grown to OD 0.4-0.6 when measured at 600nm and harvested at 3500rpm for 15mins at 4°C. The cell pellets were resuspended in 4ml ice cold 100mM $CaCl_2$. Cells were pooled and had 1ml 80% glycerol added and were gently mixed. 50µl aliquots were dispensed and flash frozen in liquid nitrogen for storage at -80°C.

2.2.6 Transformation of DNA into Calcium Competent DH5α cells

Plasmid DNA or ligation mix (described in ligation of DNA into plasmid backbone) was added to 50µl Calcium Competent DH5α cells and left on ice for 30 mins. Cells were subjected to a heat shock for 90 secs at 42°C then returned to ice for 2 mins. 300µl LB media was added and

incubated in a shaking incubator at 200rpm for 1 hour at 37°C. 250µl was then spread on an Agar plate with corresponding antibiotic to plasmid resistance and incubated overnight at 37°C.

2.2.7 Preparation of DNA

Plasmids prepared using either the QIAGEN QIAPrep Spin Mini kit or a QIAGEN Plasmid Maxi kit following the manufacturer's instructions using a 5ml or 250ml *E.coli* culture respectively.

2.2.8 DNA Quantification

Quantity of DNA and RNA was measured using a Nano-Drop Spectrometer ND-1000. A 2µl DNA sample was measured using the appropriate DNA or RNA setting at 260nm.

2.2.9 Polymerase Chain Reaction target amplification

Polymerase Chain Reaction (PCR) was performed using ThermoFisher Phusion High Fidelity Polymerase with the corresponding High Fidelity 5x buffer according to the manufacturer's instructions. 100ng complementary DNA template or 20ug plasmid DNA, 0.5µM forward and reverse primers and 10mM dNTP mix (equal parts of dATP, dTTP, dGTP and dCTP made up to 100µl with MilliQ water) were used for reactions with water added to make a total volume of 100µl. Samples were then analysed via an agarose gel to check the amplified PCR product was as expected.

PCR was used to amplify target genes using cDNA generated from CHOS cells, detailed in section 2.3.9.1, using the primers found in Table 2.2.2. Some subunits were commercially synthesised, including the E2 subunit (PEL5, 7, 8, 9, 15 and 18) and E1alpha NV5 Tag (PEL13) ordered from ThermoFisher GeneArt and the E1alpha CV5 Tag (PEL16) ordered from Twist Bioscience.

Table 2.2.1.1 Thermocycler Programme used for PCR with Phusion High Fidelity Polymerase.

X = melting point of the reaction primers used in the reaction and varied between 65-70°C.

Y = length of time required for sequence amplification, 30 secs per 1kb of amplicon size.

Temperature	**Time**	**Step**	
98°C	30 secs	Initial Denaturation	
98°C	10 secs	Denaturation	x 35 cycles
X - 5°C	30 secs	Annealing	
72°C	Y	Extension	
72°C	7 mins	Final Extension	
4°C	∞	Hold	

PCR was also used to screen *E.coli* colonies grown after a transformation for the correct plasmid DNA, instead using Promega GoTaq® G2 Flexi DNA Polymerase. A colony was picked from a LB Agar plate and mixed with 5µl nuclease free water, 5X GoTaq® Flexi buffer, 3mM $MgCl_2$, 0.5µM forward and reverse primers and 10mM dNTP mix master mix was added along with water to make up a 15µl total volume. The Thermocycler was used as detailed in Table 2.2.1.2.

Table 2.2.1.2 Thermocycler Programme used for PCR with Promega GoTaq® G2 Flexi DNA Polymerase.

Y = length of time required for sequence amplification. 1 minute per 1kb of amplicon size.

Temperature	**Time**	**Step**	
98°C	30 secs	Initial Denaturation	
98°C	10 secs	Denaturation	x 35 cycles
65°C	30 secs	Annealing	
72°C	Y	Extension	
72°C	7 mins	Final Extension	
4°C	∞	Hold	

Table 2.2.2 Primers used to amplify target genes including the addition of a tag when required.

Primer Name	Primer Sequence (5' to 3')	Restriction Sites	Annealing Temp (°C)	Relevant Section
E1alpha for	TAT **GGCGCGCC** ATGAGGAAGATG	**AscI**	64.2	3.5
E1alpha rev	ATA **TTAATTAA** TTAACTGACTGACTTAAACTTGATCCACTG	**PacI**	64.4	3.5
E1beta for	TAT **ACCGGT** ATGGCGACGCTGG	**AgeI**	64.0	3.5
E1beta rev	ATA **GGTACC** TTAGACATTCAGTGTCTTCTTTACT	**KpnI**	64.7	3.5
E2 for	TAT **CTCGAG** ATGTGGCGCGTCTGT	**XhoI**	64.4	3.5
E2 rev	ATA **GTTTAAAC** TTATAACAACATAGTTATAGGCTTTTCAAGGT	**PmeI**	64.7	3.5
E1alphaV5TagN for	TAT **CGTACG** ATGAGGAAGATGCTTGCC	**BsiWI**	65.0	3.8
E1alphaV5TagN rev	ATA **TTAATTAA** CTGACTGACTTAAACTTGATCCACTGGTT	**PacI**	65.4	3.8
E1betaHATagN for	TAT **CGTCTCA** CAGC ATGGCGACGC	**AarI**	66.1	3.8
E1betaHATagN rev	ATA **GGATCC** TTAGACATTCAGTGTCTTCTTTACT	**BamHI**	64.7	3.8
E2FLAGTagN for	TAT **GCTTAGC** ATGTGGCGCGTCTGTG	**BlpI**	66.4	3.8
E2FLAGTagN rev	ATA **TTCGAA** TTATAACAACATAGTTATAGGCTTTTCAAGGTAC	**BstBI**	65.6	3.8
E1alphaV5TagC for	TAT **ATCGAT** ATGAGGAAGATGCTTGCCGCT	**ClaI**	65.4	3.8
E1alphaV5TagC rev	ATA **CTTAAG** ACTGACTGACTTAAACTTGATCCACTT	**AflII**	64.9	3.8
E1betaHATagC for	TAT **ACCGGT** ATGGCGACGCTGGC	**AgeI**	66.0	3.8
E1betaHATagC rev	ATA **GGTACC** GACATTCAGTGTCTTCTTTACTG	**KpnI**	65.6	3.8
E2FLAGTagC for	TAT **GCGGCCGC** ATGTGGCGCGT	**NotI**	67.7	3.8
E2FLAGTagC rev	ATA **TCTAGA** TAACAACATAGTTATAGGCTTTTCAAGGTAC	**XbaI**	65.4	3.8
E1alphamutAla for	TAT **GCTAGC** ATGAGGAAGATGCTTGCC	**NheI**	65.0	3.12
E1alphamutAla rev	ATA **CTTAAG** ACTGACTGACTTAAACTTGATCCACT	**AflII**	64.8	3.12

2.2.10.1 Agarose Gel Electrophoresis

DNA fragments were separated using agarose gel electrophoresis. 50ml TAE buffer (4.84g Tris-base, 1.142ml Acetate, 2ml 0.5M Sodium EDTA made up to 1L with MilliQ water) was heated to dissolve agarose making either a 1% or 2% agarose gel. Once cooled, 3µl of Ethidium Bromide was added and the gel poured and cast with an appropriate well comb. Samples were loaded alongside either a Promega 1kb or Promega 100bp DNA ladder. Gels were run at 80V to enable separation based on molecular weight.

2.2.10.2 Purification of DNA from Agarose gel

DNA bands were cut from agarose gels using a razor blade, weighed and purified using a Promega Wizard® SV Gel and PCR Clean up kit following the manufacturer's instructions. This was also used to clean up PCR fragments. Alternatively, the QIAGEN QIAquick Nucleotide Removal Kit was used for smaller sized PCR products.

2.2.11 Restriction digests

All enzymes used were either ThermoFisher Fast digest or NEB High Fidelity enzymes according to the manufacturer's instructions.

2.2.12 Dephosphorylation of a DNA backbone

DNA backbones were dephosphorylated at the 5' end using Promega Thermosensitive Alkaline Phosphatase (TSAP) as to the manufacturer's instructions.

2.2.13 DNA ligation

DNA fragments were ligated together using Promega T4 DNA ligase. A reaction mix of 3µl backbone and 5 µl insert had 1µl T4 DNA ligase enzyme and 1µl T4 DNA ligase 10x buffer added. The ratio of backbone to insert was changed in response to DNA concentration. This was left either on the benchtop at room temperature for several hours or in the fridge at 4°C overnight before being transformed into DH5α *E.coli* cells.

2.3 Mammalian Cell culture and sampling

2.3.1 Suspension Cell lines and maintenance

Cell lines were generated using CHO-S and CHOK1 cells and were kept in CD-CHO (Gibco 10743-029) media supplemented with 8mM L-glutamine. Anti Clumping agent or ACA (Gibco 0010057AE) was often used at a 1 in 1000 dilution to prevent cell clumping and enable higher density cell numbers in culture. Invitrogen Hygromycin B selection was used for stably generated cell lines, at

a concentration 750µg/ml. After cell sampling, cells were passaged and seeded at $0.2x10^6$ viable cells in a 125ml Erlenmeyer flask with a 20ml total volume or alternatively in a 50ml falcon tube with a 10ml total volume. Cells were then gassed with 5% CO_2 for an average of 10 secs and placed into a shaking incubator at 37°C. If 50ml falcon tubes were used, a shake speed of 220rpm was used, however for larger Erlenmeyer flasks (varying from 125ml to 250ml) a shake speed of 140rpm was used.

2.3.2 Cell sampling

Cells were passaged every 3 to 4 days. Cells were measured on a Beckmann Coulter Vi-Cell with a 1ml total volume used at various dilutions depending on total culture volume with fresh media used to make up the final volume. Total cell number, viable cell number and percentage viability of the cultures were measured.

2.3.3 Cryopreservation and revival of cells

Cells were banked down in 1.8ml Fisher Scientific cryovials, with $1x10^7$ cells spun for 5mins at 1000rpm. 1ml freezing media (CD-CHO media supplemented with 8mM L-glutamine with the addition of 7.5% DMSO) was added to the cell pellet, resuspended and flash frozen on dry ice. The cryovials were kept in the -80°C freezer before being added to the cryostat full of liquid nitrogen.

To revive cryopreserved cells, vials were thawed in the water bath at 37°C before being added to a 50ml falcon tube or Erlenmeyer flask of fresh media of appropriate volume. Cells were passaged as usual with a minimum of 3 passages performed before use in experimentation.

2.3.4 Lipofectamine NovaCHOice® based Transfection of DNA in Mammalian Cells

A Merck NovaCHOice® Transfection kit was used for lipofectamine based transfections initially to investigate the potential impact of overexpressing selected PDH subunits. Both the DNA quantity used, 1µg, 2µg and 4µg, and cell seeding density, $0.5x10^6$ and $1x10^6$, was changed to optimise the transfection process. Cells were counted and centrifuged at 1000rpm for 5mins and the pellet resuspended in 75ml media to cover all 12 6 well plates used. 1.8ml cell culture was added to each well along with the DNA lipid mixture (CDCHO media, 100ng/µl plasmid at previously mentioned concentrations, 2µl NovaCHOice transfection reagent and 1µl NovaCHOice booster reagent with a total volume of 213µl per transfection.) This was added dropwise as the plate was swirled gently. The plates were kept at 37°C in a static incubator with 5% CO_2. After 72 hours, the cells were harvested. 200µl trypsin was added to each well, swirled and then left to incubate at 37°C for 5mins. 2ml well volume was pipetted up and down to dislodge cells and spun at 1000rpm for

5mins with the pellet resuspended in fresh media. A cell count was performed and $1x10^6$ cells were taken to perform protein analysis.

2.3.5 Electroporation based Transfection of DNA in Mammalian Cells

Transfections were also performed using electroporation. This was after the initial Lipofection based transient expression and was used primarily for the construction of stable cell pools described in 2.3.7. $10x10^6$ cells per transfection were centrifuged at 1000rpm for 5mins. The supernatant was removed, and the pellet resuspended in 700µl per transfection and kept at 37°C until the transfection was carried out. DNA was diluted in 100µl TE volume with 40µg used for transient and stable cell line creation and 10µg used per gRNA in CRISPR/Cas9 experiments. The cells and DNA were added together into a BIORAD cuvette and electroporated in a BIORAD Genepulser Xcell electroporator at 300 V and 900 µF with a cuvette diameter of 0.4 mm. After the electroporation, 1ml warmed media was added to the cuvette and all added to a Erlenmeyer flask or 50ml falcon tube. A further 1ml of media was used to wash the cuvette and added. One transfection was used for a 20ml total volume, either in one Erlenmeyer flask or split over two falcon tubes for transient and CRISPR/Cas9 experiments. The flask or tube was gassed with 5% CO^2 gas and incubated in a shaking incubator at 37°C at 140rpm or 220rpm respectively.

2.3.6 Linearisation of DNA and DNA precipitation

DNA was prepared using the QIAGEN Plasmid MaxiPrep kit. 50µg DNA was linearised using an overnight digest with ThermoFisher Fast Digest FspI. The DNA was then solubilised using sodium acetate, washed with ethanol and then resuspended in TE buffer. The concentration was determined via the Nano-Drop Spectrometer ND-1000 and then 20µg prepared in 100µl volumes ready for transfections.

2.3.7 Construction of Stable Cell Pools

Linearised DNA was used for the electroporation of cells as described with Invitrogen Hygromycin B selection added 24hrs after transfection to achieve an end concentration of 750µg/ml. Cells were checked after 2 weeks via a cell count and passaged once a suitable cell viability had been reached. Cell passages continued with alternate media used to continue the Invitrogen Hygromycin B selection pressure.

2.3.8 Metabolite Analysis

Cell supernatant samples were taken throughout growth curves on days 4, 6 and 8 having been centrifuged at 1000rpm for 5mins. These were processed on a CM Scientific CuBiAn HT-270 Biochemistry Analyser using the appropriate assay kits.

2.3.9.1 RNA Extraction and cDNA generation

RNAse free water and Eppendorfs were used throughout all RNA work, with surfaces, racks and pipettes cleaned with 70% IMS and then Sigma RNAsezap. $2x10^6$ cells were spun at 1000rpm for 5mins, the supernatant removed and 350µl QIAGEN RLT buffer was added. Samples were frozen on dry ice and stored in -80°C until needed. Defrosted samples were vortexed and homogenised on a QIAGEN QIAShredder column following the manufacturers instructions. The samples had the total mRNA extracted using a QIAGEN RNeasy Mini Kit. The concentration of the mRNA was measured using the Nano-Drop Spectrometer ND-1000 on the RNA setting at 260nm. mRNA was treated with Promega RQ1 RNase free DNAse to remove any genomic DNA contamination and diluted to a total concentration of 25ng/µl for use in RTqPCR.

This RNA was then used to generate cDNA which was used for target gene amplification. 4 µg RNA and 4 µl oligoDT primers were incubated at 70°C for 5 minutes and left on ice for 2 minutes. 2.6 µl of 10 mM dNTPs, 10 µl 5X MMLV buffer (Promega), 1.4 µl RNase and 2 µl MMLV reverse transcriptase (Promega) were added to the mixture and a total volume of 50 µl reached via the addition of RNase free water. The mixture was incubated at 37°C for 1 hour and the resulting cDNA purified using Promega's Wizard® SV gel and PCR clean up system and stored at -80°C.

2.3.9.2 mRNA analysis using RTqPCR

mRNA levels were measured using RTqPCR in BRAND 96 well, non-skirted, white plates using the QIAGEN QuantiFast SYBR Green RT-PCR Kit until it was discontinued and replaced by the QIAGEN QuantiNova SYBR Green RT-PCR Kit in 2021. Both were used following the manufacturer's instructions, scaling down the reaction to a 12ul total volume, on a BIORAD DNA Engine Peltier Thermocycler with a BIORAD Chromo4 real-time detection module and later a ThermoFisher QuantStudio3 real-time PCR system. ThermoFisher QuantStudio Design and Analysis Software 2.6.0 was used for analysis of the results with the relative quantification calculated following the steps in (Taylor et al., 2019). To check the DNAse treatment was successful, RTCs, RT free controls were completed with water in place of the RT enzyme. Any signal detected would be due to DNA present in the samples and not the cDNA reverse transcribed from RNA due to the absence of RT enzyme.

Table 2.3.1 Thermocycler programme used to run all RTqPCR and qPCR plates.

Step	Parameter
1	50°C for 10mins
2	95°C for 2mins
3	95°C for 5secs
4	60°C for 10secs
5	Plate read
6	Repeat steps 3-5 39 times
7	Melting curve from 58°C to 95°C. Plate read every 0.5°C

Table 2.3.2 Primer sequences used for RTqPCR analysis.

Primer Name	Primer Sequence (5’ to 3’)	Amplicon size (bp)
RTqPCR Beta-actin for	AGCTGAGAGGGAAATTGTGCG	163
RTqPCR Beta-actin rev	GCAACGGAACCGCTCATT	
RTqPCR GAPDH for	AACTTTGGCATTGTGGAAGG	223
RTqPCR GAPDH for	ACACGTTGGGGGTAGGAACA	
RTqPCR PDK1 for	GAGCTGCTTGATTTTAAGGACA	109
RTqPCR PDK1 rev	TGGTTGGAATGACATCATTGTG	
RTqPCR PDK2 for	CTGGAGTACAAGGACACCTATG	144
RTqPCR PDK2 rev	GGGTTGGTACTTCCATCAAAGA	
RTqPCR PDK3 for	TATACCAACCGCATCTCTTTCC	134
RTqPCR PDK3 rev	CTTTCACGACATCAGCTACATT	
RTqPCR E1alpha for	AGCAATTCTTGCAGAGCTAAC	102
RTqPCR E1alpha rev	GATGCCATTGCCTCCATAGAA	
RTqPCR E1beta for	ATACGGTGACAAGAGGATCATA	75
RTqPCR E1beta rev	ATAGCTGCACCAACAGCAATTC	
RTqPCR E2 for	TATAGCAGCCTTTGCAGACTAC	183
RTqPCR E2 rev	AACTTCTTTGCAAGAGGGCTAA	
RTqPCR E3BP for	GATGGGCAAGATTACAGAATCC	177
RTqPCR E3BP rev	AATAACTCTCCGAATGTTGCTG	
RTqPCR PDP for	TTACGCACATCTCCTCTGTATG	190
RTqPCR PDP rev	CTTCCTTACAGCACTTGACTTC	

2.3.10.1 gDNA extraction

$2x10^6$ cells were spun at 250g for 5mins with the pellet frozen and stored in the in -20°C until needed. The Invitrogen™ PureLink™ Genomic DNA Mini Kit was used following the manufacturer's instructions to isolate the gDNA. The concentration of the gDNA was measured using the Nano-Drop Spectrometer ND-1000 on the DNA setting at 260nm and then aliquoted into 25ng/µl.

2.3.10.2 gDNA analysis using qPCR

gDNA levels were measured using qPCR in BRAND 96 well, non-skirted, white plates using the QIAGEN QuantiFast SYBR Green RT-PCR Kit until it was discontinued and replaced by the QIAGEN QuantiNova SYBR Green RT-PCR Kit in 2021 both times excluding the RT enzyme from the reaction. Both were used following the manufacturer's instructions, scaling down the reaction to a 12ul total volume, on a BIORAD DNA Engine Peltier Thermocycler with a BIORAD Chromo4 real-time detection module and later a ThermoFisher QuantStudio3 real-time PCR system. ThermoFisher QuantStudio Design and Analysis Software 2.6.0 was used for analysis of the results.

Table 2.3.3 Primer sequences used for qPCR analysis.
*FUT8 gene used as a control CRISPR/Cas9 KO reaction. Primers taken from (Marx et al., 2021)
**LDHa qPCR primers from (M. Zhou et al., 2011)

Primer Name	Primer Sequence (5' to 3')	Amplicon size (bp)
qPCR Beta-actin for	AGCTGAGAGGGAAATTGTGCG	163
qPCR Beta-actin rev	GCAACGGAACCGCTCATT	
qPCR Fut8 for*	GAAGGAAACGAACTCCAAAGAC	107
qPCR Fut8 rev*	GCTCCATCTGTTTGACTGAGG	
qPCR GAPDH for	GCCAAGAGGGTCATCATCTC	261
qPCR GAPDH rev	CCTTCCACAATGCCAAAGTT	
qPCR PDK1 1 for	CCCATTTTGATAGTTGAGGGC	83
qPCR PDK1 1 rev	TCAGATCTGTCCCGTACACTTA	
qPCR PDK2 1 for	CTTCAGCTACATGTACTCCACA	121
qPCR PDK2 1 rev	TGGAGTATGCTTGGGAGTTAAG	
qPCR PDK3 2 for	GCTGTTAAAACTCTCGTTACTCT	642
qPCR PDK3 2 rev	TTTTCGAAGTGGGACTCCACC	
qPCR E1alpha 2 for	AGTGCTAATAGCTTCCCGTAA	788
qPCR E1alpha 2 rev	TAGTACTTGAGCCCATCTTCTC	
qPCR E1beta 1 for	TAAGGTGCTGGTTACTTACTGT	109
qPCR E1beta 1 rev	GTCTAGAAGCTTTAGGATGGGT	
qPCR E2 2 for	GTGAGCTCAAGATCCATGATTG	113
qPCR E2 2 rev	TAGTCTCATGTCAGAACTGGAC	

Primer Name	Primer Sequence (5’ to 3’)	Amplicon size (bp)
qPCR E3BP 2 for	AGGGTTTCCGAATTTACCCTAA	157
qPCR E3BP 2 rev	GCTTGAGTAGACAATGATAGCC	
qPCR PDP 2 for	CTCTGAAGCGTATCAACTCAAG	199
qPCR PDP 2 rev	GATCGTGCACATTGAGGAAAG	
qPCR LDHa for**	GCCGAGAGCATAATGAAGAA	68
qPCR LDHa rev**	CCATAGAGACCCTTAATCATGGTA	
qPCR E1alpha N for	GATGGGTAAGCCTATCCCTAA	189
qPCR E1alpha N rev	TCTTCTAGCCGATGAAGGTCAC	
qPCR E1beta N for	CAAGACCGGTATGTATCCCTATG	215
qPCR E1beta N rev	TAGCTTCTCGAACTGTCAACTG	
qPCR E2 N for	CTACAAAGACGATGACGACAAG	113
qPCR E2 N for	CTTCCTTCAAGACTGCCCAC	
qPCR E1alpha C for	GGAGGAACTAGGCTATCACATC	137
qPCR E1alpha C rev	TAGAATCGAGACCGAGGAGA	
qPCR E1beta C for	AGAAGACAACTCCATACCTCAG	137
qPCR E1beta C rev	GGTATCCAGCATAATCAGGAA	
qPCR E2 C for	GCATGATGTCTGTTACACTCAG	146
qPCR E2 C for	CTTGTCGTCATCGTCTTTGTAG	

2.4 Protein analysis via SDS-PAGE and Western blotting

2.4.1 Cell lysis

$1x10^6$ cells were spun for 5mins at 1000rpm. 100µl lysis buffer (Hepes 0.48g, NaCl 0.58 g, b-Glycerophosphate 0.216 g, triton 1 ml, pH to 7.2. For every 10 ml of this add 1 Roche inhibitor tablet plus 500 ul Naf and 50 ul Nav) was added and the sample left on ice for 30mins.

2.4.2 Bradford Assay

Prepare the cells by spinning them at 13,000rpm for 3 mins at 4°C to remove cell debris. Triplicates of protein standard concentrations of 400µg/ml, 300µg/ml, 200µg/ml, 150µg/ml, 100µg/ml, 50µg/ml, 25µg/ml and 0µg/ml, made using Promega BSA 10mg/ml and MilliQ water, were added to a 96 well plate. Dilute cell lysate samples 1 in 20 with MilliQ water and load triplicate samples into plate. Add 200µl Bradford reagent to each well and leave for 10 mins. Read the absorbance at 595nm using an Eppendorf BioPhotometer. Input these results to create the control standard curve and calculate concentration of protein in each sample in µg/ml.

2.4.3 Prepare samples for SDS-PAGE gel analysis

Protein samples were prepared for SDS-PAGE analysis using the concentrations estimated by Bradford assay with between 5-20µg of protein loaded each time. A 4x reducing laemmli buffer (1 M Tris-HCl pH 6.8, 4ml Glycerol, 0.8g SDS, 1ml β-Mercaptoethanol, 4mg Bromophenol Blue, 2.6ml MilliQ water) was added alongside MilliQ water to form a total 10ul. Samples were then boiled at 95^oC for 10mins before being loaded into an SDS-PAGE gel.

2.4.4 SDS-PAGE Gels

Sodium dodecyl sulphate polyacrylamide gel electrophoresis (SDS-PAGE) was used to separate proteins based on molecular weights. Gels were made with either 8, 10 or 12% BIORAD polyacrylamide resolving gel (1.5M Tris pH 8.8, 10% SDS, 10% Ammonium Persulfate, TEMED) depending on the target protein sizes with 5% stacking gel (1M Tris pH 6.8, 10% SDS, 10% Ammonium Persulfate, TEMED) added to hold an appropriate well comb.

Gels were run with SDS running buffer (14.44g Glycine, 1g SDS, 3g Tris base added to 1L MilliQ water and pH to 8.8) at 100V for 30mins then 150V for 1 to 1.5 hours. Depending on the well size, around 15µl sample was loaded with 5µl ThermoFisher PageRuler Plus Pre-stained Protein ladder. Gels were either stained with Coomassie or used for Western blots.

2.4.5 Western blots

After running a SDS-PAGE Gel, it was transferred to a 0.45 µM Sigma Hybond® ECLTM nitrocellulose membrane for 1 h at 0.75 A in a 2051 Midget Multiblot Electrophoretic Transfer Unit at 4°C. 1X Transfer buffer was used from a 10X stock (100 mM Glycine, 125 mM Tris + 0.5% SDS) with the addition of methanol to the 1X solution.

The nitrocellulose membrane was then blocked with 5% w/v milk in TBS buffer (20 mM Tris, 137 mM NaCl made up to 1 L with MilliQ water and pH to 7.6) on a shaker for 30 mins at room temperature. TBST buffer (1L TBS buffer with 1ml Tween added) was used for 3 x for 10mins washes. The primary antibody of choice was added and left on a shaker at 4°C overnight. This was then removed, and the membrane washed 3 x for 10mins using TBST. The secondary antibody was then added and left on a shaker for 1 hour at room temp. The membrane was then washed again, after removing the secondary antibody, 3 x for 10mins using TBST. Membranes were then incubated in GE Life Sciences Amersham ECL reagent as per the manufacturer's instructions for signal detection. Excess reagent was dabbed off the membranes before they were developed in a dark room via exposure of GE Life Sciences ECL chemiluminescence film. Exposure times vary depending on the Western blots and are detailed throughout.

Table 2.4.1 Details of Primary and Secondary Antibodies. Antibodies were diluted accordingly in 5% (w/v) BSA in TBST buffer.

*Abcam PDH Antibody cocktail Abcam, mouse, (ab110416.) contains the following antibodies at specified concentrations:

Mouse anti C-V-OSCP [4C11C10D12] monoclonal: Amount: 12.5 µg. Working concentration: 0.5 µg/ml

Mouse anti PDH-E1-alpha [9H9AF5] monoclonal: Amount: 25 µg. Working concentration: 1 µg/ml

Mouse anti PDH-E1-beta [17A5E2H8] monoclonal: Amount: 62.5 µg. Working concentration: 2.5 µg/ml

Mouse anti PDH-E2 [15D3G9C11] monoclonal: Amount: 25 µg. Working concentration: 1 µg/ml

Mouse anti PDH-E2/E3bp [13G2AE2BH5] monoclonal: Amount: 25 µg. Working concentration: 1 µg/ml

**These Tag primary antibodies were used for the immunoprecipitation of tagged protein subunits as described in section 2.4.9.

(NVC) These antibodies were not validated for performing Western blots with CHO cell samples.

Primary Antibody	**Brand and Cat No.**	**Produced In**	**Dilution**
Anti-β-actin	Sigma-Aldrich (A5441)	Mouse	1:5000
PDH Antibody cocktail* (NVC)	Abcam (ab110416)	Mouse	1:4000
Anti-GFP 3E1	Research Monoclonal Antibody Service, CRUK	Mouse	1:5000
Anti-V5**	Invitrogen (R961-25)	Mouse	1:1000
Anti-HA Tag**	Cell signalling (C29F4)	Rabbit	1:1000
Anti-DYKDDDDK (FLAG) Tag**	Invitrogen (MAI-91878)	Mouse	1:1000
Anti-PDK1 (NVC)	GeneTex (GTX105999)	Rabbit	1:10,000
Anti-PDK2 (NVC)	GeneTex (GTX105251)	Rabbit	1:10,000
Anti-PDK3 (NVC)	GeneTex (GTX104286)	Rabbit	1:1000
Anti-PDPc (D-11) (NVC)	Santa Cruz (sc-398117)	Mouse	1:500
Anti-PKLR Antibody (E-2) (Pyruvate Kinase) (NVC)	Santa Cruz (133222)	Mouse	1:500
Anti γ chain	Sigma-Aldrich (I9764)	Rabbit	1:2000
Anti-SCD1	Cell Signalling (2438)	Rabbit	1:1000
Anti-SREBP1	Abcam (ab3259)	Mouse	1:1000
Secondary Antibody	**Brand and Cat No.**	**Produced In**	**Dilution**
Anti-Mouse IgG	Sigma-Aldrich (A4416)	Goat	1:1000
Anti-Rabbit IgG	Sigma-Aldrich (A6154)	Goat	1:1000

2.4.6 Dot blots

A Bio-Dot microfiltration apparatus was used to perform dot blots for screening multiple samples. 50µl of cell lysate, prepared as mentioned previously for SDS-PAGE gels, or 100µl supernatant was loaded in each of the required 96 wells and vacuumed through to a piece of 0.45 µM Sigma Hybond® ECLTM nitrocellulose membrane pre-wetted with TBS buffer. The nitrocellulose membrane then followed the Western blot process to be developed.

2.4.7 Coomassie Staining

SDS-PAGE gels were stained with Coomassie stain (1 g comassie brilliant blue G250, add to 500 ml MeOH, 10ml glacial acetic acid and 400 ml MilliQ water) using enough to cover gel and left to shake for 1 hour at room temperature. The Coomassie stain was replaced with Destain (240 ml MeOH, 140 ml glacial acetic acid, make up to 1L MilliQ water) and left to shake for 1 hour at room temperature. The Destain was replaced with MilliQ water and left to shake before being imaged.

2.4.8 Western blot Densitometry analysis

ImageJ 1.50i software (Schneider *et al*., 2012) was used to analyse Western blot bands and dot blot dots after scanning and saving. A control sample on each blot allowed the comparison of housekeeper gene β-actin to bands of target proteins to see relative density.

2.4.9 Magnetic Immunoprecipitation using Invitrogen Dynabeads™ M-270 Epoxy

Invitrogen Dynabeads™ M-270 Epoxy beads were used for immunoprecipitation according to the manufacturer's instructions. The lyophilised beads were covalently coupled to each tag antibody, listed in Table 2.4.1, following the manufacturer's recommended concentrations. Anti-V5 and anti-HA antibodies were used at a 1 in 50 dilution whilst the anti-FLAG antibody was used at 1mg/ml. After coupling, the beads were washed with PBS and resuspended in Buffer A (0.1M sodium phosphate buffer pH 7.4.) The beads were incubated with cell lysate samples containing excess protein (10µg) for 1hour before being washed again. A magnetic tube rack was used at each stage to separate the beads and the supernatant allowing the removal of non-specific proteins. The beads were boiled in 4x reducing laemmli buffer, detailed in section 2.4.3, for 10mins with the resulting supernatant collected and loaded in SDS PAGE gels, section 2.4.4, for Western blot analysis, section 2.4.5.

2.5 CRISPR/Cas9 Knock out of target genes

This process was learnt whilst on a EPSRC Industrial Placement in Professor Nicole Borth's lab in Vienna. The same process was used but the following methods refer to equipment used at the University of Kent.

2.5.1 Annealing and phosphorylation of oligos for CRISPR/Cas9 gRNAs

gRNA pairs were designed around 500 bp upstream and downstream of the gene of interest for a paired approach, using the CCTop - CRISPR/Cas9 target online predictor. A 10µl reaction mixture of 1µl of both forward and rev gRNAs 100µM, 1µl New England Bioscience 10X T4 Ligation Buffer, 6.5µl ddH_20 and 0.5µl New England Bioscience Polynucleotide Kinase (PNK) (10,000 U/ml), was prepared for each set of gRNAs. This was annealed and phosphorylated in the Thermocycler as follows then diluted 1in10 in ddH_20 to yield an annealed oligo concentration of 1µM then stored at -20°C. A control was performed with ddH_20.

Table 2.5.1.1 Thermocycler programme used for annealing and phosphorylation of oligos for CRISPR/Cas9 gRNAs.

Temperature	Time	Temperature Change
37°C	30mins	(2°C/sec)
95°C	5mins	(2°C/sec)
25°C	14mins	(0.1°C/sec)
16°C	Pause	

Table 2.5.1.2 gRNAs sequences used for CRISPR/Cas9 targeting of specific genes of interest for KO.
Addition of CACC or AAAC amino acids to encode a BbsI/BpiI restriction site for later cloning.
*FUT8 gene used as a control CRISPR/Cas9 KO reaction. gRNA sequences taken from (Marx et al., 2021)

Primer Name	Primer Sequence (5' to 3')
FUT8_sg1 for*	**CACC** GGACACTGCGTGGAGTACTT
FUT8_sg1 rev*	**AAAC** AAGTACTCCACGCAGTGTCC
FUT8_sg6 for*	**CACC** GAGATCGCTGTGCAGTAGTA
FUT8_sg6 rev*	**AAAC** TACTACTGCACAGCGATCTC
PDK1gRNA 2 for	**CACC** GTCTCGGGGCTCCGCCTACGA
PDK1gRNA 2 rev	**AAAC** TCGTAGGCGGAGCCCCGAGAC
PDK1gRNA 3 for	**CACC** GCAAGGACCTGCGTGGTCGC
PDK1gRNA 3 rev	**AAAC** GCGACCACGCAGGTCCTTGC
PDK1gRNA 5 for	**CACC** GGTACGTGCCTATAGTATCT
PDK1gRNA 5 rev	**AAAC** AGATACTATAGGCACGTACC
PDK1gRNA 6 for	**CACC** GTTTACTCCGCTAGGGACATA
PDK1gRNA 6 rev	**AAAC** TATGTCCCTAGCGGAGTAAAC
PDK2gRNA 1 for	**CACC** GTAGCCTTGCGCTTCGACACG
PDK2gRNA 1 rev	**AAAC** CGTGTCGAAGCGCAAGGCTAC
PDK2gRNA 3 for	**CACC** GCGCGGCCATTGGCGACGTC
PDK2gRNA 3 rev	**AAAC** GACGTCGCCAATGGCCGCGC
PDK2gRNA 4 for	**CACC** GTATGCTCTGGTTGCTAGCT
PDK2gRNA 4 rev	**AAAC** AGCTAGCAACCAGAGCATAC
PDK2gRNA 6 for	**CACC** GCCAAGACGATCGATCAATCT
PDK2gRNA 6 rev	**AAAC** AGATTGATCGATCGTCTTGGC
PDK3gRNA 1 for	**CACC** GTGCACGCGCGCGCCGCTGAT
PDK3gRNA 1 rev	**AAAC** ATCAGCGGCGCGCGCGTGCAC
PDK3gRNA 2 for	**CACC** GAGCGCTAAAGATCGTGTTTC

PDK3gRNA 2 rev	**AAAC** GAAACACGATCTTTAGCGCTC
PDK3gRNA 3 for	**CACC** GAAATATAACACCTCCGGTGA
PDK3gRNA 3 rev	**AAAC** TCACCGGAGGTGTTATATTTC
PDK3gRNA 4 for	**CACC** GCCATTCACATGGTATGGTG
PDK3gRNA 4 rev	**AAAC** CACCATACCATGTGAATGGC

2.5.2 Golden Gate Assembly cloning of CRISPR/Cas9 gRNAs into Cas9 vector

A reaction mixture containing 1µl 50ng circular pX458 vector (pSpCas9(BB)-2A-GFP, #48138, Addgene) 0.5µl annealed oligos (use the ddH_20 control as a ligation control), 2.5µl 10X restriction enzyme buffer (Fast Digest, Thermo), 2µl BbsI/BpiI restriction enzyme (Fast Digest, Thermo), 2.5µl 10µM ATP (NEB), 0.9375µl T4 DNA ligase (NEB) and ddH_20 was prepared to create a 25µl total volume. This plasmid expresses the Cas9 and has another cassette with a U6 promoter for gRNA expression. This was run in the Thermocycler as follows and then stored at -20°C.

Table 2.5.2 Thermocycler Programme used for Golden Gate assembly cloning of CRISPR/Cas9 gRNAs into the Cas9 vector.

Temperature	**Time**	**Temperature Change**	
37°C	5mins	(2°C/sec)	X20 cycles
20°C	5mins	(2°C/sec)	
80°C	14mins	(0.1°C/sec)	

10µl of this was then used for a transformation into Calcium Competent DH5α cells and prepared via a QIAGEN Plasmid Maxi kit once GeneWiz sanger sequencing confirmed cloning was successful. Cells were transfected as previously described with 10ug of each gRNA pair used per transfection.

2.5.3 Single cell cloning by serial dilution

CRISPR/Cas9 cell lines were sorted using serial dilutions before being replaced by FACS based cell sorting. 96 well plates had 100µl CD CHO media added to all wells apart from well A1 which instead had 200µl of cells at $1x10^5$ viable cells/ml added. Serial dilutions were carried out vertically from A1 to H1 and then horizontally from columns 1 to 12 with 100µl being discarded from column 12. 100µl media was added to all wells to bring the total volume to 200µl. The plates were left in a 37°C static incubator and checked regularly for growth. Wells containing one colony were chosen and moved to 6 well plates and T25 flasks.

2.5.4 Fluorescence activated cell sorting

The presence of a GFP gene included in the pX458 vector used for CRISPR/Cas9 transfections allowed the sorting of cells based on fluorescence. A BD Biosciences FACSJazz™ was used with BD Rainbow Calibration Particles 8 peaks (559123) for calibration of the blue laser at 488nm and BD FACS™ Accudrop Fluorescent Beads (345249) for calibration and stream alignment ready for cell sorting. Cells were sorted 3 days after transfection with DNA free transfected CHOS or CHOK1 cells used as a control for gating populations. Cells were sorted into 96 well plates containing either 10, 100 or 1000 cells per well. CD-CHO media was used supplemented with 8mM l-glutamine, 5000 U/ml Gibco Penicillin-Streptomycin (15070063) and 2.5 mg/L Sigma-Aldrich Amphotericin B solution(A2942.) The plates were left in a 37°C static incubator and checked regularly for growth.

Chapter 3: Investigating the Overexpression of PDH Subunits and their Interactions with Endogenous Subunits

3.1 Introduction

As outlined in the introduction chapter of this thesis, CHO cells are one of the most commonly used mammalian host cell systems for the production of secreted biotherapeutic recombinant proteins due to their ability to produce 'human like' PTMs, grow in large suspension cultures and secrete proteins (Walsh & Walsh, 2022). However, when expressing novel recombinant proteins, the yield is often not comparable to a classic mAb design and they are often described as difficult to express (Saccardo et al., 2016). This is sometimes the case for new mAbs and antibody inspired formats such as bispecific antibodies. The introduction chapter of this thesis describes the targeting of the PDH complex, that acts to convert pyruvate to acetyl-CoA. The work in this thesis aimed to increase the flux of pyruvate through the complex creating more acetyl-CoA available for entry into the TCA cycle and for amino acid and lipid biosynthesis (Ku et al., 2020). This chapter describes the generation of plasmids encoding multiple subunits of the PDH complex individually and in combination for the generation of CHO cell pools and lines stably overexpressing PDH. The work set out to increase the number of copies of the PDH complex, thereby increasing PDH activity within the cell whilst reducing regulation via the activity of PDKs due to an increased number of active PDH complexes requiring phosphorylation.

CHOS and CHOK1 host cell lines were used for the work described in this thesis representing commercially relevant host cell lines. Industrial CHO cell lines originate from the CHO *ori* cell line first isolated in 1956 by Theodore Puck. Differences in both phenotype and genotype during culture have been identified (Tihanyi & Nyitray, 2020) with differences in expression quantity and quality. Different CHO cell lines have been shown to favour either biomass synthesis or production of a recombinant protein (Reinhart et al., 2019). Using CHOS and CHOK1 cells allowed the comparison of industrially relevant host cell lines and the effects of targeted engineering techniques.

The PDH complex is made up of multiple subunits that interact to convert pyruvate to acetyl-CoA in the mitochondria of the cell. Figure 1.6.1 in the introduction chapter shows a cartoon representation of the assembly of subunits forming the complex. When aiming to increase the number of copies of the complex, specific subunits were chosen as targets to be overexpressed, care was taken to choose specific subunits rather than all of the PDH subunits by aiming to reduce any potential cellular stress resulting from the engineering. E1alpha forms half of the heterotetrametric E1 PDH subunit which has TPP dependent activity. The first and rate limiting step

of PDH activity carried out by the E1 subunit is the decarboxylation of pyruvate to carbon dioxide with the formation of a 2-alpha-hydroxyethylidene-TPP intermediate occurring with the reductive acetylation of the lipoyl groups covalently attached to the E2 subunit (Patel et al., 2014). The E1alpha subunit contains three serine residues which are phosphorylated via the activity of PDKs to deactivate the enzyme complex at serine 264, 271 and 203, known as sites 1, 2 and 3 respectively (Rardin et al., 2009).

It is noted that there is a 29 amino acid difference between the serine residue numbers in the human PDH E1alpha sequence when compared to the Chinese hamster sequence so the serine residue numbers can differ depending on the described organism. A comparison between human and CHO PDH E1alpha subunit using NCBI BLAST showed a 97.95% sequence identity and highlighted the 29 amino acid sequence alignment of serine residues targeted for phosphorylation. Overexpression of the E1alpha subunit was undertaken with the aim of increasing the number of E1alpha subunits available to form PDH complexes in CHO cells leading to increased activity and limit the impact of PDK activity phosphorylating and inactivating complexes as additional complex copies are present. The same logic was applied for the overexpression of the E1beta subunit of PDH which forms the other half of the heterotetrametric E1 subunit. Although this subunit does not have serine residues which are impacted by the phosphorylating activity of PDKs, additional copies of the E1beta subunit would act to support the E1alpha subunit to form E1. There may therefore be an impact on PDH expression and activity when just E1beta is overexpressed in the cell as any endogenous E1alpha expression may also be supported to form more complex copies. Finally, the core E2 subunit of the PDH complex was selected for overexpression in CHO cells. Acting as the scaffold for the PDH complex, the E2 subunit organises and connects the other components of the PDH via flexible linkers (Yu et al., 2008). The overexpression of the E2 subunit was undertaken to support the formation of multiple additional PDH complexes. Alongside these PDH subunits with native sequences, a mutant E1alpha subunit was also expressed. Here the three serine residues, the sites of phosphorylation regulation, were mutated to alanine residues preventing the interaction of PDKs and maintaining the PDH complex in an active state (Kolobova et al., 2001b). Expression of the E1alpha mutant aimed to enable incorporation of exogenous mutant E1alpha subunits with endogenous PDH protein resulting in an increase in PDH activity and TCA cycle flux that cannot be subjected to regulation.

The overexpression of the chosen PDH subunits was undertaken individually and in combination with others to identify if the expression of all would be required to increase expression levels of the PDH complex or if expression of only one subunit would act to support endogenous expression levels. A triple cassette vector was chosen to reduce the number of transfections required for multiple subunit expression, ensure all subunits would be upregulated (rather than potential for

only some subunits to be delivered into cells if genes were on individual plasmids) and the same strong CMV promoter used for each cassette. E1alpha was expressed in the first cassette, E1beta in the second and E2 in the third. This aimed to reduce cellular stress and result in even expression levels when multiple subunits were transfected using the same plasmid. The addition of either an N- or C-terminal tag was also used with the same cassette positioning. This would enable the identification of both endogenous and exogenous expression and enable the use of immunoprecipitation to identify if exogenous protein subunits were able to form complexes with endogenous PDH subunits. Western blots and qPCR were used to analyse the impact of the overexpression of PDH subunit protein and gDNA levels respectively.

3.2 Aims of this Chapter

This chapter describes the creation of CHOS and CHOK1 cell pools stably integrated with multiple cassette vectors to allow production of recombinant copies of the PDH subunits E1alpha, E1beta and E2. These were established with, and without, an N- or C-terminal tag to allow for clear identification of endogenous and exogenous PDH subunit expression. Further to this, the chapter describes the analysis of protein and genomic DNA from the integration and expression of these vectors ready for further work investigating any impact of PDH manipulation on difficult to express protein production and cell growth phenotypes.

The overall aims therefore were to:

a. Establish multiple cassette vectors to express recombinant PDH subunits with and without N- and C-terminal tags.
b. Generate CHOS and CHOK1 cell pools stably expressing the recombinant PDH subunits using these vectors.
c. Analyse the levels of endogenous and exogenous PDH subunit protein expression.
d. Analyse genomic DNA expression after stable integration of recombinant DNA.

3.3 Generation of a Hygromycin 3-Cassette Mammalian Expression Vector

To enable the simultaneous expression of each of the three PDH subunits of interest (E1alpha, E1beta, E2), a triple cassette vector was assembled whereby each subunit was independently expressed from a CMV promoter. The construction of this vector allowed each subunit to be expressed alone and/or in combination with others from a single plasmid, reducing the number of transfections required, maintaining the ratio of each subunit during the transfection process, and ensuring all cell lines experienced the same conditions during the transfection process. The Hygro 3 Cass plasmid (PEL1) was created to contain a Hygromycin resistance marker to select for stable integration in mammalian cells and 3 cassettes each with a CMV and T7 promoter, a bGH poly(A) signal and a distinct multiple cloning site (MCS). Within the MCS, each cassette was designed to have a set of unique restriction enzyme sequences to allow the insertion of genes of interest. The plasmid also contained an ampicillin resistance marker for selection of transformed *E.coli* and an origin of replication for amplifying the plasmid in *E.coli*. A schematic of the complete plasmid is shown in Figure 3.3.1 and is described in Table 2.2.3 in the methods section. Once PEL1 had been assembled, the plasmid backbone sequence was verified via commercial Sanger sequencing through GeneWiz. For clarity, PEL1 and all the backbone or control plasmids are highlighted throughout this thesis via the use of underlining. All plasmids are shown in Appendix Table 1.

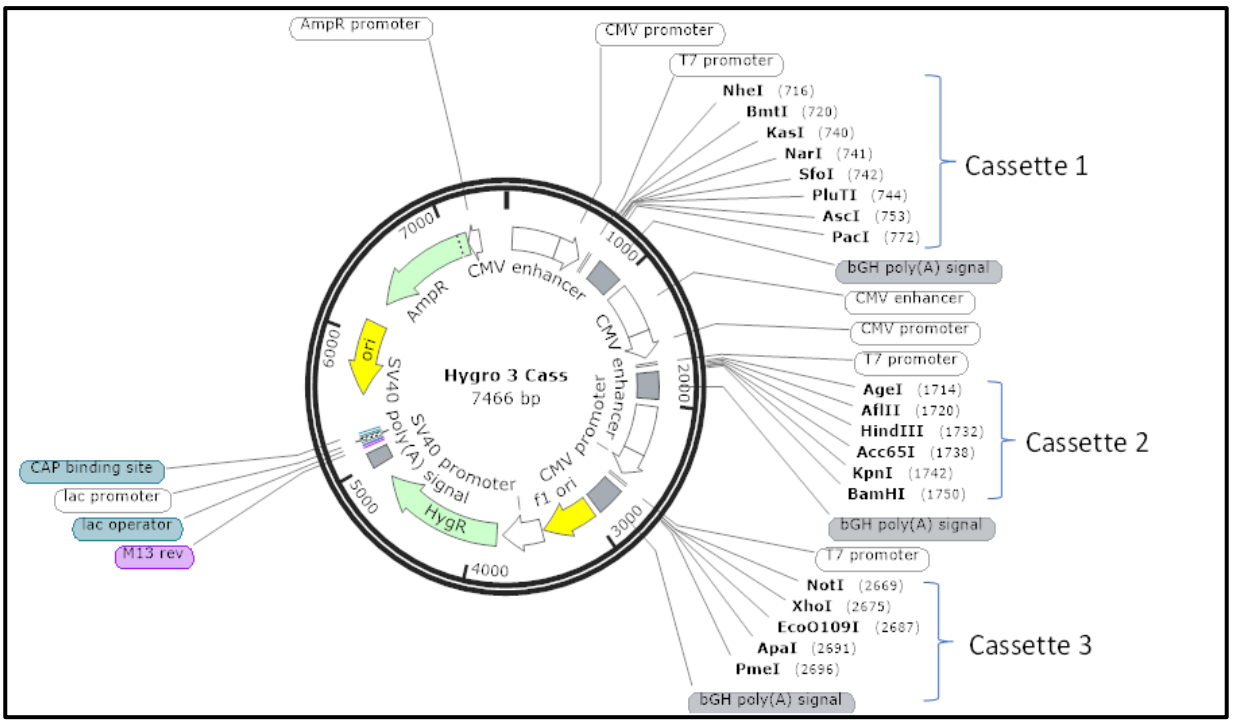

Figure 3.3.1 Schematic of the Hygro 3 Cassette plasmid PEL1 showing the unique enzymes used to clone genes into each of the separate cassettes 1, 2 and 3.

Alongside PEL1, a 3 cassette vector containing a mouse glutamine synthetase (GS) metabolic selection marker in place of the Hygromycin selection was generated (PEL2) (Appendix Table 1). This metabolic selection marker works in CHO cells with or without a GS knockout when using glutamine free medium and the addition of methionine sulfoxamine (MSX) (Lin et al., 2019). MSX binds to GS and acts to inhibit the production of glutamine which is essential for cell growth. Without the expression of the recombinant GS provided through the PEL2 plasmid, the CHO cells cannot produce glutamine and therefore die, leaving only those expressing high enough levels of the GS gene and the gene of interest. To avoid any potential impact on cell metabolism and PDH activity by the GS selection process, this plasmid was not ultimately used and the PEL1 hygromycin selection system was utilized in the studies described here.

3.4 Organisation of PDH Subunit Orientation and Order in the PEL1 Hygro 3 Cassette Vector

Each of the three individual PDH subunits could be inserted into a separate cassette in the PEL1 plasmid. In order to do this, the *E1alpha* gene was cloned into cassette 1, the *E1beta* gene in cassette 2, and *E2* gene into cassette 3. The locations, enzymes used for insertion and size of insert are described in Table 3.4.1 below.

Table 3.4.1 Restriction enzymes used for cloning of PDH subunits into different cassettes of the Hygro 3 Cass vector PEL1 and the insert size of each gene.

Cassette	PDH Subunit	Restriction enzymes	Insert size (bp)
1	E1alpha	AscI and PacI	1180
2	E1beta	AgeI and KpnI	1092
3	E2	XhoI and PmeI	1951

Constructs were created with different insert combinations to allow investigations as to whether a specific combination of subunit overexpression changed the observed cell phenotype compared to another. This would allow investigation as to whether the availability of one (or more) subunits might be restricting or if all three were required to be over-expressed to observe any phenotypic change. This resulted in the generation of the seven constructs shown in Table 3.4.2.

Table 3.4.2 The seven plasmids generated from PEL1 for overexpression of the different PDH subunits and combinations of these.

Plasmid No.	Cassette 1	Cassette 2	Cassette 3	Plasmid Size (bp)
PEL3 (E1α)	E1alpha	Empty	Empty	8631
PEL4 (E1β)	Empty	E1beta	Empty	8528
PEL5 (E2)	Empty	Empty	E2	9395
PEL6 (E1α, E1β)	E1alpha	E1beta	Empty	9689
PEL7 (E1α, E2)	E1alpha	Empty	E2	10,560
PEL8 (E1β, E2)	Empty	E1beta	E2	10,457
PEL9 (E1α, E1β, E2)	E1alpha	E1beta	E2	11,618

Although the design of PEL1 allows unique restriction sites to be used for each subunit, the presence of a XhoI restriction site in the sequence of the *E1alpha* subunit gene meant the *E2* subunit needed to be inserted into the backbone first before cloning any of the other subunits into the multiple cassette vectors.

3.5 PCR Amplification of PDH Subunit Genes

After the generation of cDNA from CHOS cells, primers were designed to allow for PCR amplification, digestion and then insertion of each gene into each of the appropriate vector cassettes of the PEL1 backbone. The methods used for the molecular cloning are detailed in the methods section 2.2.9 along with the primers used in Table 2.2.2, plasmid maps can be found in Appendix Table 1. Note that primers contained the required sequences for the restriction enzymes to ligate the PCR products into the PEL1 vector. Although the *E1alpha* and *E1beta* gene sequences were successfully amplified from the generated CHOS cDNA, issues surrounding the amplification of the *E2* subunit led to generating this by commercial synthesise by ThermoFisher GeneArt.

Once the genes were amplified with the addition of the correct restriction sites, the backbone PEL1 plasmid was digested accordingly, and the fragments ligated together. Minipreps were generated from transformed colonies of calcium competent *E.coli* DH5α cells grown on ampicillin containing LB agar plates. The plasmid DNA generated for each single cassette gene insertion, Plasmids PEL3 (E1α), 4 (E1β), and 5 (E2) were isolated and digested with the appropriate restriction enzymes to

release the gene insert and then analysed on 1% agarose gels as shown in Figures 3.5.1, 3.5.2 and 3.5.3 below.

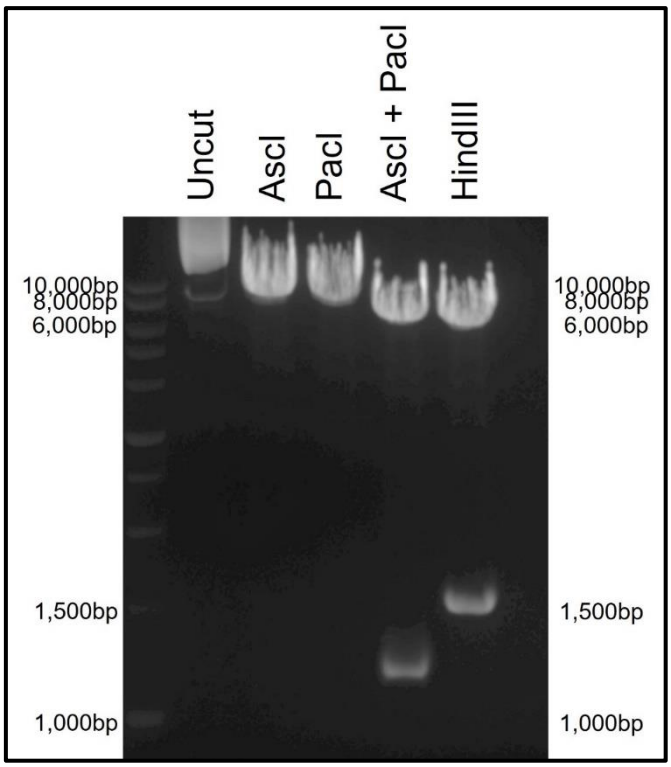

Figure 3.5.1 Restriction digest of PEL3 (E1α) Hygro 3 Cass backbone with the *E1alpha* PDH subunit in cassette 1. Lane 1, uncut plasmid. Lane 2, linearised plasmid cut with AscI only with band expected at 8631 bp. Lane 3, linearised plasmid cut with PacI showing expected band around 8631 bp. Lane 4, plasmid cut with both AscI and PacI with the *E1alpha* subunit drop out expected at 1180 bp and backbone at 7451 bp. Lane 5 shows the plasmid cut with HindIII which cuts within *E1alpha*, generating two expected bands at 7110 bp and 1521 bp.

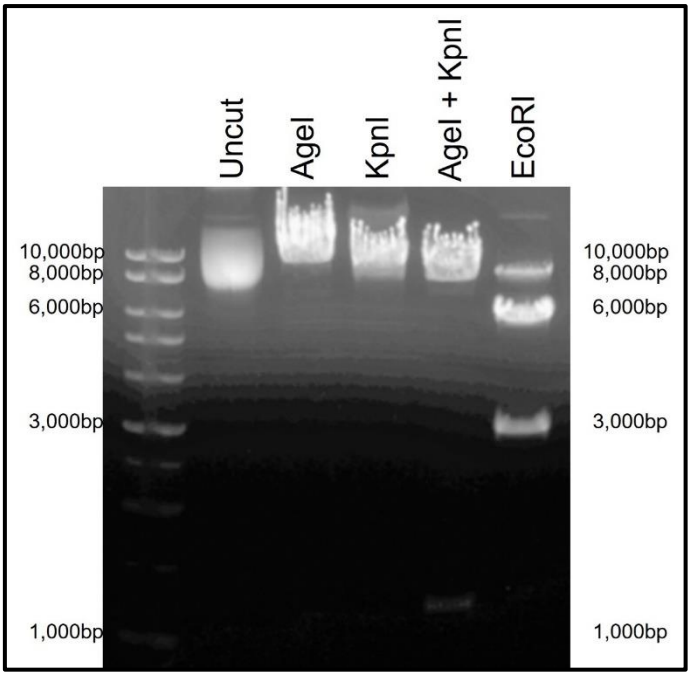

Figure 3.5.2 Restriction digest of PEL4 (E1β), Hygro 3 Cass backbone with the E1beta PDH subunit in cassette 2. Lane 1, uncut plasmid. Lane 2, linearised plasmid cut with AgeI with expected band at 8537 bp. Lane 3, linearised plasmid cut with KpnI with expected band at 8537 bp. Lane 4, plasmid cut with both AgeI and KpnI with the *E1beta* subunit drop out expected at 1099 bp and backbone at 7438 bp. Lane 5, plasmid cut with EcoRI which cuts within *E1beta*, generating two expected bands at 2860 bp and 5677 bp. A band was also observed at around 8537 bp which is linearised plasmid where only one cut has occurred.

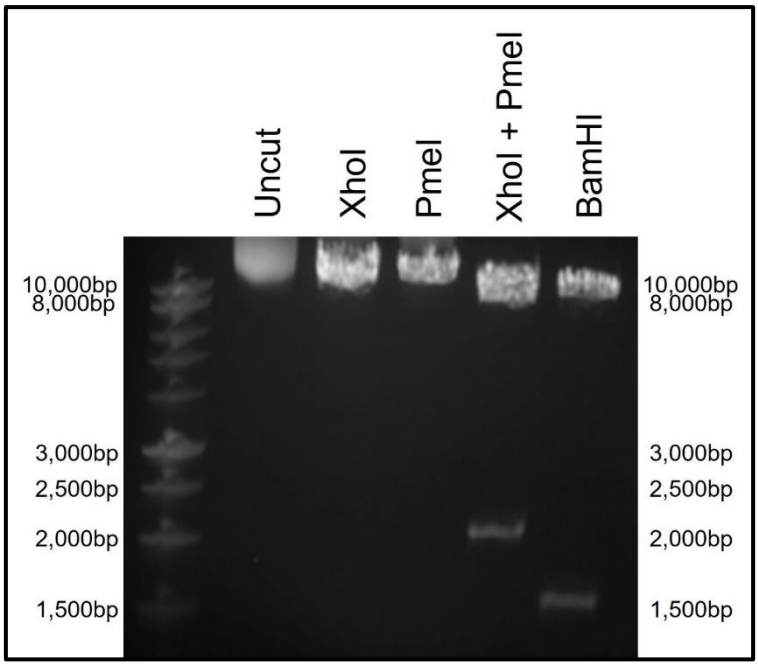

Figure 3.5.3 Restriction digest of PEL5 (E2), Hygro 3 Cass backbone with the *E2* PDH subunit in cassette 3. Lane 1, uncut plasmid. Lane 2, linearised plasmid cut with XhoI with expected band only at 9395 bp. Lane 3, linearised plasmid cut with PmeI with expected band at 9395 bp. Lane 4, plasmid cut with both XhoI and PmeI with the *E2* subunit drop out expected at 1950 bp and backbone at 7445 bp. Lane 5, the plasmid cut with BamHI which cuts within *E2*, generating two expected bands at 7990 bp and 1405 bp.

After screening for the presence of the required gene inserts by test restriction digests (Figures 3.5.1-3.5.3), the presence of the genes in the plasmids and their sequences were confirmed via commercial Sanger sequencing via GeneWiz.

Once the individual genes had been inserted into the backbone, the remaining subunits were added following the same process. Colony PCR screens and restriction digests were used to screen for the double and triple cassette vectors, PEL6-9, shown in the Figure 3.5.4 below. The presence of, and gene sequences, were once again also confirmed via commercial Sanger sequencing via GeneWiz.

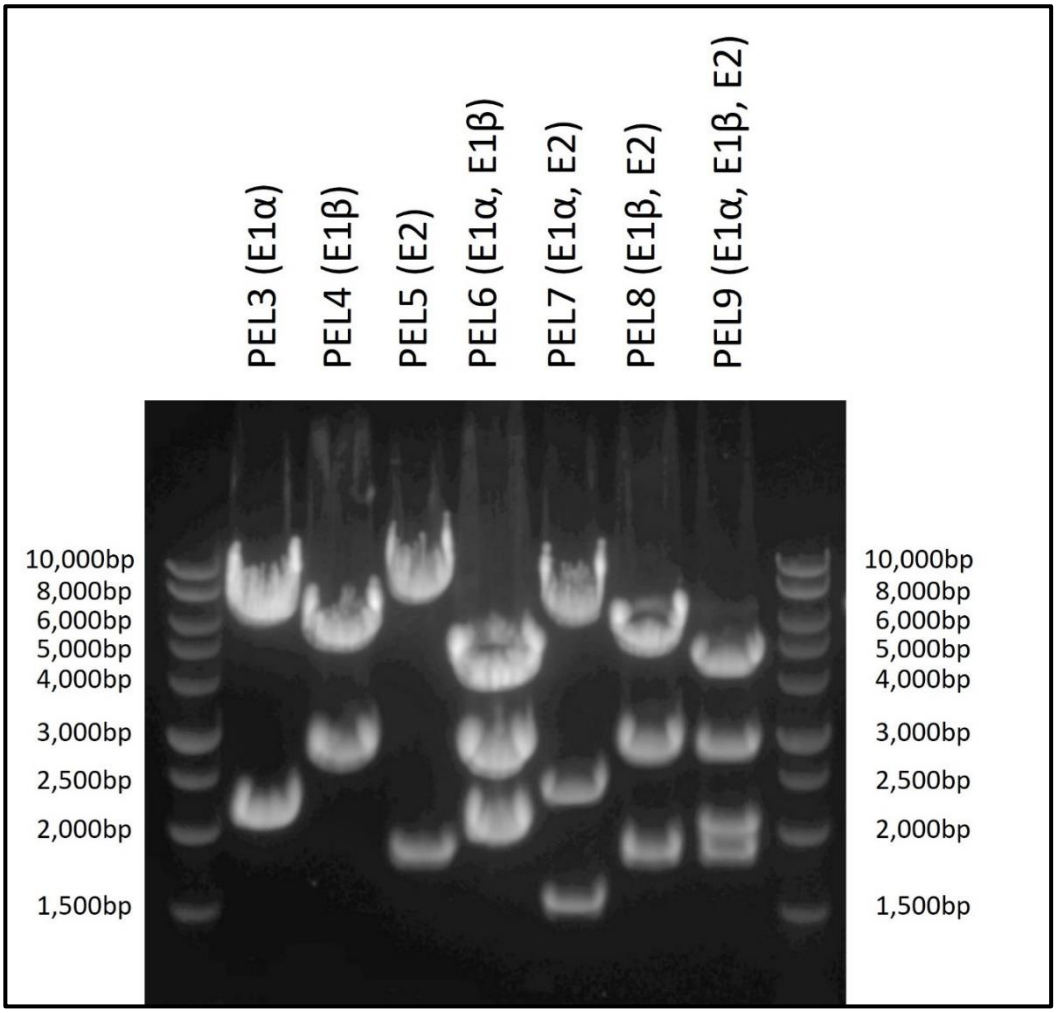

Figure 3.5.4 Restriction enzyme digest of all Hygro 3 Cass vectors with different combinations of PDH gene subunits in the three cassettes. Lane 1, PEL3 (E1α) digested with XhoI, expected bands at 8387 bp and 2173 bp. Lane 2, PEL4 (E1β) digested with EcoRI, bands expected at 5668 bp and 2860 bp. Lane 3, PEL5 (E2) digested with ApaI and PmeI, bands expected at 7543 bp and 1852 bp. Lane 4, PEL6 (E1α, E1β) digested with HindIII and EcoRI, bands expected at 2038 bp, 2860 bp and 4791 bp. Lane 5, PEL7 (E1α, E2) digested with HindIII, bands expected at 6649 bp, 1521 bp and 2390 bp. Lane 6, PEL8 (E1β, E2) digested with EcoRI and HindIII, bands expected at 1858 bp, 5668 bp and 2931 bp. Lane 7, PEL9 (E1α, E1β, E2) digested with HindIII and EcoRI, bands expected at 2038 bp, 2931 bp, 1858 bp and 4791 bp.

3.6 Evaluation of Transient Protein Expression of PDH Subunits in CHOS Cells from PDH Generated Plasmid Constructs

To confirm that the genes inserted into the PEL1 plasmid were expressed in CHOS cells, and determine whether the presence of additional cassettes, full or empty, had an impact on subsequent gene expression as determined by subunit protein expression, lipofectamine based transfections were carried out into CHOS cells. The Merck NovaCHOice® Transfection kit was used to transfect CHOS cells in 6 well plates. To optimise the system, the amount of DNA used per transfection was varied (1, 2 or 4 µg), alongside the seeding density of the cells at either $0.5x10^6$ or $1x10^6$ viable cells per well. Plasmids PEL3 (E1α), 6 (E1α, E1β) and 9 (E1α, E1β, E2) were used in initial experiments to investigate any differences that may occur during transfection due to the presence of multiple cassettes, containing 1, 2 and 3 full cassettes respectively. Control transfections were also completed, with the empty PEL1, a Hygromycin resistance containing eGFP plasmid, PEL10 (GFP), a DNA free transfection and CHOS cells that were not transfected. Cells were subsequently harvested 72 hours post-transfection to enable protein analysis via Bradford assays, western blot and Coomassie staining of SDS-PAGE gels. The methods used for protein analysis are detailed in the materials and methods section 2.4.

Figures 7.1.1, 7.1.2 and 7.1.3 in the Appendix show the resulting western blots where 20 µg of total protein cell lysate was loaded for each sample. Also loaded was a HEK293 cell lysate sample in the centre of all 6 SDS-PAGE gels. These western blots were the first to be probed with the Abcam PDH Antibody cocktail (ab110416) antibody. High sequence similarity between human and CHO PDH complex suggested reactivity but the HEK293 cell lysate sample acted to confirm this on the western blots.

A β-actin housekeeping protein control blot was also performed and is shown in Figure 7.1.2 in the Appendix. This revealed some uneven loading across the samples which was reflected in the varying levels of PDH expression observed in Figure 7.1.1. An anti-eGFP antibody western blot, Figure 7.1.3, confirmed the success of the transfections, showing protein bands for the eGFP samples, PEL10 (GFP) only at the expected size.

Figures 7.1.1, 7.1.2 and 7.1.3 combine with Figure 7.1.4, also in the Appendix, which shows the percentage viabilities after transfection, to summarise the successful expression of transfected PDH subunit containing plasmids in CHOS cells as well as the detection of protein using the Abcam PDH Antibody cocktail (ab110416) antibody. The western blot data however does not suggest that protein levels of the PDH subunits were increased as a result of the transfections with no obvious visual difference in band intensity observed in comparison to the control PEL1, PEL10 (GFP) and no

DNA transfection of CHOS cells suggesting the generation of stable cell lines may be more successful when aiming to increase PDH subunit protein expression.

3.7 Generation and Evaluation of CHOS and CHOK1 Cell Pools Stably Overexpressing the PDH Subunits

In order to establish that exogenous over-expression of the PDH subunits in CHOS cells, stably expressing CHOS cell pools were made whereby the gene is integrated into the genome and thus should be expressed in all cells constitutively. This contrasts expression resulting from a transient transfection whereby the plasmid DNA is not integrated into cellular genome and is lost as cells divide. First, each plasmid was linearised by an overnight digest with FspI, which cuts in the ampicillin gene, to facilitate integration of the DNA into the cell genome. An agarose gel was run on the digested material to confirm successful linearisation and is shown in Figure 3.7.1.

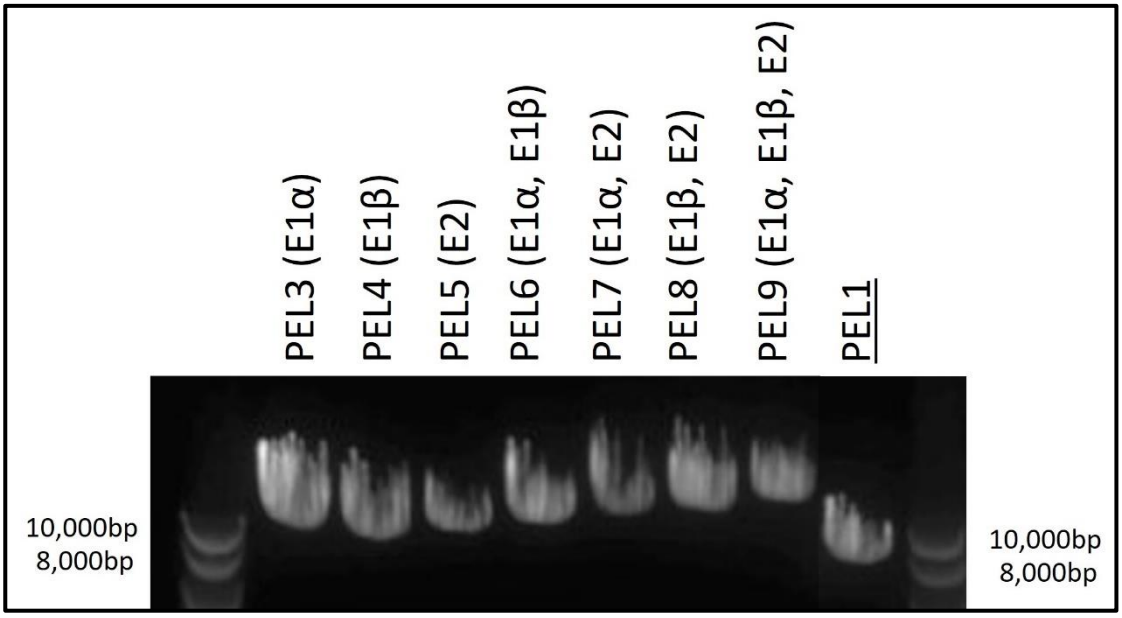

Figure 3.7.1 Overnight linearisation of plasmids PEL1, PEL3-PEL9 using FspI enzyme in preparation for the generation of PDH subunit stably expressing CHOS and CHOK1 cell lines. Expected sizes of linearisation plasmids; PEL3 (E1α) 8631 bp, PEL4 (E1β) 8528 bp, PEL5 (E2) 9395 bp, PEL6 (E1α, E1β) 9689 bp, PEL7 (E1α, E2) 10560 bp, PEL8 (E1β, E2) 10457 bp, PEL9 (E1α, E1β, E2) 11618 bp, PEL1 7466 bp.

Electroporation was used to transfect CHO cells, with one transfection split into two flasks to make technical repeats and increase the likelihood of generating a stably expressing cell pool. 24 hours post-transfection, Hygromycin B was added to a final concentration of 750 µg/ml and the cells left to recover in a 37°C static incubator. A DNA free control was also transfected to ensure the plasmid

had been successfully delivered and that the selection 'killed' all cells not expressing the plasmid and resistance marker. 2-3 weeks later, the cultures were cell counted to ensure recovery had occurred and that the no DNA control cells had died. Some repeats did not successfully recover and therefore were omitted from future work. At least one cell pool for each plasmid transfection survived and was carried forward. The cells were moved from static culture into shaking 125 ml Erlenmeyer flasks and passaged with alternating CD-CHO media containing 750 µg/ml Hygromycin B and CD-CHO without selection, both with the addition of 8 mM L-glutamine. Protein lysate samples were then generated from the resulting cell pools and analysed by western blot as described in section 2.4.5. Figure 3.7.2 shows the resulting western blot using the PDH Antibody cocktail- Abcam (ab110416) with a HEK293 cell lysate sample loaded as a control.

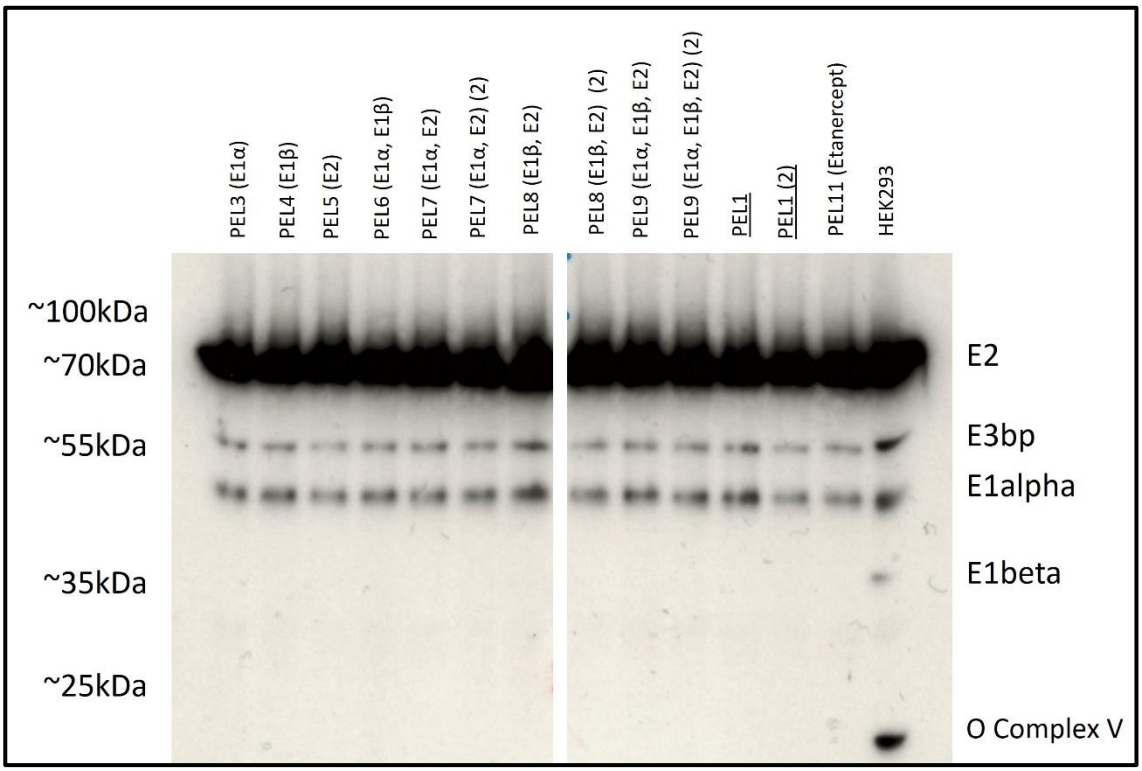

Figure 3.7.2 Western blot analysis of CHOS cells transfected with PDH subunit containing plasmids PEL3-9 and empty control plasmid PEL1, subjected to hygromycin selection to isolate stably overexpressing PDH cell pools. 10 µg total protein cell lysate loaded, and samples exposed for 5 mins. Antibody cocktail made of 5 monoclonal antibodies, multiple bands for the different subunits of the PDH enzyme complex are observed. E2 band expected at 69 kDa, E3bp band expected at 54 kDa, E1alpha band expected at 43.3 kDa, and E1beta band expected at 39.4 kDa. A band for the control Complex V antibody, 22 kDa, is seen in the HEK cell lysate sample.

The western analysis in Figure 3.7.2 suggests more-or-less even expression levels of all PDH subunits compared to the controls for all cell pools transfected with the different plasmids. This suggest little

or no expression of the recombinant, exogenous subunits or that the cell responds to ensure a 'constant' amount of the subunits and is in line with the Figure 3.5 transient transfection data. A β-actin housekeeping protein control blot was also run and is shown in Figure 3.7.3. The β-actin western blots in Figure 3.7.3, even though saturated, show similar loading of protein, further confirming that PDH subunit expression did not appear to have changed in the stable pools.

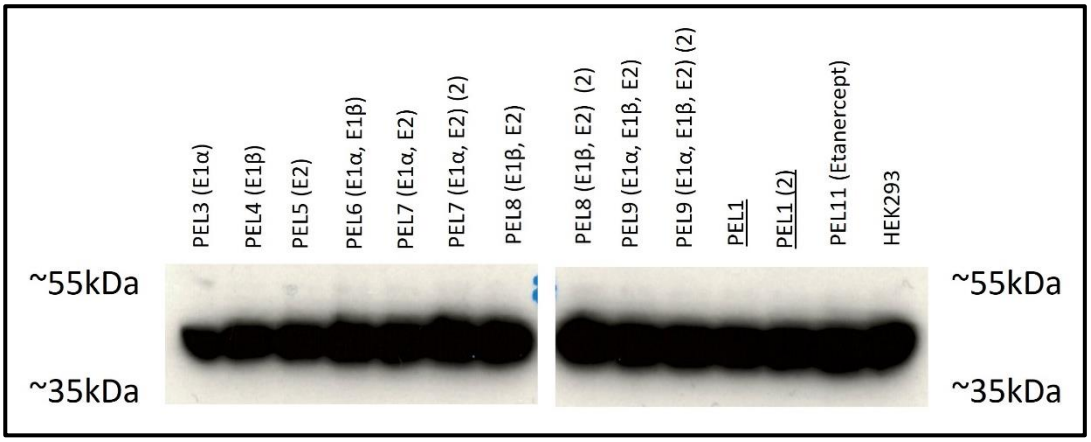

Figure 3.7.3 Western blot analysis of β-actin expression in CHOS cells transfected with PDH subunit containing plasmids PEL3-9 and empty control plasmid PEL1, subjected to hygromycin selection to isolate stably overexpressing PDH cell pools. 10 µg total protein cell lysate samples loaded and exposed for 1 min to reveal β-actin at 37 kDa.

In conclusion, the CHOS stable cell pools selected for the stable integration of the different PDH subunit genes showed no clear changes in cell phenotype or PDH subunit protein expression. Both cell growth and culture viability also remained comparable to control cell lines expressing PEL1 and un-transfected/non-engineered CHOS cells.

Stable cell pools were also created using CHOK1 host cells using plasmids PEL1 and PEL3-5. Again, no clear impact on PDH expression or cell phenotype was observed in the resulting CHOS cell pools from plasmids PEL6-9, so only the individual cassette vectors were carried forward at this stage. Figure 3.7.4 shows the western blot analysis of PDH subunit expression in the CHOK1 stable cell pools.

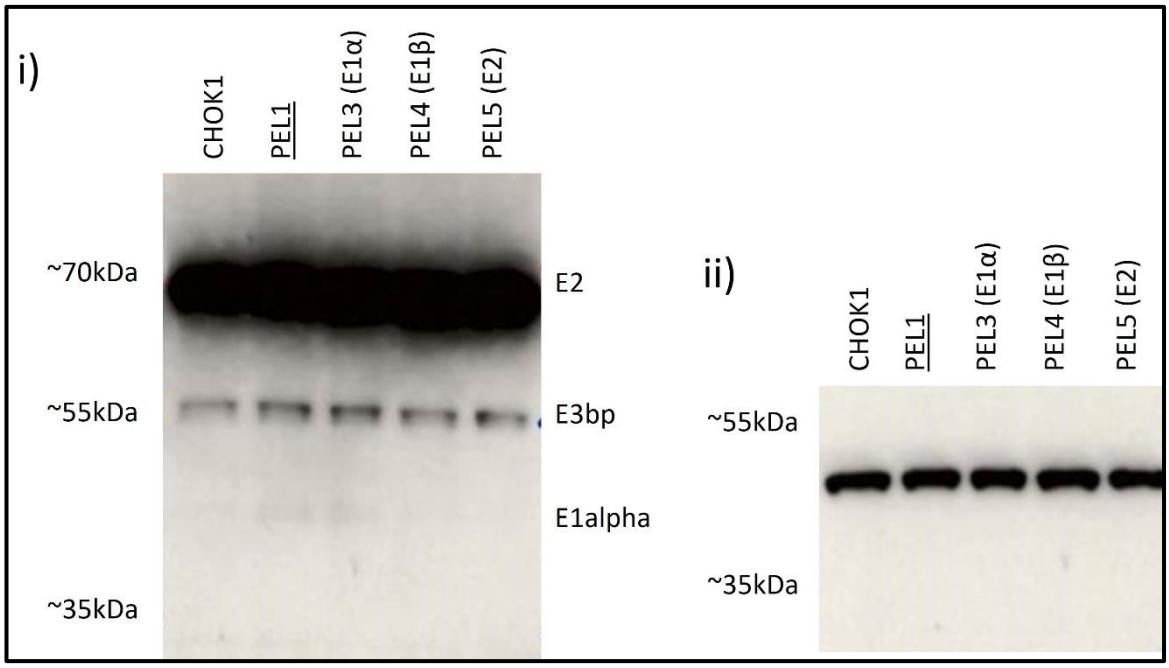

Figure 3.7.4 Western blot analysis of CHOK1 cells engineered to stably overexpress PDH enzyme subunits via the expression of plasmids PEL3-5 alongside the empty control PEL1 plasmid. 5 µg of total protein cell lysate loaded. i) Samples exposed for 5 mins. Antibody cocktail made of 5 monoclonal antibodies, multiple bands for the different subunits of the PDH enzyme complex are observed. E2 band expected at 69 kDa, E3bp band expected at 54 kDa, E1alpha band expected at 43.3 kDa and E1beta band expected at 39.4 kDa. ii) β-actin expression after exposure for 10 secs to reveal β-actin at 37 kDa.

The western blots shown in Figure 3.7.4 show more-or-less even expression for the different PDH subunits across all samples, even with the selection for integration of the exogenous plasmid DNA in CHOK1 cells. A longer exposure was used in Figure 3.7.4 i) however, unlike in the CHOS western blots in Figure 3.7.2, expression is only seen of PDH subunits E2 and E3bp. This is likely to reflect the higher protein concentration loaded for the CHOS lysate samples in Figure 3.7.2 which has double the protein concentration compared to Figure 3.7.4 and not correlate to differences between the two cell lines. Even expression of all PDH subunits is seen regardless of the stable expression of PDH subunit containing plasmids. Therefore, to confirm if it was possible to express exogenous copies of the subunits of the PDH enzyme complex in CHO cells, a tag was added to the genes of interest with a different tag for each subunit. This was done both N- and C-terminally to allow investigations as to whether the presence of the tag at one end or the other impacted recombinant subunit expression or overall PDH complex formation by endogenous subunits.

3.8 Assembly of the Hygromycin 3 Cassette Tag vector with Antigen Tags in Frame with Target Gene Open Reading Frames

The Hygromycin 3 Cassette Tag vector, PEL12, was designed to enable the N or C terminal tagging of genes of interest depending on the restriction sites used. Additional amino acids and multiple restriction enzyme sites enabled the selection of specific sites for each gene of interest and for each tag location. Cassette 1 was modified to contain a V5 Tag, cassette 2 to contain three copies of the HA Tag and cassette 3 to contain a FLAG Tag. Figure 3.8.1 shows the plasmid map with the N- and C-terminal restriction sites used to enable tagging of the PDH subunits which are also detailed in Table 3.8.1 below.

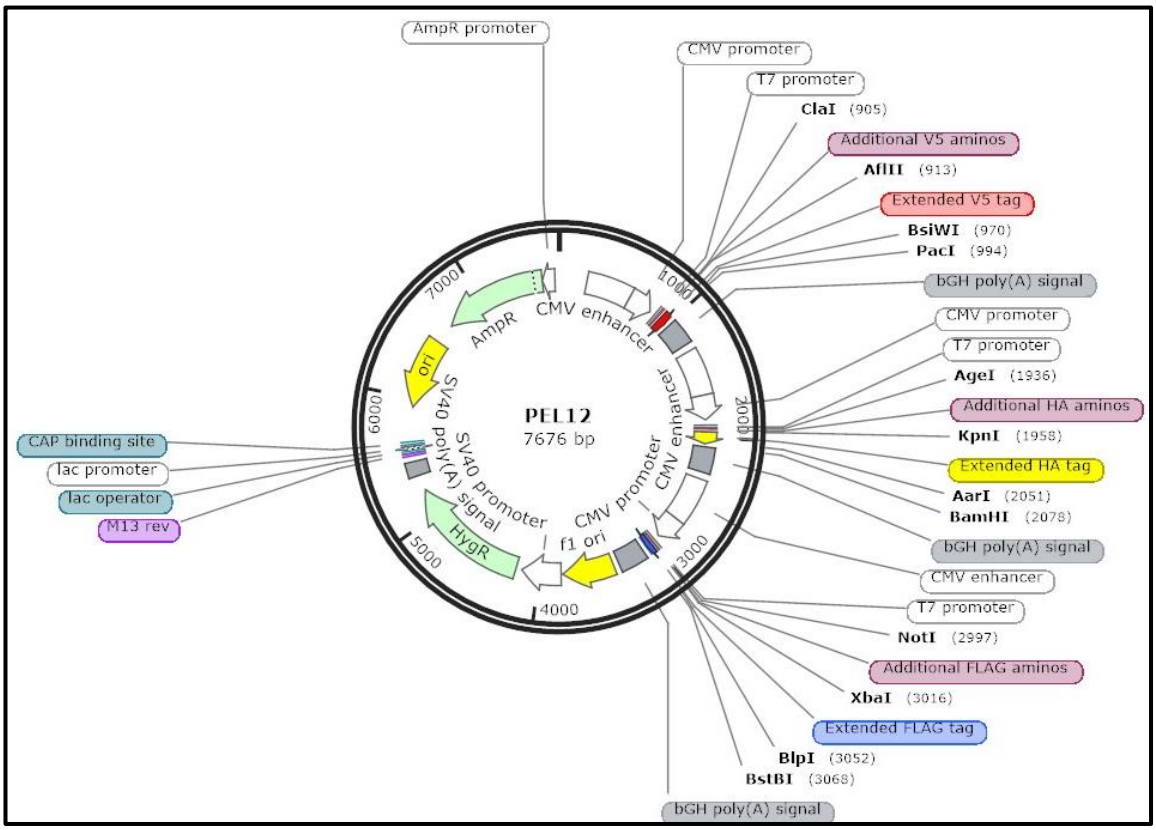

Figure 3.8.1 A schematic of the Hygro 3 Cass Tag vector PEL12 showing the unique enzymes enabling the N- or C-terminal tagging of the PDH enzyme complex genes of interest. It should be noted that it was necessary to remove stop codons from the end of the target genes of interest so that the open reading frame included the tag in frame.

Table 3.8.1 Restriction enzymes used on the end of primers for PCR amplification, and subsequent digestion and ligation of PDH subunits into PEL12 in the specific cassette locations.

Plasmid no.	Cassette	Tag	Tag position	PDH Subunit	Restriction enzymes
PEL13 (E1αNV5)	1	V5	N	E1alpha	AflII and PacI
PEL14 (E1βNHA)	2	HA	N	E1beta	AarI and BamHI
PEL15 (E2NFLAG)	3	FLAG	N	E2	BlpI and BstBI
PEL16 (E1αCV5)	1	V5	C	E1alpha	ClaI and AflII
PEL17 (E1βCHA)	2	HA	C	E1beta	AgeI and KpnI
PEL18 (E2CFLAG)	3	FLAG	C	E2	NotI and XbaI

Primers were designed to allow for PCR amplification of the genes of interest with the appropriate restriction sites on the 5' and 3' ends, the PCR products digested and then ligated into each of the appropriate vector cassettes of the Hygro 3 Cass Tags, PEL12, backbone. The methods used for the molecular cloning are detailed in section 2.2 along with the primers used in Table 2.2.2, plasmid maps can be found in Appendix Table 1.

Although several target sequences were successfully amplified from the previously generated plasmids using PCR, issues in the amplification of the *E1alpha* inserts for PEL13 (E1αNV5) and PEL16 (E1αCV5) led to the ordering of the genes for these targets. PEL13 (E1αNV5) was ordered as a string from ThermoFisherGeneArt whilst PEL16 (E1αCV5) was ordered from Twist Bioscience.

The N-terminally tagged constructs were made first with the C-terminally tagged made shortly after. Due to the small size of the 3 tags (V5 84 bp, 3 copies of the HA Tag 123 bp, and FLAG 60 bp), confirming the addition of the tag by analysis on a DNA agarose gel would not be suitable because of the small size increase and presence of restriction sites in the backbone. Therefore, the presence of the required sequences in clones were confirmed using commercial Sanger sequencing.

3.9 Investigating Transient Expression of the PDH Subunits with N-Terminal Tags

The N terminally tagged plasmids, PEL13 (E1αNV5), 14 (E1βNHA) and 15 (E2NFLAG) were initially cloned and so were transiently expressed in CHOS and CHOK1 host cell lines to confirm if the tagged PDH subunits could be expressed before stably expressing cell pools were made.

For transient expression, electroporation was used to transfect cells with 40 µg of each plasmid DNA following the process detailed in section 2.3.5. One 20 ml transfection was split across two 10 ml

falcon tubes and left to grow for three days at which time cell lysate samples were taken for protein analysis by western blot. Viable cell concentrations were also determined to ensure transfection and expression of the recombinant DNA had no detrimental impact on cell growth or culture viability. Figure 7.1.5 in the Appendix reports the percentage culture viability of the transfected cell cultures three days after transient transfection with most cultures remaining above 80% viability. Figure 7.1.6 in the Appendix shows the resulting western blot analysis after 5 µg of total protein cell lysate was loaded and probed using the relevant tag antibodies. Bands were only seen for the PEL14 (E1βNHA) expressing cells, other cells not shown, as well as some anti-HA antibody cross reactivity where higher molecular weight bands were also present in the control samples.

The data confirmed that the E1beta subunit could be exogenously expressed and that the presence of the HA tag on the E1beta PDH subunit in PEL14 at least did not seem to negatively impact cell growth or culture viability. From these results it was therefore decided to move forward with the production of stably expressing tagged cell pools using PEL12 to PEL18. This would involve developing stable cell pools with both the N- and C-terminally tagged PDH subunits with the aim of developing stably expressing PDH subunit cell pools where the exogenously expressed material was clearly visible and distinct from the endogenous (untagged) material.

3.10 Generation of Stably Expressing N- and C-Tagged PDH Subunit CHO Cell Pools

Due to the successful recovery of both CHOS and CHOK1 stable cell pools after transfection with different plasmid constructs previously, the same hygromycin selection process was used again to generate stable pools using the PDH tagged constructs. Figure 3.10.1 shows the agarose gel after plasmids PEL12 and PEL13 to 18 (that contained the tagged genes) were linearized overnight with FspI enzyme ready for transfection.

The linearised plasmids were then used in electroporation transfections to create stably expressing CHOS and CHOK1 cell pools, following the same process as for the untagged constructs PEL3-9 described previously in methods section 2.3.7.

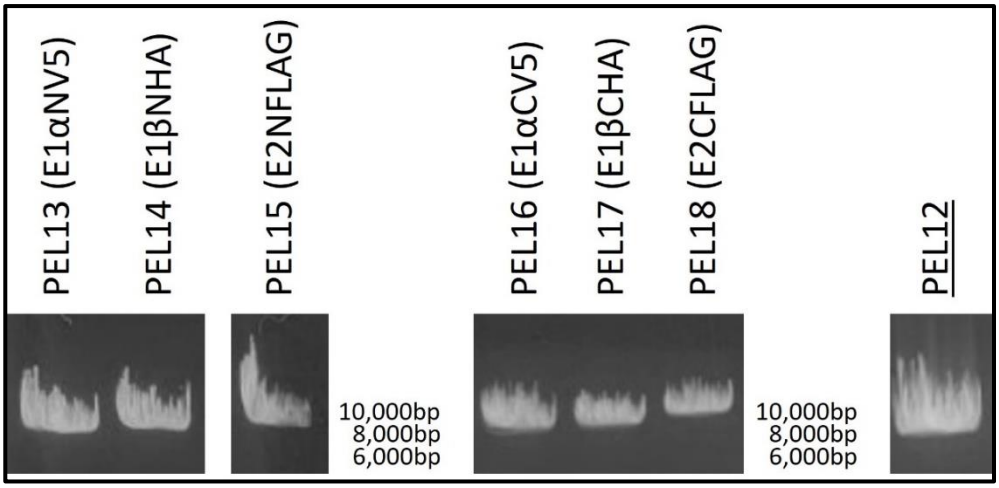

Figure 3.10.1 Agarose gel analysis after the linearisation of 50 µg plasmid DNA after an overnight digest with FspI enzyme in preparation for the generation of stably expressing CHOS and CHOK1 cell pools expressing the different N- or C-terminally tagged PDH subunits. PEL13 (E1αNV5) expected band 8819 bp, PEL14 (E1βNHA) expected band 8710 bp, PEL15 (E2NFLAG) expected band 9608 bp, PEL16 (E1αCV5) expected band 8843 bp, PEL17 (E1βCHA) expected band 8741 bp, PEL18 (E2CFLAG) expected band 9602 bp, and PEL12 expected band 7676 bp.

3.11 Evaluation of Recombinant Tagged PDH Subunit Expression in Stable CHO Cell Pools

After recovery from transfection, and Hygromycin B selection, cell pools engineered to stably express the N- and C-terminally tagged PDH E1alpha, E1beta and E2 subunits had protein lysate samples taken for protein analysis via western blotting. Cells were also banked down using cryopreservation. Western blot success varied depending on the tags and cell pools, with some revealing the presence of the expected bands, depending on the amount of protein loaded and exposure times. Figures 7.1.7, 7.1.8 and 7.1.9 in the Appendix show initial western blots confirming the presence/expression of the different PDH tagged proteins in some of the tagged cell pools. Mixed success is seen when identifying cell pools stably expressing the tagged subunits of interest as revealed by western blot for the specific tag on each subunit. There was evidence of expression of the C-terminally tagged subunits in each case with clear bands of the expected size indicating the presence of the tagged protein compared to the N-terminally tagged protein subunits. This suggests that N-terminal labelling is detrimental to the recombinant/exogenous expression of all three subunits.

Western analysis was repeated with these samples for all PDH endogenous subunits and β-actin to determine if expression of the exogenous tagged PDH subunits impacted total PDH expression, or whether endogenous protein levels were reduced as a result of the overexpression. Figures

3.11.1.1, 3.11.2.1 and 3.11.3.1 show the western blots comparing expression levels after stable integration of the different PDH genes into CHO cells.

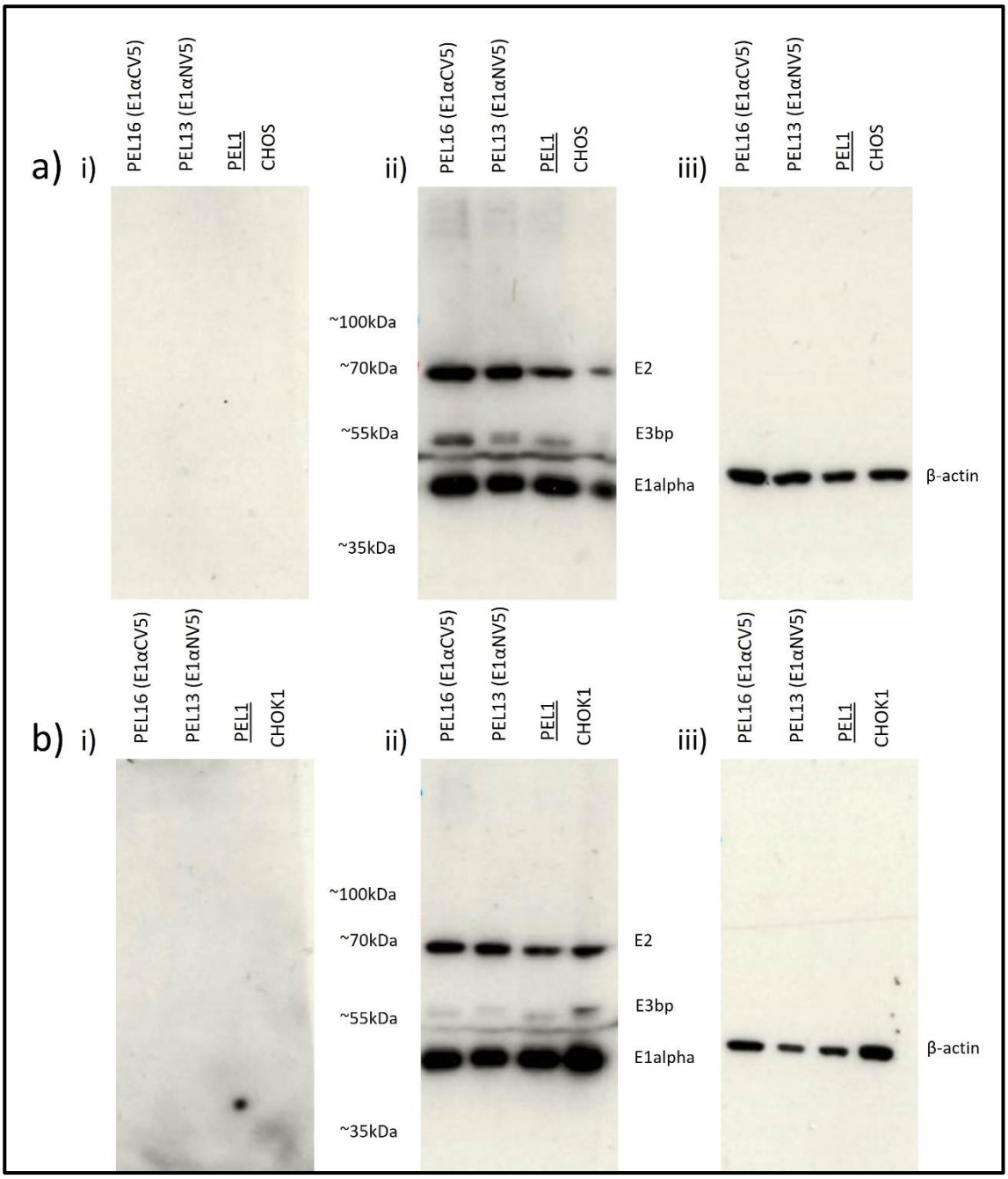

Figure 3.11.1.1 Analysis of CHOS and CHOK1 cell pools engineered to stably express E1alpha N V5- (PEL13) and C- (PEL16) terminally tagged protein. 10% SDS-PAGE run with 8 µg protein sample. a) CHOS cell lysates. b) CHOK1 cell lysates. i) Samples exposed to anti-V5 antibody for 1 hour, tagged band for cells expressing E1alpha expected at 44.3 kDa. ii) Samples exposed to anti-PDH antibody cocktail for 1 hour. Multiple bands for the different subunits of the PDH enzyme complex are seen. E2 at 69 kDa, E3bp at 54 kDa, E1alpha at 43.3 kDa and E1beta at 39.4 kDa. iii) Samples exposed to anti-β-actin antibody for 1 min to show β-actin as a loading control at 37 kDa.

Figure 3.11.1.1 shows western analysis of expression of the V5 tagged PDH E1alpha subunit, PDH subunits and β-actin in the CHOS (a) and CHOK1 (b) cells engineered to stably express the PDH subunit E1alpha N V5 (PEL13) and E1alpha C V5 (PEL16), alongside the control host cell lines. None of the CHOS or CHOK1 samples showed the presence of the V5 tagged recombinant E1alpha PDH subunits when probed with the anti-V5 antibody i). The PDH blots in ii) contained an additional band across the blot not previously seen on blots using the anti-PDH antibody cocktail, such as Figures 3.7.2 and 3.7.4. It is also seen in ii) of Figures 3.11.2.1 and 3.11.3.1 across all samples suggesting it is not of significance to protein expression. Expression of the E1beta subunit was not seen in any samples so any subunit specific impact could not be determined. Figure 3.11.1.2 shows the densitometry analysis using Image J software of the PDH and beta-actin blots shown in Figure 3.11.1.1 (ii) and (iii) for both CHOS (a) and CHOK1 (b) cell lines.

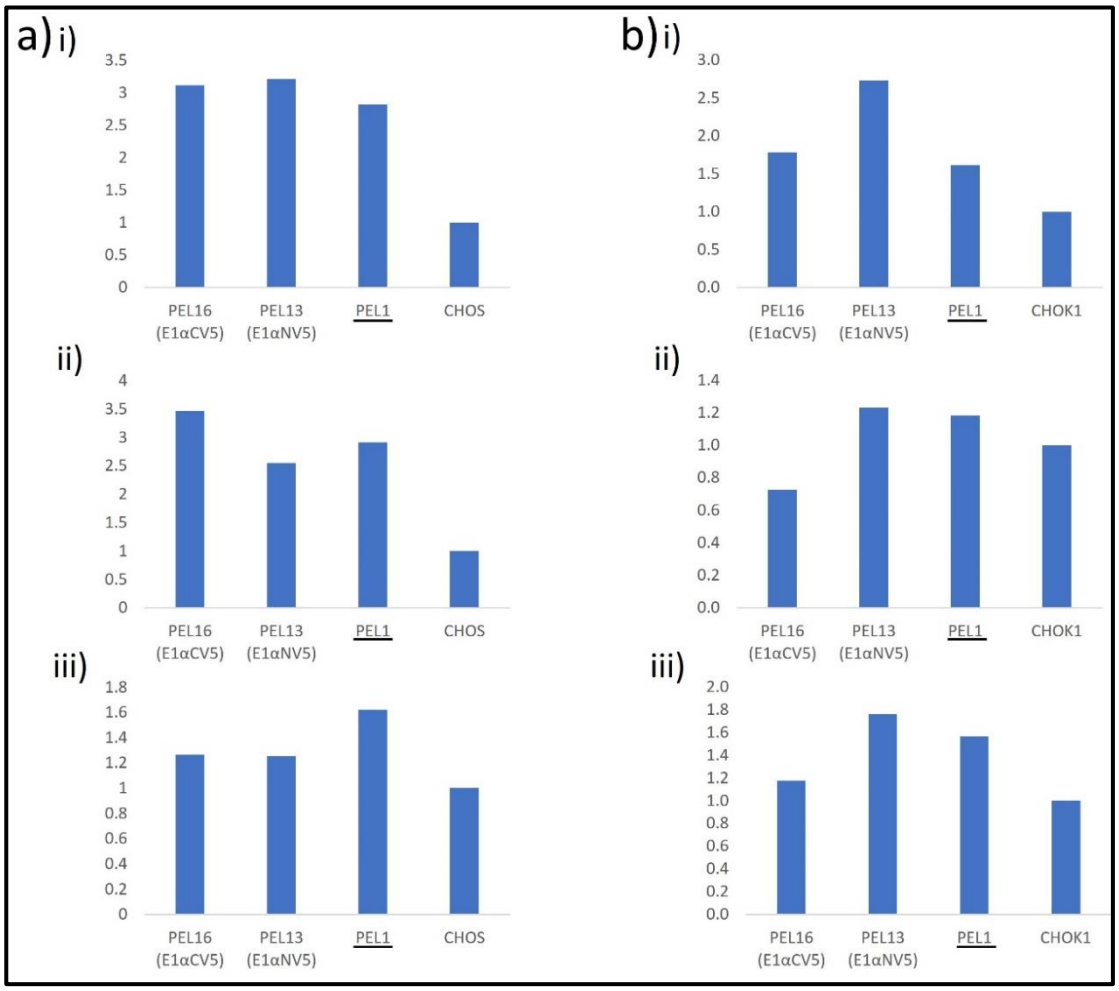

Figure 3.11.1.2 Densitometry of western blot signals showing the relative expression of E2 (i), E3bp (ii) and E1alpha (iii) subunits in CHOS (a) and CHOK1 (b) cell pools engineered to stably express E1alpha N V5- (PEL13) and C- (PEL16) terminally tagged protein compared to control host cell lines and β-actin expression. Analysis of bands presented in Figure 3.11.1.1 from PDH (ii) and β-actin (iii) blots is shown.

The CHOS PDH blots in Figure 3.11.1.1 (ii) showed increased expression of E2 and E3bp PDH subunits in E1alpha N V5 (PEL13) and E1alpha C V5 (PEL16) stably expressing cell pools when compared to the control CHOS cells. However, this was also observed in pools expressing control PEL1 and is seen in the relative expression data in Figure 3.11.1.2. The E1alpha PDH subunit, the target gene in PEL13 and PEL16, showed equal expression throughout samples (Figure 3.11.1.1). Relative expression analysis suggests a small increase in expression of E1alpha however this is a smaller increase when compared to control empty cassette vector PEL1 cells. When looking at the β-actin expression in iii), the loading was even between all samples suggesting a small over expression of these subunits in the tagged stable cell lines. This is confirmed by the relative expression comparison reported in Figure 3.11.1.2.

The CHOK1 PDH blots in Figure 3.11.1.1 (bii) show a small increase in expression of the E2 PDH subunit in E1alpha N V5 (PEL13) and E1alpha C V5 (PEL16) expressing cell pools when compared to the PEL1 and CHOK1 control cell lines but lower expression of the E3bp and E1alpha PDH subunits. When looking at the relative expression graphs in Figure 3.11.1.2, E1alpha C V5 (PEL16) expressing cells show increased E2 and E1alpha subunit expression but lower E3bp expression. E1alpha N V5 (PEL13) expressing cells show increased expression of all PDH subunits when compared to both control cell lines. However, this is also seen in the control cells expressing the empty cassette vector PEL1. The β-actin loading control blot in iii) shows an increase in expression for the PEL16 E1alpha C-terminally tagged expressing cell line compared to the others but even higher expression for the CHOK1 control cell line. This suggests the higher protein concentration of the CHOK1 control sample has led to the more intense band seen in the PDH blot ii) and that expression of the PDH subunits is relatively even for all cell pools, including those expressing E1alpha N V5 and C. Based on the β-actin expression, relative expression analysis in Figure 3.11.1.2 shows the CHOK1 control cell line to have lower overall expression of all PDH subunits compared to the other cell pools.

Overall, the CHOS cell pools stably expressing E1alpha N V5 (PEL13) and E1alpha C V5 (PEL16) show a small increase in expression of the PDH subunits, but this is not observed in the CHOK1 stable cell lines, with only cells expressing E1alpha N V5 (PEL13) showing an increase in expression of all subunits. This, however, was also seen in control cells expressing the empty cassette vector PEL1. There was no clear difference in PDH subunit expression observed between the N- and C-terminal tags of E1alpha in PEL13 and 16 respectively. Neither CHOS or CHOK1 samples showed expression of the V5 Tag attached to the recombinant E1alpha protein in PEL13 and 16 in Figure 3.11.1.1 (i). The resulting impacts to PDH subunit expression are summarised in Table 3.11.1.

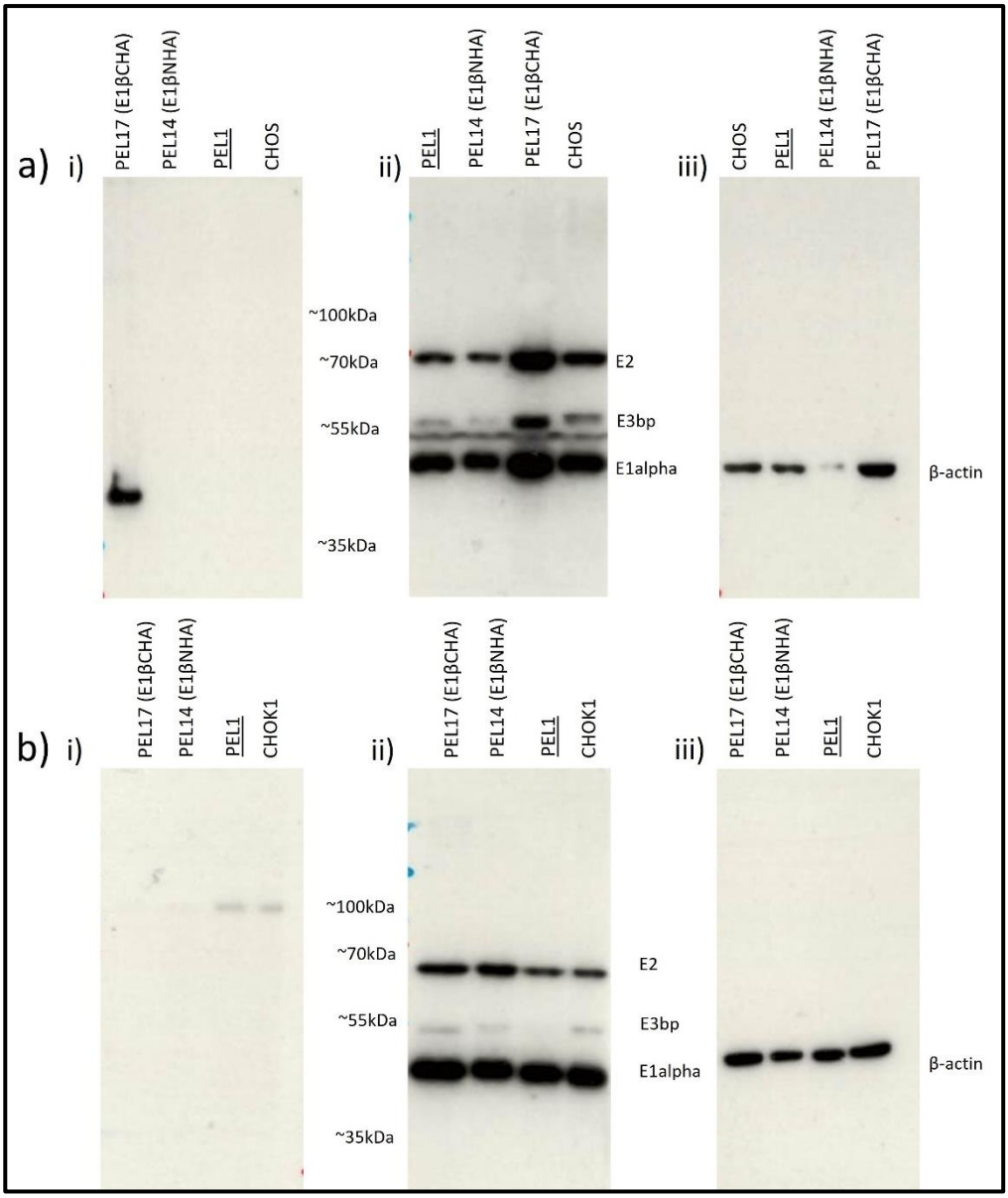

Figure 3.11.2.1 Analysis of CHOS and CHOK1 cell pools engineered to stably express E1beta N HA- (PEL14) and C- (PEL17) terminally tagged protein. 10% SDS-PAGE run with 8 µg protein sample. A) CHOS cell lysates. B) CHOK1 cell lysates. I) Samples exposed to anti-HA antibody for 1 hour, tagged band for cells expressing E1beta expected at 42.4 kDa. ii) Samples exposed to anti-PDH antibody cocktail for 1 hour. Multiple bands for the different subunits of the PDH enzyme complex are seen. E2 at 69 kDa, E3bp at 54 kDa, E1alpha at 43.3 kDa and E1beta at 39.4 kDa. iii) Samples exposed to anti-β-actin antibody for 1 min to show β-actin as a loading control at 37 kDa.

Figure 3.11.2.1 shows western blot analysis of expression of the HA tagged PDH E1beta subunit, PDH subunits and β-actin in the CHOS (a) and CHOK1 (b) cells engineered to stably express the PDH subunit E1beta N HA (PEL14) and E1beta C HA (PEL17), alongside the control host cell lines. The anti-HA tag antibody blots (i) show expression of the HA tag in CHOS cells stably expressing E1beta C HA (PEL17) only. This is similar to Appendix Figure 7.1.8, although previously both N and C

terminally tagged E1beta CHOS and CHOK1 samples showed expression of the HA Tag. The PDH blots in ii) show an additional band across the blot also observed in Figures 3.11.1.1 and 3.11.3.1. This is seen clearly in the CHOS (a) but not in the CHOK1 (b) blots. Expression of the E1beta subunit was not observed for any samples or in Figures 3.11.1.1 and 3.11.3.1. This is made clearer when aligned with the CHOS (a) anti-HA tag blot in (i) where the HA Tagged E1beta subunit was clearly seen for cells expressing E1beta C HA (PEL17). Figure 3.11.2.2 shows the densitometry analysis using Image J software of the PDH and Beta-actin blots shown in Figure 3.11.2.1 (ii) and (iii) for both CHOS (a) and CHOK1 (b) cell lines.

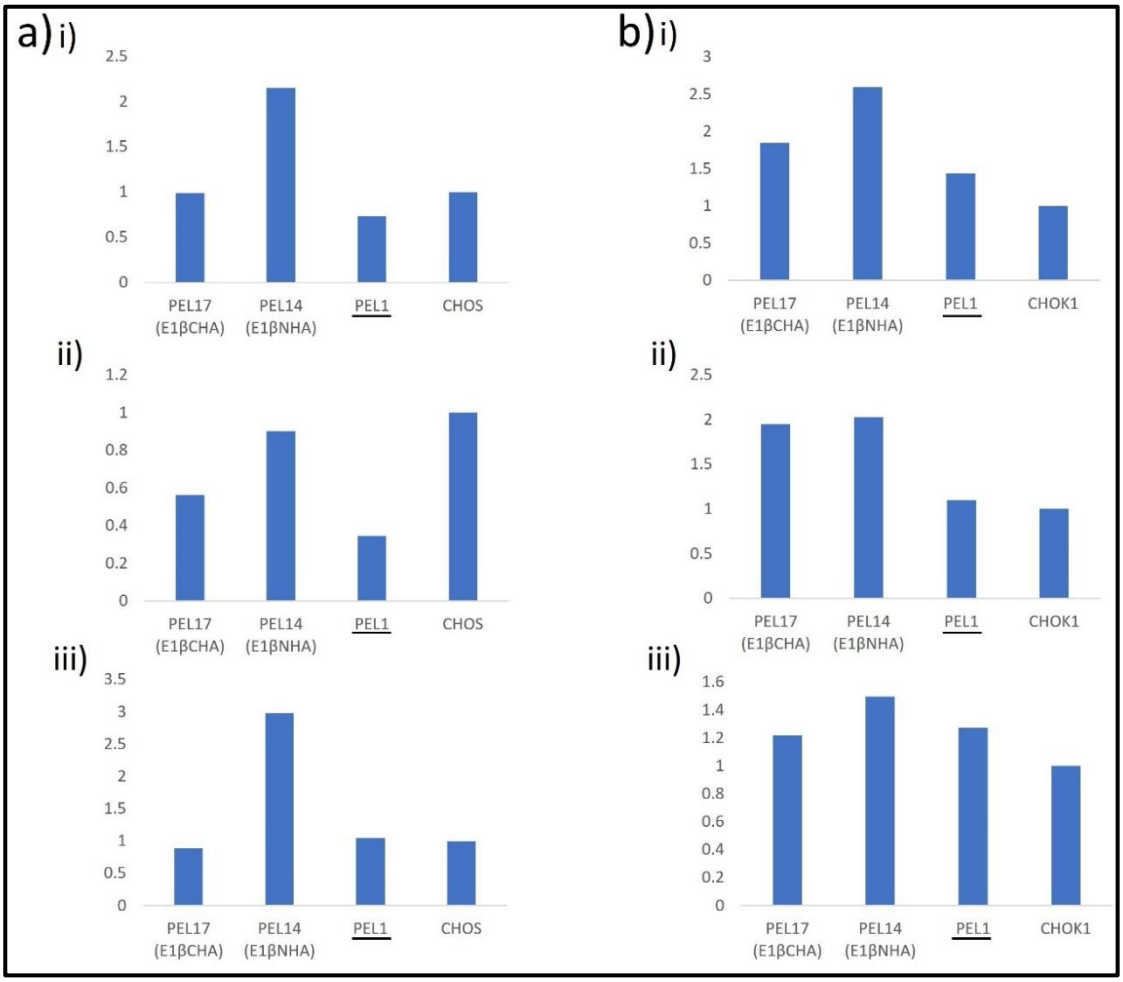

Figure 3.11.2.2 Densitometry of western blot signals showing the relative expression of E2 (i), E3bp (ii) and E1alpha (iii) subunits in CHOS (a) and CHOK1 (b) cell pools engineered to stably express E1beta N HA- (PEL14) and C- (PEL17) terminally tagged protein compared to control host cell lines and β-actin expression. Analysis of bands presented in Figure 3.11.2.1 from PDH (ii) and β-actin (iii) blots is shown.

The CHOS cells expressing E1beta C HA (PEL17) showed intense bands for all PDH subunits in Figure 3.11.2.1 (a) (ii) however also more intense β-actin (iii) suggesting this is the result of a higher protein

concentration having been loaded for this sample and not the impact of recombinant protein expression. The relative expression in Figure 3.11.2.2 also supports this as the expression of all subunits is as equal to and lower for the E3bp subunit when compared to the control cell lines. Cells stably expressing E1beta N HA (PEL14) had more evenly matched expression levels for the PDH subunits and a less intense β-actin band in Figure 3.11.2.1 (ii) and (iii.) The relative expression in Figure 3.11.2.2 supports this, showing higher expression levels for E2 and E1alpha PDH subunits and slightly reduced E3bp subunit expression when compared to the control cell lines. Empty cassette vector (PEL1) expressing cells showed reduced expression for all subunits apart from E1alpha which was more similar when compared to the CHOS control cells.

The CHOK1 samples in Figure 3.11.2.1 (b) show cells expressing E1beta N HA (PEL14) and E1beta C HA (PEL17) were more evenly matched with both showing higher expression of all PDH subunits in (ii) when compared to CHOK1 control cells. E3bp subunit expression appeared even between cell pools but more intense β-actin (iii) for CHOK1 control cell line samples suggest this is due to loading a higher protein concentration. This is supported by the relative expression analysis in Figure 3.11.2.2. E1beta C HA (PEL17) expressing cells had a lower expression of all subunits when compared to cells expressing E1beta N HA (PEL14) when normalised to beta-actin.

The CHOS and CHOK1 E1beta N HA (PEL14) and E1beta C HA (PEL17) stably expressing cell pools showed mixed impact on PDH subunit expression when compared to control cell lines, with those expressing E1beta N HA (PEL14) showing the largest increase in expression in both CHOS and CHOK1 cell lines. No expression of the E1beta PDH subunit was observed at 39.4 kDa in any samples. There was no clear difference between expression of the N- or C-terminally tagged E1beta subunits in PEL14 and PEL17 respectively. The resulting impacts to PDH subunit expression are summarised in Table 3.11.1.

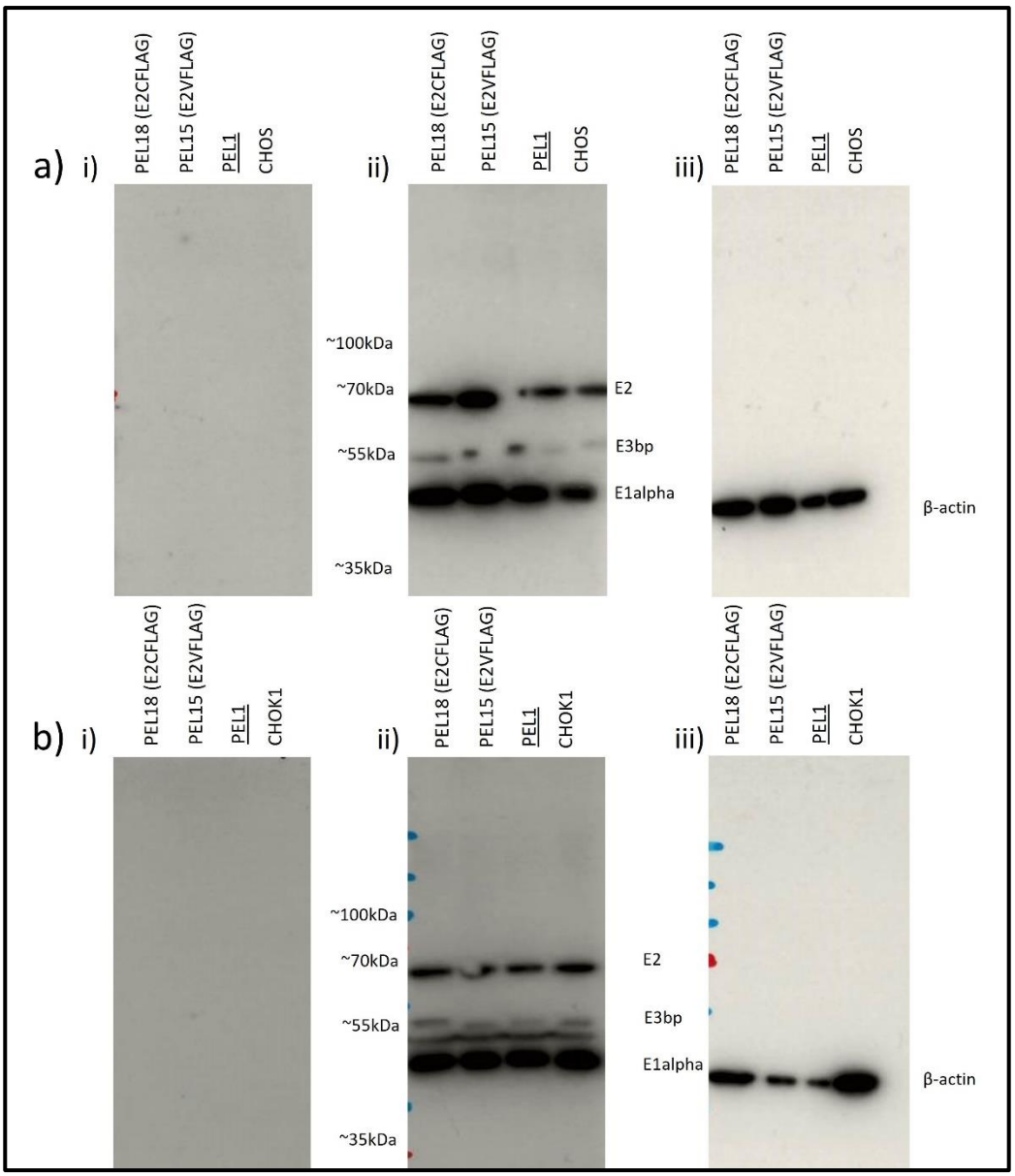

Figure 3.11.3.1 Analysis of CHOS and CHOK1 cell pools engineered to stably express E2 N FLAG- (PEL15) and C- (PEL18) terminally tagged protein. 10% SDS-PAGE run with 8 µg protein sample. a) CHOS cell lysates. b) CHOK1 cell lysates. i) Samples exposed to anti-FLAG antibody for 1 hour, tagged band for cells expressing E2 expected at 42.4 kDa. ii) Samples exposed to anti-PDH antibody cocktail for 1 hour. Multiple bands for the different subunits of the PDH enzyme complex are seen. E2 at 69 kDa, E3bp at 54 kDa, E1alpha at 43.3 kDa and E1beta at 39.4 kDa. iii) Samples exposed to anti-β-actin antibody for 1 min to show β-actin as a loading control at 37 kDa.

Figure 3.11.3.1 shows western analysis of expression of the FLAG tagged PDH E2 subunit, PDH subunits and β-actin in the CHOS (a) and CHOK1 (b) cells engineered to stably express the PDH subunit E2 N FLAG (PEL15) and E2 C FLAG (PEL18), alongside the control host cell lines. None of the CHOS or CHOK1 samples showed the presence of the FLAG tagged recombinant E2 PDH subunits when probed with the anti-FLAG antibody i). The PDH blots in ii) show an additional band across

the blot previously seen on blots in Figures 3.11.1.1 and 3.11.5.1. This was observed in the CHOK1 (b) but not in the CHOS (a) blots. Expression of the E2 subunit was clearly seen but expression of the E1beta subunit was not observed. Figure 3.11.3.2 shows the densitometry analysis using Image J software of the PDH and Beta-actin blots in Figure 3.11.3.1 (ii) and (iii) for both CHOS (a) and CHOK1 (b) cell lines.

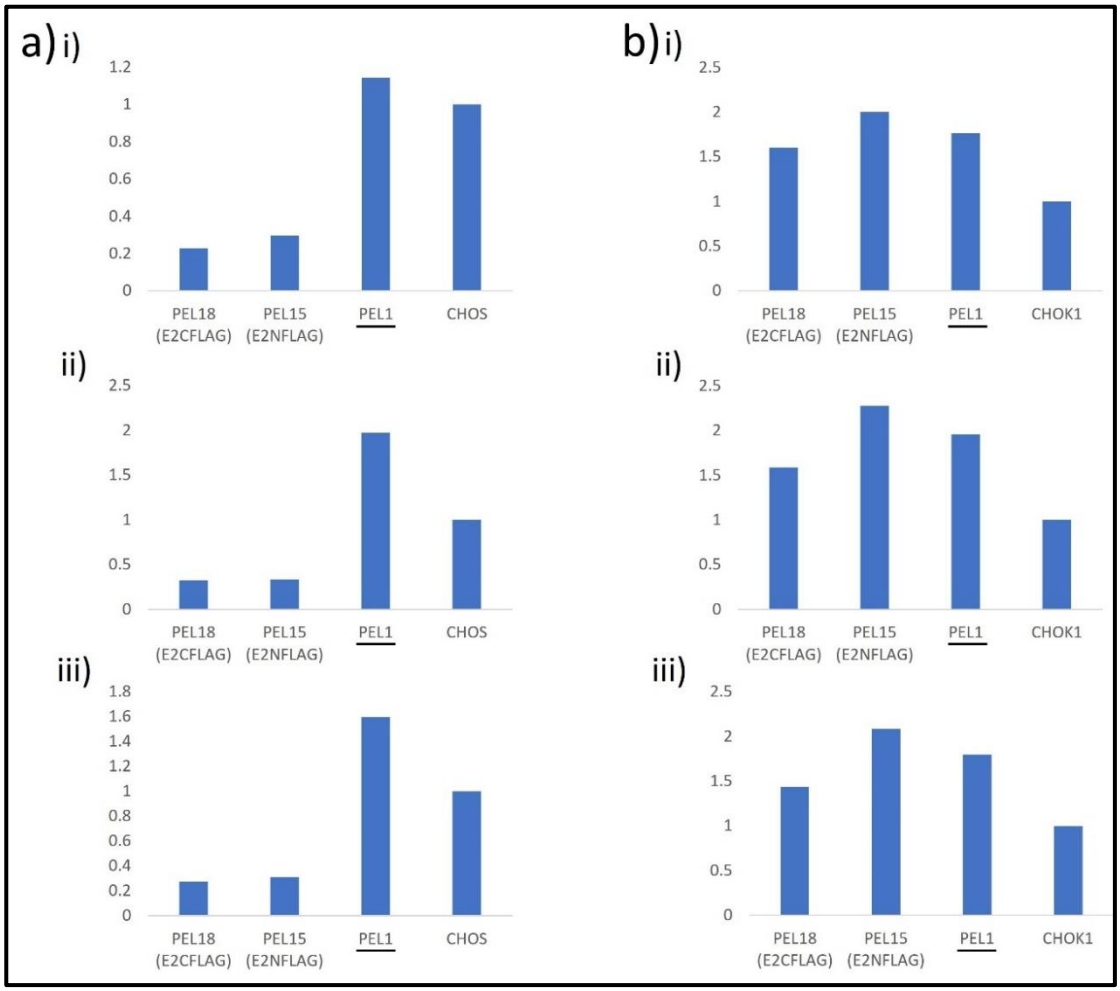

Figure 3.11.3.2 Densitometry of western blot signals showing the relative expression of E2 (i), E3bp (ii) and E1alpha (iii) subunits in CHOS (a) and CHOK1 (b) cell pools engineered to stably express E2 N FLAG- (PEL15) and C- (PEL18) terminally tagged protein compared to control host cell lines and β-actin expression. Analysis of bands presented in Figure 3.11.3.1 from PDH (ii) and β-actin (iii) blots is shown.

The CHOS blots (a) in Figure 3.11.3.1 appeared to show increased expression of all PDH subunits in both E2 N FLAG (PEL18) and E2 C FLAG (PEL15) stably expressing cell pools when compared to both the empty cassette vector (PEL1) expressing and control cell lines, with the E2 C FLAG pools showing increased expression for all subunits. However, the β-actin blots (iii) show more intense β-actin bands in these samples when compared to the CHOS control cell line and even more intense

compared to the empty cassette (PEL1) expressing cells. This was confirmed by the relative expression determined by densitometry for all subunits in Figure 3.11.3.2 as expression levels for the E2 N FLAG and C expressing cell pools (PEL15 and PEL18 respectively) was greatly reduced when normalized to β-actin loading and compared to the control cell lines. Expression levels observed for empty cassette vector (PEL1) expressing cell pools seem matched to those of the CHOS control cells but due to the lower β-actin band intensity, when looking at the relative expression of subunits, they were all expressed at a higher level.

The CHOK1 blots in Figure 3.11.3.1 show similar expression of all PDH subunits (ii), however a bubble during the transfer process impacted the expression level for the E2 subunit of the E2 N FLAG expressing cell pools. When looking at the β-actin blot (iii), the β-actin loading control in E2 C FLAG (PEL18) expressing cell samples was higher than the others, whilst the band intensity in the control cells was the highest of all samples. This is reflected in the relative expression densitometry graphs shown in Figure 3.11.3.2 where the expression of all PDH subunits in all cell pools was higher than the CHOK1 control sample. E2 C FLAG (PEL18) expressing cells showed the smallest increase in expression, followed by the empty cassette vector (PEL1) expressing control cells and finally the E2 N FLAG (PEL15) expressing cells which showed the largest increase, almost double the expression levels compared to the control.

The E2 N FLAG and C (PEL15 and PEL18 respectively) stably expressing cell pools showed contrasting impact on PDH subunit expression in the two CHO cell lines (CHOS or CHOK1). Expression of recombinant protein in CHOS cells has a negative impact on overall PDH subunit expression compared to the CHOK1 cell lines which show up to two times the expression level for multiple subunits in E2 N FLAG (PEL15) expressing cell pools. As the FLAG Tag was not observed for any samples in the anti-FLAG tag antibody probed blot it was not possible to confirm expression of the Flag-tagged subunit. There was no difference observed between expression of the N-and C-terminally tagged E2 PDH subunit in respective PEL15 and PEL18 cell pools suggesting the presence of the tag and its location did not impact expression of the tagged PDH subunits. The resulting impacts to PDH subunit expression are summarised in Table 3.11.1.

Table 3.11.1 Summary of the protein expression and resulting densitometry data of relative expression of PDH subunits presented in Figures 3.11.1.1 to 3.11.3.2.

		(Figures 3.11.1.1, 3.11.2.1 and 3.11.3.1)	Impact to Relative Expression of PDH subunit compared to host (Densitometry from Figures 3.11.1.2, 3.11.2.2 and 3.11.3.2)			
Cell Line	Target PDH subunit	Protein Expression with relevant tag antibody	E1alpha	E1beta	E2	E3bp
CHOS PEL13 (E1αNV5)	E1α	None	Increase, smaller than in PEL1	No E1beta signal seen in Western blots (Figures 3.11.1.1, 3.11.2.1 and 3.11.3.1)	Increase, similar to PEL1	Increase, smaller than in PEL1
CHOS PEL16 (E1αCV5)	E1α	None (Seen in Appendix Figure 7.1.7)	Increase, smaller than in PEL1		Increase, similar to PEL1	Increase, also seen in PEL1
CHOK1 PEL13 (E1αNV5)	E1α	None	Increase, similar to PEL1		Increase, larger than in PEL1	Increase, similar to PEL1
CHOK1 PEL16 (E1αCV5)	E1α	None (Seen in Appendix Figure 7.1.7)	Increase, smaller than in PEL1		Increase, similar to PEL1	Decrease, increase to PEL1
CHOS PEL14 (E1βNHA)	E1β	None	Large Increase, PEL1 similar to host		Large Increase, low PEL1	Small Decrease, low PEL1
CHOS PEL17 (E1βCHA)	E1β	Yes (Seen in Appendix Figure 7.1.8 also)	Similar Expression, PEL1 similar		Similar Expression, low PEL1	Large Decrease, low PEL1
CHOK1 PEL14 (E1βNHA)	E1β	None	Increase, larger than in PEL1		Increase, larger than PEL1	Large Increase, PEL1 similar to host
CHOK1 PEL17 (E1βCHA)	E1β	None (Seen in Appendix Figure 7.1.8)	Increase, similar to PEL1		Increase, larger than PEL1	Large Increase, PEL1 similar to host
CHOS PEL15 (E2NFLAG)	E2	None	Large Decrease, increase to PEL1		Large Decrease, increase to PEL1	Large Decrease, increase to PEL1
CHOS PEL18 (E2CFLAG)	E2	None (Seen in Appendix Figure 7.1.9)	Large Decrease, increase to PEL1		Large Decrease, increase to PEL1	Large Decrease, increase to PEL1
CHOK1 PEL15 (E2NFLAG)	E2	None	Increase, larger than in PEL1		Increase, similar to PEL1	Increase, larger than in PEL1
CHOK1 PEL18 (E2CFLAG)	E2	None	Increase, smaller than in PEL1		Increase, smaller than in PEL1	Increase, smaller than in PEL1

When comparing the success of overexpression of all tagged PDH subunits of in CHOS and CHOK1 cell lines, the results are mixed. E1alpha N V5 and C tags (PEL13 and 16) showed the highest expression in the CHOS cell line whereas CHOK1 cell lines had the highest PDH subunit expression when stably expressing all other subunits. Expressing N-terminally tagged PDH subunits E1alpha, E1beta and E2 (PEL13, 14 and 15) resulted in the largest increase in PDH subunit expression when compared to the equivalent C-terminally tagged PDH subunits. It should be noted that there were no clear impacts on cell growth or culture viability when either CHOS or CHOK1 cells were stably expressing the N or C terminally tagged PDH subunits, suggesting increased protein expression of the PDH subunits was not detrimental to the cells.

3.12 Generation and Evaluation of CHOS and CHOK1 Cell Pools Stably Expressing an E1alpha PDH Subunit Serine Mutant

Overexpressing the subunits of the PDH complex, as described previously, aims to increase availability of the subunits themselves allowing the formation of more complex and therefore PDH activity converting pyruvate to acetyl-CoA. The theory of this increase in metabolic flux from

pyruvate to acetyl-CoA through there being more available PDH complexes relies on there being fewer complexes inactivated due to phosphorylation via PDKs 1 to 4. The E1alpha subunit is the site of PDK mediated phosphorylation and acts as the rate limiting step of the complex enzymatic activity. E1alpha has three serine residues at amino acids 264, 271, and 203 that are phosphorylated by PDK resulting in deactivation of the enzyme. Replacement of these serine residues with alanine residues has been used as an approach to remove the potential for phosphorylation allowing an always 'active' PDH complex to form. The sequences used by (Kolobova et al., 2001a) to mutate E1alpha via site directed mutagenesis and were therefore adapted and used to create stably expressing E1alpha mutant cell lines. The mutant E1alpha sequence was ordered from Twist Bioscience and cloned into Cassette 1 of the Hygro 3 Cass Tags backbone (PEL12) to create the E1alpha mutant PEL19 (E1αmutCV5). This allowed the attachment of a C-terminal V5 tag using the enzymes listed in Table 3.12.1.

Table 3.12.1 Restriction enzymes used on the end of primers for PCR amplification, and subsequent digestion and ligation of the mutant E1alpha PDH subunit into PEL12 into cassette 1 creating PEL19 (E1αmutCV5).

Plasmid no.	Cassette	Tag	Tag position	PDH Subunit	Restriction enzymes
PEL19 (E1αmutCV5)	1	V5	C	E1alpha mutant	NheI and AflII

Similar to the presence of tags on subunits in PEL13 to 18, this approach would enable the expression of the E1alpha mutant to be identified and easily compared to endogenous expression levels. A C-terminal position for the V5 tag was selected due to the previous success when expressing C-terminal tags in comparison to N-terminal, as seen in western blots in section 3.11 and Appendix Figures 7.1.7 to 7.1.9. After amplification via PCR and insertion into the PEL12 backbone, the final E1alpha mutant PEL19 was screened using restriction digests before being sent for commercial Sanger sequencing. Figure 3.12.1 shows the results of a restriction digest confirming the presence of the PEL19 (E1αmutCV5) sequence (a) and the linearisation of PEL19 (E1αmutCV5) after an overnight digest with FspI in preparation for the creation of stably expressing cell pools.

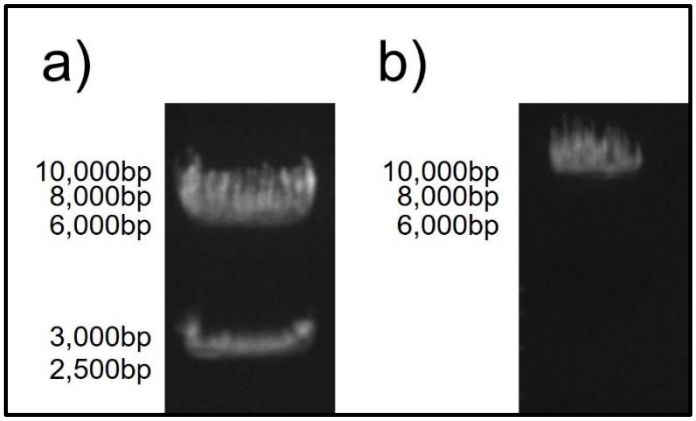

Figure 3.12.1 Restriction digests of PEL19 (E1αmutCV5), Hygro 3 Cass Tags backbone with the mutant *E1alpha* subunit in cassette 1 and linearisation using FspI in preparation for the generation of stably expressing CHOS and CHOK1 cell pools. (a) Digest with HindIII, expected bands at 2690 bp and 6144 bp. (b) 50 µg DNA linearised overnight with FspI enzyme in preparation for the creation of stably expressing CHOS and CHOK1 cell lines with expected band at 8834 bp.

The results from the commercial Sanger sequencing showed the successful mutation of all three serine residues and their replacement with alanine residues. However, it also showed a point mutation where a guanine (G) nucleotide had mutated to a thymine (T) nucleotide. This meant the TGT nucleotide sequence encoding a leucine amino acid at position 213 was instead a TTT nucleotide sequence encoding a phenylalanine amino acid. Both amino acids have polar groups but the large phenol ring in phenylalanine may cause an issue with overall protein folding. The mutation lies nineteen amino acids upstream of the phosphorylation Site 3 serine, now mutated to an alanine, at position 203. The distance between the phosphorylation site suggests that the mutation should not be an issue and as it aimed to disrupt the ability of PDKs to phosphorylate the original serine residue, the impact of the sequence change should be minimal. Alternatively, it could present an issue for protein expression due to misfolding preventing protein production and incorporation with other PDH subunits to form an active protein complex. The decision was made to continue using the mutated E1alpha mutant and identify if stable cell lines could be generated expressing the subunit analysing any impacts on protein assembly downstream.

3.13 Creation and Evaluation of E1alpha Mutant Stably Expressing Cell Pools

Despite the issues surrounding the point mutation in the E1alpha mutant PEL19 (E1αmutCV5), stably expressing cell pools were made in both CHOS and CHOK1 cell lines. After the linearisation of DNA, shown in Figure 3.12.1, cells were electroporated following the same process as the cells stably expressing untagged and tagged controls PEL1 and PEL12 and PDH subunit containing

plasmids PEL3-18 as described previously. After recovery from the transfection and addition of Hygromycin B selection, cell pools stably expressing PEL19 (E1αmutCV5) had lysate samples prepared from cell pellets for protein analysis via Bradford assays and western blot. Cells were also banked down using cryopreservation.

To identify any successful overexpression of the PDH subunits due to the stable expression of the *E1alpha mutant* gene, lysate samples were loaded onto an SDS-PAGE gel alongside lysate samples from CHOS and CHOK1 cell pools stably expressing the other tagged *E1alpha* containing subunits (plasmids PEL13 and PEL16 using PEL12 expressing cells and host cells as controls). The results of these western blots when probing with anti-PDH antibody cocktail (a) anti-V5 antibody (b) and anti-β-actin (c) are shown in Figure 3.13.1.1.

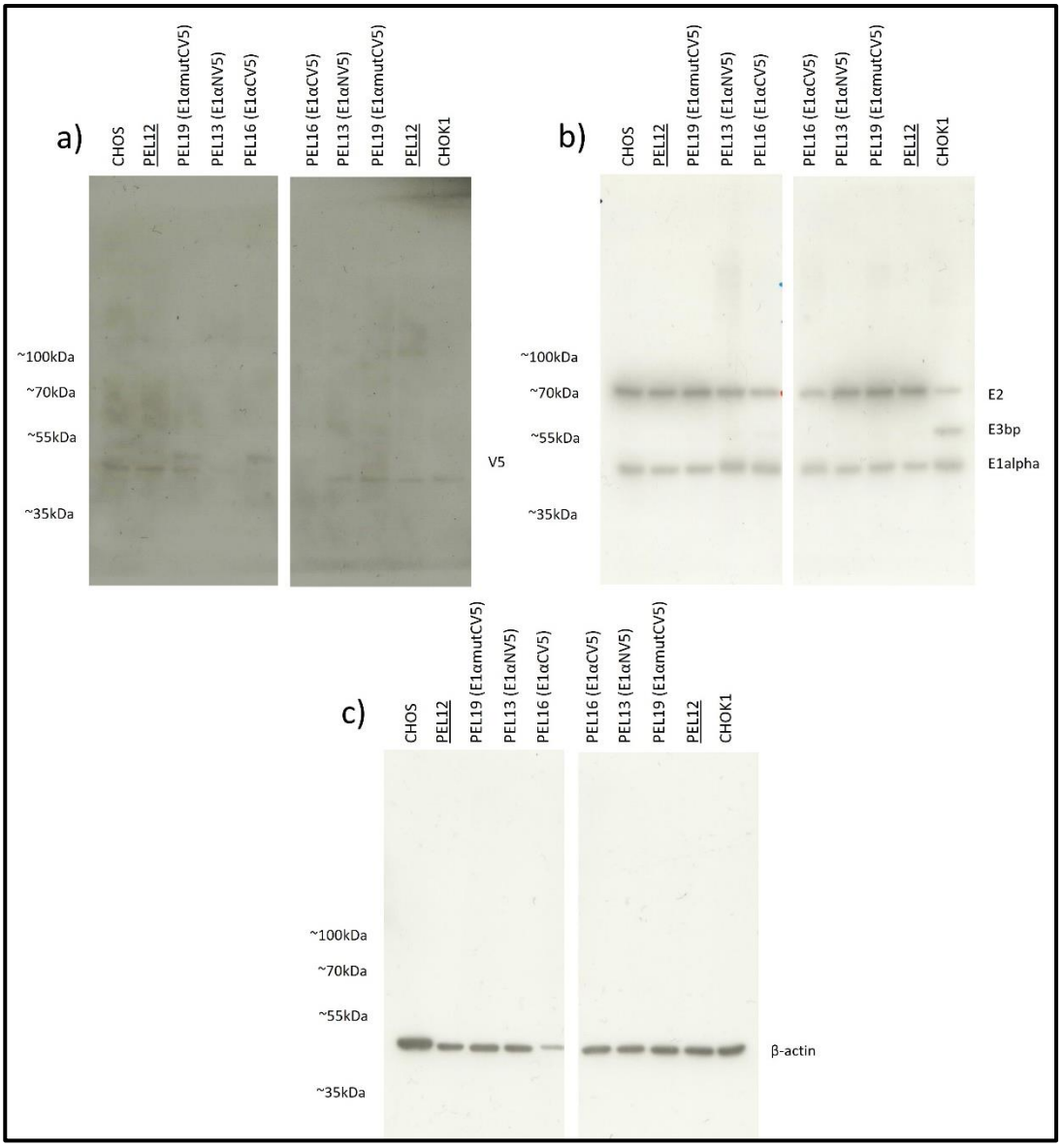

Figure 3.13.1.1. Evaluation of CHOS (left) and CHOK1 (right) cell pools engineered to stably express E1alpha N- and C-terminally V5 tagged proteins (PEL13 and PEL16 respectively) alongside C-terminally V5 tagged E1alpha mutant (PEL19 E1αmutCV5) stably expressing cells. 10% SDS-PAGE run with 8 µg protein a) Samples exposed to anti-V5 antibody for 1 hour, tagged band for cells expressing E1alpha expected at 44.3 kDa. b) Samples exposed to anti-PDH antibody cocktail for 1 hour. Multiple bands for the different subunits of the PDH enzyme complex are seen. E2 at 69 kDa, E3bp at 54 kDa, E1alpha at 43.3 kDa and E1beta at 39.4 kDa. c) Samples exposed to anti-β-actin antibody for 1 min to show β-actin as a loading control at 37 kDa.

Figure 3.13.1.1 shows faint expression of the V5 tag (a) in CHOS samples stably expressing E1alpha C V5 mutant (PEL19) and E1alpha C V5 (PEL16) expressing cell lines only. A band was observed in almost all samples around 44 kDa, the size that would be expected for the E1alpha subunit itself, however as these blots were probed with only the anti-V5 antibody this must be non-specific binding. Figure 3.13.1.2 shows the densitometry analysis using Image J software of the PDH and β-

actin blots in Figure 3.13.1.1 (a) and (b) respectively. Results are shown for both CHOS (a) and CHOK1 (b) cell lines.

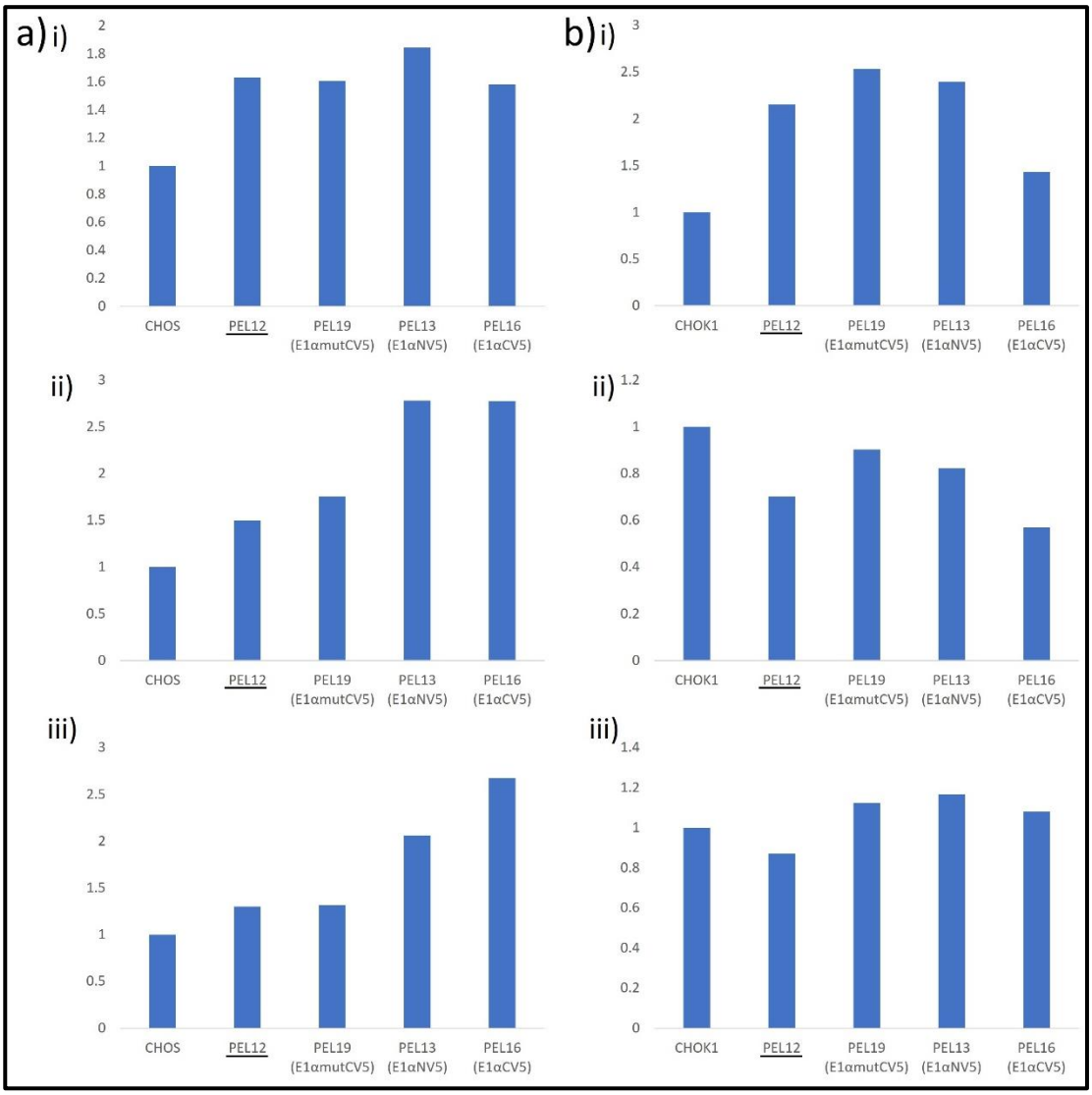

Figure 3.13.1.2 Densitometry of western blot signals showing the relative expression of E2 (i), E3bp (ii) and E1alpha (iii) subunits in CHOS (a) and CHOK1 (b) cell lines engineered to stably express E1alpha N V5- (PEL13) and C- (PEL16) terminally tagged protein and C-terminally V5 tagged E1alpha mutant (PEL19) compared to control host cell lines and β-actin expression. Analysis of bands presented in Figure 3.12.1.1 from PDH (ii) and β-actin (iii) blots is shown.

The CHOS samples (a) in Figure 3.13.1.2 showed a similar trend in PDH subunit expression with all samples having higher expression of all PDH subunits compared to the CHOS control cell line. When looking at the β-actin blots (c) in Figure 3.13.1.1. it is clear to see why this is the case as the intense β-actin band seen for the CHOS control sample suggests a higher protein concentration was loaded for these samples. Expression of E2 (i) was similar in all stably expressing cell pools, with E1alpha N V5 (PEL13) expressing cells showing the highest increase in expression of the E2 subunit. Expression

of E3bp and E1alpha subunits showed a similar pattern with cells expressing the N- and C-terminally tagged E1alpha subunits in PEL13 and PEL16 showing the largest increase in expression. These cell pools show comparable expression levels of all subunits, but PEL16 shows the largest improvement in expression of E1alpha. The V5-Tag band observed in Figure 3.13.1.1 (a) suggests expression of E1alpha C V5 mutant (PEL19) with the V5-tag was occurring.

The CHOK1 samples (b) in Figure 3.13.1.2 show different results in terms of PDH subunit expression in stable pools compared to the CHOS (a) cell lines. Expression levels of PDH subunit E2 (i) was higher in all cell pools compared to CHOK1 control cells with those expressing E1alpha C V5 (PEL16) having lower expression than empty cassette tag vector (PEL12) expressing control cells. E1alpha C V5 mutant (PEL19) and E1alpha N V5 (PEL13) expressing cells showed the highest expression levels of E2. Looking at expression levels of the E3bp PDH subunit (ii) however, showed CHOK1 control cells as having the highest expression levels. In Figure 3.13.1.1, CHOK1 host cells were the only cell line to clearly show E3bp expression however it is unclear why this is the case as similar expression levels of β-actin suggest it is not due to higher protein loading compared to other samples. E1alpha C V5 (PEL16) expressing cell pools again showed expression levels lower than the control empty cassette tag vector (PEL12) expressing cells whilst E1alpha C V5 mutant (PEL19) and empty cassette tag vector expressing cells had the next highest expression levels. E1alpha expression levels (iii) were more evenly matched, especially when compared to those of the CHOS cell lines (a iii.) All cell pools showed increased expression of the E1alpha subunit apart from the empty cassette tag vector (PEL12) expressing control cell lines. The increase in expression observed in the other cell pools was much smaller than the expression increase seen for the E2 subunit (i) or the CHOS cells (a). E1alpha C V5 mutant (PEL19) expressing cell pools showed the highest over-expression of PDH subunits. E1alpha C V5 (PEL16) expressing cells showed the smallest increase in overall PDH subunit expression. The resulting impacts to PDH subunit expression are summarised in Table 3.13.1.

Table 3.13.1 Summary of the protein expression and resulting densitometry data of relative expression of PDH subunits presented in Figures 3.13.1.1 and 3.13.1.2.

		(Figure 3.13.1.1)	Impact to Relative Expression of PDH subunit compared to host (Densitometry from Figure 3.13.1.2)			
Cell Line	Target PDH subunit	Protein Expression with relevant tag antibody	E1alpha	E1beta	E2	E3bp
CHOS PEL13 (E1αNV5)	E1α	None	Large Increase, larger than in PEL12	No E1beta signal seen in Western blots (Figures 3.13.1.1)	Increase, larger than in PEL12	Large Increase, larger than in PEL12
CHOS PEL16 (E1αCV5)	E1α	Faint band (Also seen in Appendix Figure 7.1.7)	Large Increase, larger than in PEL12		Increase, similar to PEL12	Large Increase, larger than in PEL12
CHOS PEL19 (E1αmutCV5)	E1α	Faint band	Increase, similar to PEL12		Increase, similar to PEL12	Increase, similar to PEL12
CHOK1 PEL13 (E1αNV5)	E1α	None (Seen in Appendix Figure 7.1.7)	Small Increase, decrease in PEL12		Increase, larger than in PEL12	Decrease, smaller than in PEL12
CHOK1 PEL16 (E1αCV5)	E1α	None	Small Increase, decrease in PEL12		Increase, smaller than in PEL12	Decrease, larger than in PEL12
CHOK1 PEL19 (E1αmutCV5)	E1α	None	Small Increase, decrease in PEL12		Increase, larger than in PEL12	Decrease, smaller than in PEL12

Both the CHOS and CHOK1 cells in Figure 3.13.1.2 showed some increase in the expression of PDH subunits when compared to the original host cell lines. CHOS cells expressing E1alpha N V5 or C in PEL13 and PEL16 respectively showed the greatest increase in PDH subunit expression when compared to cells expressing E1alpha C V5 mutant (PEL19) and the empty cassette tag vector control (PEL12) for the CHOK1 cells. All engineered cells grew comparably and no clear impact on growth or culture viability as a result of expressing the tagged plasmids was observed.

3.14 Magnetic Bead Immunoprecipitation of the PDH Complex

To identify whether the presence of the tag on the recombinant exogenous PDH complex proteins was impacting formation of the complex with endogenous untagged subunits, immunoprecipitation using magnetic beads was undertaken. This would determine whether the expressed tagged PDH subunit(s) were able to join with other endogenous subunits forming functional PDH complexes or whether the presence of the tag was preventing complex interactions and any resulting increase in complex activity.

To do this, Invitrogen Dynabeads™ M-270 Epoxy were covalently coupled to the relevant tag primary antibodies overnight and the supernatant collected. This was to check for any co-elution of antibody occurring during the protein elution process. After washing, the antibody coated beads were mixed with lysate samples from cells expressing tagged subunit constructs PEL13 to 19, with cells expressing empty cassette tag vector PEL12 and host cells used as controls. This enabled the binding of antibody to PDH subunits with tags before multiple wash steps to remove any unbound protein. The supernatant from the initial mixing step was kept enabling the identification of how much of

the tagged protein was binding to the beads and how much was left in the mixture. The protein was eluted off the beads using the recommended elution buffer, 0.1 M citrate pH 3.1. The beads were also boiled in sample buffer to reduce any complex still bound, breaking interactions to separate any attached PDH complex subunits. Samples were then separated from the beads using magnets to be loaded into an SDS-PAGE gel for western blot analysis. The process is described in the methods section 2.4.9. Lysate samples for the N- and C-terminally tagged E1beta subunit containing PEL14 and PEL17 respectively expressing CHOS cells were used first with the results shown in Figure 3.14.1.

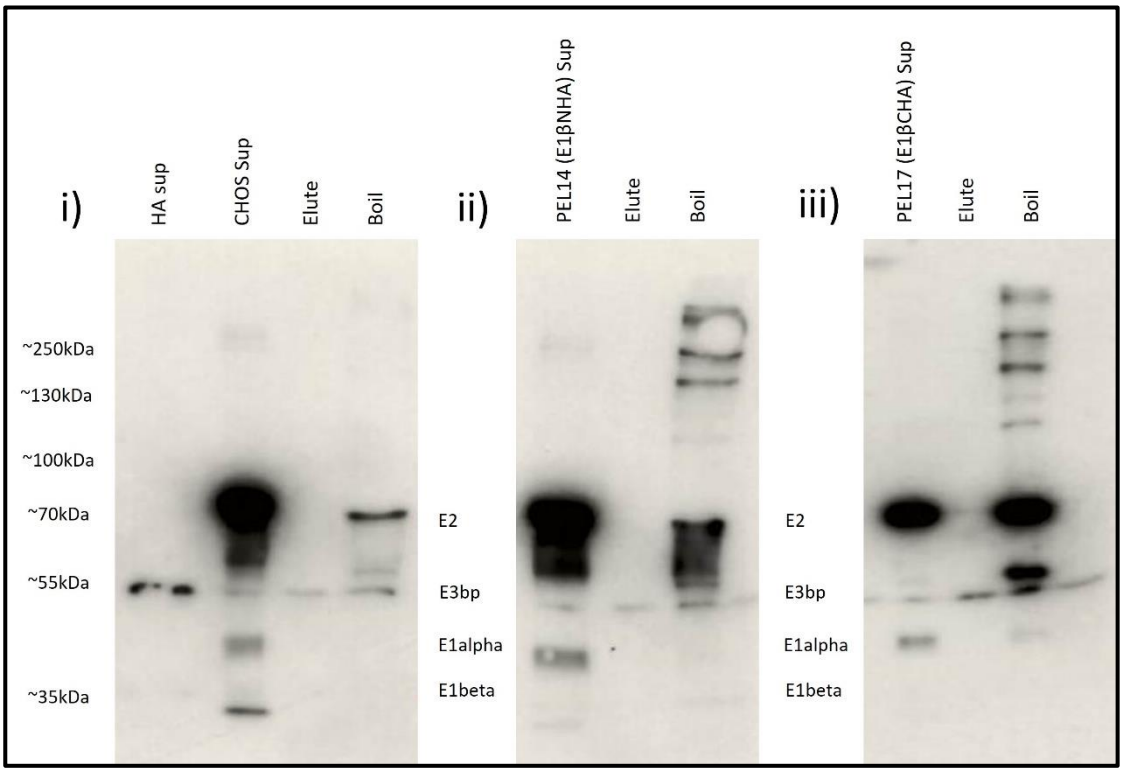

Figure 3.14.1 CHOS lysate samples from cell pools engineered to stably express E1beta N HA- (PEL14) and C- (PEL17) terminally tagged protein incubated with anti-HA antibody coupled Invitrogen Dynabeads™ M-270 Epoxy beads. 10% SDS-PAGE gel with 15 µl sample loaded**.** Beads incubated with i) CHOS host cell lysate ii) Cell lysate from CHOS cells stably expressing PEL14 iii) Cell lysate from CHOS cells stably expressing PEL17. HA supernatant collected after covalently binding antibodies to beads. Sample supernatants collected after sample incubation with beads. Elution buffer samples and samples after boiling beads to separate the bound protein. Samples exposed to anti-PDH antibody cocktail for 1 hour. Multiple bands for the different subunits of the PDH enzyme complex are seen. E2 at 69 kDa, E3bp at 54 kDa, E1alpha at 43.3 kDa and E1beta at 39.4 kDa.

Figure 3.14.1 shows the binding of the N- and C-terminally tagged E1beta subunit expressed by PEL14 and 17 respectively to the anti-HA tag antibody bound beads. To identify whether the anti-HA antibody was co-eluting with the beads when mixed with the elution buffer or boiled, the supernatant after attachment was kept and run on the gel. The signal seen for this antibody sample Lane 1 (i) is similar to the one seen in all samples with a band observed at around 55 kDa. This is

similar to the subunit band previously observed (Figures 3.11.1.1, 3.11.5.1 and 3.11.6.1) when probing with the anti-PDH antibody cocktail.

The CHOS control samples (i) in Figure 3.14.1 showed the presence of PDH subunits after boiling the beads. Expression of all PDH subunits was seen in the supernatant sample taken after mixing with the beads suggesting a high protein concentration had been exposed to the beads. Nothing was observed for the elution sample, other than the signal for all samples at 55 kDa using the suggested elution buffer, however a protein band was observed at 70 kDa for the E2 and at 55 kDa for the E3bp subunits after the beads were boiled with reducing buffer suggesting some non-specific interactions were occurring. No protein was observed at 39 kDa for the E1beta subunit which is the target of overexpression for PEL14 and 17.

CHOS cells expressing the N-terminally tagged E1beta PDH subunit (PEL14) showed an intense band, as did the CHOS control cells in the supernatant samples (ii) after mixing with the beads which is to be expected due to the overloading of lysate for the bead volume. The elution sample again showed no protein was present but multiple protein bands were observed when the beads are boiled, suggesting the elution buffer was not eluting bound protein. Much more intense banding was present between 130 kDa and 250 kDa as well as signals at 70 kDa and 55 kDa, those expected for the E2 and E3bp subunits respectively. These banding patterns suggest the formation of larger, multiple PDH subunit interactions with the exogenous N-terminally HA tagged E1beta subunits expressed from PEL14 and endogenous untagged PDH subunits.

CHOS cells expressing the C-terminally tagged E1beta subunit in PEL17 showed a similar pattern (Figure 3.14.1) to those expressing E1beta N HA (PEL14). The supernatant sample however showed weaker protein signals compared to both the CHOS control and the E1beta N HA (PEL14) expressing cell pools but more intense bands for the beads that have been boiled samples. Protein bands were observed at 70 kDa, corresponding to the E2 subunit, and 43 kDa corresponding to the E1alpha subunit for the supernatant sample. More intense protein bands were observed in the boiled samples, between 130 kDa and 250 kDa and at 70 kDa, 50 kDa and faintly at 43 kDa corresponding to the individual E2, E3bp and E1alpha subunits. Once again, the presence of these bands suggests the formation of larger, multiple PDH subunit interactions with the exogenous C-terminally HA tagged E1beta subunits expressed from PEL17 and endogenous untagged PDH subunits.

Figure 3.14.1 shows that both N- and C-terminally tagged E1beta recombinant proteins, expressed from PEL14 and 17 respectively, are able to interact with endogenous PDH subunits to form larger complexes. The recommended citrate elution buffer showed no bands for any samples however many were seen when the beads were boiled in reducing buffer. Future samples were boiled with a

longer boiling time to fully reduce bonds in the larger protein complexes to separate individual subunits. The HA tag does not negatively impact subunit integration into the complex and seems to result in similar concentrations of protein eluting off the beads independent of location. A bead only control could have been included to identify any non-specific interactions between the beads and cell lysate. It should be noted that neither E1beta N HA (PEL14) or E1beta C HA (PEL17) expressing cell pools have a clear band on Figure 3.14.1 at 39 kDa, the expected size for the targeted E1beta subunit suggesting it may be present in the larger protein complexes.

The western blots show the success of the pulldown approach to evaluate if tagged subunits interact with other endogenous PDH subunits. Samples from cells stably expressing tagged PDH subunits in PEL13 to 19 were therefore mixed with the appropriate anti-tag antibody tagged beads, washed and the supernatant collected after boiling with reducing buffer. Figures 3.14.2, 3.14.3 and 3.14.4 show the resulting western blots when these samples were run on SDS-PAGE gels and probed with the anti-PDH antibody cocktail.

Figure 3.14.2 CHOS (left) and CHOK1 (right) lysate samples from cells engineered to express N- (PEL13) terminally and C- (PEL16) terminally tagged and C-terminally tagged mutant (PEL19) E1alpha PDH subunits incubated with anti-V5 antibody coupled Invitrogen Dynabeads™ M-270 Epoxy beads. Tagged lysate samples used alongside lysate from stably expressing control PEL12 and control host cells. V5 supernatant collected after covalently binding anti-V5 antibody to beads. 10% SDS-PAGE gel run with 10 µl sample loaded. Samples exposed to anti-PDH antibody cocktail for 1 hour. Multiple bands for the different subunits of the PDH enzyme complex are seen. E2 at 69 kDa, E3bp at 54 kDa, E1alpha at 43.3 kDa and E1beta at 39.4 kDa.

Figure 3.14.2 showed very little protein in any samples. There were no signals observed for the anti-V5 supernatant sample or any other sample suggesting co-elution of the anti-V5 tag antibody with the PDH proteins when boiling the beads did not occur. The CHOS and empty tag cassette vector

(PEL12) expressing control samples had a faint band at 70 kDa for the E2 subunit but no other bands suggesting some non-specific binding is occurring between the beads and lysate samples. This was similar to the results of samples for cells expressing PEL13, 16 and 19 with N- and C-terminally tagged E1alpha and E1alpha mutant subunits. Faint signals at 55 kDa for the E3bp subunit could be seen for some samples. Bands could also be seen at the dye front of the gel for several samples. This band, around 20 kDa, had not been seen previously on other blots probed with the anti-PDH antibody and was observed in control samples alongside the tagged PDH subunit expressing cell lines in both CHOS and CHOK1 hosts. The band could be the Complex V control, but this is unlikely as this has only previously been seen for the HEK293 sample run as a control in Figure 3.6.2. This band could be a result of boiling the beads for longer but does not seem to have an impact on the results overall. The CHOK1 samples showed a similar pattern to the CHOS samples.

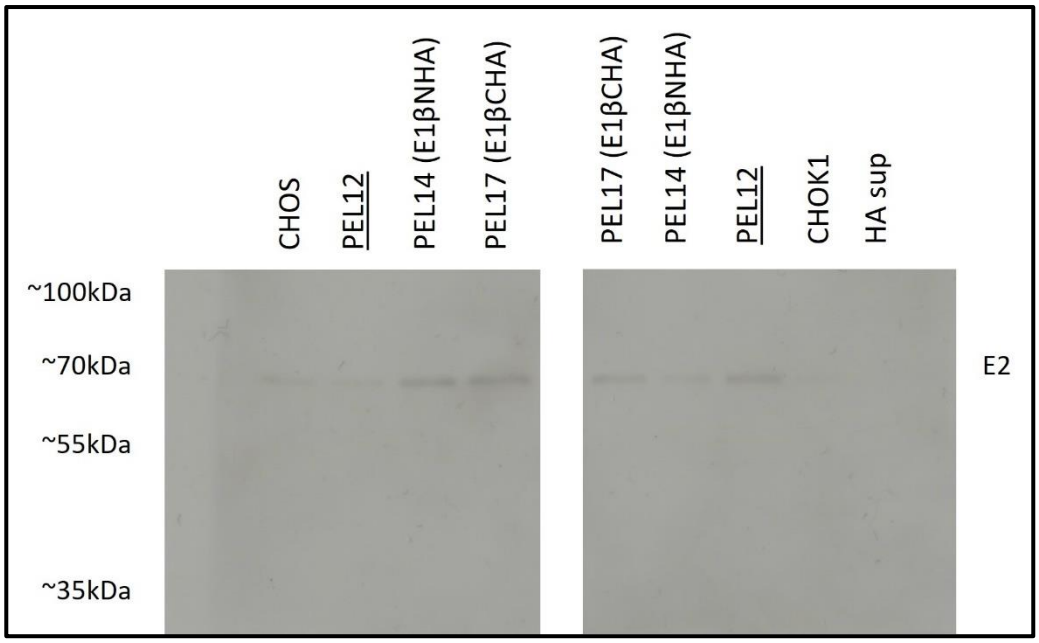

Figure 3.14.3 CHOS (left) and CHOK1 (right) lysate samples from cells engineered to express N- (PEL14) terminally and C- (PEL17) terminally tagged E1beta PDH subunits incubated with anti-HA antibody coupled Invitrogen Dynabeads™ M-270 Epoxy beads. Tagged lysate samples alongside lysate from stably expressing control PEL12 and control host cells. HA supernatant collected after covalently binding anti-HA antibody to beads. 10% SDS-PAGE gel run with 10 µl sample loaded. Samples exposed to anti-PDH antibody cocktail for 1 hour. Multiple bands for the different subunits of the PDH enzyme complex are seen. E2 at 69 kDa, E3bp at 54 kDa, E1alpha at 43.3 kDa and E1beta at 39.4 kDa.

Figure 3.14.3 shows only faint protein bands at 70 kDa for the E2 subunit for most samples. There were no bands observed for the anti-HA supernatant sample or any other sample suggesting co-elution of the anti-HA tag antibody with the protein when boiling the beads did not occur. The CHOS and empty cassette tag vector (PEL12) expressing control samples showed a faint band at 70 kDa

for the E2 subunit but no other bands. These results are similar to the results of samples for cells expressing PEL14 and PEL17 with N- and C-terminally tagged E1beta subunits respectively as well as those in Figure 3.12.2. Unlike Figure 3.14.2 however, no bands could be seen at the dye front of the gel for any samples. The CHOK1 samples showed a similar pattern to the CHOS samples but empty cassette tag vector (PEL12) expressing control cells had the strongest protein signal at 70 kDa for the E2 PDH subunit. The bands for the E1beta N HA (PEL14) and E1beta C HA (PEL17) expressing cells were fainter in comparison although the CHOK1 control cell line band was the faintest. No other protein signals were seen for any samples including at 39.3 kDa for the target E1beta subunit.

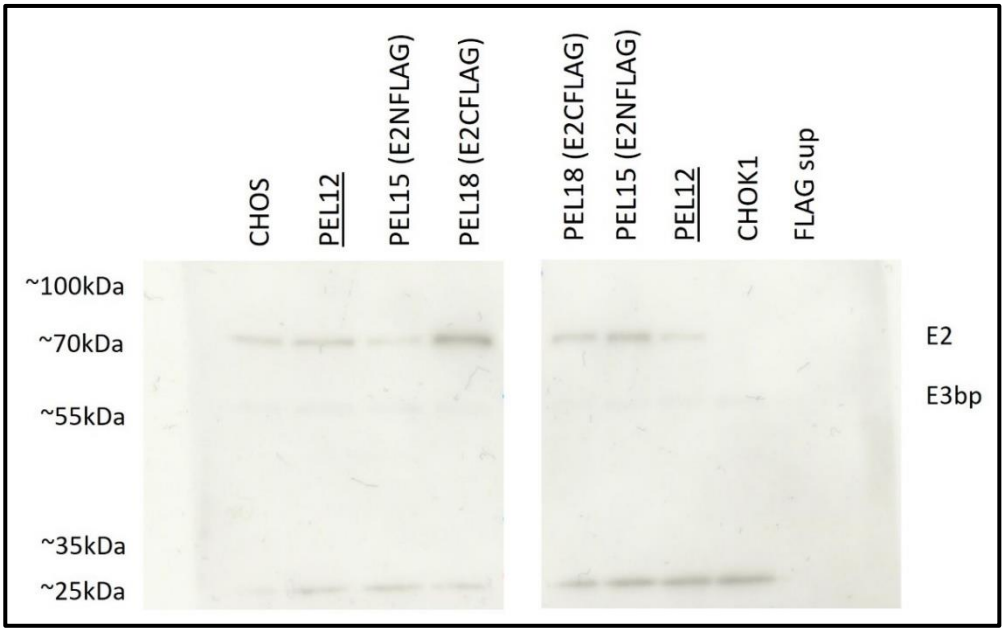

Figure 3.14.4 CHOS (left) and CHOK1 (right) lysate samples from cells engineered to express N- (PEL15) terminally and C- (PEL18) terminally tagged E2 PDH subunits incubated with anti-FLAG antibody coupled Invitrogen Dynabeads™ M-270 Epoxy beads. Tagged lysate samples alongside lysate from stably expressing control PEL12 and control host cells. FLAG supernatant collected after covalently bonding anti-FLAG antibody to beads. 10% SDS-PAGE gel run with 10 µl sample loaded. Samples exposed to anti-PDH antibody cocktail for 1 hour. Multiple bands for the different subunits of the PDH enzyme complex are seen. E2 at 69 kDa, E3bp at 54 kDa, E1alpha at 43.3 kDa and E1beta at 39.4 kDa.

Figure 3.14.4 shows bands at 70 kDa and 55 kDa, the size expected for the E2 and E3bp subunits respectively, in most samples. There were no bands observed for the anti-FLAG supernatant sample or any other sample suggesting co-elution of the anti-FLAG tag antibody with the protein when boiling the beads was not occurring. However the bands in control samples suggest some non-specific interactions are occurring. The CHOS and empty cassette tag vector (PEL12) expressing control samples contained a faint band at 70 kDa for the E2 subunit and a faint band at 55 kDa for

the E3bp subunit. This is similar to the results of samples for cells expressing E2 N FLAG (PEL15) which had a fainter band for the E2 subunit and E2 C FLAG (PEL18) which had a more intense band for the E2 subunit. Expression of PEL15 and 18 with N- and C-terminally FLAG tagged E2 recombinant PDH subunits did not result in an increase in the amount of E2 subunit binding and detaching from the beads when compared to control cell lines. As in Figure 3.14.2, bands could be observed at the dye front of the gel for all samples. It is unclear what is reacting with both the anti-V5 and anti-FLAG tags to produce this band as it is present in almost all samples for both antibodies. The CHOK1 samples showed a similar pattern to the CHOS samples but empty cassette tag vector (PEL12) expressing control cells had the faintest band at 70 kDa for the E2 subunit. The bands for the E2 N FLAG (PEL15) and E2 C FLAG (PEL18) expressing cells were more intense in comparison whilst the CHOK1 control cell line sample showed no band for the E2 subunit and only a faint band at 55 kDa for the E3bp subunit.

Unlike the samples loaded in Figure 3.14.1, Figures 3.14.2, 3.14.3 and 3.14.4 show very little protein present in samples for any PDH subunits, even after exposure for an hour. This is likely due to a low protein concentration eluting off the beads. The leftover samples not loaded into the SDS-PAGE gels were added back to the relevant beads and boiled again to ensure any remaining protein bound was separated in the supernatant. However, the resulting western blot again showed very little protein present for PDH subunits and bands remained faint for all samples. The figures do however show some PDH subunits attaching to the tagged beads and eluting off. Figure 3.14.1 shows interactions between N- and C-terminally tagged E1beta subunits expressed in PEL14 and 17 interacting with E2, E3bp and, for E1beta C HA (PEL17), E1alpha endogenous PDH subunits. This is not shown to be the case for the E1alpha N V5 (PEL13) and E1alpha C V5 (PEL16) expressing cells or E2 N FLAG (PEL15) and E2 C FLAG (PEL18) expressing cells.

3.15 Evaluation of PDH Subunit gDNA Expression in Stable CHO Cell Pools using qPCR

Western blot analysis showed expression of exogenous PDH subunits in cells stably expressing recombinant DNA, however this was only clear with the addition of a tag onto the target gene. Bands were more frequently seen when the tag was C-terminally attached compared to N-terminally. To identify whether expression of recombinant PDH was limited at the DNA level, and therefore impacting protein expression, genomic DNA was isolated from cell pools stably expressing tagged and untagged PDH subunits in PEL13-18 and PEL3-5 respectively as well as control PEL1, PEL12 and host cell lines. mRNA and transcript levels of PDH subunits could have also been looked

at but due to time constraints weren't investigated until batch cultures detailed in Chapter 5. gDNA concentration was measured on a Nano-Drop Spectrometer ND-1000 and aliquoted into 25 ng/µl volumes ready for qPCR reactions (see methods section 2.3.10.2).

qPCR primers were designed for each of the PDH subunits, *E1alpha*, *E1beta*, *E2* and *E3bp* as well as each of the tagged target genes with the addition of both N- and C-terminal tags so the sequence ran into or from the tag itself. This would allow the comparison between endogenous and exogenous PDH subunit expression levels. A primer set for the β-actin housekeeping gene was also designed to enable relative gDNA amount analysis and comparisons between cell pools. Primers were designed using NCBI PrimerBLAST which enabled the prediction and avoidance of off target primer interactions. The sequences are in methods section 2.3.10, Table 2.3.3. Initial primer tests were completed to ensure single peaks were generated for the melt curves, suggesting one binding site, and the product run on a 2% agarose gel to ensure the amplicon size was as expected (Appendix Figure 7.1.10). NTCs, non-template controls, were also completed for each primer mix on each qPCR plate to ensure any results seen weren't due to cross contamination of gDNA during preparation of the reaction master mix.

Appendix Figure 7.1.10 shows the resulting amplicons after qPCR reactions with CHOS and CHOK1 host cell gDNA. Primers for β-actin and the *E1alpha*, *E1beta*, *E2* and *E3bp* PDH subunits alongside *PDP* all produced clear single bands of the expected sizes on the gel. Appendix Figure 7.1.11 shows the resulting amplicons after qPCR reactions with CHOS host cell gDNA using the primers for tagged PDH subunits. All primer sets produced clear single bands at the expected sizes when using both CHOS and CHOK1 gDNA (CHOK1 data not shown).

Once the primers had been evaluated, they were used with CHOS and CHOK1 gDNA samples from engineered cell lines expressing individual untagged PDH subunits PEL3-5 and tagged PDH subunits PEL13-18. Sample reactions were run in triplicate with all comparable reactions being run on the same plate to avoid inter-plate variability. Relative quantification was calculated via multiple steps once the Cq values had been determined from the ThermoFisher QuantStudio Design and Analysis Software 2.6.0 following the process described in (Taylor et al., 2019). Figures 3.15.1 to 3.15.3 show the results of the qPCR analysis comparing fold change in gDNA content of PDH subunits compared to β-actin. (*N) or (*C) signals when tag specific qPCR primers are used. Error bars were generated from the standard deviation from each experimental repeat (n=3). A one-way ANOVA was also performed using Dunnett's multiple comparisons test comparing the results to relevant host cells and any significant results with a p value below 0.05 are highlighted. Large variation can be seen throughout the results due to sampling from a cell pool.

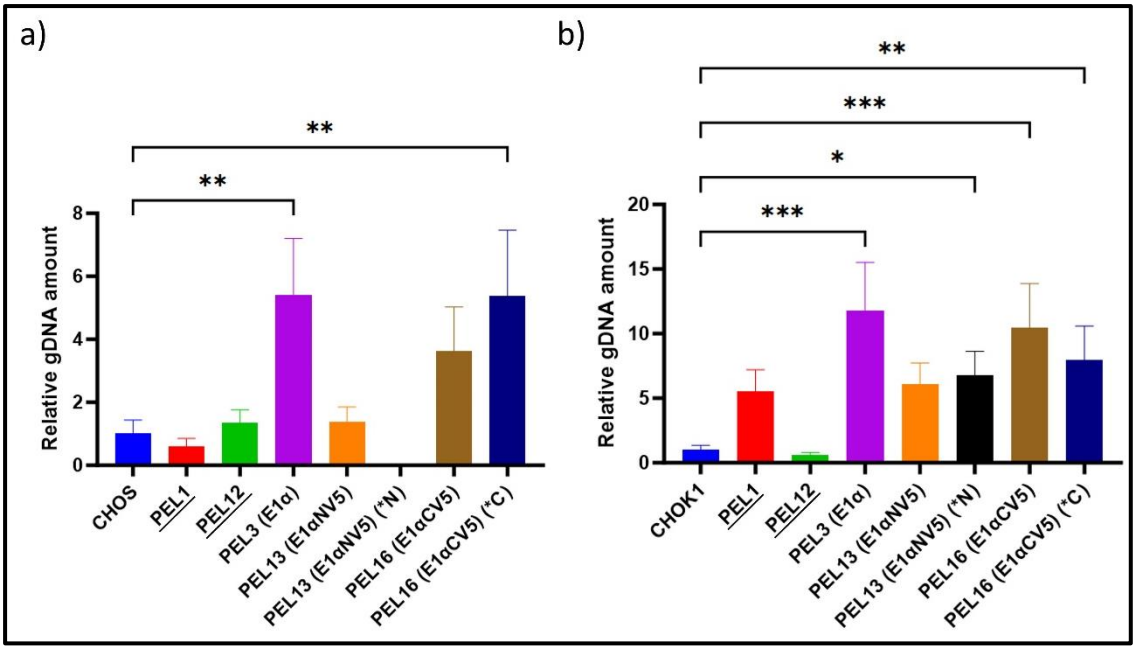

Figure 3.15.1 Fold change in relative gDNA amount of the E1alpha PDH subunit in CHOS and CHOK1 cell pools engineered to stably express E1alpha (PEL3), E1alpha N V5- (PEL13) and C- (PEL16) terminally V5 tagged proteins analysed via qPCR. a) CHOS gDNA samples b) CHOK1 gDNA samples. E1alpha specific primers used throughout unless marked to signify relevant E1alpha specific tag primers used for analysis of tagged PDH subunits (*N)/(*C). A one-way ANOVA was performed using Dunnett's multiple comparisons test comparing the results to relevant host cells. Significance shown for key results where p value was less than or equal to 0.05. Extremely significant p < 0.0001 (****), Extremely significant p = 0.0001 to 0.001 (***), Very significant p = 0.001 to 0.01 (**), Significant p = 0.01 to 0.05 (*), Not significant p ≥ 0.05 (ns). (n=3).

Figure 3.15.1 shows the fold change in amount of the *E1alpha* subunit gene in CHOS (a) and CHOK1 (b) cell pools stably expressing PEL3, 13 and 16, all containing additional copies of the *E1alpha* gene with and without the presence of an N- or C-terminal V5 tag. CHOS cells expressing control plasmids PEL1, empty cassette vector, and PEL12, empty cassette tag vector, show variation in the amount of the *E1alpha* gene with lower amounts in the PEL1 cells and higher amounts in the PEL12 expressing cells. These controls demonstrate the variability expected when sampling from a cell pool but are not significant suggesting no obvious impact on relative *E1alpha* gDNA amount when expressing either empty control plasmid when compared to the host cell line. CHOS cells engineered to express the untagged *E1alpha* gene in PEL3 showed a large increase in gDNA amount with a five-fold change in the amount of *E1alpha* gDNA when compared to the CHOS host cells. Again, variation was seen within the sample, shown by the large error bars, but a significant increase in the amount of target *E1alpha* gene is shown. Cells engineered to express the N-terminally V5 tagged *E1alpha* gene in PEL13 showed a small increase in gene amount but little to no presence of the tagged gene when using the N -terminally tagged *E1alpha* primer set (*N). Cells engineered to express the C-terminally V5 tagged *E1alpha* gene in PEL16 showed a large increase in the amount of the *E1alpha* gDNA

compared to host cell lines for when using both the untagged and C-terminally tagged (*C) primer sets. However, only the increase when using the C-terminally tagged (*C) primers is shown to be significant. Here, a similar five-fold increase in gene content when compared to the cell pool expressing untagged E1alpha in PEL3.

CHOK1 cell pools engineered to stably express *E1alpha* containing PEL3, 13 and 16 showed similar increases to *E1alpha* gene amounts. The CHOK1 control empty cassette cell line PEL1 however had a large increase in *E1alpha* gene amount compared to both the host cell and those expressing PEL12 which had a decreased gene amount. This was not seen in the equivalent CHOS cell lines but was shown to not be significant. The potential cause is unclear as similar relative gDNA amounts should be expected in all host and transfected controls. PEL3 cell pools engineered to express the untagged *E1alpha* PDH subunit gene showed a large and significant increase of almost twelve-fold in comparison to host cell lines of the target gene. Both N- and C-terminally V5 tagged engineered cell lines, PEL13 and 16 respectively, showed a large increase in *E1alpha* gene amount with and without the addition of the tag with the significance of the increase varying between cell lines.

All CHOS and CHOK1 cell pools showed increased relative gene amounts of the *E1alpha* PDH subunit after transfection with the *E1alpha* containing plasmids PEL3, 13 and 16. Cells engineered to express the C-terminally V5 tagged *E1alpha* PDH subunit in PEL16 showed the greatest fold change. Large variation was seen within the gene amounts and the significance, but this is likely due to sampling from cell pools.

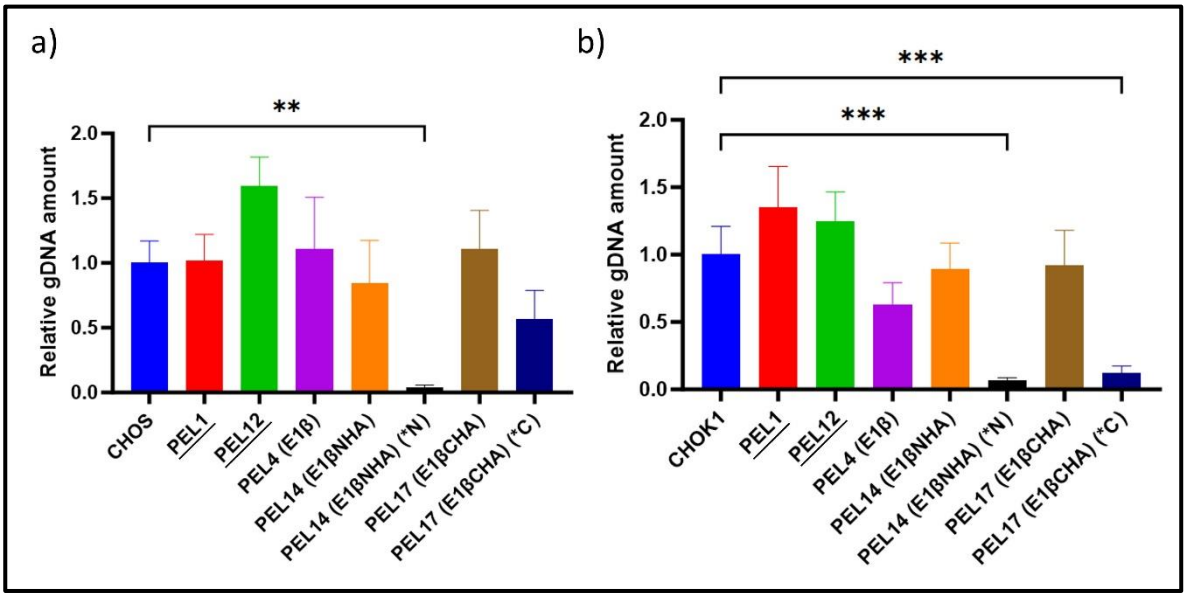

Figure 3.15.2. Fold change in relative amount of the E1beta PDH subunit in CHOS and CHOK1 cell pools engineered to stably express E1beta (PEL4), E1beta N HA- (PEL14) and C- (PEL17) terminally tagged proteins analysed via qPCR. a) CHOS gDNA samples b) CHOK1 gDNA samples. E1beta specific primers used throughout unless marked to signify relevant E1beta specific tag primers used for analysis of tagged PDH subunits (*N)/(*C). A one-way ANOVA was performed using Dunnett's multiple comparisons test comparing the results to relevant host cells. Significance shown for key results where p value was less than or equal to 0.05. Extremely significant $p < 0.0001$ (****), Extremely significant $p = 0.0001$ to 0.001 (***), Very significant $p = 0.001$ to 0.01 (**), Significant $p = 0.01$ to 0.05 (*), Not significant $p \geq 0.05$ (ns). (n=3).

Figure 3.15.2 shows the fold change in *E1beta* PDH subunit gene in CHOS (a) and CHOK1 (b) cell pools engineered to stably express PEL4, 14 and 17 all containing additional copies of the *E1beta* gene. CHOS cells stably expressing control plasmid PEL1, empty cassette vector, showed a similar *E1beta* gene amount whilst the PEL12, empty cassette tag vector, cell pool showed an increase in *E1beta* gene amount however this was shown not to be significant. Again, these control cell lines do not have additional copies of the *E1beta* gene so should have a relative gDNA similar to host cells. PEL4 cell pools expressing the untagged *E1beta* gene showed a small increase in *E1beta* gene amount but this was similar to the increase in control cell pools PEL1 and PEL12. This is especially apparent looking at the variation in the error bars for these samples. Cell pools stably expressing N-terminally HA tagged *E1beta* PDH subunit genes in PEL14 showed an apparent reduction in *E1beta* gene amounts which was shown to be significant. Whilst PEL17 (E1βCHA) cell pools showed a small increase in relative E1beta gDNA amount with results suggesting up to 50% of that was due to the presence of exogenous C-terminally HA tagged E1beta subunit gDNA.

The CHOK1 cell pools showed a similar pattern in *E1beta* gene amounts to the results seen for the CHOS cells in Figure 3.15.2. Control cell lines expressing PEL1 and PEL12 showed a small increase in

E1beta gene amount relative to host cells and similar to the CHOS control cells, was shown not to be significant. Cell pools stably expressing PEL4, untagged E1beta subunits, showed an apparent reduction in *E1beta* gene amount that was matched by the small apparent reduction of those expressing N- and C-terminally HA tagged *E1beta* genes. Neither of the tagged cell pools showed an increase in *E1beta* gene levels and the appropriate tag primers showed significantly low presence of the respective tagged *E1beta* genes. The PEL4, 14 and 17 expressing CHOS and CHOK1 cells showed varied impact on *E1beta* gene amounts but little increase compared to the host and transfected control cell lines.

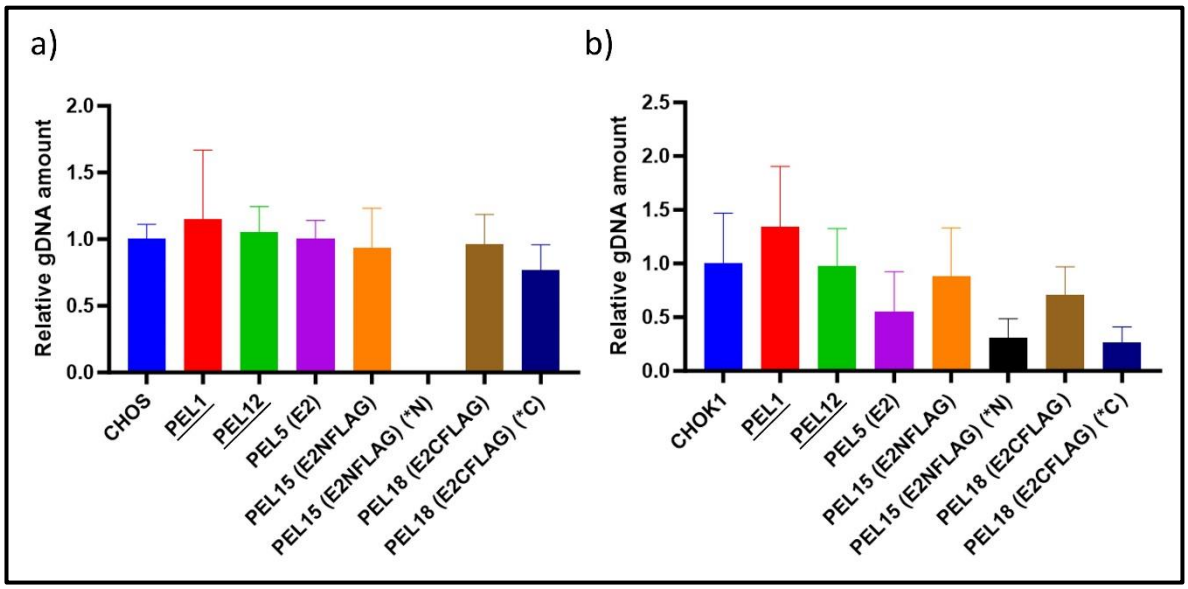

Figure 3.15.3. Fold change in relative amount of the E2 PDH subunit in CHOS and CHOK1 cell pools engineered to stably express E2 (PEL5), E2 N FLAG- (PEL15) and C- (PEL18) terminally tagged proteins analysed via qPCR. a) CHOS gDNA samples b) CHOK1 gDNA samples. E2 specific primers used throughout unless marked to signify relevant E2 specific tag primers used for analysis of tagged PDH subunits (*N)/(*C). A one-way ANOVA was performed using Dunnett's multiple comparisons test comparing the results to relevant host cells. Significance shown for key results where p value was less than or equal to 0.05. Extremely significant $p < 0.0001$ (****), Extremely significant $p = 0.0001$ to 0.001 (***), Very significant $p = 0.001$ to 0.01 (**), Significant $p = 0.01$ to 0.05 (*), Not significant $p \geq 0.05$ (ns). (n=3).

Figure 3.15.3 shows the fold change in the amount of the *E2* PDH subunit gene in CHOS (a) and CHOK1 (b) cell pools stably expressing PEL5, 15 and 18. All contain additional copies of the *E2* gene. CHOS cells stably expressing control plasmids PEL1 and PEL12 showed similar amounts of *E2* gene when compared to host cell lines. Cells expressing the untagged *E2* gene in PEL5 showed gene amounts equal to the control whilst cells expressing N- and C-terminally FLAG tagged E2 genes in PEL15 and PEL18 respectively showed similar gene amounts. The results for the PEL15 N-terminally tagged E2 expressing cells were undefined when using the specific N-terminal E2 primer set. The C-

terminal tag specific E2 primer set showed an apparent small reduction in gene amount for the PEL18 cells but this was shown not to be significant.

CHOK1 cells expressing the tagged and untagged E2 genes in PEL5, 15 and 18 showed different results when compared to the CHOS equivalent cell pools. PEL1 and PEL12 control cell pools showed increased and comparable levels of *E2* gene, respectively similar to the amount for CHOS control cell pools. PEL5 cells expressing the untagged *E2* gene showed apparently half the amount compared to the host cell line however this was shown not to be significant. Similarly, the tagged PEL15 (E2NFLAG) and PEL18 (E2CFLAG) stably expressing cell pools showed a reduction in *E2* gene levels. This was seen again when using the specific tagged *E2* gene primer sets which showed an apparent large reduction to about a third of the *E2* gene amount seen in host cell lines. None of these reductions in relative E2 gDNA amounts were shown to be significant when compared to host cells.

Both sets of cell pools showed a large amount of variability in the qPCR results which is likely due to the sampling from cell pools. CHOS cells show a maintenance of E2 gene amounts when compared to the host cell lines for all constructs. CHOK1 cell lines however all suggest an apparent reduction in E2 gene amount whilst stably expressing E2 containing PEL5, 15 and 18 however not significantly.

The qPCR results showed varied results regarding the over expression of the different subunits of the PDH complex with and without the presence of N- or C-terminal tags. CHOS cells showed the greatest increase in relevant PDH subunit amounts when compared to CHOK1 cell lines. Further work in Chapter 5 explores and describes any impact of over-expression of the subunits on cell growth and culture viability as well as recombinant protein production and metabolism in CHOS and CHOK1 cell lines stably expressing the recombinant DNA detailed in this Chapter.

3.16 Discussion

This Chapter aimed to establish CHOS and CHOK1 cell pools stably expressing recombinant DNA containing genes encoding for target PDH subunits leading to an increase in their expression. Multiple cassette vectors containing *E1alpha*, *E1beta* and *E2* PDH subunit genes were created individually and in different combinations to investigate if expression of any, or all the subunits impacted expression of the PDH complex as a whole. These were first transiently expressed and then used to generate stable cell pools expressing these genes in both CHOS and CHOK1 hosts. Expression levels were investigated using western blot analysis to identify any impact on protein

expression but no clear increase in expression levels were observed in any transient or stable pools. To allow the identification of exogenous recombinant protein expression compared to endogenous, N- or C-terminal tags were added to each of the PDH subunit genes. A V5 tag in the first cassette with *E1alpha*, a HA tag in the second cassette with *E1beta* and a FLAG tag in the third cassette with *E2*. Alongside cell pools stably expressing a mutant *E1alpha* with a C- terminal V5 tag (PEL19) were generated with the serine residues, the targets of phosphorylation via PDKs resulting in PDH complex deactivation, mutated to alanine residues. This was designed to prevent enzyme deactivation via the activity of PDKs aiming to increase PDH activity and limit regulation. A point mutation upstream of site 3 was discovered through Sanger sequencing which resulted in change of a leucine to a phenylalanine residue. These amino acids both have polar groups but differ in size due to the presence of a phenol ring in phenylalanine. As the aim of the mutant E1alpha subunit in PEL19 was to prevent the activity of PDKs to phosphorylate and inactivate the PDH complex, it was assumed that any resulting disruption to the regulation site because of the presence of a phenol ring may work as an advantage to prevent phosphorylation whilst the polar nature of phenylalanine would allow normal complex folding. It was because of this and timing constraints that the choice was made to continue with the construct generating stably expressing cells.

Once the cell pools were generated that stably expressed tagged PDH subunits, the levels of protein expression were investigated using western blot analysis. Blots were probed with the PDH antibody cocktail and the relevant anti-tag antibody to identify differences between endogenous and exogenous protein expression. The full list of constructs and the relevant target gene and tag are listed in Table 3.8.1. When probing with relevant anti-tag antibodies, expression of PDH subunits with an N-terminal tag (PEL13, 14 and 15) were less frequently visible on western blots when compared to cells stably expressing PDH subunits with a C-terminal tag (PEL16, 17, 18 and 19). The differences between the location of the tag could suggest that addition to the N-terminus of the protein is detrimental to expression and may be impacting interactions with untagged endogenous PDH subunits. This pattern was seen for experiments in both CHOS and CHOK1 cells. Importantly, there was a faint band for the C-terminally tagged *E1alpha* mutant expressing cells when probed with the anti-V5 antibody. This suggests the point mutation in the sequence was not impacting protein expression however could still interfere with its ability to integrate with endogenous PDH proteins to form the complete and active complex. This result was seen for the CHOS cells only with no band seen for CHOK1 *E1alpha* mutant (PEL19) expressing cells.

An immunoprecipitation experiment using magnetic beads was used to identify whether the expressed tagged PDH subunits were able to join with endogenous subunits to form functional PDH complexes. Results varied from this process with the CHOS cells expressing either N- or C-terminally

tagged *E1beta* in PEL14 and PEL17 respectively clearly showing protein bands indicating the presence of multiple PDH subunits detached from the beads after boiling. However, multiple protein bands of expected sizes were also seen for the control samples, whilst very faint or no bands were seen for most other samples and in repeats of the experiment. No bands were seen for either of the *E1alpha* mutant expressing cell pools PEL19 suggesting the presence of the mutation does not prevent the protein from being expressed but is detrimental to its ability to incorporate and form PDH complexes with endogenous PDH subunits. It could be suggested that the addition of the tags to the PDH subunits interferes with expression, however tags have been used previously when added to the N-terminus when expressing PDH subunits although this was mainly for purification purposes (Jiang et al., 2014).

To investigate whether gDNA expression was impacted by the exogenous expression of PDH subunits, qPCR was used. Primers were designed for each of the target PDH subunits and their tagged counterparts. Comparison to the housekeeping gene β-actin enabled the comparison between cell pools. Variation was seen in all the qPCR data which is likely the result of using cell pools where natural variation in expression will occur even after selection pressure is applied. An increase to target PDH subunit gDNA amounts was seen resulting from the expression of relevant subunits, however this varied and was often not significantly different to host cell lines or control transfected cell lines PEL1 and PEL12. CHOS cells showed the largest impact to gDNA amounts resulting from the expression of tagged and untagged PDH subunits.

The results in this thesis chapter successfully describe the generation of PDH subunit overexpressing cell pools however the resulting impact to protein and gDNA varied. The generated cell pools were used to investigate the impact overexpression of the PDH subunits had on recombinant protein production of DTE protein Etanercept, which is detailed in Chapter 5 of this thesis. A wider discussion of all results presented in the results chapter can also be found in Chapter 6 of this thesis.

Chapter 4: Investigating the Impact of CRISPR/Cas9 KO of PDKs 1-3 on CHO Cell Growth and PDH Expression

4.1 Introduction

As outlined previously in the introduction chapter of this thesis, PDKs are important kinases that post-translationally control PDH activity through its phosphorylation which acts to inactivate the PDH complex. The PDH complex acts to convert pyruvate to acetyl-CoA which can then enter several metabolic pathways such as the TCA cycle and lipid or amino acid biosynthesis. PDH activity also channels pyruvate away from the conversion to lactate via the activity of LDH. Lactate is considered a waste product and can accumulate, negatively impact cellular culture (Dean & Reddy, 2013). The E1alpha subunit of the heterotetrametric E1 PDH subunit has three serine residues that are targeted by the PDKs for the phosphorylation based control (S. Zhang et al., 2014). Phosphorylation of just one of the six total serine residues in the E1 subunit is enough to inactivate the enzyme complex. (Holness & Sugden, 2003). The activity of PDPs is required to dephosphorylate and reactivate the PDH complex. PDK activity therefore impacts the metabolic flux of glucose into pyruvate and lactate or acetyl CoA and the TCA cycle. In order to maintain the ability of active PDH to convert pyruvate to acetyl CoA, reduction of PDK activity is required. Knock down or out of the kinases that inactive the enzyme complex was therefore hypothesised to be one approach by which silencing or inactivation of the PDH complex could be avoided. This approach was undertaken with the aim of increasing the metabolic flux from pyruvate to acetyl CoA, rather than pyruvate being converted to lactate via the activity of LDH.

As described in the introduction, there are 4 PDKs that act to phosphorylate PDH but PDK 4 is reported to be expressed at low amounts in CHO cell lines (M. Zhou et al., 2011). Therefore PDKs 1-3 were targeted for CRISPR/Cas9 KO with PDK1 and 2 as the initial focus. The CRISPR/Cas9 process used in this study utilised a paired approach with gRNAs designed approximately 500 bp up and downstream of the gene of interest with the aim of removal of the whole target gene rather than simply introducing a mutation, deletion, or frameshift (Schmieder et al., 2018). These approaches can result in the production of an inactive protein which could in itself result in misfolded protein expression and further stress on the cell and endoplasmic reticulum so complete removal of the target gene is preferable. Multiple gRNA pairs were designed for each PDK target extending to PDKs 1-3 and were then transfected into both CHOS and CHOK1 cell hosts. These cell lines act as industrially relevant hosts with different phenotypes and genotypes when producing recombinant protein. Analysis of both gDNA and RNA was used to select the most suitable gRNA pairs that exhibited the most successful KO of target PDK expression. The PDKs were targeted separately

alongside the attempted creation of a triple knock out cell pool with all three gRNA pairs transfected at once. Once knock out cell pools had been generated, multiple techniques were used to sort the cells with fluorescence activated cell sorting (FACS) used to generate cell pools. Western blots and qPCR were used to confirm the KO of PDKs at the protein and gDNA levels respectively. Finally, the impact on PDH complex expression was investigated upon PDK KO using the qPCR primers from Chapter 3 of this thesis. This work aimed to determine if there were any impacts on PDH expression resulting from the KO of the target PDKs as a result of the cell trying to maintain a flux of pyruvate metabolism.

4.2 Aims of this Chapter

This chapter details the design of multiple CRIPSR/Cas9 gRNA pairs targeting PDKs 1 and 2 and the cloning approach to introduce them into an Addgene sourced Cas9 vector. These constructs were then transiently transfected into both CHOS and CHOK1 cell lines and the KO efficiency investigated by qPCR to select the best gRNA sequences. This process was then repeated with the addition of gRNA pairs targeting PDK3. The KO efficiency was compared to previous experiments and the impact on PDH subunit expression investigated. Limited dilution cloning was carried out alongside FACS based sorting in an attempt to isolate individual cells and candidates that could be screened to identify cells/populations with the most efficient KO to be isolated and carried forward. Analysis of PDK protein and genomic DNA was undertaken to identify the impact of the KO on the PDH complex and overall culture viability. Ultimately the cells would be assessed with regard to any impact on PDK KO/down on model difficult to express protein production.

The overall aims of the chapter were therefore to:

a. Design gRNA pairs for the KO of PDKs 1, 2 and 3 and clone these into the Addgene sourced Cas9 vector
b. Transiently express gRNAs in CHO cells and analyse the efficiency of the KO using qPCR to select the best pairing
c. Sort cells from pools to allow cells and population with the ‘best’ KO to be isolated
d. Analyse any impact of KO/knockdown of the PDKs on CHO cell growth and the PDH complex

4.3 Design of PDK1 and PDK2 gRNAs and assembly into the Cas9 plasmid backbone

To enable the CRIPSR Cas9 targeted KO of *PDKs 1* and *2*, the sequences of the genes were first identified using the CHOgenome J Browse Genome viewer. The transcript was compared to the most recent genome sequence using BLAST allowing the chromosome number, sequence and scaffold to be identified. A sequence of around 500 to 1000 bp either side of the gene of interest was imported into SnapGene ready for annotation with gene exons, introns and the gene start and end sites.

The CCTop- CRISPR/Cas9 prediction tool was then used to design gRNA sequences of 20 nucleotides, needed for Cas9 recognition, as well as a NGG PAM type for the *Streptococcus pyogenes* Cas9 in the pX458 vector (pSpCas9(BB)-2A-GFP, #48138, Addgene. The additional nucleotides CACC and AAAC were added to the forward and reverse sequences respectively to encode a *BbsI/BpiI* restriction site to enable Golden Gate assembly cloning into the pX458 vector after annealing and phosphorylation of the oligos. A guanine nucleotide was also placed at the start of the sequence to accommodate the use of a U6 promoter at the start of the gRNA scaffold (see Table 2.5.2 in methods section 2.5). Forward and reverse single stranded DNA oligo sequences were ordered from IDT and then annealed and phosphorylated, forming double stranded DNA sequences ready for Golden Gate assembly cloning. The entire process is detailed in methods section 2.5.1. Multiple guide pairs were designed for each target gene both up and downstream to enable the selection of gRNA pair generating the most efficient KO. It is important that the gRNAs work as pairs to cut either end of the targeted DNA to enable the removal of the entire gene sequence. There are multiple potential outcomes if only one of the gRNA pairs results in a DSB at the target site. The site may be repaired leaving no trace of the DSB maintaining target gene expression or the site may be repaired using NHEJ resulting in a mutation at the target site such as an insertion or deletion. These mutations can result in the continued expression of a functional target gene or the expression of a mutated protein of interest which can result in increased protein aggregation leading to increased cellular stress. Alternatively, these mutations can result in a reduction in the amount of gene expression however not a complete KO of the target. It is therefore preferable that both gRNAs cut efficiently to result in DSBs and the complete removal of target gene expression to create a target KO cell pool. The sequences of all screened gRNAs are listed in Table 2.5.2 in methods section 2.5.1. Figures 4.3.1 shows the positions of the target gRNA pairs up and downstream of the PDK gene sequences.

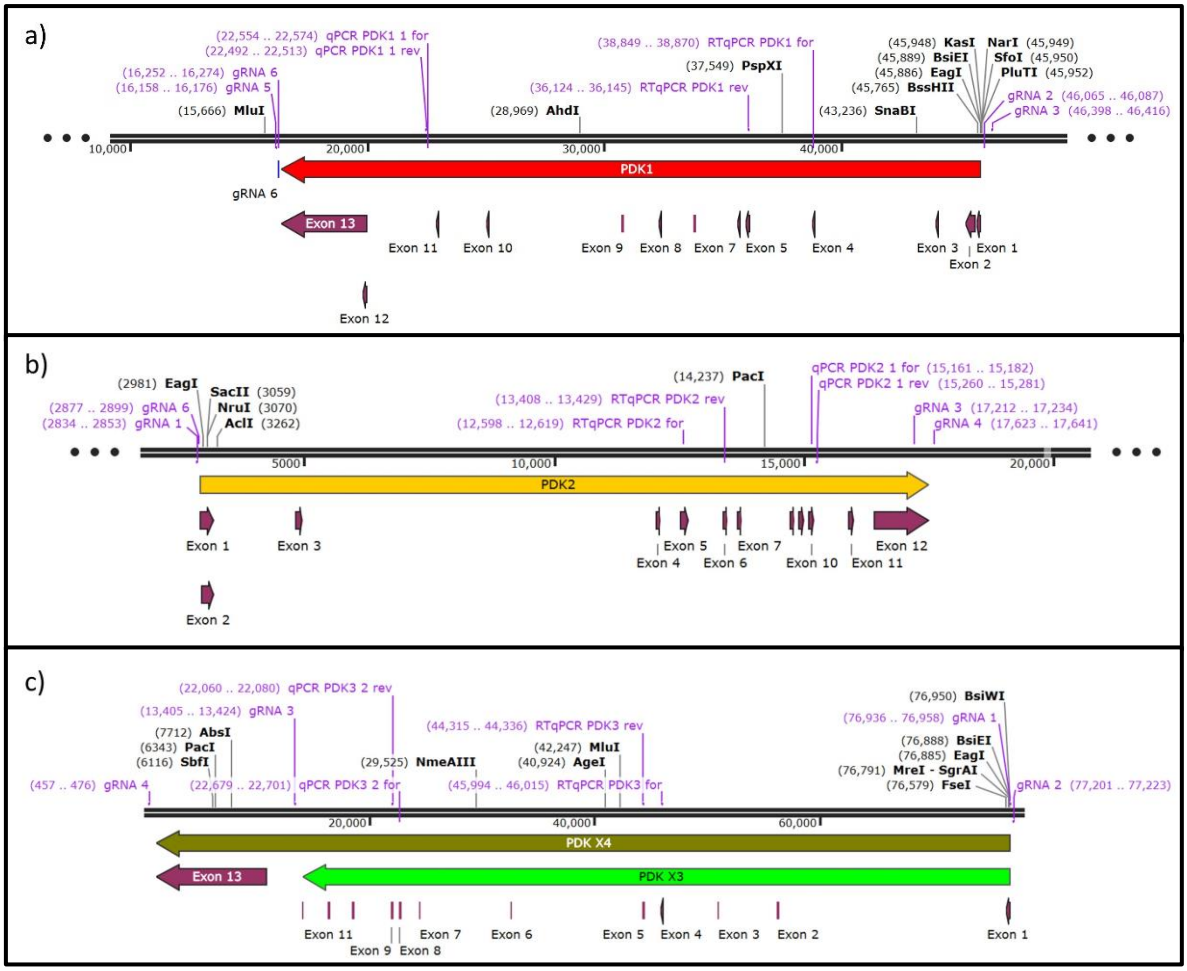

Figure 4.3.1 gRNA positions for targeted CRISPR/Cas9 double strand breaks aiming to knockout target PDK genes of interest resulting in a reduction of expression and therefore activity. a) PDK1 sequence with gRNAs 2 and 3 targeting upstream and 5 and 6 targeting downstream of the PDK1 target gene. b) PDK2 sequence with gRNAs 1 and 6 targeting upstream and 3 and 4 targeting downstream of the PDK2 target gene. c) PDK3 sequence variants X3 and X4 with gRNAs 1 and 2 targeting upstream, 3 targeting downstream of the PDK1 X3 variant and gRNA 4 targeting downstream of the X4 target gene variant. Also shown are the relevant qPCR and RTqPCR primers for each target.

Alongside the PDK KO experiments, the KO of a 150.7 kb section of the *Fut8* gene using sequences detailed in (Schmieder et al., 2018) was undertaken and acted as a positive control for the newly designed PDK gRNA sequences and the efficiency of both transfection and KO. The sequences of the *Fut8* gRNAs are detailed in Table 2.5.2 in methods section 2.5.1.

Once the oligos were annealed into double stranded gRNA sequences, they were ready for Golden Gate assembly into the pX458 vector following the steps detailed in methods section 2.5.2. One plasmid was generated for each annealed gRNA for use in a double transfection with DNA vectors prepared via minipreps before Sanger sequencing was used to confirm successful insertion into the pX458 vector.

4.4 Analysing Transient Transfection Efficiency of Cas9 Vectors into CHOK1 cells using Flow Cytometry

After sequencing, the Cas9 vectors were prepared via maxi prep ready for transient transfections. The vector contains a cassette for expression of GFP which can indicate transfection efficiency and those cells that have been successfully transfected. 10 µg of each gRNA DNA plasmid was used in combination for transfections into CHOK1 cells with one upstream targeting and one downstream targeting gRNA used. A 100 µl total volume of $5x10^6$ cells mixed with the appropriate target gRNA DNA was transfected using the Invitrogen Neon Transfection System with one pulse at a width of 20 ms at 1700 V. Cells were kept in a static incubator for one to two hours post transfection before being moved to a shaking incubator. Cell counts were completed the day after transfection to check culture viability.

On the third day after transfection, cell pool samples were taken for analysis of GFP expression using the CytoFLEX and associated CytExpert software. The results indicate the relative levels of expression of the GFP protein from transfection of the pX458 vector and give an estimation of transfection efficiency of the gRNAs. GFP expression does not accurately reflect the effectiveness expected of the KO as expression of the Cas9 complex would not guarantee cutting of the DNA and subsequent KO of the target gene after DNA repair. The flow cytometry analysis gives an indication of expected Cas9 activity to initially aid screening for successful KO cells via sorting based on GFP expression, but further screening is required. The data allows a comparison of the different gRNA sequences designed to PDKs to the known Fut8 gRNAs at an early stage in the process. Figures 4.4.1 and 4.4.2 show the fluorescence intensities of 10,000 events recorded from CHOK1 KO cell samples measured at 488 nm with the percentage of those cells expressing above the level of autofluorescence after gating at 10^4 based on CHOK1 host cells (i) and the mean fluorescence of all cells measured (ii). The histograms for all the results can be seen in Appendix Figure 1.

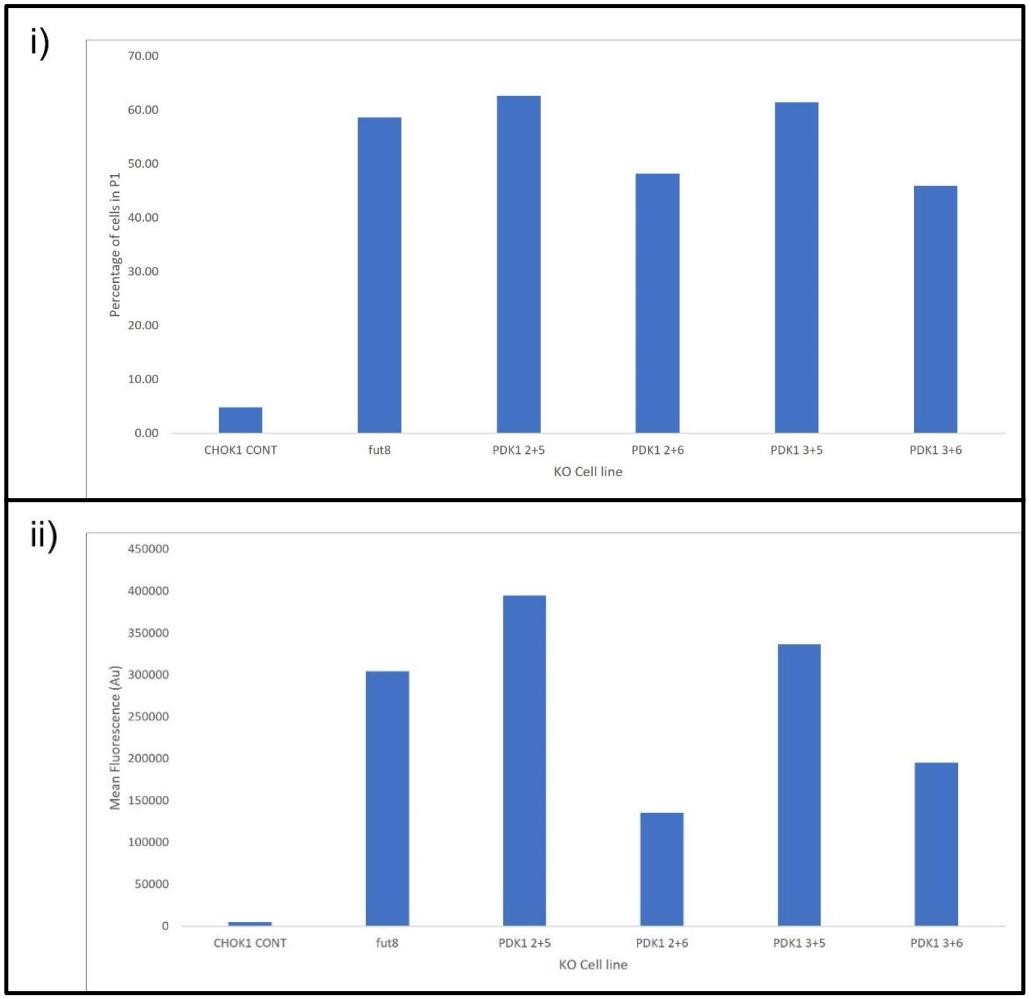

Figure 4.4.1 Flow cytometry analysis of CHOK1 cells transfected with CRISPR/Cas9 plasmids containing the GFP gene and gRNAs targeting either *Fut8* or *PDK1* genes compared to CHOK1 host cells. 10,000 events were measured at 488 nm. i) Percentage of cells over the 10^4 fluorescence intensity (P1) gated based upon CHOK1 host cells. ii) mean fluorescence of all cells measured.

Figure 4.4.1 shows the flow cytometry analysis of CHOK1 cell pools after transfection with Cas9 gRNAs targeting PDK1. Compared to the control cells, a large percentage of all cells transfected were fluorescing above the threshold of 10^4 in all transfections (i). The combination of gRNAs 2 + 5 and 3 + 5 had a higher percentage of cells above the threshold compared to the known fut8 gRNAs; this does not directly determine expression of the PDK1 gRNAs as previously explained but is a proxy measurement based upon GFP expression. The data suggests good expression of the PDK1 targeting Cas9 plasmids expressing these gRNAs and the potential for KO in these transfected cells. gRNA pairs 2 + 6 and 3 + 6 had a smaller percentage of cells over the fluorescence threshold in the P1 gate but was still much higher than the fluorescence in the CHOK1 host control. The mean fluorescence in (ii) shows a similar result with gRNA pairs 2 + 5 and 3 + 5 having the highest mean fluorescence of all samples compared to both the CHOK1 host cell control and fut8 targeted KO sample. Cells

expressing Cas9 plasmids with gRNA pairs 2 + 6 and 3 + 6 had a lower mean fluorescence compared to the other KO transfection pools. From these results the PDK1 gRNA pair 2 + 5 were selected for future CRISPR/Cas9 KO experiments.

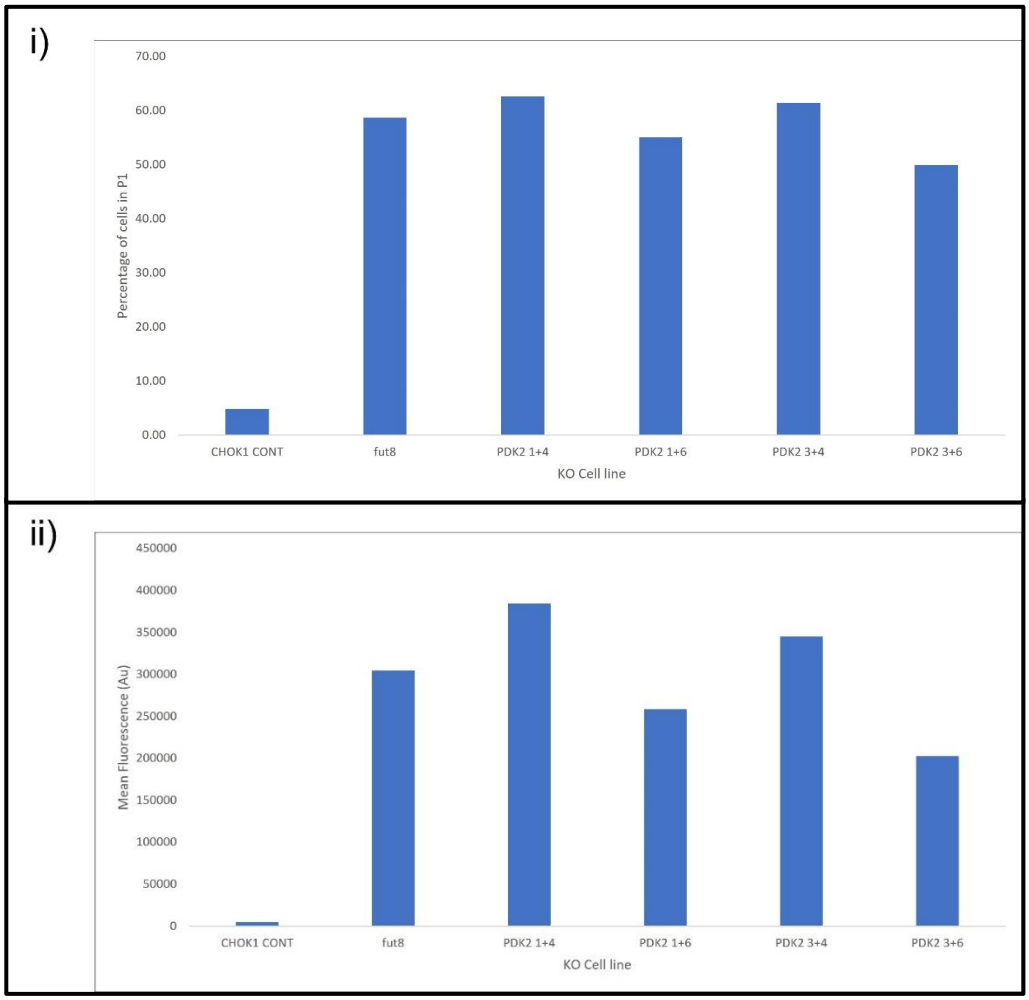

Figure 4.4.2 Flow cytometry analysis of CHOK1 cells transfected with CRISPR/Cas9 plasmids with gRNAs targeting either fut8 or PDK2 genes and with a GFP expression cassette compared to CHOK1 host cells. 10,000 events were measured at 488 nm. i) Percentage of cells over the 10^4 fluorescence intensity (P1) gated based upon CHOK1 host cells. ii) mean fluorescence of all cells measured.

Figure 4.4.2 shows the flow cytometry analysis of CHOK1 cell pools after transfection with Cas9 gRNAs targeting PDK2. All cell pools showed a high percentage of cells over the fluorescence threshold of 10^4 of gate P1 (i) when compared to host cells. gRNA pair 1 + 4 had the highest percentage of cells in P1 closely followed by 3 + 4. gRNA pair 3 + 6 had the lowest percentage of cells in gate P1 but this was higher than the lowest two gRNA pairs 2 + 6 and 3 + 6 targeting PDK1 in Figure 4.4.1. Mean fluorescence (ii) showed a similar result with gRNA pair 1 + 4 having the highest mean fluorescence compared to all other cell pool transfections, suggesting a high

transfection efficiency. gRNA pair 3 + 6 again had the lowest mean fluorescence suggesting the lowest transfection efficiency. From these results PDK2 gRNA pair 1 + 4 were selected for future CRISPR/Cas9 experiments. The flow cytometry results of the fut8 KO transfection in Figures 4.4.1 and 4.4.2 also provide evidence of expression of the Cas9 vector indirectly via GFP expression.

4.5 Evaluation of PDK gDNA in KO Cell Pools using qPCR

Cell pools were passaged four days after transfection and the culture viability checked. To further investigate the success of the transfection and KO, seven days after transfection, gDNA samples were isolated from cell pools using a Qiagen DNeasy Blood & Tissue Kit following the manufacturer's instructions. qPCR primers were designed for each of the *PDK1, 2* and *3* genes (although *PDK3* KO was not undertaken until a later date). These qPCR primers have been designed to amplify inside the target gene sequence, shown in Figure 4.3.1, so if the CRISPR/Cas9 complex and target specific gRNAs have successfully removed the target gene, no binding should occur, preventing amplification of a band of the expected size during the qPCR process. As these are cell pools, a mixture of cells will reflect varying CRISPR/Cas9 efficiencies so at this stage, before sorting of the cells is carried out, a reduction in gDNA amounts is likely to be seen instead of a complete KO. The primer set for the control *β-actin* housekeeping gene was as in Chapter 3, section 3.15 and the Fut8 primer set was that from (Schmieder et al., 2018). For the initial qPCR experiments, primers for the GAPDH housekeeping gene were used as a reference instead of *β-actin* as indicated in the figure legends. These genes are referred to as housekeeping genes due to their relatively constant expression levels in most cells. Involved in cellular function and survival, they act as a base line for the comparison of gene amounts and can help ensure reproducibility between experiment repeats. The use of relative quantification based upon the fold change compared to the housekeeping genes aims to reduce error with the potential to normalise to multiple references. The primer sequences used are described in the methods section 2.3.10, Table 2.3.3. Initial primer tests were completed to ensure single peaks were generated for the melt curves and the PCR products run on a 2% agarose gel to ensure the amplicon size was as expected (shown in Figure 4.3.3).

Sample reactions for the initial PDK1 and PDK2 KO target work were run in quadruplicate in a Qiagen Rotor-Gene Q with all comparable reactions being run at the same time to reduce impact of reaction variability. A SensiFAST™ Real-Time PCR Kit was used following the manufacturer's instructions. Non-template controls (NTCs) were also completed for each primer mix during each run to ensure any amplification products observed weren't due to cross contamination of gDNA. Figure 4.5.1

shows the resulting amplicons from qPCR reactions with CHOS and CHOK1 host cell gDNA. Primers for PDKs 1, 2 and 3 all produced clear single bands of the expected sizes.

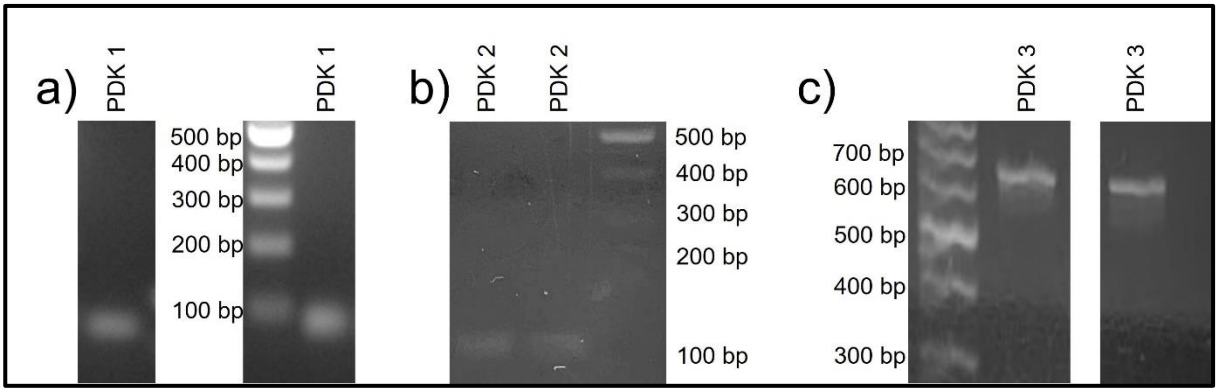

Figure 4.5.1 qPCR products when testing primers for PDK genes with CHOS and CHOK1 gDNA. a) PDK1 primer set tested with CHOS (lefthand lane) and CHOK1 (righthand lane) gDNA with expected band size of 83 bp. b) PDK2 primer set tested with CHOS (lefthand lane) and CHOK1 (righthand lane) gDNA with expected band size at 121 bp. c) PDK3 primer set tested with CHOS (lefthand lane) and CHOK1 (righthand lane) gDNA with expected band size at 642 bp.

Once the primers had been designed and evaluated, they were used with CHOK1 gDNA samples from cells transfected with the PDK1, PDK2 and fut8 Cas9 plasmids containing corresponding target gRNAs. Relative quantification was calculated from the Cq values as determined from the ThermoFisher QuantStudio Design and Analysis Software 2.6.0 following the process described in (Taylor et al., 2019). Figures 4.5.2, 4.5.3 and 4.5.4 show the results comparing fold change in amounts of PDKs 1 and 2 and fut8 compared to GAPDH and control cell lines. Error bars were generated from the standard deviation from each experimental repeat with relevant statistical analysis carried out to show significant results, (specific statistical analysis details are shown in figure legends), (n=4). Complete KO and reduction of gDNA amounts is not expected due to the nature of the cell pools generated, however after cell sorting this would be the target outcome.

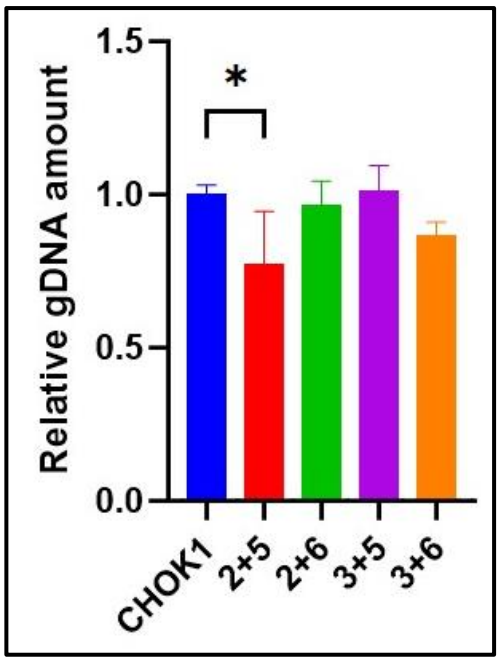

Figure 4.5.2 Relative gDNA amount of PDK1 in CHOK1 cell pools expressing CRISPR/Cas9 KO plasmids with varied combinations of PDK1 targeting gRNAs analysed via qPCR. PDK1 primers used compared to GAPDH levels. A one-way ANOVA was performed using Dunnett's multiple comparisons test comparing the results to relevant host cells. Significance shown for key results where p value was less than or equal to 0.05. Extremely significant $p < 0.0001$ (****), Extremely significant $p = 0.0001$ to 0.001 (***), Very significant $p = 0.001$ to 0.01 (**), Significant $p = 0.01$ to 0.05 (*), Not significant $p \geq 0.05$ (ns). (n=4).

Figure 4.5.2 shows the change in relative amounts of PDK1 gDNA resulting from the CRISPR/Cas9 KO of PDK1 using different gRNA combinations in CHOK1 cell pools compared to unedited cell lines. The combination of gRNAs 2 + 5 resulted in the greatest reduction in PDK1 gDNA amount, which was also shown to be significant, whilst gRNAs 3 + 6 were also successful in reducing PDK1 amounts but to a lesser extent. gRNAs 2 + 6 and 3 + 5 showed very little to no reduction in PDK1 amounts. Further work for KO of PDK1 was therefore undertaken using gRNAs 2 + 5. The results reinforce those shown in Figure 4.3.2.1 whereby the highest fluorescence expression was observed in cells transfected with gRNAs 2 + 5. Interestingly, the next greatest reduction in PDK1 gDNA amounts was in cells transfected with gRNAs 3 + 6 which, in Figure 4.4.1, had the lowest percentage of cells above the fluorescence threshold and the second lowest mean fluorescence. These results show that the flow cytometry analysis alone cannot be used to determine which gRNAs are most appropriate to use to achieve the largest reduction in target gene gDNA amounts.

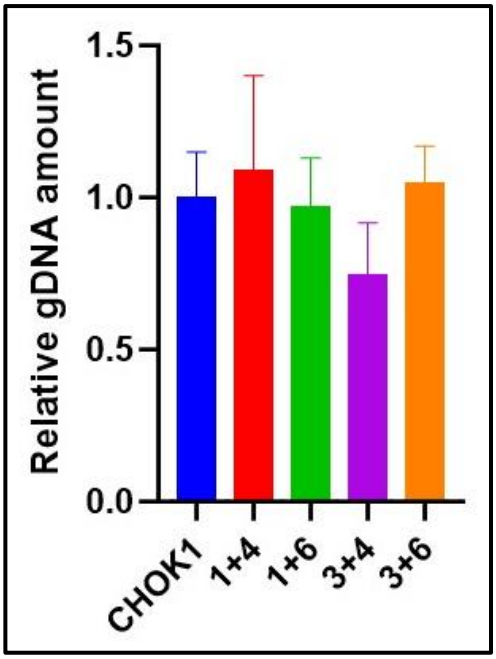

Figure 4.5.3 Relative gDNA amount of PDK2 in CHOK1 cell pools expressing CRISPR/Cas9 KO plasmids with varied combinations of PDK2 targeting gRNAs analysed via qPCR. PDK2 primers used compared to GAPDH levels. A one-way ANOVA was performed using Dunnett's multiple comparisons test comparing the results to relevant host cells. Significance shown for key results where p value was less than or equal to 0.05. Extremely significant $p < 0.0001$ (****), Extremely significant $p = 0.0001$ to 0.001 (***), Very significant $p = 0.001$ to 0.01 (**), Significant $p = 0.01$ to 0.05 (*), Not significant $p \geq 0.05$ (ns). (n=4).

Figure 4.5.3 shows the change in relative amounts of PDK2 gDNA resulting from the CRISPR/Cas9 KO of PDK2 using different gRNA combinations in CHOK1 cell pools compared to unedited cell lines. gRNA combinations 1 + 4, 1 + 6 and 3 + 6 all had little to no impact on PDK2 amounts. The combination of gRNAs 3 + 4 had the strongest impact on PDK2 amounts when compared to the others. Although shown not to be a significant reduction to PDK2 gDNA amounts, it was used for further experiments. These results again were different from the GFP flow cytometry analysis shown in Figure 4.4.2 where the gRNA pair with the largest percentage of cells above the fluorescence threshold and highest mean fluorescence, was the 1+4 gRNA pair.

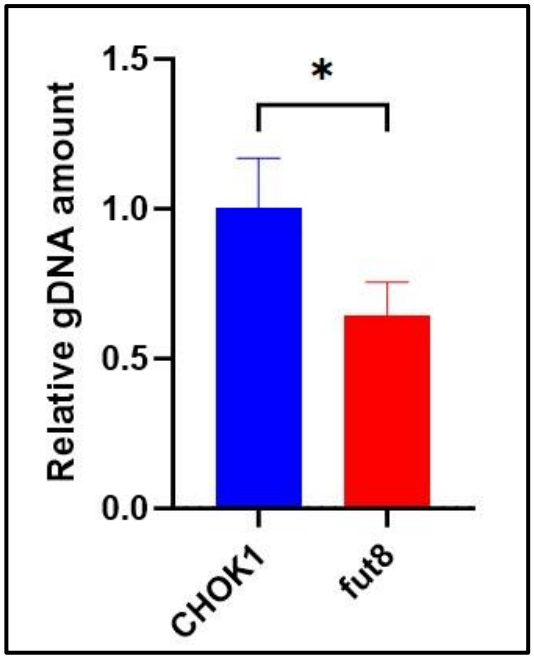

Figure 4.5.4 Relative gDNA amount of fut8 in CHOK1 cell pools expressing CRISPR/Cas9 KO plasmids with fut8 targeting gRNAs analysed via qPCR. fut8 primers taken from (Schmieder et al., 2018) used compared to GAPDH levels. A Welch's t test was performed comparing the results to relevant host cells. Significance shown for key results where p value was less than or equal to 0.05. Extremely significant $p < 0.0001$ (****), Extremely significant $p = 0.0001$ to 0.001 (***), Very significant $p = 0.001$ to 0.01 (**), Significant $p = 0.01$ to 0.05 (*), Not significant $p \geq 0.05$ (ns). (n=4).

Figure 4.5.4 shows the change in relative amount of fut8 gDNA using the known gRNAs from (Schmieder et al., 2018). This was used as a control KO. The KO of fut8 showed a greater reduction in the amount of the target gene compared to the KO of PDKs 1 and 2 in Figures 4.5.2 and 4.5.3. The reduction of fut8 amounts in Figure 4.5.4 is similar to that reported when using the same gRNAs in (Schmieder et al., 2018).

4.6 Evaluation of PDK mRNA Expression in KO Cell Pools using qRT-PCR

To investigate the impact of the KO of PDKs 1 and 2 on mRNA expression, RNA was extracted from the cell pools. For this initial work TRIzol was used to isolate RNA from cell pellets and the RNA samples then purified using a Zymo Direct-zol RNA Miniprep kit following the manufacturer's instructions. qRT-PCR primers were designed for each of the target *PDK 1, 2* and *3* mRNAs across an intron sequence (*PDK3* wasn't targeted for KO until a later date). Initial experiments used primers for the GAPDH housekeeping gene as a reference instead of β-actin. All primer sequences are detailed in section 2.3.10, Table 2.3.3. Initial primer tests were completed to ensure single peaks

were generated for the melt curves and the product run on a 2% agarose gel to ensure the amplicon size was as expected (Figure 4.6.1).

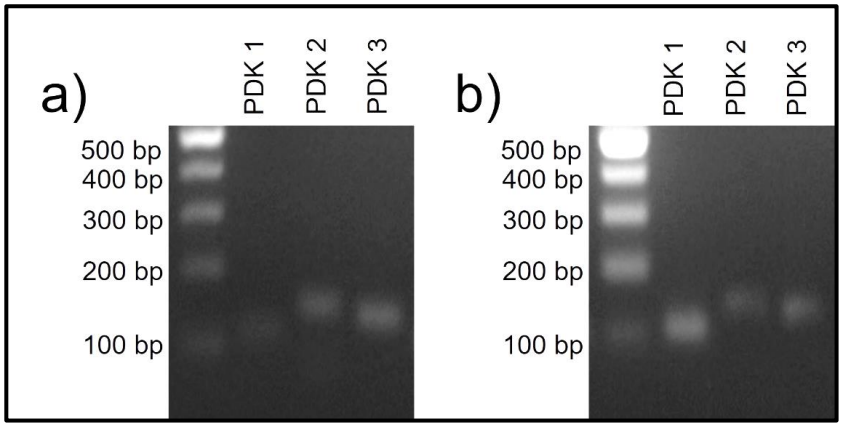

Figure 4.6.1 qRT-PCR products when testing primers for PDK genes with CHOS and CHOK1 RNA. The primer tests were completed using a one-step qRT-PCR reaction. a) CHOS RNA used for reactions. b) CHOK1 RNA used for reactions. PDK1 primer set tested with expected band size of 109 bp. PDK2 primer set tested with expected band size at 144 bp. PDK3 primer set tested with expected band size at 134 bp.

Sample reactions for the initial PDK1 and PDK2 target work were run in quadruplicate in a Qiagen Rotor-Gene Q with all comparable reactions being run at the same time to reduce impact of reaction variability. A SensiFAST™ Real-Time PCR Kit was used following the manufacturer's instructions. Non-template controls were also completed for each primer mix during each run.

Figure 4.6.1 shows the amplicons after qRT-PCR reactions with CHOS and CHOK1 host cell RNA in a one-step reaction. Primers for PDKs 1, 2 and 3 all produced clear single bands of the expected sizes on the gel.

Once the primers had been designed and evaluated, they were used with CHOK1 cDNA samples generated with mRNA from cells transfected with the PDK1, PDK2 and fut8 Cas9 plasmids containing the corresponding target gRNAs. Relative quantification was determined once the Cq values had been established from the ThermoFisher QuantStudio Design and Analysis Software 2.6.0 following the process described in (Taylor et al., 2019). Figures 4.6.2 and 4.6.3 show the results of the analysis comparing fold change in transcript (mRNA) expression of PDKs 1 and 2 compared to GAPDH and control cell lines. Error bars were generated from the standard deviation from each experimental repeat with a one way ANOVA performed using Dunnett's multiple comparisons test comparing the results to relevant host cells (n=4).

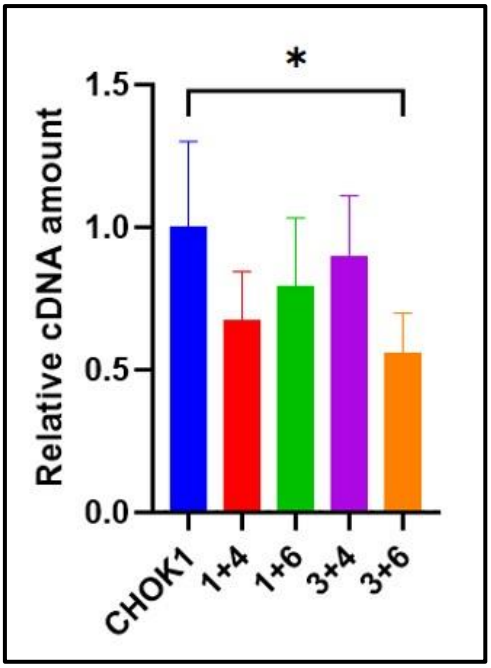

Figure 4.6.2 Relative cDNA amount of PDK1 in CHOK1 cell pools expressing CRISPR/Cas9 KO plasmids with PDK1 targeting gRNAs analysed via qPCR from cDNA samples. PDK1 primers used compared to GAPDH expression levels. A one-way ANOVA was performed using Dunnett's multiple comparisons test comparing the results to relevant host cells. Significance shown for key results where p value was less than or equal to 0.05. Extremely significant $p < 0.0001$ (****), Extremely significant $p = 0.0001$ to 0.001 (***), Very significant $p = 0.001$ to 0.01 (**), Significant $p = 0.01$ to 0.05 (*), Not significant $p \geq 0.05$ (ns). (n=4).

Figure 4.6.2 shows the change in relative PDK1 cDNA expression resulting from the CRISPR/Cas9 KO of PDK1 using different gRNA combinations in CHOK1 cell pools compared to unedited cell lines. Expression levels of PDK1 mRNA were significantly reduced when gRNA combinations of 2 + 5 (by approximately 80%) or 2 + 6 (by approximately 50%) were used. Interestingly, the use of gRNAs 3 + 5 resulted in an apparent increase of PDK1 mRNA expression of over 1.7-fold that in the control cell pool whilst gRNAs 3 + 6 resulted in no change. These results show that the combination of gRNAs 2 + 5 were the most effective in agreement with the flow cytometry data in Figure 4.4.1 and the qPCR in Figure 4.5.2.

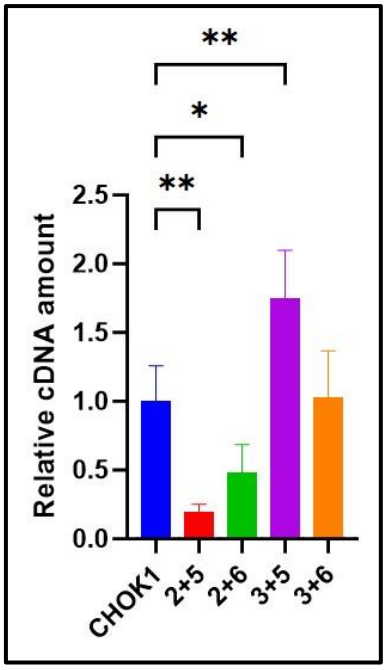

Figure 4.6.3 Relative cDNA amount of PDK2 in CHOK1 cell pools expressing CRISPR/Cas9 KO plasmids with PDK2 targeting gRNAs analysed via qPCR from cDNA samples. PDK2 primers used compared to GAPDH levels. A one-way ANOVA was performed using Dunnett's multiple comparisons test comparing the results to relevant host cells. Significance shown for key results where p value was less than or equal to 0.05. Extremely significant $p < 0.0001$ (****), Extremely significant $p = 0.0001$ to 0.001 (***), Very significant $p = 0.001$ to 0.01 (**), Significant $p = 0.01$ to 0.05 (*), Not significant $p \geq 0.05$ (ns). (n=4).

Figure 4.6.3 shows the fold change in expression of PDK2 resulting from the CRISPR/Cas9 KO of PDK2 using different gRNA combinations in CHOK1 cell pools compared to unedited cell lines with all gRNA pairs resulting in some degree of reduction of PDK2 mRNA amounts. gRNAs 1 + 4 and 3 + 6 gave the greatest reduction in PDK2 mRNA expression with a reduction of 33% and 44% respectively however only the reduction resulting from gRNAs 3 + 6 was shown to be significant. gRNAs 1 + 6 and 3 + 4 gave a smaller reduction in PDK2 mRNA expression levels in comparison. These results suggest gRNA pair 3 + 6 is the best pair for further CRISPR/Cas9 targeted KO of PDK2. This result is contrary to the flow cytometry results in Figure 4.4.2 which suggests gRNAs 1 + 4 followed by 3 + 4 would be the best option, or the qPCR based upon gDNA in Figure 4.5.3 which suggests that the combination of gRNAs 3 + 4 would be best.

Further analysis of the efficiency of the CRISPR/Cas9 KO could have been completed at this stage but as the process was going to be repeated, to also include the CHOS cell line as well as targeting PDK3 for KO, this was not undertaken and the qPCR gDNA and mRNA analysis used as a preliminary screen. The CRISPR/Cas9 experiments were therefore repeated using the same PDK1 and 2 gRNAs to determine if a different gRNA pairs resulted in a stronger KO of PDK1 or 2 activity when using an

alternative transfection system (see methods section 2.3.5) and if any potential impact would result from the targeting of PDK3.

4.7 Repeat of the CRISPR/Cas9 Process in CHOS cells and with addition of PDK3 target gRNAs

The CRISPR/Cas9 process targeting PDKs 1 and 2 was successfully assessed in CHOK1 cells and so was repeated using CHOS cells to allow comparison between different CHO cell hosts and to confirm the most suitable gRNA pair for the KO of PDK3. PDK3 was targeted with gRNA pairs designed following the same process outlined in section 4.3.1. Again, fut8 was used as a control. The details for the transfections are in methods section 2.3.5 and are noted to be different compared to those used in section 4.4 to 4.6.

4.8 Analysing Transient Transfection efficiency of Cas9 vectors into CHOS cells and comparison to CHOK1 cells using Flow Cytometry

Three days after transfection, cell samples were taken for flow cytometry analysis to monitor GFP expression from the Cas9 plasmid. One cell pool was picked for each PDK and fut8 target in each host cell line. Figure 4.3.6 shows the results of the flow cytometry analysis using a FACScalibur™ (BDbiosciences) instrument. Figures 4.8.1 and 4.8.2 show the percentage of cells expressing above the levels of autofluorescence after gating at 10^4 (P1) based on CHOS or CHOK1 host cells (i) and the mean fluorescence of all cells measured (ii).

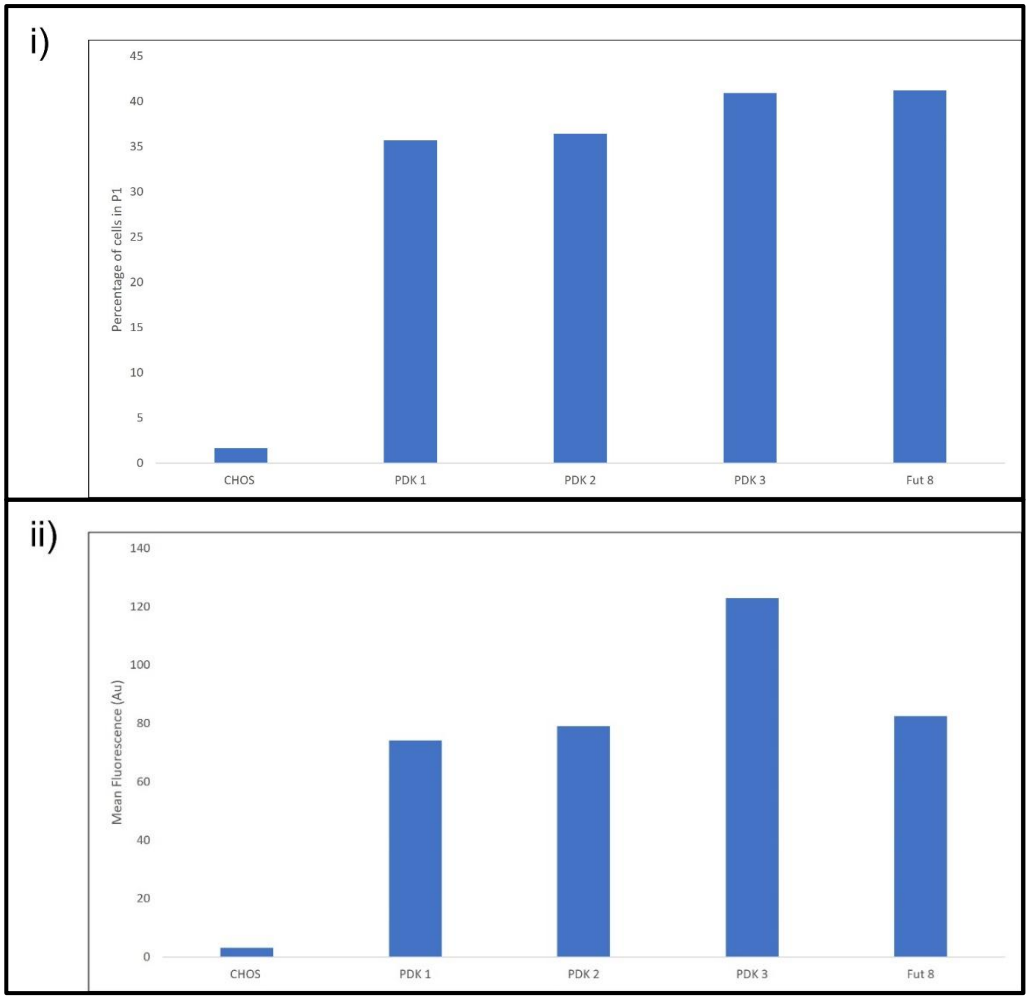

Figure 4.8.1 Flow cytometry of GFP expression from CHOS cell pools transfected with CRISPR/Cas9 gRNAs targeting PDKs 1, 2, 3 and fut8 compared to the control CHOS host cell line. 10,000 events measured at 488 nm. i) Percentage of cells over the 10^4 fluorescence intensity (P1) gated based upon CHOS host cells. ii) Mean fluorescence. PDK1 KO target cells using gRNAs 2 + 6. PDK2 KO target cells using gRNAs 1 + 6. PDK3 KO target cells using gRNAs 1 + 4.

Figure 4.8.1 shows the percentage of cells over the 10^4 fluorescence intensity (P1) gate based upon CHOS host cells (i) and mean fluorescence (ii) from 10,000 events measured from CHOS cell samples transfected with relevant target gRNAs. The flow cytometry data clearly shows all cell pools having a higher average fluorescence when compared to the control cell line. Figure 4.8.1 shows the successful transfection of the Cas9 vector into CHOS cells which would suggest that the CRISPR/Cas9 gRNAs investigated in CHOK1 cells previously should also result in KO of PDKs in the CHOS host cell line. The GFP expression in the fut8 KO CHOS cells was similar to the PDK1 and 2 target gRNA cell

lines. Cells transfected with the newly designed PDK3 gRNA pair 1 + 4 had the highest mean fluorescence in Figure 4.8.1 (ii) compared to the other Cas9 transfected cell pools.

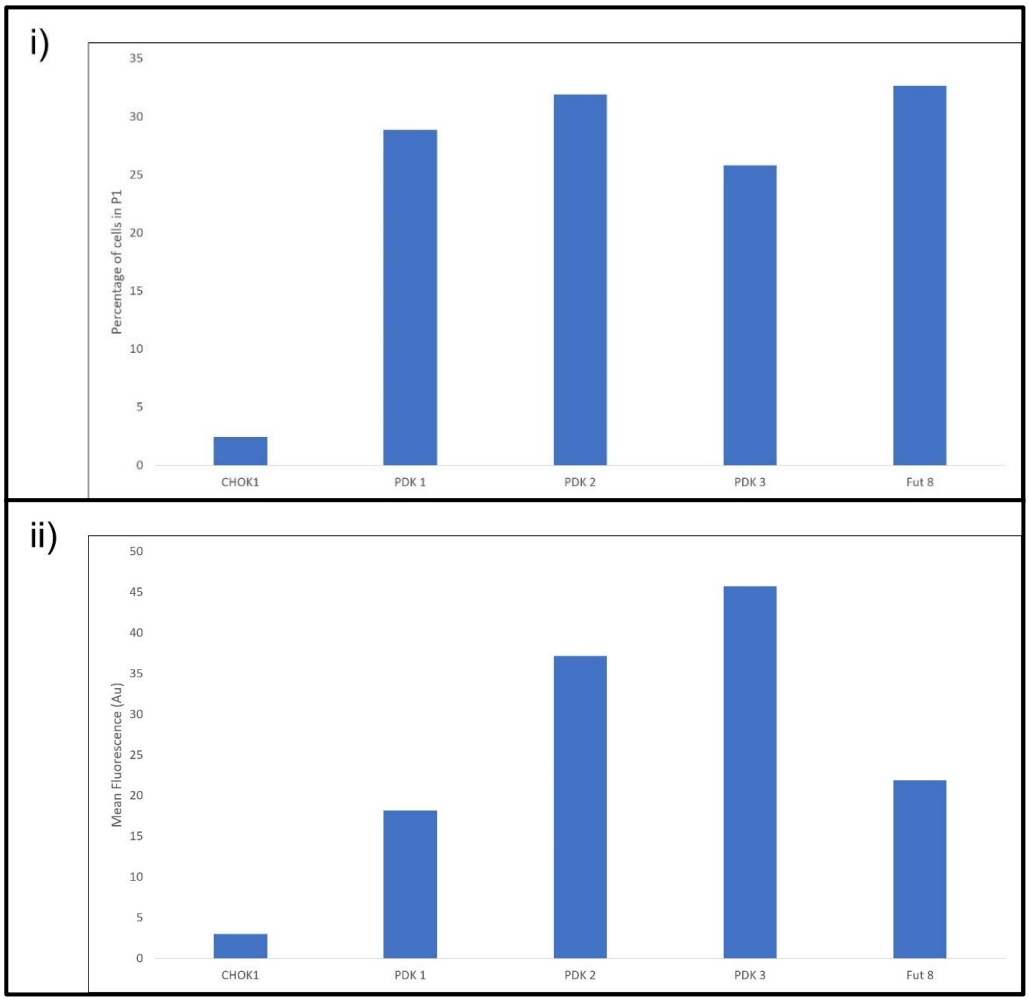

Figure 4.8.2 Flow cytometry results from analysis of CHOK1 cell pools transfected with CRISPR/Cas9 gRNAs targeting PDKs 1, 2, 3 and fut8 compared to control cell lines. 10,000 events measured at 488nm. i) Percentage of cells over the 10^4 fluorescence intensity (P1) gated based upon CHOK1 host cells. ii) Mean fluorescence. PDK1 KO target cells using gRNAs 3 + 5. PDK2 KO target cells using gRNAs 3 + 6. PDK3 KO target cells using gRNAs 2 + 4.

Figure 4.8.2 shows the percentage of cells over the 10^4 fluorescence intensity (P1) gate based upon CHOK1 host cells (i) and mean fluorescence (ii) from 10,000 events measured from CHOK1 cell samples transfected with relevant target gRNAs. All cell pools showed an increase in average fluorescence when compared to the control cell line suggesting the expression of GFP from the Cas9 plasmids. Cells transfected with the PDK3 gRNA pair 2 + 4 had the highest mean fluorescence in Figure 4.8.2 (ii) when compared to the other Cas9 transfected cell pools, similar to the results for the CHOS cell pools in Figure 4.8.1.

Direct comparison to the previous CHOK1 cell line CRISPR Cas9 experiment results in Figure 4.4.1(i) and 4.4.2(i) revealed a lower percentage of cells over the 10^4 fluorescence intensity (P1) gate for all PDK gRNAs. This is likely to be due to the different transfection equipment used between the experiments. Comparing the results of the CHOS Cas9 transfections in Figure 4.8.1 to the CHOK1 Cas9 transfections in Figure 4.8.2 highlights the difference in both the percentage of cells in the P1 gate and mean fluorescence of the cell pools. Transfected CHOS cells had a higher fluorescence, around 2.5 times the amount in transfected CHOK1 cell pools. This may be due to the transfection process which had previously been optimised for CHOS cells. Nevertheless, to keep the process simple, the transfection methodology was kept the same for both cell lines for future experiments.

4.9 Evaluation of PDK gDNA Amounts in KO Cell Pools using qPCR

After the flow cytometry data confirmed the expression of GFP from transfection of the Cas9 plasmids into the CHOS and CHOK1 cells, further investigation into the KO of the PDKs was undertaken. Cells were passaged four days following the transfection and samples for protein, gDNA and mRNA analysis were taken eight days after transfection. Cells were then banked down using cryopreservation following the steps in method section 2.3.3. Culture viabilities varied between cell pools and repeats but at least one pool of each transfection was cryopreserved.

qPCR analysis of the KO impact used the same primer sequences as those used previously to target the PDK1, 2 and 3 genes. Section 4.5 describes the primer design process with Figure 4.5.1 showing the initial primer tests and amplicon sizes after running the qPCR products on a 2% agarose gel. The qPCR process differed from that described previously and the full process is described in methods section 2.3.10.2. Both β-actin and GAPDH housekeeping genes were used for the qPCR analysis however future experiments focus predominantly on the β-actin gene due to issues with the GAPDH primers in some experiments. For this reason, the GAPDH specific qPCR results can be found in Appendix Figures 7.2.2. Figures 4.9.1 to 4.9.3 show the gDNA expression levels of KO targeted genes in CHOS and CHOK1 cell pools with each of the gRNA pairs used. A one-way ANOVA was performed using Dunnett's multiple comparisons test comparing the results to relevant host cells. Significance is shown for key results where p value was less than or equal to 0.05 otherwise results displayed are not significant. Figure 4.9.4 shows the results of the Fut8 KO control where a Welch's t test was performed comparing the results to relevant host cells.

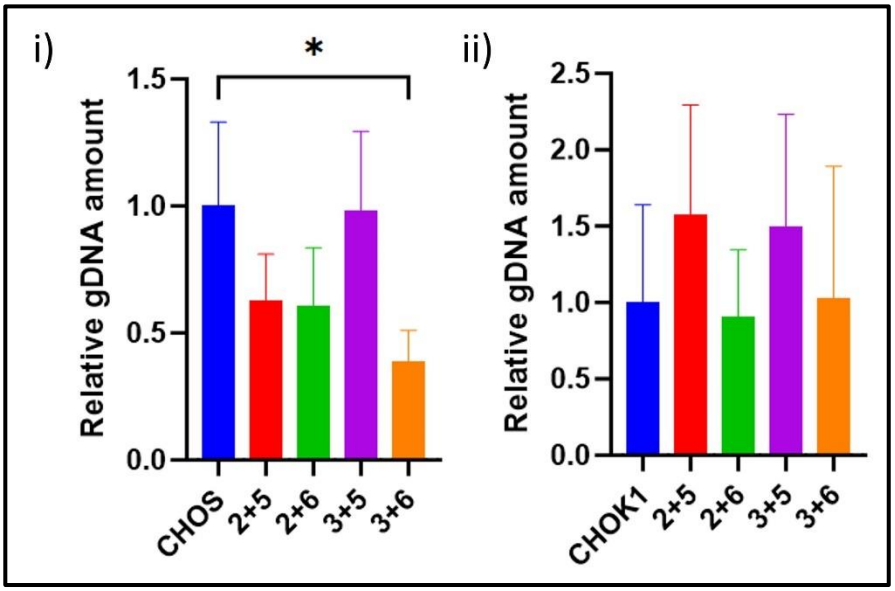

Figure 4.9.1 Relative gDNA amount of PDK1 in CHOS (i) and CHOK1 (ii) cell pools transfected with CRISPR/Cas9 KO plasmids with PDK1 targeting gRNAs analysed via qPCR from gDNA samples. PDK1 primers used to compare to β-actin levels. A one-way ANOVA was performed using Dunnett's multiple comparisons test comparing the results to relevant host cells. Significance shown for key results where p value was less than or equal to 0.05. Extremely significant $p < 0.0001$ (****), Extremely significant $p = 0.0001$ to 0.001 (***), Very significant $p = 0.001$ to 0.01 (**), Significant $p = 0.01$ to 0.05 (*), Not significant $p \geq 0.05$ (ns). (n=3).

Figure 4.9.1 reports the relative gDNA amounts of KO target gene PDK1 in CHOS and CHOK1 cells expressing CRISPR/Cas9 plasmids and relevant gRNAs when compared to β-actin levels. Comparison to GAPDH levels can be seen in Appendix Figure 7.2.2. CHOS cells transfected with the gRNA pair 3 + 5 showed the smallest reduction in PDK1 gDNA amounts, similar to the host cell amounts. gRNA pairs 2 + 5 and 2 + 6 showed a similar level of reduction to PDK1 amounts in CHOS cells with gRNAs 3 + 6 showing a large and significant reduction to gDNA amounts when compared to host cells. When these gRNA pairs were transfected in CHOK1 cells, a different pattern is seen. No gRNA pair shows a reduction in PDK1 gDNA amounts when compared to host cells, with gRNAs 2 + 5, 3 + 5 and 3 + 6 resulting in an increased in PDK1 gDNA amounts. All results for both CHOS and CHOK1 cells have notably large error bars which is likely the result of sampling from a cell pool suggesting the isolation of single cell clones will be required. The significant reduction in PDK1 gDNA amounts in CHOS cells transfected with gRNAs 3 + 6 suggests this pair is a viable option to use for the KO of the PDK1 target gene in CHOS cells (i), however the CHOK1 results (ii) suggest gRNA pair 2 + 6 would result in the most effective KO of PDK1.

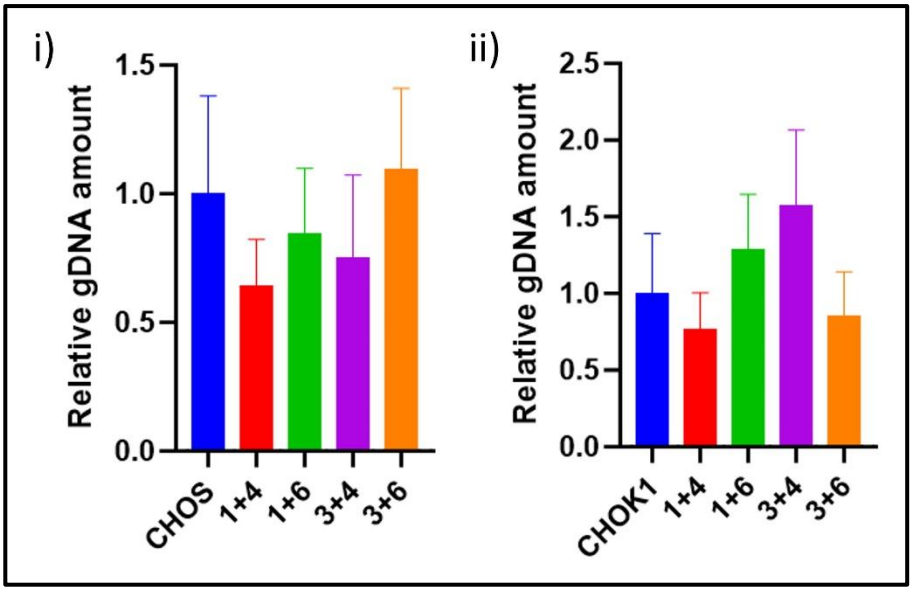

Figure 4.9.2 Relative gDNA amount of PDK2 in CHOS (i) and CHOK1 (ii) cell pools transfected with CRISPR/Cas9 KO plasmids with PDK2 targeting gRNAs analysed via qPCR from gDNA samples. PDK2 primers used to compare to β-actin levels. A one-way ANOVA was performed using Dunnett's multiple comparisons test comparing the results to relevant host cells. Significance shown for key results where p value was less than or equal to 0.05. Extremely significant $p < 0.0001$ (****), Extremely significant $p = 0.0001$ to 0.001 (***), Very significant $p = 0.001$ to 0.01 (**), Significant $p = 0.01$ to 0.05 (*), Not significant $p \geq 0.05$ (ns). (n=3).

Figure 4.9.2 shows the relative gDNA amounts of KO target gene PDK2 in CHOS (i) and CHOK1 (ii) cells transfected with CRISPR/Cas9 plasmids and relevant gRNAs compared to β-actin levels. Comparison to GAPDH levels can be seen in Appendix Figure 7.2.3. CHOS cells (i) transfected with the Cas9 construct with gRNA pair 1 + 4 show the largest reduction in PDK2 gDNA amounts however this was shown not to be significant. gRNA pairs 1 + 6 and 3 + 4 also show a reduction but to a smaller extent. When transfected in CHOS cells, gRNA pair 3 + 6 shows a slight increase in PDK2 gDNA amounts. Conversely in the CHOK1 cells (ii) gRNA pair 3 + 6 shows a slight decrease in PDK2 gDNA amounts with gRNA pairs 1 + 6 and 3 + 4 resulting in an increase in PDK2 gDNA levels when compared to β-actin. Both cell lines show the largest impact to PDK2 gDNA levels when gRNA pair 1 + 4 is used however in neither case is it shown to be a significant reduction.

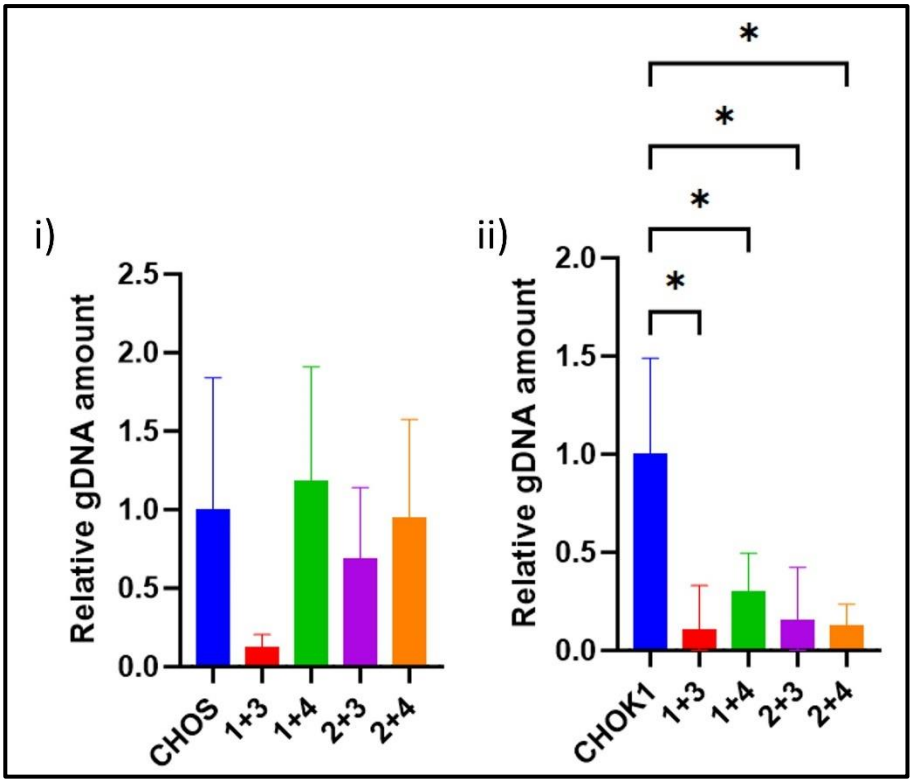

Figure 4.9.3 Relative gDNA amount of PDK3 in CHOS (i) and CHOK1 (ii) cell pools transfected with CRISPR/Cas9 KO plasmids with PDK3 targeting gRNAs analysed via qPCR from gDNA samples. PDK3 primers used to compare to β-actin levels. A one-way ANOVA was performed using Dunnett's multiple comparisons test comparing the results to relevant host cells. Significance shown for key results where p value was less than or equal to 0.05. Extremely significant $p < 0.0001$ (****), Extremely significant $p = 0.0001$ to 0.001 (***), Very significant $p = 0.001$ to 0.01 (**), Significant $p = 0.01$ to 0.05 (*), Not significant $p \geq 0.05$ (ns). (n=3).

Figure 4.9.3 shows the relative gDNA amounts of KO target gene PDK3 in CHOS (i) and CHOK1 (ii) cells transfected with CRISPR/Cas9 plasmids and relevant gRNAs when compared to β-actin levels. Comparison to GAPDH levels can be seen in Appendix Figure 7.2.4. CHOS cells transfected with the Cas9 construct with gRNA pairs 1 + 4 or 2 + 4 both showed a similar amount, or increase, in PDK3 gDNA relative to β-actin levels. A slight reduction in PDK3 gDNA amounts was seen when using gRNA pair 2 + 3 but a much larger reduction was seen for gRNA pair 1 + 3 however this was shown not to be significant. In the CHOK1 cells (ii) all gRNA pairs showed a greater reduction in PDK3 gDNA amounts compared to β-actin with all reductions shown to be significant. gRNA pair 1 + 3 shows a similar reduction to PDK3 gDNA amounts in both cell lines so this pair was selected for further CRISPR/Cas9 experiments.

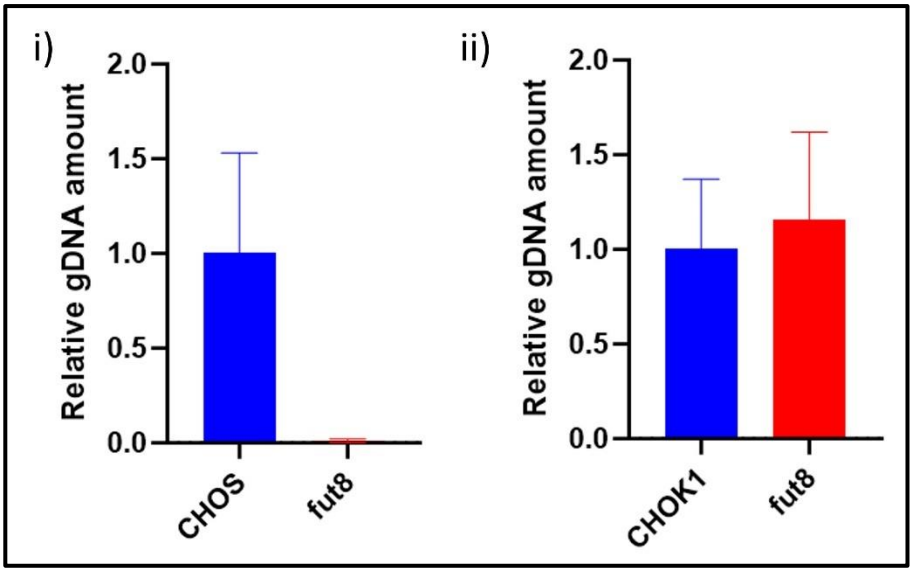

Figure 4.9.4 Relative gDNA amount of fut8 in CHOS (i) and CHOK1 (ii) cell pools expressing CRISPR/Cas9 KO plasmids with fut8 targeting gRNAs analysed via qPCR. fut8 primers taken from (Schmieder et al., 2018) used compared to β-actin levels. A Welch's t test was performed comparing the results to relevant host cells. Significance shown for key results where p value was less than or equal to 0.05. Extremely significant $p < 0.0001$ (****), Extremely significant $p = 0.0001$ to 0.001 (***), Very significant $p = 0.001$ to 0.01 (**), Significant $p = 0.01$ to 0.05 (*), Not significant $p \geq 0.05$ (ns). (n=3).

Finally, the data in Figure 4.5.4 shows the relative gDNA amounts of KO target gene fut8 in CHOS (i) and CHOK1 (ii) cells respectively transfected with CRISPR/Cas9 plasmids and relevant gRNAs when compared to β-actin levels. Comparison to GAPDH levels can be seen in Appendix Figure 7.2.5. A large reduction in fut8 gDNA amounts was observed in CHOS cells (i) in comparison to the β-actin housekeeping gene however this was not observed in the CHOK1 cells (ii) where a slight increase in gDNA amounts is seen however neither is seen to be significant.

The data presented in Figures 4.9.1 to 4.9.3 highlights gRNA pairs that give a reduction in target gene gDNA amounts in the CHOS or CHOK1 cells pools. Large variation was seen in many samples with large error bars which is likely to be due to the use of cell pools at this initial screening stage. To ensure the 'best' gRNA pairs were selected, the impact on PDK mRNA levels of the target genes was also investigated and is discussed in the next section.

4.10 Evaluation of PDK RNA Expression in KO Cell Pools using RTqPCR

To ensure the most appropriate gRNA pair was selected for the CRISPR/Cas9 targeted KO of PDKs 1 to 3, RTqPCR was undertaken on the cell pools showing the best reduction to target gene gDNA expression. RNA samples were extracted on the same day as gDNA samples, eight days post transfection, and RNA isolated following as in section 2.3.9.1 followed by RTqPCR as in methods

section 2.3.9.2. The same primer sequences were used for the RTqPCR reactions as those previously having been validated. Figures 4.10.1 to 4.10.3 show the subsequent results of the RTqPCR focused on the CRIPSR/Cas9 targeted genes in both CHOS (i) and CHOK1 (ii) cell lines, relative to expression of housekeeping gene β-actin. A one-way ANOVA was performed using Dunnett's multiple comparisons test comparing the results to relevant host cells. Significance is shown for key results where p value was less than or equal to 0.05 otherwise results displayed are not significant.

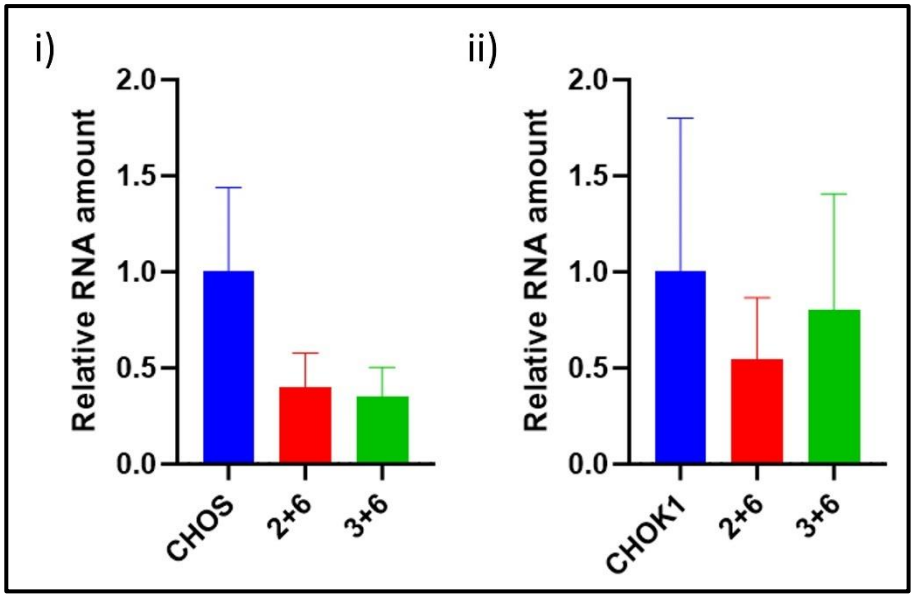

Figure 4.10.1 Relative amount of PDK1 mRNA in CHOS (i) and CHOK1 (ii) cell pools transfected with CRISPR/Cas9 KO plasmids with PDK1 targeting gRNAs analysed via RTqPCR from RNA samples. PDK1 primers used compared to β-actin expression levels. A one-way ANOVA was performed using Dunnett's multiple comparisons test comparing the results to relevant host cells. Significance shown for key results where p value was less than or equal to 0.05. Extremely significant $p < 0.0001$ (****), Extremely significant $p = 0.0001$ to 0.001 (***), Very significant $p = 0.001$ to 0.01 (**), Significant $p = 0.01$ to 0.05 (*), Not significant $p \geq 0.05$ (ns). (n=3).

Figure 4.10.1 shows the relative mRNA expression of KO target gene PDK1 in CHOS (i) and CHOK1 (ii) cells transfected with CRISPR/Cas9 plasmids and relevant gRNAs when compared to β-actin mRNA expression. A successful reduction of gDNA amounts in both CHOS and CHOK1 cells transfected with gRNA pairs 2 + 6 or 3 + 6 (Figure 4.9.1) meant these were targeted for mRNA expression analysis using RTqPCR. Figure 4.10.1 shows use of either gRNA pair reduced the expression of PDK1 mRNA relative to the housekeeping gene β-actin however neither result was shown to be significant. From this data and the qPCR data in Figure 4.9.1, gRNA pair 3 + 6 was selected for further studies in CHOS cells as this resulted in the largest decrease in PDK1 amounts in CHOS cells at both the gDNA and mRNA expression level. CHOK1 cells (ii) transfected with gRNA pair 2 + 6 showed a larger reduction in relative PDK1 RNA expression compared to the 3 + 6 pair

however neither was shown to be significant. It was for this reason that for CHOK1 cells, the gRNA pair 2 + 6 was chosen for further PDK1 KO approaches. Samples from both cell lines show large variation and error bars for most samples highlighting the diversity expected within a cell pool. Further sorting of these cells is likely to be required to isolate a cell line with a higher KO and reduction in target PDK gDNA or mRNA expression levels.

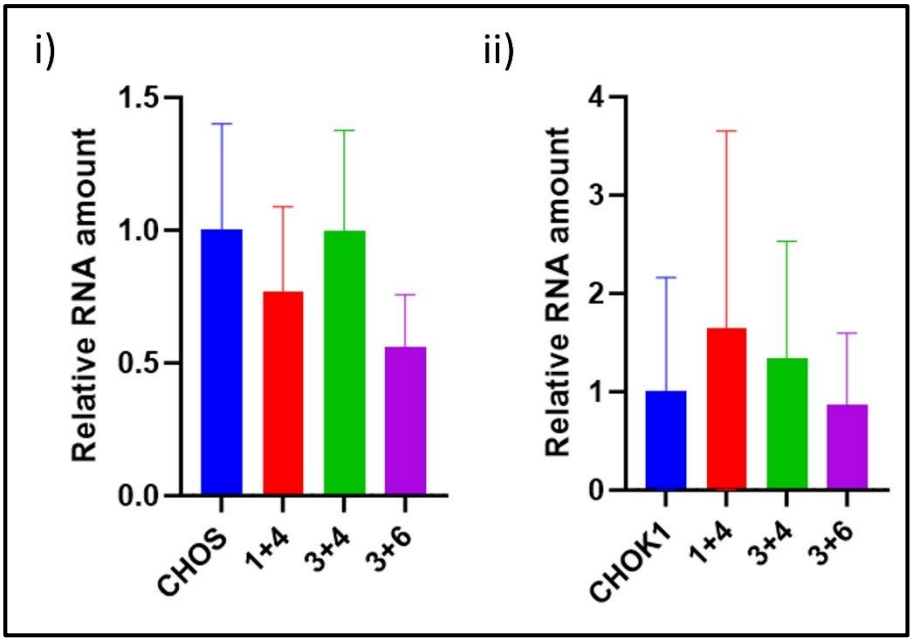

Figure 4.10.2 Relative amount of PDK2 mRNA in CHOS (i) and CHOK1 (ii) cell pools transfected with CRISPR/Cas9 KO plasmids with PDK2 targeting gRNAs analysed via RTqPCR from RNA samples. PDK2 primers used compared to β-actin expression levels. A one-way ANOVA was performed using Dunnett's multiple comparisons test comparing the results to relevant host cells. Significance shown for key results where p value was less than or equal to 0.05. Extremely significant $p < 0.0001$ (****), Extremely significant $p = 0.0001$ to 0.001 (***), Very significant $p = 0.001$ to 0.01 (**), Significant $p = 0.01$ to 0.05 (*), Not significant $p \geq 0.05$ (ns). (n=3).

Figure 4.10.2 shows the relative mRNA expression of KO target gene PDK2 in CHOS (i) and CHOK1 (ii) cells transfected with CRISPR/Cas9 plasmids and relevant gRNAs when compared to β-actin mRNA expression levels. The varied results and limited reduction of relative gDNA amounts in cells transfected with PDK2 targeting gRNA pairs shown in Figure 4.9.2 meant multiple gRNA pairs were assessed for impact on PDK2 mRNA expression. Figure 4.10.2 shows the greatest reduction to PDK2 mRNA expression levels in CHOS cells (i) transfected with gRNA pair 3 + 6 relative to β-actin mRNA expression however this was not shown to be significant. This contrasts with the gDNA qPCR data presented in Figure 4.9.2, which suggests gRNA pair 1 + 4 or 3 + 4 gave the largest reduction in amounts of PDK2 gDNA suggesting a more efficient KO. When looking at the CHOK1 cells (ii), the largest reduction to PDK2 mRNA expression relative to β-actin mRNA was in the cell pools

transfected with gRNA pair 3 + 6. This was relatively even to CHOK1 host cell expression however and was shown to be not significant. This also differs from the results from the gDNA qPCR in Figure 4.9.2 which shows the largest reduction to PDK2 gDNA amounts in cells transfected with gRNA pair 1 + 4. The mRNA results for this pool however shows an increase in PDK2 mRNA expression to over 1.5 times the levels in the control cell line. Combining the qPCR and RTqPCR data in Figures 4.9.2 and 4.10.2 respectively, the gRNA pair 3 + 6 in CHOK1 cells resulted in the largest reduction in PDK2 gDNA amounts or mRNA expression when compared to the other gRNA pairs. Although the CHOS pool data in these figures revealed no clear gRNA pair that gave appropriate reduction in gDNA and mRNA, gRNA pair 3 + 6 was selected for use in both CHOS and CHOK1 cells lines primarily based upon the CHOK1 results.

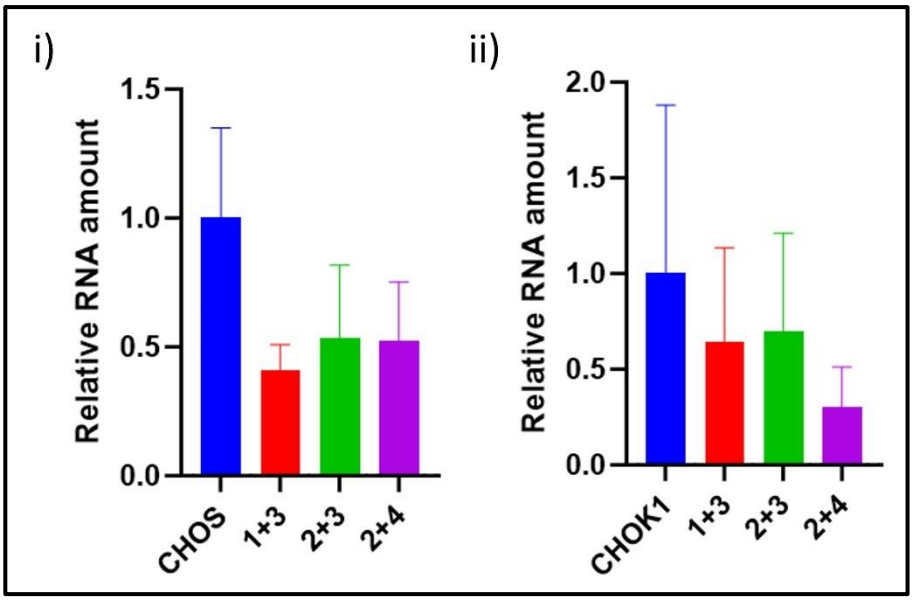

Figure 4.10.3 Relative amount of PDK3 mRNA in CHOS (i) and CHOK1 (ii) cell pools transfected with CRISPR/Cas9 KO plasmids with PDK3 targeting gRNAs analysed via RTqPCR from RNA samples. PDK3 primers used compared to β-actin expression levels. A one-way ANOVA was performed using Dunnett's multiple comparisons test comparing the results to relevant host cells. Significance shown for key results where p value was less than or equal to 0.05. Extremely significant $p < 0.0001$ (****), Extremely significant $p = 0.0001$ to 0.001 (***), Very significant $p = 0.001$ to 0.01 (**), Significant $p = 0.01$ to 0.05 (*), Not significant $p \geq 0.05$ (ns). (n=3).

Figure 4.10.3 reports the relative mRNA expression of KO target gene PDK3 in CHOS (i) and CHOK1 (ii) cell pools transfected with CRISPR/Cas9 plasmids and relevant gRNAs when compared to β-actin mRNA expression levels. Although the data presented in Figure 4.9.3 suggested that gRNA pair 1 + 3 results in the largest reduction to CHOS PDK3 gDNA amounts, mRNA samples from cells transfected with gRNA pairs 2 + 3 or 2 + 4 was also analysed by RTqPCR. The data in Figure 4.10.3

shows a similar result with the cells transfected with gRNA pair 1 + 3 resulting in the largest reduction in PDK3 mRNA expression levels with a reduction of approximately 60%. A reduction in PDK3 mRNA expression of approximately 50% was observed in cells transfected with gRNA pairs 2 + 3 or 2 + 4 however none of these reductions were shown to be significant. This, combined with the gDNA results reported in Figure 4.9.3 suggest that gRNA pair 1 + 3 were best for KO of PDK3 in

CHOS cells. The CHOK1 cell results in Figure 4.10.3 show transfection with gRNA pair 2 + 4 results in the greatest reduction in PDK3 mRNA expression. However, this, along with all the results in Figure 4.10.3, was shown not to be significant and in order to use the same pair in both host cells, gRNA pair 1 + 3 was selected for future CRISPR/Cas9 experiments for CHOK1 and CHOS cells.

Table 4.10.1 reports the final gRNA pairs selected for the CRISPR/Cas9 targeted KO of PDKs 1 to 3 based upon the qPCR and RTqPCR experiments described in sections 4.9 and 4.10.

Table 4.10.1 The final gRNA pairs chosen for CRISPR/Cas9 targeted KO of PDKs 1, 2 and 3 in both CHOS and CHOK1 cell lines.

	gRNA Target		
Cell line	*PDK1*	*PDK2*	*PDK3*
CHOS	gRNAs 3 + 6	gRNAs 3 + 6	gRNAs 1 + 3
CHOK1	gRNAs 2 + 6	gRNAs 3 + 6	gRNAs 1 + 3

4.11 Evaluation of PDK Protein Expression in KO Cell Pools

The results of the impact of CRISPR/Cas9 KO with different gRNAs on gDNA amounts and mRNA expression levels in the CHO cell pools were further investigated at the protein level. A reduction in mRNA expression levels should impact protein expression of targeted PDKs however the extent and relationship between the two needs to be determined. Samples for protein analysis were taken from the cell pools for those transfected with the gRNAs in Table 4.10.1 and processed following the steps described in methods section 2.4. At this stage a TRIPLE KO cell pool in both CHOS and CHOK1 hosts was generated. 5 µg of each final selected gRNA Cas9 plasmid was mixed and transfected into cells. The same process was used as for the previous KO cell pools with lysate samples taken for protein analysis eight days after transfection. Figures 4.11.1 to 4.11.3 show the results of western blot analysis of the cell lysates probed with anti-PDK and anti-β-actin antibodies.

Control lysate samples from host cells and PEL1, empty cassette, expressing cell pools were also investigated.

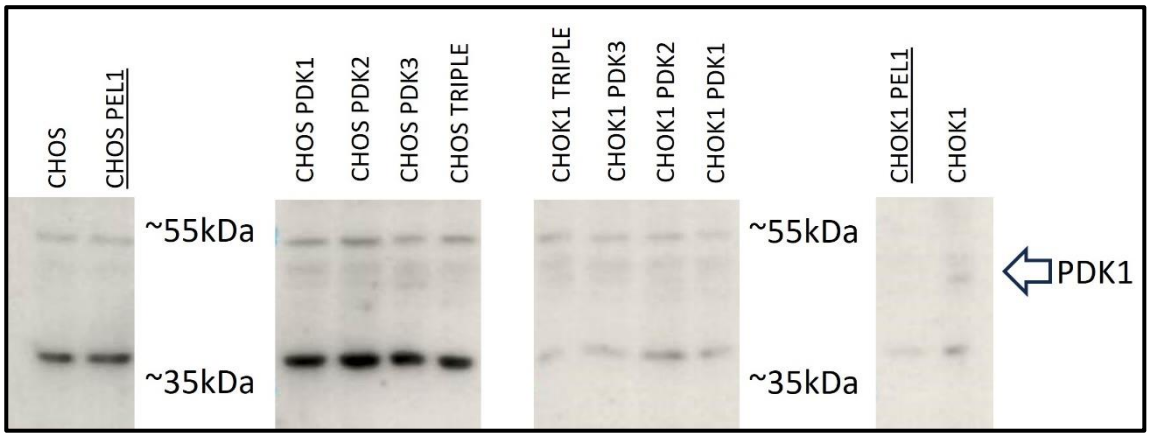

Figure 4.11.1 Western blot analysis of CHOS and CHOK1 cells transfected with CRISPR/Cas9 plasmids with gRNAs targeting PDKs 1, 2, 3 or all three (TRIPLE) when probed with an anti-PDK1 antibody. 20 µg protein loaded and blot exposed for 20 mins. PDK1 KO cell pools using gRNAs 2 + 5. PDK2 KO cell pools using gRNAs 1 + 4. PDK3 KO cell pools using gRNAs 1 + 3. TRIPLE KO cell pools using all three sets of gRNAs. PDK1 can be seen around 49 kDa, the expected size.

Figure 4.11.1 shows the presence of multiple bands in all samples when probed with the anti-PDK1 antibody. The expected size for PDK1 is 49 kDa, where a faint band is observed. There was no obvious difference observed between the band intensities in pools transfected with the CRISPR/Cas9 targeted KO gRNAs for PDK1 in either host cell line pool compared to the control. Figure 4.11.1 also confirmed that transfections with CRISPR/Cas9 plasmids with gRNAs targeting PDK2, 3 or all three PDKs did not impact expression of PDK1 to a large extent. Thus, the differences observed at the gDNA and RNA level of PDK1 (see sections 4.9 and 4.10) are not observed at protein level, possibly due to the pool nature of the samples.

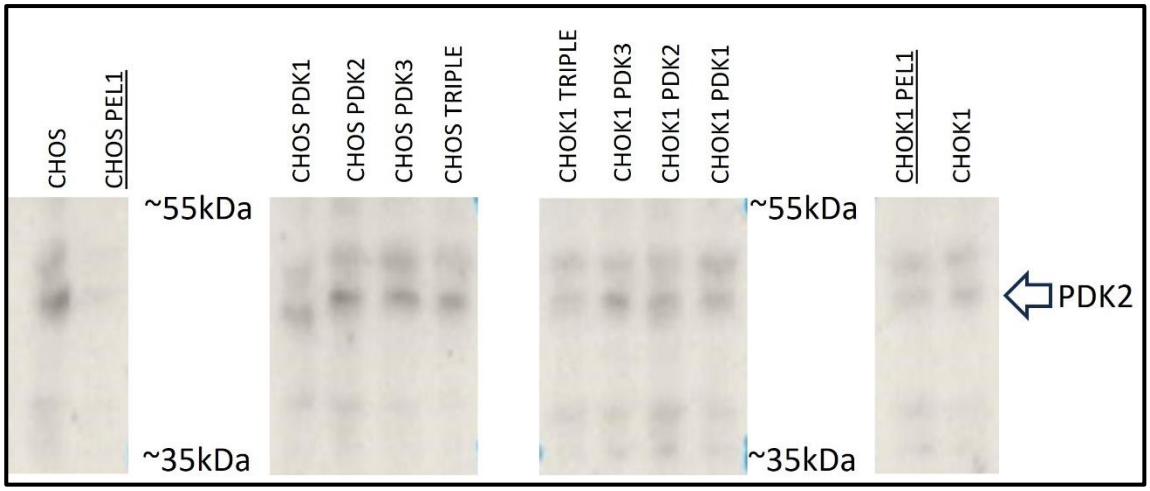

Figure 4.11.2 Western blot protein analysis of CHOS and CHOK1 cells transfected with CRISPR/Cas9 plasmids with gRNAs targeting PDKs 1, 2, 3 or all three (TRIPLE) when probed with an anti-PDK2 antibody. 20 µg protein loaded and blot exposed for 20 mins. PDK1 KO cell pools using gRNAs 2 + 5. PDK2 KO cell pools using gRNAs 1 + 4. PDK3 KO cell pools using gRNAs 1 + 3. TRIPLE KO cell lines using all three sets of gRNAs. PDK2 can be seen around 46 kDa, the expected size.

Figure 4.11.2 shows bands in all samples at the expected PDK2 size of 46 kDa. The CHOS control sample shows the most prominent band when compared to all other samples with the sample from cells transfected with PDK2 targeting Cas9 plasmids also showing an intense band. The data in Figure 4.11.2 suggests no difference at a pool level in PDK2 expression when cells were transfected with Cas9 plasmids with gRNAs targeting PDK1, 3 or all three PDKs does not seem to impact expression levels of PDK2. The results suggest expressing the Cas9 plasmids targeting PDK1, 3 or all three PDKs might impact PDK2 protein expression but is shown to a larger extent in CHOS cell lines compared to CHOK1.

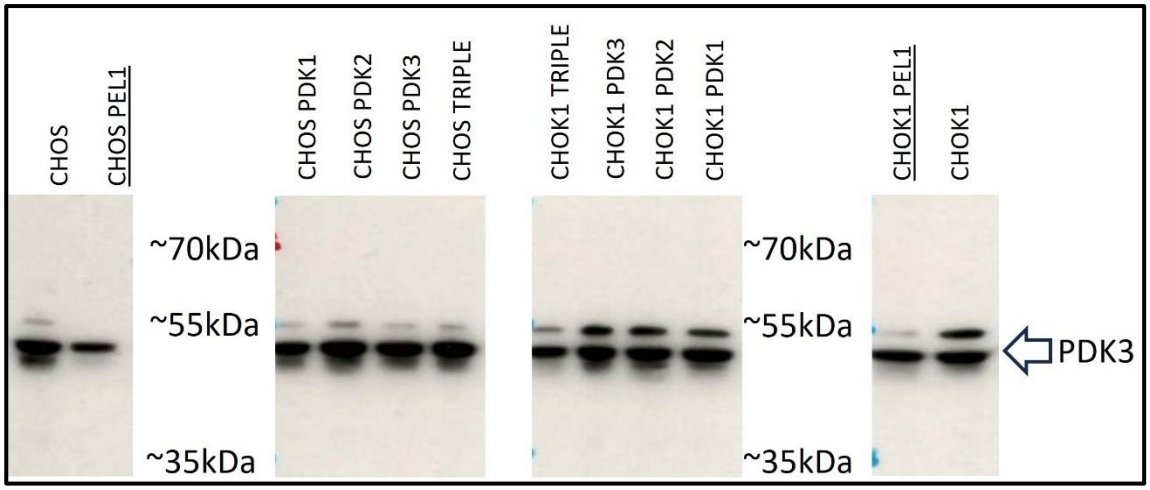

Figure 4.11.3 Western blot protein analysis of CHOS and CHOK1 cells transfected with CRISPR/Cas9 plasmids with gRNAs targeting PDKs 1, 2, 3 or all three (TRIPLE) when probed with an anti-PDK3 antibody. 20 µg protein loaded and blot exposed for 20 mins. PDK1 KO cell pools using gRNAs 2 + 5. PDK2 KO cell pools using gRNAs 1 + 4. PDK3 KO cell pools using gRNAs 1 + 3. TRIPLE KO cell lines using all three sets of gRNAs. PDK3 can be seen around 47 kDa, the expected size.

Figure 4.11.3 shows one major band and several minor bands for all samples including at the expected PDK3 size of 47 kDa. CHOS cell pool samples transfected with the Cas9 plasmids showed similar bands compared to the CHOS control, apart from PDK1 KO cells which showed some evidence of a small reduction in band intensity for PDK3 expression. CHOS PEL1 transfected cells had the weakest intensity band for PDK3 expression levels. CHOK1 cells showed a similar pattern with all KO cell pools having similar PDK3 expression levels apart from PDK1 KO cells which had a marginally reduced intensity band. The data in Figure 4.11.3 suggests cells transfected with the CRISPR/Cas9 plasmids with gRNAs targeting PDK3 did not impact expression of PDK3 at the protein level but that its expression might be impacted when PDK1 is targeted for KO. The strong reduction in expression seen of PDK3 gDNA amounts and mRNA expression seen in Figures 4.9.3 and 4.10.3 in both CHOS and CHOK1 cells is not suggested by the protein expression levels in Figure 4.11.3.

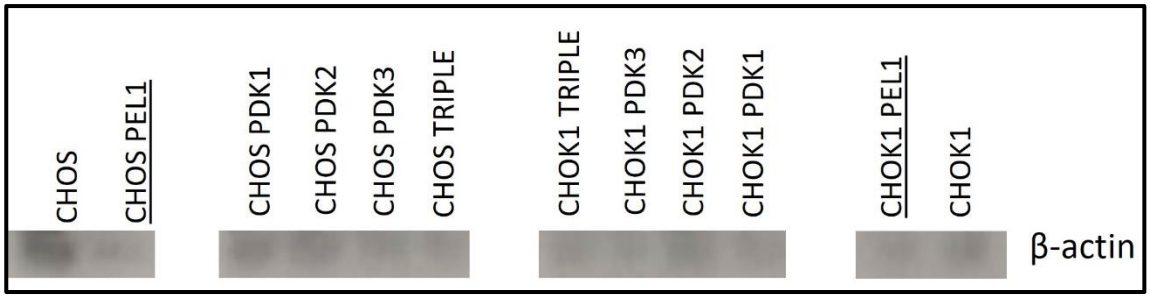

Figure 4.11.4 Western blot protein analysis of CHOS and CHOK1 cells transfected with CRISPR/Cas9 plasmids with gRNAs targeting PDKs 1, 2, 3 or all three (TRIPLE) when probed with an anti-β-actin antibody. 20 μg protein loaded and blot exposed for 20 mins. PDK1 KO cell pools using gRNAs 2 + 5. PDK2 KO cell pools using gRNAs 1 + 4. PDK3 KO cell pools using gRNAs 1 + 3. TRIPLE KO cell pools using all three sets of gRNAs. β-actin can be seen around 37 kDa, the expected size.

Figure 4.11.4 shows the same samples loaded in Figures 4.11.1 to 4.11.3 when probed with anti-β-actin antibody. Bands are seen for all samples at the expected 37 kDa, with even loading suggested for most samples other than the CHOS control lysate sample which has a darker band compared to other samples. CHOS and CHOK1 PEL1 cell lines show a fainter band when compared to the other samples which could relate to the weaker bands seen previously in Figures 4.11.1, 4.11.2 and 4.11.3.

Western blot analysis was also undertaken to assess protein expression levels of PDP and Pyruvate Kinase (PK). PDP acts to dephosphorylate the E1alpha subunit to reactivate the PDH complex whilst PK acts to convert PEP to pyruvate as the last step of glycolysis. PK activity is of interest due to its role supplying the PDH complex with its substrate pyruvate. This analysis aimed to determine any changes in expression, and therefore potential supply of pyruvate to the PDH complex, upon the KO of target PDKs as an alternate approach of controlling PDH complex activity. Figures 4.11.5 and 4.11.7 show the western blots of these analyses and details of the antibodies used can be found in methods section 2.4.5 Table 2.4.1.

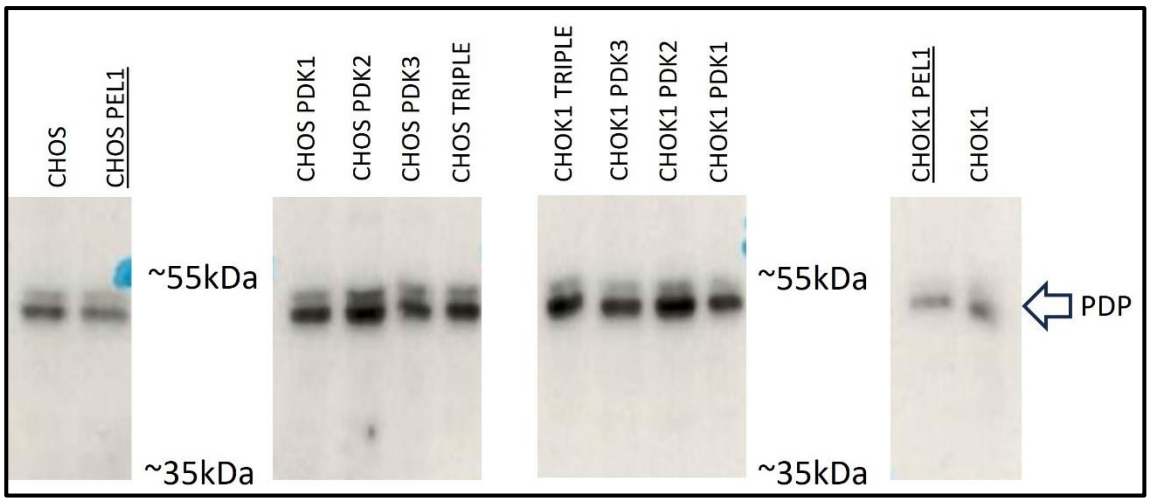

Figure 4.11.5.1 Western blot protein analysis of CHOS and CHOK1 cells transfected with CRISPR/Cas9 plasmids with gRNAs targeting PDKs 1, 2, 3 or all three (TRIPLE) when probed with an anti-PDPc (D-11) antibody. 20 µg protein loaded and blot exposed for 20 mins. PDK1 KO cell pools using gRNAs 2 + 5. PDK2 KO cell pool using gRNAs 1 + 4. PDK3 KO cell pools using gRNAs 1 + 3. TRIPLE KO cell pools using all three sets of gRNAs. The PDP band can be seen around 53 kDa, the expected size.

Figure 4.11.5.1 shows expression of PDP in all cell pools with a suggested increase observed in cell pools transfected with CRISPR/Cas9 plasmids targeting all PDKs compared to both CHOS and CHOK1 control cell lines. This is more clearly demonstrated in the densitometry analysis in Figure 4.11.5.2.

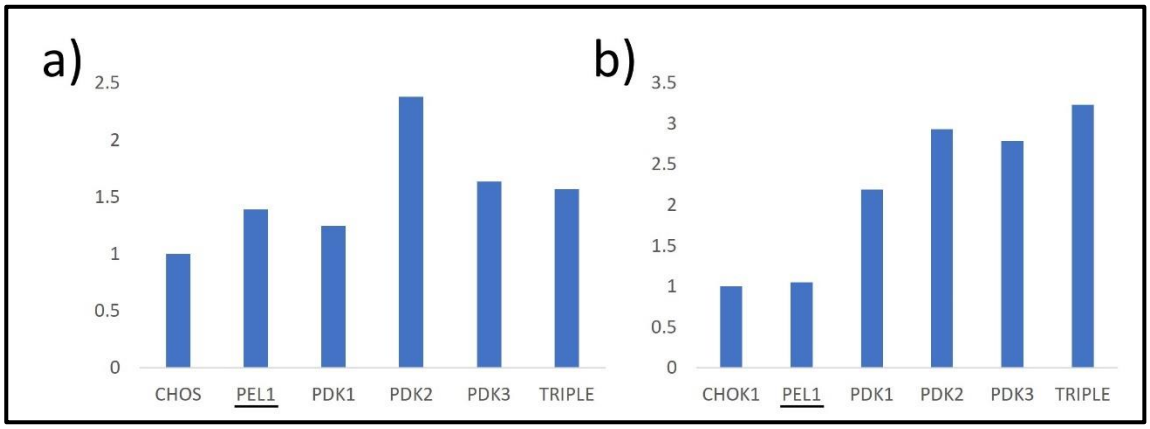

Figure 4.11.5.2 Densitometry of western blot signals in Figure 4.11.5.1 showing the relative expression of PDP in CHOS (a) and CHOK1 (b) cell pools transfected with CRISPR/Cas9 plasmids with gRNAs targeting PDKs 1, 2, 3 or all three (TRIPLE) compared to control host cell lines and β-actin expression. Analysis of bands presented in Figure 4.11.5.1 and 4.11.4 from PDP and β-actin blots respectively is shown.

Figure 4.11.5.2 shows the densitometry analysis of the PDP bands in Figure 4.11.5.1. and the β-actin bands in Figure 4.11.4 from CHOS (a) and CHOK1 (b) cell pool samples. All cell pools transfected

with CRISPR/Cas9 plasmids targeting PDKs suggest an increase in PDP expression relative to the control cell lines. Edited CHOS cells (a) had an average increase in expression of around 1.5 times the level compared to the control cells, although a similar increase in expression was also seen in control CHOS cells transfected with the control PEL1 plasmid suggesting potential variation within the cell pool is likely to be impacting the results. Cells transfected with PDK2 targeting gRNA containing CRISPR/Cas9 plasmids had the largest increase in expression levels suggested to be over twice the level of control cells. CHOK1 cells (b) showed similar results with all PDK1, 2 and 3 targeted KO cell pools expressing over twice the amount of PDP in comparison to host cell lines. Although this is not seen in control PEL1 cells, it is still likely that cell pool variation is having a key impact here.

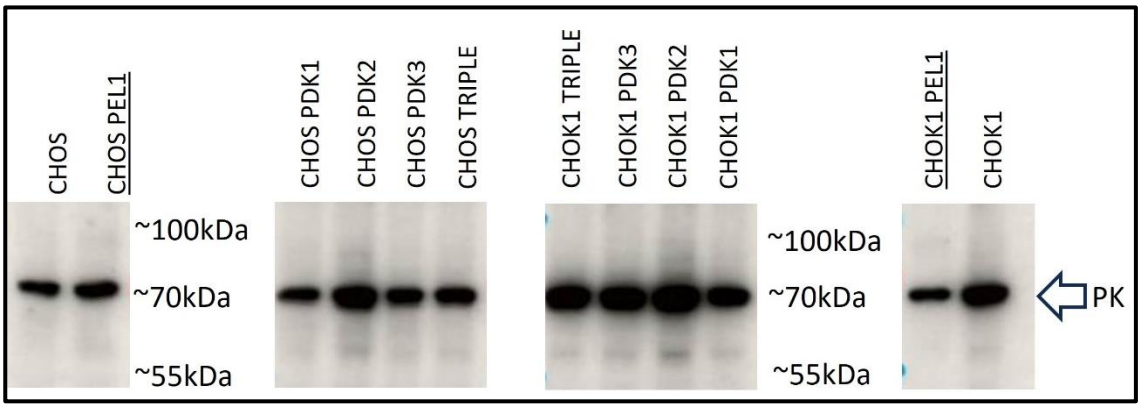

Figure 4.11.6.1 Western blot protein analysis of CHOS and CHOK1 cells transfected with CRISPR/Cas9 plasmids with gRNAs targeting PDKs 1, 2, 3 or all three (TRIPLE) when probed with an anti-PKLR antibody. 20 µg protein loaded and blot exposed for 20 mins. PDK1 KO cell pools using gRNAs 2 + 5. PDK2 KO cell pools using gRNAs 1 + 4. PDK3 KO cell pools using gRNAs 1 + 3. TRIPLE KO cell pools using all three sets of gRNAs. PK bands can be seen around 63/59 kDa, the expected sizes.

Figure 4.11.6.1 reveals bands for all samples at the expected sizes which appear in a range between 63 to 59 kDa. CHOS cell samples show similar expression levels of PK apart from those transfected with PDK2 targeting Cas9 plasmids which had a slightly larger, more prominent band. CHOK1 cell pools all had a higher expression level of PK compared to the CHOS samples apart from the CHOK1 PEL1 transfected cell pool. Figure 4.11.6.2 shows the densitometry analysis of these results.

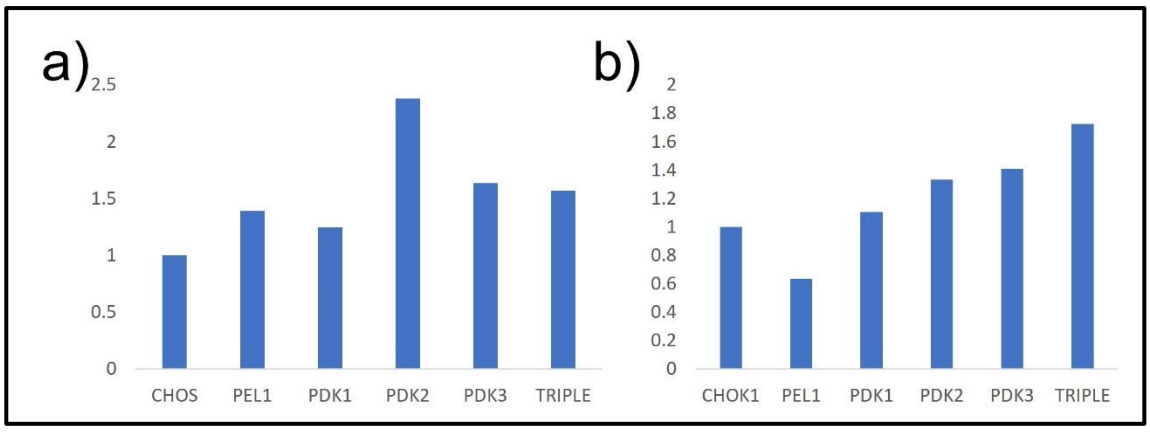

Figure 4.11.6.2 Densitometry of western blot signals in Figure 4.11.6.1 showing the relative expression of PK in CHOS (a) and CHOK1 (b) cell pools transfected with CRISPR/Cas9 plasmids with gRNAs targeting PDKs 1, 2, 3 or all three (TRIPLE) compared to control host cell lines and β-actin expression. Analysis of bands presented in Figure 4.11.6.1 and 4.11.4 from PK and β-actin blots respectively is shown.

Figure 4.11.6.2 shows the densitometry analysis of the PK bands observed in Figure 4.11.6.1 and the β-actin bands in Figure 4.11.4 from CHOS (a) and CHOK1 (b) cell pool samples. CHOS cell samples (a) show an increase in expression of PK in all samples including the control PEL1 cell pool. PDK2 KO cells suggest the largest increase in expression compared to host cell lines. CHOK1 cell samples (b) had an increased expression of PK in all samples apart from PEL1 control cell pool where a reduction in expression was seen. The TRIPLE KO cell pool had the largest increase in expression levels compared to the host cell line.

The western blot data suggests that the CRISPR/Cas9 plasmid transfected cell pools generally had changes in protein expression when the different PDK targeting KOs were undertaken. However not to the extent suggested by some of the reduction in mRNA levels seen resulting from RTqPCR analysis in Figures 4.10.1 to 4.10.3. Multiple repeats of the western blots should be completed to limit the impact of the large variation seen within the cell pools. It is likely that cell sorting would enable a clearer picture of the impact had on protein expression resulting from the targeted CRISPR/Cas9 KO of PDKs.

4.12 Evaluation of KO impact on PDH subunit gDNA Amounts in CHOS KO Cell Pools using qPCR

The results of the qPCR and RTqPCR reported in sections 4.9 and 4.10 report the impact on gDNA amounts and RNA expression levels of PDK targets in KO pools. qPCR was also used to investigate any impact the KO had on the relative gDNA amounts of the PDH complex subunits impacted by the

activity of PDKs. Although it was expected that there might be an impact at the mRNA level but not at the gDNA level, gDNA amounts were investigated by qPCR with the aim of repeating the analysis for mRNA expression levels at a later date. gDNA samples from CHOS cells transfected with PDK1 targeting gRNA pair 2 + 5, PDK2 targeting gRNA pair 1 + 4 and PDK3 targeting gRNA pair 1 + 3 were used in qPCR reactions with primers specific for PDH subunits E1alpha, E1beta, E2, E3bp and the phosphatase PDP which acts to remove the phosphorylation activity of PDKs to enable activity of the PDH complex. These primers had been used previously and tested in qPCR reactions to ensure single peaks were generated of the expected amplicon size (Appendix Figure 7.1.10). Figures 4.12.1 to 4.12.5 show the results of the qPCR focused on the PDH subunits in the specific CHOS cell pools transfected with CRIPSR/Cas9 PDK targeted gRNAs. These results are all shown relative to housekeeping genes β-actin. Comparisons to GAPDH gDNA amounts are shown in Appendix Figure 7.2.6. A one-way ANOVA was performed using Dunnett's multiple comparisons test comparing the results to relevant host cells. Significance is shown for key results where p value was less than or equal to 0.05 otherwise results displayed are not significant.

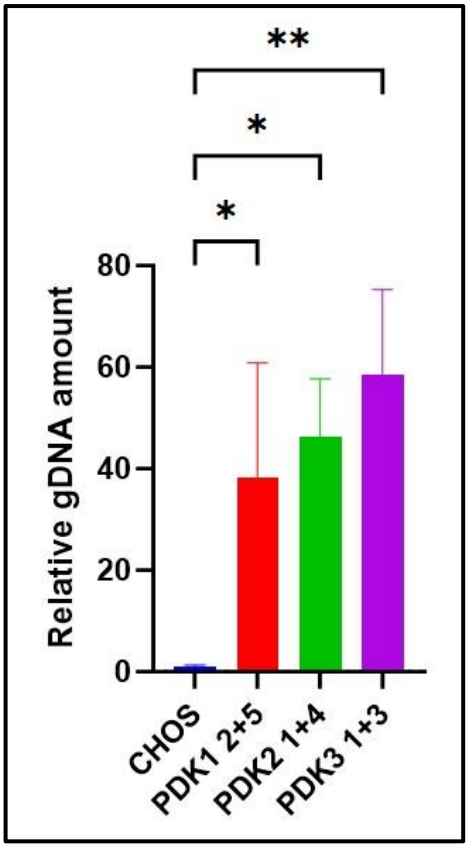

Figure 4.12.1 Relative gDNA amount of PDH subunit E1alpha in CHOS cell pools transfected with CRISPR/Cas9 KO plasmids with PDK1, 2 and 3 targeting gRNAs analysed via qPCR from gDNA samples. E1alpha primers used to compare to β-actin levels. PDK1 KO cell pools using gRNAs 2 + 5. PDK2 KO cell pools using gRNAs 1 + 4. PDK3 KO cell pools using gRNAs 1 + 3. A one-way ANOVA was performed using Dunnett's multiple comparisons test comparing the results to relevant host cells. Significance shown for key results where p value was less than or equal to 0.05. Extremely significant $p < 0.0001$ (****), Extremely significant $p = 0.0001$ to 0.001 (***), Very significant $p = 0.001$ to 0.01 (**), Significant $p = 0.01$ to 0.05 (*), Not significant $p \geq 0.05$ (ns). (n=3).

Figure 4.12.1 shows the relative gDNA amounts of PDH subunit E1alpha in CHOS cells transfected with CRISPR/Cas9 plasmids and relevant gRNAs targeting PDKs 1, 2 and 3 when compared to β-actin gDNA amounts. Surprisingly, all three KO cell pools showed large and significant increases in gDNA amounts of the E1alpha subunit when compared to β-actin gDNA amounts with the PDK3 KO cell pool transfected with gRNAs 1 + 3 showing the largest increase of almost 60 fold. E1alpha is the target of the phosphorylation activity of PDKs which act to inactivate the PDH complex regulating its activity. The increase in gDNA amounts in Figure 4.12.1 compared to control host cell lines suggests the cell is responding to the KO by increasing gene copy number in the genome to give a higher gDNA amount.

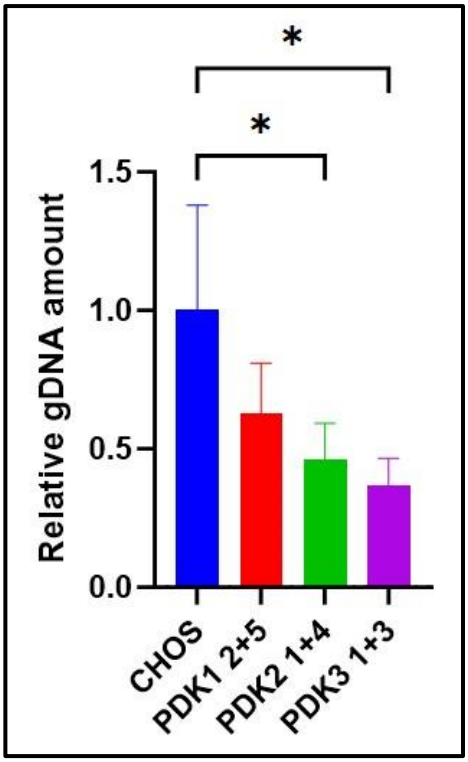

Figure 4.12.2 Relative gDNA amount of PDH subunit E1beta in CHOS cell pools transfected with CRISPR/Cas9 KO plasmids with PDK1, 2 and 3 targeting gRNAs analysed via qPCR from gDNA samples. E1beta primers used to compare to β-actin levels. PDK1 KO cell pools using gRNAs 2 + 5. PDK2 KO cell pools using gRNAs 1 + 4. PDK3 KO cell pools using gRNAs 1 + 3. A one-way ANOVA was performed using Dunnett's multiple comparisons test comparing the results to relevant host cells. Significance shown for key results where p value was less than or equal to 0.05. Extremely significant $p < 0.0001$ (****), Extremely significant $p = 0.0001$ to 0.001 (***), Very significant $p = 0.001$ to 0.01 (**), Significant $p = 0.01$ to 0.05 (*), Not significant $p \geq 0.05$ (ns). (n=3).

Figure 4.12.2 reports the relative gDNA amounts of PDH subunit E1beta in CHOS cells transfected with CRISPR/Cas9 plasmids and relevant gRNAs targeting PDKs 1, 2 and 3 when compared to β-actin gDNA. All cell pools had reduced gDNA of the PDH subunit E1beta with cells transfected with gRNAs targeting PDK2 and 3 showing a large and significant reduction. The reduction of gDNA amounts seen follows an opposite trend to that of E1alpha in Figure 4.12.1, which increased when PDKs were targeted for KO. The E1alpha subunit joins with E1beta to form the heterotetrametric E1 subunit of the PDH complex however is not the site of regulation via the activity of PDKs.

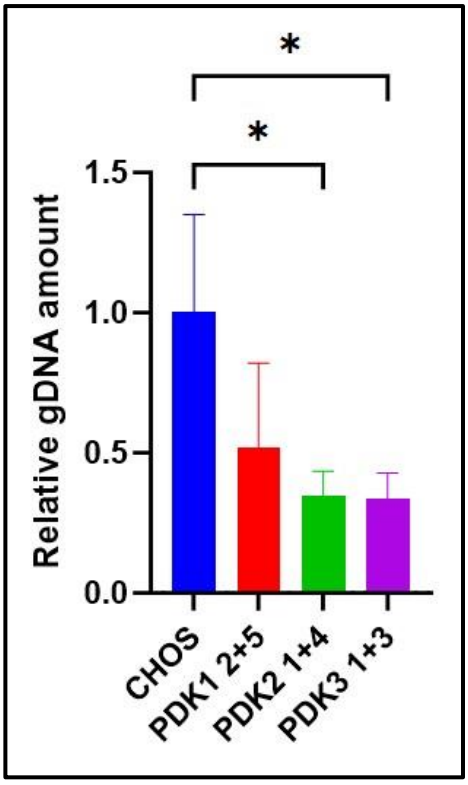

Figure 4.12.3 Relative gDNA amount of PDH subunit E2 in CHOS cell pools transfected with CRISPR/Cas9 KO plasmids with PDK1, 2 and 3 targeting gRNAs analysed via qPCR from gDNA samples. E2 primers used to compare to β-actin levels. PDK1 KO cell pools using gRNAs 2 + 5. PDK2 KO cell pools using gRNAs 1 + 4. PDK3 KO cell pools using gRNAs 1 + 3. A one-way ANOVA was performed using Dunnett's multiple comparisons test comparing the results to relevant host cells. Significance shown for key results where p value was less than or equal to 0.05. Extremely significant $p < 0.0001$ (****), Extremely significant $p = 0.0001$ to 0.001 (***), Very significant $p = 0.001$ to 0.01 (**), Significant $p = 0.01$ to 0.05 (*), Not significant $p \geq 0.05$ (ns). (n=3).

Figure 4.12.3 shows the relative gDNA amounts of PDH subunit E2 in CHOS cells transfected with CRISPR/Cas9 plasmids and relevant gRNAs targeting PDKs 1, 2 and 3 when compared to β-actin levels. Similar to those results presented in Figure 4.12.3, the gDNA levels of the PDH subunit E2 were reduced in all cell pools although no results were significant. Cells transfected with gRNAs targeting PDK2 and 3 showed the largest decrease in PDH subunit gDNA.

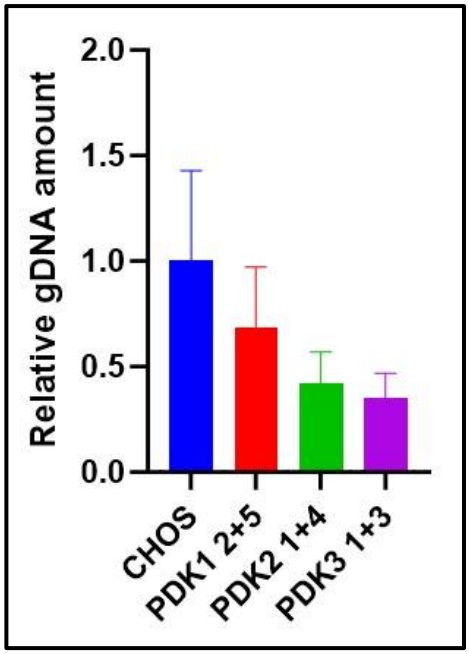

Figure 4.12.4 Relative gDNA amount of PDH subunit E3bp in CHOS cell pools transfected with CRISPR/Cas9 KO plasmids with PDK1, 2 and 3 targeting gRNAs analysed via qPCR from gDNA samples. E3bp primers used to compare to β-actin levels. PDK1 KO cell pools using gRNAs 2 + 5. PDK2 KO cell pools using gRNAs 1 + 4. PDK3 KO cell pools using gRNAs 1 + 3. A one-way ANOVA was performed using Dunnett's multiple comparisons test comparing the results to relevant host cells. Significance shown for key results where p value was less than or equal to 0.05. Extremely significant $p < 0.0001$ (****), Extremely significant $p = 0.0001$ to 0.001 (***), Very significant $p = 0.001$ to 0.01 (**), Significant $p = 0.01$ to 0.05 (*), Not significant $p \geq 0.05$ (ns). (n=3).

Figure 4.12.4 shows the relative gDNA amounts of PDH subunit E3bp in CHOS cells transfected with CRISPR/Cas9 plasmids and relevant gRNAs targeting PDKs 1, 2 and 3 when compared to β-actin. Following the trends in Figures 4.12.2 and 4.12.3, the gDNA levels of PDH subunit E3bp were reduced in cell pools transfected with CRISPR/Cas9 plasmids with gRNAs targeting PDKs 1, 2 and 3 with those targeting PDK3 showing the largest reduction compared to β-actin although no result was shown to be significant.

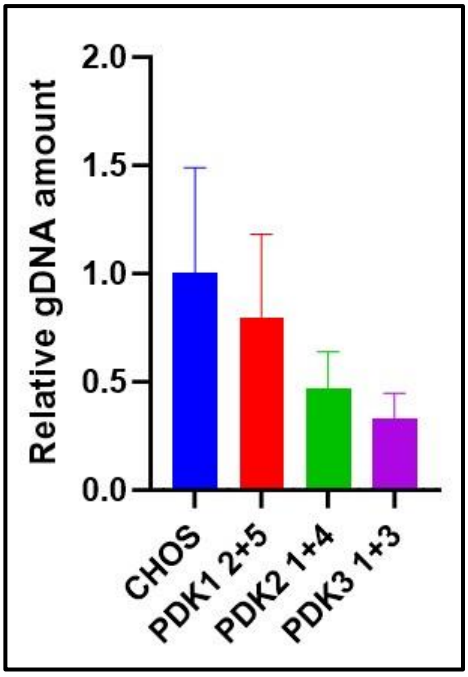

Figure 4.12.5 Relative gDNA amount of PDP in CHOS cell pools transfected with CRISPR/Cas9 KO plasmids with PDK1, 2 and 3 targeting gRNAs analysed via qPCR from gDNA samples. PDP primers used to compare to β-actin levels. PDK1 KO cell pools using gRNAs 2 + 5. PDK2 KO cell pools using gRNAs 1 + 4. PDK3 KO cell pools using gRNAs 1 + 3. A one-way ANOVA was performed using Dunnett's multiple comparisons test comparing the results to relevant host cells. Significance shown for key results where p value was less than or equal to 0.05. Extremely significant $p < 0.0001$ (****), Extremely significant $p = 0.0001$ to 0.001 (***), Very significant $p = 0.001$ to 0.01 (**), Significant $p = 0.01$ to 0.05 (*), Not significant $p \geq 0.05$ (ns). (n=3).

Figure 4.12.5 shows the relative gDNA amounts of PDP in CHOS cells transfected with CRISPR/Cas9 plasmids and relevant gRNAs targeting PDKs 1, 2 and 3 compared to β-actin levels. All three PDK KO cell pools showed a reduction in gDNA of PDP compared to β-actin gDNA although these reductions were not significant. PDK3 targeted KO cell pools showed the largest impact on PDP gDNA amounts.

It is noted that samples were taken on the same day, from cell pools, so do not reflect individual clonal cell impacts. The data in Figures 4.12.1 to 4.12.5 shows changes to the gDNA amounts of PDH subunits and PDP in cells transfected with CRISPR/Cas9 gRNAs targeted to PDKs 1, 2 or 3 compared to host CHOS cells. The increased gDNA amount of the E1alpha subunit of PDH, the site of regulation via PDKs, in Figure 4.12.1 combined with the decrease in gDNA levels of PDH subunits E1beta, E2 and E3bp and PDP, seen in Figures 4.12.2 to 4.12.5, suggest cells respond to the KO of PDKs by regulating gDNA amounts of the complex subunits. Further analysis of PDH subunit mRNA expression was planned but not completed due to time constraints. Impacts to mRNA expression resulting from the targeted PDK KO would suggest PDH complex expression was being downregulated in response to maintain a similar level of PDH activity and reduce the impact on complex activity had by the KO.

4.13 Single Cell Sorting for Selection of Monoclonal Cell Lines

As outlined above, the KO data assessment so far considered the 'average' from pools of cells which does not reflect that of individual cells. The process of single cell cloning was therefore used to isolate individual cells for the generation of monoclonal cell lines. This would ensure that any KO was present in all future cell generations and allow the identification of any phenotypic changes that resulted from the KO by selecting cells where KO had occurred.

The first approach used to isolate monoclonals was single cell cloning using serial dilutions (see methods section 2.5.3). One cryovial of each of the PDK KO cell pools was revived alongside the TRIPLE KO cell pool and passaged for two weeks in CD-CHO media with 8 mM L-glutamine. Once the cell pools were at a culture viability >90%, the cells were diluted in series over four 96 well plates to provide wells with single cells. Those wells with single cells were then identified and marked before serial dilution plates were left for three to four weeks and checked under a light microscope for daughter cells growing from a single host. These cells could then be screened using qPCR for those where KO of target gene expression had occurred.

The first attempt at serial dilution was unsuccessful for all KO cell pools and individual cells failed to recover/divide and grow in the 96 well plates. This may have been due to the use of ACA in the cell culture media which acts to prevent cells clumping, a step favoured by cells as they try to grow up from a small number of cells. To ensure this wasn't the case, when cells were revived from cryovials, fresh CD-CHO media was used for cell passaging that was free of ACA. Amphotericin B solution (Sigma-Aldrich A2942) was also added at a 1 in 100 dilution to the CD-CHO media to prevent any fungal contamination. To support growth from single cells the additive ClonaCell™-CHO ACF Supplement (STEMCELL Technologies) was also added to the CD-CHO media at a forty times dilution attempting to improve single cell cloning efficiency. This additive was successful in aiding the recovery of cells but due when cells were moved to 24 well plates for further issues around cell growth and recovery from single cells remained.

To address this ongoing issue, cell pools were generated instead of single cells to see if this improved the recovery process. This was more successful, but when adapting cells from 2 ml cultures in 6 well plates in static incubators to 10 ml cultures in falcon tubes in an incubator shaking at 220 rpm, the cell lines did not survive the process. An alternative approach of FACS based sorting of the cells, instead of serial dilutions, was therefore also attempted.

4.14 FACS Sorting of Cell Pools

Due to the difficulty of cells reviving from single cells after limited dilution cloning, FACS was used to sort cells into pools of 10, 100 and 1000 cells per well with the aim of more cells in the wells helping with cell recovery. Although this would not isolate single edited cells, if it was not possible to isolate these the next best approach was to develop minipools that came from a small number of cells. A BD FACSJazz™ was used for this purpose (see section 2.5.4).

The CRISPR/Cas9 KO process was started again with both CHOS and CHOK1 host cell lines transfected with the selected gRNA pairs and the GFP expression from the Cas9 plasmid used to sort cells based on fluorescence intensities. Cells with a fluorescence intensity above 10^3 were selected and sorted into 96 well plates. Both Amphotericin B and Penicillin-Streptomycin were added to the media. Once in 96 well plates, cells were left to recover in a 37°C static incubator and regularly checked for growth and confluence. Cells were moved from 96 well plates to 24 well plates when evidence of increased confluence to approximately 50% was observed.

Dot blots to determine PDK expression in KO pools were used to screen and select the wells with the best KO comparing the protein expression levels for target PDKs and control β-actin. Although this process is less specific than individual western blots, it allows a higher throughput for screening samples. Figures 4.14.1 to 4.14.3 show the results of the dot blots where 5 µg of protein was loaded from cell lysate samples. If a sample had a lower protein concentration, 50 µl of lysate was loaded and the β-actin dot size/intensity used to determine whether a lack of signal for the PDK target was due to KO or lack of protein entirely. TRIPLE KO cell lysate samples were loaded on each of the PDK blots for comparison and can be seen on the right-hand side of each blot.

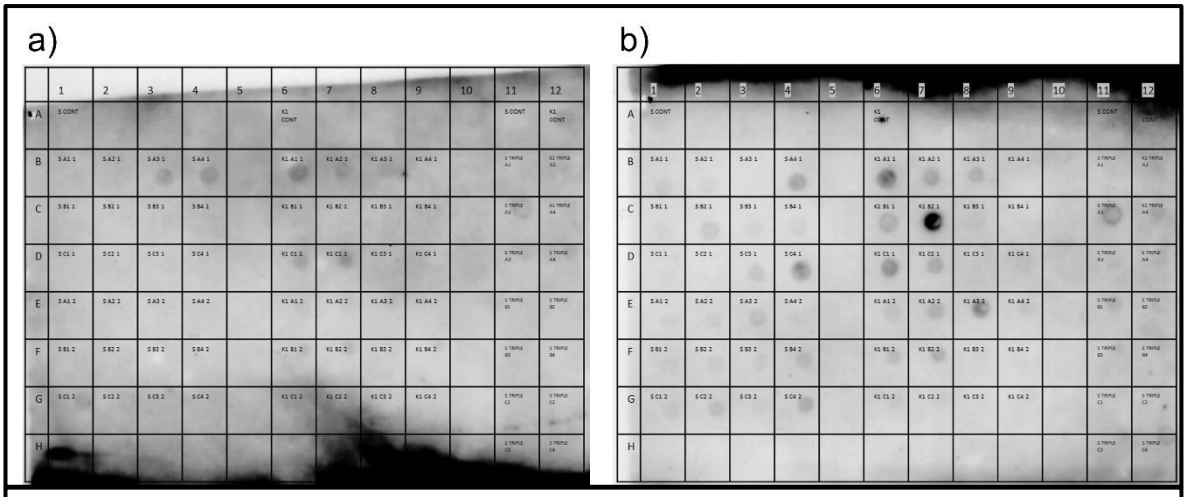

c)i)

	1	2	3	4	5	6	7	8	9	10	11	12
A	S CONT					K1 CONT					S CONT	K1 CONT
B	S A1 1	S A2 1	S A3 1	S A4 1		K1 A1 1	K1 A2 1	K1 A3 1	K1 A4 1		S TRIPLE A1	K1 TRIPLE A2
C	S B1 1	S B2 1	S B3 1	S B4 1		K1 B1 1	K1 B2 1	K1 B3 1	K1 B4 1		S TRIPLE A2	K1 TRIPLE A4
D	S C1 1	S C2 1	S C3 1	S C4 1		K1 C1 1	K1 C2 1	K1 C3 1	K1 C4 1		S TRIPLE A3	S TRIPLE A4
E	S A1 2	S A2 2	S A3 2	S A4 2		K1 A1 2	K1 A2 2	K1 A3 2	K1 A4 2		S TRIPLE B1	S TRIPLE B2
F	S B1 2	S B2 2	S B3 2	S B4 2		K1 B1 2	K1 B2 2	K1 B3 2	K1 B4 2		S TRIPLE B3	S TRIPLE B4
G	S C1 2	S C2 2	S C3 2	S C4 2		K1 C1 2	K1 C2 2	K1 C3 2	K1 C4 2		S TRIPLE C1	S TRIPLE C2
H											S TRIPLE C3	S TRIPLE C4

c)ii)

PDK1 CHOS Cells		PDK1 CHOK1 Cells	
Dot blot	Cell line	Dot blot	Cell line
S C3 1	100 G5	K1 B1 1	10 C7
S C4 1	100 G6	K1 B2 1	10 C9
S A3 2	100 G9	K1 A1 2	10 H11
S B1 2	100 G11	K1 A3 2	100 A4
S B4 2	100 H10	K1 C1 2	100 B10
S C4 2	1000 B4	K1 C2	1000 A2

Figure 4.14.1 Dot blot analysis of CHOS and CHOK1 cells transfected with CRISPR/Cas9 plasmids with gRNAs targeting PDK1 or all three PDKs (TRIPLE) when probed with an anti-PDK1 antibody (a) or an anti-β-actin antibody (b). The chosen cell pools are highlighted in green (ci) and listed for each cell line host along with the originating cell pool number sorted into the well (cii). 5 μg protein loaded and blots exposed for 1 hour. TRIPLE KO cell lines transfected using all three sets of gRNA pairs.

Figure 4.14.1 shows results of dot blots of cell lysate samples from PDK1 KO cell pools recovered from the FACS process and moved into 24 well plates. The dots seen for samples on the anti-PDK1 antibody dot blot (a) vary in intensity suggesting differences in PDK1 expression in both the CHOS and CHOK1 KO cell pools. However, for a signal to be relevant, a β-actin signal also needed to be observed. Faint signals could be seen for the TRIPLE KO cell lines, specifically the CHOS TRIPLE A2 well C11, suggesting reduced PDK1 protein expression compared to other cell pools. The anti-β-actin antibody blot (b) shows a signal for more cell samples with CHOK1 B2 2 in well C7 showing the strongest signal. The top six cell pools were picked based on a strong signal for β-actin (b) but little to no signal for the corresponding PDK1 blot (a). These cell pools are highlighted in green (ci) relating to the position in the 96 well plate layout for the dot blots. The original pool name and cell seeding

number from which the cells originated after FACS is shown in (cii) and reveals CHOS cells with the most pool candidates coming from those sorted into 100 cells per well and CHOK1 selected cells coming from 10, 100 or 1000 cells per well.

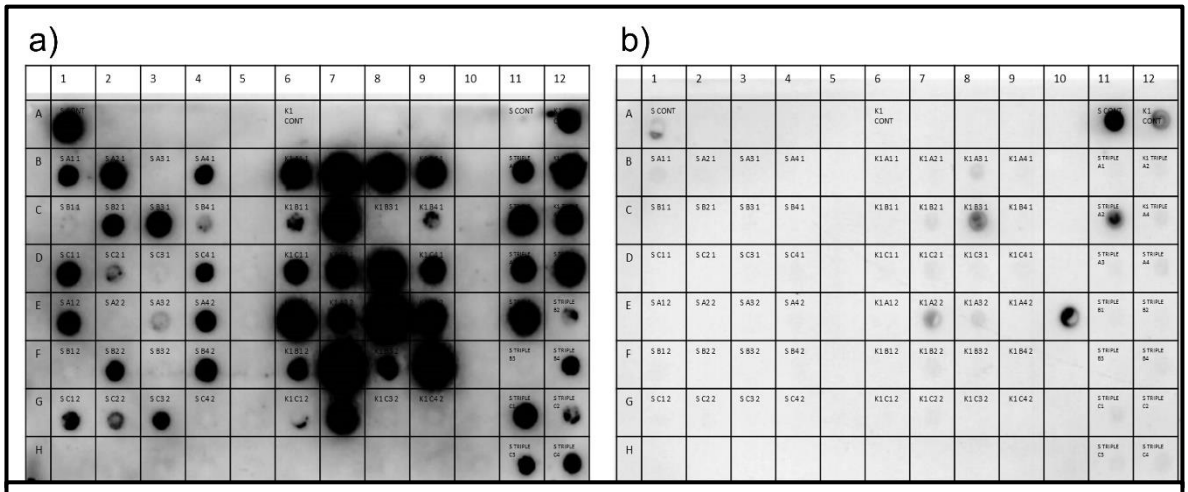

c)i)

	1	2	3	4	5	6	7	8	9	10	11	12
A	S CONT					K1 CONT					S CONT	K1 CONT
B	S A1 1	S A2 1	S A3 1	S A4 1		K1 A1 1	K1 A2 1	K1 A3 1	K1 A4 1		S TRIPLE A1	K1 TRIPLE A2
C	S B1 1	S B2 1	S B3 1	S B4 1		K1 B1 1	K1 B2 1	K1 B3 1	K1 B4 1		S TRIPLE A2	K1 TRIPLE A4
D	S C1 1	S C2 1	S C3 1	S C4 1		K1 C1 1	K1 C2 1	K1 C3 1	K1 C4 1		S TRIPLE A3	S TRIPLE A4
E	S A1 2	S A2 2	S A3 2	S A4 2		K1 A1 2	K1 A2 2	K1 A3 2	K1 A4 2		S TRIPLE B1	S TRIPLE B2
F	S B1 2	S B2 2	S B3 2	S B4 2		K1 B1 2	K1 B2 2	K1 B3 2	K1 B4 2		S TRIPLE B3	S TRIPLE B4
G	S C1 2	S C2 2	S C3 2	S C4 2		K1 C1 2	K1 C2 2	K1 C3 2	K1 C4 2		S TRIPLE C1	S TRIPLE C2
H											S TRIPLE C3	S TRIPLE C4

c)ii)

PDK2 CHOS Cells		PDK2 CHOK1 Cells	
Dot blot	Cell line	Dot blot	Cell line
S A3 1	10 E3	K1 B1 1	10 G10
S C3 1	100 C3	K1 B3 1	10 H6
S A2 2	100 C12	K1 B4 1	10 H9
S B1 2	100 D5	K1 B3 2	100 B9
S B3 2	100 E3	K1 C1 2	1000 A3
S C4 2	1000 B3	K1 C3 2	1000 C4

Figure 4.14.2 Dot blot analysis of CHOS and CHOK1 cells transfected with CRISPR/Cas9 plasmids with gRNAs targeting PDK2 or all three PDKs (TRIPLE) when probed with an anti-PDK2 antibody (a) or an anti-β-actin antibody (b). The chosen cell pool are highlighted in green (ci) and listed for each cell pool along with the originating cell pool number (cii). 5 µg protein loaded and blots exposed for 1 hour. TRIPLE KO cell lines transfected using all three sets of gRNA pairs.

Figure 4.14.2 shows the results of dot blots of cell lysate samples from PDK2 KO cell pools having recovered from the FACS process and moved into 24 well plates. Signals for PDK2 protein expression (a) were much more intense than those observed in Figure 4.14.1 for PDK1 expression and were present for most samples. Much fewer signals were observed for the β-actin blot (b) with only a few samples, including the controls, showing evidence of β-actin. A signal was observed in well E10 where no sample was loaded suggesting some sample bleeding. For this reason, six cell pools were carried forward to allow final cell pool selection after further screening of these. Cell pools were

selected based on the lowest intensity PDK2 protein expression observed in green in (ci). The original pool name and cell seeding number after the FACS is listed in (cii) and shows both CHOS and CHOK1 cell pools recovering and potential PDK2 KO from pools of 10, 100 and 1000 cells per well.

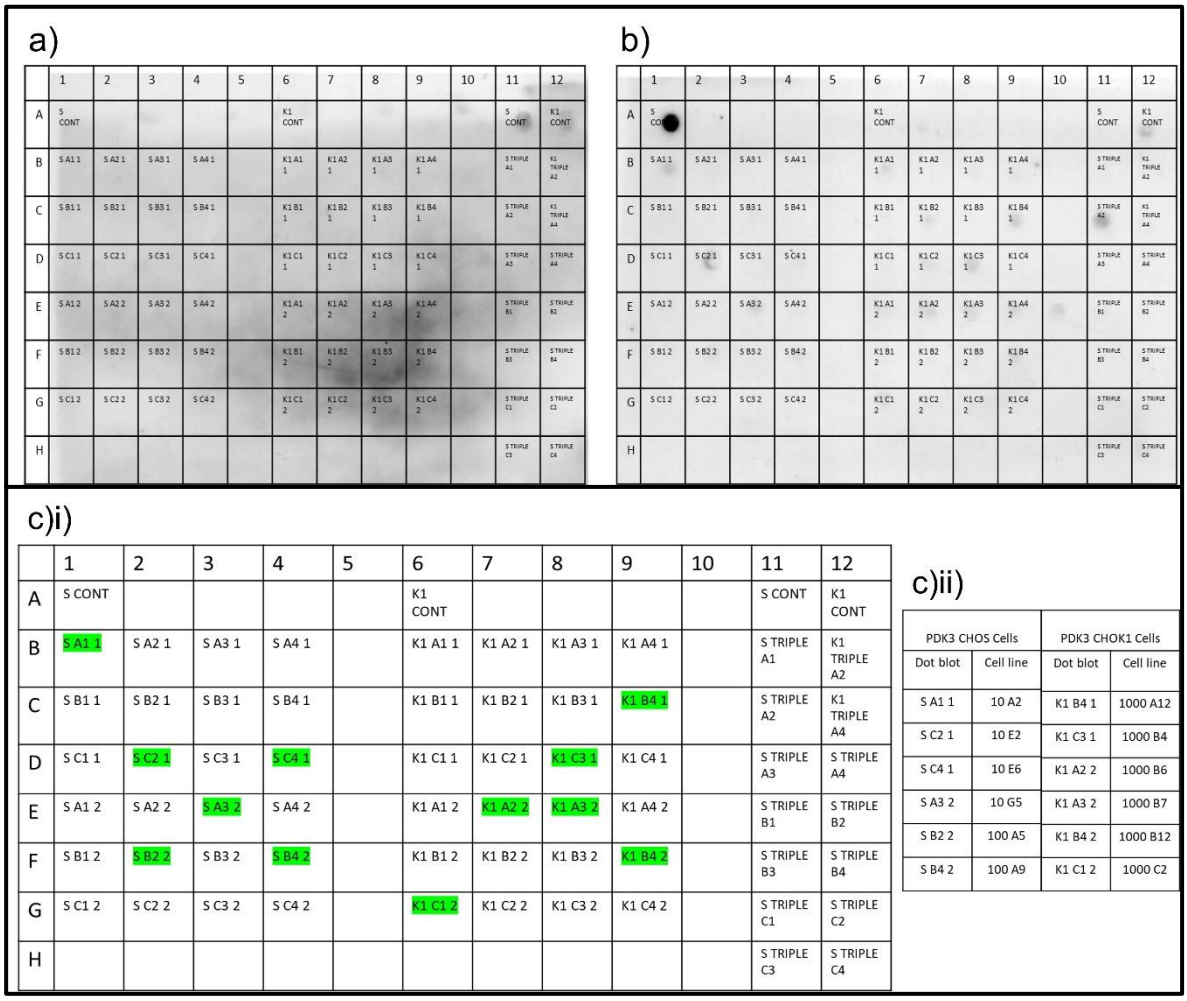

	1	2	3	4	5	6	7	8	9	10	11	12
A	S CONT					K1 CONT					S CONT	K1 CONT
B	S A1 1	S A2 1	S A3 1	S A4 1		K1 A1 1	K1 A2 1	K1 A3 1	K1 A4 1		S TRIPLE A1	K1 TRIPLE A2
C	S B1 1	S B2 1	S B3 1	S B4 1		K1 B1 1	K1 B2 1	K1 B3 1	K1 B4 1		S TRIPLE A2	K1 TRIPLE A4
D	S C1 1	S C2 1	S C3 1	S C4 1		K1 C1 1	K1 C2 1	K1 C3 1	K1 C4 1		S TRIPLE A3	S TRIPLE A4
E	S A1 2	S A2 2	S A3 2	S A4 2		K1 A1 2	K1 A2 2	K1 A3 2	K1 A4 2		S TRIPLE B1	S TRIPLE B2
F	S B1 2	S B2 2	S B3 2	S B4 2		K1 B1 2	K1 B2 2	K1 B3 2	K1 B4 2		S TRIPLE B3	S TRIPLE B4
G	S C1 2	S C2 2	S C3 2	S C4 2		K1 C1 2	K1 C2 2	K1 C3 2	K1 C4 2		S TRIPLE C1	S TRIPLE C2
H											S TRIPLE C3	S TRIPLE C4

PDK3 CHOS Cells		PDK3 CHOK1 Cells	
Dot blot	Cell line	Dot blot	Cell line
S A1 1	10 A2	K1 B4 1	1000 A12
S C2 1	10 E2	K1 C3 1	1000 B4
S C4 1	10 E6	K1 A2 2	1000 B6
S A3 2	10 G5	K1 A3 2	1000 B7
S B2 2	100 A5	K1 B4 2	1000 B12
S B4 2	100 A9	K1 C1 2	1000 C2

Figure 4.14.3 Dot blot analysis of CHOS and CHOK1 cell pools transfected with CRISPR/Cas9 plasmids with gRNAs targeting PDK3 or all three PDKs (TRIPLE) when probed with an anti-PDK3 antibody (a) or an anti-β-actin antibody (b). The selected cell pools are highlighted in green (ci) and listed for each cell pool along with the originating cell pool number (cii). 5 µg protein loaded and blots exposed for 1 hour. TRIPLE KO cell pools transfected using all three sets of gRNA pairs.

Figure 4.14.3 shows the results of dot blots of cell lysate samples from PDK3 KO cell pools having recovered from the FACS process and moved into 24 well plates. Very few signals were observed for PDK3 protein expression on the anti-PDK3 antibody blot (a) for any samples other than the CHOS and CHOK1 host control samples. There were also few signals on the β-actin blot (b) suggesting low protein levels were present in samples from the wells. Cell pools were therefore selected based upon the most prominent β-actin protein expression levels and are highlighted in green in (ci). The

original pool name and cell seeding number from which the cells originated after FACS is detailed in (cii) and shows CHOS cells originating from pools of 10 or 100 cells per well while the CHOK1 cell pools all came from wells with 1000 cells per well.

The TRIPLE KO cell pools showed mixed success when looking at the PDK antibody blots in Figures 4.14.1 to 4.14.3. Only two CHOK1 TRIPLE KO cell pools recovered from the selection process compared to twelve CHOS cell pools, so both were carried forward for further analysis. CHOS TRIPLE A2 was one of the only TRIPLE KO cell pools to show a signal for PDK1 expression in Figure 4.14.1 compared to all others. CHOK1 TRIPLE B3 had a signal for PDK2 protein expression (Figure 4.14.2) but no TRIPLE KO cell pools had a signal for PDK3 protein expression in Figure 4.14.3. and the β-actin signals were weak or non-essential too. The decision was made to continue with all TRIPLE KO cell pools in both CHOS and CHOK1 hosts to screen them further for evidence of multiple PDK KOs. Figure 4.14.4 reports the original pool name and cell seeding number from which the pools originated after FACS.

a)

TRIPLE CHOS Cells	
Dot blot	Cell line
S TRIPLE A1	10 C9
S TRIPLE A2	10 D4
S TRIPLE A3	10 H4
S TRIPLE A4	100 A5
S TRIPLE B1	100 A8
S TRIPLE B2	100 A9

TRIPLE CHOS Cells	
Dot blot	Cell line
S TRIPLE B3	100 D3
S TRIPLE B4	100 E2
S TRIPLE C1	100 E5
S TRIPLE C2	100 E6
S TRIPLE C3	100 F5
S TRIPLE C4	100 F7

b)

TRIPLE CHOK1 Cells	
Dot blot	Cell line
K1 TRIPLE A2	100 A2
K1 TRIPLE A4	100 A4

Figure 4.14.4 The chosen CHOS (a) and CHOK1 (b) TRIPLE KO cell pools and the originating cell pool size.

Once the six, or fourteen in the case of the TRIPLE KO cell pools, had been selected, the cell pools were moved to a 6 well plate and allowed to proliferate further. Viable cell numbers were then determined and varied between cell pools. The total well was then cryopreserved and then revived into 6 well plates at a later date. This was done in two batches to allow time for recovery and screening of two PDK targets as the others recovered. However, some cell pools failed to recover or maintained low viability and cell number. For those cell pools that did revive from cryopreservation,

the cells were subsequently moved to a T25 flask and finally to 10 ml culture in a 50 ml falcon tube with shaking at 220 rpm. This was also an issue for some of the cell pools when adapting from the static to shaking conditions.

In total eleven of the fifty selected PDK KO cell pools recovered and grew in 10 ml cultures in shaking falcon tubes. Lysate samples were taken from these cell pools to gather further evidence of any reduced target PDK protein expression and to identify if the creation of mini pools reduced the variation previously seen within sample pools to produce a clearer impact on target PDK expression. Figures 4.14.5 to 4.14.7 show the results of these western blots where individual KO cell pools were loaded next to TRIPLE KO lysate samples and probed with the KO target anti-PDK antibody (a) and then anti-β-actin antibody (b.)

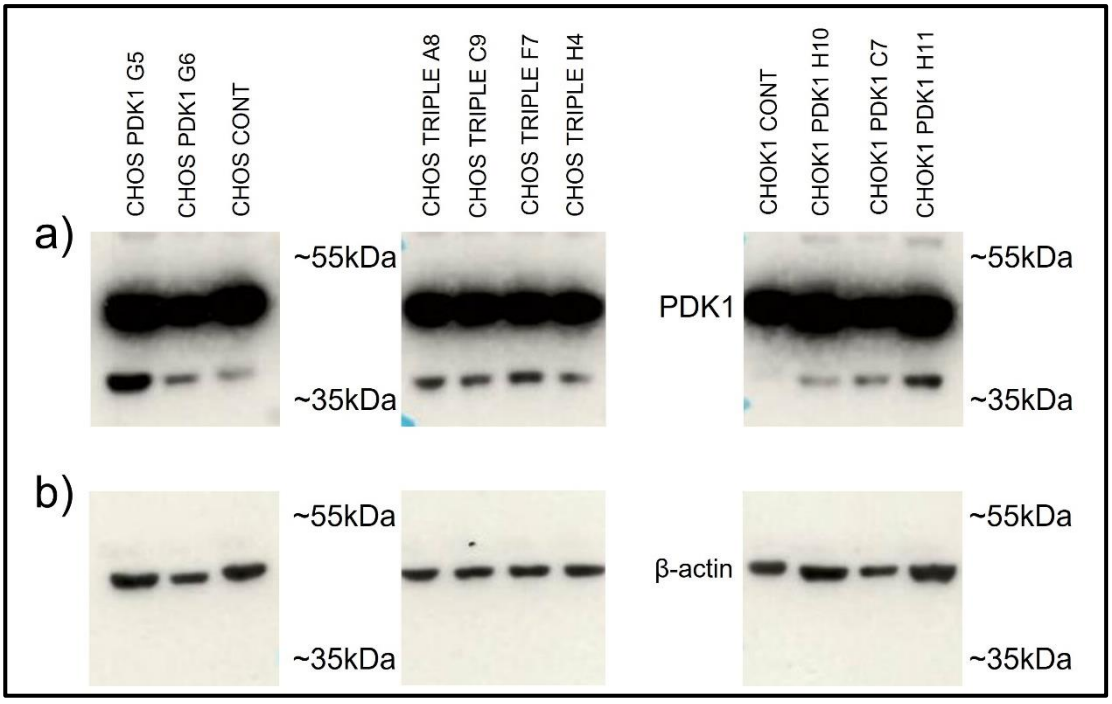

Figure 4.14.5 Western blot protein analysis of CHOS and CHOK1 cells transfected with CRISPR/Cas9 plasmids with gRNAs targeting PDK 1 or all three PDKs (TRIPLE) when probed with an anti-PDK1 antibody (a) and an anti-β-actin antibody (b). 5 µg protein was loaded and the blot exposed for 10 mins (a) and 5 secs (b). PDK1 can be seen around 49 kDa and β-actin can be seen around 37 kDa, the expected sizes.

Figure 4.14.5 reveals the presence of multiple bands in most samples when probed with the anti-PDK1 antibody (a), similar to those present in Figure 4.11.1.1, including a band at the expected size for PDK1 at 49 kDa. The blot was overexposed to allow visualisation of PDK1 expression in each sample however a shorter exposure time might have been clearer. PDK1 protein expression appeared similar in most samples with no obvious reduction in the cell pools transfected with

CRISPR/Cas9 plasmids targeting PDK1 or the TRIPLE KO cell pools when compared to host cell lines. There was also no clear difference in PDK1 expression when comparing CHOS or CHOK1 cell hosts. The β-actin blots (b) confirmed even protein loading.

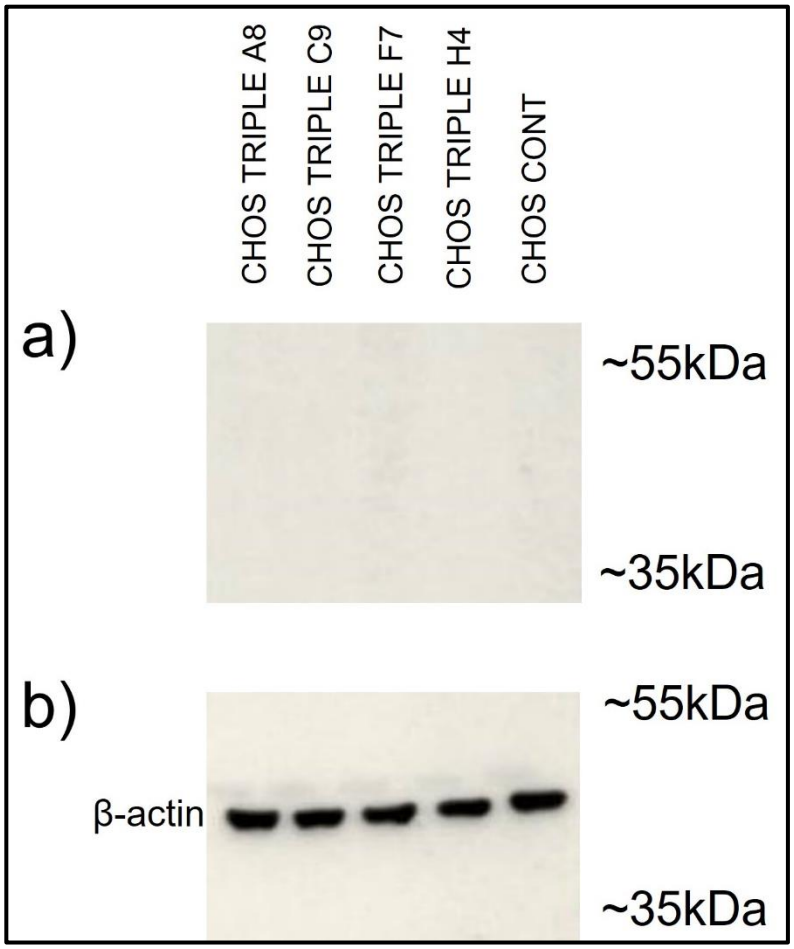

Figure 4.14.6 Western blot protein analysis of CHOS cells transfected with CRISPR/Cas9 plasmids with gRNAs targeting all three PDKs (TRIPLE) when probed with an anti-PDK2 antibody (a) and an anti-β-actin antibody (b). 5 µg protein was loaded and the blot exposed for 45 mins (a) and 5 secs (b). Bands for PDK2 are not seen around the expected size of 46 kDa but β-actin bands can be seen around 37 kDa as expected.

Figure 4.14.6 shows no bands were observed for any samples when using the anti-PDK2 antibody (a – including the control). Bands had been observed previously when using this antibody (Figure 4.11.2.1), although they were faint. The presence of β-actin was observed for all samples (b), suggesting protein was present at similar concentrations and therefore the lack of a PDK2 band (a) is likely due to low concentration in all samples and a weak antibody.

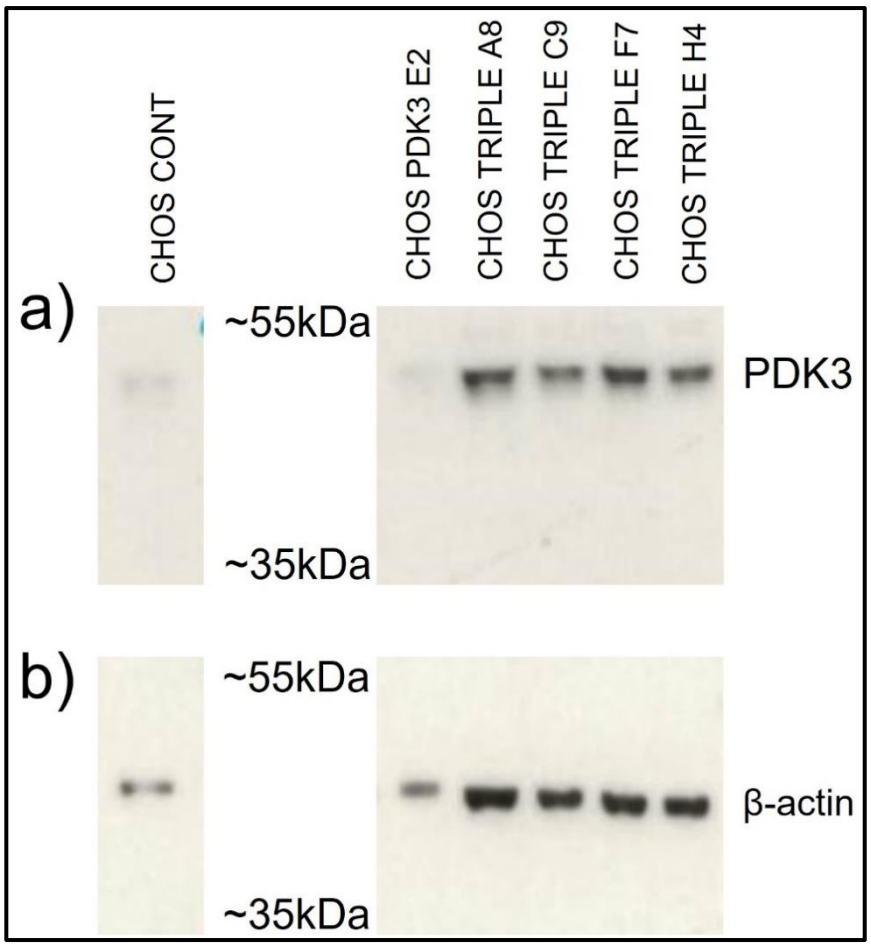

Figure 4.14.7 Western blot protein analysis of CHOS and CHOK1 cells transfected with CRISPR/Cas9 plasmids with gRNAs targeting PDK 3 or all three PDKs (TRIPLE) when probed with an anti-PDK3 antibody (a) and an anti-β-actin antibody (b). 5 µg protein was loaded and the blot exposed for 45 mins (a) and 5 secs (b). PDK3 can be seen around 47 kDa and β-actin can be seen around 37 kDa, the expected sizes.

Figure 4.14.7 (a) reveals the presence of bands in all samples at 47 kDa, the expected size of PDK3, when probed with the anti-PDK3 antibody. The bands for the CHOS control cell line and CHOS PDK3 KO E2 were both fainter in comparison to those from the TRIPLE KO samples. However, when looking at the signal from the anti-β-actin antibody (b), this was also fainter for these samples suggesting a lower concentration of protein was present to start with. Figure 4.14.7 suggests little difference in protein expression in the KO cell pools when compared to the host CHOS cells.

Figures 4.14.5 to 4.14.7 suggest little impact on PDK protein expression from transfection of the CRISPR/Cas9 plasmids targeting the relevant PDKs. This result was seen for the TRIPLE KO cell pools also. The results presented in Figures 4.14.5 to 4.14.7 were similar to those from the dot blot analysis presented in Figures 4.14.1 to 4.14.3 suggesting the creation of the mini pools did not select cell lines with a higher target PDK KO and instead large variation is seen within samples.

Alternatively, it could suggest that the mini pool process selects for cells with a lower level of target PDK KO suggesting the process of individual cell sorting is required to identify and isolate cells with a higher impact to protein expression resulting from the CRISPR/Cas9 process.

4.15 Evaluation of PDK Expression in KO Cell Pools with Differences in Recovery

Recovering cell pools generated via the FACS process had gDNA samples taken from them. Large differences in culture viability had been noted, whilst some that had adapted to shaking suspension culture had an average culture viability of 85-95%, other cell pools that were growing in T25 flasks with a lower viability and cell number. This variation was seen across cell pools independent of the starting number of cells sorted to create the pool. Samples were then used for qPCR analysis, following the process detailed in methods section 2.3.10.2, to evaluate the gDNA amount of relevant KO PDK target compared to β-actin in relevant host cells. Further analysis using mRNA expression levels was planned but not completed due to time constraints and sample availability especially for the slower growing cells. Figure 4.15.1 highlights the key trends in the results of the qPCR reactions with CHOS (a) and CHOK1 (b) cell lines transfected with PDK2 targeting CRISPR/Cas9 gRNAs with further data in Appendix Figures 7.2.7 and 7.2.8 showing other surviving KO cell lines. Samples taken from cell pools of lower culture viability in T25 flasks are marked with an asterisk (*). A one-way ANOVA was performed using Dunnett's multiple comparisons test comparing the results to relevant host cells. Significance is shown for key results where p value was less than or equal to 0.05 otherwise results displayed are not significant.

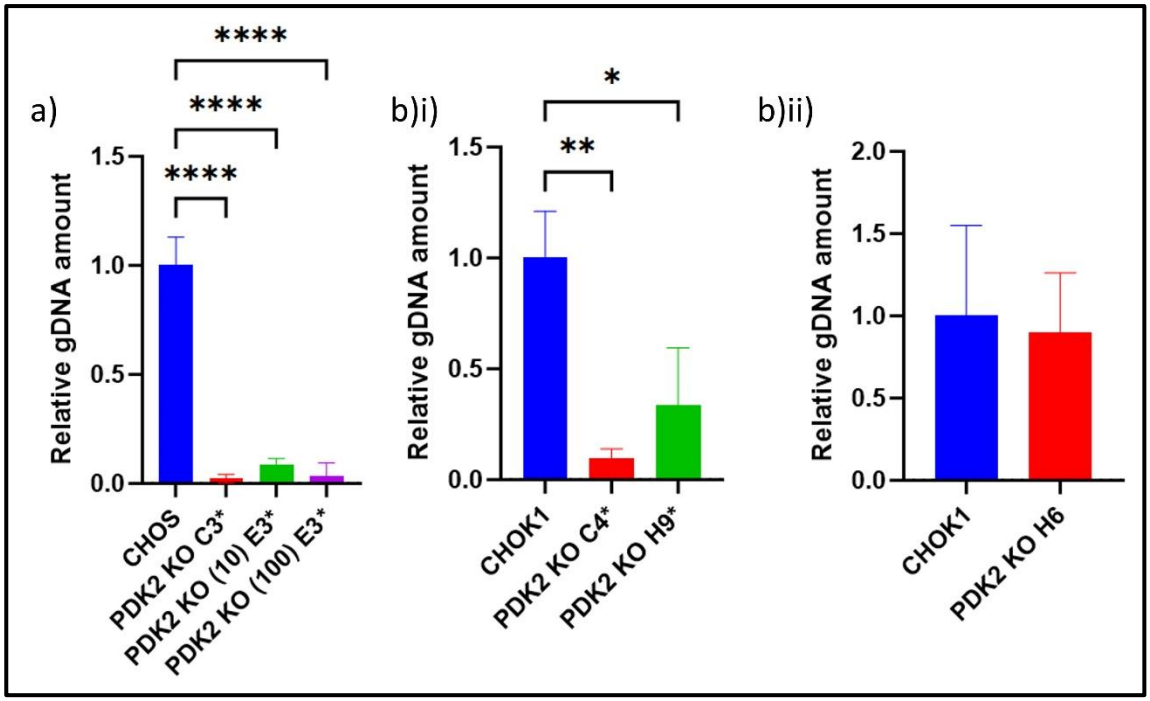

Figure 4.15.1 Relative gDNA amount of PDK2 in selected CHOS (a) and CHOK1 (b) cell pools expressing CRISPR/Cas9 KO plasmids with PDK1 targeting gRNAs analysed via qPCR from gDNA samples. PDK1 primers used to compare β-actin levels. Samples marked with an asterisk (*) are from pools with lower cell viability. A one-way ANOVA was performed using Dunnett's multiple comparisons test comparing the results to relevant host cells. Significance shown for key results where p value was less than or equal to 0.05. Extremely significant $p < 0.0001$ (****), Extremely significant $p = 0.0001$ to 0.001 (***), Very significant $p = 0.001$ to 0.01 (**), Significant $p = 0.01$ to 0.05 (*), Not significant $p \geq 0.05$ (ns). (n=3).

Figure 4.15.1 shows the relative gDNA amounts of KO target gene PDK2 in FACs sorted, screened and selected CHOS (a) and CHOK1 (b) cells transfected with CRISPR/Cas9 plasmids when compared to β-actin gDNA levels. No CHOS PDK2 KO cell pools recovered to larger shaking cultures from the cryopreservation process so gDNA samples were taken from cell pools with lower culture viability in T25 flasks (*). All CHOS PDK2 KO cell pools (a) show a large reduction in PDK2 gDNA amounts compared to the host cell lines with the starting size of the pool also shown (10/100). CHOK1 KO cell pools (b) had one pool adapt to shaking culture after revival (bii) and two that remained in T25 flasks at a lower culture viability (bii). The reduction in PDK2 gDNA amounts in lower viability cell pools C4 and H9 (bi) was much larger than the reduction observed in the H6 cell line (bii) that maintained a high culture viability.

These trends of a higher KO efficiency, suggested by a lower gDNA amount of KO target PDK, in cell pools not recovering after FACs are also suggested in the results in Appendix Figure 7.7.7 and 7.7.8 for both CHOS and CHOK1 cells including TRIPLE KO cell pools. When cells were growing in shaking cultures with a higher cell viability and number, a smaller reduction in gDNA amounts of target PDKs

was seen, with some results suggesting an increase in relative target PDK gDNA amounts. Issues occurred during this process as the PDK3 qPCR primers were not always binding correctly so were not producing valid results. However, the overall suggestion of the PDK KO impacting cell viability and recovery after FACs was seen in all PDK KO cells sampled, including the TRIPLE KO cells. These results could suggest the cells with a more efficient CRISPR/Cas9 KO of the target PDKs are not surviving leading to those with a lower efficiency KO to out compete them skewing the results of the qPCR, RTqPCR and protein level analysis. Repeats of these analytical methods would enable the investigation into this further.

4.16 Attempt Two at FACS Sorting of PDK KO Cell Pools

Due to the limited success of generating viable PDK KO cell lines shown in 4.15, the CRISPR/Cas9 experiment process was repeated. The same process as described previously in this Chapter was used with transfections of the selected gRNA pairs in both CHOS and CHOK1 cells to create individual KO and TRIPLE KO cell pools. Three days after transfection cells were selected into pools using FACS, isolating cells expressing a GFP fluorescence intensity above 10^3 which were sorted into two 96 well plates of 10 cells per well for each host cell line and PDK target. Both Amphotericin B solution and Penicillin-Streptomycin were added to the media after cell sorting. The cell pools were then left in the plates to recover at 37°C, 5% CO_2 and checked weekly for growth and confluence, moving the recovering cell pools from the 96 well plate up to 24 well plates and finally 6 well plates.

Screening of cell pools was then undertaken using western blot analysis of PDK protein expression. The western blots of CHOS and CHOK1 PDK1 KO cell pools probed with the anti-PDK1 antibody had no bands for any samples, including the control host samples, even after an exposure of an hour. This may have been due to the limited lysate sample taken and the low protein concentration of PDK1 combined with the antibody not being strong. The western blot was probed with an anti-β-actin antibody and bands were observed for control and some PDK KO cell pool samples at the expected 37 kDa size, suggesting that there was differential protein loading. Therefore, a dot blot was undertaken, and the results are shown in Figure 4.16.1.

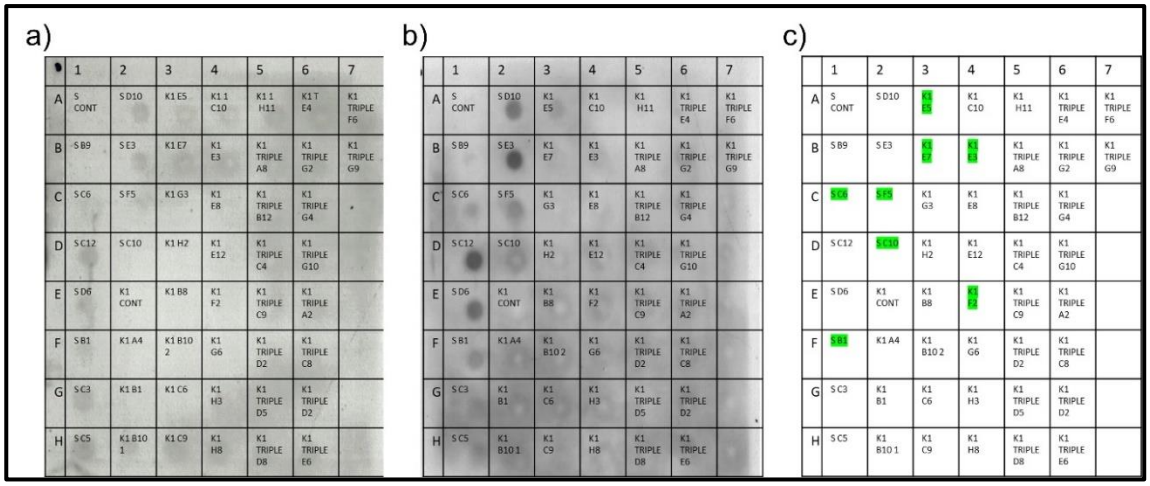

Figure 4.16.1 Dot blot analysis of CHOS and CHOK1 cells transfected with CRISPR/Cas9 plasmids with gRNAs targeting PDK1 or all three PDKs (TRIPLE) when probed with an anti-PDK1 antibody (a) or an anti-β-actin antibody (b). The chosen cell pools are highlighted in green (c) 5 µg protein loaded. PDK1 blot exposed for 1 hour and β-actin blot exposed for 40 mins. TRIPLE KO cell pools transfected using all three sets of gRNA pairs.

Figure 4.16.1 shows the results of dot blots of lysate samples from PDK1 KO cell pools having recovered from the FACS process and subsequently expanded into 24 and 6 well plates. Some faint signals could be seen when probing with the anti-PDK1 antibody (a) with clearer signals observed for the β-actin blot (b), although neither control sample shows a signal on either blot. Cell pools were selected based on a high β-actin signal but low PDK1 signal as in the previous rounds of cell pool generation. The CHOS and CHOK1 cell pools selected are outlined in 4.16.1 (c) and were as follows; CHOS PDK1 KO C6, C10, F5, B1 and CHOK1 PDK1 KO E5, E7, E3, F2.

The western blot analysis of the CHOS and CHOK1 PDK2 KO cell pools were more successful than PDK1 as shown in Figure 4.16.2 with at least a band for β-actin being observed in the cell samples. When probed with anti-PDK2 antibody, all samples, apart from the CHOS and CHOK1 control cell lines, only showed a band at a higher molecular weight than the expected size for PDK2 at 46 kDa (not shown in Figure 4.16.2). The expected PDK2 band was observed in the CHOS and CHOK1 control samples (Figure 4.16.2 (a)) suggesting expression levels of PDK2 protein in the KO cell pools was lower than the control cell lines. This analysis was used to select the KO cell pools with high β-actin expression levels and no PDK2.

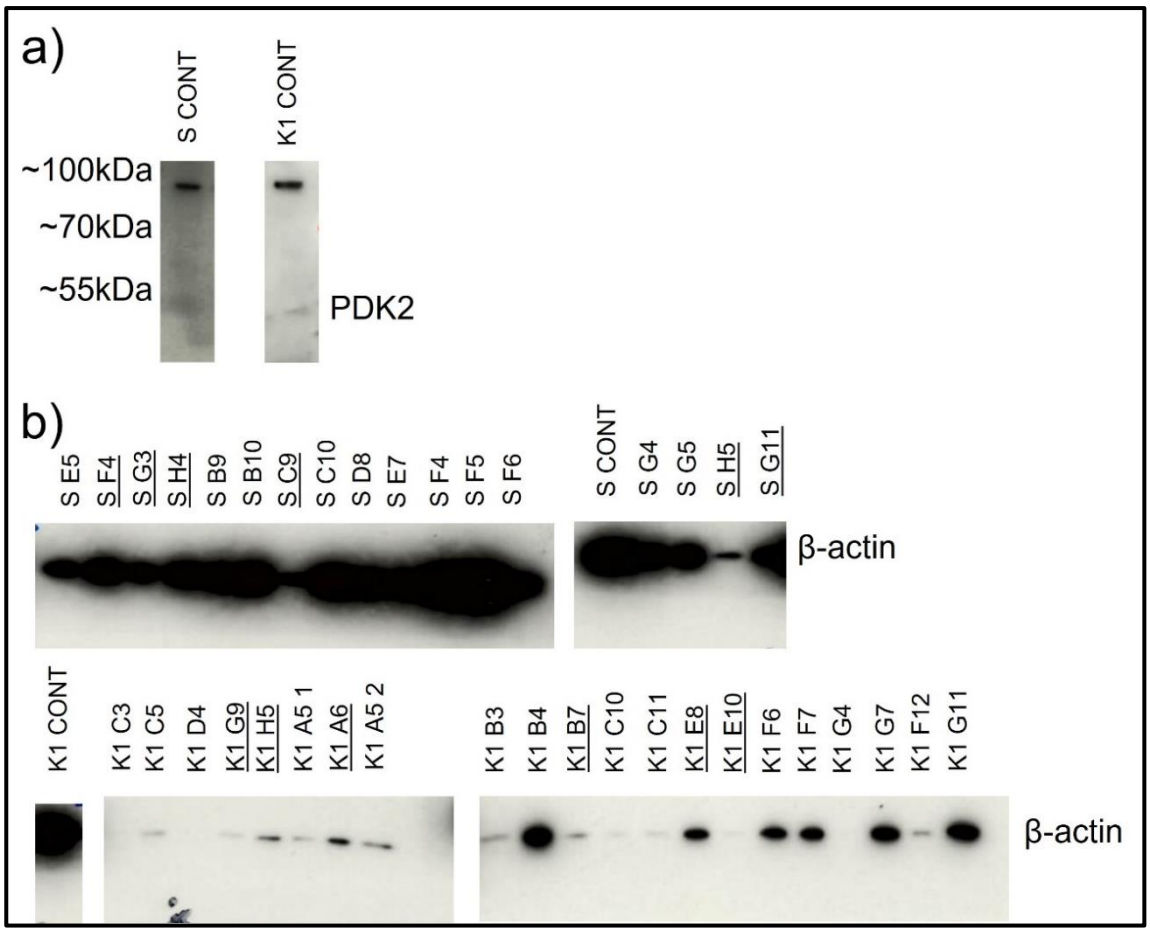

Figure 4.16.2 Western blot analysis of CHOS and CHOK1 cells transfected with CRISPR/Cas9 plasmids with gRNAs targeting PDK2 when probed with an anti-PDK2 antibody (a) or an anti-β-actin antibody (b). 5 μg protein loaded PDK2 blots exposed for 1 hour, β-actin for 10 mins. A band at 46 kDa is seen for PDK2 and at 37 kDa for the β-actin blots respectively. The cell pools underlined were carried forward.

Figure 4.16.2 shows the results of western blot analysis of lysate samples from PDK2 KO cell pools having recovered from the FACS process and subsequently moved into 24 and 6 well plates. The two bands observed in the PDK2 blot (a) were at around 100 kDa and 46 kDa, the smaller being the expected size of PDK2. None of the PDK2 KO cell pools had signals for PDK2 smaller 46 kDa band (data not shown) so the results from the β-actin blot (b) were used to select cell pools as follows; CHOS PDK2 KO F4, G3, H4, C9, H5, G11 and CHOK1 PDK2 KO G9, H5, A6, B7, E8, E10.

A similar pattern with the PDK1 KO western blots was observed as for the PDK3 KO lysate western blot. When PDK3 pools were probed with the anti-PDK3 antibody there were no bands for any samples including the control host samples even after an hour of exposure. This probably reflects the limited lysate sample available and low protein concentration. The western blot was also probed

with anti-β-actin antibody and bands were observed for control samples and some cell pool samples at the expected 37 kDa size (data not shown). A dot blot was therefore also undertaken shown in Figure 4.16.3.

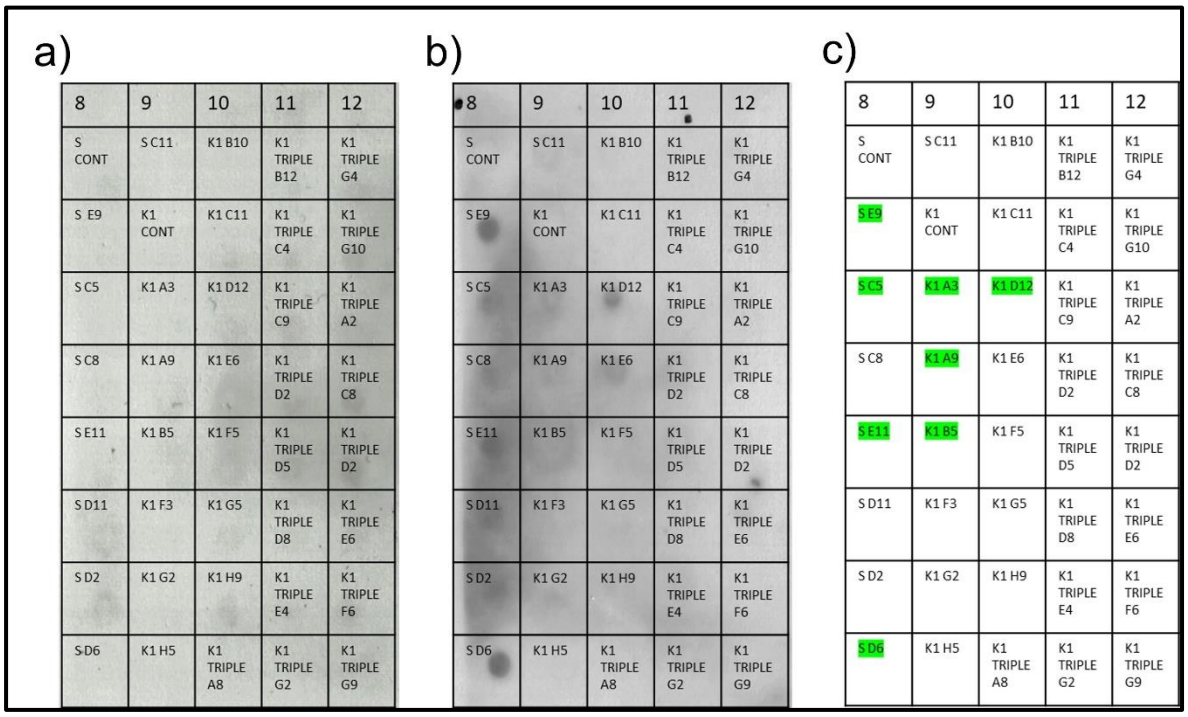

Figure 4.16.3 Dot blot analysis of CHOS and CHOK1 cells transfected with CRISPR/Cas9 plasmids with gRNAs targeting PDK3 or all three PDKs (TRIPLE) when probed with an anti-PDK3 antibody (a) or an anti-β-actin antibody (b). The chosen cell pools are highlighted in green (c) 5 µg protein loaded. PDK3 blot exposed for 1 hour and β-actin blot exposed for 40 mins. TRIPLE KO cell pools transfected using all three sets of gRNA pairs.

Figure 4.16.3 shows the results of dot blot analysis of lysate samples from PDK3 KO cell pools having recovered from the FACS process and expanded into 6 well plates. Some cell pools had a faint signal for the PDK3 blot (a), however more intense signals were present in the β-actin blot (b.) Signals were not observed for either CHOS or CHOK1 control samples for either antibody. Cell pools were selected based on a high β-actin signal but low PDK3 signal. The selected CHOS and CHOK1 cell pools are detailed in 4.16.3 (c) and are as follows; CHOS PDK3 KO E9, C5, E11, D6 and CHOK1 PDK3 A3, A9, B5, D12. CHOS PDK3 cell pools C11 and D11 were also expanded into shaking culture.

The dot blot analysis of the TRIPLE KO cell pool lysates are shown on the right-hand side of Figures 4.16.1 and 4.16.3. Unfortunately, analysis of the TRIPLE KO samples revealed no bands for the PDK2 and hence are absent in Figure 4.16.2. Ultimately all the CHOS TRIPLE KO cell pools were lost and did not recover from the sorting. By combining the results from Figures 4.16.1 and 4.16.3, Figure 4.16.4 shows the results and selection of CHOK1 TRIPLE KO cell pools.

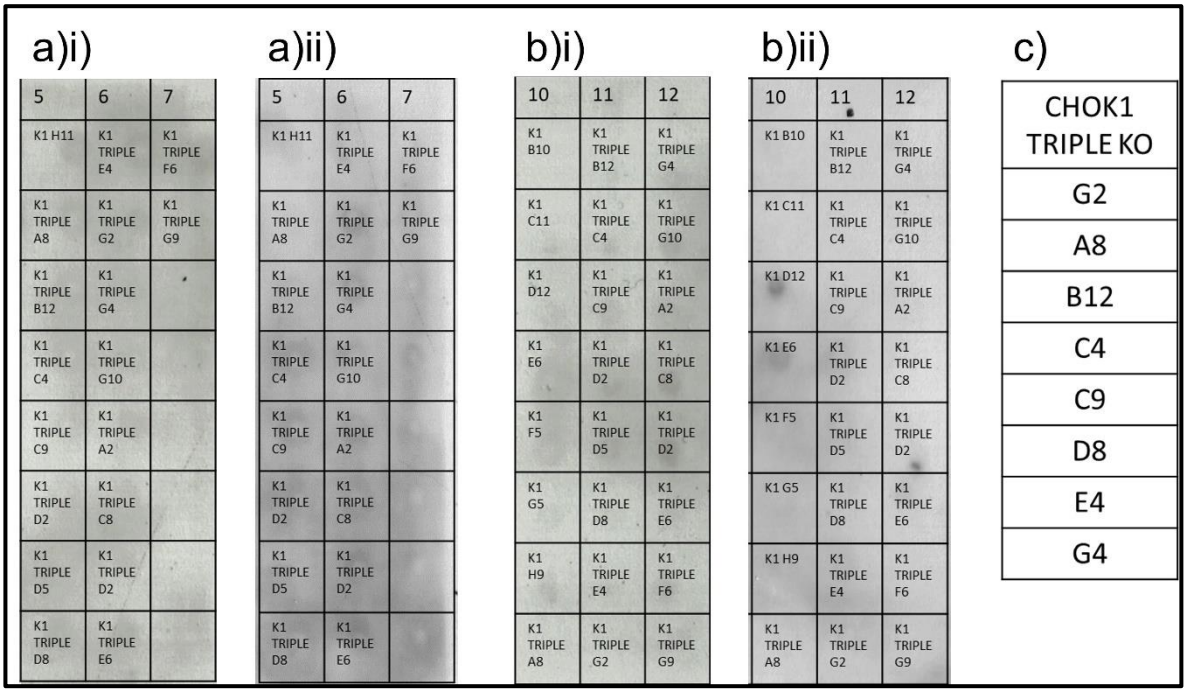

Figure 4.16.4 Dot blot analysis of CHOS and CHOK1 cells transfected with CRISPR/Cas9 plasmids with gRNAs targeting all three PDKs (TRIPLE) when probed with an anti-PDK1 antibody (a)i) or an anti-β-actin antibody (a)ii) or when probed with an anti-PDK3 antibody (a)i) or an anti-β-actin antibody (a)ii). The selected cell pools are listed (c) 5 µg protein loaded. PDK1 and PDK3 blots exposed for 1 hour and β-actin blots exposed for 40 mins. TRIPLE KO cell pools transfected using all three sets of gRNA pairs. The full dot blot results can be seen in Figures 4.16.1 and 4.16.3 for PDK1 and PDK3 screening respectively.

Figure 4.16.4 shows the selection of CHOK1 TRIPLE KO cell pools based upon dot blots probed with anti-PDK1, anti-PDK3 and anti-β-actin antibodies taken from Figures 4.16.1 and 4.16.3. CHOK1 TRIPLE KO cell pools were selected that showed little to no signal for the PDK antibody blots but signals for the anti-β-actin probed dot blots. CHOK1 TRIPLE KO cell pools G2, A8, B12, C4, C9, D8, E4 and G4 were selected.

Although the method of screening via dot blot is less specific compared to bands on a western blot, the layout allows simple identification of cell lines with lower protein expression levels of PDKs targeted for KO. It also allows for high throughput screening which is especially useful when screening multiple cell line pools.

4.17 qPCR Screening of PDK gDNA Levels in Selected Cell Pools

To investigate whether the PDK KO cell pools described and selected in section 4.16 had impacted gDNA levels of the target PDKs, gDNA samples were taken and qPCR used for analysis. Previously, in section 4.15, qPCR data showed a larger reduction in gDNA amounts of PDK KO targets in cell pools growing at a lower cell number and viability than in those that were growing in shaking culture at higher cell numbers. To investigate whether this trend continued, qPCR was again performed. RTqPCR based analysis of mRNA expression levels was planned to complement the qPCR results but was not completed due to time constraints. PDK3 KO cell pools and the CHOK1 TRIPLE KO cell pools were unable to be fully investigated for their PDK3 gDNA levels as the assay was not reproducible enough for this target. Figure 4.17.1 highlights the key trends in the results of the qPCR reactions with CHOS (a) and CHOK1 (b) cell lines transfected with PDK2 targeting CRISPR/Cas9 gRNAs with further data in Appendix Figures 7.2.9 and 7.2.10 showing other surviving KO cell lines. Cells maintained in 6 well plates, at lower viability and cell number compared to shaking cultures, are indicated by the presence of an asterisk (*) after the cell pool name. A one-way ANOVA was performed using Dunnett's multiple comparisons test comparing the results to relevant host cells. Significance is shown for key results where p value was less than or equal to 0.05 otherwise results displayed are not significant.

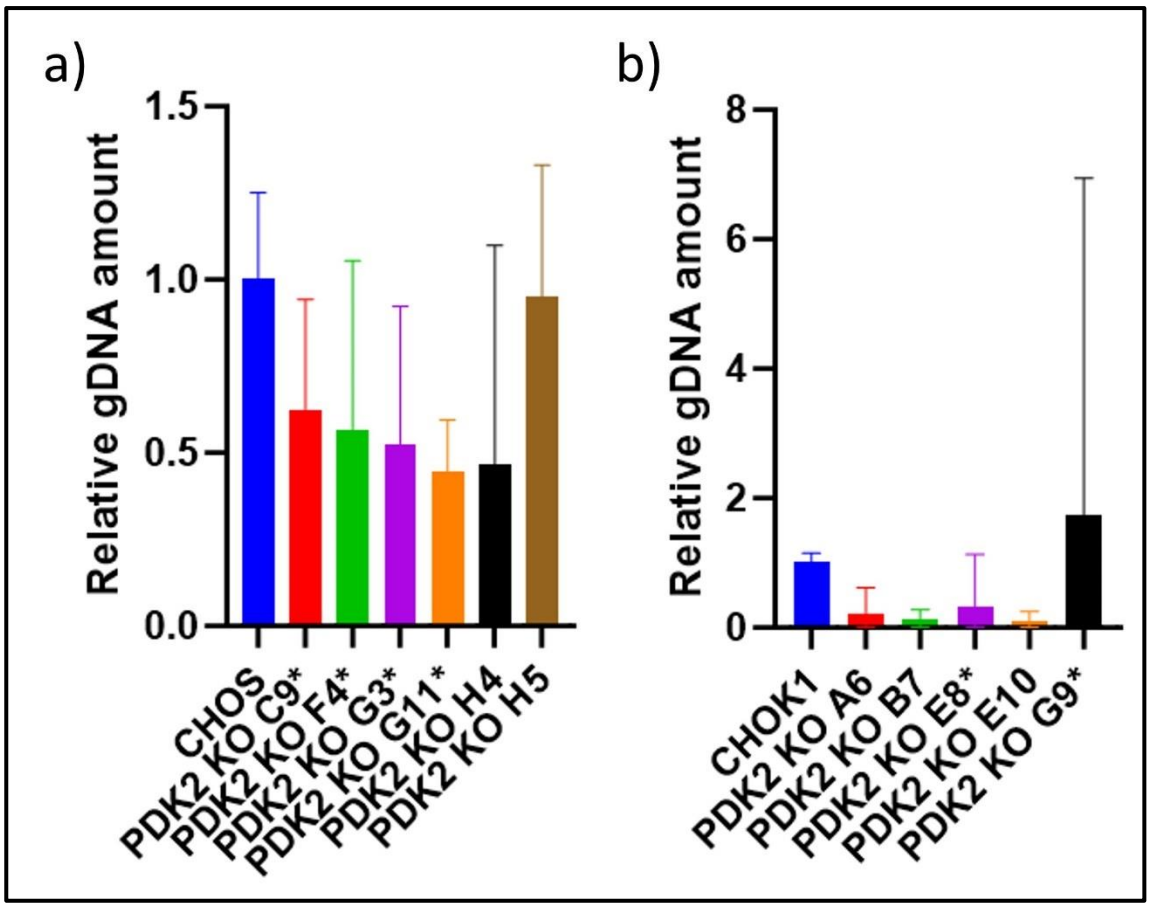

Figure 4.17.1 Relative gDNA amount of PDK2 in selected CHOS (a) and CHOK1 (b) cell pools transfected with CRISPR/Cas9 KO plasmids with PDK2 targeting gRNAs analysed via qPCR from gDNA samples. PDK2 primers used to compare β-actin levels. Samples marked with an asterisk (*) are from pools with lower culture viability. A one-way ANOVA was performed using Dunnett's multiple comparisons test comparing the results to relevant host cells. Significance shown for key results where p value was less than or equal to 0.05. Extremely significant $p < 0.0001$ (****), Extremely significant $p = 0.0001$ to 0.001 (***), Very significant $p = 0.001$ to 0.01 (**), Significant $p = 0.01$ to 0.05 (*), Not significant $p \geq 0.05$ (ns). (n=3).

Figure 4.17.1 shows the relative gDNA amounts of KO target gene PDK2 in selected CHOS (a) and CHOK1 (b) PDK2 KO cells transfected with CRISPR/Cas9 plasmids and relevant gRNAs when compared to β-actin gDNA amounts. Two of the six CHOS PDK2 KO cell pools were at high culture viabilities in suspension in falcon tubes, pools H4 and H5, whilst the other four cell pools had lower culture viability and were maintained in 6 well plates. PDK2 KO cell pool H4 had a large reduction in PDK2 gDNA amounts compared to the other high culture viability cell pool H5 and was comparable to the reduction in PDK2 gDNA amounts seen in the cell pools of lower culture viability in 6 well plates. CHOK1 cell pools (b), CHOK1 PDK2 KO E10, B7 and A6, were maintained at higher culture viability in suspension shaking cultures in falcon tubes whilst the others, CHOK1 PDK2 KO G9 and E8, were maintained at a lower culture viability in 6 well plates. Figure 4.17.1 suggests a greater reduction in target PDK gDNA amount in the higher culture viability cell pools compared to the lower

culture viability which is opposite the trend reported in section 4.15. The CHOK1 PDK2 KO G9 pool had an increase in PDK2 gDNA amounts compared to the host cell lines but was a low viability cell pool. All other cell pools, including CHOK1 PDK2 KO E10, B7 and A6 which were of a higher culture viability, had a large reduction in PDK2 gDNA amounts. The CHOS (a) and CHOK1 (b) PDK2 KO cell pools show different results with some supporting the trends of a larger reduction in target PDK gDNA amounts in lower viability cell pools seen in section 4.15 and others showing the opposite with lower viability cell pools having a smaller reduction of target gDNA amounts. There are noticeably large error bars on all samples including those in Appendix Figures 7.2.9 and 7.2.10 suggesting large variability was seen in results likely to be the impact of taking lower quality samples from cells of lower viability and limited cell numbers.

Issues with the PDK3 qPCR primers meant the expression of PDK3 gDNA could not be determined in either CHOS or CHOK1 cell pools or the CHOK1 TRIPLE KO cell pools so only PDK1 and PDK2 KO impact on gDNA amounts could be investigated limiting the potential to fully analyse the impact to target gDNA amounts resulting from CRISPR/Cas9 targeted KO.

Cell pools were cryopreserved and revived a few weeks later to explore the impact of the CRISPR/Cas9 targeted KO of PDKs on the cell pool phenotype and expression of a model difficult to express biotherapeutic protein. CHOS PDK2 KO H4 and CHOS PDK3 D11 cell pools were the only two that survived revival from cryopreservation and so were assessed in characterisation experiments described in Chapter 5.

4.18 General Discussion

A full discussion of all the results from this thesis is provided in Chapter 6. The aim of this Chapter (Chapter 4) was to design and assemble CRISPR/Cas9 gRNA plasmids targeting the PDKs 1-3 that phosphorylate and deactivate the PDH enzyme complex, transiently express them in CHO cells and analyse their efficiency using qPCR. When designing gRNAs, care must be taken to avoid unwanted off target effects due to sequence similarities to other genes or non-coding sequences (Mohr et al., 2016). The publication of the CHO genome and chromosome scaffolds along with the development of multiple target predictors such as CCTop has streamlined the design process and is a key factor of the widespread adoption of the CRISPR genome editing process (Hilliard et al., 2020). The use of a paired approach aims to remove the entire gene preventing the formation of indels that could result in misfolded or mutated protein production. Multiple sets of gRNAs were designed for PDKs 1-3 and transfected into cells. Their KO efficiency was analysed using qPCR and enabled the selection of a single pair for each target. Initial experiments targeting PDKs 1 and 2 were performed in

Professor Nicole Borth's lab in Vienna using CHOK1 cells whereas the following experiments targeting all three PDKs were performed at the University of Kent in Canterbury using both CHOS and CHOK1 cell hosts. Different methods were used for the transfection of cells and the resulting analysis and might provide an explanation for the differences observed alongside the use of both β-actin and GAPDH housekeeping genes for qPCR and RTqPCR analysis. The final selection for gRNA sequences is displayed in Table 4.10.1.

Protein expression levels of PDKs, PDP and PK were investigated using western blots to identify any difference in the KO cell pools compared to the hosts. When using relevant anti-PDK antibodies, results showed mixed success at detecting reduced protein expression of the targeted PDKs. Interestingly, all KO cells showed an increase in protein expression of PDP which acts to remove the phosphorylation of the PDH complex via the activity of the PDKs. Protein expression levels of PK, that acts to convert PEP to pyruvate, were similar in host cells compared to KO cells apart from those with a PDK2 targeted KO which showed a more prominent band. Changes to protein expression were identified as a result of targeted PDK KO but small changes with large variation between cell pools were seen suggesting the need for clonal selection.

These pools were also used to investigate any impact on gDNA amounts of PDH subunits *E1alpha*, *E1beta*, *E2* and *E3BP* as well as *PDP*. The KO cell pools showed an increase in gDNA amounts of the PDH subunit E1alpha whilst the other PDH subunits and PDP showed a decrease in gDNA amounts. These results suggest the cells might be responding to the KO of the PDKs and trying to regulate the expression of the PDH complex to maintain activity levels and flux from pyruvate to acetyl-CoA.

Once gRNAs had been selected to target each PDK, the transfection process was repeated, and the KO cell pools were sorted using both limiting dilutions and FACS. Initially limiting dilutions was used but cell recovery was an issue after multiple attempts. Repetition of the transfection process allowed the expression of GFP, in the Cas9 encoding backbone from Addgene, to be used for FACS based cell sorting and so this process was used instead. Due to the issues with clonal cell recovery, minipools were generated of the KO cell pool with 10, 100 and 1000 cells per well sorted into several plates. Dot blot analysis enabled the quick screening of multiple minipools to select the final KO cell pools for evaluation. Western blot analysis was used to investigate modulated PDK protein expression in the pools more clearly for the TRIPLE KO cell pools. Recovery from the cell sorting process continued to be an issue with some cell pools recovering quickly and others maintaining low viable cell numbers and culture viabilities. A selection of cells were sampled for gDNA analysis via qPCR which showed the cells recovering slowly had a higher reduction of gDNA amounts compared to those growing faster which showed gDNA levels more comparable to host cells.

Difficulties with the PDK3 targeting qPCR primers also proved to be an issue and so full analysis of the TRIPLE KO cell pools was not possible.

A further attempt at generating PDK KO cell pools was more successful with their recovery. A similar trend of recovery and higher PDK gDNA levels was seen in some but not all samples after qPCR analysis, however two CHOS KO cell pools were successfully generated, CHO PDK2 H4 which showed a reduction to about 47% of host PDK2 gDNA levels, and CHOS PDK3 D11 whose PDK3 gDNA levels could not be analysed due to issues with the relevant qPCR primers.

The results in this thesis chapter successfully describe the generation of two CHOS PDK KO cell pools, however the resulting impact to protein and gDNA amounts of relevant PDK targets varied. Although described as a KO pool, it is likely to be a mix of cells including some KO cells and some wild type cells, with the potential for wild type cells to out compete KO cell lines where the KO is impacting growth phenotypes. This mixture of cell genotypes is likely a key cause of the variation seen within the results presented in this Chapter and highlights the need for the creation of clonal cell pools for full analysis of KO impact. Unfortunately, only PDK2 and PDK3 KO CHOS minipools were able to be generated after multiple rounds of CRISPR/Cas9 suggesting either the KO itself, or an aspect of the recovery process was impacting cell survival. These cell pools were then used to investigate the impact KO of the PDKs had on cell growth and secretory recombinant protein production of DTE protein Etanercept which is detailed in Chapter 5 of this thesis. A fuller discussion of all the results chapters from the thesis is provided in Chapter 6 of the thesis.

Chapter 5: Investigating the Impact of PDH Cell Line Engineering on CHO Cell Phenotype and Difficult to Express (DTE) Protein Yields

5.1 Introduction

Chapters 3 and 4 of this thesis detailed the specifics of cell line engineering based approaches in an attempt to modify PDH expression and activity in CHO cells generating multiple cell pools. Chapter 3 describes the development of cell pools overexpressing PDH subunits E1alpha, E1beta and E2 in combinations and individually, with and without the addition of tags, alongside an E1alpha serine/alanine mutant cell pool. Chapter 4 describes the use of CRISPR/Cas9 to generate PDK KO cell minipools with a CHOS PDK2 and PDK3 KO cell pool successfully made. This chapter investigated these modified cell pools made in Chapters 3 and 4, to analyse the impact the cell engineering subsequently had on cell growth, metabolite flux and finally the production of a model DTE biotherapeutic protein used in the clinic, Etanercept. Having originally been approved for use in the clinic to treat rheumatoid arthritis in 1998 under the drug name Enbrel, the producers Amgen had the patent further extended from 2012 to 2028 (Harrison, 2012). This extended patent however is only relevant in the US market and hasn't prevented the development of multiple biosimilars for the European market where the patent ended in 2015 (Walsh & Walsh, 2022). Biosimilars are designed to act with no clinically meaningful differences from the originating medicine (US Food & Administration, n.d.) and help to provide market competition, reducing costings and increase the availability of medicines (Azevedo et al., 2015). Etanercept is considered a DTE protein, being a tumour necrosis factor receptor (TNFR)-Fc-fusion protein where the Fc is derived from an IgG1 (Duivelshof et al., 2021). Etanercept is both N- and O-glycosylated and is prone to aggregation during manufacturing. It was therefore used as a model DTE protein in the studies described here.

Engineered cell pools from Chapters 3 and 4 were grown in 10 ml batch cultures. During the culture their growth was analysed measuring viable cell concentrations and culture viabilities throughout the 240 hour culture period. Samples were taken at 96, 144 and 192 hours into the culture relating to the exponential, stationary and the decline phases of cell culture growth. These samples were used to analyse changes in the metabolites glucose, lactate, ammonia, glutamine and glutamate throughout the culture to determine if any changes in their metabolism as a result of the PDH targeted cell engineering was observable. After this, the batch culture process was repeated, however this time the engineered cells were transiently transfected to express the Etanercept Fc-fusion protein. Samples were again taken at the 96, 144 and 192 hour timepoints with cell growth and culture viability determined. Western blot analysis was used to identify differences in

Etanercept expression in both the engineered and host cell lines with cell specific production calculated. Samples were taken for metabolite analysis however this was not possible due to the unavailability of the Cubian Metabolite Analyser used previously. A selection of these host cell samples were used to analyse gDNA levels of PDH subunits E1alpha, E1beta, E2 and E3BP as well as LDHa and PDP when, and when not, producing the model DTE Etanercept. These results showed the biggest changes in gDNA levels observed whilst producing Etanercept were in relation to the levels of PDH subunit E1alpha and LDHa. The qPCR process was therefore repeated with all samples taken at the 144 hour mark of batch culture. Samples from the PDK KO cell pools generated in Chapter 4 were also used to analyse differences in gDNA amounts of PDH subunits as well as LDHa, PDP and PDK1 and PDK2.

Finally, western blot analysis was used to identify any changes in expression of lipid gene targets SCD1 and SREBF1. SCD1 and SREBF1 were previously identified as lipid metabolism targets that led to an increase in cell growth, ER size and recombinant protein production when their expression was increased (Budge et al., 2020). SCD1 acts to desaturate saturated fatty acids to monounsaturated fatty acids to increase membrane fluidity. It also influences the activity of acetyl-CoA carboxylase (ACC) which acts to convert acetyl-CoA to malonyl-CoA in the first and rate limiting step in *de novo* fatty acid synthesis (Y. Wang et al., 2022). SREBF1 is a transcriptional activator which influences multiple genes involved in lipid metabolism (Van Meer & De Kroon, 2011). An increase in PDH activity could lead to the generation of more acetyl-CoA and therefore may influence SCD1 and/or SREBF1 expression.

A summary of all the cell pools generated detailed in Chapters 3 is shown in Table 5.1 for reference throughout this chapter. PDK KO cell pools generated in Chapter 4 are referenced as such.

Table 5.1 Stable CHOS and CHOK1 cell pools generated in Chapter 3 of this thesis and the gene engineered. Y = gene is present, blank box signifies that cassette was left empty.

Plasmid Number	Plasmid Name	E1alpha Cassette 1	E1beta Cassette 2	E2 Cassette 3
PEL1	Hygro 3 Cass	3 Empty Cassettes		
PEL3 (E1α)	Hygro 3 Cass E1alpha	Y		
PEL4 (E1β)	Hygro 3 Cass E1beta		Y	
PEL5 (E2)	Hygro 3 Cass E2			Y
PEL6 (E1α, E1β)	Hygro 3 Cass E1alpha E1beta	Y	Y	
PEL7 (E1α, E2)	Hygro 3 Cass E1alpha E2	Y		Y
PEL8 (E1β,E2)	Hygro 3 Cass E1beta E2		Y	Y
PEL9 (E1α, E1β,E2)	Hygro 3 Cass E1alpha E1beta E2	Y	Y	Y
PEL11	Hygromycin Etanercept	Etanercept, Single Cassette		
PEL12	Hygromycin 3 Cass Tags	3 Empty Cassettes with Tags		
PEL13 (E1αNV5)	Hygromycin 3 Cass E1alpha N V5 Tag	Y N V5 Tag		
PEL14 (E1αCV5)	Hygromycin 3 Cass E1alpha C V5 Tag	Y C V5 Tag		
PEL15 (E1βNHA)	Hygromycin 3 Cass E1beta N HA Tag		Y N HA Tag	
PEL16 (E1βCHA)	Hygromycin 3 Cass E1beta C HA Tag		Y C HA Tag	
PEL17 (E2NFLAG)	Hygromycin 3 Cass E2 N FLAG Tag			Y N FLAG Tag
PEL18 (E2CFLAG)	Hygromycin 3 Cass E2 C FLAG Tag			Y C FLAG Tag
PEL19 (E1αmutCV5)	Hygromycin 3 Cass Tags E1alpha serine/alanine mutant C V5 Tag	Y, Mutant C V5 Tag		

5.2 Aims of this Chapter

The aim of this chapter was to determine any impact on cell phenotype and production of the model DTE biotherapeutic protein Etanercept as a result of the engineering approaches to manipulate PDH complex activity described in Chapters 3 and 4. The overall aims of the work in this chapter were therefore to:

a. Analyse any differences between the PDH subunit overexpression cell pools generated as described in Chapter 3 during batch culture in terms of growth and basic carbon (glucose) metabolism
b. Transiently express the model DTE biotherapeutic protein Etanercept in a batch culture in the PDH overexpression cell pools generated in Chapter 3 and the PDK KO cell pools generated in Chapter 4
c. Analyse the cell phenotype (growth, basic glucose metabolism) and Etanercept production from the PDH subunit overexpression cell pools generated in Chapter 3 and the PDK KO cell pools generated in Chapter 4
d. Start to investigate if there were any impacts on lipid metabolism in the engineered cell pools generated in Chapters 3 and 4.

5.3 Analysis of cell growth during batch culture of CHO cell pools engineered to express tagged and untagged exogenous PDH subunits described in Chapter 3

The overexpression cell pools generated in Chapter 3 include CHOS and CHOK1 cell pools stably expressing untagged and N- or C-terminally tagged PDH subunits E1alpha, E1beta or E2. Chapter 3 details their generation and the analysis of gDNA amounts and protein expression levels of the PDH subunits when compared to host and empty cassette plasmid (PEL1 or PEL12) stable control cell lines with a summary shown in Table 5.1. To investigate any impact the expression of these PDH subunits had on cell concentrations and culture viability, batch cultures were setup and monitored. CHOS and CHOK1 cell pools expressing untagged and N- and C-terminally tagged E1alpha, E1beta and E2 PDH subunits were grown in 10 ml cultures with shaking at 220 rpm in Corning™ Mini Bioreactor Centrifuge Tubes alongside control cell lines and seeded at $0.2x10^6$ viable cells per ml. Growth profiles were determined in biological triplicate for all cell pools and compared to the host, PEL1 (empty cassette) and PEL12 (empty tag cassette) control cell lines/pools. Figures 5.3.1 to 5.3.4 report the viable cell numbers of the CHOS and CHOK1 host cell lines and engineered cell pools.

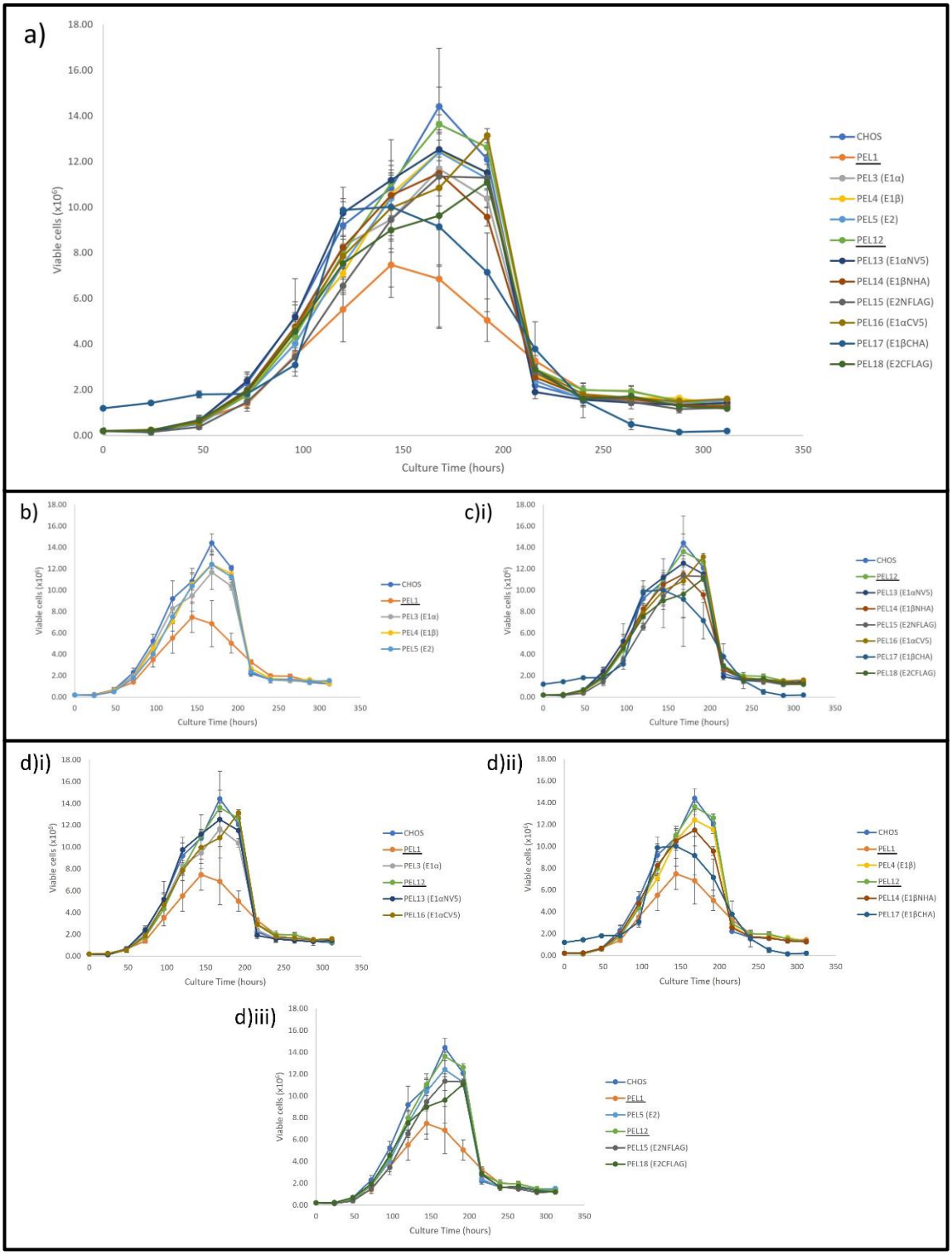

Figure 5.3.1 Viable cell number (x10^6) for CHOS cell pools stably expressing untagged and N- or C-terminally tagged PDH subunits E1alpha, E1beta or E2 generated in Chapter 3 over a 312 hour batch culture time course. (a) All cell lines, (b) untagged PDH subunit expressing cell pools only, (c) N- or C-terminally tagged PDH subunit expressing cell pools only. Untagged and N- or C-terminally tagged PDH subunit expressing cell pools (di) E1alpha only, (dii) E1beta only, (diii) E2 only. (n=3). PEL1 empty cassette control, PEL3 (E1α), PEL4 (E1β), PEL5 (E2), PEL12 empty tag cassette control, PEL13 (E1αNV5), PEL14 (E1βNHA), PEL15(E2NFLAG), PEL16 (E1αCV5), PEL17 (E1βCHA), PEL18 (E2CFLAG).

Figure 5.3.1 shows the viable cell numbers for CHOS cell pools stably expressing untagged and N- or C-terminally tagged PDH subunits E1alpha, E1beta or E2 over a 312 hour batch culture time course when compared to host, PEL1 (empty cassette) and PEL12 (empty tag cassette) control cell lines/pools. All cells outperformed the PEL1 empty cassette control. The untagged and N- and C-terminally tagged cell pool results are displayed in graphs 5.3.1(b) and 5.3.1(c) respectively to allow for clearer comparison. Results in 5.3.1(d) show the viable cell numbers for untagged and tagged individual PDH subunit expressing cell pools, allowing comparisons between cell pools expressing specific PDH subunits E1alpha (di), E1beta (dii) and E2 (diii) with and without the tag and in each position (N- or C-terminal). All cell pools show a similar trend in viable cell number (a) with peak viable cell number reached around 170 hours of batch culture and a steep reduction observed after 200 hours. The CHOS host control cell line reached the highest viable cell number over the culture with the PEL12 control (empty tag cassette) cell pool reaching a similar viable cell number. When compared, the edited cell pools expressing untagged or tagged individual PDH subunits all obtained a lower peak viable cell number as shown in Figure 5.3.2. Control cell pools expressing the empty cassette (PEL1) obtained the lowest viable cell number over the culture time. Comparing the viable cell numbers of cell pools expressing untagged PDH subunits in PEL1 (empty cassette control), 3 (E1alpha), 4 (E1beta) and 5 (E2) in 5.3.1(b) shows similar viable cell numbers were obtained for all three untagged cell pools across the time course. The tagged subunit expressing cell lines PEL12 to PEL18 5.3.1(c) also showed no clear change in the viable cell number obtained when compared to host cells over the batch culture. Thus, the expression of any of the exogenous PDH subunits did not seem to have a detrimental effect on viable cell number.

The results presented in Figure 5.3.1(d) show the individual PDH subunit specific expression impact compared to control cell lines. The untagged and tagged E1alpha expressing cell lines, PEL3 (E1α), 13 (E1αNV5) and 16 (E1αCV5) 5.3.1 (di) obtained similar viable cell numbers with the N-terminally V5 tagged E1alpha PEL13 cell pool obtaining viable cell numbers closest to the control cell line and the C-terminally V5 tagged E1alpha PEL16 cell pool showing the highest peak viable cell number before the steep reduction after 200 hours. E1beta untagged and tagged expressing cell lines PEL4 (E1β), 14 (E1βNHA) and 17 (E1βCHA) (dii) also showed a similar trend in terms of viable cell numbers when compared to control cell lines. The C-terminally HA tagged (PEL17) cell pools expressing the E1beta subunit with a C-terminal HA tag showed a small increase in viable cell number 120 hours into the batch culture. E2 untagged and tagged expressing cell pools PEL5 (E2), 15 (E2NFLAG) and 18 (E2CFLAG) 5.3.1(diii) obtained similar viable cell numbers over the batch culture. In summary, the data in Figure 5.3.1 show similar viable cell numbers reached by all edited CHOS cell pools however these were not as high as the CHOS host or PEL12 (empty tag cassette) control cells. When

comparing the individual PDH subunits 5.3.1(d) and their expression either untagged or with N- or C-terminal tags, there was no clear difference between these cells. The presence and position of the tag was therefore not seen to impact viable cell numbers.

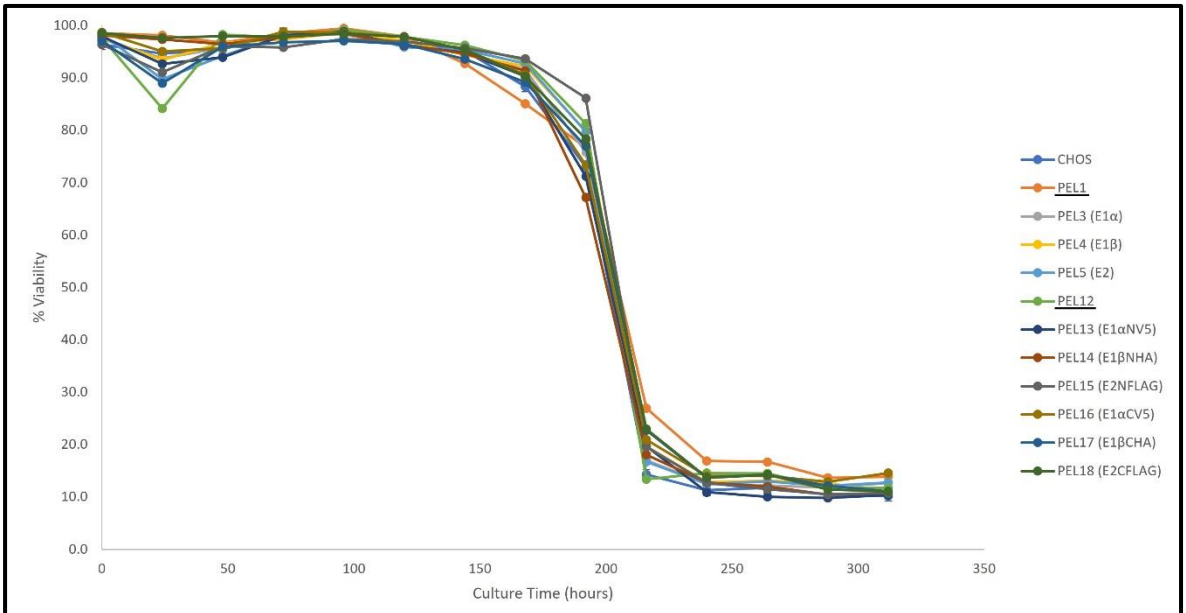

Cell Line	CHOS	PEL1	PEL3 (E1α)	PEL4 (E1β)	PEL5 (E2)	PEL12	PEL13 (E1αNV5)	PEL14 (E1βNHA)	PEL15 (E2NFLAG)	PEL16 (E1αCV5)	PEL17 (E1βCHA)	PEL18 (E2CFLAG)
Doubling Time (Hours)	20.42	23.24	20.98	21.28	22.22	21.61	20.45	21.10	23.45	21.18	22.80	21.30
Peak Cell Density ($x10^6$)	14.42	7.48	11.67	12.44	12.42	13.63	12.53	11.50	11.35	13.14	10.01	11.09

Figure 5.3.2 Average percentage culture viability for CHOS cell pools stably expressing untagged and N- or C-terminally tagged PDH subunits E1alpha, E1beta or E2 generated in Chapter 3 over a 312 hour batch culture time course together with the doubling time (Hours) over the first 96 hours of batch culture and peak cell density ($x10^6$). (n=3). PEL1 empty cassette control, PEL3 (E1α), PEL4 (E1β), PEL5 (E2), PEL12 empty tag cassette control, PEL13 (E1αNV5), PEL14 (E1βNHA), PEL15(E2NFLAG), PEL16 (E1αCV5), PEL17 (E1βCHA), PEL18 (E2CFLAG).

Figure 5.3.2 shows the average percentage culture viability between the triplicates of each engineered CHOS cell pool over the course of the batch culture (viable cell numbers reported in Figure 5.3.1). Alongside is the doubling time over the first 96 hours of the culture (during growth phase) and the peak cell density obtained for each cell pool. All engineered CHOS cell pools had similar culture viabilities across the batch culture when compared to the control cell lines. The pattern in Figure 5.3.1 was mirrored in terms of with the culture viability falling after 200 hours of batch culture. The doubling times of each cell pool reflect the similarities in growth profiles in Figure 5.3.1 and 5.3.2. CHOS host cell lines had the fastest doubling time at 20.42 hours with N-terminally V5 tagged E1alpha PEL13 cells having a similar doubling time of 20.45 hours. PEL12 empty tag cassette control cell pools had a slower doubling time of 21.61 hours (Figure 5.3.2), although they

obtained the second highest viable cell number after the CHOS host cells. The low doubling time over the first 96 hours is a reflection of the reduction culture viability at the 24 hour time point. The doubling time was calculated over the first 96 hours of the batch culture whilst the cells were growing exponentially suggesting the PEL12 empty tag cassette control cells recovered to achieve high viable cell numbers. When looking at data for the untagged and N-terminally tagged PDH subunit expressing cell pools, E1alpha targeted cell pools (PEL13) had the shortest doubling time followed by E1beta (PEL14) and the E2 (PEL15) expressing cell pools in their relevant groupings. C-terminally tagged PDH subunit expressing cell lines PEL16 (E1αCV5), 17 (E1βCHA) and 18 (E2CFLAG) did not follow this pattern with all C-terminally tagged subunits having a similar doubling time.

Figure 5.3.3 shows the viable cell numbers for CHOK1 cell pools stably expressing untagged and N- or C-terminally tagged PDH subunits E1alpha, E1beta or E2 over a 312 hour batch culture compared to host, PEL1 (empty cassette) and PEL12 (empty tag cassette) control cell pools. The untagged and N- and C-terminally tagged cell pool results are split into 5.3.3(b) and 5.3.3(c) respectively for clearer comparison. Results in 5.3.3(d) show the viable cell numbers for untagged and tagged individual PDH subunit expressing cell pools for comparisons between pools expressing specific PDH subunits E1alpha 5.3.3(di), E1beta 5.3.3(dii) and E2 5.3.3(diii) with and without the tag and in each position. The CHOK1 host cells grew well at the start of the culture but dipped in viable cell number around 170 hours before increasing in number and finally decreasing again at the end of the culture. The error bars from the standard deviation of these results are large and therefore these results should be considered carefully when making comparisons to the engineered cell pools. Control cell pools PEL1 (empty cassette) and PEL12 (empty tag cassette) showed opposite trends in viable cell number. PEL1 cells obtained higher viable cell numbers initially which decreased around 150 hours into the batch culture before a small increase before falling again at end of culture whereas PEL12 cells initially had a lower viable cell number which increased around 150 hours before falling at the end of culture. These trends were followed by other CHOK1 cells expressing PDH subunits. Untagged E1alpha (PEL3), E1beta (PEL4) and E2 (PEL5) and C-terminally tagged E1alpha (PEL16) and E1beta (PEL17) cell pools had similar viable cell numbers over the culture when compared to the PEL1 control.

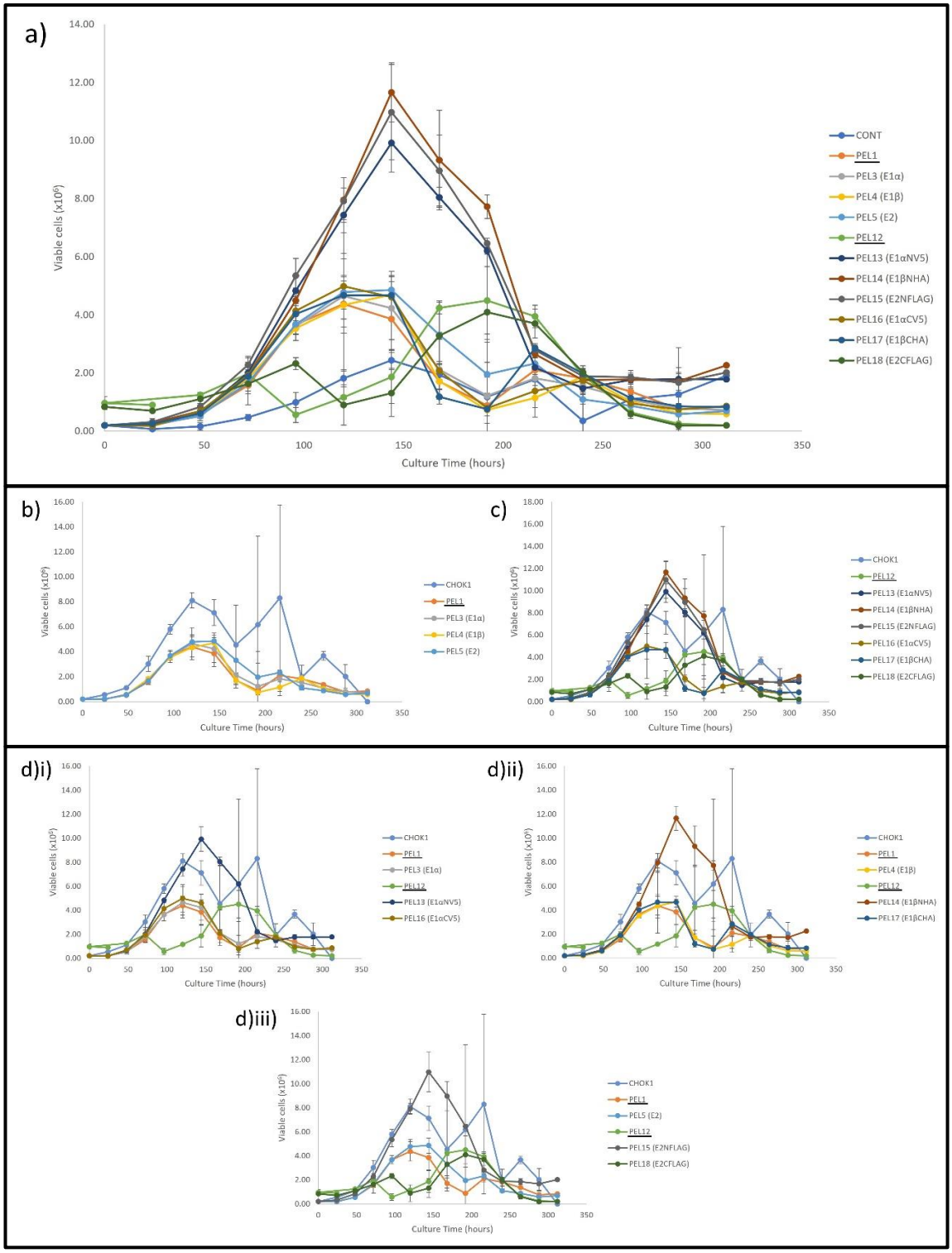

Figure 5.3.3 Viable cell number (x10^6) for CHOK1 cell pools stably expressing untagged and N- or C-terminally tagged PDH subunits E1alpha, E1beta or E2 generated in Chapter 3 over a 312 hour batch culture time course. (a) All cell pools, (b) untagged PDH subunit expressing cell pools only, (c) N- or C-terminally tagged PDH subunit expressing cell pools only. Untagged and N- or C-terminally tagged PDH subunit expressing cell pools (di) E1alpha only, (dii) E1beta only, (diii) E2 only. (n=3) PEL1 empty cassette control, PEL3 (E1α), PEL4 (E1β), PEL5 (E2), PEL12 empty tag cassette control, PEL13 (E1αNV5), PEL14 (E1βNHA), PEL15(E2NFLAG), PEL16 (E1αCV5), PEL17 (E1βCHA), PEL18 (E2CFLAG).

C-terminally FLAG tagged E2 expressing cell line (PEL18) achieved viable cell numbers similar to that of the PEL12 control cell pool throughout the batch culture. These similarities are clearly seen in the subunit specific viable cell number data (Figure 3.3.3(d)). These results also indicate differences in viable cell number between the cell pools and those expressing any of the PDH subunits with an N-terminal tag (PEL13, 14 and 15) which grew to much higher (almost double), viable cell numbers than all other engineered and control CHOK1 cell lines. This distinct enhancement in viable cell numbers is shown to the greatest extent with PEL14 (E1βNHA) cells followed by PEL18 (E2NFLAG) and finally PEL13 (E1αNV5) cell pools. The CHOK1 host control cell line had a similar viable cell number profile compared to the N-terminally tagged PDH expressing cell pools PEL13, 14 and 15 at the start of the batch culture, however from 120 hours the control cells decreased in viable cell number.

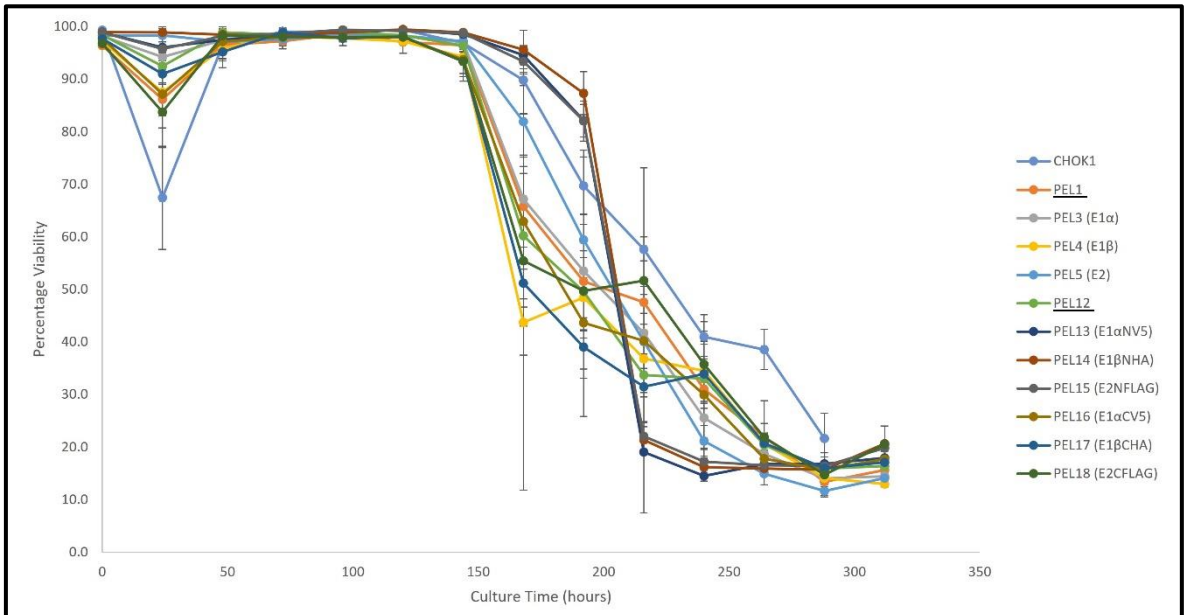

Cell Line	CHOK1	PEL1	PEL3 (E1α)	PEL4 (E1β)	PEL5 (E2)	PEL12	PEL13 (E1αNV5)	PEL14 (E1βNHA)	PEL15 (E2NFLAG)	PEL16 (E1αCV5)	PEL17 (E1βCHA)	PEL18 (E2CFLAG)
Doubling Time (Hours)	19.77	22.88	22.99	23.17	22.85	22.32	20.91	21.39	20.25	22.05	22.16	22.95
Peak Cell Density ($x10^6$)	8.11	4.38	4.65	4.70	4.86	4.50	9.92	11.66	10.98	4.99	4.68	4.10

Figure 5.3.4 Average Percentage Viability for CHOK1 cell lines stably expressing untagged and N- or C-terminally tagged PDH subunits E1alpha, E1beta or E2 generated in Chapter 3 over a 312 hour batch culture time course together with the doubling time (Hours) over the first 96 hours of batch culture and peak cell density ($x10^6$). (n=3) PEL1 empty cassette control, PEL3 (E1α), PEL4 (E1β), PEL5 (E2), PEL12 empty tag cassette control, PEL13 (E1αNV5), PEL14 (E1βNHA), PEL15(E2NFLAG), PEL16 (E1αCV5), PEL17 (E1βCHA), PEL18 (E2CFLAG).

The average culture viabilities are shown alongside the average doubling time over the first 96 hours of the batch culture and peak density for each cell pool in Figure 5.3.4 and highlights the differences

between CHOK1 cell pools expressing untagged and C-terminally tagged PDH subunits compared to those expressing N-terminally tagged subunits as previously shown in Figure 5.3.3. The cell pools expressing N-terminally tagged E1alpha (PEL13), E1beta (PEL14) and E2 (PEL15) remained at a higher culture viability up to 200 hours whereas the other engineered cell pools showed a decline in culture viability after around 170 hours. The N-terminally tagged PDH subunit expressing cell pools however decreased to a culture viability lower than the other engineered cell lines with a much steeper decline. Also shown are the differences between the N-terminally tagged PDH subunit expressing cell pools and the control host CHOK1 cells. These failed to maintain a high culture viability but did not exhibit a rapid decline in culture viability at 200 hours of culture. The other edited cell pools maintained a high culture viability until decreasing at 150 hours. These cell pools followed a similar pattern apart from the untagged E1alpha PDH subunit expressing cells (PEL3) which showed a small increase in culture viability.

The start of the batch culture was also of interest as many cell pools showed a reduction in culture viability after 24 hours. This was especially clear in the CHOK1 host cell pools; however all cell pools showed a recovery to reach high (>90%) culture viability after 48 hours. When determining the doubling time of the cell pools, CHOK1 host cells had the shortest over the first 96 hours of the batch culture. The N-terminally tagged expressing cell lines PEL13 (E1αNV5), 14 (E1βNHA) and 15 (E2NFLAG) had similar doubling times but the rapid increase in viable cell number observed in host CHOK1 cells in Figure 5.3.3 was not matched by any cell pools. Similarly, the peak cell density of CHOK1 host cell lines was much higher than the other control cell lines and edited cell pools apart from the cell pools expressing N-terminally tagged PDH subunits. The cells expressing N-terminally tagged PEL13 (E1αNV5), 14 (E1βNHA) and 15 (E2NFLAG), obtained peak cell density around double that achieved in most other cell pools and up to 1.4 times the density of the control cell line. The other edited cell pools achieved peak cell densities similar to the other PEL1 (empty cassette) and PEL12 (empty tag cassette) control cell pools. These results suggest the expression of the N-terminally tagged PDH subunits could potentially impact the pools growth phenotype leading to a higher viable cell concentration being achieved and that the culture viability was maintained at higher levels for longer in the batch culture compared to control cells and those expressing the untagged or C-terminally tagged PDH subunits.

Comparing the CHOS and CHOK1 cell lines and pools highlights the differences in growth phenotype between the two hosts. CHOS cell pools grew to a much higher viable cell number, around $13x10^6$ viable cells per ml compared to CHOK1 cells that grew to around $8x10^6$ viable cells per ml. It could therefore be suggested that the expression of the N-terminally tagged E1alpha, E1beta and E2 subunits in PEL13, 14 and 15 respectively in CHOK1 cells impacts the cell phenotype to increase the

viable cell number to one that is higher than control CHOK1 cells and comparable to that of the CHOS cell pools.

5.4 Analysis of untagged and tagged PDH subunit overexpression cell pool IVC values across batch culture

After investigating any impact on growth phenotype of the expression of untagged and tagged PDH subunits in both CHOS and CHOK1 cell pools generated in Chapter 3, extracellular cell culture metabolite analysis was undertaken to identify any impact on metabolism resulting from the engineering during batch culture. A CM Scientific CuBiAn HT-270 Biochemistry Analyser was used to measure the levels of glucose, lactate, ammonia, glutamine and glutamate in supernatant samples taken at 96, 144 and 192 hours of batch culture. This would potentially allow identification of any changes in glucose metabolism associated with the overexpression of target PDH subunits and therefore activity of the PDH complex in the engineered cell pools. Sample details are reported in methods section 2.3.8. GraphPad Prism 10.0.0 software was used to display and analyse the data for statistically significant differences between cell pools.

Before calculating the cumulative utilisation or production of metabolites from the cell pools, the integral of viable cell concentration (IVC) over the batch culture time period was calculated (detailed in methods section 2.3.9). The IVC calculates the area under the viable cell concentration curve shown in Figures 5.3.1 and 5.3.3 for CHOS and CHOK1 cells respectively. IVC is also used to calculate cell line/pool productivity and can be used to calculate specific utilisation or production rates of metabolites. The IVC values are reported for CHOS (a) and CHOK1 (b) cell pools in Figure 5.4.1.

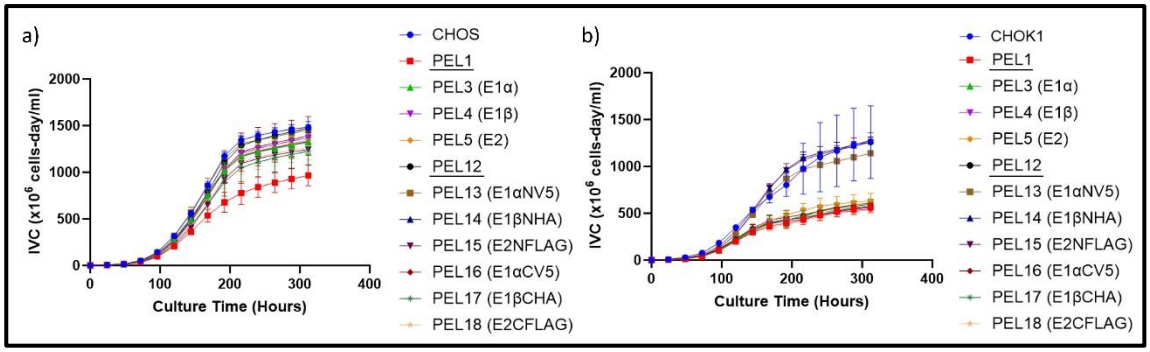

Figure 5.4.1 Integral of Viable Cell Concentration (IVC) of CHOS (a) and CHOK1 (b) cell pools over a 312 hour batch culture time course. (n=3) PEL1 empty cassette control, PEL3 (E1α), PEL4 (E1β), PEL5 (E2), PEL12 empty tag cassette control, PEL13 (E1αNV5), PEL14 (E1βNHA), PEL15(E2NFLAG), PEL16 (E1αCV5), PEL17 (E1βCHA), PEL18 (E2CFLAG).

Figure 5.4.1 shows the IVC values for the PDH subunit engineered cell pools over the batch culture time course for both CHOS (a) and CHOK1 (b) cells. Similar to the CHOS cell pool viable cell numbers reported in Figure 5.3.1, the IVC values in Figure 5.4.1(a) show one main grouping of most cell pools and the PEL1 empty cassette control cell pool sitting below the group with lower viable cell numbers and IVC values throughout the batch culture. Control CHOS cell pools had the highest IVC values with all PDH subunit overexpression cell pools having lower IVC values across the culture. CHOK1 cell pools profiles 5.4.1(b) also reflect the results reported in Figure 5.3.3 with cell pools expressing PDH subunits E1alpha (PEL13), E1beta (PEL14) and E2 (PEL15) with an N-terminal tag having the highest IVC values compared to untagged and C-terminally tagged PDH subunit expressing cell pools (PEL16, 17 and 18). Figure 5.4.1 also shows the similarities between these N-terminally tagged PDH subunit expressing cell pools and the CHOS host control cells which all had similar IVC values at the end of culture, although the CHOS host cells had much larger variation between replicates. The IVC values were used to calculate the specific production or utilisation rates of each metabolite based upon the cumulative production or utilisation over the culture period. These values are reported alongside their concentrations over the course of the culture and compared to host cell lines.

5.5 Analysis of glucose concentrations in overexpression cell lines during batch culture

Figure 5.5.1 reports the glucose concentrations (i) in the culture supernatant over the course of the batch culture at 96, 144 and 192 hours in both CHOS (a) and CHOK1 (b) PDH subunit overexpression cell pools as well as the cumulative concentration compared to IVC values (ii).

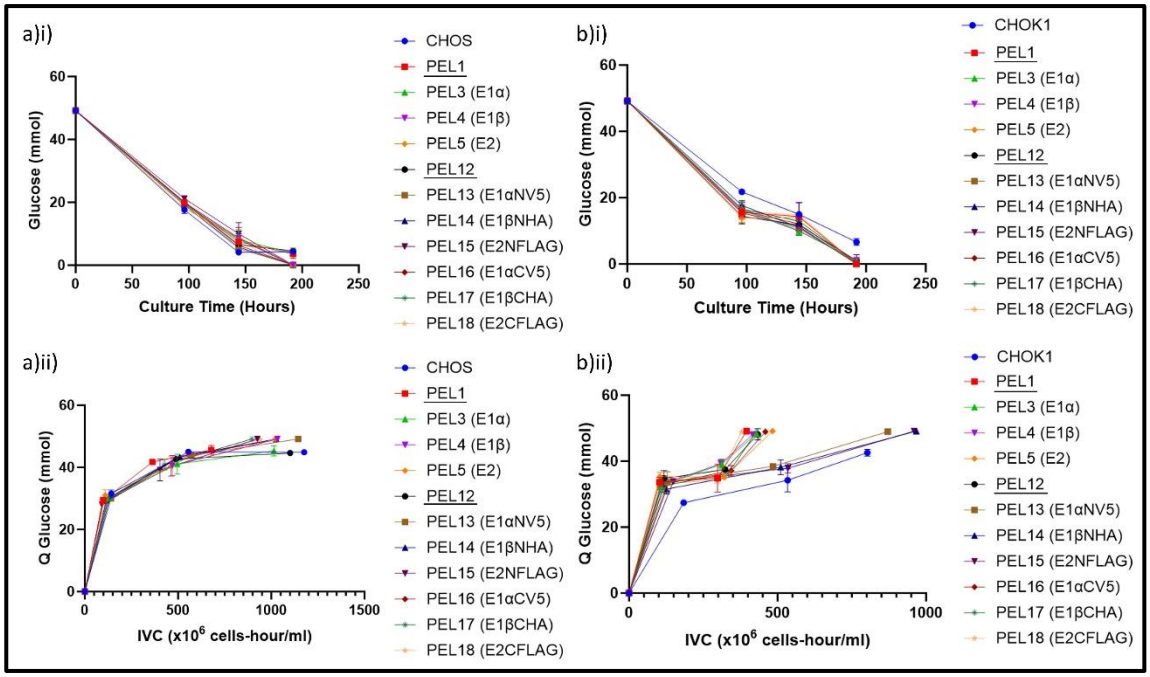

Figure 5.5.1 Glucose concentration (mmol) over culture time (i) and cumulative glucose utilisation (QGlucose) over IVC (ii) for CHOS (a) and CHOK1 (b) overexpression cell pools generated in Chapter 3 over a 312 hour batch culture. (n=3) PEL1 empty cassette control, PEL3 (E1α), PEL4 (E1β), PEL5 (E2), PEL12 empty tag cassette control, PEL13 (E1αNV5), PEL14 (E1βNHA), PEL15(E2NFLAG), PEL16 (E1αCV5), PEL17 (E1βCHA), PEL18 (E2CFLAG).

The CHOS cell line results in Figure 5.5.1(a) show similar glucose concentrations in all cell pool culture supernatants over the batch culture (i) with a steady decline in glucose and almost all of the glucose being used by most cell pools by the 192 hour time point. Only the control CHOS host, PEL1 (empty cassette) control, PEL12 (empty tag cassette) control and untagged E1alpha expressing PEL3 cell pools had appreciable glucose remaining at the final measurement, but at an approximate tenth of the concentration as at the start of culture. The cumulative glucose utilisation of CHOS cell pools (ii) showed all CHOS cells had similar glucose utilisation throughout the batch culture. CHOK1 cell pools (b) also showed a decrease in glucose concentration with culture time as expected (i). CHOK1 host cells maintained a higher glucose concentration throughout culture (albeit marginally) compared to other cell pools which all had depleted glucose concentration after 192 hours. The cumulative glucose utilisation of CHOK1 pools (ii) split into the two groupings of cell pools also observed when considering viable cell numbers and IVC reported in Figures 5.3.3 and 5.4.1 respectively. CHOK1 host cells were clustered together with cell pools expressing N-terminally tagged PDH subunits E1alpha, E1beta and E2 in PEL13, 14 and 15 respectively whilst those expressing untagged and C-terminally tagged PDH subunits were in a separate profile cluster. All cell

pools had similar cumulative glucose utilisation, however the N-terminally tagged expressing cell pool and host control cell lines had much higher IVC values in comparison.

When comparing the cumulative glucose utilisation to IVC in Figure 5.5.1 (ii), the trend lines can be used to calculate average specific glucose utilisation rates for each cell line/pool. These are shown in Figure 5.5.2. A one-way ANOVA using Dunnett's multiple comparisons test was performed comparing the results for each cell pool to the relevant host cells.

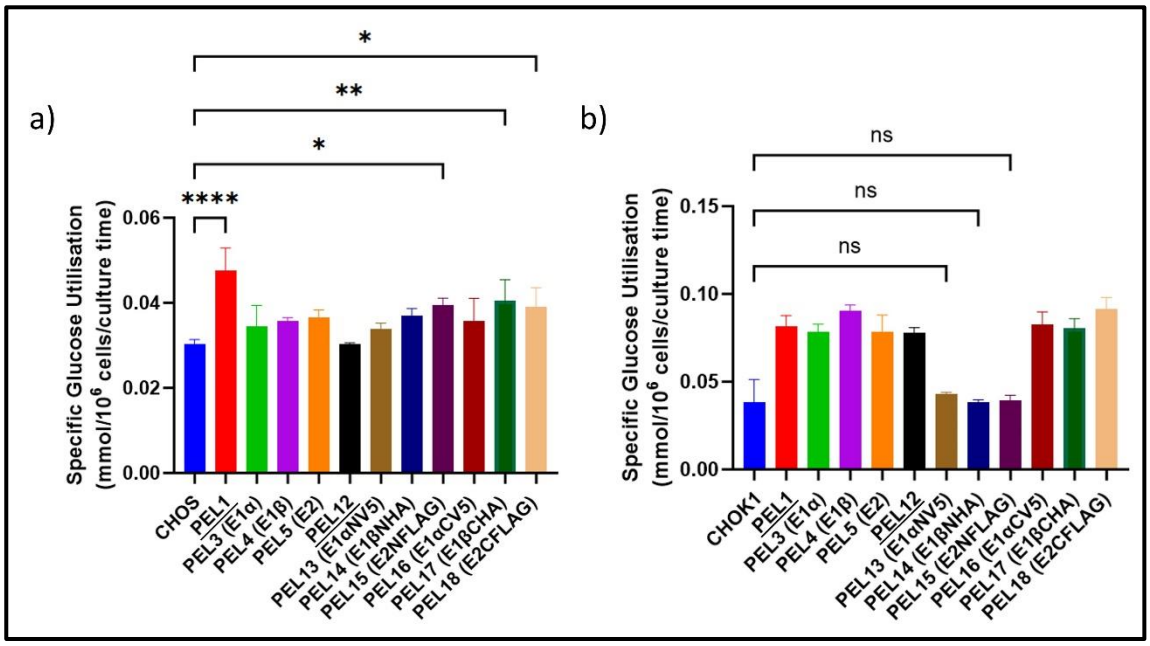

Figure 5.5.2 Specific utilisation of glucose for CHOS (a) and CHOK1 (b) PDH subunit overexpression cell pools. A one-way ANOVA was performed using Dunnett's multiple comparisons test comparing the results to relevant host cells. Significance shown for key results, Extremely significant $p < 0.0001$ (****), Extremely significant $p = 0.0001$ to 0.001 (***), Very significant $p = 0.001$ to 0.01 (**), Significant $p = 0.01$ to 0.05 (*), Not significant $p \geq 0.05$ (ns). (n=3) PEL1 empty cassette control, PEL3 (E1α), PEL4 (E1β), PEL5 (E2), PEL12 empty tag cassette control, PEL13 (E1αNV5), PEL14 (E1βNHA), PEL15(E2NFLAG), PEL16 (E1αCV5), PEL17 (E1βCHA), PEL18 (E2CFLAG).

Figure 5.5.2 reports the results for specific glucose utilisation rates in CHOS (a) and CHOK1 (b) cell pools and whether the results are statistically significant different compared to the controls using a one-way ANOVA and Dunnett's multiple comparisons test at $p<0.05$ confidence levels. The results for the CHOS cell pools (a) show all cell pools having a higher specific glucose utilisation compared to the CHOS host cells with cells engineered with empty cassette control plasmid PEL1 in particular showing statistically significantly higher glucose utilisation rates than the control host cells due to the similar glucose utilisation for lower viable cell numbers over the course of the culture. CHOK1 cells (b) showed a similar increase in glucose utilisation rates in all cell pools other than those

expressing PEL13 (E1αNV5), 14 (E1βNHA) and 15 (E2NFLAG) respectively which also showed similar IVC values to control cells. However, the difference was shown not to be statistically significant when compared to the CHOK1 host cells with similar glucose utilisation as the host control. All other cell pools showed statistically significant increases to glucose utilisation suggesting that when compared to host cells, the approach to overexpress untagged or C-terminally tagged PDH subunits made the cells less efficient with glucose utilisation whilst those overexpressing N-terminally tagged PDH subunits remained more similar to the hosts.

5.6 Analysis of lactate concentrations in PDH subunit overexpression cell pools during batch culture

Figure 5.6.1 reports the lactate concentrations (i) in the culture supernatant over the batch culture at 96, 144 and 192 hours in both CHOS (a) and CHOK1 (b) PDH subunit overexpression cell pools as well as the cumulative concentration compared to IVC values (ii).

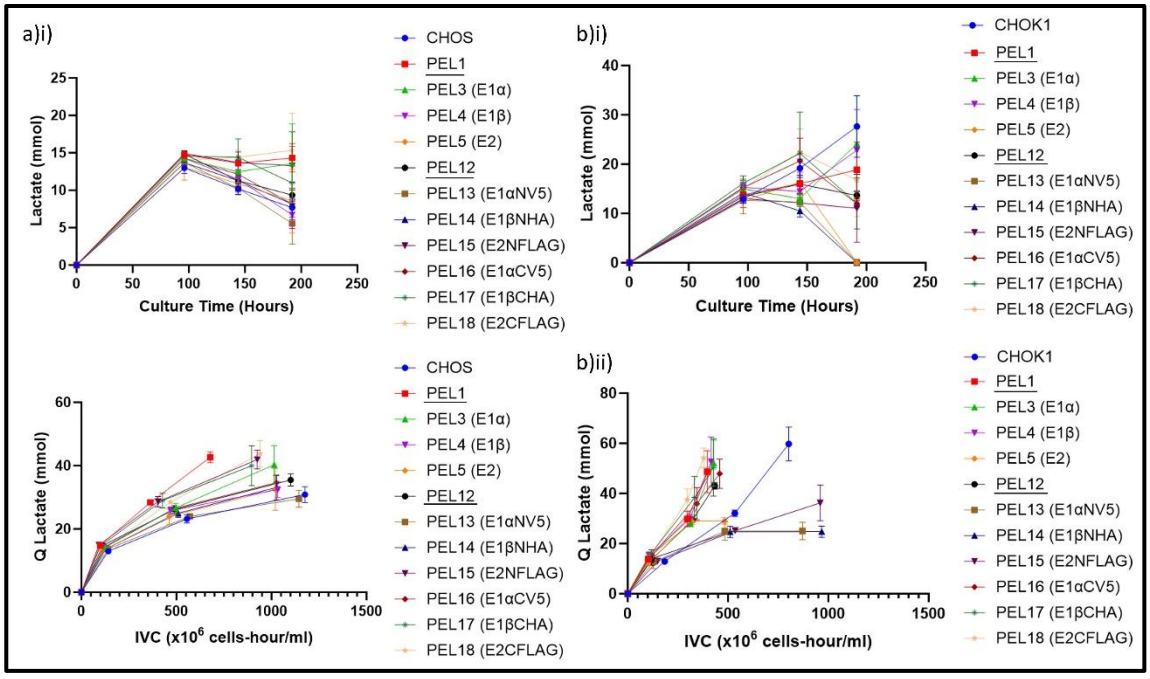

Figure 5.6.1 Lactate concentration (mmol) over culture time (i) and cumulative lactate production (QLactate) over IVC (ii) for CHOS (a) and CHOK1 (b) PDH subunit overexpression cell pools generated in Chapter 3 across a 312 hour batch culture. (n=3) PEL1 empty cassette control, PEL3 (E1α), PEL4 (E1β), PEL5 (E2), PEL12 empty tag cassette control, PEL13 (E1αNV5), PEL14 (E1βNHA), PEL15(E2NFLAG), PEL16 (E1αCV5), PEL17 (E1βCHA), PEL18 (E2CFLAG).

The CHOS cell pools (a) in Figure 5.6.1 showed a similar production of lactate (i) and QLactate (ii) for the first 96 hours of batch culture. After this, the lactate concentration in the supernatant samples varied with some cell pools such as untagged cassette control PEL1, PEL3 (E1α) and PEL18

(E2CFLAG) cell pools maintaining similar lactate concentration whilst all other cell pools started to consume lactate leading to a reduced lactate concentration at the end of culture. This is clearly seen between the samples taken at 144 and 192 hours of the culture when the glucose levels were also reduced, (Figure 5.5.1). CHOS cell pools varied in cumulative lactate production (ii) with PEL13 (E1αNV5) cell pools having production levels most similar to that of control host cells. CHOS cell line derived pool results, unsurprisingly showed similar groupings as for glucose utilisation and viable cell analysis in Figures 5.5.1 and 5.3.1 respectively.

CHOK1 cell pools (b) also had similar lactate production levels in the first 96 hours of culture (i). Similar to the CHOS cell pools, the CHOK1 cell pools had varied lactate concentrations at 144 hours with further variation at 192 hours. CHOK1 host cells continued producing lactate throughout the culture and had a distinct cumulative lactate production and utilisation. CHOK1 cell pools expressing untagged PDH subunit E2 (PEL5) and N-terminally HA tagged E1beta (PEL14) or N-terminally FLAG tagged E2 (PEL15) all showed a complete reduction of lactate in the supernatant where the switch to lactate consumption was likely occurring. Although PEL15 (E2NFLAG) cell pools had an increase in viable cell number in Figure 5.3.3 as for the other N-terminally tagged PDH subunit expressing cells PEL13 (E1αNV5) and PEL14 (E1βNHA), the lactate concentration in these samples showed a steadier maintenance and no obvious consumption of lactate towards the end of the culture. The CHOK1 cell pools (b) had a larger spread of final lactate concentrations in the supernatant compared to the CHOS cell pools. The CHOK1 cumulative lactate production (ii) had groupings as seen previously for the glucose consumption (Figure 5.5.1) with the N-terminally tagged PDH subunit expressing cell pools grouped apart from all other cell pools.

Figure 5.6.2 shows the results for specific lactate production rates in CHOS (a) and CHOK1 (b) cell pools and whether the results are statistically significant using a one-way ANOVA and Dunnett's multiple comparisons test with $p<0.05$ confidence levels.

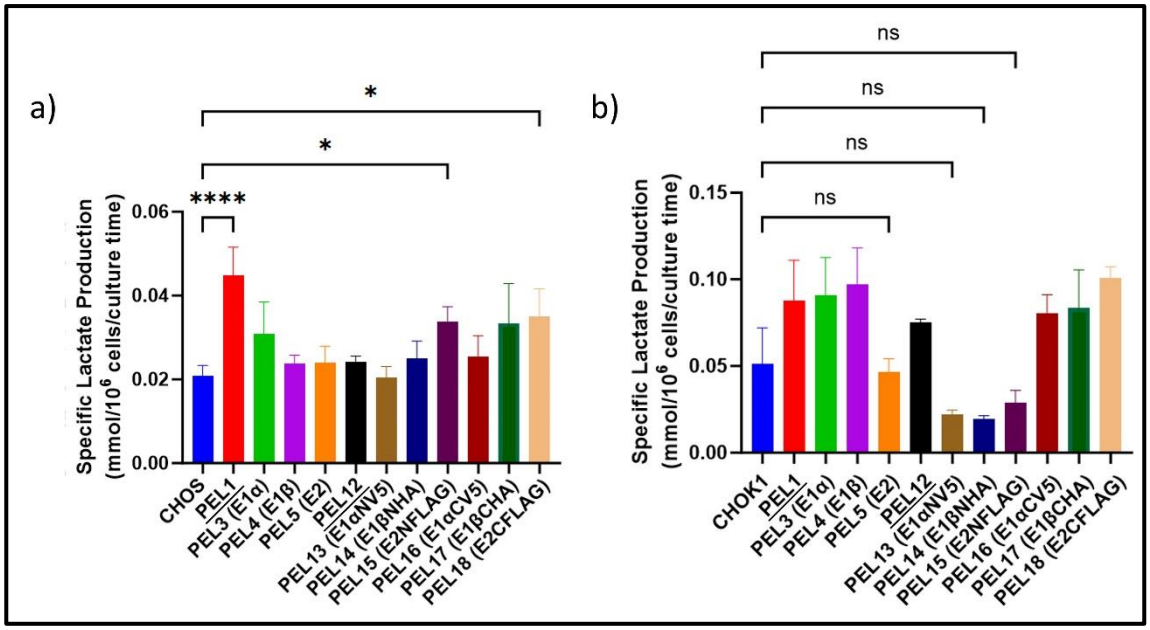

Figure 5.6.2 Specific production of lactate for CHOS (a) and CHOK1 (b) PDH subunit overexpression cell pools. A one-way ANOVA was performed using Dunnett's multiple comparisons test comparing the results to relevant host cells. Significance shown for key results, Extremely significant $p < 0.0001$ (****), Extremely significant $p = 0.0001$ to 0.001 (***), Very significant $p = 0.001$ to 0.01 (**), Significant $p = 0.01$ to 0.05 (*), Not significant $p \geq 0.05$ (ns). (n=3) PEL1 empty cassette control, PEL3 (E1α), PEL4 (E1β), PEL5 (E2), PEL12 empty tag cassette control, PEL13 (E1αNV5), PEL14 (E1βNHA), PEL15(E2NFLAG), PEL16 (E1αCV5), PEL17 (E1βCHA), PEL18 (E2CFLAG).

The results for the CHOS cell pools (a) show statistically significant increase in lactate production rates when comparing empty cassette control PEL1 cells and N- and C-terminally tagged E2 subunit expressing cell pools PEL15 and 18 to CHOS host controls. No CHOS cell pools show a reduction in lactate production rates (a) after the overexpression of PDH subunits either with or without the presence of a tag. In the CHOK1 cell pools (b), N-terminally tagged PDH subunit expressing cell pools PEL13, 14 and 15 showed a reduced lactate production rate compared to the CHOK1 host cells although this was, similar to the glucose utilisation rates (Figure 5.5.2), shown not to be statistically significant. PEL5 (E2) cells, showed a lactate production rate similar to CHOK1 host cells and were shown to start utilising lactate by the end of the culture, however this was also shown not to be statistically significant.

5.7 Analysis of the yield of viable cells and lactate from glucose in PDH overexpression cell pools across batch culture

Figure 5.7 reports the cell number generated per glucose (i) and the lactate produced per glucose (ii) in the supernatant over the course of the batch culture at 96, 144 and 192 hours in both CHOS (a) and CHOK1 (b) PDH subunit overexpression cell pools. The cell specific rate of lactate production was divided by the cell specific glucose utilisation rate to calculate the lactate produced per glucose. Towards the end of the culture cell pools are consuming lactate as the glucose levels fall instead of producing it so an increase in the number of samples taken earlier in the culture would have helped improve this analysis.

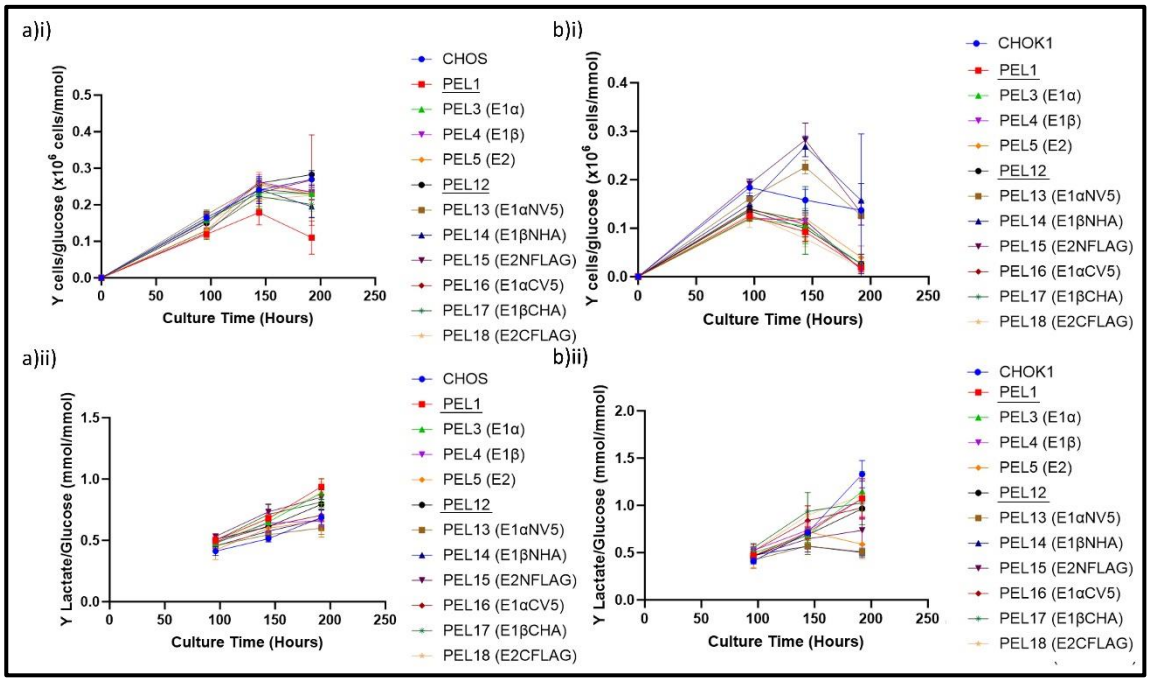

Figure 5.7 Yield of viable cells per glucose (mmol) (i) and yield of lactate (mmol) per glucose (mmol) (ii) over culture for CHOS (a) and CHOK1 (b) PDH subunit overexpression cell pools generated in Chapter 3 from a 312 hour batch culture. (n=3) PEL1 empty cassette control, PEL3 (E1α), PEL4 (E1β), PEL5 (E2), PEL12 empty tag cassette control, PEL13 (E1αNV5), PEL14 (E1βNHA), PEL15(E2NFLAG), PEL16 (E1αCV5), PEL17 (E1βCHA), PEL18 (E2CFLAG).

Figure 5.7 shows the CHOS cell pools (a) and the yield of viable cells from glucose (mmol) (i), with most cell pools matching the yield per glucose of CHOS control cells throughout the batch culture. PEL1 empty cassette control cells had a lower yield of cells per glucose reflecting the reduced number of viable cells in Figure 5.3.1. Control cell line PEL12 expressing the empty tag cassette had the highest yield of cells per glucose at 192 hours. Most cell pools showed an increase in the yield of cells per glucose until 144 hours into the culture after which the yield was shown to decrease at

hour 192. The CHOS host, PEL12 empty tag cassette control and PEL17 (E1βCHA) cell pools continued to exhibit an increase in yield of cells per glucose compared to all other cell pools that showed a reduced yield at the end of culture. No tagged or untagged PDH subunit overexpression cell pools showed any enhancement in the cells yielded per glucose compared to the control cell line. The yield of lactate per glucose (ii) in CHOS cells increased in all cell pools over culture with the PEL1 empty cassette control cell pool showing the largest yield of lactate per glucose towards the end of culture.

CHOK1 cells 5.7 (b) showed a similar number of viable cells produced per glucose (i) 96 hours into the culture, after this the cell pools varied with PEL13 (E1αNV5), PEL16 (E1αCV5) and PEL14 (E1βNHA) cell pools showing the highest yield of viable cells at 144 hour. All other untagged and C-terminally tagged PDH subunit expressing cell pools grouped together below the CHOK1 host control cells with a lower yield of viable cells per glucose. The yield of lactate per glucose (ii) for CHOK1 cells (b) was similar to the results for CHOS cells (a) at 96 and 144 hours. However, after 192 hours, the CHOK1 cell pools exhibited a larger spread of lactate yield results. The N- and C-terminally V5 tagged E1alpha subunit expressing cell lines PEL13 and PEL16 had the lowest yield of lactate per glucose at the 192 hour time point. There was large variation in the results at the 192 hour time point and some cell pools were shown to be consuming lactate by this point in the culture.

5.8 Analysis of ammonia concentrations in PDH subunit overexpression CHO cell pools during batch culture

Figure 5.8.1 reports the ammonia concentrations (i) in the supernatant over the course of the batch culture at 96, 144 and 192 hours in both CHOS (a) and CHOK1 (b) PDH subunit overexpression cell pools as well as the cumulative concentration compared to IVC values (ii).

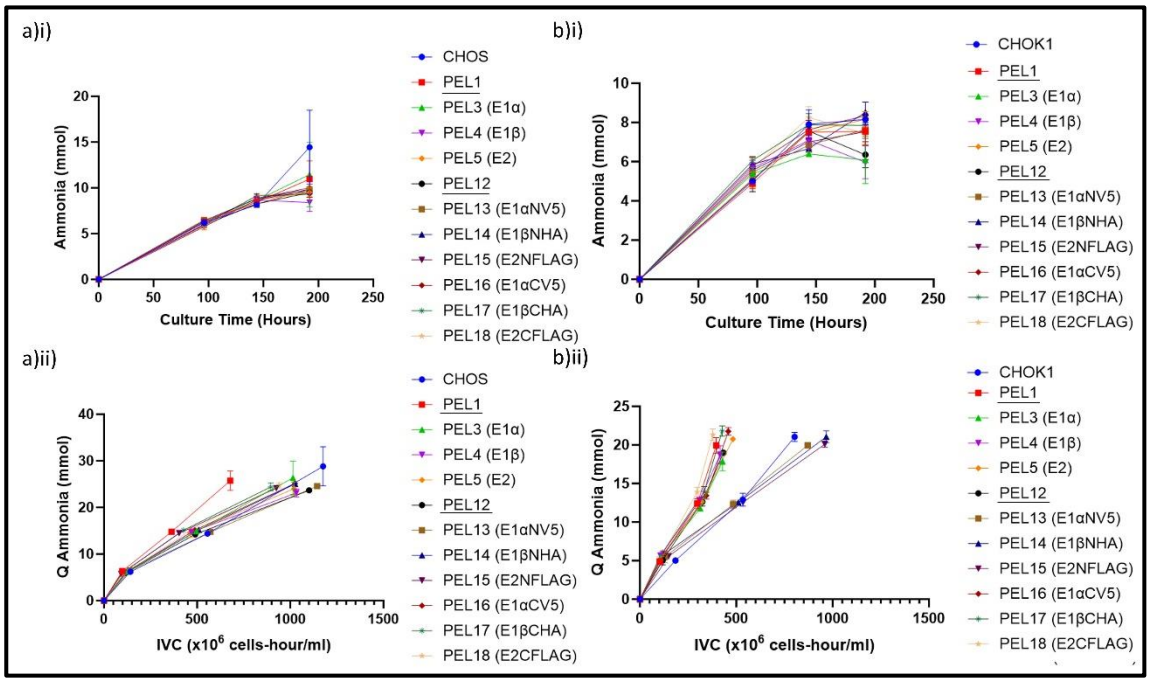

Figure 5.8.1 Ammonia concentration (mmol) over culture time (i) and cumulative ammonia production (QAmmonia) over IVC (ii) for CHOS (a) and CHOK1 (b) PDH subunit overexpression cell pools generated in Chapter 3 from a 312 hour batch culture. (n=3) PEL1 empty cassette control, PEL3 (E1α), PEL4 (E1β), PEL5 (E2), PEL12 empty tag cassette control, PEL13 (E1αNV5), PEL14 (E1βNHA), PEL15(E2NFLAG), PEL16 (E1αCV5), PEL17 (E1βCHA), PEL18 (E2CFLAG).

The CHOS cell pools (a) in Figure 5.8.1 (i) had similar ammonia concentrations over the course of the batch culture until hour 192, whereupon the CHOS host control cells had a larger ammonia concentration compared to all other cell pools. Control empty cassette cell line PEL1, which had higher lactate concentrations (Figure 5.6.1), had lower ammonia concentrations throughout the batch culture compared to the host cell line. However, when looking at the cumulative ammonia production (ii), the CHOS PEL1 empty cassette control cells had a higher production of ammonia compared to the IVC value of other cell pools. All the other PDH subunit overexpression cell pools had similar cell specific ammonia production rates compared to the host cell pools.

The CHOK1 cell pools (b) had similar ammonia production trends throughout the batch culture, with PEL3 (E1α), PEL4 (E1β) and empty tag cassette control PEL12 cell pools having the lowest ammonia

concentration at 192 hours. The other PDH subunit overexpression cell pools had similar ammonia production profiles compared to the CHOK1 host cells. The rate of ammonia production over the batch culture (ii) again had the distinct pool groupings observed in Figures 5.5.1 and 5.6.1 (b) (ii) when investigating cell specific utilisation and production of glucose and lactate respectively.

When comparing the cumulative ammonia production to IVC in Figure 5.8.1 (ii), the trend lines can be used to calculate average specific ammonia production rates for each cell line. These are shown in Figure 5.8.2. A one-way ANOVA using Dunnett's multiple comparisons test was performed comparing the results for each cell line to the relevant host cells.

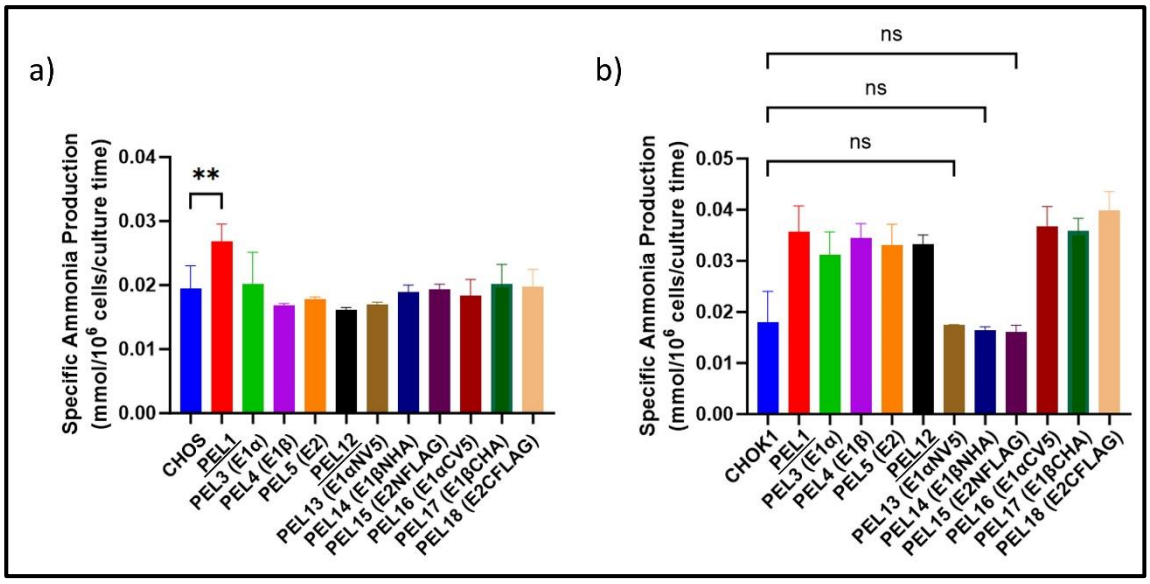

Figure 5.8.2 Specific production of ammonia from CHOS (a) and CHOK1 (b) PDH subunit overexpression cell pools. A one-way ANOVA was performed using Dunnett's multiple comparisons test comparing the results to relevant host cells. Significance shown for key results, Extremely significant $p < 0.0001$ (****), Extremely significant $p = 0.0001$ to 0.001 (***), Very significant $p = 0.001$ to 0.01 (**), Significant $p = 0.01$ to 0.05 (*), Not significant $p \geq 0.05$ (ns). (n=3) PEL1 empty cassette control, PEL3 (E1α), PEL4 (E1β), PEL5 (E2), PEL12 empty tag cassette control, PEL13 (E1αNV5), PEL14 (E1βNHA), PEL15(E2NFLAG), PEL16 (E1αCV5), PEL17 (E1βCHA), PEL18 (E2CFLAG).

All CHOS cell pools in Figure 5.8.2 (a) had comparable cell specific ammonia production rates when compared to CHOS host control cells other than the PEL1 empty cassette control cell pool which had a statistically significant increase. This is due to the lower viable cell number, shown in Figure 5.3.1, of the CHOS PEL1 empty cassette cell pool over the batch culture compared to the control. The CHOK1 cell pools (b) in Figure 5.8.2 all showed increased cell specific ammonia production rate compared to control host cells apart from those expressing N-terminally tagged PDH subunits in cell pools expressing PEL13 (E1αNV5), PEL14 (E1βNHA) and PEL15 (E2NFLAG).

5.9 Analysis of glutamine concentrations in PDH subunit overexpression CHO cell pools during batch culture

Figure 5.9.1 reports glutamine concentrations (i) in the culture supernatant over the course of the batch cultures at 96, 144 and 192 hours in both CHOS (a) and CHOK1 (b) PDH subunit overexpression cell pools as well as the cumulative concentration compared to IVC values (ii).

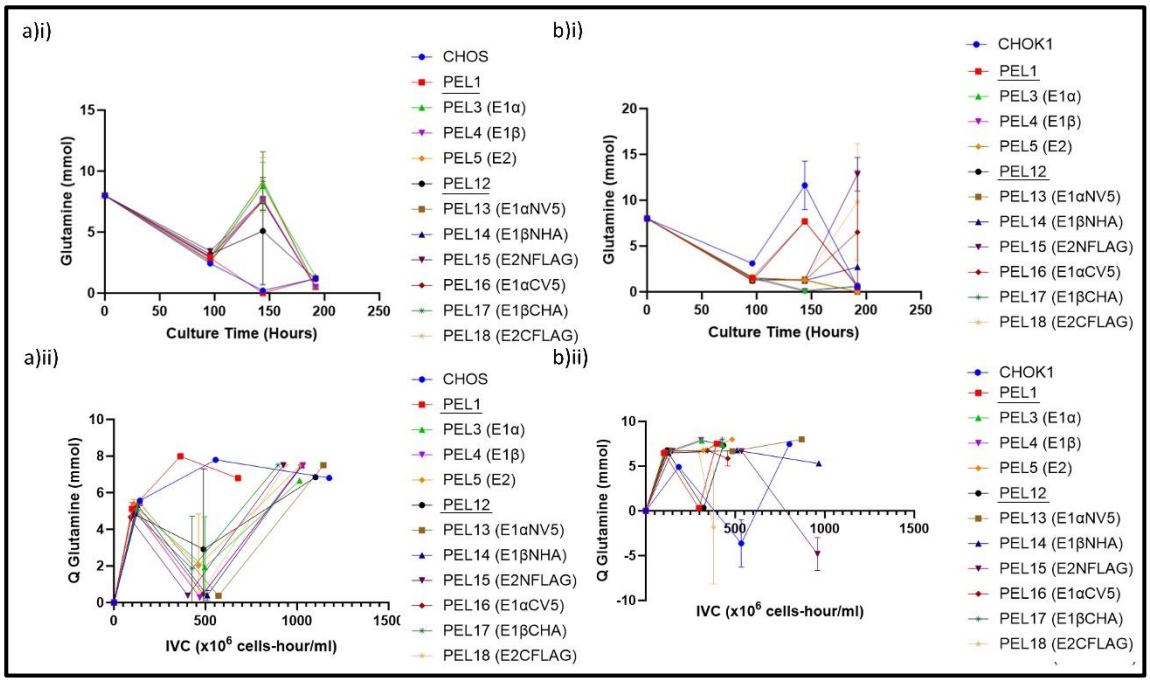

Figure 5.9.1 Glutamine concentration (mmol) over culture time (i) and cumulative glutamine production (QGlutamine) over IVC (ii) for CHOS (a) and CHOK1 (b) PDH subunit overexpression cell pools generated in Chapter 3 from a 312 hour batch culture. (n=3) PEL1 empty cassette control, PEL3 (E1α), PEL4 (E1β), PEL5 (E2), PEL12 empty tag cassette control, PEL13 (E1αNV5), PEL14 (E1βNHA), PEL15(E2NFLAG), PEL16 (E1αCV5), PEL17 (E1βCHA), PEL18 (E2CFLAG).

The CHOS cell pools (a) in Figure 5.9.1 had similar glutamine concentrations at the 96 hour time point of batch culture (i) however after 144 hours there was large variation in cell pool glutamine concentrations. CHOS host and PEL12 empty tag cassette control cells had a complete reduction of glutamine in the supernatant and all other cell pools had an increase in glutamine. Many of these measurements have large error bars with variation seen in most of the samples taken at the 144 hour time point. All cell pools had a similar final glutamine concentration after 192 hours. When looking at cumulative glutamine concentration in (ii), the CHOS cell pools had variable results with groupings of the CHOS host and PEL12 empty tag cassette control cells and all other cell pools. All cells other than the PEL12 empty tag cassette control cells ended at a similar cumulative glutamine concentration and IVC value at the end of culture.

The CHOK1 cell pools (b) also showed large variation in the glutamine concentration measurements (i) taken after the first 96 hours of batch culture. The CHOK1 host cells had a difference in glutamine concentration compared to all other cell pools until the final measurement at 192 hours. Again, there was a similar trend in glutamine concentration compared to PEL1 empty cassette and PEL12 empty tag cassette control cell lines with an increase in glutamine concentration at the 144 hour time point which then decreased at 192 hours. All PDH subunit overexpression cell pools had a decrease or maintained glutamine concentration between the 96 and 144 hour time points although the concentrations varied at 192 hours. PEL14 (E1βNHA), PEL17 (E1βCHA) and PEL18 (E2CFLAG) cell pools had a large to moderate increase in glutamine concentration at the end of culture. All other cell pools had low glutamine concentrations at the end of culture. At the 192 hour time point, similar to the CHOS cells (a), there were large error bars for all replicate samples. Once again, when comparing the cumulative glutamine utilisation to IVC in Figure 5.9.1 (ii), the trend lines can be used to calculate average specific glutamine utilisation rates for each cell pool. These are shown in Figure 5.9.2. A one-way ANOVA using Dunnett's multiple comparisons test was performed comparing the results for each cell line to the relevant host cells.

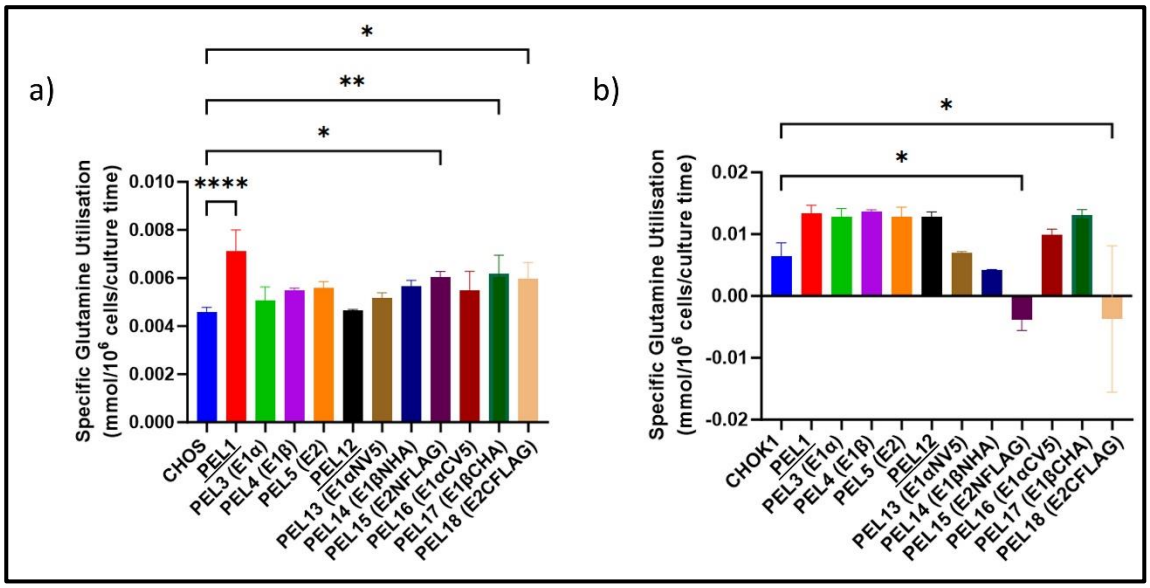

Figure 5.9.2 Specific utilisation of glutamine for CHOS (a) and CHOK1 (b) PDH subunit overexpression cell pools. A one-way ANOVA was performed using Dunnett's multiple comparisons test comparing the results to relevant host cells. Significance shown for key results, Extremely significant $p < 0.0001$ (****), Extremely significant $p = 0.0001$ to 0.001 (***), Very significant $p = 0.001$ to 0.01 (**), Significant $p = 0.01$ to 0.05 (*), Not significant $p \geq 0.05$ (ns). (n=3) PEL1 empty cassette control, PEL3 (E1α), PEL4 (E1β), PEL5 (E2), PEL12 empty tag cassette control, PEL13 (E1αNV5), PEL14 (E1βNHA), PEL15(E2NFLAG), PEL16 (E1αCV5), PEL17 (E1βCHA), PEL18 (E2CFLAG).

The specific glutamine utilisation of CHOS cells shown in Figure 5.9.2(a), shows most PDH subunit overexpression cell pools had increased glutamine utilisation compared to CHOS host cells, with those highlighted that are statistically significant. The control PEL1 empty cassette cell pools as well as PEL15 (E2NFLAG), PEL17 (E1βCHA) or PEL18 (E2CFLAG) pools all showed a significant increase in glutamine utilisation. As expected, control PEL12 empty tag cassette pools had a cell specific glutamine utilisation rate most similar to the CHOS control cells. CHOK1 overexpression cell pools in Figure 5.9.2(b) reveal a mixed impact to cell specific glutamine utilisation when compared to CHOK1 host cells with most showing an increase in glutamine utilisation rate. PEL14 (E1βNHA), PEL15 (E1βCHA) and PEL18 (E2CFLAG) all exhibited a lower cell specific glutamine utilisation rate compared to CHOK1 host cells. None of the reductions however are statistically significant.

5.10 Analysis of glutamate concentrations in PDH subunit overexpression CHO cell pools during batch culture

Figure 5.10.1 reports the glutamate concentrations (i) in the culture supernatant over the course of the batch culture at 96, 144 and 192 hours in both CHOS (a) and CHOK1 (b) PDH subunit overexpression cell pools as well as the cumulative concentration compared to IVC values (ii).

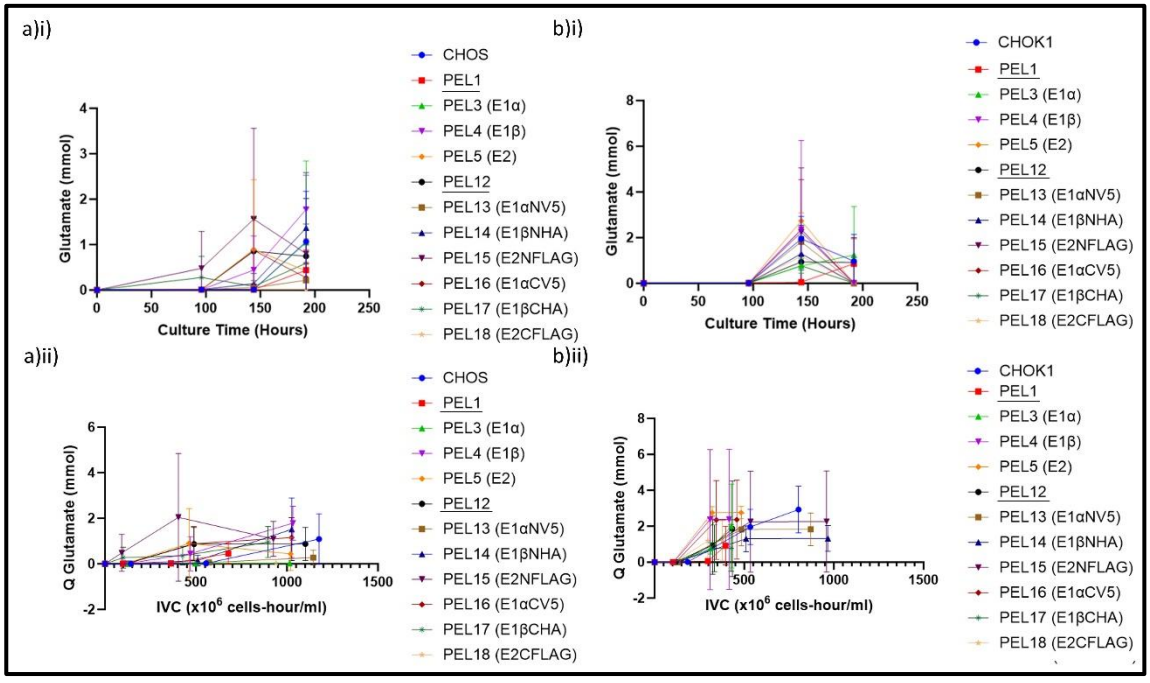

Figure 5.10.1 Glutamate concentration (mmol) over culture time (i) and cumulative glutamate production (QGlutamate) over IVC (ii) for CHOS (a) and CHOK1 (b) PDH subunit overexpression cell pools generated in Chapter 3 from a 312 hour batch culture. (n=3) PEL1 empty cassette control, PEL3 (E1α), PEL4 (E1β), PEL5 (E2), PEL12 empty tag cassette control, PEL13 (E1αNV5), PEL14 (E1βNHA), PEL15(E2NFLAG), PEL16 (E1αCV5), PEL17 (E1βCHA), PEL18 (E2CFLAG).

The CHOS cell pools in Figure 5.10.1(a) show different glutamate production (i) across most cell pools, with the CHOS host cell pools generally maintaining a low glutamate concentration until 192 hours into batch culture. PEL3 (E1α) cell pools had glutamate concentrations in the media most similar to the CHOS control host. CHOS cell pools expressing C-terminally FLAG tagged E2 in PEL15 had an increase in glutamate concentration until 192 hours but large variation between samples. There was no clear pattern to the glutamate metabolism in the CHOS cell pools which is highlighted in the cumulative glutamate results (ii).

The CHOK1 results 5.10.1(b) had much more uniform glutamate concentrations (i) when compared to the CHOS cell pools (a) although large variation and error bars were again prevalent for most of the measurements taken at 144 and 192 hours. All cells showed similar glutamate concentrations at 96 hours but some differentiation by 192 hours which either decreased (PEL13 (E1αNV5), 14 (E1βNHA) and 15 (E2NFLAG)) or increased in concentration (CHOK1 control cell lines, host, PEL1 and PEL12 and PEL3 (E1α)). When looking at the cumulative glutamate concentration, figure (ii) shows the CHOK1 cell pools grouping together as seen for other metabolite utilisation and production rates. As previously described, when comparing the cumulative glutamate utilisation to IVC in Figure 5.10.1(ii), the trend lines can be used to calculate average specific glutamine utilisation rates for each cell pool. These are shown in Figure 5.10.2. A one-way ANOVA using Dunnett's multiple comparisons test was performed comparing the results for each cell line to the relevant host cells.

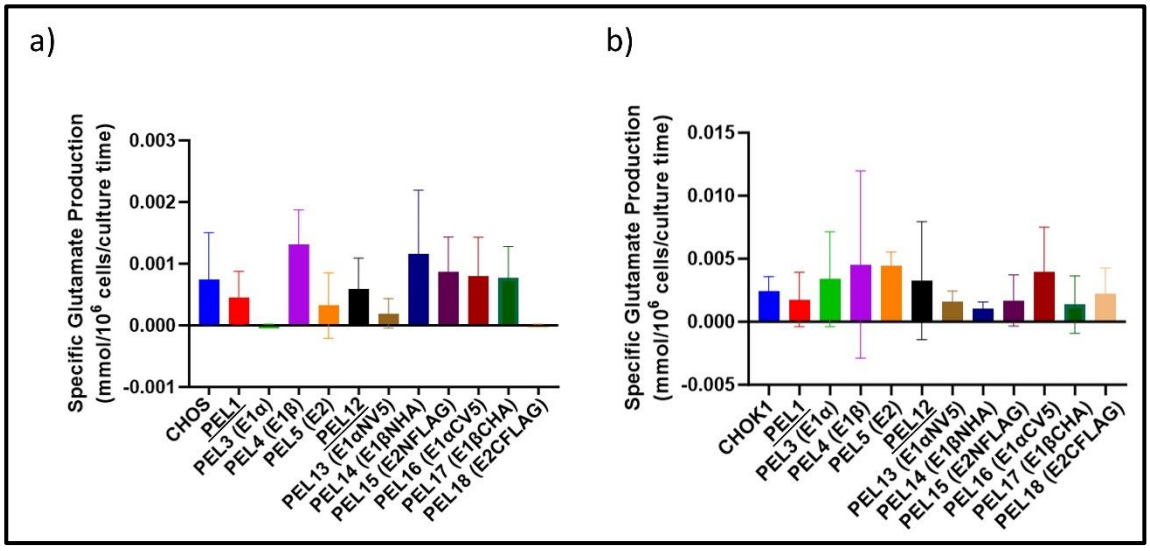

Figure 5.10.2 Specific production of glutamate for CHOS (a) and CHOK1 (b) PDH subunit overexpression cell pools. A one-way ANOVA was performed using Dunnett's multiple comparisons test comparing the results to relevant host cells. Significance shown for key results, Extremely significant $p < 0.0001$ (****), Extremely significant $p = 0.0001$ to 0.001 (***), Very significant $p = 0.001$ to 0.01 (**), Significant $p = 0.01$ to 0.05 (*), Not significant $p \geq 0.05$ (ns). (n=3) PEL1 empty cassette control, PEL3 (E1α), PEL4 (E1β), PEL5 (E2), PEL12 empty tag cassette control, PEL13 (E1αNV5), PEL14 (E1βNHA), PEL15(E2NFLAG), PEL16 (E1αCV5), PEL17 (E1βCHA), PEL18 (E2CFLAG).

The cell specific production of glutamate in CHOS cells were shown to vary (Figure 5.10.2(a)). Untagged E1alpha expressing cell line PEL3 showed an overall lower utilisation of glutamate compared to all other cell pools and the CHOS host. However, large variation is present across all samples and the changes in cell specific production or utilisation of glutamate in all cell pools were shown not to be statistically significant when compared to the CHOS host cell line. CHOK1 cell pools (b) also showed large variation and there were no statistically significant differences observed.

5.11 Analysis of batch culture cell growth during transient Etanercept expression in the PDH subunit overexpression and PDK KO CHO cell pools

Once the impact of both the expression of untagged and tagged exogenous PDH subunits on cell growth phenotype had been investigated, a production run of a model DTE was performed, detailed in methods section 2.3.8. Etanercept was used as the model DTE protein for reasons previously described. This was carried out using selected engineered cell pools from Chapter 3, the CHOS PDK2 and PDK3 KO cell pools generated and described in Chapter 4, and the E1alpha Serine to Alanine mutant expressing PEL19 cell pools.

For the production run, an Etanercept construct, PEL11, was generated which also had a Hygromycin based selection system. Figure 5.11.1 shows the test restriction digest on the PEL11 Etanercept plasmid using enzymes AvrII and BamHI to result in three bands of sizes 1394 bp, 701 bp and 5028 bp.

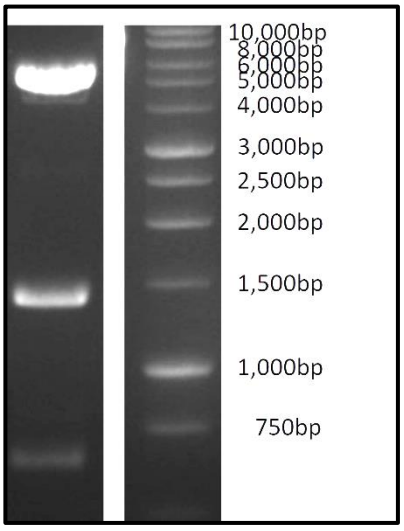

Figure 5.11.1 Restriction test digest of Etanercept PEL11 plasmid (left hand lane) using AvrII and BamHI fast digest enzymes. Bands are seen at expected sizes of 1394 bp, 701 bp and 5028 bp. Right hand lane shows size marker with sizes of bands indicated.

For the Etanercept production run, although stable pools could have been produced, cells were transiently transfected by electroporation with the PEL11 Etanercept plasmid following the methods detailed in section 2.3.5. A batch culture production was then undertaken with transfected cell pools grown for 240 hours post-transfection in 10 ml cultures shaking at 220 rpm in Corning™ Mini Bioreactor Centrifuge Tubes alongside control cell pools/lines. No obvious change to cell growth or culture viability was seen in any CHOS engineered cell pools during the previous batch culture experiment so CHOS cell pools expressing C-terminally tagged PDH subunits E1alpha, E1beta and E2 in PEL16, 17 and 18 respectively generated in Chapter 3 were used for this study. The C-terminally tagged versions were selected as the presence of the C-terminal tagged versions of these subunits was observed on western blots to be expressed more strongly compared to the subunits with an N-terminal tag. Alongside, the surviving CHOS PDK KO cell pools, generated in Chapter 4, were also investigated. CHOK1 cells expressing either the N- or C-terminally tagged PDH subunits were also investigated due to the increased viable cell number observed in the previous batch culture experiments. The growth profiles were characterised in biological triplicate for all cell pools and compared to host, PEL1 empty cassette and PEL12 empty tag cassette control cell pools. Dot blots were used to semi-quantify production levels of Etanercept in the supernatant at the end of the batch culture. A dot blot was used for initial production screening purposes with the aim to use a more quantitative method to measure titre however this was not completed due to time constraints.

Figures 5.11.2 to 5.11.5 report the viable cell numbers throughout the batch cultures post-transfection with the Etanercept plasmid of the selected CHOS and CHOK1 cell pools expressing N- or C-terminally tagged PDH subunits including the Serine Alanine mutant E1alpha PEL19 alongside the CHOS PDK2 or PDK3 KO cell pools when compared to control cell lines. Figure 5.11.2 reports the viable cell numbers of the transiently Etanercept transfected CHOS cell pools stably expressing C-terminally tagged PDH subunits alongside PDK2 and PDK3 KO cell pools over a 240 hour batch culture time course compared to host and PEL12 empty tag cassette control cell pools. The C-terminally tagged cell pool results are shown in 5.11.2(b) whilst the results in 5.11.2(c) show the viable cell numbers for PDK2 or PDK3 KO cell pools. C-terminally V5 tagged E1alpha expressing PEL16 pools did not recover after transfection. Figure 5.11.2 shows that most cell pools, apart from those expressing E1beta with a C-terminal HA tag (PEL17) or the Serine/Alanine E1alpha mutant (PEL19) had higher viable cell numbers throughout the production run compared to CHOS host cells.

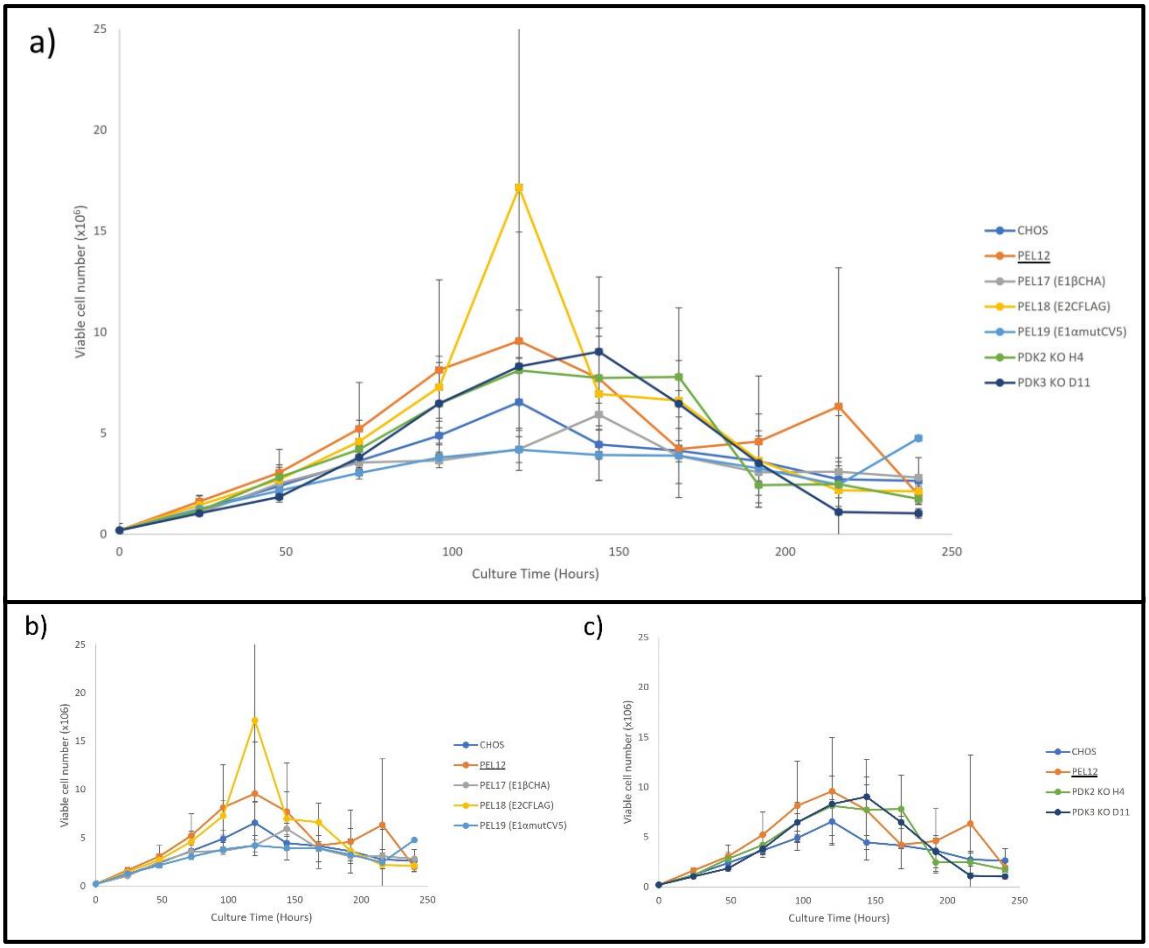

Figure 5.11.2 Viable cell number (x10^6) for CHOS cell pools stably expressing C-terminally tagged PDH subunits E1beta (PEL17) or E2 (PEL18) and E1alpha mutant (PEL19) alongside CHOS PDK2 and PDK3 KO cell pools generated transiently expressing Etanercept over a 240 hour batch culture. (a) All cell lines, (b) C-terminally tagged PDH subunit expressing cell pools and E1alpha mutant PEL19 only. (c) PDK2 and PDK3 KO cell pools only. PEL12 empty tag cassette control, PEL17 (E1βCHA), PEL18 (E2CFLAG), PEL19 (E1αmutCV5). (n=3).

The empty tag cassette control cell pool (PEL12) had the second highest viable cell number up until 120 hours. These control cell pools, along with the host control cells, had large error bars for most sample points suggesting large variation between the triplicates. The C-terminal tagged PDH subunit expressing pools, E1beta (PEL17), and E2 (PEL18) are shown alongside the E1alpha mutant (PEL19) cell pool, where the Serine residue phosphorylation site regulation was mutated to Alanine residues. An apparent increase in viable cell numbers of PEL18 (E2CFLAG) expressing cells was observed 120 hours into the production run, however large variation in the triplicate data was also observed. The PEL17 (E1βCHA) and the PEL19 (E1αmutCV5) cell pools maintained lower viable cell numbers throughout the culture. The viable cell numbers of CHOS PDK2 and PDK3 KO cell pools had similar viable cell numbers, higher than host cells but lower than the PEL12 empty tag cassette control cell pools. No detrimental impact to viable cell number was observed from the KO of either

target PDK2 or PDK3 when compared to host cells and the viable cell numbers were comparable to the engineered cell pools investigated in the transient Etanercept production run.

The average culture viabilities during the production run are shown alongside the average doubling time over the first 96 hours of the time course and peak density for each cell pool across the replicates in Figure 5.11.3.

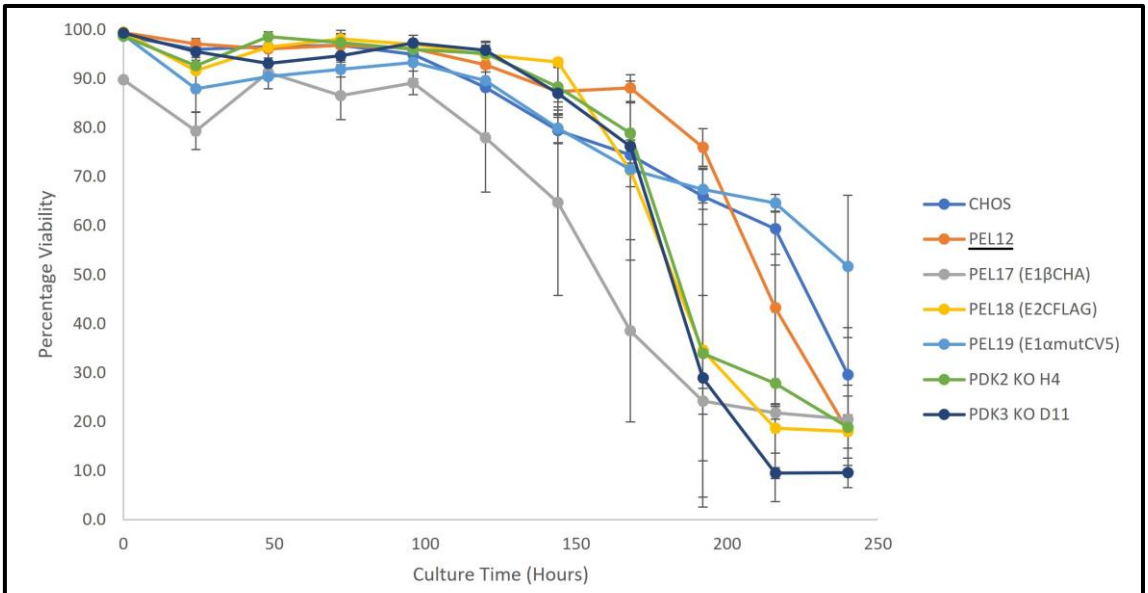

Cell Line	CHOS	PEL12	PEL17 (E1βCHA)	PEL18 (E2CFLAG)	PEL19 (E1αmutCV5)	PDK2 KO H4	PDK3 KO D11
Doubling Time (Hours)	20.84	18.65	22.97	18.64	22.62	19.51	19.19
Peak Cell Density ($x10^6$)	6.54	9.57	5.153	17.17	4.19	8.12	9.04

Figure 5.11.3 Average culture viability for CHOS cell pools stably expressing C-terminally tagged PDH subunits E1beta (PEL17) or E2 (PEL18) and E1alpha mutant (PEL19) alongside CHOS PDK2 and PDK3 KO cell pools transiently expressing Etanercept over a 240 hour batch culture. The doubling time (Hours) over the first 96 hours of batch culture and peak cell density ($x10^6$) is also reported. (n=3).

Figure 5.11.3 reports the average culture viability of the CHOS cell pool triplicates throughout the Etanercept production run. CHOS host cells and PEL12 empty tag cassette control cells maintained a high percentage culture viability throughout the production run until 200 hours. The PEL17 (E1βCHA) cell line had the lowest viability throughout most of the production run. This cell pool had one of the lowest viable cell numbers throughout the culture (Figure 5.11.2) suggesting that the expression of E1beta with a C-terminal HA tag is detrimental to cell growth and proliferation. This is supported by the longest doubling time and low peak cell density in Figure 5.11.3. The PEL18

(E2CFLAG) cell pools had a higher culture viability throughout the production run although a steep decline was observed around 170 hours into the culture. These cells had the shortest doubling time in the first 96 hours. They also showed the highest peak cell density of all cell pools at $17.17x10^6$ cells/ml. PEL19 (E1αmutCV5) cells had high culture viability and maintained this throughout the culture. However, they also had one of the longest doubling times and the lowest peak cell density. PDK2 and PDK3 KO cell pools (H4 and D11 respectively) had similar culture viability throughout the culture to the PEL18 (E2CFLAG) cell pools. The KO cell pools also had similar doubling times and peak viable cell densities. The culture viability of these cell pools had great variation which was considerably different to the viability of the cell pools during the batch culture in Figure 5.3.3. The expression of the model DTE Etanercept protein is possibly impacting the viability.

The results for the CHOK1 cell pools investigated for Etanercept production are shown in Figures 5.11.4 and 5.11.5. Due to the increased viable cell number observed when expressing the N-terminally tagged E1alpha (PEL13), E1beta (PEL14) and E2 (PEL15) PDH subunits in Figure 5.3.3, these and the cell pools expressing C-terminally tagged PDH subunits (PEL16, 17 and 18) were investigated.

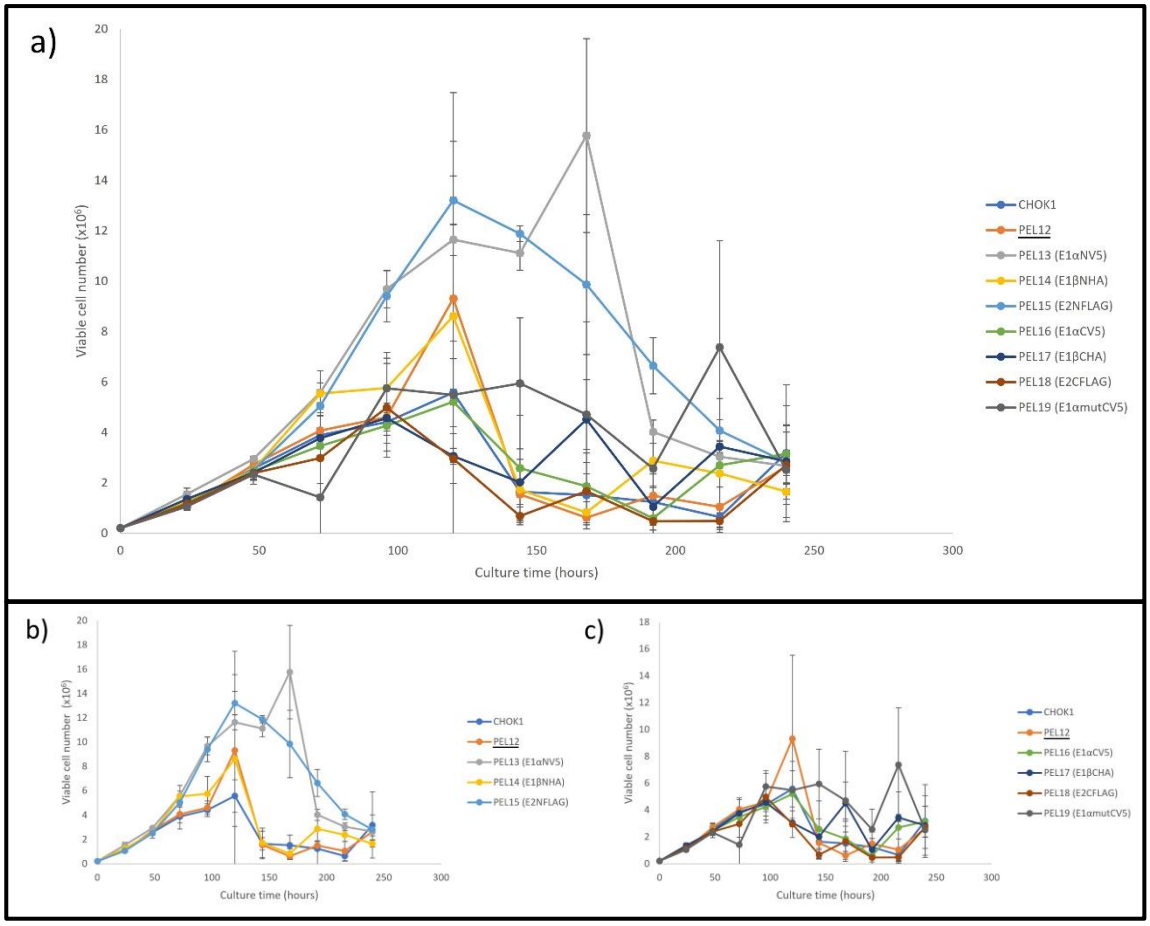

Figure 5.11.4 Viable cell number (x10^6) for CHOK1 cell pools stably expressing N- or C-terminally tagged PDH subunits E1alpha (PEL13 & PEL16), E1beta (PEL14 & PEL17) or E2 (PEL15 & PEL18) and E1alpha Serine/Alanine mutant PEL19 transiently expressing Etanercept over a 240 hour batch culture. (a) All cell lines, (b) N-terminally tagged PDH subunit expressing cell lines (c) C-terminally tagged PDH subunit and E1alpha mutant (PEL19) expressing cell pool only. (n=3)

Figure 5.11.4 reports the viable cell numbers for CHOK1 cell pools stably expressing N- or C-terminally tagged PDH subunits E1alpha, E1beta or E2 and E1alpha Serine/Alanine mutant (PEL19) over a 240 hour batch culture compared to host and the PEL12 empty tag cassette control cell pool whilst transiently producing model DTE protein Etanercept. The N-terminally tagged PDH subunit expressing cell pools are shown in (b) whilst the C-terminally tagged PDH subunit expressing cell pools, including the E1alpha Serine/Alanine mutant (PEL19) cell pool, viable cell numbers are shown in (c). Similar to the results in Figure 5.3.3, Figure 5.11.4 shows high viable cell numbers throughout the production run in cell pools expressing the PDH subunits with a N-terminal tag. N-terminally tagged E1alpha and E2 expressing cell lines (PEL13 and PEL15) respectively are seen (b) with up to 3 times the viable cell number achieved in the CHOK1 host control cells. PEL14 (E1βNHA) cells however had viable cell numbers more comparable to those of the PEL12 empty tag cassette control

cell pool although both of these cell pools had viable cell numbers higher than CHOK1 host control cells at multiple points throughout the batch culture.

The viable cell numbers of cell pools expressing C-terminally tagged PDH subunits PEL16 (E1αCV5), 17 (E1βCHA) and 18 (E2CFLAG) and the E1alpha Serine/Alanine mutant PEL19 are shown in (c). Here the cell pools had varied viable cell numbers throughout the batch culture however the PEL12 empty tag cassette control cell pools achieved the highest peak cell number 120 hours into the culture. PEL19 (E1αmutCV5) cells had the next highest viable cell numbers which increase, fall and then increased again towards the end of culture. C-terminally tagged E1alpha, E1beta and E2 in PEL16, 17 and 18 respectively followed a similar pattern when compared to the CHOK1 host control cells at the start of the culture however all varied after 96 hours of batch culture. PEL16 (E1αCHA) cells had a trend similar to the viable cell numbers of the CHOK1 host control cells for most of the culture. PEL17 (E1βCHA) cells had a reduction and then peak in viable cell numbers between time points at 144 and 168 hours into the culture whilst C-terminally FLAG tagged E2 PEL18 showed a reduction after the peak 96 hours into the culture. The large variability in the viable cell numbers of all triplicates may reflect the transient nature of the Etanercept expression.

The average culture viabilities during the production run are also shown alongside the average doubling time over the first 96 hours of the culture and peak density for each cell pool across the replicates in Figure 5.11.5.

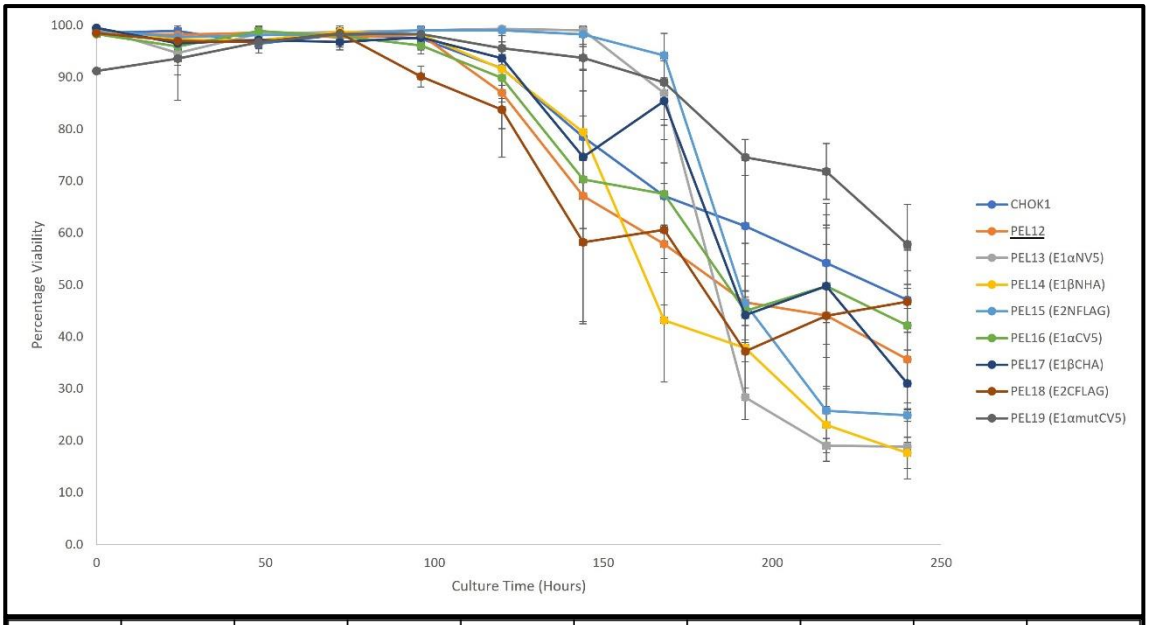

Cell Line	CHOK1	PEL12	PEL13 (E1αNV5)	PEL14 (E1βNHA)	PEL15 (E2NFLAG)	PEL16 (E1αCV5)	PEL17 (E1βCHA)	PEL18 (E2CFLAG)	PEL19 (E1αmutCV5)
Doubling Time (Hours)	21.57	21.27	17.16	20.00	17.30	21.85	21.59	21.18	19.91
Peak Cell Density ($x10^6$)	5.57	9.31	15.137	8.60	13.21	5.21	4.56	4.98	5.154

Figure 5.11.5 Average culture viability for CHOK1 cell pools stably expressing N- or C-terminally tagged PDH subunits E1alpha (PEL13 & PEL16), E1beta (PEL14 & PEL17) or E2 (PEL15 & PEL18) and E1alpha Serine/Alanine mutant PEL19 transiently expressing Etanercept over a 240 hour batch culture. The doubling time (Hours) over the first 96 hours of batch culture and peak cell density ($x10^6$) are also reported. (n=3)

Figure 5.11.5 reports the average culture viability of the CHOK1 cell pool triplicates throughout the Etanercept transient expression batch culture production run. PEL15 (E2NFLAG) cells maintained a high percentage culture viability for the longest time period when compared to other cell pools. This was similar to the pattern of culture viability observed in CHOK1 PEL13 (E1αNV5) cells. Both N-terminally tagged E1alpha and E2 (PEL13 and PEL15) expressing cell pools had the fastest doubling times and achieved the highest peak cell densities. The higher number of viable cells in each of these cell pools could therefore lead to an improvement in model DTE Etanercept production levels if the transient cell specific productivity was maintained. The PEL19 (E1αmutCV5) cell pools had a similar culture viability which was maintained throughout the culture time. These E1alpha Serine/Alanine mutant expressing cells had a faster doubling time when compared to CHOK1 host control cells but obtained a lower peak cell density. Fewer viable cells that remain at a higher viability throughout the culture could also lead to improved Etanercept production levels as a result. PEL14 (E1βNHA) had a steady decline in culture viability after the 96 hour time point, with a similar doubling time and peak cell density to that of the CHOK1 host control cells. Cell pools expressing C-

terminally tagged E1alpha (PEL16), E1beta (PEL17) or E2 (PEL18) all had doubling times and peak cell densities similar to the CHOK1 host cell line and PEL12 empty tag cassette controls. The cell pools all followed a similar pattern to both the control cell lines in culture viability until 72 hours into the culture when PEL18 (E2CFLAG) started to decline in culture viability. Generally, the C-terminally tagged PDH subunit expressing cell pools did not achieve the viable cell numbers as the cell pools expressing PDH subunits with N-terminal tags.

5.12 Investigating model DTE Etanercept expression from PDH subunit overexpression cell pools and PDK KO cell pools

To enable qualitative determination of Etanercept production levels from the batch culture production run described in section 5.11, supernatant samples were taken on the last day of the culture for analysis. After 240 hours, the supernatant was harvested and analysed by dot blot. This was intended to be an initial screen to check for expression levels before analysing titre and product quality however these approaches were not completed due to time restraints. 100 µl of supernatant sample was loaded twice for each cell pool, with an average taken for the sample and that used to generate an average for the triplicate biological repeats. Figure 5.12 reports the densitometry analysis comparing expression levels relative to those from control CHOS or CHOK1 host cells. A one-way ANOVA using Dunnett's multiple comparisons test was performed comparing the results for each cell line to the relevant host cells.

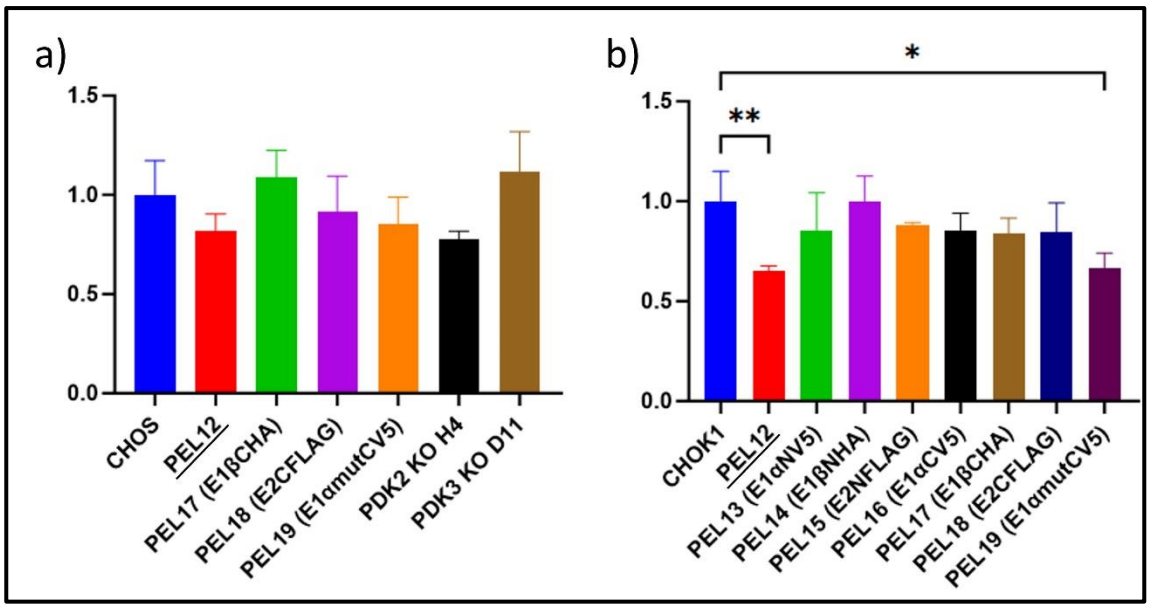

Figure 5.12 Densitometry analysis from dot blot analysis of transient Etanercept production from edited CHOS (a) and CHOK1 (b) cells generated in Chapters 3 and 4 when probed with anti-γ chain antibody. 100 µl supernatant sample loaded twice for each cell line and exposed for 1 hour. The densitometry analysis based on dot signal of CHOS overexpression and PDK KO cell lines only (a) and CHOK1 overexpression cell lines only (b). A one-way ANOVA was performed using Dunnett's multiple comparisons test comparing the results to relevant host cells. Significance shown for key results, Extremely significant $p < 0.0001$ (****), Extremely significant $p = 0.0001$ to 0.001 (***), Very significant $p = 0.001$ to 0.01 (**), Significant $p = 0.01$ to 0.05 (*), Not significant $p \geq 0.05$ (ns). (n=3) PEL12 empty tag cassette control, PEL13 (E1αNV5), PEL14 (E1βNHA), PEL15 (E2NFLAG), PEL16 (E1αCV5), PEL17 (E1βCHA), PEL18 (E2CFLAG), PEL19 (E1αmutCV5), PDK2 and PDK3 KO cell pools.

Figure 5.12 reports the densitometry analysis of Etanercept amounts from the different samples. There was some impact on Etanercept production as determined from the dot blot analysis of the engineering/editing of the CHOS cell lines, although this unfortunately tended to be a negative impact.

The empty tag cassette (PEL12) control cell pools had a reduced expression of Etanercept compared to the host CHOS cells. PEL17 (E1βCHA) showed a small increase in Etanercept production compared to CHOS host cells which was shown not to be statistically significant. PEL18 (E2CFLAG) or PEL19 (E1αmutCV5) CHOS cell pools gave similar levels of Etanercept production, although both were lower than the expression from the CHOS host cells, but this difference was not significant. The CHOS PDK2 KO H4 cell pool yielded the lowest Etanercept expression of all cell pools. PDK3 KO D11 cell pools however showed an increased level of Etanercept production when compared to host CHOS cell lines and the highest expression of all CHOS cell samples which was shown to be statistically not significant.

The engineered CHOK1 cell pools also showed a large amount of variation between cell pool samples. This probably reflects the transient nature of the Etanercept expression experiment. The results were broadly similar to those of the CHOS engineered cell pool results, with no positive increase in the amount of secreted Etanercept observed when analysed using dot blots in the transient expression studies and only a significant decrease seen in some samples.

5.13 Investigating transient cell specific model DTE Etanercept expression from tagged and untagged PDH subunit overexpression cell pools and PDK KO cell pools

To calculate the cell specific production of Etanercept in the engineered/edited cell pools generated from Chapter 3 and 4, the IVC of the cells was first calculated and then used to calculate the cell specific expression. The calculated IVC for CHOS and CHOK1 cell pools assessed in the Etanercept production experiment is shown in Figure 5.13.1.

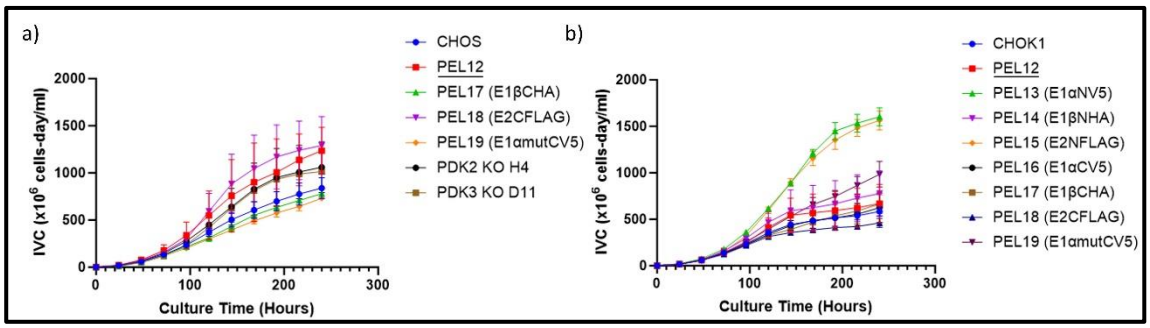

Figure 5.13.1 Integral of viable cell concentration (IVC) of CHOS (a) and CHOK1 (b) cells transiently producing Etanercept in a production run over a 240 hour batch culture time course. (n=3) PEL12 empty tag cassette control, PEL13 (E1αNV5), PEL14 (E1βNHA), PEL15 (E2NFLAG), PEL16 (E1αCV5), PEL17 (E1βCHA), PEL18 (E2CFLAG), PEL19 (E1αmutCV5), PDK2 and PDK3 KO cell pools.

The IVC values reported in Figure 5.13.1 show the increased growth of CHOS (a) PEL18 (E2CFLAG) cell pools over the culture time compared to the other cell pools previously highlighted by the short doubling time, which was similar to empty tag cassette control cell pool PEL12, (Figure 5.11.3). The CHOS host control cells (Figure 5.13.1) had some of the lowest IVC values except for PEL17 (E1βCHA) and PEL19 (E1αmutCV5) cells. CHOS PDK KO cell pools PDK2 KO H4 and PDK3 KO D11 had similar IVC values throughout the culture. The IVC values for all CHOS cell pools at the start of the culture were similar and only started to vary after 96 hours. The engineered CHOK1 cell pools (b) had larger variation in their IVC when compared to the CHOS cell pools (a) with an increase in IVC seen for cells

expressing N-terminally tagged E1alpha and E2 PDH subunits (PEL13 and PEL15 respectively). PEL14 (E1βNHA) cells had a lower IVC value than other N-terminally tagged PDH expressing cell pools.

The IVC values at the end of culture were used to calculate the relative specific production of Etanercept based upon the intensity from the dot blot analysis. Again this calculation would have been preferable using a more quantitative titre analysis method. These values are reported for each of the cell pools compared to host cell lines in Figure 5.13.2. A one-way ANOVA using Dunnett's multiple comparisons test was performed comparing the results for each cell pool to the relevant host cells.

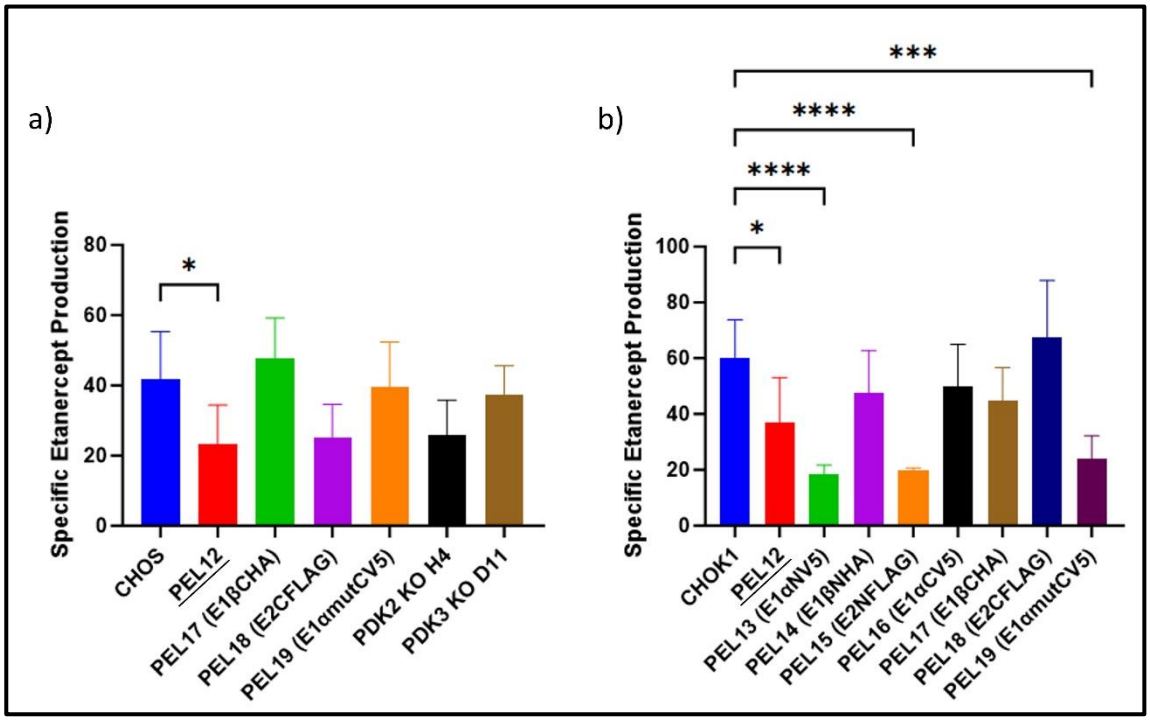

Figure 5.13.2 Relative cell specific Etanercept production in CHOS (a) and CHOK1 (b) cell pools generated in Chapters 3 and 4. A one-way ANOVA was performed using Dunnett's multiple comparisons test comparing the results to relevant host cells. Significance shown for key results, Extremely significant $p < 0.0001$ (****), Extremely significant $p = 0.0001$ to 0.001 (***), Very significant $p = 0.001$ to 0.01 (**), Significant $p = 0.01$ to 0.05 (*), Not significant $p \geq 0.05$ (ns). (n=3) PEL12 empty tag cassette control, PEL13 (E1αNV5), PEL14 (E1βNHA), PEL15 (E2NFLAG), PEL16 (E1αCV5), PEL17 (E1βCHA), PEL18 (E2CFLAG), PEL19 (E1αmutCV5), PDK2 and PDK3 KO cell pools.

Figure 5.13.2 shows the relative cell specific production rates of Etanercept in CHOS (a) and CHOK1 cell pools. The CHOS (a) cell pools showed different impacts of cell manipulation with empty tag cassette control cells (PEL12), C-terminally FLAG tagged E2 expressing cell pools (PEL18) and PDK2 KO H4 cells showing lower specific Etanercept production compared to the CHOS host cells. These

cell pools all had higher IVCs compared to the CHOS host cells which is likely the cause of the reduction in relative cell specific production of Etanercept. CHOS cell pools PEL15 (E2NFLAG) had a small increase in relative cell specific Etanercept production compared to the CHOS host cell line but this was, along with all reductions in the other CHOS cell pools, shown to not be statistically significant. The CHOK1 cell pool results (b) showed a similar mixture of results. Cells expressing the N-terminally tagged PDH subunits E1alpha and E2 (PEL13 and PEL15) had lower relative cell specific Etanercept production, similar to the C-terminally tagged E1alpha Serine/Alanine mutant expressing PEL19 cells, when compared to the CHOK1 host cells. No cell pools showed a statistically significant improvement to relative cell specific Etanercept production compared to the relevant CHOS or CHOK1 host cells.

5.14 Evaluation of PDH subunit gDNA in CHOS and CHOK1 control cell pools during the Etanercept production run using qPCR

Expression of protein products (e.g. Etanercept) can lead to a large amount of stress put upon the cell lines (Chevallier et al., 2020). This is reflected in the changes to peak cell density in CHOS and CHOK1 cell pools when comparing Figures 5.3.2, 5.3.4, 5.11.3 and 5.11.5 over the course of batch cultures and Etanercept production runs. To confirm that this pressure did not impact the stability of the previously targeted and engineered/edited genes for the PDH complex and pyruvate metabolism during the batch culture transient production of Etanercept, samples for gDNA analysis were taken after 144 hours of the batch culture growth analysis in section 5.3 and the Etanercept production run in section 5.5. Figure 5.14.1 summaries the key results of relative gDNA amounts of *E1alpha*, *E1beta*, *E2*, *E3BP, PDP* and *LDHa* compared to β-actin gDNA amounts in the equivalent cell pools during batch culture. This was used to compare gDNA amounts in the batch culture and the Etanercept production run in CHOS and CHOK1 host and control cell lines and determine if the engineering resulted in instability in the gDNA amounts. Samples marked with an (E) signify those taken from the Etanercept production run from section 5.5 whereas samples without the (E) were taken from the batch culture in section 5.3. A Welch's t test was performed comparing the results to relevant host cells. Statistically significant results are marked accordingly.

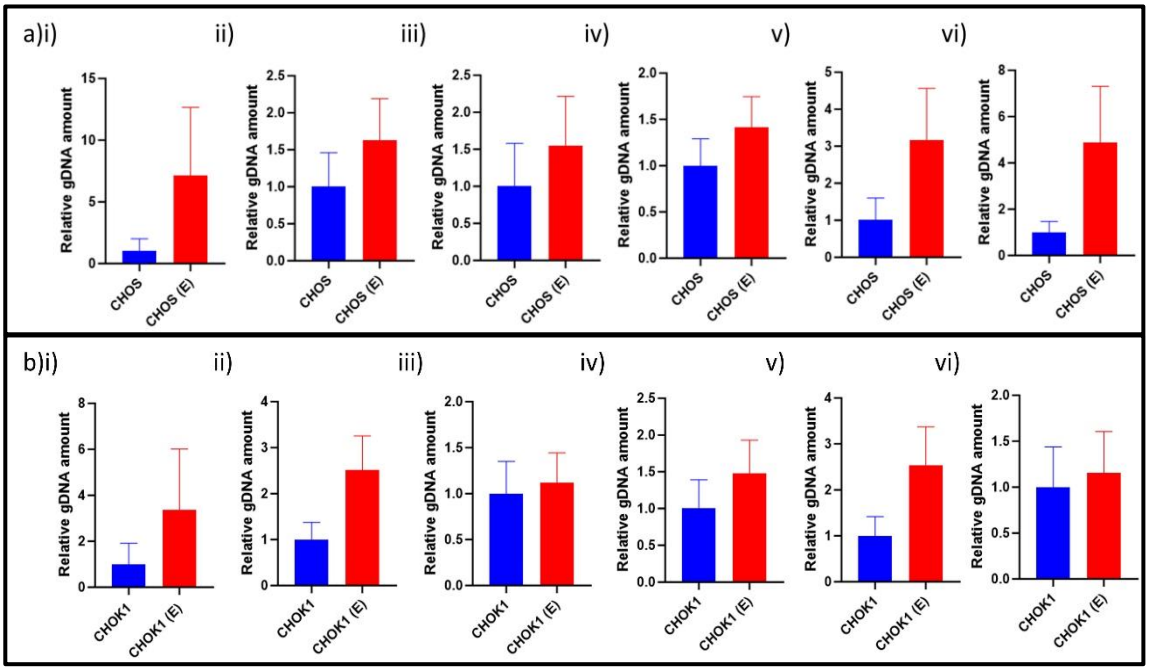

Figure 5.14.1 Relative gDNA amount of PDH subunits E1alpha (i), E1beta (ii), E2 (iii), E3BP (iv), LDHa (v) and PDP (vi) in CHOS host (a) and CHOK1 host (b) control cell pools during batch culture compared to an Etanercept production run (E) analysed via qPCR from gDNA samples taken 144 hours into culture time. Relevant E1alpha, E1beta, E2, E3BP, LDHa or PDP primers used to compare to β-actin gDNA in host cell lines CHOS (a) and CHOK1 (b) to their equivalent from an Etanercept production run. Samples marked with an (E) are from an Etanercept production batch culture detailed in Section 5.5. A Welch's t test was performed comparing the results to relevant host cells. Significance shown for key results where p value was less than or equal to 0.05. Extremely significant $p < 0.0001$ (****), Extremely significant $p = 0.0001$ to 0.001 (***), Very significant $p = 0.001$ to 0.01 (**), Significant $p = 0.01$ to 0.05 (*), Not significant $p \geq 0.05$ (ns). (n=3).

Figure 5.14.1 shows the relative gDNA of PDH subunits as well as LDHa and PDP in CHOS (a) and CHOK1 (b) cell pools during a batch culture when compared to the equivalent cell pool during the Etanercept production (E) batch culture. β-actin gDNA amounts were used to analyse relative gDNA amounts. Comparing gDNA of the E1alpha subunit (i) in CHOS cells (a) in batch culture and the Etanercept production run revealed that CHOS host cell pools had a relative increased gDNA amount when producing Etanercept. The same was observed for the CHOK1 cell pools (b) although to a lesser extent and neither result was shown to be significant. CHOS host cells showed an increase in relative E1beta gDNA (ii) when producing Etanercept as for the E1alpha data. CHOK1 cells (b) had a large increase in relative E1beta gDNA amounts when expressing Etanercept but both increases in gDNA amounts seen in CHOS and CHOK1 cells were shown not to be significant. All samples from both CHOS (a) and CHOK1 (b) cell pools show an increase in E2 (iii) and E3BP (iv) PDH subunit gDNA amounts when producing Etanercept in batch culture although none of these results were shown to be significant. All subunits of the PDH complex were shown to have increased relative gDNA in cell pools when producing Etanercept but not significantly. It is not apparent why gDNA amounts

might have increased during a Etanercept production run unless the expression of Etanercept applies a pressure that results in cells in the pool with higher gDNA amounts of the gene (or copies) out-growing those with lower gDNA amounts, offering such cells a competitive advantage. Cells with increased gDNA amounts of differing PDH subunits could have an advantage in terms of complex activity and availability of Acetyl-CoA to be used in processes such as the TCA cycle to support protein production. Further analysis, including that of mRNA expression levels during cultures would assist with confirming these potential impacts to cell genotype.

Figure 5.14.1 also reports the relative gDNA amounts of the LDHa gene (v) and PDP gene (vi) in CHOS (a) and CHOK1 (b) cell lines. PDP acts to remove the phosphorylation on serine residues in PDH subunit E1alpha to reactivate the complex allowing activity. The data shows that PDP gDNA (vi) amounts increase, potentially due to selection pressure again from the Etanercept providing an advantage to those cells with increased copy number of these genes however these results were shown not to be significant in either the CHOS (a) or CHOK1 (b) cell lines. Also shown is the relative gDNA amounts of LDHa (v). Lactate Dehydrogenase (LDHa) acts to convert Pyruvate to Lactate (Ying et al., 2019), a waste product in terms of energy production. It is therefore thought that reduced LDH activity in favour of PDH complex activity is best to increase Acetyl-CoA production. The results show an increased relative LDHa gDNA amount in all cell pools when producing Etanercept however this was not significant. Similarly to the PDH subunit gDNA analysis, further testing should be completed to fully analyse the impact had on cell lines when expressing a DTE such as Etanercept in batch culture.

5.15 Evaluation of impact of Etanercept production on PDH subunit gDNA amounts in CHOS PDK KO cell pools using qPCR

Although the impact on PDH subunit gDNA amounts observed in section 5.14 was shown to not be significant, qPCR analysis was used to investigate any potential impact seen in PDK KO cell lines during the batch production cultures. Samples were taken from CHOS PDK2 KO H4 and PDK3 KO D11 cell lines 144 hours into the Etanercept production run from section 5.5 and had gDNA isolated following the process in methods section 2.3.11 for qPCR analysis. These cell pools were only used in the Etanercept production run so were compared to host control cells also expressing Etanercept during the production run. gDNA amounts of PDH subunits E1alpha, E1beta, E2 and E3BP were investigated alongside PDP and LDHa due to their role in Pyruvate metabolism and compared to β-actin gDNA in the equivalent host control cell lines during batch culture. Figure 5.15.1 shows the results. A one-way ANOVA was also performed using Dunnett's multiple comparisons test

comparing the results to relevant host cells and any significant results with a p value below 0.05 are highlighted.

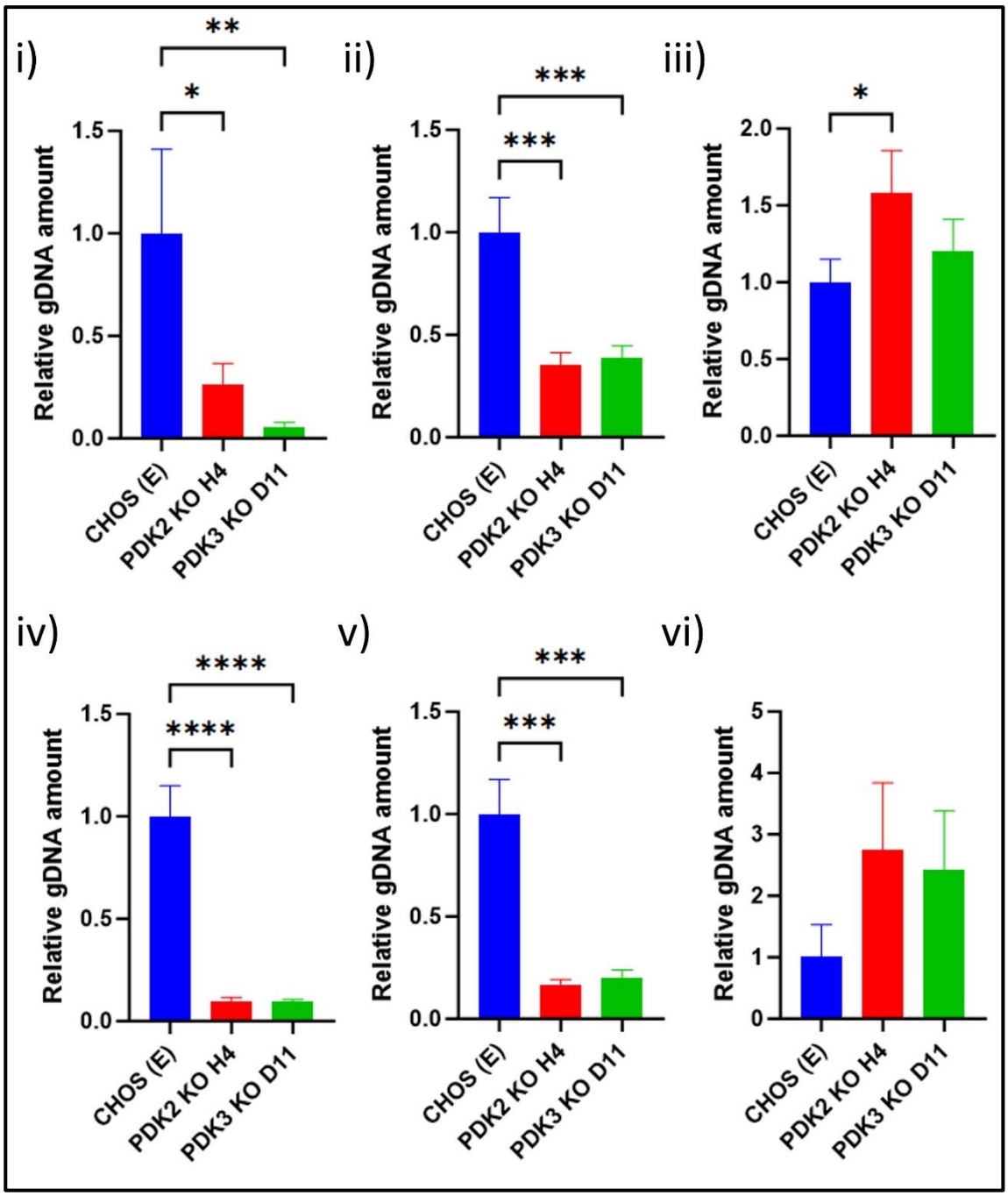

Figure 5.15.1 Relative gDNA amount of PDH subunits E1alpha (i), E1beta (ii), E2 (iii) and E3BP (iv), LDHa (v) and PDP (vi) in CHOS PDK KO cell lines during an Etanercept production run compared to CHOS host analysed via qPCR from gDNA samples taken 144 hours into culture time. Relevant E1alpha, E1beta, E2, E3BP, LDHa or PDP primers used to compare to β-actin gDNA in host cell lines CHOS (a) and CHOK1 (b) to their equivalent from an Etanercept production run. Samples marked with an (E) are from an Etanercept production batch culture detailed in Section 5.5. A one-way ANOVA was performed using Dunnett's multiple comparisons test comparing the results to relevant host cells. Significance shown for key results, Extremely significant $p < 0.0001$ (****), Extremely significant $p = 0.0001$ to 0.001 (***), Very significant $p = 0.001$ to 0.01 (**), Significant $p = 0.01$ to 0.05 (*), Not significant $p \geq 0.05$ (ns). (n=3).

Figure 5.15.1 shows the relative gDNA amounts of PDH subunits as well as LDHa and PDP in CHOS PDK KO cell lines during an Etanercept production run when compared to CHOS host cells also in an Etanercept production batch culture. β-actin gDNA amounts were used to analyse relative gDNA amounts. The Etanercept producing CHOS cells show much higher levels of E1alpha gDNA (i) when compared to KO cell lines with both the CHOS PDK2 and PDK3 cells showing a much smaller gDNA amount which is shown to be statistically significant. A reduction in PDH E1alpha subunit gDNA amounts in these cell lines could suggest a reduction in gDNA expression of other PDH complex subunits and lead to a reduction in activity in these cell lines.

Both CHOS PDK2 KO H4 and PDK3 KO D11 cells show a similar reduction in E1beta gDNA amounts (ii) when compared to CHOS host cells producing Etanercept and are both shown to be significant. A reduction of overall PDH subunit gDNA may be occurring in these cell pools when producing Etanercept due to the engineered PDK KO in these CHOS cell lines. Alternatively, cells with lower gDNA amounts (or copies) might outgrow those with higher amounts and thus this appears as an overall reduction.

CHOS KO cell pools PDK2 KO H4 and PDK3 KO D11 both show an increase in E2 gDNA amounts (iii) when compared to CHOS host cells producing Etanercept. CHOS PDK2 KO H4 had an increase to 1.5 times the amount seen in control cells, whilst CHOS PDK3 KO D11 cells show a smaller increase to E2 gDNA levels to 1.2 times the amount with both increases seen as significant. These results differ from those for other PDH subunits E1alpha (i) and E1beta (ii). The increase in gDNA amounts of PDH subunit E2 when these KO cell pools are producing Etanercept suggests the reduction of overall gDNA amounts of subunits of the PDH complex is not applicable to all subunits and is instead subunit specific. The E1alpha and E1beta subunits are involved in PDH complex regulation, possibly resulting in cells with reduced gDNA performing better and outgrowing others in the pool in these KO cell pools compared to the E2 subunit which forms the inner complex core.

Both CHOS PDK KO cell lines PDK2 KO H4 and PDK3 KO D11 show a large and significant reduction in relative gDNA amounts of E3bp (iv) when compared to CHOS cells producing Etanercept. Although PDH subunit E3bp is not involved in regulation of the complex like E1alpha and E1beta, the data in Figure 5.15.1 shows a significant reduction in gDNA amounts in PDK KO cell lines unlike the E2 subunit. It is therefore likely that the impacts to gDNA amounts are subunit specific and investigation using mRNA analysis and RTqPCR might help to further explain these responses to the targeted KO.

Figure 5.15.1 also shows the relative gDNA amounts of LDHa (v) and PDP (vi) in CHOS PDK KO cell pools during an Etanercept production run when compared to CHOS host cells also in an Etanercept

production batch culture. PDP acts to reverse the activity of PDKs, removing the phosphorylation from the Serine residues on the E1alpha subunit of the PDH complex to reactivate complex activity. Figure 4.12.5 (i) previously showed that in CHOS PDK KO cell pools when compared to β-actin gDNA amounts of CHOS host cells, the gDNA amount of PDP was reduced. When compared to CHOS host cells also producing Etanercept however, a different result was seen with the relative amount of PDP gDNA increased when compared to host cell amounts in both PDK KO cell pools. An increase in PDP gDNA levels when compared to host cell lines suggests that PDH complex activity may not be negatively impacted by the PDK KO in these cell pools. This increase is shown not to be significant so this may not be the case.

Figure 5.15.1 shows a large and significant reduction in LDHa gDNA in both PDK KO cell pools when amounts are compared to CHOS host cells also producing Etanercept in batch culture (v). A reduction in LDHa gDNA levels during the Etanercept production run when compared to host cell lines could suggest that cell metabolism is moving away from the waste product lactate to focus on PDH complex activity converting Pyruvate to Acetyl-CoA where there is reduced PDK based regulation occurring. This might occur due to cells with reduced LDHa outgrowing those with higher LDHa gDNA (or copy) amounts and explain the observed reduction. Levels of LDHa for the PDK KO cell pools were not determined in Chapter 4 so no comparisons to base line gDNA expression could be performed.

Figures 5.15.1 shows the results of CHOS PDK KO cell pools PDK2 KO H4 and PDK3 KO D11 gDNA amounts during an Etanercept production run when compared to host cell lines. PDH subunits E1alpha, E1beta and E3BP showed a reduction in gDNA levels in PDK KO cell pools when compared to host cell lines also producing Etanercept however PDH subunit E2 showed an increase in these cell pools. The PDH subunit specific impact on gDNA amounts suggests changes in PDH activity may reflect differences in the population of cells within the KO cell pools. PDP and LDHa gDNA amounts suggest PDH complex activity may be increased in these PDK KO cell pools with higher PDP gDNA levels. This could lead to increased dephosphorylation and reactivation of the complex. Comparing these results to the PDK KO cell pools whilst in batch culture but not producing model DTE Etanercept would enable the full impact of the PDK KO engineering to be examined on gDNA amounts of PDH subunits. As outlined elsewhere, it is likely that in the pool population there are subsets of cells with different gDNA amounts that outgrow other cells when specific stresses are imposed (e.g. a secretory recombinant protein load) and thus the enrichment of these populations during culture suggests an apparent change in gDNA amounts.

5.16 Evaluation of impact of Etanercept production on PDK gDNA amounts in CHOS PDK KO cell pools using qPCR

The qPCR process was also used to analyse impact to relative PDK gDNA levels in the KO cell pools during the Etanercept production run. The gDNA samples from 144 hours into the batch culture production run were used to analyse relative DNA amounts of PDK1, 2 and 3, however the PDK3 primers did not successfully amplify a product. Figure 5.16.1 shows the qPCR results compared to CHOS host cells in batch cultures producing the model DTE protein Etanercept. Unfortunately, no data was gathered for the PDK KO cell pool in batch culture for a direct comparison of changes to PDK gDNA amounts when producing Etanercept. A one-way ANOVA was also performed using Dunnett's multiple comparisons test comparing the results to relevant host cells and any significant results with a p value below 0.05 are highlighted.

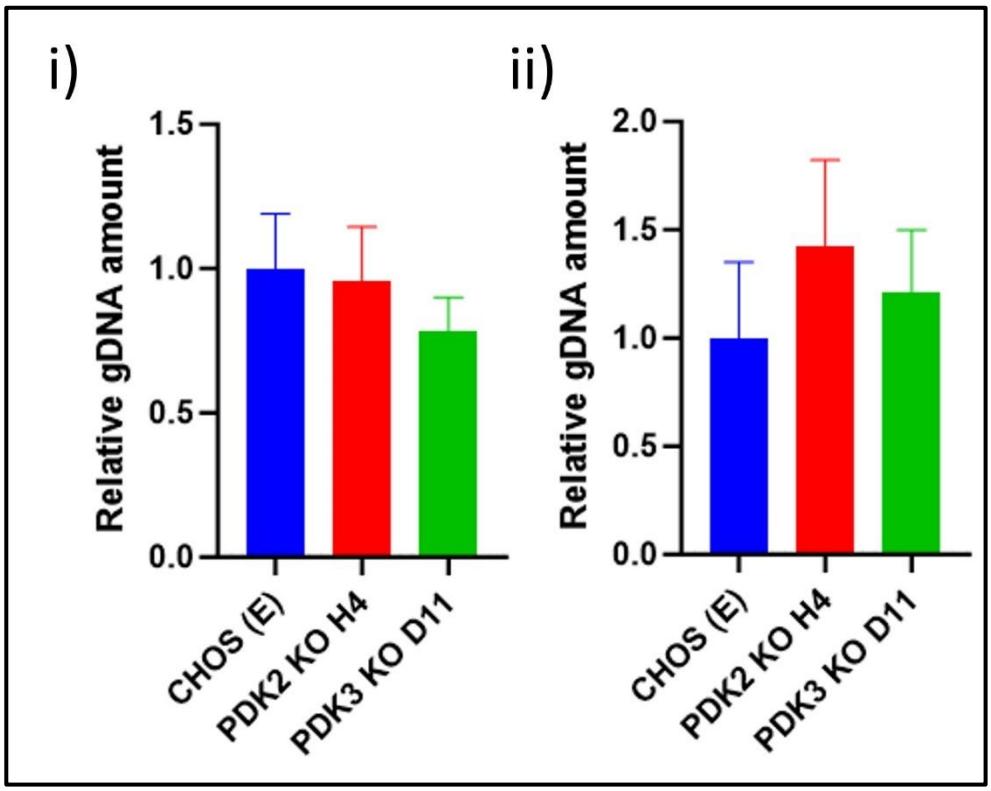

Figure 5.16.1 Relative gDNA amount of PDK1 (i) and PDK2 (ii) in CHOS PDK KO cell pools during an Etanercept production run compared to CHOS host cells during an Etanercept production run analysed via qPCR from gDNA samples taken 144 hours into culture time. PDK1 primers used to compare to β-actin gDNA levels in host cell lines in an Etanercept production run (i). CHOS samples marked with an (E) are from an Etanercept production batch culture detailed in Section 5.5. A one-way ANOVA was performed using Dunnett's multiple comparisons test comparing the results to relevant host cells. Significance shown for key results, Extremely significant $p < 0.0001$ (****), Extremely significant $p = 0.0001$ to 0.001 (***), Very significant $p = 0.001$ to 0.01 (**), Significant $p = 0.01$ to 0.05 (*), Not significant $p \geq 0.05$ (ns). (n=3).

Figure 5.16.1 shows the relative gDNA amounts of PDK1 (i) and PDK2 (ii) in CHOS PDK KO cell lines during an Etanercept production run when compared to CHOS host cells also in an Etanercept production batch culture. β-actin gDNA amounts were used to analyse relative gDNA amounts. Although PDK1 is not the target of the CRISPR/Cas9 based targeted KO in either of these cell lines, it is of interest if it's gDNA level changes in these KO cell lines acting in place of the specific KO target PDK. CHOS PDK2 KO H4 cells show a similar gDNA level of PDK1 when compared to CHOS host cells also producing Etanercept. CHOS PK3 KO D11 cells show a slight reduction in PDK1 gDNA expression when compared to host cells. As neither cell line has been selected for a KO of PDK1, the impact to PDK1 gDNA expression levels was not expected to be large unless PDK1 activity was acting in place of specific the PDK KO target.

PDK2 KO H4 cells were selected for the targeted PDK2 KO during the processes described in Chapter 4. The results in Figure 5.16.1 suggest the reduced PDK2 gDNA levels previously observed in Appendix Figure 7.2.9 were not maintained during the Etanercept production run. An increase in PDK2 gDNA amounts can be seen when comparing results to CHOS host cells also producing Etanercept. A similar gDNA amount was observed of PDK2 in CHOS PDK3 KO D11 cells when compared to host cells also producing Etanercept. The results in Figure 5.16.1 shows changes in PDK gDNA levels resulting from the expression of model DTE Etanercept when compared to host cells also producing Etanercept. Unfortunately, the full qPCR analysis of PDK3 gDNA was not successful so changes to PDK3 KO D11 cells could not be fully investigated. Similarly, any potential changes in PDK gDNA levels in cell pools where other PDKs were targeted could not be completed in full.

5.17 Evaluation of impact to expression of Lipid metabolism targets SCD1 and SREBF1 in PDH subunit overexpression cell pools and PDK KO cell pools

To investigate whether any impacts to lipid metabolism occurred as a result of the PDH targeted cell line engineering, western blots were performed to investigate protein expression levels of targets SCD1 and SREBF1. Samples from all tagged and untagged PDH overexpressing cell pools were taken on the last day of culture and analysed. PDK KO cell samples were not used. 20 µg total protein was loaded for all samples unless a low protein concentration was harvested. These samples are marked with (*), instead the maximum volume of lysate was loaded.

Western blot analysis of SCD1 expression resulted in blank blots (data not shown), with no bands seen for any samples including the controls. This was previously reported in (Budge et al., 2020), where endogenous expression of SCD1 was not identified via western blots.

Western blot analysis of SREBF1 expression was observed as shown in Figure 5.18.1 and 5.18.2. Full length SREBF1 has an expected size of 127 kDa and nuclear SREBF1 has an expected band size of 70 kDa.

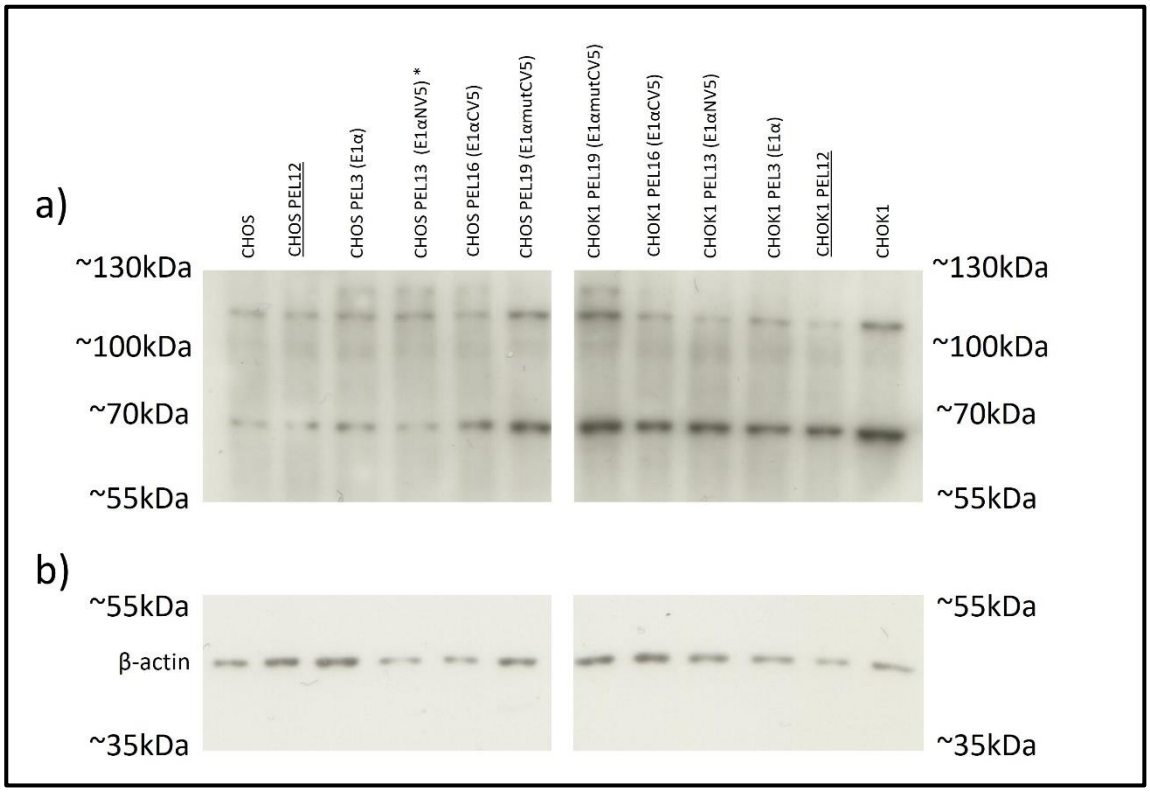

Figure 5.17.1 Evaluation of SREBF1 (a) and β-actin (b) protein expression in CHOS (left) and CHOK1 (right) cell pools engineered to stably express E1alpha N V5- and C-terminally tagged and untagged proteins PEL3 (E1α), PEL13 (E1αNV5) and PEL16 (E1αCV5) alongside PEL19 (E1αmutCV5) cells. The expected band for full length SREBF1 should be observed at 127 kDa and nuclear SREBF1 should be observed at 70 kDa. 10% SDS PAGE run with 20 µg protein unless sample is marked (*) here as much protein as possible was loaded and a) probed with anti-SREBF1 antibody and exposed for 1 hr b) probed with an anti- β-actin antibody and exposed for 30 secs.

Figure 5.17.1 shows the presence of multiple bands when samples were probed with the anti-SREBF1 antibody (a). A band ~70 kDa was seen for all samples including the controls suggesting the presence of nuclear SREBF1. Bands were observed in all samples at ~110 kDa size, slightly smaller than the expected full length SREBF1 size of 127 kDa. In some samples, CHOS PEL3 (E1α), 13 (E1αNV5) and 16 (E1αCV5) and CHOK1 PEL19 (E1αmutCV5) expressing cell pools, faint bands were present towards the top of the blot at ~130 kDa suggesting this second but fainter band is the full length SREBF1 protein. None of the CHOS or CHOK1 cell lines show this additional higher molecular weight band. When looking at the expression of β-actin (b), bands appear even in most samples although for CHOS PEL13 (E1αNV5) and 16 (E1αCV5) these were less intense although both

displayed the additional higher molecular weight band (a) suggesting that an increase in SREBF1 expression might be present in these samples. When comparing the results for the CHOS and CHOK1 cells the CHOK1 cells had higher expression of the nuclear SREBPF1. The host cells and PEL19 (E1αmutCV5) cell pool both had a higher expression of the band at ~110 kDa, but only the PEL19 cell pools showed the presence of the additional higher molecular weight band. The β-actin loading in these cells (b) was higher than the CHOK1 control cells which may explain this.

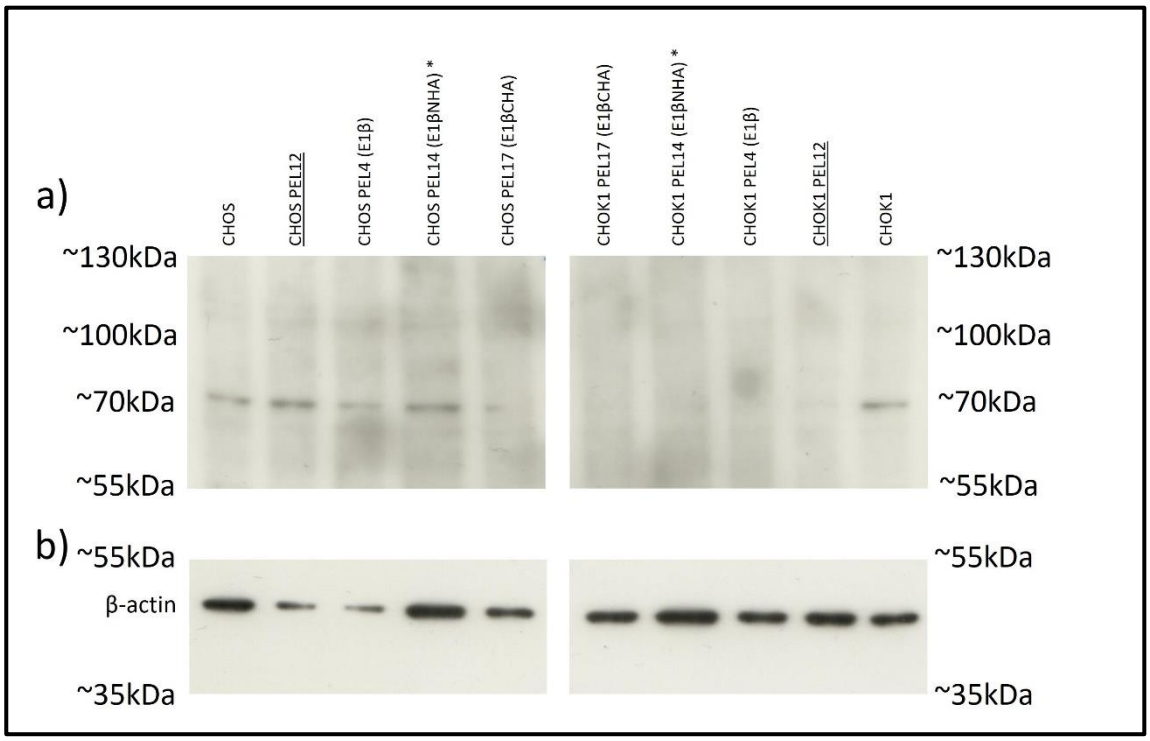

Figure 5.17.2 Evaluation of SREBF1 (a) and β-actin (b) protein expression in CHOS (left) and CHOK1 (right) cell pools engineered to stably express E1beta N HA- and C-terminally tagged and untagged proteins PEL4 (E1β), PEL14 (E1βNHA) and PEL17 (E1βCHA). The expected band for full length SREBF1 should be observed at 127 kDa and nuclear SREBF1 should be observed at 70 kDa. 10% SDS PAGE run with 20 µg total protein unless sample is marked (*) where as much protein as possible was loaded and a) probed with anti-SREBF1 antibody and exposed for 1 hr b) probed with an anti- β-actin antibody and exposed for 30 secs.

Figure 5.17.2 shows the presence of multiple bands when samples were probed with the anti-SREBF1 antibody (a). Only some of the samples had a band at ~70 kDa suggesting expression of nuclear SREBF1. All of the CHOS samples had faint bands compared to the CHOK1 host cells. No cell pools had any band around ~127 kDa, the expected band size of full length SREBF1. When looking at the β-actin loading (b), there was large variation in the CHOS cell samples. High loading was obvious for CHOS host and PEL14 (E1βNHA), whereas the other samples had lower actin intensities and thus had a lower total protein load. Even with higher β-actin loading (reflecting higher total

protein load) in these samples only faint nuclear SREBPF1 bands were observed (a). The same western blot was performed with samples from the E2 tagged and untagged overexpressing CHOS and CHOK1 cell pools, however no bands were observed for any samples including host controls when it was probed with the anti-SREBF1 antibody. Bands were observed for all samples when probed with anti-β-actin antibody. This western blot was repeated but again resulted in no SREBF1 bands being observed.

5.18 Discussion

This chapter aimed to investigate the cell pools with engineered PDH activity generated in Chapters 3 and 4 and analyse their growth, specific metabolite profiles and ability to transiently express a model DTE recombinant protein alongside investigating for any changes to lipid metabolism that may have resulted from the cell engineering strategies employed.

When considering the impact stably expressing the tagged and untagged PDH subunits had on the growth phenotype of the cell pools across a 240 hour culture, there was a marked difference between cells and particularly between the CHOS and CHOK1 hosts. Figure 5.3.1 and 5.3.2 show CHOS cells expressing any PDH subunits, tagged or untagged, and that there was little difference in viable cell number or culture viability over the course of the culture when compared to control cell lines PEL1, PEL12 and host cells. However, Figure 5.3.3 and 5.3.4 show CHOK1 cells expressing N-terminally tagged PDH subunits, PEL13 (E1αNV5), 14 (E1βNHA) and 15 (E2NFLAG). In these CHOK1 engineered cells there was an obvious increase in viable cell number at 144 hours of culture which remained at a high culture viability for an additional 48 hours when compared to host cells. This was followed by a steep drop in culture viability over the next 24 hours that was more gradual for other cell pools and spread over a 96 hour time period. This increase in maximum viable cell number was accompanied by a shorter doubling time and higher peak cell density. The CHOS cells grew to higher viable cell number compared to CHOK1 cells, however those CHOK1 cells expressing the N-terminally tagged PDH subunits grew to a more comparable viable cell number when compared to the CHOS cell profiles.

To enable evaluation of any changes in extracellular metabolites over the course of the culture between cell pools and the host cell lines, the integral viable cell concentration (IVC) over culture was first calculated as shown in Figure 5.4.1. The CHO cells all had similar IVC values although the CHOK1 N-terminally tagged PDH subunit expressing cells PEL13 (E1αNV5), 14 (E1βNHA) and 15 (E2NFLAG) had a distinct increase when compared to other CHOK1 cell pools. This was reflected in the results of the cumulative metabolite calculations in sections 5.5 to 5.10. Glucose utilisation,

shown in Figure 5.5.1 and 5.5.2, by CHOS cells was comparable with almost all glucose in the media used by the final measurement at 196 hours of culture with no clear impact resulting from the overexpression of PDH subunits with or without tags on glucose utilisation. Some PDH engineered cell pools were shown to have significantly worse specific glucose utilisation when compared to CHOS host cells.

CHOK1 cells showed similar glucose utilisation with only control cells showing any glucose remaining in the culture media at the final time point. Cumulative utilisation of glucose analysis showed two distinct groupings with the cells expressing N-terminally tagged PDH subunits, PEL13 (E1αNV5), 14 (E1βNHA) and 15 (E2NFLAG), grouped together with a lower specific glucose utilisation. Interestingly, the control CHOK1 host cell line also was within this grouping with no significant difference between engineered and host cells. This suggests the resulting impact on glucose utilisation of expressing N-terminally tagged PDH subunits in CHOK1 cells is more comparable to CHOK1 host cells whilst the other untagged and C-terminally tagged PDH subunit expressing cell pools are less efficient with their glucose utilisation. High glucose utilisation and therefore glycolytic flux is linked to the Warburg effect and lactate production and is considered to be a negative trait of recombinant protein producing cell lines (Rogatzki et al., 2015). The PDH engineering aimed to increase metabolic flux away from lactate production and instead through PDH towards acetyl-CoA production. The high glycolytic flux in these cell lines and close comparison to host cells suggests this was not occurring.

Lactate production analysis, shown in Figures 5.6.1 and 5.6.2, were more varied with some, but not all CHOS cells starting to consume lactate towards the end of the culture. This switch to lactate consumption is considered a favourable metabolic feature of industrial cell lines and is linked to increased recombinant protein production (Mulukutla et al., 2015). CHOK1 cell pools show varied results for lactate concentrations with most cells continuing to produce lactate until the 196 hour time point. PEL13 (E1αNV5), 14 (E1βNHA) and 15 (E2NFLAG) cells had a complete utilisation of any lactate in the media by this time point. This suggests these cells have made the metabolic switch and consumed lactate. When looking at cumulative and specific lactate production, these N-terminally tagged subunit expressing cells had a reduced specific lactate production, however it was not significantly different when compared to the CHOK1 host cells.

Combining the results of glucose consumption and lactate production generates the yield of viable cells per glucose and lactate yield per glucose over the culture span shown in Figure 5.7. The aim of overexpressing the PDH subunits was to have a higher yield of viable cells per glucose and specifically a lower yield of lactate per glucose due to a funnelling of pyruvate into acetyl-CoA. This

however was not the case for the CHOS cells as all cells had similar profiles to the controls. The CHOK1 PEL13 (E1αNV5), 14 (E1βNHA) and 15 (E2NFLAG) cells had a higher yield of cells per glucose at the 144 hour time point, however at the final 196 hour time point the yield was matched to the CHOK1 control cells. When considering the yield of lactate per glucose, the CHOK1 host cell line had the highest yield at the 196 hour time point. The PEL13 (E1αNV5), 14 (E1βNHA) and 15 (E2NFLAG) cell pools had a lower yield of lactate per glucose over the time course which was maintained towards the end of culture.

The accumulation of ammonia and utilisation of glutamine and glutamate were also measured during the batch cultures, shown in Figures 5.8.1 and 5.8.2, 5.9.1 and 5.9.2 and 5.10.1 and 5.10.2 respectively. Ammonia is produced as a result of glutamine metabolism which acts as one of the main nitrogen supplies for cells during culture and can be used as an alternative energy source to glucose (Yoo et al., 2020). Ammonia accumulation in cell culture can have negative effects on both the cells and product during a batch culture, impacting culture viability and glycosylation patterns (Savizi et al., 2021). Ammonia accumulated in all cell pools over the culture time with similar accumulation levels seen for both CHOS and CHOK1 host and engineered cells. All CHOS cells had similar profiles whilst CHOK1 PEL13 (E1αNV5), 14 (E1βNHA) and 15 (E2NFLAG) cells grouped together with CHOK1 host cells, having similar cumulative ammonia production. The results for the glutamine and glutamate concentrations during cell culture had large variation in all cell lines. The Cubian metabolite analyser struggled taking both glutamine and glutamate measurements with many samples being at the limits of detection. Unlike for the measurement of the other metabolites, there were no clear groupings even with the CHOK1 cells expressing N-terminally tagged subunits *E1alpha, E1beta* and *E2* in PEL13, 14 and 15 respectively that had shown potential improvements to metabolism with other metabolites.

It is noted that during the growth experiments, the metabolites of other control cells PEL1 expressing an empty cassette vector, and PEL12 expressing an empty TAG cassette vector, were also investigated. The CHOS PEL1 cell pool achieved a lower peak cell density and higher doubling time whilst the PEL12 cell pool was more comparable to the host CHOS cells. CHOS PEL1 cells also showed significantly higher glucose consumption, higher lactate and ammonia production when compared to CHOS host cells. The CHOK1 PEL1 and PEL12 cell pools both achieved a lower peak cell density around half of that of the CHOK1 host cells. These differences between all sample results demonstrate the variation between samples and cell pools and the justification for using clonal cell lines for production.

After the generation of the *E1alpha* serine/alanine mutant PEL19 stably expressing cells, the cells were transfected to transiently express the model DTE recombinant protein Etanercept. Etanercept is considered a DTE protein, being a tumour necrosis factor receptor (TNFR)-Fc-fusion protein where the Fc is derived from IgG1 (Duivelshof et al., 2021). Expression of the molecule often results in issues with glycosylation and aggregation during its production. Here the PDH engineered CHOS cells, expressing C-terminally tagged PDH subunits *E1alpha, E1beta* and *E2* in PEL17, 18 and 19 respectively were investigated. This was because of the results of the western blot analysis in Chapter 3 where protein expression of C-terminally tagged PDH subunits was more frequently observed. This was undertaken alongside transfection of the CHOS PDK KO cell pools generated in Chapter 4, CHOS PDK2 KO H4 and CHOS PDK3 KO D11 as well as the *E1alpha* serine/alanine mutant PEL19 cell pool. The successful improvement to the cell viability of CHOK1 cell pools expressing N-terminally tagged PDH subunits during the previous culture meant that all CHOK1 PDH engineered cell pools were transfected with the Etanercept plasmid. Unfortunately issues with the Cubian metabolite analyser meant that the metabolite analysis of samples could not be carried out, however the viable cell numbers and culture viability was investigated, reported in Figure 5.11.2 and 5.11.3 and 5.11.4 and 5.11.5 for CHOS and CHOK1 cells respectively.

CHOS C-terminally tagged PDH overexpressing cells PEL16 (E1αCV5) and PEL17 (E1βCHA) had similar trends in their growth characteristics compared to the previous growth curve, however PEL18 (E2CFLAG) cells had a higher viable cell number midway through the culture. This peak immediately fell and showed large variation suggesting it was not significant. The PDK KO cell pools both achieved higher viable cell numbers compared to CHOS control cells with a faster doubling time. CHOK1 cells showed large variation in viable cell numbers reached with the control cells showing some of the highest numbers compared to the others. The PEL13 (E1αNV5), 14 (E1βNHA) and 15 (E2NFLAG) cells did not show such an obvious increase to viable cell number as seen previously, however all had higher peak cell densities and shorter doubling times compared to the CHOK1 host although this was most prominent in the PEL13 (E1αNV5) cell pool. PEL19 (E1αmutCV5) cells had a peak culture viability similar to the host cell line but maintained this higher culture viability throughout the culture. All CHOK1 cells finished the culture run around or above 50% culture viability, a considerable improvement from the results presented in Figure 5.3.4 where the cultures finished around 20% viability. This was not as apparent with the CHOS cell pools but a marked improvement to final culture viability was noticed. Due to this prolonged culture viability, it may have been possible to extend the culture to potentially increase the yield of secreted Etanercept, but other factors such as exhaustion of metabolites may have impacted this. As only transient expression was investigated this is likely to be low towards the end of culture when cells will have lost the ability to

produce recombinant material. Further, the potential for cell death and waste accumulation may result in changes to product quality if culture duration was further increased.

The integral of viable cell concentration of all cell pools was calculated (Figure 5.13.1). CHOS cells had large variation in IVC and overlap between cell lines. CHOK1 cells however did present as two separate IVC groupings similar to those seen in Figure 5.4.1. This group consists of PEL13 (E1αNV5) and PEL15 (E2NFLAG) cells whereas previously PEL14 (E1βNHA) cells and CHOK1 host cells also featured. These results suggest that the improvements to viable cell number are observed during a transient recombinant protein production culture and could therefore lead to an improvement in recombinant protein production compared to CHOK1 host cells.

A dot blot was used to analyse Etanercept production for each cell pool with cell specific Etanercept production then calculated. Unfortunately, no cell pool from either the CHOS or CHOK1 host produced more Etanercept as a result of the PDH engineering process using this approach to estimate relative Etanercept production. The CHOS PDK KO cell pools were also found to have produced less than the CHOS host. PEL13 (E1αNV5) and PEL15 (E2NFLAG) CHOK1 cells had a significant reduction in cell specific Etanercept production showing that the increase to viable cell numbers did not result in a higher production of Etanercept.

Samples from the CHOS and CHOK1 host cells were then used to investigate if any significant changes in PDH subunit gDNA amounts occurred during the production culture compared to the growth culture. gDNA expression of PDH subunits E1alpha, E1beta, E2, E3BP were analysed alongside PDP and LDHa. Results in Chapter 4 showed that the gDNA levels of some PDH subunits were apparently lowered in response to the PDK KO process whilst apparent gDNA amounts of E1alpha, the subunit containing the site of the phosphorylation based regulation, was increased. This might suggest the cells were responding to PDK KO to try and maintain a level of PDH activity, or more likely that cells with particular gDNA copies or amounts had an advantage under these conditions and so are enriched, under the conditions of the experiment. To identify if this was also observed during the Etanercept production run, samples from the control cell lines were subjected to qPCR analysis. The largest changes occurred in the gDNA levels of the E1alpha subunit as well as LDHa (M. Zhou et al., 2011) however these were shown not to be significant.

This experiment was repeated using samples taken from the CHOS PDK KO cell pools CHOS PDK2 KO H4 and PDK3 KO D11. All PDH subunits were investigated as well as PDP, LDHa and the relative gDNA amounts of PDKs 1 and 2. During the Etanercept production culture, both cell pools showed a reduction in *E1alpha* gDNA amounts compared to the host CHOS cells. E1beta and E3BP PDH subunits, as well as LDHa gDNA, was reduced compared to CHOS host cells during Etanercept

production with a greater reduction seen for E3BP and LDHa compared to E1beta. These results show variation in the responses to gDNA levels in PDK KO cell pools compared to host cells when producing Etanercept. This suggests that the cells may be responding to the PDK KO by changing the gDNA levels of PDH subunits and related genes such as LDHa however not to the clear extent seen previously in Chapter 4. As outlined above, this result may reflect the pool nature of the cells investigated and may be achieved by the cells with the appropriate copies or 'best' number of copies of target genes for the conditions outgrowing those with a 'less desirable' copy number, thereby giving the impression of an increase or decrease in gDNA amounts in the pools.

Finally, western blot analysis was used to investigate expression of lipid metabolism targets SCD1 and SREBF1. These were investigated due to their role in lipid biosynthesis when increased expression resulted in increased ER size and recombinant protein production (Budge et al, 2020). As these cells were engineered with the aim of increasing the flux of pyruvate through the PDH complex producing acetyl-CoA, a key precursor for both fatty acid and lipid biosynthesis, the expression of these targets was of interest. Unfortunately, expression of SCD1 was not able to be observed on western blots which was also previously reported to be an issue, where endogenous protein expression was not shown (Budge et al., 2020). SREBF1 protein expression was observed on western blots. PEL3 (E1α), PEL13 (E1αNV5) and PEL16 (E1αCV5) CHOS and CHOK1 cells showed bands of expected sizes for both nuclear and full length SREBF1 protein. CHOS cells expressing tagged or untagged E1alpha showed a faint band ~127 kDa at the expected size of the full length SREBF1 whilst only CHOK1 PEL19 (E1αmutCV5) cells had this band. Another lower molecular weight band was observed for all samples although it seemed to be closer to ~110 kDa in size. The CHOK1 cells did show a larger band for the nuclear SREBF1 protein when compared to the CHOS cells. PEL4 (E1β), PEL14 (E1βNHA) and PEL17 (E1βCHA) CHOS and CHOK1 cells showed fewer bands for any samples with only nuclear SREBF1 observed. All CHOS cell samples showed a band of the expected size however only the CHOK1 host cell showed a band for nuclear SREBF1 expression. The results suggest that SREBF1 protein is present but that there was no clear impact to SREBF1 expression when compared to host cells resulting from the PDH subunit overexpression engineering.

Chapter 6: Overall Discussion

Recombinant protein based therapeutics are produced by the expression of recombinant DNA in a host cell system. Mammalian cells are the most commonly used host due to their ability to secrete complex molecules, performing 'human like' glycosylation patterns and PTMs in large culture volumes (J. Zhu, 2011c). There are also disadvantages of using mammalian systems which typically relate to their production and process development costs (Shanmugaraj et al., 2020). CHO cells are one of the most frequently used mammalian cell expression hosts with 89% of recombinant protein products produced in a mammalian host from 2018 to 2022 made in CHO cells along with seven of the top ten bestselling biopharmaceutical products from 2022 (Walsh & Walsh, 2022). Developments in cell culture processes and media designs have resulted in an increased production yield for a typical mAb based recombinant protein product to 1-10 g/L depending on the mAb (Kunert & Reinhart, 2016). However, novel and more complex recombinant protein designs do not always reach such high yields and are often considered DTE. The introduction of this thesis details improvements made to the classic mAb design as well as examples of recombinant protein based biotherapeutics available in the clinic. The overall aim of the work described in this thesis was the design and production of new, engineered CHO cell chassis to help improve the yield of biotherapeutic recombinant proteins, both standard and those considered to be DTE recombinant protein products.

Both CHOS and CHOK1 host cell lines were used for the work described in this thesis as a representation of commercially relevant host cell lines. Multiple CHO cell lines are used in industry for the production of recombinant proteins originating from the CHO *ori* cell line first isolated in 1956 by Theodore Puck, each displaying differences in both phenotype and genotype during culture due to genetic modifications over time (Tihanyi & Nyitray, 2020). Specific differences in expression quantity and quality have been identified with some CHO cell lines shown to favour either production of a recombinant protein or biomass synthesis (Reinhart et al., 2019). Often described as prone to clumping, the CHOS cell line is less commonly used compared to the CHOK1 host when expressing recombinant proteins in industrially relevant settings. The use of both CHOS and CHOK1 cells allowed the comparison between host cell lines and to identify if any engineering approaches impacted cell phenotype in either a positive or negative manner and was conserved across different hosts.

The PDH enzyme complex was selected as a target for the work due to its key metabolic role linking glycolysis and the TCA cycle in cellular glucose metabolism (Yiew & Finck, 2022). Detailed in Figures 1.6.1 and 1.6.2 in the introduction of this thesis is the structure of the PDH complex and activity

respectively. PDH acts to convert pyruvate to acetyl-CoA which can then enter the TCA cycle and oxidative phosphorylation for the generation of ATP or act as a precursor for fatty acid and lipid biosynthesis (Patel & Korotchkina, 2001). Alternatively, pyruvate can be converted to lactate, via the activity of LDH, which is considered a waste product. Accumulation of lactate and other waste products such as ammonia can be detrimental to cell culture health impacting pH and recombinant protein product quality (Ley et al., 2019). These pathways are therefore often targeted to reduce activity through cell line engineering and/or media and additive optimisation (Noh et al., 2017). PDH function is regulated via the activity of PDKs that act to phosphorylate and inactivate the enzyme complex (Gray et al., 2014). Three serine residues on the E1alpha subunit of PDH are the sites of phosphorylation with phosphorylation of one site enough to inactivate the whole complex (Holness & Sugden, 2003). PDP acts to dephosphorylate and reactivate the complex balancing the activity and function to suit the energy requirements of the cell (Roche & Hiromasa, 2007). The work in this thesis aimed to increase the flux of pyruvate through the PDH complex into the TCA cycle and lipid biosynthesis whilst channelling pyruvate away from LDH. Two approaches were used to achieve this and are detailed in Chapters 3 and 4 of this thesis with the resulting impact on cell growth and production of a model DTE protein Etanercept detailed in Chapter 5.

The work described in Chapter 3 details the creation of multiple triple cassette plasmids for the overexpression of PDH subunits. *E1alpha*, *E1beta* and *E2* were chosen to be expressed individually and in multiple combinations in a triple cassette vector, *E1alpha* in the first cassette, *E1beta* in the second cassette and *E2* in the third cassette generating eight vector constructs alongside a control empty cassette vector. The full plasmid list and details of the genes expressed in each cassette can be found in Appendix Table 1. The PDH subunits were kept in the same cassette and orientation throughout, with and without the addition of tags. Differences in expression between cassette positions was not investigated but could have influenced the impact on engineered cells. All three cassettes had the same design layout and CMV promoter with varied restriction sites used, however differences in expression resulting from vector position within the same plasmid have previously been reported (Beal et al., 2023b). This plasmid backbone was designed to examine if overexpression of a single PDH subunit was sufficient to increase overall protein complex expression and therefore activity, whilst limiting the number of transfections necessary for the expression of multiple target genes. After the assessment of transiently expression of each subunit, no impact to PDH subunit protein expression was observed and therefore (Figure 3.6.1), stably expressing cell pools were created. These stable cell pools showed no evidence of impact to PDH subunit protein expression (Figure 3.7.2 and 3.7.4). Had there been an obvious difference in expression between PDH subunits at this stage, the positional impact of genes in the triple cassette vector may have

been investigated. Alternatively, the strength of promoters in each cassette and pairing specific strength promoters with specific PDH subunits could have been investigated if results had favoured expression of a particular subunit.

To enable the identification of endogenous and exogenous subunit expression levels, tags were added to both the N- and C-terminus of each gene target. The same vector backbone structure was used but with the addition of the tags. A V5 tag was used in cassette one for *E1alpha*, a HA tag in cassette two for *E1beta* and a FLAG tag in cassette three for *E2*. Antibodies for these tag sequences are commercially available. PDH subunit E1alpha had previously been N-terminally His tagged (Korotchkina & Patel, 1995) and E1alpha and E1beta had previously been N-terminally FLAG tagged (Jiang et al., 2014). In both of these situations the addition of the tag was for purification purposes, however Jiang detailed the co-purification of both PDH subunits suggesting the presence of the tag was not interfering with complex formation. Both N- and C-terminally tagged PDH sequences were designed, and stable cell pools generated.

Also generated was an *E1alpha* mutant (PEL19) detailed in 3.13. Here primers for site directed mutagenesis were adapted from (Kolobova et al., 2001a) to enable the mutation of the *E1alpha* serine residues to alanine residues. This process has been used previously to identify the binding kinetics and specificities of PDKs for each of the serine phosphorylation sites (Möller et al., 2020). Sanger sequencing results showed a point mutation where a leucine residue was exchanged for a phenylalanine upstream of the site 3 serine residue. As both of these residues are polar and the alanine mutation was designed to remove the possibility for phosphorylation, cell pools stably expressing the mutant were generated. Alternatively, further cloning could have been performed to repeat the generation of the plasmid, but for the sake of time the mutant PEL19 *E1alpha* mutant was used.

Western blot analysis of the tags (section 3.11) showed mixed results with signals for the subunits with a C-terminal tag more frequently observed when probing with the relevant antibodies. The aim of these blots with antibodies to the tags was to determine exogenous expression levels, however the weak or absent signals from the anti-tag antibodies prevented this process. Similarly, the use of an anti-PDH antibody cocktail may not have suited this purpose. The PDH protein complex core is made up of 60 copies of the E2 subunit whilst fewer E1alpha and E1beta subunits attach via the lipoyl domains. Westen blot analysis often shower the higher amounts of E2 subunit expression resulting in overexposed signals whilst E1alpha and E1beta signals were not identified. The use of subunit specific antibodies may have been better suited to comparing endogenous and exogenous expression levels. No clear overexpression was observed for any samples. There was a faint band

for the PEL19 (E1αmutCV5) cell pools (Figure 3.13.1), indicating expression of the *E1alpha* mutant despite the point mutation. Immunoprecipitation was used to examine whether exogenous tagged PDH subunits were able to interact and form complexes with endogenous subunits (section 3.14). This process had mixed success and required large quantities of antibody. CHOS cells expressing N- or C-terminally HA tagged *E1beta* (PEL14 and PEL17 respectively) confirmed the interaction with additional PDH subunits (Figure 3.14.1), however control samples also showed the presence of these protein bands. The *E1alpha* mutant PEL19 cells also showed no evidence of interaction with other PDH subunits (Figure 3.14.2), possibly because the point mutation interferes with its incorporation to PDH complexes. In conclusion, the addition of the tags and their detection by antibodies had mixed success with regard to detecting exogenous subunit protein expression. The C-terminally tagged subunits were detected in more samples compared to N-terminally tagged subunits, suggesting the positioning of the tag may impact expression or incorporation into larger multi-subunit PDH complexes. Unfortunately, the immunoprecipitation using magnetic beads did not provide an answer and showed attachment to beads resulting from untagged host control cells.

gDNA analysis via qPCR was also used to investigate gDNA amounts. Primers were designed for all PDH subunits as well as their tagged counterparts to allow the comparison between untagged and tagged or endogenous and exogenous gDNA levels. Large variation was seen with these analyses and although an increase in relative gDNA was observed in engineered cell pools, it was not significant in comparison to the host cells. The use of single cell cloning at this stage may have enabled the isolation of cell lines over-expressing different amounts of the various PDH subunits. Isolating cells with high, medium and low expression of different PDH target subunits, and analysing any resulting phenotypic changes would potentially provide a clearer understanding of the impact of overexpressing the PDH subunits on CHO cell phenotype.

The results presented in Chapter 3 described the generation of PDH subunit overexpressing cell lines in both CHOS and CHOK1 cell hosts with the aim of increasing PDH complex copies and therefore activity, ultimately generating more acetyl-CoA from pyruvate. The results presented suggest that phenotypic differences between engineered and host cells were subtle at best. Exogenous overexpression of a host protein has been shown to result in a reduction of endogenous protein levels (Bernhem et al., 2018). As the activity of the PDH complex is key in channelling glucose metabolism and linking both glycosylation and the TCA cycle, high levels of regulation occur. It is therefore likely that cells act to respond to exogenous overexpression of the native PDH sequences and reduce the expression of endogenous protein resulting in a limited impact to total protein expression. This would be in line with the results reported in Chapter 3 and, if correct, confirm that

manipulation of PDH is not well tolerated by CHO cells and the amount and activity of the complex remains tightly regulated.

The material in Chapter 4 describes a CRISPR/Cas9 gene editing approach in an attempt to generate PDK KO cell pools and investigate the impact of such a KO on CHO cell growth phenotype. Although PDKs 1-4 act to phosphorylate and inactivate the PDH complex, low expression levels of PDK4 in CHO cells has previously been reported so this was not targeted (M. Zhou et al., 2011). The CRISPR/Cas9 method utilised a paired gRNA approach with one gRNA 500 bp up and downstream of the target sites aiming to remove the whole gene whilst avoiding the potential for frameshift and point mutations (Bauer et al., 2015). The availability of the CHO genome enhanced this process and made the design of gRNAs simpler whilst avoiding other potential recognition sites to reduce off target effects. Initially this process was learnt and performed in Professor Borth's lab in Vienna with CHOK1 cells and then transferred to and repeated at Kent with both CHOS and CHOK1 cells. Once multiple target gRNAs were designed and generated, the CRISPR/Cas9 transfection process was completed and the CHOK1 cells sorted into pools for high GFP expression after 48 hours using FACS. GFP expression is used as a marker of successful pX458 vector transfection into a cell, however this does not guarantee KO has occurred in such cells. Expression of GFP from just one of the Cas9 gRNA plasmids can result in high GFP expression but does not report on whether the Cas9 nuclease has efficiently caused a double stranded DNA break resulting in gene KO or if both or just break has been performed. The use of two CRISPR/Cas9 plasmids with different fluorescence markers could enable a better understanding of the CRISPR/Cas9 transfection efficiency measuring the ratio of expression of each reporter. Multiple Cas9 plasmids are commercially available including equivalent versions of the Abcam pX458 plasmid used in this thesis encoding different fluorescent proteins. Although again, expression of the Cas9 complex with the target gRNA does not guarantee a double strand break will occur. Instead, the cell DNA repair machinery may repair the Cas9 complex DNA double strand break resulting in no KO or gene removal. Alternatively, the use of multiple CRISPR/Cas9 Nickases could enable site specific cutting of DNA instead resulting from two single strand breaks via the activity of two mutated Cas9 Nickases (Villiger et al., 2024b). This approach may be more precise and limit off target effects but would require use of multiple plasmids during transfections which could impact efficiency compared to transfections with fewer plasmids. These CRIPSR/Cas9 approaches require post transfection screening to identify a successful KO and multiple gRNAs should be used before selecting the most suitable.

PDK KO generated cells were sorted into pools and qPCR and RTqPCR was used to analyse relative gDNA amounts and RNA expression respectively using primers for PDKs 1 and 2. The qPCR results (Figure 4.5.2 and 4.5.3) showed some reduction in relative gDNA amounts of targets PDK1 and 2,

but this was less than the reduction in gDNA observed in the fut8 KO control experiment (Figure 4.5.4). The reduction in fut8 gDNA was similar to that reported previously with the same gRNA pairs suggesting transfection efficiency was not a limiting factor (Schmieder et al., 2018). A reduction in relative RNA expression was more successful for PDK1 targeting gRNAs (Figure 4.6.2) compared to those targeting PDK2 (Figure 4.6.3). These results show the potential for variation and the important of screening in CRISPR/Cas9 KO targeting with different gRNA designs resulting in variable impacts to both relative gDNA and RNA levels in resulting cell pools when compared to host cells. The cell pools thus show likely have a mix of original, non-edited host cells that dominate the population and different proportions of single and multiple gRNA induced modification. This may also explain why there were no distinct observable differences in cell phenotype resulting from either the PDK1 or 2 targeted CRISPR/Cas9 KO suggesting the cell pools were still able to grow at pre-KO levels.

The KO process was then repeated alongside a PDK3 targeted KO in both CHOS and CHOK1 cells at Kent. Strong GFP expression was seen three days after the transfection in all cell lines and the fut8 control suggesting the alternative transfection system was successful in delivering the Cas9 plasmids into the cells. The same qPCR and RTqPCR methods and relevant primers were used to analyse the gRNA pair that led to the largest reduction in target PDK, however different pairs were identified as causing the largest reduction in relative PDK gDNA and RNA amounts. In the first experiments with only PDK1 and PDK2 targeted for KO in CHOK1 cells, the PDK1 KO gDNA and RNA analysis showed the PDK1 2 + 5 gRNA pair was most successful whilst for the PDK2 KO relative gDNA analysis showed 3 + 4 and relative RNA analysis showed 3 + 6 to be the best gDNA pairings. These results were analysed relative to the GAPDH housekeeping gene, however issues developed with these primers when trying to repeat the process after transfer to Kent so amount relative to the β-actin housekeeping gene was the main focus of the second experiment set. Figures 4.9.1 to 4.9.4 show relative gDNA amounts in both CHOS and CHOK1 cells with different reductions to target PDK gDNA when using the same target gRNAs. The results from the relative gDNA analysis were reflected in the relative RNA analysis. Relative RNA expression of selected samples is shown in Figures 4.10.1 to 4.10.3. CHOS PDK1 KO cell pools showed the best potential KO with gRNA pair 3 + 6 when both relative gDNA and RNA was analysed whilst CHOK1 PDK1 KO cells showed gRNA pair 2 + 5 and 2 + 6 were the most promising at reducing PDK1 when relative gDNA amounts and relative RNA expression was analysed respectively. The gRNA pairs selected for further experiment for CHOS and CHOK1 were therefore different in the two host cell lines for the targeting of PDK1 with gRNA pair 3 + 6 selected for PDK1 KO in CHOS and gRNA pair 2 + 6 chosen for PDK1 KO in CHOK1 cells. Due to similar results in both relative gDNA and RNA for CHOS and CHOK1 PDK2 and PDK3 KO experiments from the same gRNA pairs, PDK2 3 + 6 and PDK3 1 + 3 were selected for the KO in both host cell

lines. These results show that differences in outcomes between host cell lines should be considered during cellular engineering and that a one size fits all approach may not be appropriate. That being said, the possibilities for gRNA design are large, however early selection of gRNA candidates was prioritised ensuring the CRISPR/Cas9 method transfer was successful.

After gRNA selection, a TRIPLE KO cell pool was created for both hosts. Although the generation of a multi-KO cell pool would normally be approached in a sequential process, with thorough screening in between, all three PDK targeting gRNA pairs were transfected simultaneously maintaining a 1:1:1 ratio of each plasmid DNA. If single PDK KO cell pools had been successfully cloned, a sequential process could have been used alongside as a comparison although this process involves cells surviving multiple transfection and selection processes.

Protein analysis of PDK expression was performed by western blot on the selected KO cell pools and TRIPLE KO cells (Figures 4.11.1 to 4.11.3). All samples were probed with anti-PDK1, 2 and 3 antibodies as well as anti-PDP and anti-PK antibodies. This approach was taken to assess any crosstalk within and between metabolic sensing pathways as a result of the targeted PDK KO. Varied protein expression levels were observed in all cell pools with no obvious impact on PDK protein expression resulting from the CRISPR/Cas9 KOs. The results suggest that although relative gDNA and/or RNA was impacted, this is not reflected at the protein level. This was also the case in the TRIPLE KO cell pools. Densitometry analysis of band intensities from the anti-PDP and anti-PK western blots revealed a small increase in protein expression in most PDK KO cells when compared to host cells although this was sometimes also observed in PEL1 control cells. At this stage the KO of PDK expression in the pool is best described as a knock down instead of a KO as a general reduction in target PDK expression was observed in the wider pool although this was not reflected at the protein level. A large proportion of the differences seen in PDK relative gDNA amount and RNA and protein expression are thus likely to be due to variation within the cell pools. The isolation of clonal cell lines would therefore be required to generate PDK KO cell lines and fully analyse the impact of the PDK KO on phenotype and genotype.

To analyse any potential wider impacts on PDH expression and activity resulting from the PDK KO, relative gDNA expression of PDH subunits E1alpha, E1beta, E2 and E3BP were investigated alongside PDP (Figures 4.12.1 to 4.12.5). Only samples from individual KO cell pools were investigated and compared to relative gDNA amounts in host cells. This analysis suggested that the PDK KO did impact the apparent relative gDNA PDH subunit amounts. The relative gDNA amount of PDH subunit E1alpha was increased in CHOS and CHOK1 PDK KO cell pools. This is in contrast to the reduction in relative gDNA of PDH subunits E1beta, E2 and E3BP observed in CHOS cells, and to a lesser extent,

in CHOK1 cells. PDP, that acts to dephosphorylate PDH and reverse the inactivation as a result of PDK activity was found to have lower relative gDNA amounts in CHOS PDK KO cell pools, however this was less apparent in CHOK1 PDK KO cell pools. The trends observed in the CHOS PDK KO cells show that those with PDK3 targeted KO had the most extreme responses in terms of relative PDH subunit gDNA amounts followed by PDK2 KO and PDK1 KO cell pools. This trend was not as obvious in CHOK1 cell KOs apart from for the relative gDNA amount of E1alpha. Once again, the results showed large differences in relative gDNA amounts with variation within cell pools and between host cells.

The work reported in Chapter 4 suggests that for KO experiments cell pools are limited in terms of the information these can provide on KO impacts and ideally the generation of clonal KO cell lines should be generated. In this regard, limiting dilution cloning was first attempted and the process repeated multiple times with no success in terms of isolating recovered KO clones. A FACS based approach was therefore used to generate minipools. Difficulties in the generation of clonal cell lines showed that the CHOS and CHOK1 cells did not recover from a single cell in a well under the conditions used in this study and that cells only recovered when multiple cells were grown together. It was because of this that minipools were used with 10, 100 and 1000 cells per well isolated by FACS and left to recover. This isolation or selection process was based upon GFP expression in cells after transfection so was limited to those cells with successful GFP expression and not a direct measurement or selection based on successful CRISPR/Cas9 double strand breaks and target PDK gene removal. Several plates were generated and those wells that recovered were screened for their target PDK protein expression when compared to β-actin protein expression using dot blots (Figures 4.14.1 to 4.14.3). This process has limitations as cells often show no or very faint dots for the relevant anti-PDK antibody signal. Pools were therefore selected that showed a positive dot for presence of β-actin protein but a faint or no dot for target PDK protein expression. The 'best' six cell minipools in each host and PDK KO target were selected alongside fourteen TRIPLE KO cell minipools. Only two CHOK1 TRIPLE KO cell pools survived the selection and recovery process compared to twelve CHOS TRIPLE cell pools suggesting differences between the hosts. A mix of minipool origin sizes were selected with cells growing up from 10, 100 and 1000 cells per well. The TRIPLE KO cell pools showed mixed results for the dot blots (right hand side of Figures 4.14.1 to 4.14.3) with all fourteen carried forward. Individual full SDS-PAGE blots were carried out to obtain a clearer picture of the PDK protein expression levels in the TRIPLE KO cells (Figures 4.14.5 to 4.14.7) although again mixed results were observed for the selected CHOS TRIPLE KO cell pools. Protein expression of PDK1 was equivalent to host cells in CHOS TRIPLE KO cell pools, whilst no expression was observed when samples were probed with anti-PDK2 antibody. Unexpectedly, an increase in

PDK3 protein expression was observed in the CHOS TRIPLE KO cell pools compared to the CHOS host and a CHOS PDK3 KO cell pool although this apparent change may be due to a reduced β-actin signal suggesting lower protein loading.

PDK KO cell pools from both CHOS and CHOK1 hosts struggled to recover, grow and obtain high culture viability during the recovery process. To identify if this was due to the PDK KOs, relative gDNA amounts of targeted PDKs were investigated in cell pools growing/recovering more rapidly and achieving higher culture viabilities compared to those 'surviving but not growing' at low culture viabilities and viable cell numbers. The key results highlighted in Figure 4.15.1 shows that in CHOS and CHOK1 individually targeted PDK KO cell pools that were actively growing there was little to no reduction of target PDK gDNA. In those cell pools that either did not grow or grew very slowly and at lower viable cell numbers, the target PDK gDNA amount was considerably lower than the hosts, suggesting that KO compromises the cell's ability to proliferate under the conditions investigated. The results for the TRIPLE KO cells (Appendix Figure 7.2.8) show mixed success in terms of the KO of any PDK. CHOS TRIPLE KO cell pools had a small decrease in gDNA amounts of PDK1 and 2 and a strong reduction in relative gDNA amounts of PDK3 except for one (C9) mini pool. Both CHOK1 TRIPLE KO cell pools showed poor growth and had a noticeable reduction in gDNA amount of target PDK gDNA in both mini pools. These results again suggest that in more successful PDK KO cell pools, this reduction negatively impacts cell growth and recovery from the mini pool sorting. Interestingly, there was no trend in terms of the starting size of the mini pool impacting recovery and subsequent growth.

During the KO recovery process, cells were cryopreserved and grown in a T25 flask then moved to shake flasks. This process proved to be more difficult on some PDK KO cell pools compared to others, with some not recovering from low culture viabilities and staying at low viable cell numbers Although PDK KO is likely to have played a major role in this, it is unlikely the sole cause of the impacted growth phenotype due to the previous generation of PDK KO CHO cell pools reported in the literature (M. Zhou et al., 2011), (Yip et al., 2014). Further, a recent patent has been published describing the creation of a CHO cell line with a complete KO of LDH and PDKs 1-4 which was previously suggested to be lethal to cells (Yip et al., 2014). In the patent it describes the use of CRISPR/Cas9 to target activity of LDH and PDKs 1-4 to generate a cell line that exclusively shuttles pyruvate through the PDH complex to produce acetyl-CoA for entry into the TCA cycle (Hefzi Hooman & Lewis Nathan, 2017) The details surrounding the patent and experimental work to generate the CHO cell line are limited and have yet, to my current knowledge, to be published. This work poses questions surrounding the gRNA sequences used for the KOs and the development process, reaffirming that gRNA design and targeting are key factors in the design and success of a

CRISPR/Cas9 KO. The media and conditions used for recovery are also likely to be important. The patent states that to create the cell line all target gRNAs were transfected together, supporting the approach used here to try and generate a TRIPLE KO cell pool/line. Due to the difficulties of recovering KO cell pools the decision was made to restart the CRISPR/Cas9 process again using FACS to isolate minipools. For this purpose, plates were sorted to contain 10 cells per well as the starting cell number had previously been shown to have no effect on cell recovery. Again, there was mixed success with recovery and fewer minipools were generated from both CHOS and CHOK1 hosts. Dot and western blot analysis of PDK protein expression was performed (Figures 4.16.1 to 4.16.4). Low cell numbers in many samples led to the generation of low protein concentrations in lysate samples so many samples showed few or faint bands other than those for β-actin. Multiple cell pools were lost during this process and didn't recover from the sorting procedure; this was observed for both CHOS and CHOK1 host cell lines. Nevertheless, analysis of the gDNA amount of target PDKs was performed on the surviving cell pools. Again, the results revealed that high viable cell numbers correlated with a smaller reduction in gDNA amount of the PDK target compared to slower growing cells with lower culture viabilities that had a larger reduction in relative gDNA amount.

From the data presented in Chapter 4 there was evidence that PDK KO cell pools were isolated, however ultimately after multiple rounds of CRISPR/Cas9 transfections only two minipools survived the sorting process, CHOS PDK2 H4 and CHOS PDK3 D11. Multiple repeats of the process with associated gDNA analysis showed around a 50% reduction to PDK2 gDNA amounts relative to the CHOS host in CHOS PDK2 H4 KO cells (Figure 4.17.3), and no change in gDNA was able to be detected in CHOS PDK3 D11 cells due to issues with the qPCR primers. It is possible that the PDK KO approach with the specific gRNA sequences used resulted in off target effects which in turn led to the death of cells. Primers were designed for PCR reactions to generate the sequence adjacent to the target PDK genes therefore identifying the resulting DNA repair after the double stranded Cas9 break occurred; unfortunately, these reactions were not run due to time constraints. Alternative methods could be used to determine the presence of any off-target effects such as the use of whole genome sequencing (Guo et al., 2023). Another approach could have been the use of a surveyor assay such as a T7 Endonuclease assay to screen for base substitutions and indel mutations resulting from CRISPR/Cas9 activity (Sentmanat et al., 2018) and is of use when considering off target effects that may be detrimental to the cells.

After generating the PDH engineered cells with the aim of increasing the flux through the PDH complex in Chapters 3 and 4, Chapter 5 analysed any impact on cell phenotype. Due to the limited impact on protein expression when PDH subunits were expressed in multiple combinations (Figure 3.7.2 and 3.7.4), only the individual untagged subunit and N- or C-terminally tagged PDH

overexpression cell pools generated in Chapter 3 were investigated. Importantly, the work in Chapter 5 also investigated the production of a model DTE protein, Etanercept in the original host and selected engineered cells. Etanercept is a tumour necrosis factor receptor (TNFR)-Fc-fusion protein where the Fc is derived from IgG1 and is both N- and O-glycosylated (Duivelshof et al., 2021). It is prone to aggregation during manufacturing (Walsh & Walsh, 2022).

Initially impacts to cell growth phenotype as a result of the cell line engineering in Chapters 3 and 4 were analysed. This would also provide a reference growth data to compare against for the cell pools when transiently producing Etanercept in a production culture. Over a 240 hour batch culture the growth profile of engineered CHOS cells were consistent with the original host in terms of culture viability and viable cell number whilst the CHOK1 pools expressing N-terminally tagged PDH subunits PEL13 (E1αNV5), PEL14 (E1βNHA) and PEL15 (E2NFLAG) showed an increase in viable cell numbers compared to host cells (Figures 5.3.1 and 5.3.3) respectively. It is noted that during this process the CHOS cells grew to distinctly higher viable cell numbers compared to CHOK1 cells with the expression of N-terminally tagged PDH subunits in CHOK1 cells increasing viable cell numbers to comparable numbers to CHOS (Figure 5.3.2 and 5.3.4). Differences in CHO host growth phenotypes have been widely reported with higher viable cell densities in some compared to others suggesting natural variation is likely to occur (Reinhart et al., 2019). Whether this higher cell density results in an increased yield of recombinant protein was to be investigated.

Metabolite analysis was performed on extracellular glucose, lactate, ammonia, glutamine and glutamate levels during growth phase after the calculation of IVC (Figure 5.4.1). Glucose and lactate analysis showed engineered CHOS cell pools had similar glycolytic fluxes compared to host cells whilst there were differences between CHOK1 engineered cell pools (Figures 5.5.1, 5.5.2, 5.6.1 and 5.6.2). Those expressing the N-terminally tagged PDH subunits that achieved a higher viable cell number had a corresponding higher cumulative glucose utilisation and lower cumulative lactate production. The CHOK1 host cell line had a similar, but different glucose and lactate utilisation; the fact there were small differences may reflect again the pool nature of the engineered cells. This was confirmed by calculation of specific utilisation and production analysis of glucose and lactate (Figures 5.5.2 and 5.6.2). Analysis of the cell numbers generated per glucose utilised and lactate produced per glucose molecule further confirmed these findings (Figure 5.7). In these analyses PDH engineered CHOS cell pools had similar data to CHOS host cells suggesting little to no impact on glucose metabolism resulting from the expression of exogenous PDH subunits. CHOK1 cells engineered to express N-terminally tagged PDH subunits had a higher yield of cells per glucose utilised when compared to CHOK1 host cells but a lower yield of lactate per glucose. Although these results appear promising in terms of reducing lactate production and enhancing the cell yield from

glucose, (Figure 5.6.1) at the later time point cells had started to consume lactate which is likely to have skewed the calculated yield of lactate per glucose molecule. The remaining CHOK1 engineered cells all had lower yields of cells per glucose utilised and more lactate per glucose molecule than the original host CHOK1 cell line.

Cumulative ammonia production and utilisation of glutamine and glutamate over the culture were also measured (Figures 5.8.1 and 5.8.2, 5.9.1 and 5.9.2 and 5.10.1 and 5.10.2). Accumulation of ammonia in the media is regarded as a waste product and can negatively impact cell growth and product critical quality attributes such as glycosylation (Savizi et al., 2021). It is produced via glutamine metabolism and can be used as an alternative energy source to glucose (Cruzat et al., 2018). Ammonia accumulated in all cell lines and pools over the batch culture with similar values observed for both CHOS and CHOK1 cell pools (Figure 5.8.1). All CHOS cells had similar accumulation of ammonia whilst N-terminally tagged PDH subunit expressing CHOK1 cells were a distinct grouping with similar ammonia accumulation but with a higher IVC value. This grouping also included host CHOK1 cells and were more similar to those values for CHOS cells. Glutamine and glutamate utilisation were also measured (Figures 5.9.1 and 5.10.1) but the measurement detection limits of the Cubian Metabolite analyser meant no clear groupings of results were observed for CHOS or CHOK1 cells.

The results of the metabolite analysis suggest little impact on glucose metabolism or PDH flux in CHOS cells overexpressing PDH subunits. However, CHOK1 cells expressing N-terminally tagged PDH subunits showed evidence of improvement to glucose utilisation and accumulation of lactate and ammonia, although these differences were not significant when compared to CHOK1 host cells. These results are of note because of the results from the tagged PDH protein expression western blots presented in Chapter 3 (section 3.11). When probed with relevant anti-tag antibodies often signals were only observed for PDH subunits with a C-terminal tag and not for those with the N-terminal tag and in Chapter 3 it was suggested that the presence of an N-terminal tag impacted expression levels. However, these results suggest that the engineering with N-tagged PDH subunits had a larger impact on CHOK1 cells than the C-tagged subunits despite an apparent lower expression of these forms of subunit. It is possible that the positioning of the N-terminal tag was shielded due to inclusion in a PDH complex assembly and therefore, unlike the C-terminal positioned tags, were not detected by the western blot analysis. This seems unlikely as the analysis was undertaken under SDS-PAGE conditions but could be further investigated. The isolation of clonal cell lines may have allowed a more direct analysis of the impact of PDH subunit over expression although this has to be balanced with the clear diversity that already exists within the host cell population and separating engineering impacts from cell specific impacts remains challenging.

PDH E1alpha serine/alanine mutant PEL19 cell pools were also generated and assessed alongside CHOS and CHOK1 cell pools to transiently express the model DTE biotherapeutic recombinant protein Etanercept. Industrial production processes usually involve the creation of a cell line stably expressing the target recombinant protein for use in fed batch cultures to enable the high yields required for clinical applications (Zhu et al., 2017). Transient transfections enabled the rapid analysis of Etanercept production yields and any changes resulting from the PDH cell engineering approaches described in Chapters 3 and 4 with the possibility to generate stably expressing cell lines at a later date. Cell pools assessed in the Etanercept production process were specifically selected from the results reported in Chapter 3 where protein expression of the C-terminally tagged PDH subunits was more frequently seen compared to those with N-terminal tags. CHOK1 cells were assessed with both N- and C-terminal tags to further investigate any impact to viable cell numbers during the growth batch culture analysis (section 5.3). CHOS PDK2 H4 and PDK3 D11 KO cells generated in Chapter 4 were also assessed alongside the E1alpha mutant (PEL19) cell pools. When looking at viable cell numbers and percentage culture viability (Figures 5.11.2 and 5.11.3) all CHOS cells showed similar trends with large overlap and variance within culture repeats. E1alpha mutant (PEL19) expressing cell pools had an extended culture viability at the end of the culture but also lower viable cell numbers throughout when compared to all other cells suggesting nutrient availability was not a limiting factor in these cell cultures compared to others. The CHOS PDK KO cell pools had a slight improvement in maximum viable cell numbers compared to host cells, but this was not accompanied by a prolonged high culture viability which declined rapidly after 168 hours of culture. The CHOK1 cells (Figure 5.11.4 and 5.11.5) also had large variation within culture repeats with cells expressing N-terminally tagged PDH subunits not grouping together as clearly as previously and only those expressing E1alpha (PEL13) and E2 (PEL15) showing an increase in maximum viable cell numbers. The large variation between results is likely to be the result of the use of cell pools. Some cell pools had relatively high culture viabilities at the end of the culture suggesting an extension of the culture duration could have been utilised to generate more recombinant protein product whilst viability remained high. This could however lead to issues with downstream protein purification due to cell death and release of proteases that can act to impact recombinant protein product quality. Alternatively, a feeding strategy could have been used with these cells in a fed batch culture to reduce any impact of limiting nutrients in the culture. This could be further assessed in future studies.

Samples were taken for metabolite analysis for comparison to the previous growth culture however issues with the Cubian metabolite analyser meant that the analysis of these samples could not be carried out. The lack of this metabolite data meant that a full picture of the impact of PDH

engineering on glucose metabolism whilst expressing a recombinant protein in culture could not be generated. One of the aims of the work described here was to investigate the impact of PDH engineering on pyruvate metabolism and its conversion to acetyl-CoA although neither metabolite concentration was directly measured. This was due to unavailability of equipment to take these measurements. A commercial acetyl-CoA assay kit was used in an attempt to generate an estimate of acetyl-CoA concentrations but the data generated was not robust. Importantly however, model DTE Etanercept expression was able to be analysed using a dot blot to give a qualitative estimate of expression. Ideally protein titre would have been measured but instead the densitometry of signals on the dot blot and IVC was used to generate relative cell specific Etanercept production data (Figure 5.13.2). No cell pool generated from either the CHOS or CHOK1 cell line host led to an increase in Etanercept production including the CHOS PDK KO cell pools. The increase in viable cell number in CHOK1 cell pools expressing N-terminally tagged PDH subunits did not result in an increase in relative cell specific Etanercept production. It appears that these cell pools favour cell growth and biomass accumulation over the production of recombinant protein. Investigations into the quality of produced protein were not performed although could be of interest as changes to PDH metabolism may also have resulted in changes to critical quality attributes such as aggregates and particularly glycosylation patterns which are key for model DTE Etanercept which exhibits both N- and O-linked glycosylation patterns (Martínez et al., 2020).

Although any specific impact on pyruvate and acetyl-CoA concentrations as a result of PDH engineering was not measured, the impact to the surrounding and related metabolic pathways was. Expansion of the analysis of cell engineering on metabolism has been actively encouraged by others to improve the understanding of linking multiple metabolic pathways and metabolomic and proteomic analysis in a systems biology approach (Richelle & Lewis, 2017). The relative gDNA amounts of PDH subunits as well as PDP and LDHa and PDKs 1 and 2 were analysed in samples (Figure 5.16.1). Cell pool specific responses to relative PDH gDNA amounts were observed for PDH subunits with a large decrease in E1alpha, E1beta and E3BP subunits observed during Etanercept production but an increase in relative E2 gDNA . Relative PDP gDNA increased in both KO cell pools compared to CHOS cell hosts during production. There was large variation in responses, however similar trends were observed for both PDK2 and PDK3 KO targeted cell minipools. It is proposed that cells with a lower level of target PDK KO are able to outgrow those with a larger reduction in PDK expression. Generating monoclonal cell lines would be an approach to isolate clonal cell lines with a complete target PDK KO in all cells in the population ensuring the full impact of the KO can be analysed.

Although the resulting impact from PDH engineering on PDH flux and surrounding metabolic pathways seems limited (at least at the pool level), impact on lipid metabolism targets was also investigated. Acetyl-CoA acts as a precursor to lipid biosynthesis, in which SCD1 and SREBF1 play a key role. SCD1 expression is partly regulated by SREBF1 transcriptional activation and acts to prevent the phosphorylation of ACC which acts to convert acetyl-CoA to malonyl-CoA for the rate limiting step of lipid biosynthesis (Y. Wang et al., 2022). If more acetyl-CoA is being produced, then both SCD1 and SREBF1 expression may be influenced to increase or regulate steps in the lipid biosynthesis pathway. Unfortunately, no SCD1 bands were observed in western blots; this has previously been the case for endogenous CHO cell expression in other studies (Budge et al., 2020). SREBF1 western blot analysis (Figures 5.17.1 and 5.17.2) revealed signals for both nuclear and/or full length SREBF1 in CHOS and CHOK1 cells overexpressing tagged or untagged E1alpha and E1beta PDH subunits, however no bands were seen for any cells overexpressing the E2 PDH subunit. There was no clear impact on SREBF1 expression as a result of the PDH targeted engineering.

The work in this thesis aimed to generate CHO cell lines and pools overexpressing PDH subunits or with PDK targeted KOs resulting in an increased flux of pyruvate through the PDH complex to acetyl-CoA and into the TCA cycle. Multiple cell pools were generated to address these aims, however there was large variation in resulting impacts to PDH subunit and PDK expression probably as a direct result of the pool nature. The evidence of the cellular responses to the engineering is that cells look to modulate endogenous expression levels to maintain the status quo and allow the tight regulation of PDH complex activity suggesting an alternative approach to increasing PDH flux may be required. Although a patent has shown the generation of CHO cells with no PDK or LDH activity (Hefzi Hooman & Lewis Nathan, 2017) this work has not been published to my knowledge and the results presented in this thesis suggest that the screening and clonal cell line generation recovery conditions are important factors that need to be addressed to generate PDK deficient CHO cells.

Key future work would therefore be to try and generate clonal cell lines from each of the PDH overexpression stable cell pools as well as the PDK KO cell pools. Isolating clonal cell lines with high, medium and low expression levels of PDH subunits would identify whether additional copies of PDH subunits have an impact on PDH activity or whether the cell acts to maintain activity levels through complex regulation. The redesign of CRIPSR/Cas9 gRNAs for target PDKs could also remove or evaluate any limitations of off target effects. However, first the sequencing of the target KO site should be performed to analyse the impact current gRNAs are having on the cells and whether whole gene KO is occurring instead of indels or mutations. These approaches would also answer whether increased PDH activity in the cell is possible or whether these approaches are lethal. Analysis of multiple metabolites including pyruvate and acetyl-CoA concentrations at multiple time

points throughout both batch and fed-batch cell culture would help to build a larger picture of the impact of the described cell engineering techniques on PDH activity and glycolytic flux. Finally, the expression of a less complex highly expressed mAb molecule to be used as a control recombinant protein would show whether PDH engineering approaches impacted standard mAb expression but not that of a DTE protein such as Etanercept or if any improvements to production are molecule specific.

Bibliography

Abil, Z., Xiong, X., & Zhao, H. (2015). Synthetic Biology for Therapeutic Applications. Molecular Pharmaceutics, 12(2), 322. https://doi.org/10.1021/MP500392Q

Abudayyeh, O. O., Gootenberg, J. S., Essletzbichler, P., Han, S., Joung, J., Belanto, J. J., Verdine, V., Cox, D. B. T., Kellner, M. J., Regev, A., Lander, E. S., Voytas, D. F., Ting, A. Y., & Zhang, F. (2017). RNA targeting with CRISPR-Cas13. Nature, 550(7675), 280–284. https://doi.org/10.1038/NATURE24049

Alden, N., Raju, R., McElearney, K., Lambropoulos, J., Kshirsagar, R., Gilbert, A., & Lee, K. (2020). Using Metabolomics to Identify Cell Line-Independent Indicators of Growth Inhibition for Chinese Hamster Ovary Cell-Based Bioprocesses. Metabolites, 10(5). https://doi.org/10.3390/METABO10050199

Azevedo, V. F., Galli, N., Kleinfelder, A., D'Ippolito, J., & Urbano, P. C. M. (2015). Etanercept biosimilars. Rheumatology International, 35(2), 197–209. https://doi.org/10.1007/S00296-014-3080-5

Baeshen, M. N., Al-Hejin, A. M., Bora, R. S., Ahmed, M. M. M., Ramadan, H. A. I., Saini, K. S., Baeshen, N. A., & Redwan, E. M. (2015). Production of Biopharmaceuticals in E. coli: Current Scenario and Future Perspectives. Journal of Microbiology and Biotechnology, 25(7), 953–962. https://doi.org/10.4014/JMB.1412.12079

Barzadd, M. M., Lundqvist, M., Harris, C., Malm, M., Volk, A. L., Thalén, N., Chotteau, V., Grassi, L., Smith, A., Abadi, M. L., Lambiase, G., Gibson, S., Hatton, D., & Rockberg, J. (2022). Autophagy and intracellular product degradation genes identified by systems biology analysis reduce aggregation of bispecific antibody in CHO cells. New Biotechnology, 68, 68–76. https://doi.org/10.1016/J.NBT.2022.01.010

Bauer, D. E., Canver, M. C., & Orkin, S. H. (2015). Generation of genomic deletions in mammalian cell lines via CRISPR/Cas9. Journal of Visualized Experiments, 95, 52118. https://doi.org/10.3791/52118

Beal, K. M., Bandara, K. R., Ali, S. R., Sonak, R. G., Barnes, M. R., Scarcelli, J. J., & Zhang, L. (2023a). The impact of expression vector position on transgene transcription allows for rational expression vector design in a targeted integration system. Biotechnology Journal, 18(9). https://doi.org/10.1002/BIOT.202300038

Beal, K. M., Bandara, K. R., Ali, S. R., Sonak, R. G., Barnes, M. R., Scarcelli, J. J., & Zhang, L. (2023b). The impact of expression vector position on transgene transcription allows for rational expression vector design in a targeted integration system. Biotechnology Journal, 18(9), 2300038. https://doi.org/10.1002/BIOT.202300038

Beck, A., Goetsch, L., Dumontet, C., & Corvaïa, N. (2017). Strategies and challenges for the next generation of antibody–drug conjugates. Nature Reviews Drug Discovery 2017 16:5, 16(5), 315–337. https://doi.org/10.1038/nrd.2016.268

Bernhem, K., Blom, H., & Brismar, H. (2018). Quantification of endogenous and exogenous protein expressions of Na,K-ATPase with super-resolution PALM/STORM imaging. PLoS ONE, 13(4). https://doi.org/10.1371/JOURNAL.PONE.0195825

Bielser, J. M., Wolf, M., Souquet, J., Broly, H., & Morbidelli, M. (2018). Perfusion mammalian cell culture for recombinant protein manufacturing – A critical review. Biotechnology Advances, 36(4), 1328–1340. https://doi.org/10.1016/J.BIOTECHADV.2018.04.011

Booth, B. J., Ramakrishnan, B., Narayan, K., Wollacott, A. M., Babcock, G. J., Shriver, Z., & Viswanathan, K. (2018). Extending human IgG half-life using structure-guided design. MAbs, 10(7), 1098. https://doi.org/10.1080/19420862.2018.1490119

Boti, M. A., Athanasopoulou, K., Adamopoulos, P. G., Sideris, D. C., & Scorilas, A. (2023). Recent Advances in Genome-Engineering Strategies. Genes 2023, Vol. 14, Page 129, 14(1), 129. https://doi.org/10.3390/GENES14010129

Bryan, L., Clynes, M., & Meleady, P. (2021). The emerging role of cellular post-translational modifications in modulating growth and productivity of recombinant Chinese hamster ovary cells. Biotechnology Advances, 49, 107757. https://doi.org/10.1016/j.biotechadv.2021.107757

Buchsteiner, M., Quek, L., Gray, P., & Nielsen, L. K. (2018). Improving culture performance and antibody production in CHO cell culture processes by reducing the Warburg effect. Biotechnology and Bioengineering, 115(9), 2315–2327. https://doi.org/10.1002/bit.26724

Budge, J. D., Knight, T. J., Povey, J., Roobol, J., Brown, I. R., Singh, G., Dean, A., Turner, S., Jaques, C. M., Young, R. J., Racher, A. J., & Smales, C. M. (2020). Engineering of Chinese hamster ovary cell lipid metabolism results in an expanded ER and enhanced recombinant biotherapeutic protein production. Metabolic Engineering, 57, 203. https://doi.org/10.1016/J.YMBEN.2019.11.007

Bulté, D. B., Palomares, L. A., Parra, C. G., Martínez, J. A., Contreras, M. A., Noriega, L. G., & Ramírez, O. T. (2020). Overexpression of the mitochondrial pyruvate carrier reduces lactate production and increases recombinant protein productivity in CHO cells. Biotechnology and Bioengineering, 117(9), 2633–2647. https://doi.org/10.1002/BIT.27439

Carter, P. J., & Lazar, G. A. (2017). Next generation antibody drugs: pursuit of the “high-hanging fruit.” Nature Publishing Group, 17. https://doi.org/10.1038/nrd.2017.227

Chen, J. P., Gong, J. S., Su, C., Li, H., Xu, Z. H., & Shi, J. S. (2023). Improving the soluble expression of difficult-to-express proteins in prokaryotic expression system via protein engineering and synthetic biology strategies. Metabolic Engineering, 78, 99–114. https://doi.org/10.1016/J.YMBEN.2023.05.007

Chevallier, V., Andersen, M. R., & Malphettes, L. (2020). Oxidative stress-alleviating strategies to improve recombinant protein production in CHO cells. Biotechnology and Bioengineering, 117(4), 1172–1186. https://doi.org/10.1002/BIT.27247

Coulet, M., Kepp, O., Kroemer, G., & Basmaciogullari, S. (2022). Metabolic Profiling of CHO Cells during the Production of Biotherapeutics. Cells, 11(12). https://doi.org/10.3390/CELLS11121929/S1

Cruzat, V., Rogero, M. M., Keane, K. N., Curi, R., & Newsholme, P. (2018). Glutamine: Metabolism and Immune Function, Supplementation and Clinical Translation. Nutrients, 10(11). https://doi.org/10.3390/NU10111564

Dahodwala, H., & Lee, K. H. (2019). The fickle CHO: a review of the causes, implications, and potential alleviation of the CHO cell line instability problem. Current Opinion in Biotechnology, 60, 128–137. https://doi.org/10.1016/J.COPBIO.2019.01.011

Davy, A. M., Kildegaard, H. F., & Andersen, M. R. (2017). Cell Factory Engineering. Cell Systems, 4(3), 262–275. https://doi.org/10.1016/J.CELS.2017.02.010

Dean, J., & Reddy, P. (2013). Metabolic analysis of antibody producing CHO cells in fed-batch production. Biotechnology and Bioengineering, 110(6), 1735–1747. https://doi.org/10.1002/BIT.24826

Deckers, M., Deforce, D., Fraiture, M. A., & Roosens, N. H. C. (2020). Genetically Modified Micro-Organisms for Industrial Food Enzyme Production: An Overview. Foods, 9(3). https://doi.org/10.3390/FOODS9030326

Doyon, Y., Vo, T. D., Mendel, M. C., Greenberg, S. G., Wang, J., Xia, D. F., Miller, J. C., Urnov, F. D., Gregory, P. D., & Holmes, M. C. (2010). Enhancing zinc-finger-nuclease activity with improved obligate heterodimeric architectures. Nature Methods. https://doi.org/10.1038/nmeth.1539

Duivelshof, B. L., Murisier, A., Camperi, J., Fekete, S., Beck, A., Guillarme, D., & D'Atri, V. (2021). Therapeutic Fc-fusion proteins: Current analytical strategies. Journal of Separation Science, 44(1), 35–62. https://doi.org/10.1002/JSSC.202000765

Dumont, J., Euwart, D., Mei, B., Estes, S., & Kshirsagar, R. (2016). Human cell lines for biopharmaceutical manufacturing: history, status, and future perspectives. Critical Reviews in Biotechnology, 36(6), 1110. https://doi.org/10.3109/07388551.2015.1084266

Ebrahimi, S. B., & Samanta, D. (2023). Engineering protein-based therapeutics through structural and chemical design. Nature Communications 2023 14:1, 14(1), 1–11. https://doi.org/10.1038/s41467-023-38039-x

Fan, L., Kadura, I., Krebs, L. E., Hatfield, C. C., Shaw, M. M., & Frye, C. C. (2012). Improving the efficiency of CHO cell line generation using glutamine synthetase gene knockout cells. Biotechnology and Bioengineering, 109(4), 1007–1015. https://doi.org/10.1002/BIT.24365

Fan, L., Kadura, I., Krebs, L. E., Larson, J. L., Bowden, D. M., & Frye, C. C. (2013). Development of a highly-efficient CHO cell line generation system with engineered SV40E promoter. Journal of Biotechnology, 168(4), 652–658. https://doi.org/10.1016/J.JBIOTEC.2013.08.021

Farid, S. S., Baron, M., Stamatis, C., Nie, W., & Coffman, J. (2020). Benchmarking biopharmaceutical process development and manufacturing cost contributions to R&D. MAbs, 12(1). https://doi.org/10.1080/19420862.2020.1754999

Fauser, F., Kadam, B. N., Arangundy-Franklin, S., Davis, J. E., Vaidya, V., Schmidt, N. J., Lew, G., Xia, D. F., Mureli, R., Ng, C., Zhou, Y., Scarlott, N. A., Eshleman, J., Bendaña, Y. R., Shivak, D. A., Reik, A., Li, P., Davis, G. D., & Miller, J. C. (2024). Compact zinc finger architecture utilizing toxin-derived cytidine deaminases for highly efficient base editing in human cells. Nature Communications, 15(1), 1181. https://doi.org/10.1038/S41467-024-45100-W

Fischer, S., Handrick, R., & Otte, K. (2015). The art of CHO cell engineering: A comprehensive retrospect and future perspectives. Biotechnology Advances, 33(8), 1878–1896. https://doi.org/10.1016/J.BIOTECHADV.2015.10.015

Food, U., & Administration, D. (n.d.). WHAT IS A BIOSIMILAR? Retrieved March 11, 2024, from www.FDA.gov

Freund, N. W., & Croughan, M. S. (2018). A Simple Method to Reduce both Lactic Acid and Ammonium Production in Industrial Animal Cell Culture. International Journal of Molecular Sciences, 19(2). https://doi.org/10.3390/IJMS19020385

Fu, T., Zhang, C., Jing, Y., Jiang, C., Li, Z., Wang, S., Ma, K., Zhang, D., Hou, S., Dai, J., Kou, G., & Wang, H. (2016). Regulation of cell growth and apoptosis through lactate dehydrogenase C over-expression in Chinese hamster ovary cells. Applied Microbiology and Biotechnology, 100(11), 5007–5016. https://doi.org/10.1007/S00253-016-7348-4/FIGURES/6

Gaidukov, L., Wroblewska, L., Teague, B., Nelson, T., Zhang, X., Liu, Y., Jagtap, K., Mamo, S., Allen Tseng, W., Lowe, A., Das, J., Bandara, K., Baijuraj, S., Summers, N. M., Lu, T. K., Zhang, L., & Weiss, R. (2018). A multi-landing pad DNA integration platform for mammalian cell engineering. Nucleic Acids Research, 46(8), 4072. https://doi.org/10.1093/NAR/GKY216

Gaj, T., Sirk, S. J., Shui, S. L., & Liu, J. (2016). Genome-Editing Technologies: Principles and Applications. Cold Spring Harbor Perspectives in Biology, 8(12). https://doi.org/10.1101/CSHPERSPECT.A023754

Genzel, Y., Ritter, J. B., König, S., Alt, R., & Reichl, U. (2005). Substitution of Glutamine by Pyruvate To Reduce Ammonia Formation and Growth Inhibition of Mammalian Cells. Biotechnology Progress, 21(1), 58–69. https://doi.org/10.1021/BP049827D

Ghaderi, D., Zhang, M., Hurtado-Ziola, N., & Varki, A. (2012). Production platforms for biotherapeutic glycoproteins. Occurrence, impact, and challenges of non-human sialylation. Biotechnology and Genetic Engineering Reviews , 147–176. https://doi.org/10.5661/bger-28-147

Giddens, J. P., Lomino, J. V., DiLillo, D. J., Ravetch, J. V., & Wang, L. X. (2018). Site-selective chemoenzymatic glycoengineering of Fab and Fc glycans of a therapeutic antibody. Proceedings of the National Academy of Sciences of the United States of America, 115(47), 12023–12027. https://doi.org/10.1073/PNAS.1812833115/-/DCSUPPLEMENTAL

Gifre, L., Arís, A., Bach, À., & Garcia-Fruitós, E. (2017). Trends in recombinant protein use in animal production. Microbial Cell Factories, 16(1), 40. https://doi.org/10.1186/S12934-017-0654-4

Goebeler, M. E., & Bargou, R. C. (2020). T cell-engaging therapies — BiTEs and beyond. Nature Reviews Clinical Oncology 2020 17:7, 17(7), 418–434. https://doi.org/10.1038/s41571-020-0347-5

Gomes, A. M. V., Carmo, T. S., Carvalho, L. S., Bahia, F. M., & Parachin, N. S. (2018). Comparison of Yeasts as Hosts for Recombinant Protein Production. Microorganisms, 6(2). https://doi.org/10.3390/MICROORGANISMS6020038

Goulet, D. R., & Atkins, W. M. (2020). Considerations for the Design of Antibody-Based Therapeutics. Journal of Pharmaceutical Sciences, 109(1), 74. https://doi.org/10.1016/J.XPHS.2019.05.031

Government Accountability Office US. (2023). Science & Tech Spotlight: Synthetic Biology. GAO-23-106648. www.gao.gov/copyright.

Gray, L. R., Tompkins, S. C., & Taylor, E. B. (2014). Regulation of pyruvate metabolism and human disease. In Cellular and Molecular Life Sciences (Vol. 71, Issue 14, pp. 2577–2604). Birkhauser Verlag AG. https://doi.org/10.1007/s00018-013-1539-2

Gulce Iz, S., Inevi, M. A., Metiner, P. S., Tamis, D. A., & Kisbet, N. (2018). A BioDesign Approach to Obtain High Yields of Biosimilars by Anti-apoptotic Cell Engineering: a Case Study to Increase the Production Yield of Anti-TNF Alpha Producing Recombinant CHO Cells. Applied Biochemistry and Biotechnology, 184(1), 303–322. https://doi.org/10.1007/S12010-017-2540-2/FIGURES/8

Guo, C., Ma, X., Gao, F., & Guo, Y. (2023). Off-target effects in CRISPR/Cas9 gene editing. Frontiers in Bioengineering and Biotechnology, 11. https://doi.org/10.3389/FBIOE.2023.1143157/FULL

Gupta, S. K., Sharma, A., Kushwaha, H., & Shukla, P. (2017). Over-expression of a Codon optimized yeast cytosolic pyruvate carboxylase (PYC2) in CHO cells for an augmented lactate metabolism. Frontiers in Pharmacology, 8(JUL). https://doi.org/10.3389/FPHAR.2017.00463/FULL

Gutiérrez-González, M., Latorre, Y., Zúñiga, R., Aguillón, J. C., Molina, M. C., & Altamirano, C. (2019). Transcription factor engineering in CHO cells for recombinant protein production. Critical Reviews in Biotechnology, 39(5), 665–679. https://doi.org/10.1080/07388551.2019.1605496

Ha, T. K., & Lee, G. M. (2014). Effect of glutamine substitution by TCA cycle intermediates on the production and sialylation of Fc-fusion protein in Chinese hamster ovary cell culture. Journal of Biotechnology, 180, 23–29. https://doi.org/10.1016/J.JBIOTEC.2014.04.002

Hamaker, N. K., & Lee, K. H. (2018). Site-specific integration ushers in a new era of precise CHO cell line engineering. Current Opinion in Chemical Engineering, 22, 152–160. https://doi.org/10.1016/J.COCHE.2018.09.011

Han, J., & Kaufman, R. J. (2016). The role of ER stress in lipid metabolism and lipotoxicity. Journal of Lipid Research, 57(8), 1329. https://doi.org/10.1194/JLR.R067595

Hansen, H. G., Nilsson, C. N., Lund, A. M., Kol, S., Grav, L. M., Lundqvist, M., Rockberg, J., Lee, G. M., Andersen, M. R., & Kildegaard, H. F. (2015). Versatile microscale screening platform for improving recombinant protein productivity in Chinese hamster ovary cells. Scientific Reports 2015 5:1, 5(1), 1–12. https://doi.org/10.1038/srep18016

Harris, R. A., Bowker-Kinley, M. M., Huang, B., & Wu, P. (2002). Regulation of the activity of the pyruvate dehydrogenase complex. In Advan. Enzyme Regul (Vol. 42). https://ac.els-cdn.com/S0065257101000619/1-s2.0-S0065257101000619-main.pdf?_tid=c00c2a7c-11eb-4f8e-9a7d-016940e50b22&acdnat=1540910296_9a57eaf781dadb373844d9980e71fe55

Harrison, C. (2012). Enbrel patent surfaces. Nature Biotechnology, 30(2), 123. https://doi.org/10.1038/NBT0212-123

Hartley, F., Walker, T., Chung, V., & Morten, K. (2018). Mechanisms driving the lactate switch in Chinese hamster ovary cells. Biotechnology and Bioengineering, 115(8), 1890–1903. https://doi.org/10.1002/BIT.26603

Hefzi Hooman, & Lewis Nathan. (2017). Mammalian Cells Devoid of Lactate Dehydrogenase Activity (Patent WO 2017/192437 A1).

Henry, M. N., MacDonald, M. A., Orellana, C. A., Gray, P. P., Gillard, M., Baker, K., Nielsen, L. K., Marcellin, E., Mahler, S., & Martínez, V. S. (2020). Attenuating apoptosis in Chinese hamster ovary cells for improved biopharmaceutical production. Biotechnology and Bioengineering, 117(4), 1187–1203. https://doi.org/10.1002/BIT.27269

Hilliard, W., MacDonald, M. L., & Lee, K. H. (2020). Chromosome-scale scaffolds for the Chinese hamster reference genome assembly to facilitate the study of the CHO epigenome. Biotechnology and Bioengineering, 117(8), 2331–2339. https://doi.org/10.1002/BIT.27432

Hmiel, L. K., Brorson, K. A., & Boyne, M. T. (2015). Post-translational structural modifications of immunoglobulin G and their effect on biological activity. Analytical and Bioanalytical Chemistry, 407(1), 79–94. https://doi.org/10.1007/S00216-014-8108-X/TABLES/2

Ho, S. C. L., Wang, T., Song, Z., & Yang, Y. (2015). IgG Aggregation Mechanism for CHO Cell Lines Expressing Excess Heavy Chains. Molecular Biotechnology, 57(7), 625–634. https://doi.org/10.1007/S12033-015-9852-7/FIGURES/6

Holkers, M., Maggio, I., Liu, J., Janssen, J. M., Miselli, F., Mussolino, C., Recchia, A., Cathomen, T., & Gonçalves, M. A. F. V. (2013). Differential integrity of TALE nuclease genes following adenoviral and lentiviral vector gene transfer into human cells. Nucleic Acids Research, 41(5), e63. https://doi.org/10.1093/NAR/GKS1446

Holness, M. J., & Sugden, M. C. (2003). Regulation of pyruvate dehydrogenase complex activity by reversible phosphorylation.

Hwang, T. J., Trinh, Q. D., Tibau, A., & Vokinger, K. N. (2022). Reforms to accelerated approval of new medicines: long overdue. The Lancet, 400(10349), 357–358. https://doi.org/10.1016/S0140-6736(22)01276-4

Jefferis, R. (2016). Posttranslational Modifications and the Immunogenicity of Biotherapeutics. Journal of Immunology Research, 2016. https://doi.org/10.1155/2016/5358272

Jemli, S., Ayadi-Zouari, D., Ben Hlima, H., & Bejar, S. (2016). Critical Reviews in Biotechnology Biocatalysts: application and engineering for industrial purposes Biocatalysts: application and engineering for industrial purposes. Crit Rev Biotechnol, 36(2), 246–258. https://doi.org/10.3109/07388551.2014.950550

Jiang, Y., Wang, J., Zhang, G., Oza, K., Myers, L., Holbert, M. A., & Sweitzer, S. (2014). Component co-expression and purification of recombinant human pyruvate dehydrogenase complex from baculovirus infected SF9 cells. Protein Expression and Purification, 97, 9–16. https://doi.org/10.1016/j.pep.2014.02.002

Kallunki, T., Barisic, M., Jäättelä, M., & Liu, B. (2019). How to Choose the Right Inducible Gene Expression System for Mammalian Studies? Cells, 8(8). https://doi.org/10.3390/CELLS8080796

Karki, U., Fang, H., Guo, W., Unnold-Cofre, C., & Xu, · Jianfeng. (2021). Cellular engineering of plant cells for improved therapeutic protein production. Plant Cell Reports, 40, 1087–1099. https://doi.org/10.1007/s00299-021-02693-6

Kato, M., Wynn, R. M., Chuang, J. L., Tso, S.-C., Machius, M., Li, J., & Chuang, D. T. (2008). Structural Basis for Inactivation of the Human Pyruvate Dehydrogenase Complex by

Phosphorylation: Role of Disordered Phosphorylation Loops. Structure, 16(12), 1849–1859. https://doi.org/10.1016/J.STR.2008.10.010

Kim, E., Kim, S., Kim, D. H., Choi, B.-S., Choi, I.-Y., & Kim, J.-S. (2010). Precision genome engineering with programmable DNA-nicking enzymes. https://doi.org/10.1101/gr.138792.112

Kim, S. H., & Lee, G. M. (2007). Down-regulation of lactate dehydrogenase-A by siRNAs for reduced lactic acid formation of Chinese hamster ovary cells producing thrombopoietin. Applied Microbiology and Biotechnology, 74(1), 152–159. https://doi.org/10.1007/S00253-006-0654-5

Kinch, M. S. (2015). An overview of FDA-approved biologics medicines. Drug Discovery Today, 20(4). https://doi.org/10.1016/j.drudis.2014.09.003

Kolobova, E., Tuganova, A., Boulatnikov, I., & Popov, K. M. (2001a). Regulation of pyruvate dehydrogenase activity through phosphorylation at multiple sites. The Biochemical Journal, 358(Pt 1), 69–77. http://www.ncbi.nlm.nih.gov/pubmed/11485553

Kolobova, E., Tuganova, A., Boulatnikov, I., & Popov, K. M. (2001b). Regulation of pyruvate dehydrogenase activity through phosphorylation at multiple sites. In Biochem. J (Vol. 358). https://www.ncbi.nlm.nih.gov/pmc/articles/PMC1222033/pdf/11485553.pdf

Komatsu, K., Kumon, K., Arita, M., Onitsuka, M., Omasa, T., & Yohda, M. (2020). Effect of the disulfide isomerase PDIa4 on the antibody production of Chinese hamster ovary cells. Journal of Bioscience and Bioengineering, 130(6), 637–643. https://doi.org/10.1016/J.JBIOSC.2020.08.001

Korotchkina, L. G., & Patel, M. S. (1995). Mutagenesis studies of the phosphorylation sites of recombinant human pyruvate dehydrogenase. Site-specific regulation. Journal of Biological Chemistry, 270(24), 14297–14304. https://doi.org/10.1074/jbc.270.24.14297

Kovalev, M. A., Davletshin, A. I., & Karpov, D. S. (2024). Engineering Cas9: next generation of genomic editors. Applied Microbiology and Biotechnology, 108(1), 209. https://doi.org/10.1007/S00253-024-13056-Y

Kozak, B. U., van Rossum, H. M., Luttik, M. A. H., Akeroyd, M., Benjamin, K. R., Wu, L., de Vries, S., Daran, J. M., Pronk, J. T., & van Maris, A. J. A. (2014). Engineering acetyl coenzyme A supply: functional expression of a bacterial pyruvate dehydrogenase complex in the cytosol of Saccharomyces cerevisiae. MBio, 5(5). https://doi.org/10.1128/MBIO.01696-14

Ku, J. T., Chen, A. Y., & Lan, E. I. (2020). Metabolic Engineering Design Strategies for Increasing Acetyl-CoA Flux. Metabolites, 10(4), 166. https://doi.org/10.3390/metabo10040166

Kumaran, S., Patel, M. S., & Jordan, F. (2013). Nuclear Magnetic Resonance Approaches in the Study of 2-Oxo Acid Dehydrogenase Multienzyme Complexes—A Literature Review. Molecules, 18(10), 11873. https://doi.org/10.3390/MOLECULES181011873

Kunert, R., & Reinhart, D. (2016). Advances in recombinant antibody manufacturing. Applied Microbiology and Biotechnology, 100(8), 3451. https://doi.org/10.1007/S00253-016-7388-9

Lalonde, M. E., & Durocher, Y. (2017). Therapeutic glycoprotein production in mammalian cells. Journal of Biotechnology, 251, 128–140. https://doi.org/10.1016/J.JBIOTEC.2017.04.028

Lanigan, T. M., Kopera, H. C., & Saunders, T. L. (2020). Principles of Genetic Engineering. Genes 2020, Vol. 11, Page 291, 11(3), 291. https://doi.org/10.3390/GENES11030291

Latorre, Y., Torres, M., Vergara, M., Berrios, J., Sampayo, M. M., Gödecke, N., Wirth, D., Hauser, H., Dickson, A. J., & Altamirano, C. (2023). Engineering of Chinese hamster ovary cells for co-overexpressing MYC and XBP1s increased cell proliferation and recombinant EPO production. Scientific Reports, 13(1). https://doi.org/10.1038/S41598-023-28622-Z

Le, H., Vishwanathan, N., Jacob, N. M., Gadgil, M., & Hu, W. S. (2015). Cell line development for biomanufacturing processes: recent advances and an outlook. Biotechnology Letters, 37(8), 1553–1564. https://doi.org/10.1007/S10529-015-1843-Z/FIGURES/2

Leader, B., Baca, Q. J., & Golan, D. E. (2008). Protein therapeutics: a summary and pharmacological classification. Nature Reviews. Drug Discovery, 7(1), 21–39. https://doi.org/10.1038/NRD2399

Lee, J., Bayarsaikhan, D., Bayarsaikhan, G., Kim, J. S., Schwarzbach, E., & Lee, B. (2020). Recent advances in genome editing of stem cells for drug discovery and therapeutic application. Pharmacology & Therapeutics, 209, 107501. https://doi.org/10.1016/J.PHARMTHERA.2020.107501

Lee, J. H., Kang, H. I., Kim, S., Ahn, Y. Bin, Kim, H., Hong, J. K., & Baik, J. Y. (2023). NAD+ supplementation improves mAb productivity in CHO cells via a glucose metabolic shift. Biotechnology Journal, 18(4), 2200570. https://doi.org/10.1002/BIOT.202200570

Lee, K. H., & Kim, D. M. (2018). Recent advances in development of cell-free protein synthesis systems for fast and efficient production of recombinant proteins. FEMS Microbiology Letters, 365(17). https://doi.org/10.1093/FEMSLE/FNY174

Ley, D., Pereira, S., Pedersen, L. E., Arnsdorf, J., Hefzi, H., Davy, A. M., Ha, T. K., Wulff, T., Kildegaard, H. F., & Andersen, M. R. (2019). Reprogramming AA catabolism in CHO cells with CRISPR/Cas9 genome editing improves cell growth and reduces byproduct secretion. Metabolic Engineering, 56, 120–129. https://doi.org/10.1016/J.YMBEN.2019.09.005

Li, H., Yang, Y., Hong, W., Huang, M., Wu, M., & Zhao, X. (2020). Applications of genome editing technology in the targeted therapy of human diseases: mechanisms, advances and prospects. Signal Transduction and Targeted Therapy, 5(1). https://doi.org/10.1038/S41392-019-0089-Y

Li, Z. M., Fan, Z. L., Wang, X. Y., & Wang, T. Y. (2022). Factors Affecting the Expression of Recombinant Protein and Improvement Strategies in Chinese Hamster Ovary Cells. Frontiers in Bioengineering and Biotechnology, 10, 880155. https://doi.org/10.3389/FBIOE.2022.880155/BIBTEX

Lin, P. C., Chan, K. F., Kiess, I. A., Tan, J., Shahreel, W., Wong, S. Y., & Song, Z. (2019). Attenuated glutamine synthetase as a selection marker in CHO cells to efficiently isolate highly productive stable cells for the production of antibodies and other biologics. MAbs, 11(5), 965–976. https://doi.org/10.1080/19420862.2019.1612690

Liste-Calleja, L., Lecina, M., Lopez-Repullo, J., Albiol, J., Solà, C., & Cairó, J. J. (2015). Lactate and glucose concomitant consumption as a self-regulated pH detoxification mechanism in HEK293 cell cultures. Applied Microbiology and Biotechnology, 99(23), 9951–9960. https://doi.org/10.1007/S00253-015-6855-Z/FIGURES/5

Liu, C., Zhang, L., Liu, H., & Cheng, K. (2017). Delivery Strategies of the CRISPR-Cas9 Gene-Editing System for Therapeutic Applications. Journal of Controlled Release : Official Journal of the Controlled Release Society, 266, 17. https://doi.org/10.1016/J.JCONREL.2017.09.012

Liu, H., Saxena, A., Sidhu, S. S., & Wu, D. (2017). Fc Engineering for Developing Therapeutic Bispecific Antibodies and Novel Scaffolds. Frontiers in Immunology, 8(JAN), 1. https://doi.org/10.3389/FIMMU.2017.00038

Liu, X., Cooper, D. E., Cluntun, A. A., Warmoes, M. O., Zhao, S., Reid, M. A., Liu, J., Lund, P. J., Lopes, M., Garcia, B. A., Wellen, K. E., Kirsch, D. G., & Locasale, J. W. (2018). Acetate Production from Glucose and Coupling to Mitochondrial Metabolism in Mammals. Cell. https://doi.org/10.1016/J.CELL.2018.08.040

Lopes, R., & Prasad, M. K. (2023). Beyond the promise: evaluating and mitigating off-target effects in CRISPR gene editing for safer therapeutics. Frontiers in Bioengineering and Biotechnology, 11. https://doi.org/10.3389/FBIOE.2023.1339189

Macarrón Palacios, A., Korus, P., Wilkens, B. G. C., Heshmatpour, N., & Patnaik, S. R. (2024). Revolutionizing in vivo therapy with CRISPR/Cas genome editing: breakthroughs, opportunities and challenges. Frontiers in Genome Editing, 6. https://doi.org/10.3389/FGEED.2024.1342193

Maeder, M. L., Thibodeau-Beganny, S., Osiak, A., Wright, D. A., Anthony, R. M., Eichtinger, M., Jiang, T., Foley, J. E., Winfrey, R. J., Townsend, J. A., Unger-Wallace, E., Sander, J. D., Müller-Lerch, F., Fu, F., Pearlberg, J., Göbel, C., Dassie, J. P. P., Pruett-Miller, S. M., Porteus, M. H., … Joung, J. K. (2008). Rapid "open-source" engineering of customized zinc-finger nucleases for highly efficient gene modification. Molecular Cell, 31(2), 294. https://doi.org/10.1016/J.MOLCEL.2008.06.016

Makurvet, F. D. (2021). Biologics vs. small molecules: Drug costs and patient access. Medicine in Drug Discovery, 9, 100075. https://doi.org/10.1016/J.MEDIDD.2020.100075

Marigliani, B., Balottin, L. B. L., & Augusto, E. de F. P. (2019). Adaptation of Mammalian Cells to Chemically Defined Media. Current Protocols in Toxicology, 82(1), e88. https://doi.org/10.1002/CPTX.88

Martínez, V. P. M., Tierrablanca-Sánchez, L., Espinosa-de la Garza, C. E., Juárez-Bayardo, L. C., Piña-Lara, N., Santoyo, G. G., & Pérez, N. O. (2020). Functional analysis of glycosylation in Etanercept: Effects over potency and stability. European Journal of Pharmaceutical Sciences : Official Journal of the European Federation for Pharmaceutical Sciences, 153. https://doi.org/10.1016/J.EJPS.2020.105467

Marx, N., Dhiman, H., Schmieder, V., Freire, C. M., Nguyen, L. N., Klanert, G., & Borth, N. (2021). Enhanced targeted DNA methylation of the CMV and endogenous promoters with dCas9-DNMT3A3L entails distinct subsequent histone modification changes in CHO cells. Metabolic Engineering, 66, 268–282. https://doi.org/10.1016/J.YMBEN.2021.04.014

Mathias, S., Wippermann, A., Raab, N., Zeh, N., Handrick, R., Gorr, I., Schulz, P., Fischer, S., Gamer, M., & Otte, K. (2020). Unraveling what makes a monoclonal antibody difficult-to-express: From intracellular accumulation to incomplete folding and degradation via ERAD. Biotechnology and Bioengineering, 117(1), 5–16. https://doi.org/10.1002/BIT.27196

McAtee Pereira, A. G., Walther, J. L., Hollenbach, M., & Young, J. D. (2018). 13 C Flux Analysis Reveals that Rebalancing Medium Amino Acid Composition can Reduce Ammonia Production while Preserving Central Carbon Metabolism of CHO Cell Cultures. Biotechnology Journal, 13(10). https://doi.org/10.1002/BIOT.201700518

McCommis, K. S., & Finck, B. N. (2015). Mitochondrial pyruvate transport: a historical perspective and future research directions. The Biochemical Journal, 466(3), 443. https://doi.org/10.1042/BJ20141171

McHugh, K. P., Xu, J., Aron, K. L., Borys, M. C., & Li, Z. J. (2020). Effective temperature shift strategy development and scale confirmation for simultaneous optimization of protein productivity and quality in Chinese hamster ovary cells. Biotechnology Progress, 36(3), e2959. https://doi.org/10.1002/BTPR.2959

Mckenzie, E. A., & Abbott, W. M. (2018). Expression of recombinant proteins in insect and mammalian cells. https://doi.org/10.1016/j.ymeth.2018.05.013

Mohr, S. E., Hu, Y., Ewen-Campen, B., Housden, B. E., Viswanatha, R., & Perrimon, N. (2016). CRISPR guide RNA design for research applications. The Febs Journal, 283(17), 3232. https://doi.org/10.1111/FEBS.13777

Möller, J., Bhat, K., Guhl, L., Pörtner, R., Jandt, U., & Zeng, A. P. (2020). Regulation of pyruvate dehydrogenase complex related to lactate switch in CHO cells. Engineering in Life Sciences, 21(3–4). https://doi.org/10.1002/elsc.202000037

Mulukutla, B. C., Yongky, A., Grimm, S., Daoutidis, P., & Hu, W. S. (2015). Multiplicity of Steady States in Glycolysis and Shift of Metabolic State in Cultured Mammalian Cells. PLoS ONE, 10(3). https://doi.org/10.1371/JOURNAL.PONE.0121561

Mussolino, C., Alzubi, J., Fine, E. J., Morbitzer, R., Cradick, T. J., Lahaye, T., Bao, G., & Cathomen, T. (2014). TALENs facilitate targeted genome editing in human cells with high specificity and low cytotoxicity. Nucleic Acids Research, 42(10), 6762. https://doi.org/10.1093/NAR/GKU305

Noh, S. M., Park, J. H., Lim, M. S., Kim, J. W., & Lee, G. M. (2017). Reduction of ammonia and lactate through the coupling of glutamine synthetase selection and downregulation of lactate dehydrogenase-A in CHO cells. Applied Microbiology and Biotechnology, 101(3), 1035–1045. https://doi.org/10.1007/S00253-016-7876-Y/FIGURES/6

Özcan, A., Krajeski, R., Ioannidi, E., Lee, B., Gardner, A., Makarova, K. S., Koonin, E. V., Abudayyeh, O. O., & Gootenberg, J. S. (2021). Programmable RNA targeting with the single-protein CRISPR effector Cas7-11. Nature 2021 597:7878, 597(7878), 720–725. https://doi.org/10.1038/s41586-021-03886-5

Pan, X., Streefland, M., Dalm, C., Wijffels, R. H., & Martens, D. E. (2017). Selection of chemically defined media for CHO cell fed-batch culture processes. Cytotechnology, 69(1), 39–56. https://doi.org/10.1007/S10616-016-0036-5/FIGURES/11

Patel, M. S., & Korotchkina, L. G. (2001). Regulation of mammalian pyruvate dehydrogenase complex by phosphorylation: complexity of multiple phosphorylation sites and kinases. In EXPERIMENTAL and MOLECULAR MEDICINE (Vol. 33, Issue 4). https://www.nature.com/articles/emm200132.pdf

Patel, M. S., Nemeria, N. S., Furey, W., & Jordan, F. (2014). The pyruvate dehydrogenase complexes: structure-based function and regulation. The Journal of Biological Chemistry, 289(24), 16615–16623. https://doi.org/10.1074/jbc.R114.563148

Perham, R. N. (2000). SWINGING ARMS AND SWINGING DOMAINS IN MULTIFUNCTIONAL ENZYMES: Catalytic Machines for Multistep Reactions. www.annualreviews.org

Posner, J., Barrington, P., Brier, T., & Datta-Mannan, A. (2019). Monoclonal antibodies: Past, present and future. Handbook of Experimental Pharmacology, 260, 81–141. https://doi.org/10.1007/164_2019_323/COVER

Rardin, M. J., Wiley, S. E., Naviaux, R. K., Murphy, A. N., & Dixon, J. E. (2009). Monitoring phosphorylation of the pyruvate dehydrogenase complex. Analytical Biochemistry, 389(2), 157–164. https://doi.org/10.1016/j.ab.2009.03.040

Rath, T., Baker, K., Dumont, J. A., Peters, R. T., Jiang, H., Qiao, S. W., Lencer, W. I., Pierce, G. F., & Blumberg, R. S. (2015). Fc-fusion proteins and FcRn: structural insights for longer-lasting and more effective therapeutics. Critical Reviews in Biotechnology, 35(2), 235–254. https://doi.org/10.3109/07388551.2013.834293

Read, A., & Schröder, M. (2021). The Unfolded Protein Response: An Overview. Biology, 10(5). https://doi.org/10.3390/BIOLOGY10050384

Reinhart, D., Damjanovic, L., Kaisermayer, C., Sommeregger, W., Gili, A., Gasselhuber, B., Castan, A., Mayrhofer, P., Grünwald-Gruber, C., & Kunert, R. (2019). Bioprocessing of Recombinant CHO-K1, CHO-DG44, and CHO-S: CHO Expression Hosts Favor Either mAb Production or Biomass Synthesis. Biotechnology Journal, 14(3). https://doi.org/10.1002/BIOT.201700686

Richelle, A., & Lewis, N. E. (2017). Improvements in protein production in mammalian cells from targeted metabolic engineering. Current Opinion in Systems Biology, 6, 1–6. https://doi.org/10.1016/J.COISB.2017.05.019

Rish, A. J., Drennen, J. K., & Anderson, C. A. (2022). Metabolic trends of Chinese hamster ovary cells in biopharmaceutical production under batch and fed-batch conditions. Biotechnology Progress, 38(1), e3220. https://doi.org/10.1002/BTPR.3220

Ritacco, F. V., Wu, Y., & Khetan, A. (2018). Cell culture media for recombinant protein expression in Chinese hamster ovary (CHO) cells: History, key components, and optimization strategies. Biotechnology Progress, 34(6), 1407–1426. https://doi.org/10.1002/BTPR.2706

Roche, T. E., & Hiromasa, Y. (2007). Pyruvate dehydrogenase kinase regulatory mechanisms and inhibition in treating diabetes, heart ischemia, and cancer. Cellular and Molecular Life Sciences, 64(7–8), 830–849. https://doi.org/10.1007/s00018-007-6380-z

Rogatzki, M. J., Ferguson, B. S., Goodwin, M. L., & Gladden, L. B. (2015). Lactate is always the end product of glycolysis. Frontiers in Neuroscience, 9(FEB). https://doi.org/10.3389/FNINS.2015.00022

Rudge, S. R., & Ladisch, M. R. (2020). Industrial Challenges of Recombinant Proteins. Advances in Biochemical Engineering/Biotechnology, 171, 1–22. https://doi.org/10.1007/10_2019_120/FIGURES/4

Saccardo, P., Corchero, J. L., & Ferrer-Miralles, N. (2016). Tools to cope with difficult-to-express proteins. Applied Microbiology and Biotechnology, 100(10), 4347–4355. https://doi.org/10.1007/s00253-016-7514-8

Sasso, J. M., Tenchov, R., Bird, R., Iyer, K. A., Ralhan, K., Rodriguez, Y., & Zhou, Q. A. (2023). The Evolving Landscape of Antibody-Drug Conjugates: In Depth Analysis of Recent Research Progress. Bioconjugate Chemistry, 34(11), 1951–2000. https://doi.org/10.1021/ACS.BIOCONJCHEM.3C00374

Savizi, I. S. P., Motamedian, E., E. Lewis, N., Jimenez del Val, I., & Shojaosadati, S. A. (2021). An integrated modular framework for modeling the effect of ammonium on the sialylation process of monoclonal antibodies produced by CHO cells. Biotechnology Journal, 16(8), 2100019. https://doi.org/10.1002/BIOT.202100019

Schmieder, V., Bydlinski, N., Strasser, R., Baumann, M., Kildegaard, H. F., Jadhav, V., & Borth, N. (2018). Enhanced Genome Editing Tools For Multi-Gene Deletion Knock-Out Approaches Using Paired CRISPR sgRNAs in CHO Cells. Biotechnology Journal, 13(3), 1700211. https://doi.org/10.1002/biot.201700211

Schmieder, V., Novak, N., Dhiman, H., Nguyen, L. N., Serafimova, E., Klanert, G., Baumann, M., Kildegaard, H. F., & Borth, N. (2021). A pooled CRISPR/AsCpf1 screen using paired gRNAs to induce genomic deletions in Chinese hamster ovary cells. Biotechnology Reports, 31, e00649. https://doi.org/10.1016/J.BTRE.2021.E00649

Sentmanat, M. F., Peters, S. T., Florian, C. P., Connelly, J. P., & Pruett-Miller, S. M. (2018). A Survey of Validation Strategies for CRISPR-Cas9 Editing. Scientific Reports 2018 8:1, 8(1), 1–8. https://doi.org/10.1038/s41598-018-19441-8

Shanmugaraj, B., Malla, A., & Phoolcharoen, W. (2020). Emergence of Novel Coronavirus 2019-nCoV: Need for Rapid Vaccine and Biologics Development. Pathogens 2020, Vol. 9, Page 148, 9(2), 148. https://doi.org/10.3390/PATHOGENS9020148

Sharma, R., Harrison, S. T. L., & Tai, S. L. (2022). Advances in Bioreactor Systems for the Production of Biologicals in Mammalian Cells. ChemBioEng Reviews, 9(1), 42–62. https://doi.org/10.1002/CBEN.202100022

Sheikholeslami, Z., Jolicoeur, M., & Henry, O. (2014). Elucidating the effects of postinduction glutamine feeding on the growth and productivity of CHO cells. Biotechnology Progress, 30(3), 535–546. https://doi.org/10.1002/BTPR.1907

Spiess, C., Zhai, Q., & Carter, P. J. (2015). Alternative molecular formats and therapeutic applications for bispecific antibodies. Molecular Immunology, 67(2), 95–106. https://doi.org/10.1016/J.MOLIMM.2015.01.003

Sutendra, G., Kinnaird, A., Dromparis, P., Paulin, R., Stenson, T. H., Haromy, A., Hashimoto, K., Zhang, N., Flaim, E., & Michelakis, E. D. (2014). A Nuclear Pyruvate Dehydrogenase Complex Is Important for the Generation of Acetyl-CoA and Histone Acetylation. https://doi.org/10.1016/j.cell.2014.04.046

Tan, J. G. L., Lee, Y. Y., Wang, T., Yap, M. G. S., Tan, T. W., & Ng, S. K. (2015). Heat shock protein 27 overexpression in CHO cells modulates apoptosis pathways and delays activation of caspases to improve recombinant monoclonal antibody titre in fed-batch bioreactors. Biotechnology Journal, 10(5), 790–800. https://doi.org/10.1002/BIOT.201400764

Tang, D., Lam, C., Bauer, N., Auslaender, S., Snedecor, B., Laird, M. W., & Misaghi, S. (2022). Bax and Bak knockout apoptosis-resistant Chinese hamster ovary cell lines significantly improve culture viability and titer in intensified fed-batch culture process. Biotechnology Progress, 38(2). https://doi.org/10.1002/BTPR.3228

Tang, D., Subramanian, J., Haley, B., Baker, J., Luo, L., Hsu, W., Liu, P., Sandoval, W., Laird, M. W., Snedecor, B., Shiratori, M., & Misaghi, S. (2019). Pyruvate Kinase Muscle-1 Expression Appears to Drive Lactogenic Behavior in CHO Cell Lines, Triggering Lower Viability and Productivity: A Case Study. Biotechnology Journal, 14(4). https://doi.org/10.1002/BIOT.201800332

Taylor, S. C., Nadeau, K., Abbasi, M., Lachance, C., Nguyen, M., & Fenrich, J. (2019). The Ultimate qPCR Experiment: Producing Publication Quality, Reproducible Data the First Time. https://doi.org/10.1016/j.tibtech.2018.12.002

Templeton, N., Dean, J., Reddy, P., & Young, J. D. (2013). Peak antibody production is associated with increased oxidative metabolism in an industrially relevant fed-batch CHO cell culture. Biotechnology and Bioengineering, 110(7), 2013–2024. https://doi.org/10.1002/BIT.24858

Tihanyi, B., & Nyitray, L. (2020). Recent advances in CHO cell line development for recombinant protein production. Drug Discovery Today: Technologies, 38, 25–34. https://doi.org/10.1016/J.DDTEC.2021.02.003

Tripathi, N. K., & Shrivastava, A. (2019). Recent Developments in Bioprocessing of Recombinant Proteins: Expression Hosts and Process Development. Frontiers in Bioengineering and Biotechnology, 7, 496566. https://doi.org/10.3389/FBIOE.2019.00420/BIBTEX

Van Meer, G., & De Kroon, A. I. P. M. (2011). Lipid map of the mammalian cell. Journal of Cell Science, 124(1), 5–8. https://doi.org/10.1242/JCS.071233

Vidarsson, G., Dekkers, G., & Rispens, T. (2014). IgG subclasses and allotypes: from structure to effector functions. Frontiers in Immunology, 5(OCT). https://doi.org/10.3389/FIMMU.2014.00520

Villiger, L., Joung, J., Koblan, L., Weissman, J., Abudayyeh, O. O., & Gootenberg, J. S. (2024a). CRISPR technologies for genome, epigenome and transcriptome editing. Nature Reviews Molecular Cell Biology 2024, 1–24. https://doi.org/10.1038/s41580-023-00697-6

Villiger, L., Joung, J., Koblan, L., Weissman, J., Abudayyeh, O. O., & Gootenberg, J. S. (2024b). CRISPR technologies for genome, epigenome and transcriptome editing. Nature Reviews Molecular Cell Biology 2024, 1–24. https://doi.org/10.1038/s41580-023-00697-6

Walsh, G., & Walsh, E. (2022). Biopharmaceutical benchmarks 2022. Nature Biotechnology 2022 40:12, 40(12), 1722–1760. https://doi.org/10.1038/s41587-022-01582-x

Wang, W., & Roberts, C. J. (2018). Protein aggregation – Mechanisms, detection, and control. International Journal of Pharmaceutics, 550(1–2), 251–268. https://doi.org/10.1016/J.IJPHARM.2018.08.043

Wang, Y., Yu, W., Li, S., Guo, D., He, J., & Wang, Y. (2022). Acetyl-CoA Carboxylases and Diseases. Frontiers in Oncology, 12. https://doi.org/10.3389/FONC.2022.836058

Wang, Z., Zhu, J., & Lu, H. (2020). Antibody glycosylation: impact on antibody drug characteristics and quality control. Applied Microbiology and Biotechnology 2020 104:5, 104(5), 1905–1914. https://doi.org/10.1007/S00253-020-10368-7

Warburg, O., Wind, F., & Negelein, E. (1927). THE METABOLISM OF TUMORS IN THE BODY. The Journal of General Physiology, 8(6), 519–530. https://doi.org/10.1085/JGP.8.6.519

Wei, M., Mi, C. L., Jing, C. Q., & Wang, T. Y. (2022). Progress of Transposon Vector System for Production of Recombinant Therapeutic Proteins in Mammalian Cells. Frontiers in Bioengineering and Biotechnology, 10. https://doi.org/10.3389/FBIOE.2022.879222

Williams, D. 0, Borer, J., Braunwald, E., Chesebro, J. H., Cohen, L. S., Dalen, J., Dodge, H. T., Francis, C. K., Knatterud, G., Ludbrook, P., Markis, J. E., Desvigne-Nickens, P., Passamani, E. R., Powers, E. R., Rao, A. K., Roberts, R., Ross, A., Ryan, T. J., Sobel, B. E., … Zaret, B. (1986). Intravenous recombinant tissue-type plasminogen activator in patients with acute myocardial infarction: A report from the NHLBI thrombolysis in myocardial infarction trial. Circulation, 73(2), 338–346. https://doi.org/10.1161/01.CIR.73.2.338

Xiao, S., Li, Q., Jiang, J., Huo, C., Chen, H., & Guo, M. (2023). Rapid Identification of Chinese Hamster Ovary Cell Apoptosis and Its Potential Role in Process Robustness Assessment. Bioengineering, 10(3). https://doi.org/10.3390/BIOENGINEERING10030357

Xiong, K., Marquart, K. F., la Cour Karottki, K. J., Li, S., Shamie, I., Lee, J. S., Gerling, S., Yeo, N. C., Chavez, A., Lee, G. M., Lewis, N. E., & Kildegaard, H. F. (2019). Reduced apoptosis in Chinese hamster ovary cells via optimized CRISPR interference. Biotechnology and Bioengineering, 116(7), 1813–1819. https://doi.org/10.1002/BIT.26969

Xu, S., Gavin, J., Jiang, R., & Chen, H. (2017). Bioreactor productivity and media cost comparison for different intensified cell culture processes. Biotechnology Progress, 33(4), 867–878. https://doi.org/10.1002/btpr.2415

Xu, T., Zhang, J., Wang, T., & Wang, X. (2022). Recombinant antibodies aggregation and overcoming strategies in CHO cells. Applied Microbiology and Biotechnology, 106(11), 3913–3922. https://doi.org/10.1007/S00253-022-11977-0/FIGURES/2

Yang, G., Wang, Q., Chen, L., Betenbaugh, M. J., & Zhang, H. (2021). Glycoproteomic Characterization of FUT8 Knock-Out CHO Cells Reveals Roles of FUT8 in the Glycosylation. Frontiers in Chemistry, 9. https://doi.org/10.3389/FCHEM.2021.755238

Yiew, N. K. H., & Finck, B. N. (2022). The mitochondrial pyruvate carrier at the crossroads of intermediary metabolism. American Journal of Physiology - Endocrinology and Metabolism, 323(1), E33. https://doi.org/10.1152/AJPENDO.00074.2022

Ying, M., Guo, C., & Hu, X. (2019). The quantitative relationship between isotopic and net contributions of lactate and glucose to the tricarboxylic acid (TCA) cycle. The Journal of Biological Chemistry, 294(24), 9615. https://doi.org/10.1074/JBC.RA119.007841

Yip, S. S. M., Zhou, M., Joly, J., Snedecor, B., Shen, A., & Crawford, Y. (2014). Complete Knockout of the Lactate Dehydrogenase A Gene is Lethal in Pyruvate Dehydrogenase Kinase 1, 2, 3 Down-Regulated CHO Cells. Molecular Biotechnology, 56(9), 833–838. https://doi.org/10.1007/s12033-014-9762-0

Yoo, H. C., Yu, Y. C., Sung, Y., & Han, J. M. (2020). Glutamine reliance in cell metabolism. Experimental & Molecular Medicine 2020 52:9, 52(9), 1496–1516. https://doi.org/10.1038/s12276-020-00504-8

Yu, X., Hiromasa, Y., Tsen, H., Stoops, J. K., Roche, T. E., & Zhou, Z. H. (2008). Structures of the Human Pyruvate Dehydrogenase Complex Cores: A Highly Conserved Catalytic Center with Flexible N-Terminal Domains. Structure (London, England : 1993), 16(1), 104. https://doi.org/10.1016/J.STR.2007.10.024

Yue, K., Chen, J., Li, Y., & Kai, L. (2023). Advancing synthetic biology through cell-free protein synthesis. Computational and Structural Biotechnology Journal, 21, 2899. https://doi.org/10.1016/J.CSBJ.2023.05.003

Zamaraev, A. V., Kopeina, G. S., Prokhorova, E. A., Zhivotovsky, B., & Lavrik, I. N. (2017). Post-translational Modification of Caspases: The Other Side of Apoptosis Regulation. Trends in Cell Biology, 27(5), 322–339. https://doi.org/10.1016/J.TCB.2017.01.003

Zangari, J., Petrelli, F., Maillot, B., & Martinou, J. C. (2020). The Multifaceted Pyruvate Metabolism: Role of the Mitochondrial Pyruvate Carrier. Biomolecules, 10(7), 1–18. https://doi.org/10.3390/BIOM10071068

Zhang, H. X., Zhang, Y., & Yin, H. (2019). Genome Editing with mRNA Encoding ZFN, TALEN, and Cas9. Molecular Therapy, 27(4), 735–746. https://doi.org/10.1016/J.YMTHE.2019.01.014

Zhang, Q., Mi, C., & Wang, T. (2023). Effects and mechanism of small molecule additives on recombinant protein in CHO cells. Applied Microbiology and Biotechnology, 107(9), 2771–2781. https://doi.org/10.1007/S00253-023-12486-4/FIGURES/1

Zhang, S., Hulver, M. W., McMillan, R. P., Cline, M. A., & Gilbert, E. R. (2014). The pivotal role of pyruvate dehydrogenase kinases in metabolic flexibility. Nutrition & Metabolism, 11(1), 10. https://doi.org/10.1186/1743-7075-11-10

Zhang, X., Han, L., Zong, H., Ding, K., Yuan, Y., Bai, J., Zhou, Y., Zhang, B., & Zhu, J. (2018). Enhanced production of anti-PD1 antibody in CHO cells through transient co-transfection with anti-apoptotic genes Bcl-xL and Mcl-1. Bioprocess and Biosystems Engineering, 41(5), 633–640. https://doi.org/10.1007/S00449-018-1898-Z/FIGURES/5

Zhang, X., Jiang, R., Lin, H., & Xu, S. (2020). Feeding tricarboxylic acid cycle intermediates improves lactate consumption and antibody production in Chinese hamster ovary cell cultures. Biotechnology Progress, 36(4), e2975. https://doi.org/10.1002/BTPR.2975

Zhang, Y., Baycin-Hizal, D., Kumar, A., Priola, J., Bahri, M., Heffner, K. M., Wang, M., Han, X., Bowen, M. A., & Betenbaugh, M. J. (2017). High-Throughput Lipidomic and Transcriptomic Analysis to Compare SP2/0, CHO, and HEK-293 Mammalian Cell Lines. Analytical Chemistry, 89(3), 1477–1485. https://doi.org/10.1021/ACS.ANALCHEM.6B02984/ASSET/IMAGES/LARGE/AC-2016-029849_0006.JPEG

Zhong, X., D'antona, A. M., Karagiannis, S., & White, A. (2021). Recent Advances in the Molecular Design and Applications of Multispecific Biotherapeutics. https://doi.org/10.3390/antib10020013

Zhou, M., Crawford, Y., Ng, D., Tung, J., Pynn, A. F. J., Meier, A., Yuk, I. H., Vijayasankaran, N., Leach, K., Joly, J., Snedecor, B., & Shen, A. (2011). Decreasing lactate level and increasing antibody

production in Chinese Hamster Ovary cells (CHO) by reducing the expression of lactate dehydrogenase and pyruvate dehydrogenase kinases. Journal of Biotechnology, 153(1–2), 27–34. https://doi.org/10.1016/J.JBIOTEC.2011.03.003

Zhou, Q., & Qiu, H. (2019). The Mechanistic Impact of N-Glycosylation on Stability, Pharmacokinetics, and Immunogenicity of Therapeutic Proteins. Journal of Pharmaceutical Sciences, 108(4), 1366–1377. https://doi.org/10.1016/J.XPHS.2018.11.029

Zhou, Y., Raju, R., Alves, C., & Gilbert, A. (2018). Debottlenecking protein secretion and reducing protein aggregation in the cellular host. Current Opinion in Biotechnology, 53, 151–157. https://doi.org/10.1016/J.COPBIO.2018.01.007

Zhu, J. (2011a). Mammalian cell protein expression for biopharmaceutical production. https://doi.org/10.1016/j.biotechadv.2011.08.022

Zhu, J. (2011b). Mammalian cell protein expression for biopharmaceutical production. https://doi.org/10.1016/j.biotechadv.2011.08.022

Zhu, J. (2011c). Mammalian cell protein expression for biopharmaceutical production. https://doi.org/10.1016/j.biotechadv.2011.08.022

Zhu, M. M., Mollet, M., Hubert, R. S., Kyung, Y. S., & Zhang, G. G. (2017). Industrial Production of Therapeutic Proteins: Cell Lines, Cell Culture, and Purification. https://doi.org/10.1007/978-3-319-52287-6_29

Appendix

Appendix Table 1 Plasmid maps used throughout this thesis.

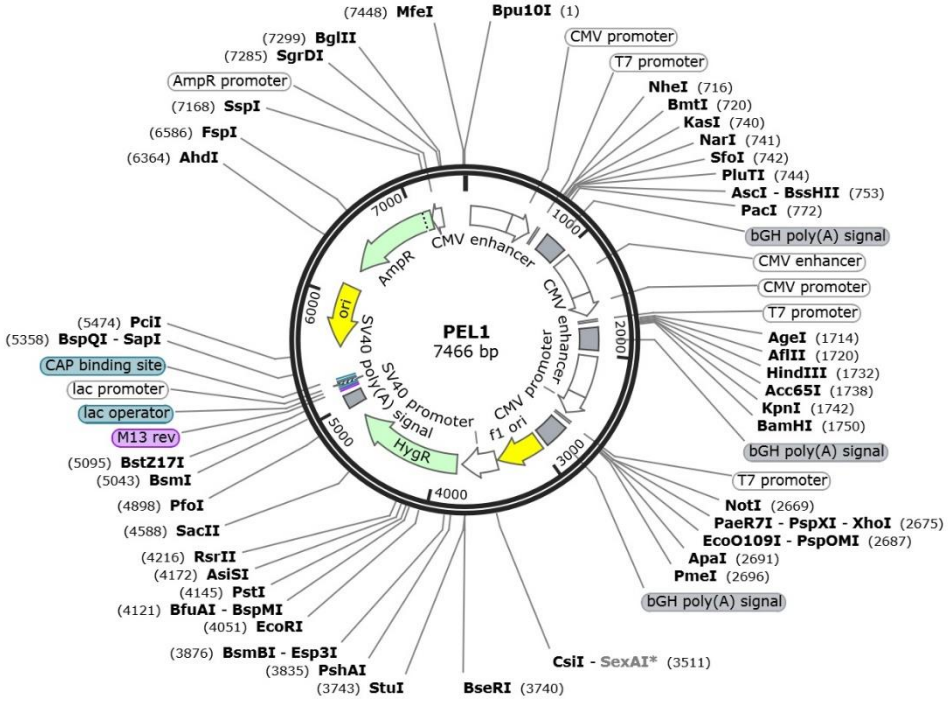

PEL1
3 Empty Cassettes, Hygromycin selection

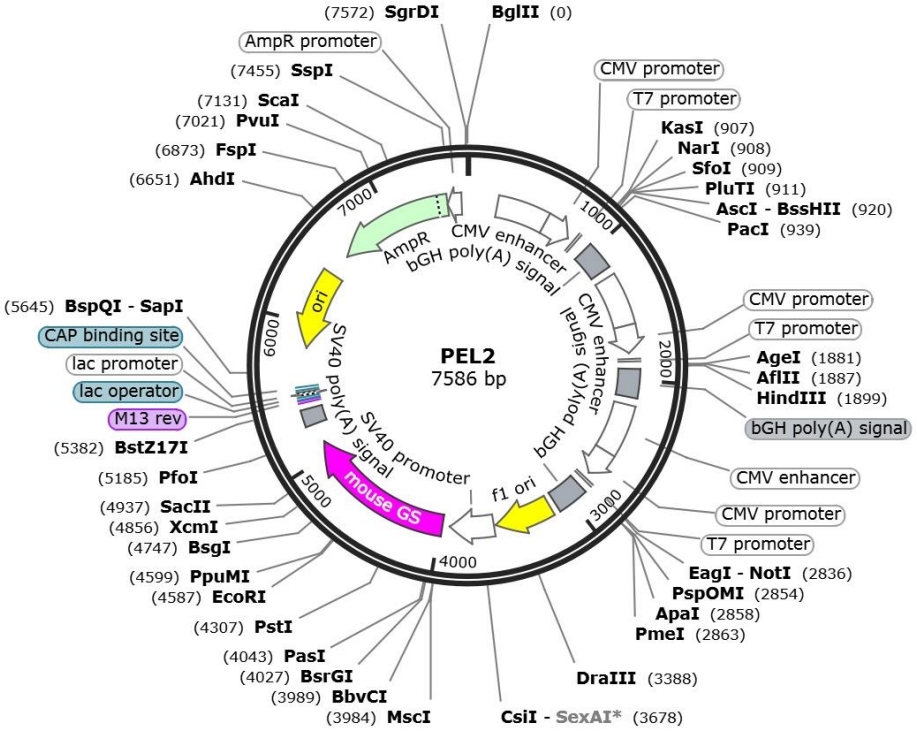

PEL2
3 Empty Cassettes, GS selection

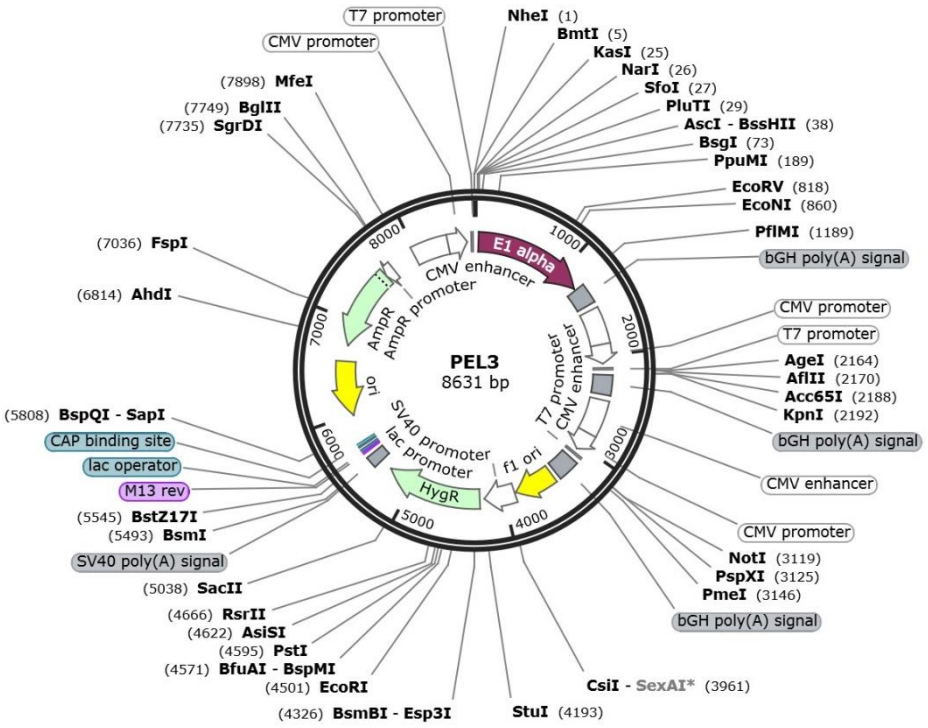

PEL3

3 Cassettes: E1alpha, Empty Cassette, Empty Cassette

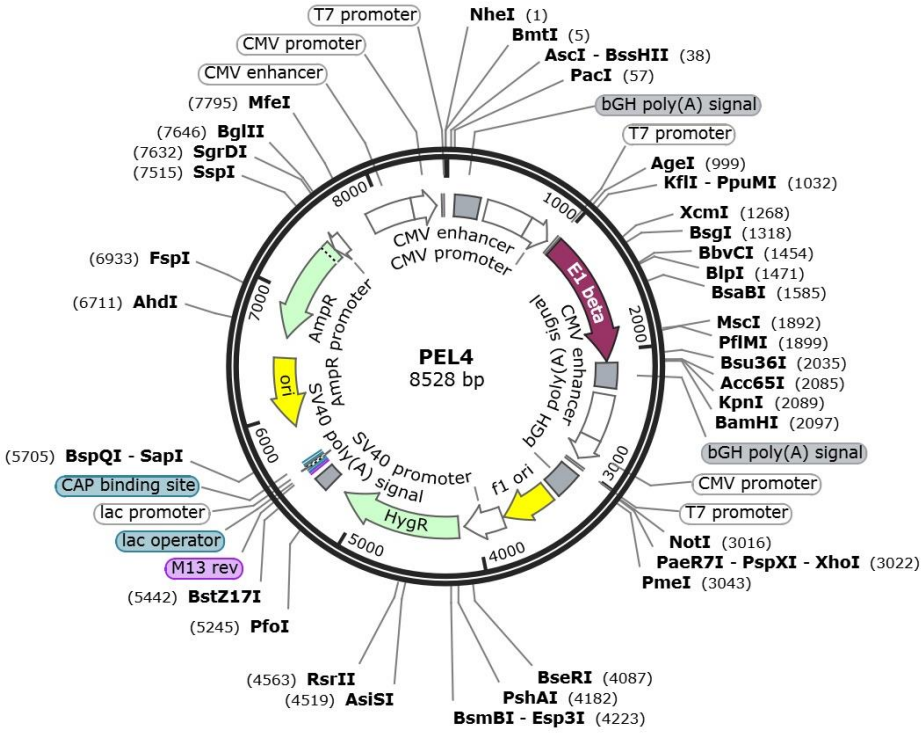

PEL4

3 Cassettes: Empty Cassette, E1beta, Empty Cassette

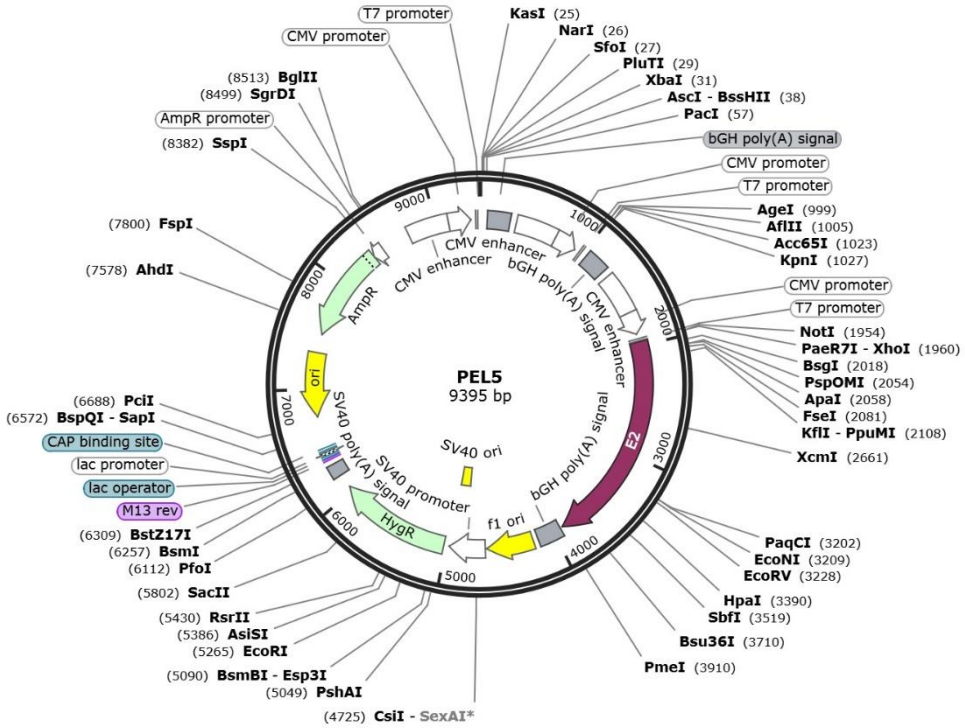

PEL5

3 Cassettes: Empty Cassette, Empty Cassette, E2

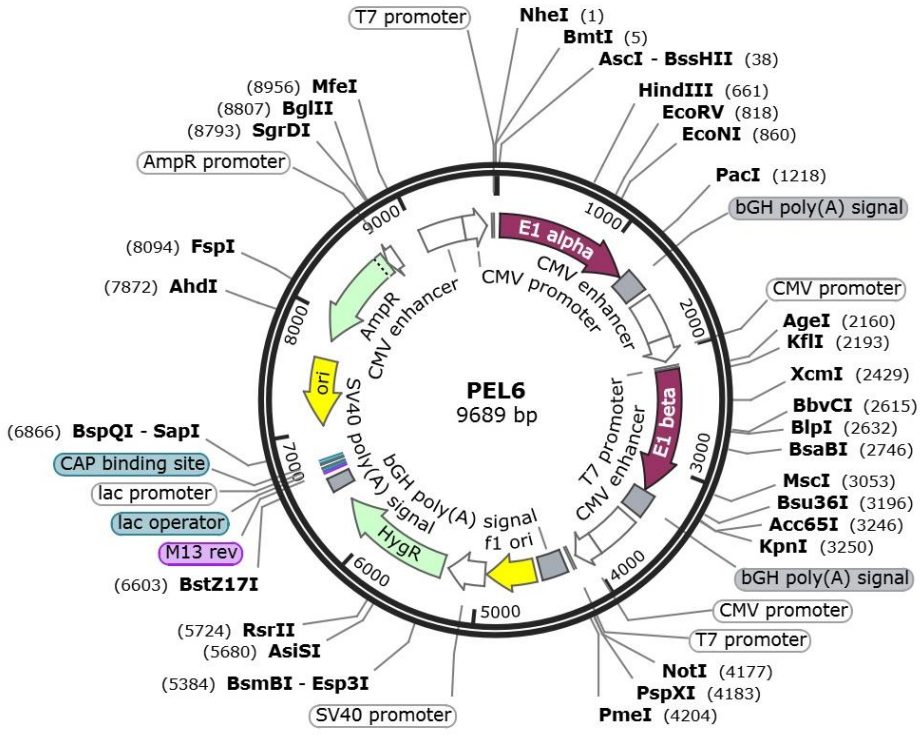

PEL6

3 Cassettes: E1alpha, E1beta, Empty Cassette

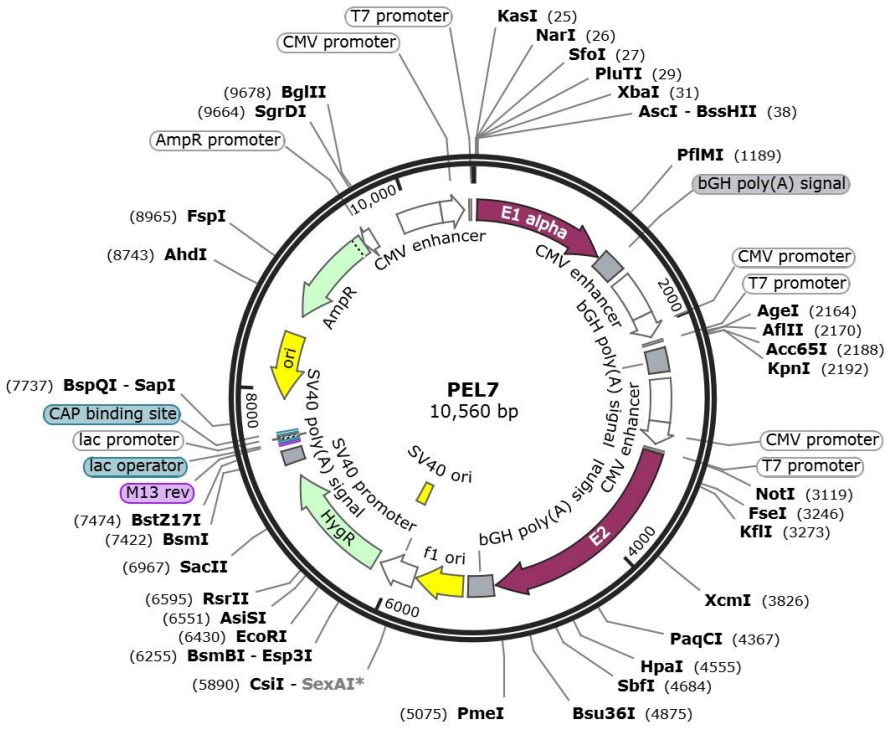

PEL7

3 Cassettes: E1alpha, Empty Cassette, E2

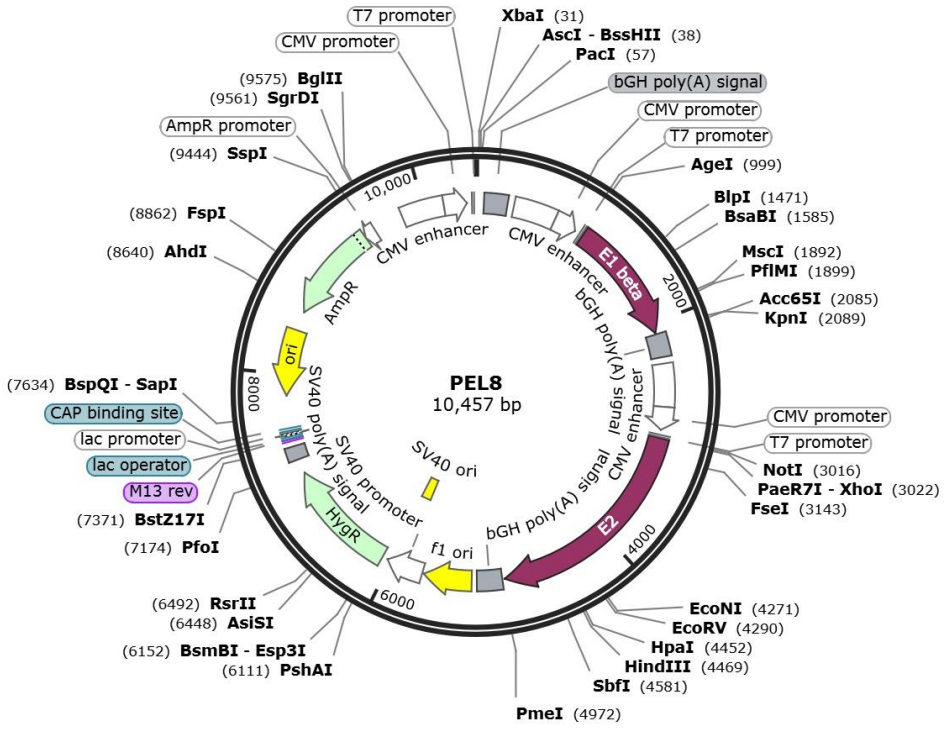

PEL8

3 Cassettes: Empty Cassette, E1beta, E2

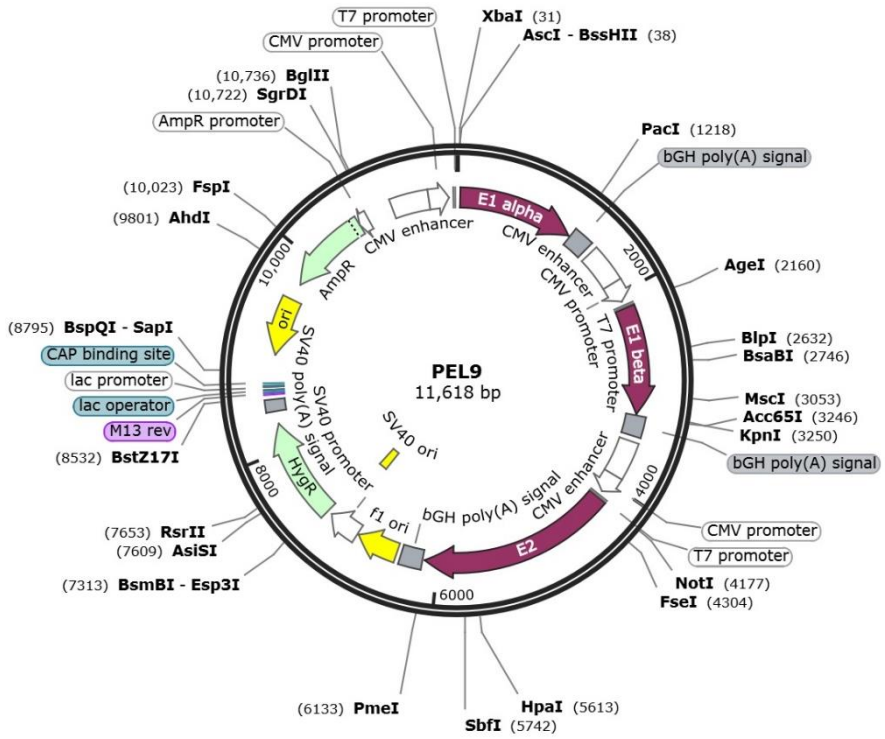

PEL9
3 Cassettes: E1alpha, E1beta, E2

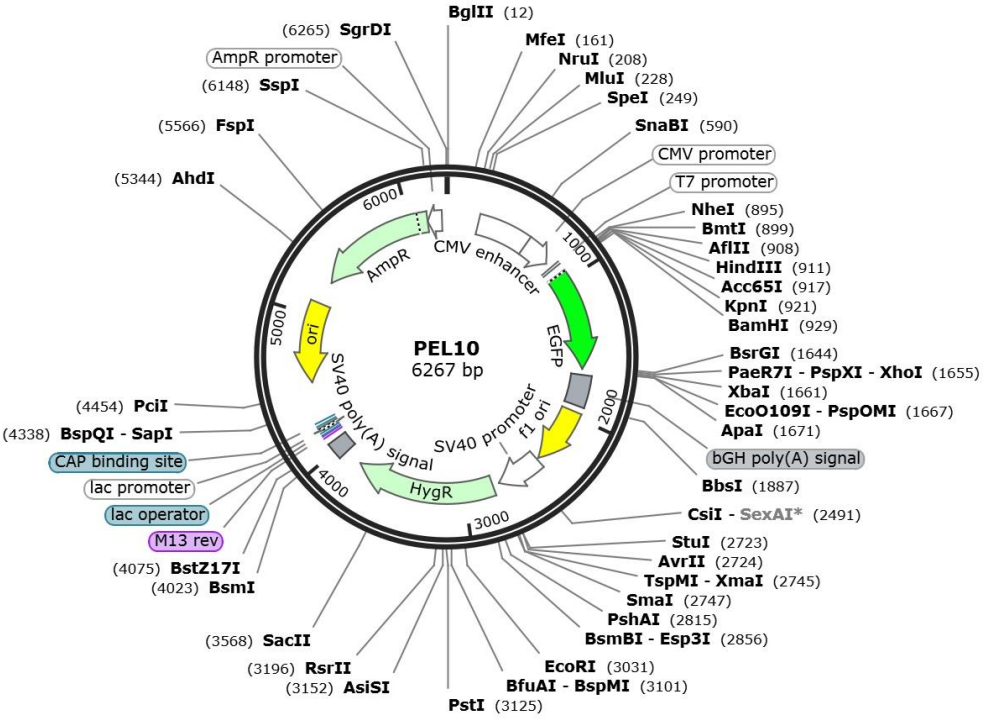

PEL10
1 Cassette: eGFP

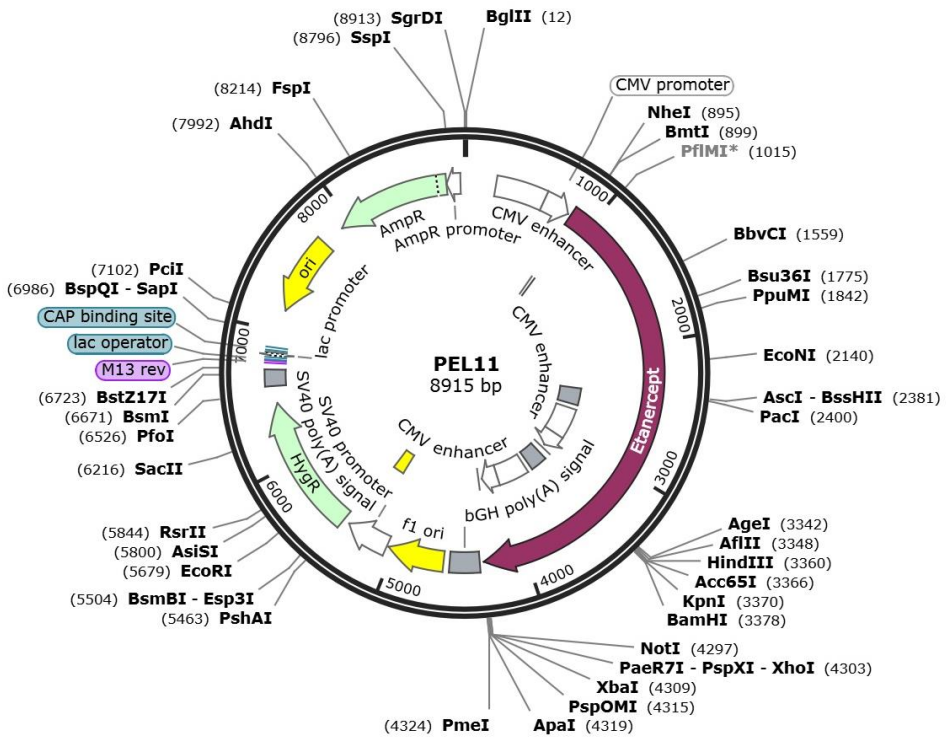

PEL11
1 Cassette: Etanercept

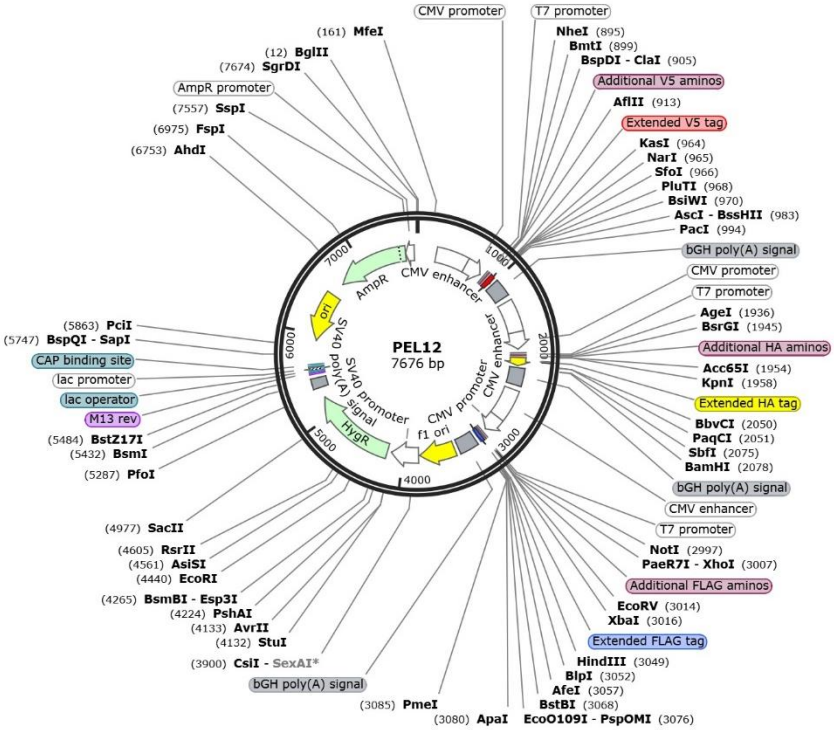

PEL12
3 Empty Tag Cassettes

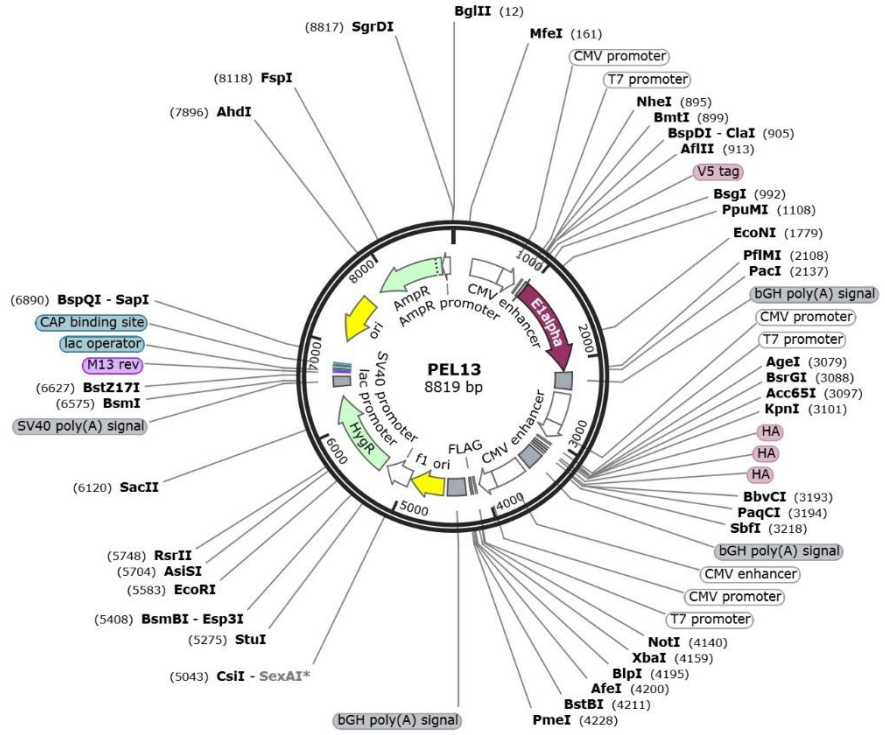

PEL13

3 Tag Cassettes: E1alpha N-terminal V5 Tag, Empty Cassette, Empty Cassette

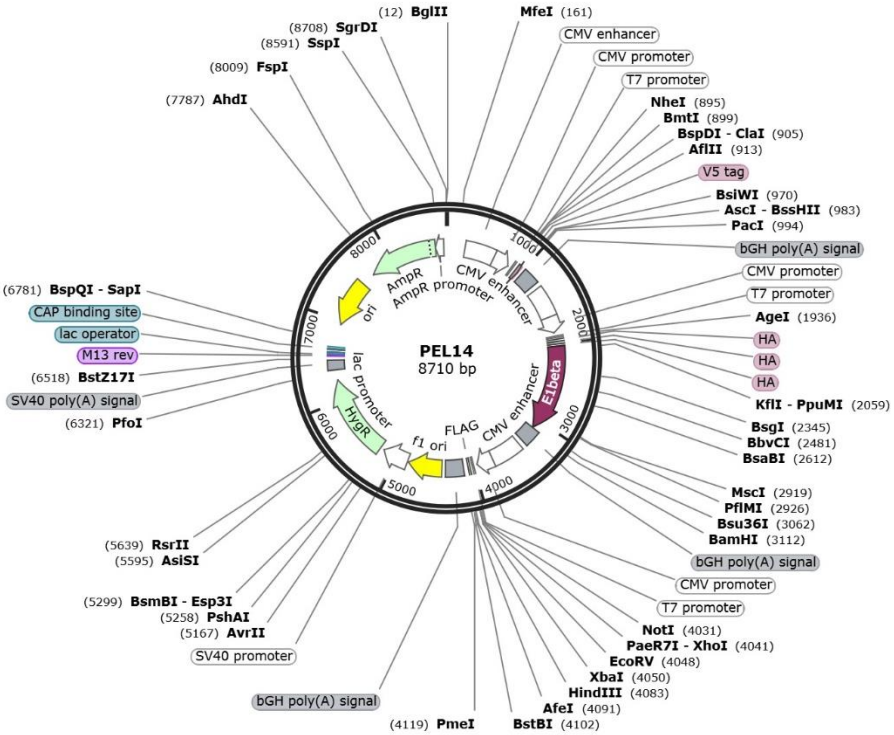

PEL14

3 Tag Cassettes: Empty Cassette, E1beta N-terminal HA Tag, Empty Cassette

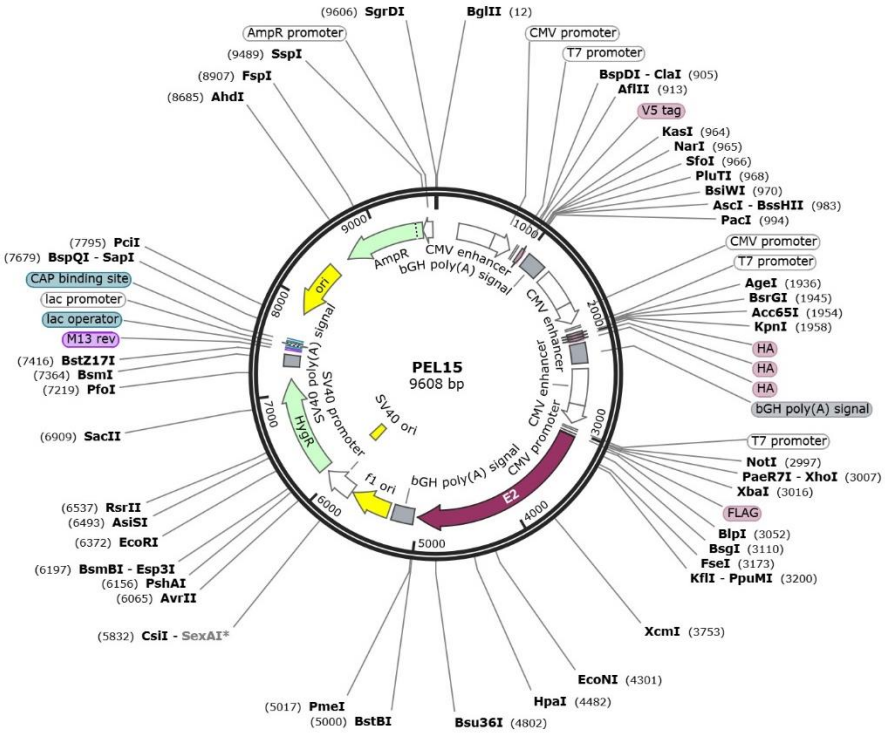

PEL15

3 Tag Cassettes: Empty Cassette, Empty Cassette, E2 N-terminal FLAG Tag

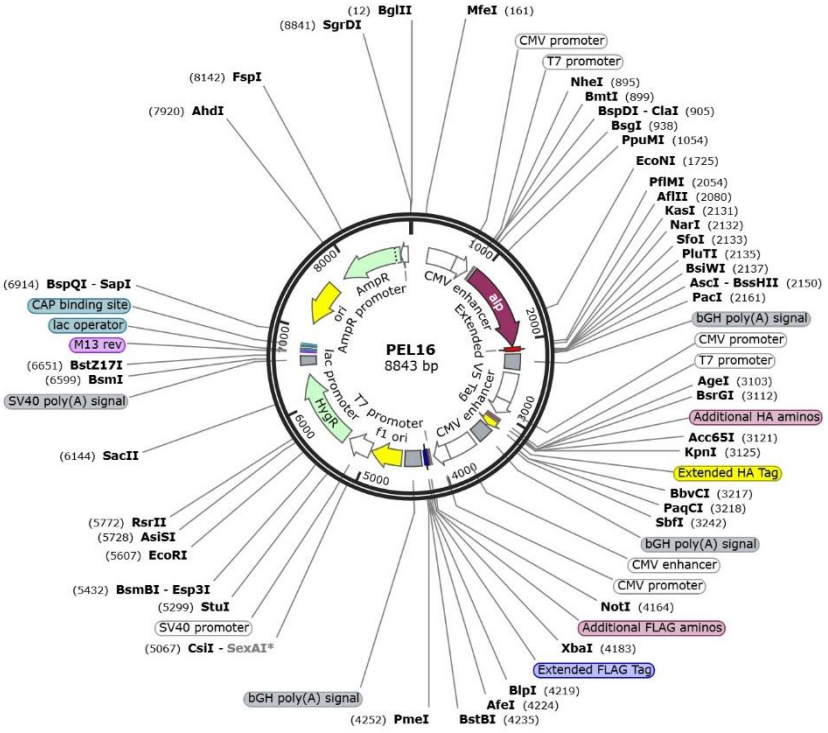

PEL16

3 Tag Cassettes: E1alpha C-terminal V5 Tag, Empty Cassette, Empty Cassette

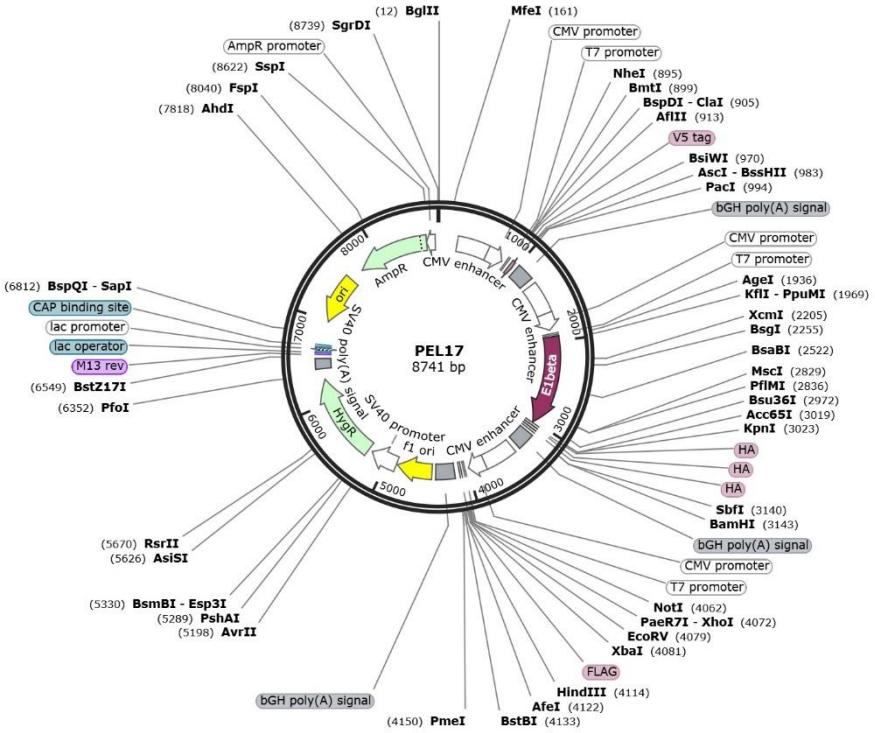

PEL17

3 Tag Cassettes: Empty Cassette, E1beta C-terminal HA Tag, Empty Cassette

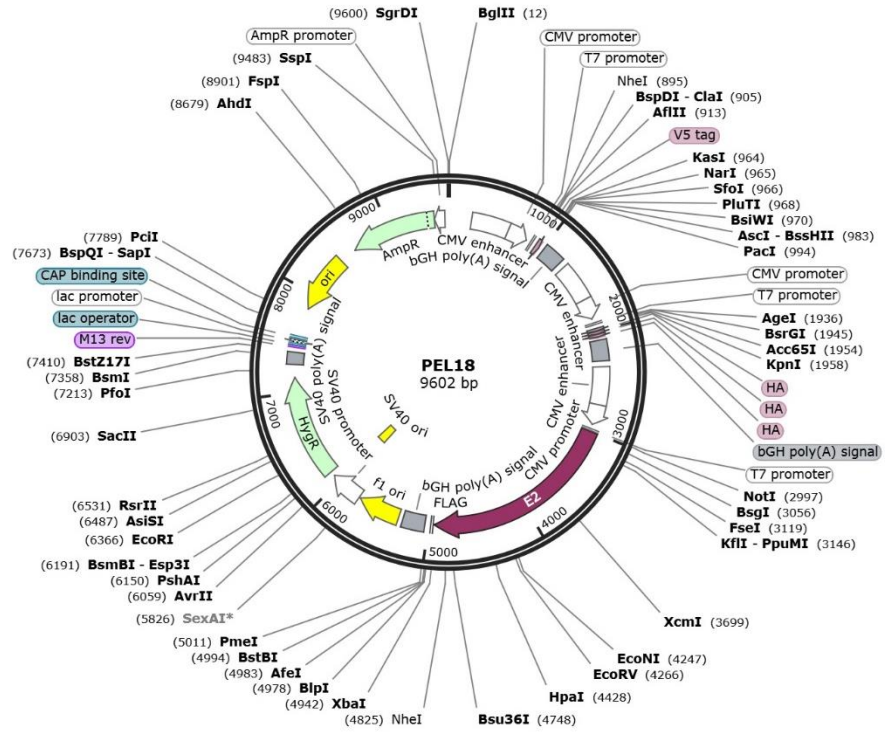

PEL18

3 Tag Cassettes: Empty Cassette, Empty Cassette, E2 C-terminal FLAG Tag

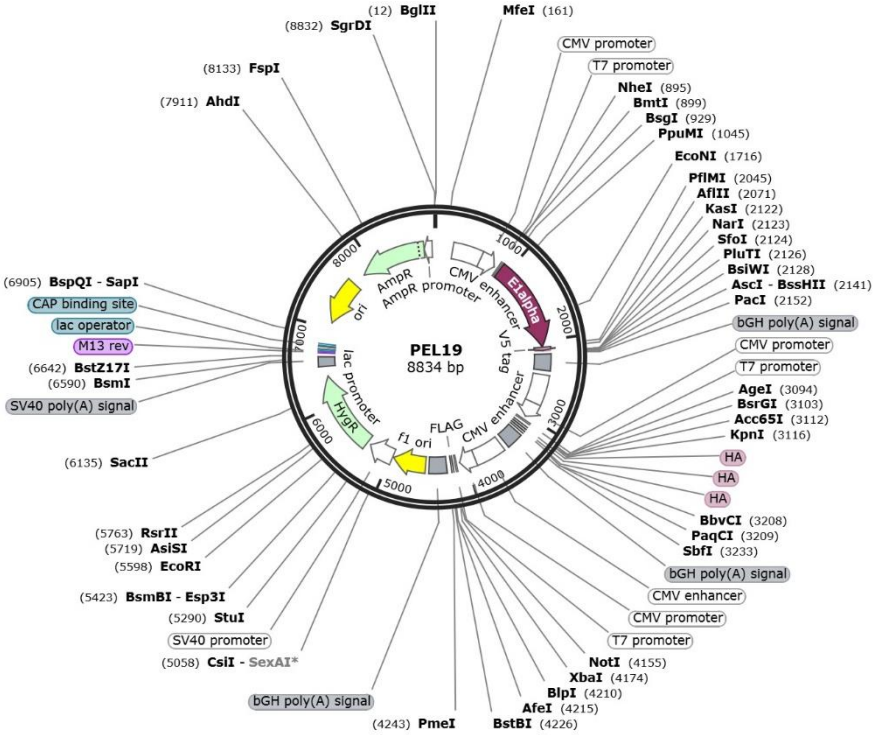

PEL19

3 Tag Cassettes: E1alpha serine/alanine mutant C-terminal V5 Tag, Empty Cassette, Empty Cassette

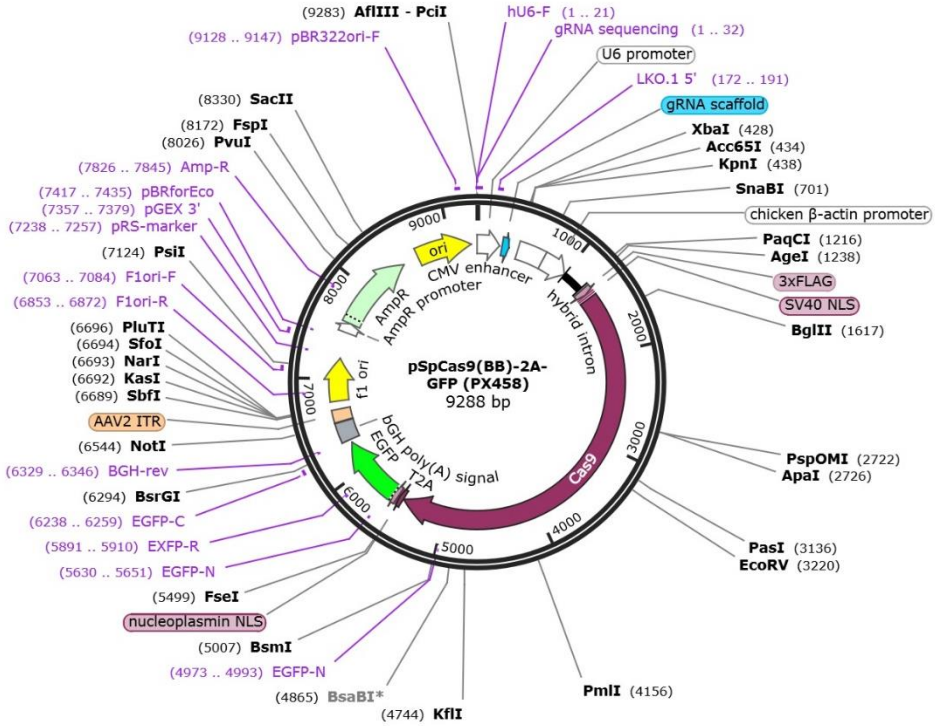

pX458 vector (pSpCas9(BB)-2A-GFP, #48138, Addgene

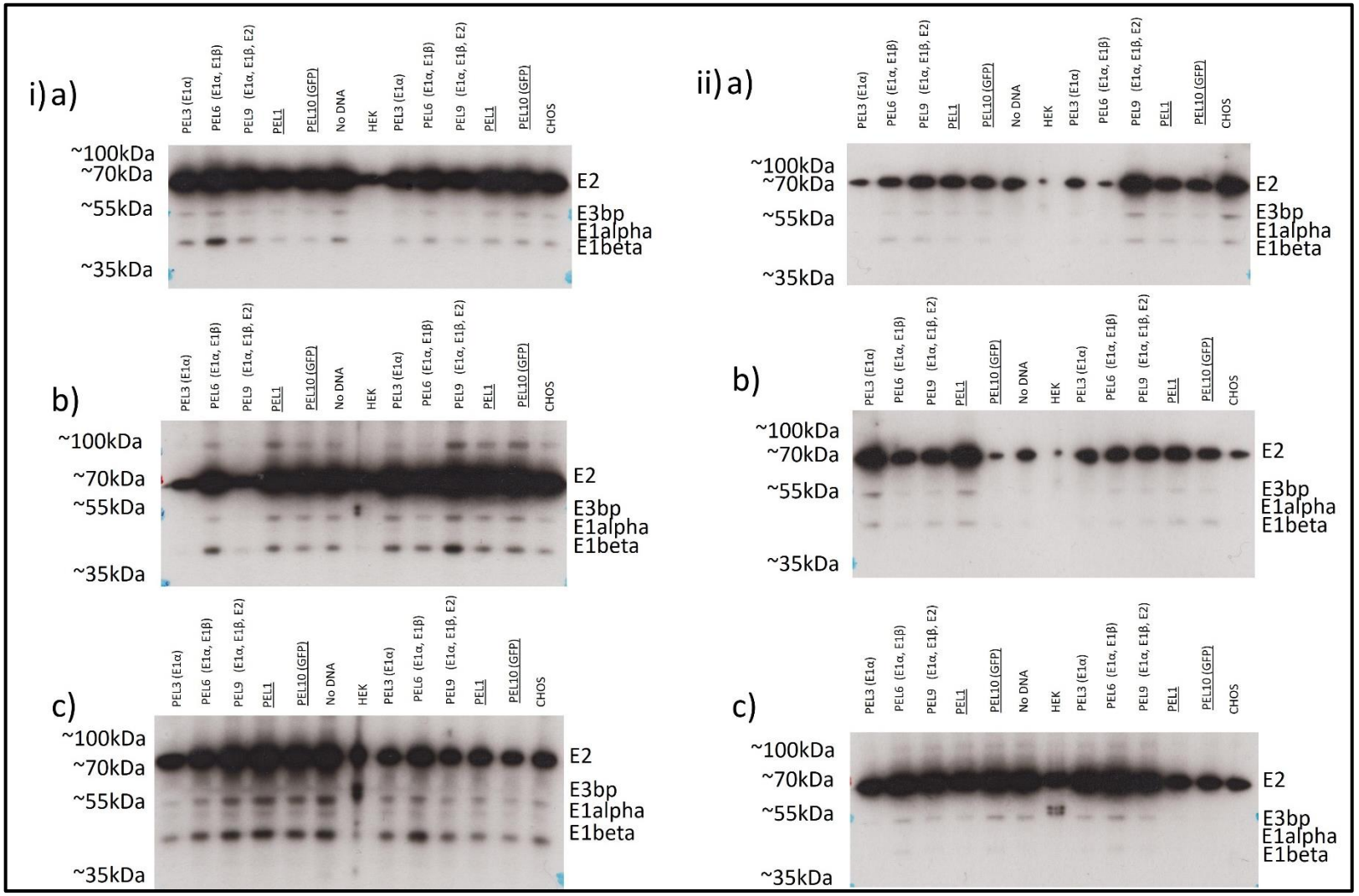

Appendix Figure 7.1.1 Western blot analysis of PDH subunit expression in CHOS cells harvested 72 hours after transfection with plasmids for the expression of individual, or a combination of, subunits via Merck NovaCHOice lipofectamine. 20 µg total protein cell lysate sample loaded and blot exposed for 5 mins. A HEK293 cell control for the PDH antibody cocktail- Abcam (ab110416) was also run. The cocktail is made of 5 monoclonal antibodies, listed in Antibody 2.4.1, section 2.4.5, multiple bands are observed corresponding to the different subunits of the PDH enzyme complex. E2 at 69 kDa, E3bp at 54 kDa, E1alpha at 43.3 kDa and E1beta at 39.4 kDa. A band for the control Complex V antibody, 22 kDa, is not seen in any samples, including the HEK293 cell lysate. i) Seeding density of $0.5x10^6$ viable cells per well, ii) Seeding density of $1x10^6$ viable cells per well. a) 1 µg DNA per transfection, b) 2 µg DNA per transfection, c) 4 µg per transfection.

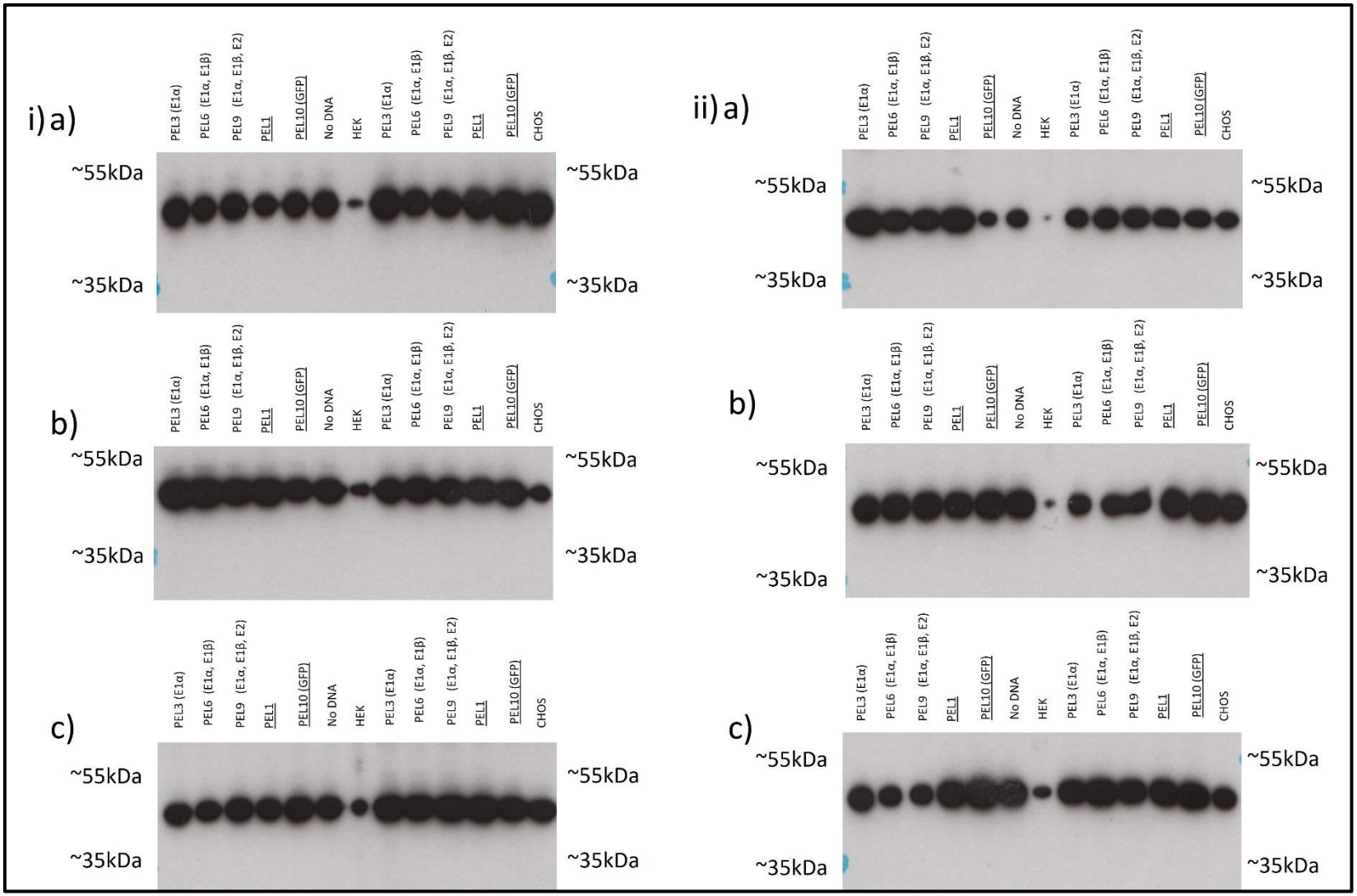

Appendix Figure 7.1.2 Western blot analysis of β-actin expression in CHOS cells harvested 72 hours after transfection with plasmids for the expression of individual, or a combination of, subunits via Merck NovaCHOice lipofectamine. 20 µg total protein cell lysate sample loaded and exposed for 30 secs, showing β-actin at 37 kDa and run alongside a HEK293 cell control. i) Seeding density of $0.5x10^6$ viable cells per well, ii) Seeding density of $1x10^6$ viable cells per well. a) 1 µg DNA per transfection, b) 2 µg DNA per transfection, c) 4 µg per transfection.

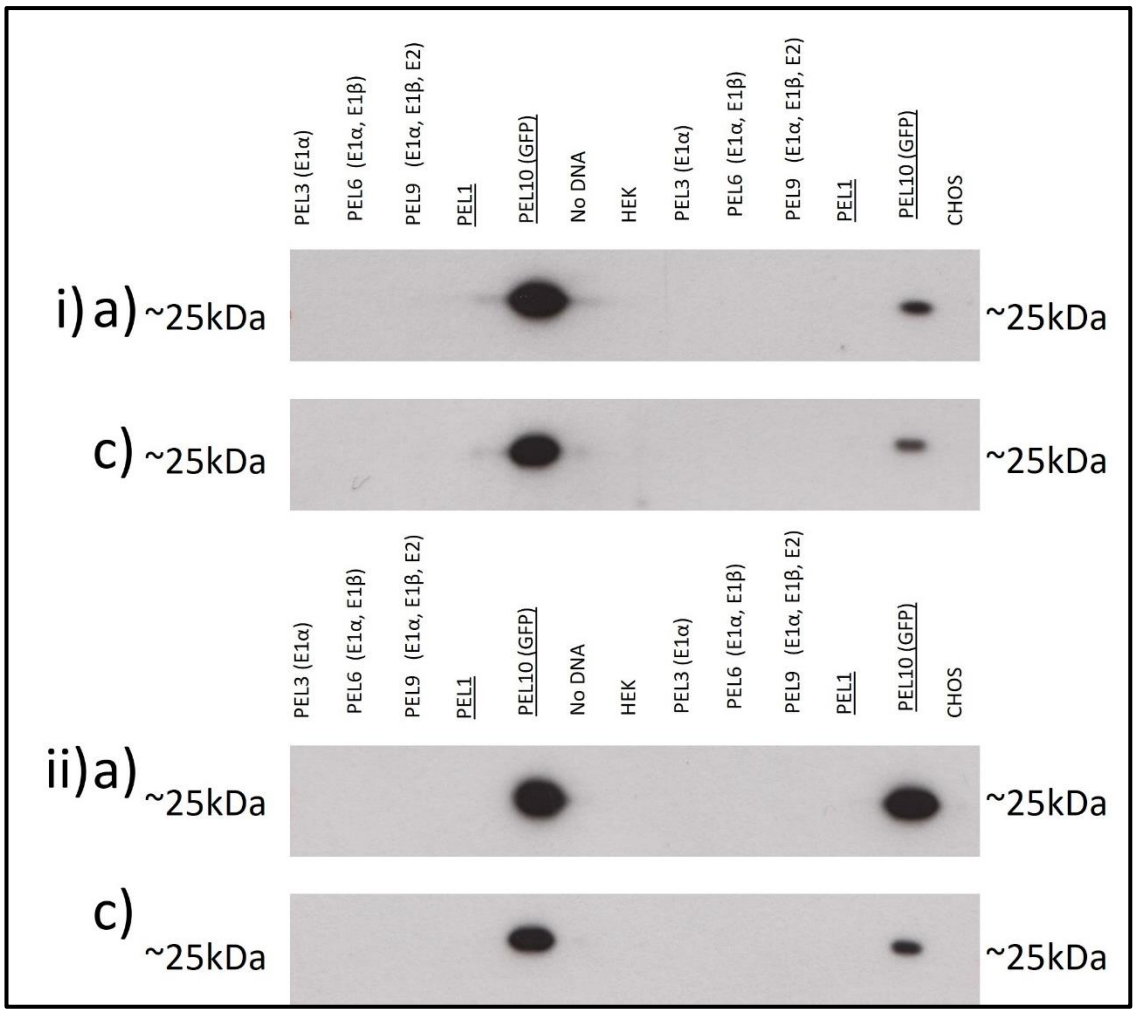

Appendix Figure 7.1.3 Western blot analysis of eGFP expression in CHOS cells harvested 72 hours after transfection with plasmids for the expression of individual, or a combination of, subunits via Merck NovaCHOice lipofectamine. 20 µg total protein cell lysate sample loaded and exposed for 1 min, showing eGFP at 27 kDa and run alongside a HEK293 cell control. i) Seeding density of $0.5x10^6$ viable cells per well, ii) Seeding density of $1x10^6$ viable cells per well. a) 1 µg DNA per transfection, b) 2 µg DNA per transfection, c) 4 µg per transfection. Western blots i)b) and ii)b) seen in Figure 3.6.1 and 3.6.2 were cut too close to the marker and therefore the expected eGFP band in PEL10 (GFP) was not able to be probed for.

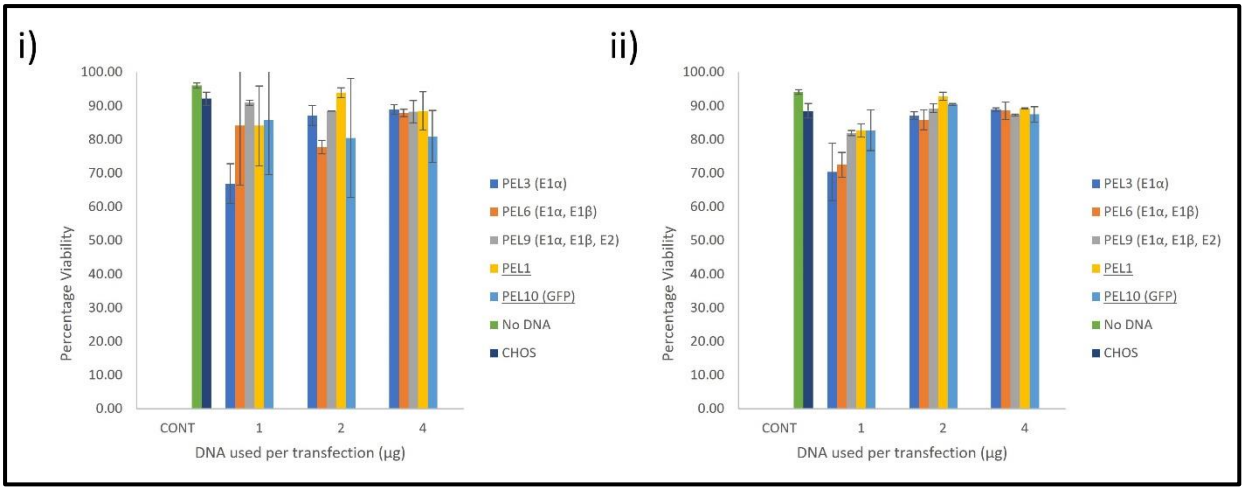

Appendix Figure 7.1.4 Culture viability (%) of CHOS cells transfected with the different PDH constructs or a control 72 hours post-transfection. i) Seeding density of $0.5x10^6$ viable cells per well, ii) Seeding density of $1x10^6$ viable cells per well. Error bars generated from the standard deviation from each experimental repeat (n=2.)

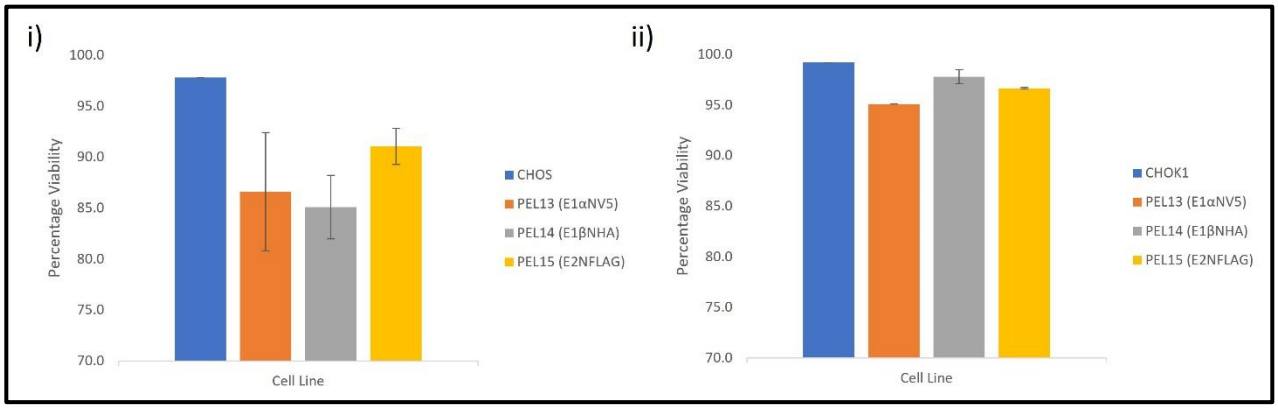

Appendix Figure 7.1.5 Culture viability of i) CHOS, and ii) CHOK1 cells three days after transient transfection with the N-terminally tagged PDH subunit containing PEL13 (E1αNV5), 14 (E1βNHA) and 15 (E2NFLAG). Alongside a 10 ml falcon of each CHOS and CHOK1 non-transfected host cells was cultured at $0.2x10^6$ viable cells per ml to act as a control. Error bars generated from the standard deviation from each experimental repeat (n=2.)

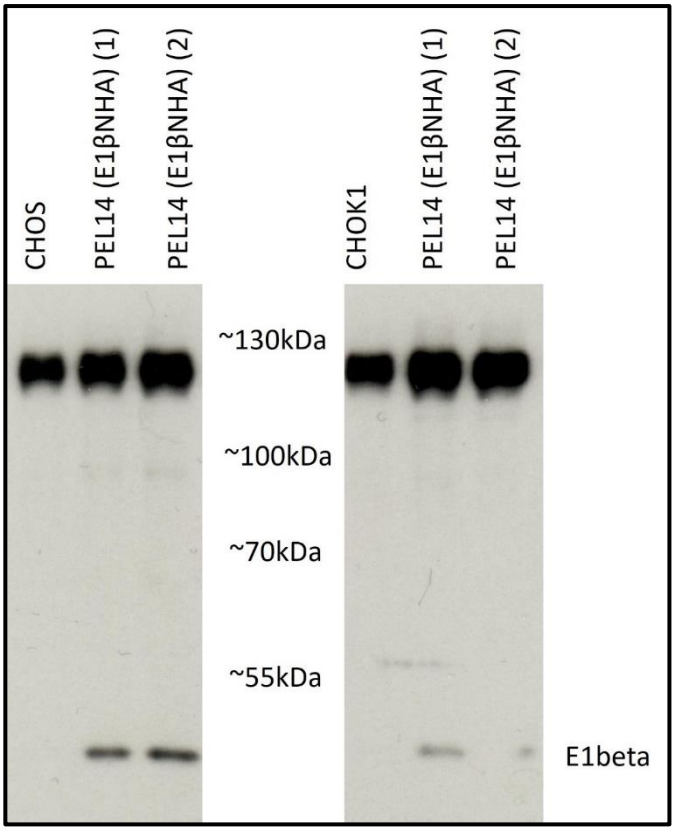

Appendix Figure 7.1.6 Western blot protein analysis of CHOS and CHOK1 cells for transient expression of an N-terminally HA tagged E1beta subunit PEL14 when probed with an anti-HA antibody. 5 µg protein loaded and blot exposed for 5 mins. The tagged E1beta subunit can be seen around 39.4 kDa, the expected size.

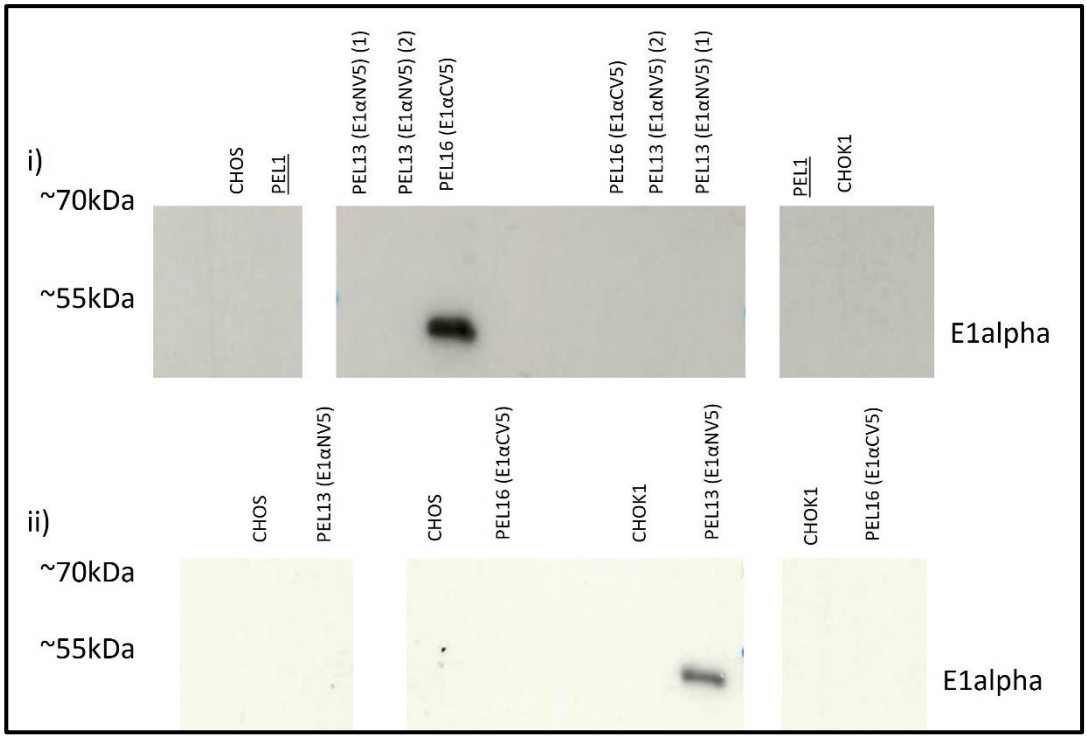

Appendix Figure 7.1.7 Evaluation of CHOS (left) and CHOK1 (right) cell pools engineered to stably express E1alpha N V5- and C-terminally tagged proteins (N – PEL13, C - PEL16) respectively. The expected band for cells expressing the PDH tagged E1alpha proteins should be observed at an apparent molecular weight of 43.3 kDa plus 1 kDa from addition of the V5 Tag (44.3 kDa). i) 10 µg protein loaded and probed with anti-V5 antibody and exposed for 2 mins. ii) 10% SDS PAGE gel with 20 µg protein sample and probed with V5 antibody and exposed for 90 secs.

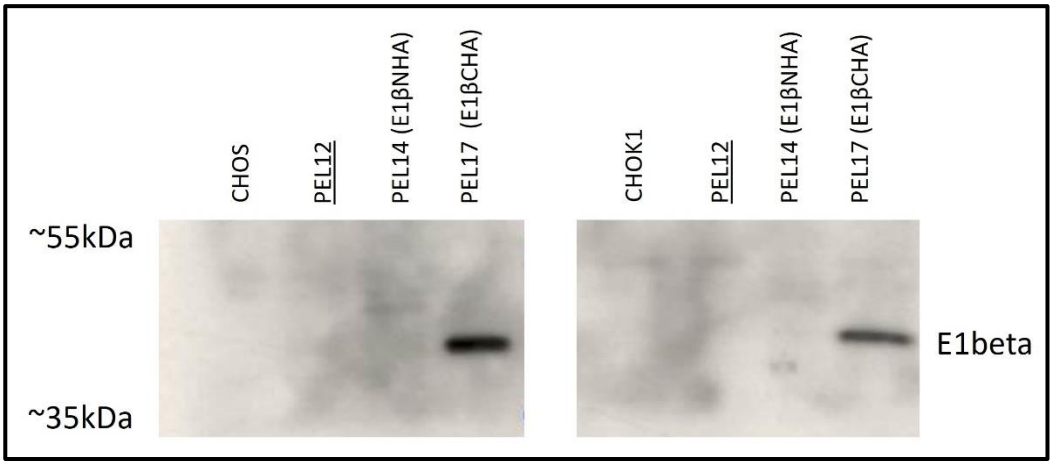

Appendix Figure 7.1.8 Evaluation of CHOS (left) and CHOK1 (right) cell pools engineered to stably express E1beta N HA- and C- terminally tagged proteins (N- PEL14 and C- PEL17) respectively. The expected band for cells expressing the PDH E1beta tagged proteins should be observed at an apparent molecular weight of 39.4 kDa plus 3 kDa from the addition of the HA Tag (42.4 kDa.) 10% SDS PAGE run with 5 µg protein sample and probed with anti-HA antibody and exposed for 5 mins.

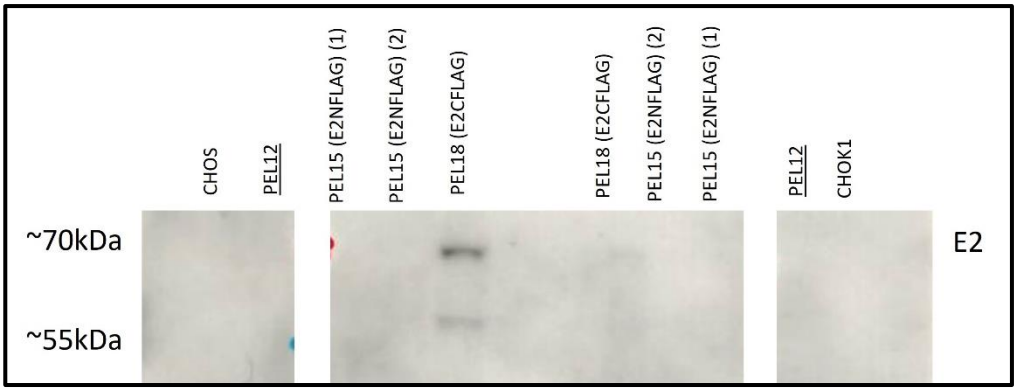

Appendix Figure 7.1.9 Evaluation of CHOS (left) and CHOK1 (right) cell pools engineered to stably express E2 N FLAG- and C -terminally tagged proteins (N-PEL15 and C-PEL18) respectively. The expected band for cells expressing the tagged PDH E2 protein should be observed at an apparent molecular weight of 69 kDa plus 1 kDa from the addition of the FLAG Tag (70 kDa.) 10% SDS PAGE run with 10 µg protein and probed with anti-FLAG antibody and exposed for 30 mins.

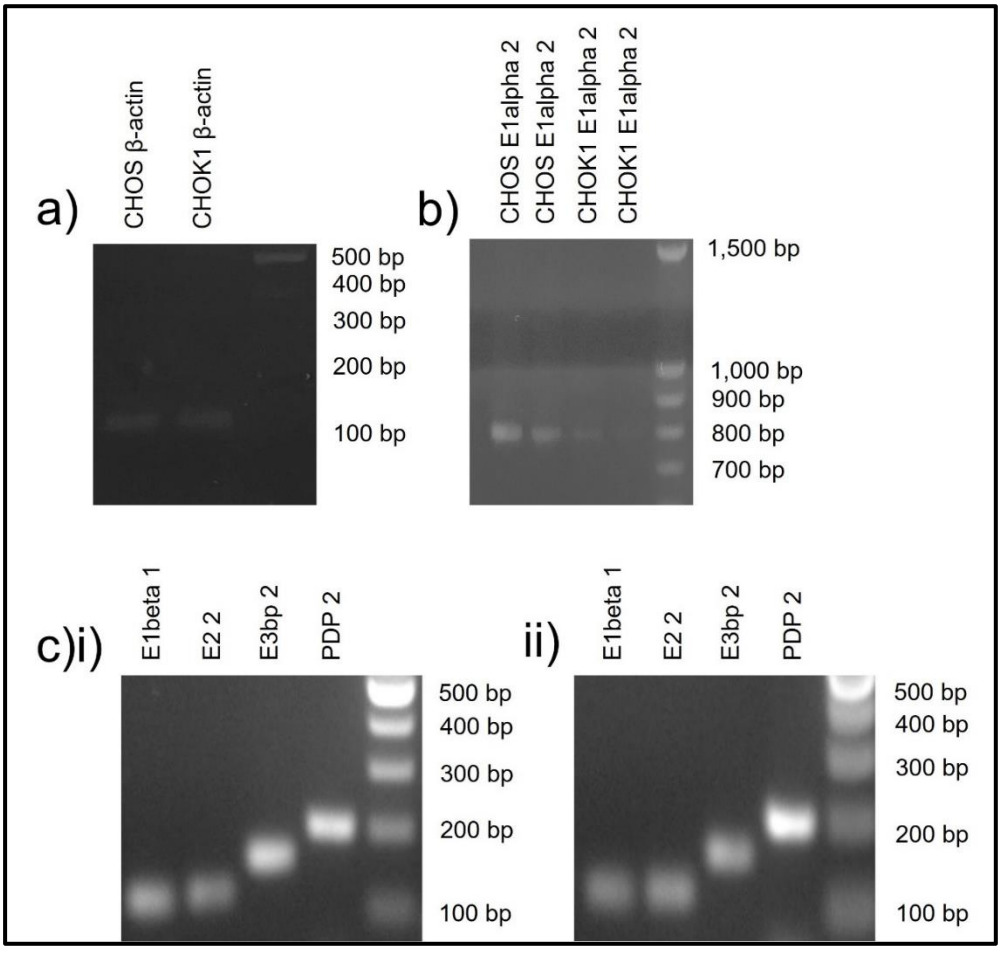

Appendix Figure 7.1.10 qPCR products when testing primers for PDH subunit genes with CHOS and CHOK1 gDNA. a) β-actin primer set tested with CHOS and CHOK1 gDNA with expected band size of 163 bp. b) E1alpha 1 primer set tested with CHOS and CHOK1 gDNA with expected band size at 788 bp. c) E1beta 1 primer set with expected band size at 109 bp. E2 2 primer set with expected band size of 113 bp. E3bp 2 primer set with expected band size at 157 bp. PDP 1 primer set with expected band size at 199 bp. i) reactions using CHOS gDNA ii) reactions using CHOK1 gDNA. Primers were used for qPCR reactions with both tagged and untagged, endogenous and exogenously expressed PDH subunits.

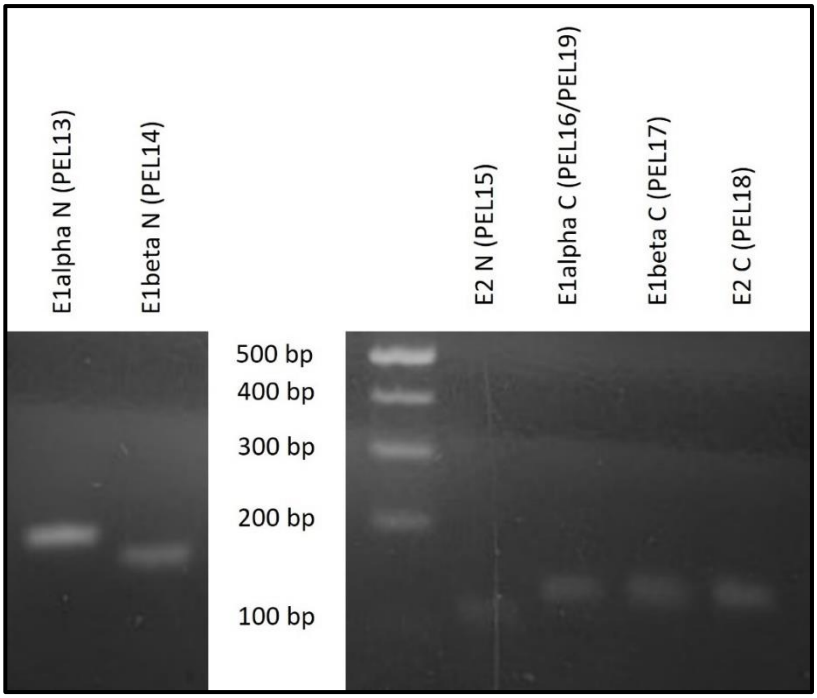

Appendix Figure 7.1.11 qPCR products when testing primers for PDH subunit genes with CHOS gDNA. E1alpha N-terminal V5 tag primer set test with expected band at 189 bp. E1beta N-terminal HA tag primer set test with expected band at 158 bp. E2 N-terminal FLAG tag primer set test with expected band at 113 bp. E1alpha C-terminal V5 tag primer set test with expected band at 137 bp. E1beta C-terminal HA tag primer set test with expected band at 137 bp. E2 C-terminal FLAG tag primer set test with expected band at 146 bp. Shown in brackets is the relevant PEL plasmid.

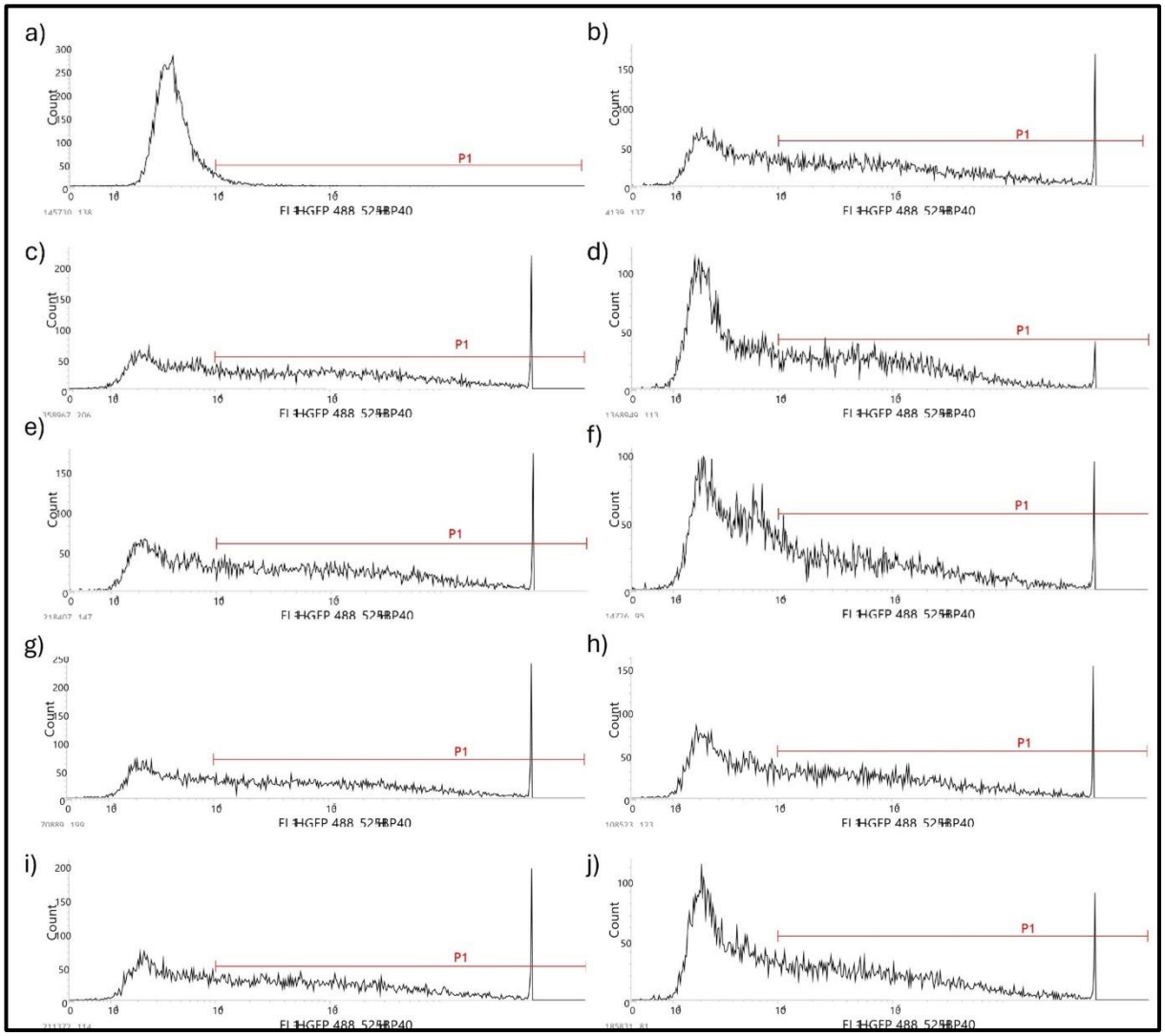

Appendix Figure 7.2.1 Histogram analysis from flow cytometry of PDK KO cell lines showing GFP expression as a result of the expression of CRISPR/Cas9 plasmids targeting PDK1 and PDK2 with a variety of gRNAs. A) CHOK1 host cells, B) Fut8 control KO cells, C) PDK1 KO with gRNAs 2 + 5, D) PDK1 KO with gRNAs 2 + 6, E) PDK1 KO with gRNAs 3 + 5, F) PDK1 KO with gRNAs 3 + 6, G) PDK2 KO with gRNAs 1 + 4, H) PDK2 KO with gRNAs 3 + 4, I) PDK2 KO with gRNAs 1 + 6, J) PDK2 KO with gRNAs 3 + 6.

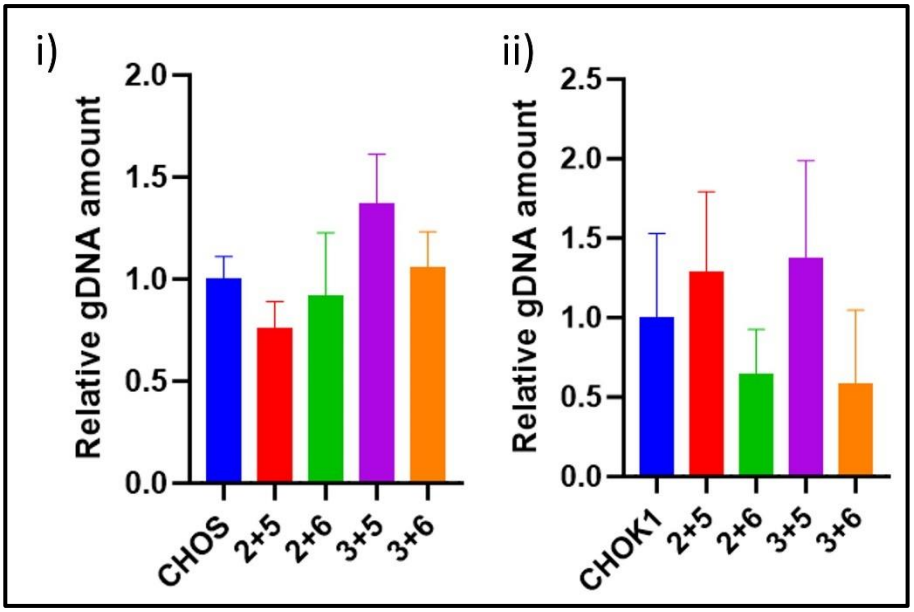

Appendix Figure 7.2.2 Relative gDNA amount of PDK1 in CHOS (i) and CHOK1 (ii) cell pools transfected with CRISPR/Cas9 KO plasmids with PDK1 targeting gRNAs analysed via qPCR from gDNA samples. PDK1 primers used to compare to GAPDH levels. A one-way ANOVA was performed using Dunnett's multiple comparisons test comparing the results to relevant host cells. Significance shown for key results where p value was less than or equal to 0.05. Extremely significant $p < 0.0001$ (****), Extremely significant $p = 0.0001$ to 0.001 (***), Very significant $p = 0.001$ to 0.01 (**), Significant $p = 0.01$ to 0.05 (*), Not significant $p \geq 0.05$ (ns). (n=3).

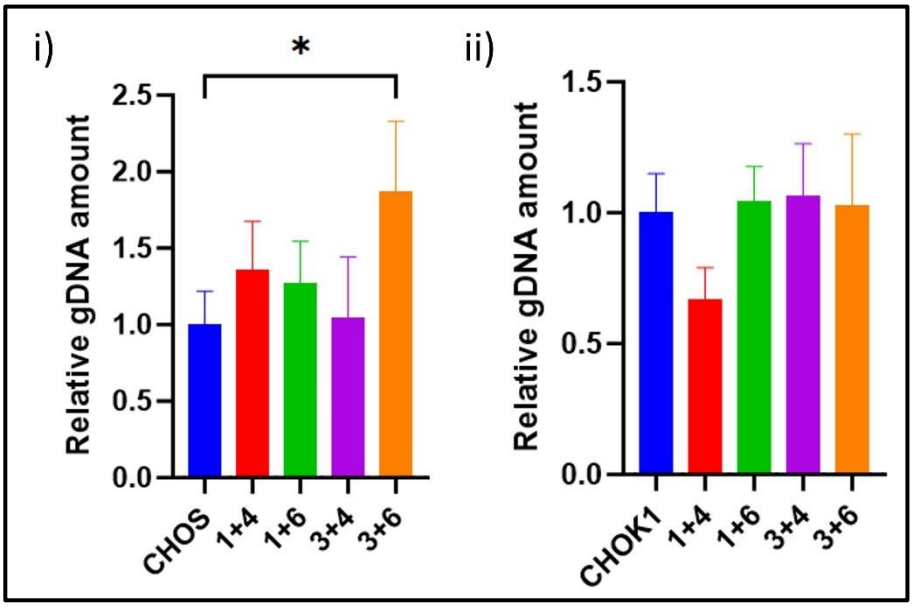

Appendix Figure 7.2.3 Relative gDNA amount of PDK2 in CHOS (i) and CHOK1 (ii) cell pools transfected with CRISPR/Cas9 KO plasmids with PDK2 targeting gRNAs analysed via qPCR from gDNA samples. PDK2 primers used to compare to GAPDH levels. A one-way ANOVA was performed using Dunnett's multiple comparisons test comparing the results to relevant host cells. Significance shown for key results where p value was less than or equal to 0.05. Extremely significant $p < 0.0001$ (****), Extremely significant $p = 0.0001$ to 0.001 (***), Very significant $p = 0.001$ to 0.01 (**), Significant $p = 0.01$ to 0.05 (*), Not significant $p \geq 0.05$ (ns). (n=3).

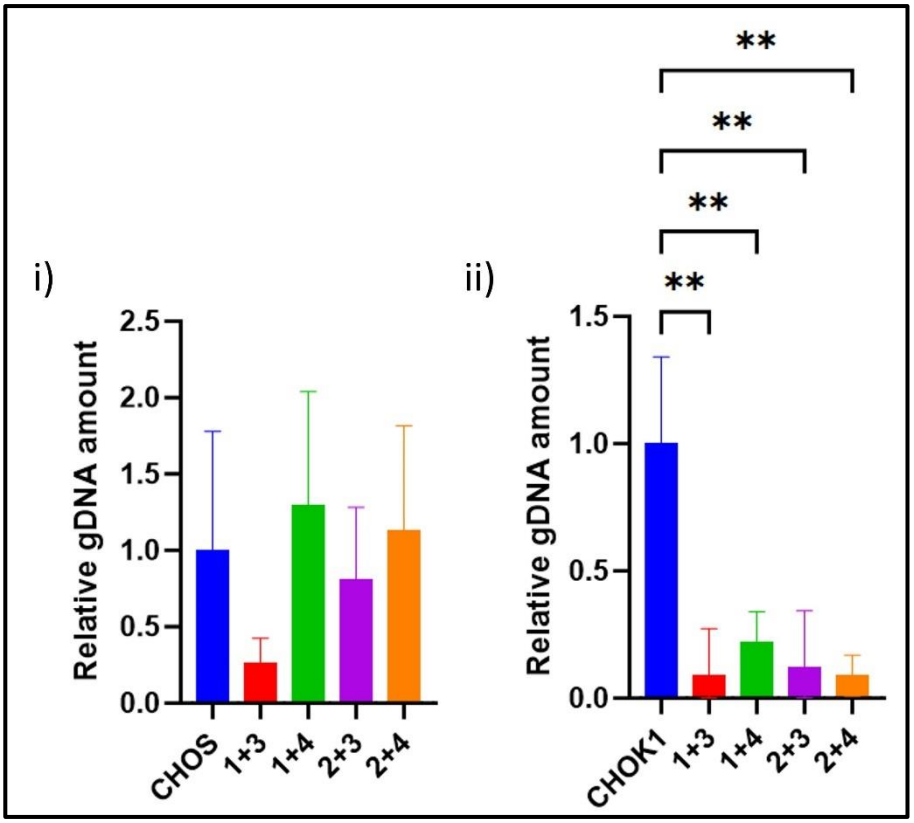

Appendix Figure 7.2.4 Relative gDNA amount of PDK3 in CHOS (i) and CHOK1 (ii) cell pools transfected with CRISPR/Cas9 KO plasmids with PDK3 targeting gRNAs analysed via qPCR from gDNA samples. PDK3 primers used to compare to GAPDH levels. A one-way ANOVA was performed using Dunnett's multiple comparisons test comparing the results to relevant host cells. Significance shown for key results where p value was less than or equal to 0.05. Extremely significant $p < 0.0001$ (****), Extremely significant $p = 0.0001$ to 0.001 (***), Very significant $p = 0.001$ to 0.01 (**), Significant $p = 0.01$ to 0.05 (*), Not significant $p \geq 0.05$ (ns). (n=3).

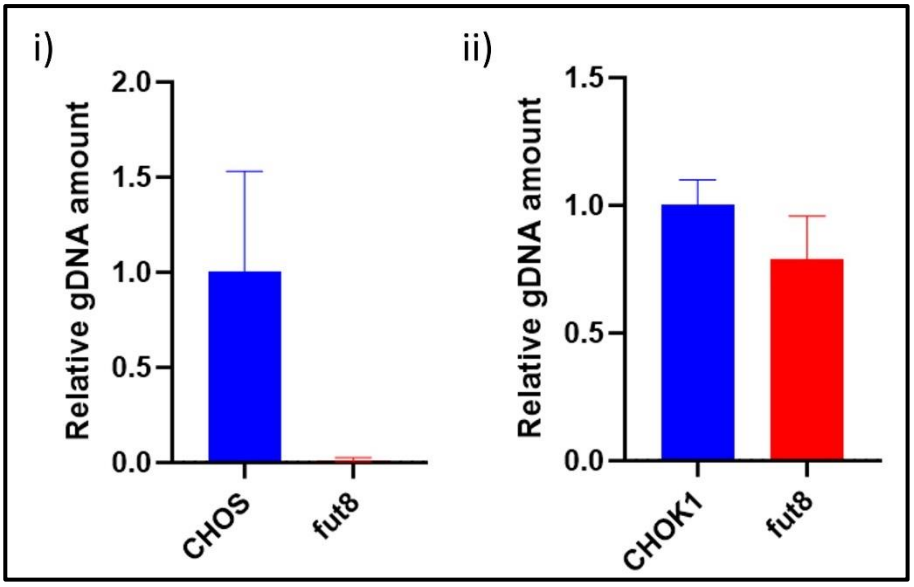

Appendix Figure 7.2.5 Relative gDNA amount of fut8 in CHOS (i) and CHOK1 (ii) cell pools expressing CRISPR/Cas9 KO plasmids with fut8 targeting gRNAs analysed via qPCR. fut8 primers taken from (Schmieder et al., 2018) used compared to GAPDH levels. A Welch's t test was performed comparing the results to relevant host cells. Significance shown for key results where p value was less than or equal to 0.05. Extremely significant $p < 0.0001$ (****), Extremely significant $p = 0.0001$ to 0.001 (***), Very significant $p = 0.001$ to 0.01 (**), Significant $p = 0.01$ to 0.05 (*), Not significant $p \geq 0.05$ (ns). (n=3).

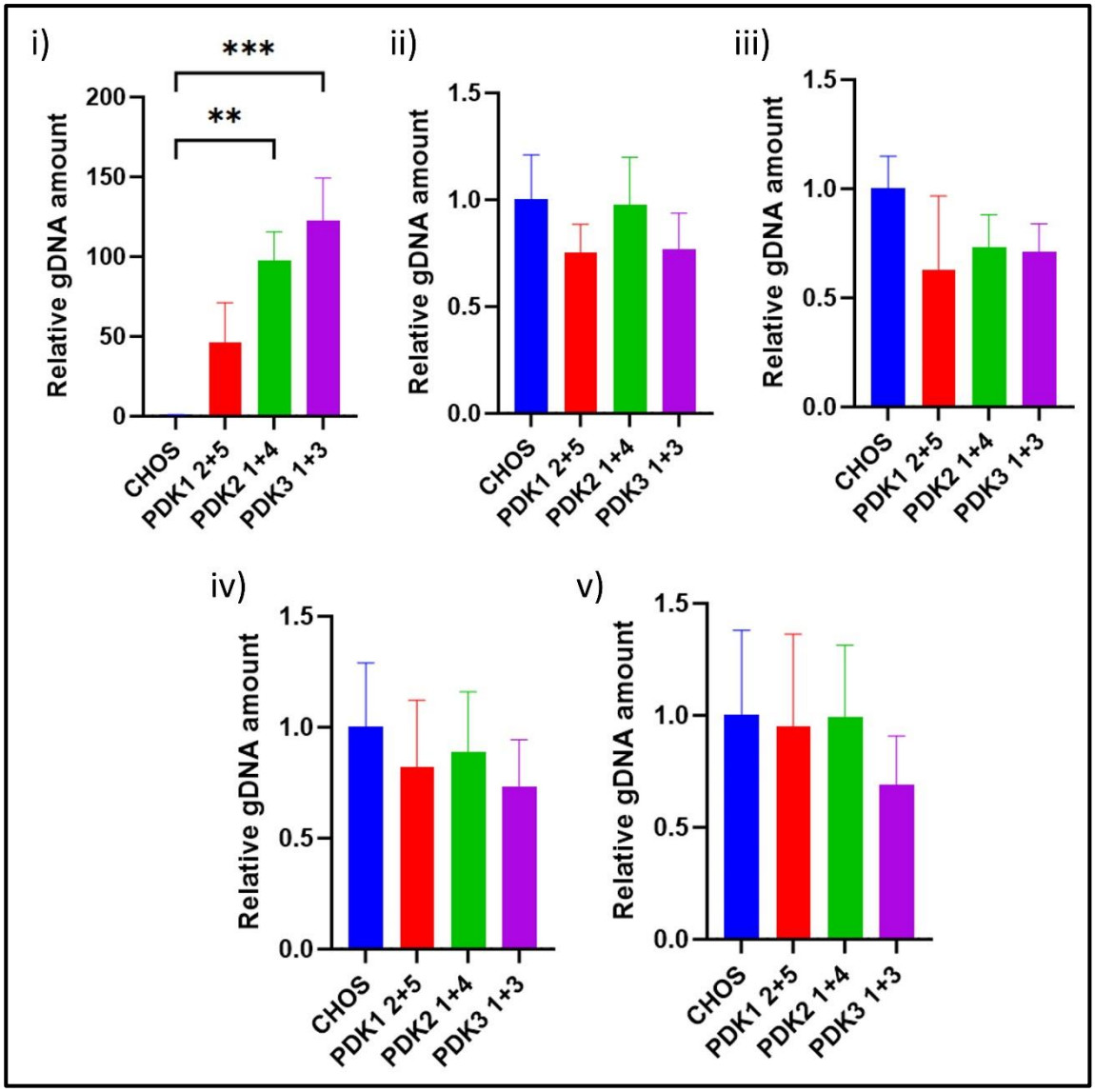

Appendix Figure 7.2.6 Relative gDNA amount of PDH subunit E1alpha (i), E1beta (ii), E2 (iii), E3BP (iv) and PDP (v) in CHOS cell pools transfected with CRISPR/Cas9 KO plasmids with PDK1, 2 and 3 targeting gRNAs analysed via qPCR from gDNA samples. E1alpha (i), E1beta (ii), E2 (iii), E3BP (iv) and PDP (v) primers used to compare to β-actin levels. PDK1 KO cell pools using gRNAs 2 + 5. PDK2 KO cell pools using gRNAs 1 + 4. PDK3 KO cell pools using gRNAs 1 + 3. A one-way ANOVA was performed using Dunnett's multiple comparisons test comparing the results to relevant host cells. Significance shown for key results where p value was less than or equal to 0.05. Extremely significant $p < 0.0001$ (****), Extremely significant $p = 0.0001$ to 0.001 (***), Very significant $p = 0.001$ to 0.01 (**), Significant $p = 0.01$ to 0.05 (*), Not significant $p \geq 0.05$ (ns). (n=3).

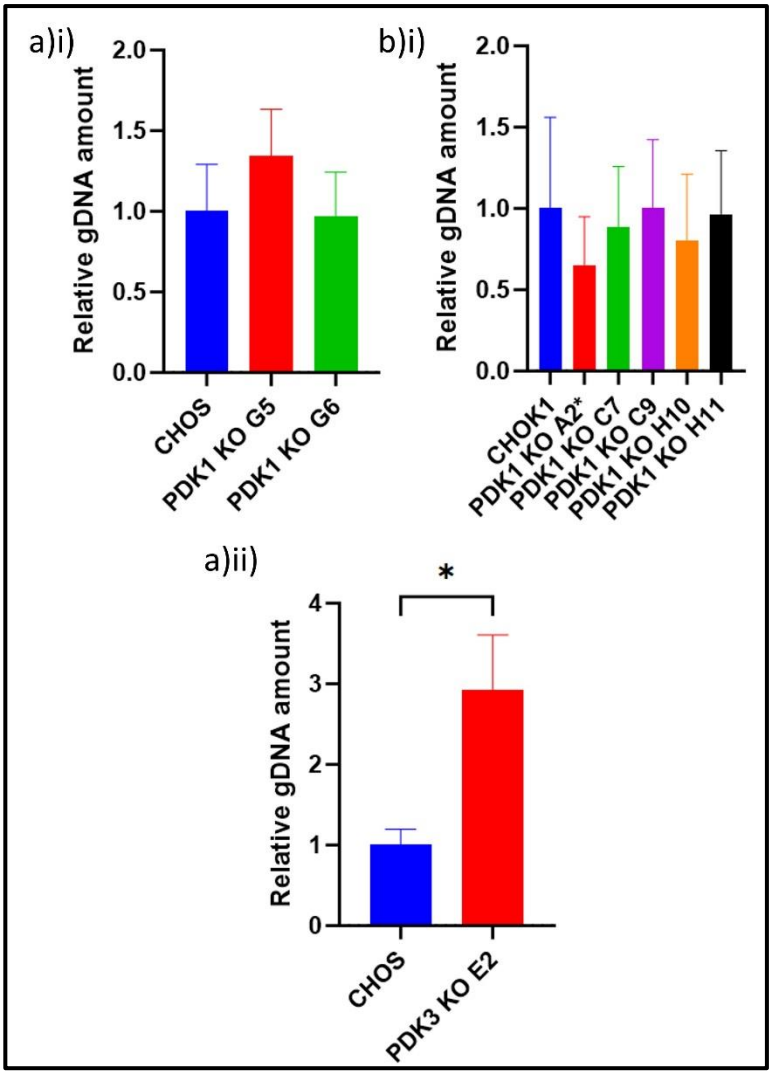

Appendix Figure 7.2.7 Relative gDNA amount of PDKs 1 (i) and 3 (ii) in CHOS (a) and CHOK1 (b) cell pools transfected with CRISPR/Cas9 KO plasmids with relevant PDK1 or PDK3 targeting gRNAs analysed via qPCR from gDNA samples. PDK1 (i) and PDK3 (ii) primers used to compare to β-actin levels in relevant host cells. Samples marked with an asterisk (*) are from pools with lower cell viability. A one-way ANOVA was performed using Dunnett's multiple comparisons test comparing the results to relevant host cells. Significance shown for key results where p value was less than or equal to 0.05. Extremely significant $p < 0.0001$ (****), Extremely significant $p = 0.0001$ to 0.001 (***), Very significant $p = 0.001$ to 0.01 (**), Significant $p = 0.01$ to 0.05 (*), Not significant $p \geq 0.05$ (ns). (n=3).

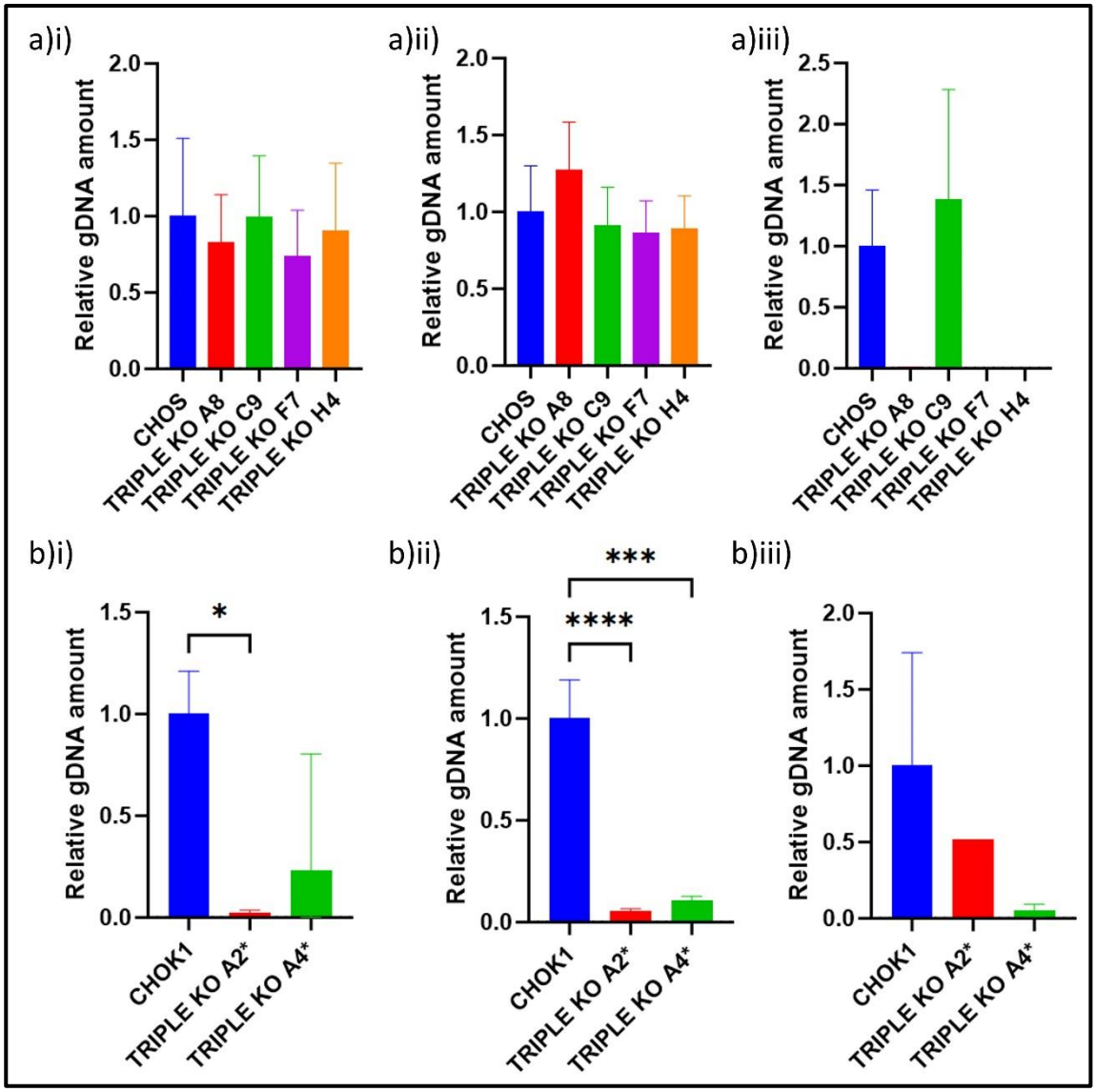

Appendix Figure 7.2.8 Relative gDNA amount of PDKs 1 (i), 2 (ii) and 3 (iii) in CHOS (a) and CHOK1 (b) cell pools transfected with CRISPR/Cas9 KO plasmids with PDK1, 2 and 3 targeting gRNAs to create a TRIPLE KO cell line analysed via qPCR from gDNA samples. PDK1 (i), PDK2 (ii) and PDK3 (iii) primers used to compare to β-actin levels in relevant host cells. Samples marked with an asterisk (*) are from pools with lower cell viability. A one-way ANOVA was performed using Dunnett's multiple comparisons test comparing the results to relevant host cells. Significance shown for key results where p value was less than or equal to 0.05. Extremely significant $p < 0.0001$ (****), Extremely significant $p = 0.0001$ to 0.001 (***), Very significant $p = 0.001$ to 0.01 (**), Significant $p = 0.01$ to 0.05 (*), Not significant $p \geq 0.05$ (ns). (n=3).

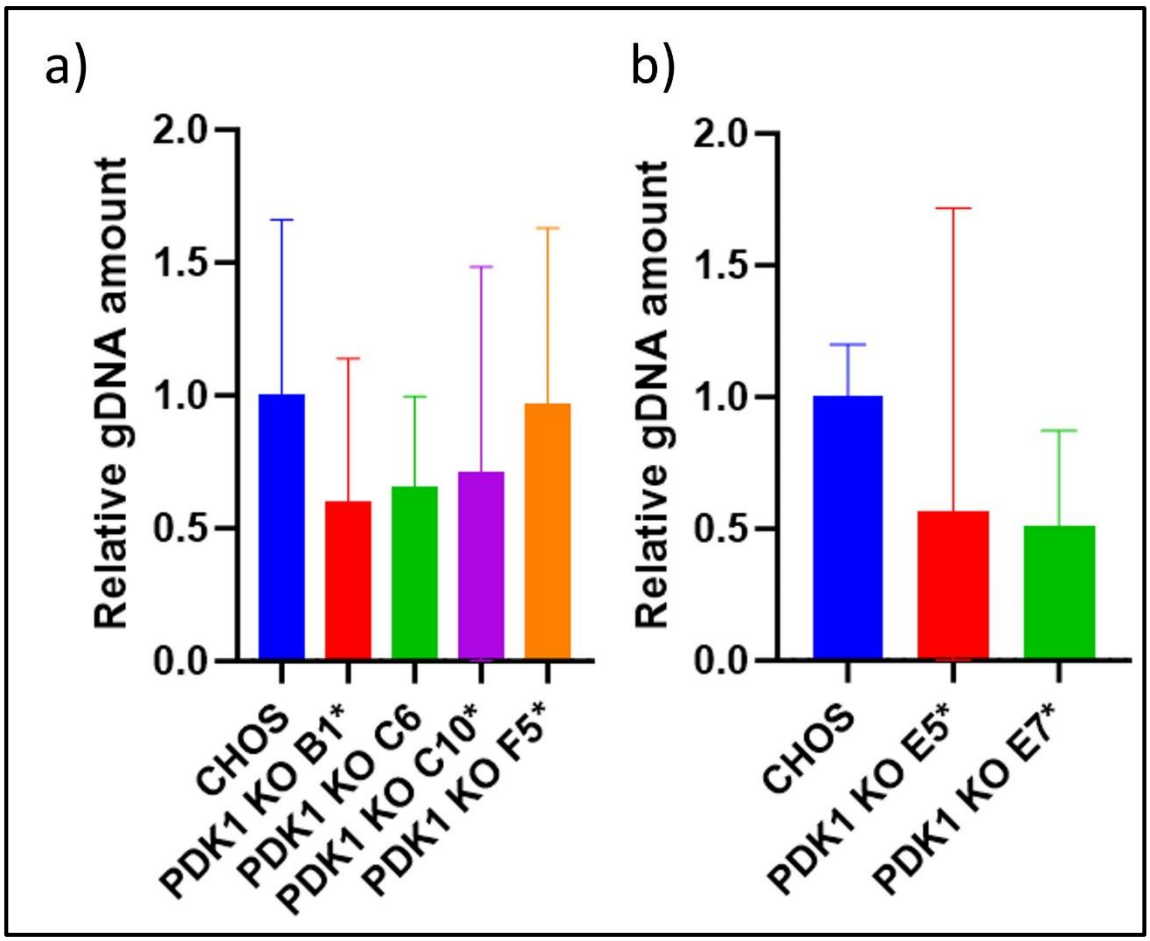

Appendix Figure 7.2.9 Relative gDNA amount of PDK1 in selected CHOS (a) and CHOK1 (b) cell pools transfected with CRISPR/Cas9 KO plasmids with PDK1 targeting gRNAs analysed via qPCR from gDNA samples. PDK1 primers used to compare β-actin levels. Samples marked with an asterisk (*) are from pools with lower culture viability. A one-way ANOVA was performed using Dunnett's multiple comparisons test comparing the results to relevant host cells. Significance shown for key results where p value was less than or equal to 0.05. Extremely significant $p < 0.0001$ (****), Extremely significant $p = 0.0001$ to 0.001 (***), Very significant $p = 0.001$ to 0.01 (**), Significant $p = 0.01$ to 0.05 (*), Not significant $p \geq 0.05$ (ns). (n=3).

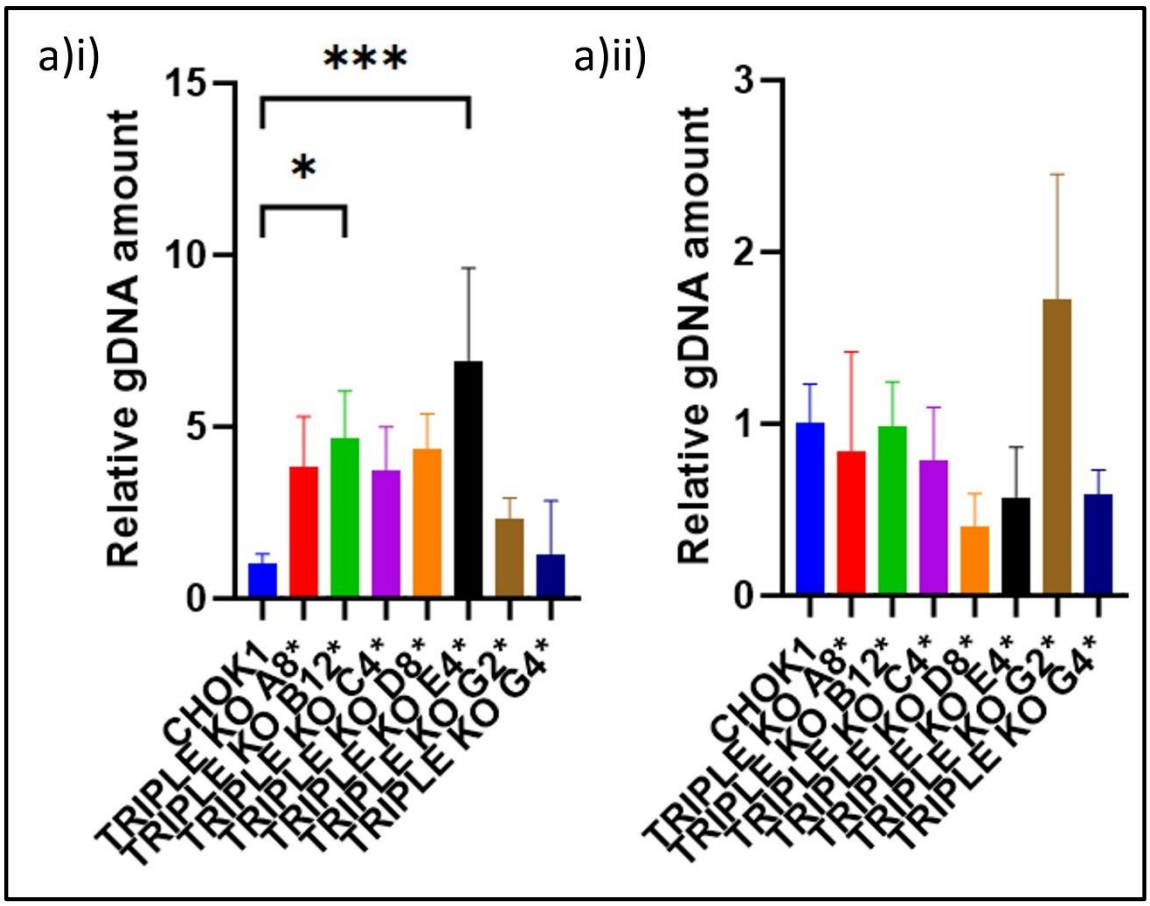

Appendix Figure 7.2.10 Relative gDNA amount of PDK1 (i) and PDK2 (ii) in selected and CHOK1 TRIPLE KO cell pools transfected with CRISPR/Cas9 KO plasmids with PDK1, 2 and 3 targeting gRNAs analysed via qPCR from gDNA samples. PDK1 (i) and 2 (ii) primers used to compare β-actin levels. Samples marked with an asterisk (*) are from pools with lower culture viability. A one-way ANOVA was performed using Dunnett's multiple comparisons test comparing the results to relevant host cells. Significance shown for key results where p value was less than or equal to 0.05. Extremely significant $p < 0.0001$ (****), Extremely significant $p = 0.0001$ to 0.001 (***), Very significant $p = 0.001$ to 0.01 (**), Significant $p = 0.01$ to 0.05 (*), Not significant $p \geq 0.05$ (ns). (n=3).